Characterisation of huntingtin localisation and transcriptional regulation in response to growth factor stimulation in an immortalised cell model of Huntington's Disease

by

Kathryn Rosemary Bowles

A thesis submitted to Cardiff University

for the degree of

Doctor of Philosophy

September 2013

MRC centre for Neuropsychiatric Genetics and Genomics

Cardiff University School of Medicine

Cathays

Cardiff

CF24 4HQ

DECLARATION

This work has not previously been accepted in substance for any degree and is not concurrently submitted in candidature for any degree.

Signed ……………………………………… (candidate)   Date …………………………

STATEMENT 1

This thesis is being submitted in partial fulfilment of the requirements for the degree of PhD.

Signed ……………………………………… (candidate)   Date …………………………

STATEMENT 2

This thesis is the result of my own independent work/investigation, except where otherwise stated.

Other sources are acknowledged by explicit references.

Signed ……………………………………… (candidate)   Date …………………………

STATEMENT 3

I hereby give consent for my thesis, if accepted, to be available for photocopying and for inter-library loan, and for the title and summary to be made available to outside organisations.

Signed ………………………………………… (candidate)   Date …………………………

STATEMENT 4: PREVIOUSLY APPROVED BAR ON ACCESS

I hereby give consent for my thesis, if accepted, to be available for photocopying and for inter-library loans **after expiry of a bar on access previously approved by the Graduate Development Committee.**

Signed ………………………………………… (candidate)   Date …………………………

Acknowledgements

First of all, I would like to thank my supervisors, Professor Lesley Jones and Professor Stephen Dunnett, for their invaluable support and encouragement throughout this project, and for having faith in my work and ability.

Many thanks also to Dr. Christopher George for taking the time to train a complete beginner in confocal microscopy, and to Dr. Claudia Consoli for teaching me how to perform qRTPCR. Also many thanks to Megan Musson in Cardiff Biotechnology Services for carrying out the microarray experiment for me.

I would particularly like to thank Yateen Patel, David Harrison and Emma Yhnell for their priceless help with mouse breeding, and for fitting me into their already busy schedules without complaint. Also thank you to everyone in the Biosciences department for their patience with me, and for accommodating me into their lab space at the most inconvenient times.

My wonderful colleagues have made it an absolute pleasure for me to come to work every day, in particular I would like to thank Lyn Elliston, Dr. Alis Hughes and Dr. Caroline Tinsley for always being ready to help, for their constant moral support, and for providing excellent company on all those essential coffee breaks.

Thank you to my parents for never failing to support and encourage me throughout my PhD. Finally, I would like to thank my husband, Eliot, for listening to countless presentation practices, for acting as taxi driver between labs on the weekends and for his never ending patience.

Thank you all ever so much.

Publications and presentations as a result of this project

Publications

- Bowles, K.R., Brooks, S.P., Dunnett, S.B. & Jones, L., 2012. Gene expression and behaviour in animal models of HD. *Brain Research Bulletin*, 88 (2-3), 276-284

Oral presentations

- Investigating the pathways leading to transcriptional dysregulation in a dynamic cell model of Huntington's disease (2012). NeuroDem Cymru annual conference, Cardiff, UK.

Poster presentations

- Bowles, K.R., Brooks, S.P., Thompson, L., Steffan, J., Dunnett, S.P. & Jones, L., 2011. The effect of growth factor stimulation on the phosphorylation and localisation of huntingtin. Gordon Research Seminar and Conference on CAG triplet repeat disorders. Barga, Italy

- Bowles, K.R., Dunnett, S.B. & Jones, L., 2012. Differential response to epidermal growth factor stimulation in an immortalised cell model of Huntington's Disease. Huntington's Disease Foundation 'Milton Wexler Celebration of life' conference, Boston, Massachusetts, USA.

- Bowles, K.R., Dunnett, S.B. & Jones, L., 2013. Differential gene expression and signalling responses to growth factor stimulation in an immortalised cell model of Huntington's Disease. Gordon Research Seminar and Conference on CAG triplet repeat disorders. Waterville Valley, New Hampshire, USA.

Abbreviations

3-NP	-	Nitropropionic acid
a.a.	-	Amino acid
Abs	-	Absorbance
Adamts5	-	A disintegrin-like and metallopeptidase (reprolysin type) with thrombospondin type 1 motif 5
Ahr	-	Aryl-hydrocarbon receptor
AKT	-	Protein kinase B
ANOVA	-	Analysis of variance
AP1	-	Activator protein 1
Arc	-	Activity-regulated cytoskeleton-associated protein
Arl4c	-	ADP-ribosylation factor-like 4C
Arntl	-	Aryl hydrocarbon receptor nuclear translocator-like
ASK1	-	Apoptosis signal-regulating kinase 1
asp	-	Aspartic acid
Atf3	-	Activating transcription factor 3
Bach1	-	BTB and CNC homology 1
BACHD	-	Bacterial artificial chromosome model of Huntington's Disease
BAD	-	B-cell lymphoma-2 associated death promoter
BAX	-	Bcl2-associated X protein
BCA	-	Bicinchoninic acid assay
Bcl2l1	-	BCL2-like 11 (apoptosis facilitator)
Bcl6b	-	B-cell CLL/lymphoma 6, member B
BCL-XL	-	B-cell lymphoma - extra-large
BDNF	-	Brain derived neurotrophic factor

BGP	-	Beta-glycerophosphate
BHLH	-	Basic helix-loop-helix
Bhlhe40	-	Basic helix-loop-helix family, member e40
Bis-Tris	-	Bis(2-hydroxyethyl)-amino-tris(hydroxymethyl)-methane
Bmp4	-	Bone morphogenic protein
bp	-	Base pairs
BSA	-	Bovine serum albumen
BSS	-	Balanced salt solution
CAAT	-	CCAAT binding factors
cAMP	-	Cyclic adenosine monophosphate
CBP	-	CREB-binding protein
CBS	-	Cardiff Biotechnology Services
Ccng2	-	Cyclin G2
Cdc42ep3	-	CDC42 effector protein (RHO GTPase binding) 3
Cdkn1α	-	Cyclin-dependent kinase inhibitor 1A (P21)
cDNA	-	Complementary deoxyribonucleic acid
Ceacam1	-	Carcinoembryonic antigen-related cell adhesion molecule 1
CK2	-	Casein kinase 2
CoSMAD	-	Common-mediator SMAD
CpG	-	Cytosine-phosphate-guanine
Crem	-	cAMP responsive element modulator
CRM1	-	Chromosome region maintenance 1
CSF	-	Cerebrospinal fluid
Csf1	-	Colony stimulating factor 1 (macrophage)
CSK	-	C-Src tyrosine kinase

C-SRC	-	Proto-oncogene tyrosine-protein kinase Src
C_t	-	Cycle threshold
Ctgf	-	Connective tissue growth factor
Cxb4	-	Chromobox homolog 4 (Drosophila Pc class)
Cyr16	-	Cysteine rich protein 61
DAG	-	Diacyl-glycerol
DAPI	-	4',6-diamidino-2-phenylindole
DARPP-32	-	Dopamine- and cAMP-regulated neuronal phosphoprotein
Ddit4	-	DNA-damage-inducible transcript 4
DEPC	-	Diethylpyrocarbonate
dH_2O	-	Distilled water
DMEM	-	Dulbecco's modified eagle medium
DMSO	-	Dimethyl sulfoxide
DNA	-	Deoxyribonucleic acid
dNTP	-	Deoxyribonucleotide triphosphate
DOK2	-	Docking protein 2
DTI	-	Diffusion tensor imaging
E14	-	Embryonic day 14
E2FF	-	E2F-homolog cell cycle regulators
EDTA	-	Ethylenediaminetetraacetic acid
EGF	-	Epidermal growth factor
EGFR	-	Epidermal growth factor receptor
Egr1	-	Early growth response 1
EGRF	-	Early growth response factor
EGTA	-	Ethylene glycol tetraacetic acid

ELISA	-	Enzyme-linked immunosorbent assay
ELK1	-	ETS-domain containing protein
Ereg	-	Epiregulin
ERK	-	Extracellular signal-regulated kinase
ESC	-	Embryonic stem cell
Ets2	-	E26 avian leukaemia oncogene 2, 3' domain
ETSF	-	E-twenty six factors
Etv5	-	Ets variant gene 5
FBS	-	Fetal bovine serum
FDR	-	False discovery rate
Fgf2	-	Fibroblast growth factor
FI	-	Fluorescence intensity
fMRI	-	Functional magnetic resonance imaging
Fosl1	-	Fos-like antigen 1
Foxa1	-	Forkhead box A1
Foxc2	-	Forkhead box C2
FOXO	-	Forkhead box proteins
Fzd8	-	Frizzled homolog 8 (Drosophila)
Gadd45g	-	Growth arrest and DNA-damage-inducible, gamma interacting protein
Gapdh	-	Glyceraldehyde 3-phosphate dehydrogenase
GDP	-	Guanosine diphosphate
GO	-	Gene ontology
Grasp	-	General receptor for phosphoinositides 1- associated scaffold protein
GRB2	-	Growth factor receptor bound protein 2
GTP	-	Guanosine triphosphate

H3	-	Histone 3
H$_3$BO$_3$	-	Boric acid
HAND	-	Twist subfamily of class B bhlh transcription factors
HAP1	-	Huntingtin-associated protein 1
HD	-	Huntington's Disease
HDCRG	-	Huntington's Disease Collaborative Research Group
Hdh	-	Huntington's Disease homolog
HEAT	-	Huntingtin, elongation factor 3, protein phosphatase 2A, and Tor1
Hivep1	-	Human immunodeficiency virus type 1 enhancer binding protein 1
Hmga2	-	High mobility group AT-hook 2
HOMF	-	Homeodomain transcription factors
Hoxa	-	Homeobox
HSD	-	Honestly significant difference
HTT	-	Huntingtin
Id	-	Inhibitor of DNA binding
IE	-	Immediate-early
IF	-	Immunofluorescence
Igfbp3	-	Insulin-like growth factor binding protein 3
IKK	-	Inhibitor of kappa-β kinase
IKKβ	-	Inhibitor of kappaB kinase-β
IKKγ	-	Inhibitor of kappaB kinase-γ
iPSC	-	Induced pluripotent stem cells
Irf2bp2	-	Interferon regulatory factor 2 binding protein 2
IT15	-	Interesting transcript 15
Jarid2	-	Jumonji, AT rich interactive domain

JNK	-	c-jun N-terminal kinase
Jub	-	Ajuba
K	-	Lysine
KCl	-	Potassium chloride
kDa	-	Kilodalton
Kdm6b	-	KDM1 lysine - specific demethylase 6B
Kitl	-	Kit ligand
Klf5	-	Kruppel-like factor 5
LDS	-	Lithium dodecyl sulphate
LEFF	-	Lymphoid enhancer factor-1/T-cell factor family
MAPK	-	Mitogen activated protein kinase
MAZF	-	MYC-associated zinc finger protein
MEK	-	Mitogen activated protein kinase kinase
MEKK	-	MAP kinase kinase kinase
$MgCl_2$	-	Magnesium chloride
mHTT	-	Mutant huntingtin
mins	-	Minutes
miRNA	-	Micro RNA
MKK	-	Mitogen activated protein kinase kinase
ml	-	Millilitres
MLK2	-	Mixed lineage kinase 2
MMP	-	Matrix metalloproteinases
MOPS	-	3-(N-morpholino)propanesulfonic acid
MRI	-	Magnetic resonance imaging
mRNA	-	Messenger RNA
MSN	-	Medium spiny neurons

Mxi1	-	Max interacting protein 1
Mybl1	-	Myeloblastosis oncogene-like 1
Myc	-	myelocytomatosis oncogene
N/C	-	Nuclear/Cytoplasmic
N/P	-	Nuclear/Perinuclear
Na_2EDTA	-	Disodium-EDTA
Na_3VO_4	-	Sodium orthovanadate
$Na_4P_2O_7$	-	Sodium pyrophosphate
NaCl	-	Sodium chloride
NES	-	Nuclear export signal
Nfil3	-	Nuclear factor, interleukin 3, regulated
NFκβ	-	Nuclear factor kappa-light-chain-enhancer of activated B-cells
ng	-	Nanograms
NGF	-	Nerve growth factor
Ngfib	-	Nerve growth factor IB
NH_4	-	Ammonium
NII	-	Neuronal intranuclear inclusions
NLS	-	Nuclear localisation signal
nm	-	Nanometres
nM	-	Nanomolar
NOLF	-	Neuron-specific-olfactory factor
NR2F	-	Nuclear receptor subfamily 2 factors
Nr4a	-	Nuclear receptor subfamily 4, Group A
NRSF	-	Neuron-restrictive silencing factor
OAZF	-	Oligodenylate synthetase

P/C	-	Perinuclear/Cytoplasmic
P300	-	Binding protein 300
P53	-	Tumour suppressor protein 53
P75 NTR	-	P75 neurotrophin receptor
PARP	-	Poly (ADP-ribose) polymerase
PAX5	-	Paired box protein 5 binding sites
Pax9	-	Paired box gene 9
PBS	-	Phosphate buffered saline
PBS-T	-	Phosphate buffered saline-Tween
PC12	-	Pheochromocytoma 12
PCA	-	Principal components analysis
PCR	-	Polymerase chain reaction
PDK-1	-	Pyruvate dehydrogenase lipoamide kinase isozyme 1, mitochondrial
Pdk4	-	Pyruvate dehydrogenase kinase, isoenzyme 4
PHLPP1	-	PH domain leucine-rich repeat protein phosphatase 1
PI3K	-	Phosphatidylinositide 3-kinases
PIP	-	Phosphatidylinositol phosphate
PKC	-	Protein kinase C
PLAG	-	Pleiomorphic a denoma gene
PLCγ	-	Phospholipase C, gamma
PML	-	Promyelocytic leukaemia
PMSF	-	Phenylmethanesulfonylfluoride
PMT	-	Photomultiplier tube
polyQ	-	Polyglutamine
Ppargc1α	-	Peroxisome proliferative activated receptor, gamma, coactivator 1 alpha

PPI	-	Pre-pulse inhibition
Prl2c	-	Prolactin family 2, subfamily C
Ptger4	-	Prostaglandin E receptor 4
Ptgfr	-	Prostaglandin F receptor
Ptgs2	-	Prostaglandin-endoperoxide synthase 2
Pthlh	-	Parathyroid hormone-like peptide
Ptp4α1	-	Protein tyrosine phosphatase 4a 1
PVDF	-	Polyvinylidene difluoride
PY-NLS	-	Proline-tyrosine NLS
qRTPCR	-	Quantitative reverse transcription PCR
RAF	-	Rapidly accelerated fibrosarcoma
Ramp3	-	Receptor (calcitonin) activity modifying protein 3
RAS	-	Rat sarcoma
Rasa1	-	RAS p21 protein activator 1
RasGAP	-	RAS GTPase activating protein
RE1/NRSE	-	Repressor element 1/neuron-restrictive silencing element
REST/NRSF	-	Repressor element 1-silencing transcription factor/neuron-restrictive silencing factor
Rgs	-	Regulator of G-protein signalling
Rims2	-	Regulating synaptic membrane exocytosis 2
RIN	-	RNA integrity number
RIPA	-	Radioimmunoprecipitation assay
RMA	-	Robust multi-array average
RNA	-	Ribonucleic acid
Rnd3	-	Rho family GTPase
RQ	-	Relative quantification

RREB	-	Ras-responsive element binding protein
Rrs1	-	Regulator of ribosome synthesis
RSMAD	-	Receptor-regulated SMAD
RXRF	-	RXR heterodimer binding sites
S	-	Serine
SAPK	-	Stress-activated protein kinase
Scmh1	-	Sex comb on midleg homolog 1
SDS	-	Sodium dodecyl sulfate
SDS-PAGE	-	Sodium dodecyl sulphate - polyacrylamide gel electrophoresis
SEM	-	Standard error of the mean
ser	-	Serine
SETDB1	-	SET-domain, bifurcated 1
SGK	-	Serine/threonine protein kinase
SH3	-	SRC-homology 3
Sik1	-	Salt inducible kinase 1
siRNA	-	Small interfering RNA
SMAD	-	Mothers against decapentaplegic homolog
Smurf	-	Smad specific E3 ubiquitin protein ligase 2
Socs3	-	Suppressor of cytokine signalling 3
SORY	-	Sox/SRY-sex/testis determining and related HMG box factors
SOS	-	Son of sevenless
SOX	-	Sex-determining region Y-box
SP1	-	Specificity protein 1
Spry2	-	Sprouty homolog 2
SRSF6	-	Serine/arginine-rich splicing factor 6

STAT	-	Signal transducer and activator of transcription
StHdh	-	Striatal Huntington's Disease homolog
SUMO	-	Small ubiquitin like modifier
SV40	-	Simian vacuolating 40
T3	-	Threonine 3
TBE	-	Tris/borate/EDTA
TBP	-	TATA-binding protein
Tead4	-	TEA domain family member 4
TF	-	Transcription factor
TGFβI	-	Transforming growth factor beta-induced
TGFβ	-	Transforming growth factor beta
Tgfβr	-	Transforming growth factor beta receptor
Thbs1	-	Thrombos pondin 1
thr	-	Threonine
Tlr2	-	Toll-like receptor 2
TPR	-	Translocated promoter region
TRAF6	-	TNF receptor associated factor 6
TR-FRET	-	Time resolved - fluorescence resonance energy transfer
Tris	-	Trisaminomethane
Tris-HCl	-	Tris-Hydrochloride
TRKA	-	Tyrosine kinase A
TRKB	-	Tyrosine kinase B
Tsc22d3	-	TSC22 domain family, member 3
Tshz1	-	Teashirt zinc finger family member 1
TSS	-	Transcription start site
Twist1	-	Twist homolog 1 (Drosophila)

tyr	-	Tyrosine
Ubc	-	Ubiquitin C
UHDRS	-	Unified Huntington's Disease Rating Scale
Usp43	-	Ubiquitin specific protease 43
UV	-	Ultraviolet
V	-	Volts
Vdr	-	Vitamin D receptor
Vegfa	-	Vascular endothelial growth factor A
WB	-	Western blot
WT	-	Wild-type
YAC	-	Yeast artificial chromosome
ZF	-	C2H2 zinc finger transcription factors
ΔC_t	-	Delta cycle threshold
μm	-	Micrometre
μM	-	Micromolar
μs	-	Microsecond

Summary

Huntington's Disease (HD) is an autosomal dominant neurodegenerative disease caused by a CAG expansion on the HD gene on chromosome 4, which gives rise to an expanded polyglutamine (polyQ) tract in the huntingtin protein. HD is characterised primarily by motor abnormalities, but is also commonly associated with cognitive impairments and psychiatric disturbances.

Huntingtin (HTT) dynamically shuttles between subcellular compartments, however the mutant huntingtin protein (mHTT) is mislocalised to cell nuclei, where it may interfere with nuclear functions, such as transcription. The phosphorylation of HTT has been implicated with the regulation of its subcellular localisation; however the mechanism by which the mislocalisation of mHTT occurs is currently unknown.

The localisation of HTT in an immortalised embryonic striatal cell model of HD ($StHdh^{Q111}$) was identified as being more nuclear with a longer polyQ length. Additionally, stimulation of $StHdh^{Q111}$ lines with a panel of growth factors alters the apparent subcellular localisation of HTT in a polyQ length-dependent manner.

Aberrant kinase responses to growth factor stimulation were identified by ELISA assay. Inhibition of AKT1 and MEK1 phosphorylation indicated that their activation may be involved in mHTT mislocalisation and immediate-early gene expression.

Transcriptional dysregulation is a characteristic feature of HD pathogenesis that may be directly influenced by HTT localisation. Microarray analysis of differential gene expression responses to growth factor stimulation uncovered a potential role for SMAD transcription factor activity and the transforming growth factor-β pathway in HD pathogenesis. Primary embryonic striatal cells from the Hdh^{Q111} and Hdh^{Q150} mouse models of HD showed similarities to the $StHdh^{Q111}$ cell model in terms of HTT localisation, kinase signalling and gene expression.

Cellular dysfunction may therefore be an early HD phenotype that is present from embryogenesis, and potentially alters HD development and progression; aberrant control of kinase signalling may regulate mHTT mislocalisation, which in turn modulates transcriptional dysregulation and contributes to HD pathogenesis.

Contents

List of tables and figures

Tables

Chapter 1: General introduction

Chapter 2: Materials and methods

Chapter 3: The localisation and phosphorylation of huntingtin in immortalised murine knock-in embryonic striatal cell lines

Chapter 4: Characterisation of the signalling pathways induced by growth factor stimulation in immortalised embryonic striatal cells

Chapter 5: Comparing differential gene expression changes in an immortalised cell model of HD in response to either NGF or EGF stimulation

Chapter 6: Recapitulating the effects of EGF stimulation on HTT localisation, kinase signalling pathways and transcriptional control in primary embryonic striatal cells from the Hdh^{Q111} and Hdh^{Q150} mouse models of HD

Figures

Chapter 1: General introduction

Chapter 2: Materials and methods

Chapter 3: The localisation and phosphorylation of huntingtin in immortalised murine knock-in embryonic striatal cell lines

Chapter 4: Characterisation of the signalling pathways induced by growth factor stimulation in immortalised embryonic striatal cells

Chapter 5: Comparing differential gene expression changes in an immortalised cell model of HD in response to either NGF or EGF stimulation

Chapter 6: Recapitulating the effects of EGF stimulation on HTT localisation, kinase signalling pathways and transcriptional control in primary embryonic striatal cells from the Hdh^{Q111} and Hdh^{Q150} mouse models of HD

Chapter 7: General discussion

Chapter 1: General introduction

1.1   Background to HD

   1.1.1   Historical background

In 1872, George Huntington provided the first comprehensive description of a 'hereditary chorea'; his detailed and vivid description meant that this disorder would later become known as 'Huntington's Disease' (HD). The inheritance of HD was subsequently found to be autosomal dominant (Hayden 1981), and the disease gene was localised to chromosome 4p16.3 (Gusella et al. 1983). However, it wasn't until 1993 that the HD gene itself (IT15) was identified, and the polymorphic expansion of a trinucleotide 'CAG' repeat on the 5' end of the gene was recognised as the genetic cause of HD (HDCRG 1993). CAG repeat lengths found in the unaffected general population are between 9 - 39, although individuals suffering from HD have been found to have CAG expansions of between 35 – 86 repeats with a median repeat size of around 46. However, expansions over 100 CAG repeats have also been identified in rare cases (De Rooij, De Koning Gans, Skraastas et al. 1993; Duyao et al. 1993; HDCRG 1993; Nørremølle et al 1993; Read 1993; Snell et al.1993; Rubinsztein et al. 1996).

The detection of the gene was largely aided by the discovery of large HD-affected families in the Lake Maracaibo region of Venezuela by Dr. Americo Negrette in 1955 (Okun & Thommi 2004), who were consequently a rich source of genetic information following a sustained and intensive collaborative research effort (Wexler 1995; Wexler 2012). Since its discovery, there has been a plethora of research that has aimed to fully characterise the HD gene and its function, and to develop effective interventions and treatments for HD. However, despite knowing the genetic basis for HD, the causal sequence leading to manifestation of the disease still remains unclear.

   1.1.2 Clinical phenotypes

HD is characterised primarily by motor disturbances, but is commonly accompanied by cognitive impairments and psychiatric abnormalities (Buckley et al. 2010; Myers et al.

1985; Martin et al. 1986; Folstein 1989; Vonsattel & DiFiglia 1998; Novak & Tabrizi 2010; Wexler 2012). HD noticeably manifests in the third to fourth decades of life, with the average age of onset being around 40 years (Novak & Tabrizi 2010). However, there is a substantial spread in the age of onset; this ranges from 2 to over 80 years old, with CAG repeat length accounting for only 40-70% of this variability (Hayden 1981; HDCRG 1993; Kremer et al. 1993; Novak & Tabrizi 2010; Wexler 2012). Despite being a monogenic, autosomal dominant disease, there is a wide range of severity and rates of progression following disease onset (MacMillan et al. 1993), and individuals may live with HD for 10-20 years before death (Vonsattel & DiFiglia 1998).

1.1.2.1 Motor symptoms

Involuntary choreiform movements are among the most common motor abnormalities that occur in HD, and become progressively more severe with time (Myers et al. 1985; Vonsattel & DiFiglia 1998; Bates & Murphy 2002; Buckley et al. 2010). This may also be accompanied by incoordination, motor impersistence and slow saccadic eye movements (Reiner et al. 1988; Reilmann et al. 2001; Walker 2007), as well as difficulty maintaining gaze and a lack of balance (Bates & Murphy 2002). Despite the prevalence of chorea in HD patients, it may not be a suitable marker for the severity of progression (Young et al. 1986; Mahant et al. 2003); in many cases, the incidence of chorea may be transient, or it may not develop in patients at all. In later stages of the disease, patients can also develop rigidity and dystonia, which make the chorea appear less prominent (Berardelli et al. 1999; Squitieri et al. 2000). In addition, some individuals experience an atypical onset of HD motor phenotypes, such as Parkinsonism, ataxia and dystonia, as well as bradykinesia and rigidity (Berardelli et al. 1999; Squitieri et al. 2000); these patients tend to have larger CAG repeat lengths and an earlier age of onset, and these atypical onsets have been associated with a more severe course of progression (Squitieri et al. 2000).

1.1.2.2 Cognitive symptoms

Cognitive impairments may also be present as early as during the prodromal stages of HD (Kirkwood et al. 2000; Ho et al. 2003; Holl et al. 2013), and tend to worsen following motor symptom onset (Stout et al. 2001; Campbell et al. 2004; Buckley et al.

2010; Novak & Tabrizi 2010). For example, individuals with HD often experience a deficit in executive function, such as a decreased ability for organisation and planning, and have delayed acquisition of learning new tasks (Crauford & Snowden 2002; Folstein 1989; Novak & Tabrizi 2010). In addition, their performance on the Stroop test (a measure of prepotent response inhibition) and verbal fluency are impaired from early disease development (Holl et al. 2013), and impairments of risky decision making, as measured by the Iowa gambling task, may also worsen with disease progression (Stout et al. 2001; Campbell et al. 2004). Many individuals may also develop problems with working memory and emotion recognition (Tabrizi et al. 2009; Duff et al. 2010; Stout et al. 2011; Labuschagne et al. 2013). These cognitive and emotional deficits can be some of the most concerning for patients, and can be highly disruptive to their general ability to function, independent of motor impairments (Rothlind et al. 1993).

1.1.2.3 Psychiatric symptoms

Emotional, behavioural and psychiatric disturbances are common in HD, and their development often precedes, and are more distressing than, motor symptoms (Myers et al. 1985; Martin et al. 1986; Dimaio et al. 1993; Rothlind et al. 1993; Klöppel et al. 2010; Novak & Tabrizi 2010; Labuschagne et al. 2013). These changes typically include increased irritability, forgetfulness, and anxiety (Folstein 1989; Klöppel et al. 2010).

Depressive symptoms are estimated as affecting as many as 33-69% of HD sufferers (Paulsen et al. 2008; Novak & Tabrizi 2010; Wexler 2012; Chisholm et al. 2013), and this has been associated with an increased suicide rate in individuals with HD; suicide was identified as a major feature of the illness by George Huntington in 1872, and the risk of attempting suicide in HD populations has been estimated to be between 5-10 times higher than in the general population (Schoenfeld et al. 1984; Dimaio et al. 1993; Robins Wahlin et al. 2000; Baliko et al. 2004). The largest proportion of those either attempting suicide or with suicidal ideation in the HD population were in the very early stages of the disease, or were gene carriers approaching the threshold for diagnosis (Schoenfeld et al. 1984; Paulsen et al. 2005). Other severe psychiatric conditions that may also develop in HD-affected individuals include hallucinations, delusions, paranoia

and obsessive-compulsive behaviour, although these are less common (Novak & Tabrizi 2010; Wexler 2012).

1.1.2.4 Monitoring progression

In order to monitor the progression of HD in individuals, both prior to and following diagnosis, the Unified Huntington's Disease Rating Scale (UHDRS) was developed to assess the clinical features of HD (Huntington Study Group 1996). The scale includes quantifiable measures of motor, cognitive, behavioural and functional components within the HD phenotype; further details of which can be found in Table 1.1.

Motor Assessment	Cognitive Assessment	Behavioural Assessment
Ocular pursuit	Verbal fluency test	Sad/Mood
Saccade initiation	Symbol digit modalities test	Low self esteem
Saccade velocity	Stroop interference test	Anxiety
Dysarthria		Suicidal thoughts
Tongue protrusion		Disruptive or aggressive behaviour
Maximal dystonia (trunk and extremities)	Functional Capacity	Irritable behaviour
Maximal chorea (face, mouth, trunk and extremities)	Occupation	Obsessions
Retropulsion pull test	Finances	Compulsions
Finger taps	Domestic chores	Delusions
Pronate/supinate hands (right and left)	Activities of daily living	Hallucinations
Luria (fist-hand-palm test)	Care level	I: Confused?
Rigidity (arms)		I: Demented?
Bradykinesia (body)		I: Depressed
Tandem walking		I: Require pharmacotherapy for depression?
Gait		

Table 1.1 Continued on next page

Functional Assessment
Can the subject…
Engage in gainful employment in accustomed work?
Engage in any gainful employment?
Engage in any volunteer work?
Manage finances?
Shop for groceries without help?
Handle money in cash transactions?
Supervise children without help?
Operate an automobile safely?
Do housework without help?
Do laundry without help?
Prepare meals without help?
Use the telephone without help?
Take medication without help?
Feed themselves without help?
Dress themselves without help?
Bathe themselves without help?
Use public transportation without help?
Walk within neighbourhood without help?
Walk without falling?
Walk without help?
Comb hair without help?
Transfer between chairs without help?
Get in and out of bed without help?
Use the toilet without help?
Care still be provided at home?

Independence Scale	
100	No special care needed
90	No physical care needed if difficult tasks are avoided
80	Pre-disease level of employment changes or ends, cannot perform chores to pre-disease level, may need help with finances
70	Self-care maintained for bathing, limited household duties, driving terminates, unable to manage finances
60	Needs minor assistance in dressing, toileting, bathing, food must be cut
50	24-hour supervision, assistance required for bathing, eating, toileting
40	Chronic care facility needed, limited self-feeding, liquefied diet
30	Patient provides minimal assistance in own feeding, bathing, toileting
20	No speech, must be fed
10	Tube fed & bed care

Table 1.1 The unified Huntington's disease rating scale (UHDRS) (Huntington Study Group 1996). Motor assessments are graded from 0 (normal) to 4 (unable to complete task). The cognitive assessments are based on the raw scores from each test, and each point within the behavioural assessment is graded for severity (0 = Absent – 4 = severe) and frequency (0 = almost never – 4 = almost always). The last four points prefixed 'I:' are based on the investigator's opinion of the subject's behaviour. Functional capacity is graded from 0 (unable/total care) to 3 (normal), and functional assessment requires yes/no responses. The most accurate level reflecting the subject's independence is selected from the independence scale.

More recently, a battery of tests has been assembled that is more sensitive to the development of subtle HD phenotypes in the prodromal stages of the disease prior to a formal diagnosis, and in early stages of progression, in order to provide reliable measures for clinical trial end points (Tabrizi et al. 2012; Tabrizi et al. 2013). Progression can be ascertained by the monitoring of fine motor skills, such as speeded finger tapping (Bechtel et al. 2010), as well as several measures of cognitive performance and the use of imaging techniques to assess brain atrophy; Table 1.2 outlines the array of tests sensitive to early HD progression in this study (Tabrizi et al. 2009; Tabrizi et al. 2011; Tabrizi et al. 2012; Tabrizi et al. 2013).

	Prodromal	Early-HD
Neuroimaging measures		
Whole brain atrophy	✓	✓
Ventricular expansion	✓	✓
Caudate atrophy		✓
Putamen atrophy		✓
White matter atrophy	✓	✓
Grey matter atrophy	✓	✓
Cognitive measures		
Symbol digit modality test		✓
Stroop test		✓
Emotion recognition		✓
UHDRS		
Motor assessment	✓	✓
Functional capacity		✓
Quantitative motor measures		
Chorea position index		✓
Chorea orientation index		✓
Grip force variability		✓
Speed-tapping tap duration		✓
Speed-tapping inter-tap interval	✓	✓
Psychiatric measures		
Problem behaviours assessment, Apathy		✓

Table 1.2 HD assessment measures utilised in the TRACK-HD study (Tabrizi et al. 2012; Tabrizi et al. 2013) that exhibited significant progression compared to controls in prodromal and/or early stage HD individuals over a period of 24-36 months.

1.1.2.5 Peripheral symptoms

The progression of HD is also associated with a variety of peripheral effects; one of the most marked is weight loss, often despite an increased appetite and an increase in calorie intake (Farrer & Meaney 1985; Morales et al. 1989; Pratley et al. 2000; Robbins et al. 2006; Aziz et al. 2008; van der Burg et al. 2009). A higher body weight has been associated with slower progression (Myers et al. 1991), and the extent of weight loss has been correlated with CAG repeat length (Aziz et al. 2008). Even in the very early stages of disease, the body mass index (BMI) of HD patients tends to be lower than in matched controls (Djoussé et al. 2002). This weight loss has been attributed to metabolic effects (Mochel et al. 2007; Goodman et al. 2008), including higher sedentary energy expenditure (Pratley et al. 2000). Many other peripheral symptoms are also characteristic of HD, including osteoporosis (Bonelli et al. 2002), skeletal muscle wasting (Ribchester et al. 2004), cardiac failure (Lanska et al. 1988), gastrointestinal abnormalities (van der Burg et al. 2009), and increased immune activation (Dalrymple et al. 2007; Bjorkqvist et al. 2008); all of which significantly contribute to the poor quality of life of individuals with HD, as well as to morbidity and mortality (van der Burg et al. 2009).

1.1.2.6 CAG repeat length and age of onset

A correlation between CAG repeat length and age of onset has been consistently identified in the literature (Andrew et al. 1993; De Rooij, De Koning Gans, Skraastas et al. 1993; Telenius et al. 1993; Lee et al. 2013), however for any repeat number there is a wide range of associated onset ages (MacMillan et al. 1993). However, under-representative sampling, such as the omission of individuals with 36-39 repeats who don't develop HD within their lifetime, and the use of inappropriate statistical analyses may have biased the current literature to over-estimate the risk associated with lower CAG expansions (Langbehn et al. 2010), making this correlation of limited clinical relevance. For repeat lengths of 40-50 CAGs, which is the range in which 90% of the world wide HD population lie, CAG repeat size accounts for only 40% of the variation of the age of onset (Wexler 2012). However, for juvenile HD, which is associated with much larger repeat sizes, this increases to 73% of the variation (Kremer et al. 1993). In

contrast, when the age of onset is higher than 60 years of age, there is no correlation with CAG repeat length (Kremer et al. 1993). In some cases, individuals with only 34 CAG repeats have developed HD, whereas other individuals have been found to have up to 39 repeats and remain unaffected (Rubinsztein et al. 1996; DiFiglia & Lombroso 2000); although the exact mechanisms contributing to the differences in penetrance are unknown, much of the variance has been found to be heritable, supporting the existence of genetic modifiers (Langbehn et al. 2010; Lee et al. 2012). However, the contribution of several of these modifying genes has failed to be replicated in large HD cohorts (Ramos et al. 2013; Lee et al. 2012), although population stratification and differences in genetic ancestry may be critical factors that contribute to the investigation of disease modifying genes, and that influence age of onset (Ramos et al. 2012).

1.1.2.7 Juvenile HD

In 1-10% of cases, HD can manifest before 20 years of age (Hayden 1981), which is known as juvenile HD. Juvenile HD is associated with considerably longer CAG repeat lengths, typically of around 60 or more (Douglas et al. 2013), although it has been found to manifest with a repeat expansion as low as 48 (Ribai et al. 2007); the largest expansion that has been identified was 250 CAG repeats, with an age of onset of just 2.5 years of age (Nance et al. 1999). Similar to adult HD, it is often behavioural and psychiatric disturbances that manifest prior to motor abnormalities, sometimes by a matter of years (Duesterhus et al. 2004). This can include depression, changes in conduct and personality, school performance decline, as well as isolation and aggression (Hayden 1981; Rasmussen et al. 2000; Duesterhus et al. 2004). Unlike adult HD, juvenile HD does not usually manifest with chorea, and has a higher incidence of bradykinesia, dystonia and rigidity as the initial motor manifestations (Jervis 1963; Vandjik et al. 1986; Rasmussen et al. 2000; Ribai et al. 2007). There is an increased incidence of seizures, myoclonus and epilepsy (Rasmussen et al. 2000; Douglas et al. 2013). In addition, juvenile HD may have a more rapid and severe rate of progression than adult HD (Hayden 1981).

1.1.2.8 Late onset HD

In contrast, 10-25% of HD cases are considered as 'late onset' HD (Davenport & Muncey 1916; Kremer et al. 1993), in whom symptom onset does not occur until after 50 years of age (Kremer et al. 1993). The progression of symptoms tends to be slower, with milder chorea and less prominent intellectual decline (Hayden 1981; Faught et al. 1983; Myers et al. 1985; Kremer et al. 1993). In cases where there is a CAG repeat length >39, it is unknown what the protective mechanism may be that delays symptom onset. However, there are limited cases of individuals who develop HD as late as 65 years of age, but carry only intermediate CAG repeat lengths of 30 - 31 (Groen et al. 2010); late symptom development at these lengths is consistent with the negative correlation of CAG repeat size and age of onset. As the HD gene is not fully penetrant at these lengths, there must be additional contributing factors that lead to the development of the HD phenotype in these individuals. For these rare cases, there are therefore implications for the diagnosis and management of HD, as well as requirements for family genetic counselling in case of CAG instability and expansion (Groen et al. 2010).

1.1.2.9 Homozygous HD carriers

The majority of HD cases are heterozygous for the HD gene, and therefore individuals carry one allele with a CAG repeat in the non-pathogenic range. However, there are some very rare cases of individuals that are homozygous for the HD gene. No difference in the age of onset has been identified in these people compared to those carrying a single expanded CAG repeat. However, despite initial reports suggesting no HD gene dosage effect (Wexler et al. 1987), it has been suggested that there may be a more rapid decline in motor, cognitive and behavioural symptoms in HD homozygotes compared to heterozygous individuals, and they may reach severe disability in a shorter time frame (Squitieri 2003). In concordance with the more severely progressing heterozygote phenotypes, 50% of homozygous individuals present with non-choreiform motor abnormalities at symptom onset (Squitieri et al. 2000; Squitieri 2003).

1.1.3 Neuropathological features

1.1.3.1 Gross neuropathology

There is evidence for widespread neuropathology in HD brain, by both post-mortem examination and *in vivo* imaging techniques (Scahill et al. 2013). The areas that exhibit the most prominent cell loss and astrogliosis are the caudate and putamen (Lange et al. 1976; Vonsattel et al. 1985; Roos et al. 1986; Vonsattel & DiFiglia 1998), which was the basis for the original 5 stage grading system of HD progression (Vonsattel et al. 1985); the extent of this atrophy has been found to be a function of CAG repeat length and age of death (Furtado et al. 1996; Penney et al. 1997). Atrophy of the striatum has also been found to begin prior to overt symptom onset by magnetic resonance imaging (MRI) (Harris et al. 1999; Aylward et al. 2004; Ciarmiello et al. 2006). In addition to caudate and putaminal atrophy, there is also widespread degeneration of cortical structures (Rosas et al. 2003; Rosas et al. 2005; Rosas et al. 2008) such as the angular gyrus in the parietal lobe (Macdonald et al. 1997; MacDonald & Halliday 2002), as well as of subcortical brain regions such as the hypothalamus (Kremer et al. 1991; Heinsen et al. 1999; Politis et al. 2008), globus pallidus, subthalamic nucleus, substantia nigra and hippocampus (Spargo et al. 1993; Vonsattel & DiFiglia 1998).

The development of imaging techniques, such as functional magnetic resonance imaging (fMRI) and diffusion tensor imaging (DTI) has allowed the development of *in vivo* quantitative measurement of HD brain atrophy, which can also be associated with disease progression and symptom severity. Imaging data has confirmed that there is a loss of striatal volume, and a consequent increase in the volume of the lateral ventricles (Aylward et al. 1997; Aylward et al. 2004; Hobbs et al. 2009; Tabrizi et al. 2009; Tabrizi et al. 2011; Tabrizi et al. 2012; Tabrizi et al. 2013), and that this atrophy can begin up to 11 years prior to estimated symptom onset in the caudate, and 9 years in the putamen (Aylward et al. 2004; Paulsen et al. 2004; Kipps et al. 2005; Tabrizi et al. 2012). In addition to striatal volume loss, there is also global brain atrophy (Thieben et al. 2002; Henley et al. 2009; Squitieri et al. 2009; Tabrizi et al. 2012) and cortical thinning (Rosas et al. 2002; Rosas et al. 2005; Nopoulos et al. 2010); these structural

losses have consequently been correlated with the clinical phenotype (Rosas et al. 2005; Henley et al. 2008; Rosas et al. 2008).

Global grey and white matter loss has also been identified in HD patient brains, and this atrophy has been correlated with performance on motor, oculomotor and emotion recognition tasks (Scahill et al. 2013). For example, the extent of the loss in the occipital and frontal lobes is correlated with anti-saccadic error rates (Scahill et al. 2013); cortical thinning is associated with visuomotor impairment (Rosas et al. 2008); a reduction in white matter integrity is correlated with tongue force coordination (Dumas et al. 2012), and bilateral atrophy of the caudate and putamen can be associated with worsened tapping precision (Scahill et al. 2013). The use of white and grey matter measures as markers for disease progression has also been proposed; the atrophy of each follows distinct patterns leading up to the estimated age of onset (Squitieri et al. 2009). However, the volume of cerebral spinal fluid (CSF) has also been suggested as a useful biomarker due to the linear increase in volume with disease progression, which strongly relates to age of onset predictions (Squitieri et al. 2009).

1.1.3.2 Cellular pathogenesis

The GABAergic medium spiny neurons (MSNs) within the striatum are most vulnerable to degeneration in HD, whereas cholinergic medium aspiny interneurons are relatively spared until the late stages of disease (Ferrante et al. 1985; Ferrante et al. 1987; Reiner et al. 1988; Vonsattel et al. 2008). Within the MSN population, there also appears to be certain subsets of neurons that are more vulnerable to degeneration than others (Figure 1.1); enkephalin containing neurons that project to the external segment of the globus pallidus showed increased cell death compared to substance-P containing neurons projecting to the internal pallidal segment (Reiner et al. 1988). However, substance-P containing neurons with afferents to the substantia nigra pars compacta were more resistant to cell death than those with afferents to the substantia nigra pars reticular until the late stages of disease (Reiner et al. 1988).

Within the cortex, loss of volume initially develops in posterior cortical regions during early stages of the disease, such as the middle occipital and middle temporal lobes, as well as the angular and supramarginal gyri (Rosas et al. 2002). With disease

progression, loss of volume extends to more anterior cortical regions, until the frontal lobes are also severely affected (Rosas et al. 2002). Cortical pyramidal neurons within the middle to deep layers (layers III, V and VI) are the most susceptible to degeneration (Cudkowicz & Kowall 1990; Hedreen et al. 1991; MacDonald & Halliday 2002). Brain derived neurotrophic factor (BDNF) production occurs largely within cortical cells, and is transported to striatal cells via corticostriatal afferents (Baquet et al. 2004); degeneration of both cortical cells and corticostriatal afferents during HD progression therefore reduces the amount of BDNF available in the striatum and contributes to striatal cell death (Zuccato & Cattaneo 2007).
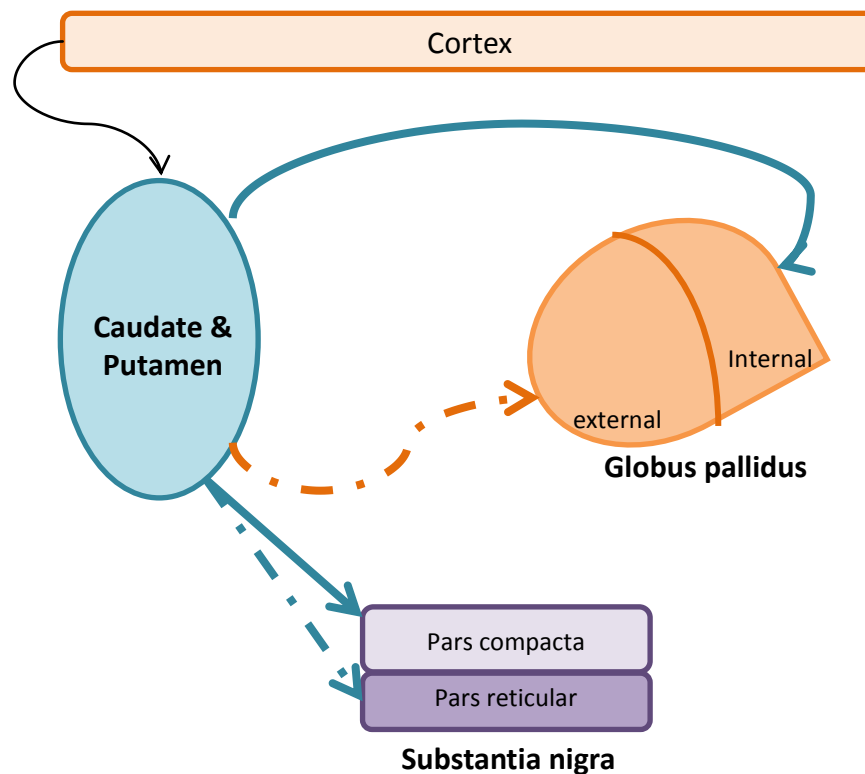
Figure 1.1 Simplified cartoon showing the differentially affected MSNs in HD pathogenesis. The orange arrow depicts enkephalin-containing neurons, and the blue arrows represent substance-P containing neurons. In early and middle stages of HD, MSNs projecting to the external segment of the globus pallidus and substantia nigra pars reticular are lost at a greater rate (dashed arrows). MSNs projecting to the substantia nigra pars compacta and internal globus pallidus are most resistant to degeneration (solid arrows) (Reiner et al. 1988).

1.1.3.3 Molecular pathogenesis

It is highly likely that dysfunction occurs before death in HD-affected neuronal cells (Levine et al. 2004). Neuronal intranuclear inclusions (NIIs) are a characteristic feature of HD that are apparent prior to symptom onset (Gomez-Tortosa et al. 2001); N-terminal fragments of the huntingtin protein (HTT) containing the expanded polyglutamine (polyQ) stretch is translated from the elongated CAG repeat and aggregates within cell nuclei. However, these have been found to occur in only 3-6% of cortical neurons in post-mortem adult HD brain, although they are more frequent (38-52% neurons) in juvenile HD brain (DiFiglia 1997). These inclusions are also present in MSNs, but not in the globus pallidus or cerebellum (DiFiglia 1997). NII presence has been correlated with neuropathological severity (Davies et al. 1997; DiFiglia 1997); for example, preventing the clearance of the mutant protein may enhance cellular toxicity (Tsvetkov et al. 2013). However, it has also been asserted that NIIs may be protective against mutant HTT (mHTT) toxicity and cell death (Saudou et al. 1998; Gutekunst et al. 1999; Kuemmerle et al. 1999; Arrasate et al. 2004); the concentration of the diffuse form of mHTT has been found to more closely correlate with cell death than NII formation (Arrasate et al. 2004), and thus sequestration into aggregates may be a compensatory strategy to reduce the availability of soluble toxic mHTT species within the cell.

NIIs were found to be disproportionately present in interneurons that tend to be spared during striatal degeneration, compared to the more vulnerable MSN population (Kuemmerle et al. 1999). In addition, smaller neuropil and cytoplasmic inclusions were present in more than 50% of the striatal cell population that are resistant to mHTT insult, whereas they were present in only 4% of MSNs (Kuemmerle et al. 1999), supporting the assertion that aggregation pathology does not correspond to disease severity (Gutekunst et al. 1999; Kuemmerle et al. 1999; Arrasate et al. 2004).

In addition to NII pathology, early stages of HD progression exhibit a diphasic pattern of dendritic alterations (Ferrante et al. 1991); initially, MSNs show proliferative dendritic activity, such as an increase in the number and size of dendritic spines, which may be indicative of a compensatory response in order to remodel degenerating

contacts (Ferrante et al. 1991). However by the severe grades of HD, there is dendritic swelling and marked spine loss, which is indicative of degenerative processes (Ferrante et al. 1991). Dystrophic neurites are also present in an uneven distribution throughout cortical layers V and VI, and are more prevalent in adult HD brain than juvenile (DiFiglia 1997; Sapp et al. 1999).

1.1.4 Epidemiology and inheritance

The incidence of HD is highest in European populations, where it affects 5-10 in 100,000 people (Reiner et al. 1988; Sackley et al. 2011), although more recent estimates suggest an incidence as high as 12.3 per 100,000 people in the UK (Evans et al. 2013). The prevalence of HD is considerably lower in African and Asian populations, at 0.5 per 100,000 people (Takano et al. 1998; Harper 2002; Warby et al. 2011). This may be due to a higher frequency of larger CAG repeat alleles in white European populations that are more predisposed to expansion (Harper 2002). Additionally, European and East-Asian populations can be characterised by different *HTT* haplotypes that confer differential HD risk; *cis*-acting elements within each haplotype may therefore contribute to the instability of the CAG repeat and help to explain variations in HD prevalence between populations (Warby et al. 2011).

Despite the dominant inheritance of the HD gene, there is a window of CAG repeat lengths where there is not complete penetrance of the HD phenotype; unaffected individuals up to the age of 95 years old with 36 - 39 CAG repeats have been identified (De Rooij, De Koning Gans, Losekoot et al. 1993; Goldberg et al. 1993; Rubinsztein et al. 1996); in contrast, there are also limited cases of individuals exhibiting HD phenotypes with CAG repeat lengths as low as 31-34 (Andrich et al. 2008; Groen et al. 2010). In these cases, known HD phenocopies have been ruled out, although post-mortem neuropathological examination has not yet been possible to confirm the HD diagnosis. Together, these cases suggest that within this intermediate repeat size range, there may be additional factors modulating HD penetrance, and may therefore also alter disease severity in the presence of longer repeats; these factors may also contribute to the variation in age of onset observed for all CAG repeat lengths. Over 39 repeats, there appears to be complete penetrance (DiFiglia & Lombroso 2000).

The expanded CAG repeat has been found to be particularly unstable during parental transmission, with around 80% of inherited alleles undergoing an alteration in CAG repeat length (Duyao et al. 1993; Myers et al. 1993; Wheeler et al. 2007; Gonitel et al. 2008). This instability is subject to both expansions (about 73% of events) and contractions (about 23% of events) (Djoussé et al. 2004; Wheeler et al. 2007). The more common CAG expansion events have contributed to the occurrence of 'anticipation' in HD families; offspring inheriting the HD gene tend to have a lower age of onset in comparison to the affected parent (Ridley et al. 1988). However, there is not a clear association between the degree of expansion and the extent of anticipation (Andrew et al. 1993). The majority of CAG expansions are paternally transmitted, and are associated with larger increases in CAG repeat length (Andrew et al. 1993; Duyao et al. 1993; Cannella et al. 2004). This expansion most likely occurs during spermatogenesis (MacDonald et al. 1993; Kremer et al. 1995; Ranen et al. 1995), as there is a high degree of CAG length mosaicism within patient spermatocytes, and repeats much larger than those found in patient lymphocytes have been identified in these cells (Duyao et al. 1993; MacDonald et al. 1993; Wheeler et al. 2007).

It has been suggested that paternal transmission of the HD allele therefore also leads to a stronger anticipation effect, and therefore an earlier age of onset in offspring (Ridley et al. 1988; Roos et al. 1991; Farrer et al. 1992; Snell et al. 1993); in a Welsh cohort of HD-affected families, the anticipation of maternally transmitted HD alleles was on average 2.75 years, whereas for paternally transmitted alleles, this was significantly earlier at 9.11 years (Snell et al. 1993). However, this was not replicated in an Italian population, despite also identifying larger CAG expansions in paternally transmitted HD alleles (Cannella et al. 2004). Nevertheless, this supports the supposition that there are additional mechanisms contributing to the age of onset other than CAG repeat length.

Due to the increased incidence of CAG expansion during gametogenesis in male germlines, both juvenile and sporadic forms of HD are also more highly associated with transmission of a paternal allele rather than with a maternal allele (Ridley et al. 1988; De Rooij, De Koning Gans, Skraastas et al. 1993; Goldberg et al. 1993; HDCRG 1993; Telenius et al. 1993; Cannella et al. 2004). Juvenile HD is associated with very large

CAG repeats, and age of onset can occur from as young as 2 years old (Hayden 1981; HDCRG 1993); 70-80% of juvenile HD cases are paternally transmitted, and this figure increases to 90% when considering an age of onset below 10 years (Telenius et al. 1993; Cannella et al. 2004). Similarly, sporadic cases of HD have been found to arise from expansions in the paternal allele (Goldberg et al. 1993); in several families experiencing sporadic HD, the paternal allele was found to lie within the intermediate allele range of 36-39 CAG repeats in unaffected fathers (Goldberg et al. 1993), which had been expanded to the fully penetrant 41-42 repeats in their offspring (Myers et al. 1993). The frequency of a new HD mutation is rare, but may be as high as 10% in some populations (Warby et al. 2011). In European populations, the majority of HD cases share the same haplotype, of which two variants are most highly associated with CAG length instability (Warby et al. 2011), these particular 'HD-haplotypes' are therefore more prone to expansion, and account for many sporadic cases of HD (Myers et al. 1993; Goldberg et al. 1995; Warby et al. 2011).

1.2 The *HTT* gene

    1.2.1 Expression

The *HTT* gene is expressed widely throughout the body (Strong et al. 1993; DiFiglia et al. 1995; Sharp et al. 1995; Cattaneo et al. 2005), and is particularly enriched in neurons and testes (Strong et al. 1993; DiFiglia et al. 1995; Sharp et al. 1995; Ferrante et al. 1997; Cattaneo et al. 2005). Within the brain, *HTT* expression is higher in neurons than glial cells, and is most strongly expressed in the pyramidal neurons of cortical layers III and V that project to the striatum (Strong et al. 1993; Fusco et al. 1999), although there is no enrichment of its expression in the striatum itself (Sharp et al. 1995). In peripheral tissues, although there is high *HTT* expression in testes, which is highest in immature spermatogonia (Strong et al. 1993), there are also high levels of expression in the liver, heart and lungs (Li et al. 1993; Landwehrmeyer et al. 1995).

Two different *HTT* mRNA species have been identified; one is a 10.3kb transcript, which is expressed throughout peripheral tissues, and the other is a longer 13.7kb transcript with an extended untranslated region at the 3' end of the mRNA sequence,

and is expressed in brain (Lin et al. 1993). These alternate transcripts are thought to be produced by differential polyadenylation sites on the 3' end of the *HTT* mRNA, although the reason for this is yet to be elucidated (Lin et al. 1993). However, the presence of alternate transcripts may be a mechanism for the tissue specific degeneration observed in HD. More recently, an alternatively spliced variant of *HTT* was also identified; in the presence of the expanded CAG repeat, serine/arginine-rich splicing factor 6 (SRSF6) binds to *HTT* and leads to a small polyadenylated exon1-intron1 mRNA transcript, which is then translated into a small polyQ-containing N-terminal fragment of the HTT protein (Sathasivam et al. 2013). This alternate processing of *HTT* expression may account for some of the observed differences in the subcellular localisation of the HTT protein.

The expression of *HTT* has also been found to be altered by the presence of the expanded CAG; in lymphoblast cultures from heterozygote juvenile HD patients, the expression of the mutant HD gene was found to be relatively reduced in comparison to the 'normal' gene (Gutekunst et al. 1995; Persichetti et al. 1996). A similar observation has also been made in an immortalised embryonic striatal cell line model of HD (Pouladi et al. 2010) and in expanded CAG-transfected rat striatal cultures (J. Miller et al. 2010); however it has not been fully elucidated whether this reduction is truly a result of reduced transcription and mRNA processing, or to altered processing of the subsequent HTT protein.

1.2.2 Somatic mosaicism

There is increasing evidence for the presence of somatic mosaicism in both models of HD, and in human HD tissues. Somatic expansion of the CAG repeat has been noted in liver, kidneys, stomach, blood and brain (Wheeler 1999; Ishiguro et al. 2001; Nørremølle et al. 2004); however, CAG repeat length exhibits the greatest variability in brain tissues (Telenius et al. 1994; Aronin et al. 1995; Giovannone et al. 1997; Kennedy et al. 2003; Shelbourne et al. 2007; Cannella et al. 2009). Although expansion of the CAG repeat has been observed in cortical neurons, the largest expansions have occurred within the striatum; expansions of up to 100 additional CAG repeats have been found in human HD striatal cells in comparison to other neuronal cells (Kennedy

et al. 2003; Shelbourne et al. 2007), and in pre-symptomatic HD gene carriers expansions of up to 200 CAG repeats were present (Kennedy et al. 2003). In contrast, late stage HD brain exhibits higher CAG instability in the cortex, implying that the early instability in striatal neurons is likely to lead to cell death before the end stage of the disease (Shelbourne et al. 2007). Somatic CAG instability has not been found to occur in the cerebellum (Ishiguro et al. 2001; Kennedy et al. 2003), and occurs to a larger extent in neurons than in glia (Shelbourne et al. 2007). CAG instability also has a greater tendency for expansion in the presence of initially larger CAG repeat lengths (Cannella et al. 2009). Instability of the CAG repeat in somatic cells, particularly large expansions in striata that accumulate with disease progression (Shelbourne et al. 2007), may be a mechanism by which cell-specific neurodegeneration occurs in HD, and therefore inhibiting CAG instability may be a therapeutic target.

1.3 The HTT protein
1.3.1 Structure

The *HTT* gene encodes for the ~348kDa protein HTT; to date, the high molecular weight of HTT has prevented the elucidation of a detailed structure of the full length protein, although it has been asserted that HTT forms a large α-helical solenoid (Seong et al. 2010). Therefore, much of the current work has focused on the structure and function of the polyQ containing N-terminus of HTT. Due to the wide variety of potential cellular functions with which HTT is associated, the polyQ stretch is thought to assume several dynamic and flexible conformations in a manner dependent on the required protein binding partners available, its subcellular localisation and cell type in order to regulate its many functions (Trettel et al. 2000; Wheeler 2000; Kim et al. 2009; Lotz et al. 2010; Seong et al. 2010; Zuccato et al. 2010; Długosz & Trylska 2011). N-terminus HTT was first described as having a 'polar zipper' structure; a motif that promotes binding with transcription factors, which suggested HTT may play a role in transcriptional regulation (Perutz et al. 1994). The N-terminus of HTT is considered to form an α-helical structure (Kim et al. 2009; Długosz & Trylska 2011), which can be altered by mutations to amino acids 1-17 (Atwal et al. 2007), post-translational

modifications such as phosphorylation events (Aiken et al. 2009; Atwal et al. 2011), and by a pathogenic expanded polyQ tract (Legleiter et al. 2009; Długosz & Trylska 2011; Peters-Libeu et al. 2012; Vachharajani et al. 2012). Alternate epitopes can be detected by using different antibodies against HTT; a more thorough discussion of this can be found in Chapter 3.

The alteration in its N-terminal structure is considered one of the pathogenic mechanisms for mHTT aggregate formation and cellular toxicity; increasing the length of the polyQ substantially reduces the stability of HTT and promotes aggregation (Vachharajani et al. 2012). One mechanism by which this may occur is by increasing the exposure of amino acids 1-17; the α-helical structure of non-pathogenic HTT is stabilised by interactions between amino acids 1-17 and the polyproline rich region that follows the polyQ tract (Długosz & Trylska 2011). When the polyQ tract is expanded in the context of mHTT, the structure is 'loosened' by preventing this interaction, and the N-terminus is more able to form aberrant associations and structures (Li et al. 2007; Długosz & Trylska 2011). Alterations to the structure of HTT by the expanded polyQ may also lead to specific conformations that are toxic in soluble monomeric and oligomeric forms, which may be particularly dynamic and heterogeneous in their structure (Lotz et al. 2010; Długosz & Trylska 2011).

The HTT protein also contains several huntingtin, elongation factor 3, protein phosphatase 2A, and Tor1 (HEAT) repeats; 16 repeats arranged into four clusters along the length of the protein have been identified (Tartari et al. 2008), although up to 36 putative HEAT repeats have been identified on HTT (Takano & Gusella 2002). HEAT repeats are binding regions that promote protein-protein interactions, therefore their multiple appearances may support a multi-functional role for HTT (Andrade & Bork 1995).

1.3.2 Cleavage and proteolysis

Caspases and calpains have been identified as potential regulators of HTT proteolysis, which plays a role in modulating HTT binding partner interactions, subcellular localisation, degradation, as well as mHTT aggregation in models of HD (Ehrnhoefer et al. 2011). Several caspase and calpain proteolytic cleavage sites have been identified

within HTT, which all lie between amino acids 469 and 586 (Figure 1.2) (Goldberg et al. 1996; Wellington et al. 1998; Kim et al. 2001; Gafni & Ellerby 2002; Graham, Deng, et al. 2006; Landles et al. 2010). 70-80kDa N-terminal fragments of HTT have been identified in several mouse and cell models, as well as in human brain (DiFiglia 1997; Wellington et al. 1998; Gafni & Ellerby 2002; Gafni et al. 2004; Sawa et al. 2005; Thompson et al. 2009; Warby et al. 2009; Landles et al.2010), which may be a result of these cleavage events. Although the cleavage of mHTT has been associated with increased cellular toxicity and neurodegeneration (DiFiglia 1997; Wellington et al. 2000; Graham, Deng et al. 2006; Schilling et al. 2006; Warby et al. 2009), whether mHTT has an increased affinity for either caspase or calpain binding, or may modulate cleavage activity, is still under debate. Several authors suggest that mHTT is more readily cleaved (Goldberg et al. 1996; Gafni & Ellerby 2002; Gafni et al. 2004), and neuronal cells containing mHTT have enhanced caspase and calpain activity (Gafni & Ellerby 2002; Gafni et al. 2004; Graham et al. 2010). In contrast, others suggest that mHTT is either more resistant to cleavage and caspase binding than wild type HTT (Dyer & McMurray 2001; Zhang et al. 2006), or no association with polyQ length has been identified at all (Wellington et al. 1998; Kim et al. 2001; Sawa et al. 2005; Landles et al. 2010).

The cleavage of HTT is regulated by its phosphorylation, and this in turn may alter the toxicity of mHTT and aggregation kinetics (Luo et al. 2005; Schilling et al. 2006; Thompson et al. 2009; Warby et al. 2009). For example, phosphorylation of serine 421 (S421) prevents caspase-6 cleavage of mHTT, thus reducing the availability of shorter N-terminal fragments that may translocate to cell nuclei, consequently reducing mHTT toxicity (Warby et al. 2009). In addition, enhanced phosphorylation of serine 434 (S434) prevents caspase-3 cleavage (Luo et al. 2005), and a phosphomimetic mutation of serine 536 (S536) prevents calpain cleavage (Schilling et al. 2006); both of which reduced mHTT toxicity and associated cell death. The cleavage-associated toxicity of mHTT is likely to act through the increased availability of smaller N-terminal fragments that can more readily translocate to cell nuclei and can more rapidly form aggregates (Sawa et al. 2005; Tanaka et al. 2006; Warby et al. 2009).
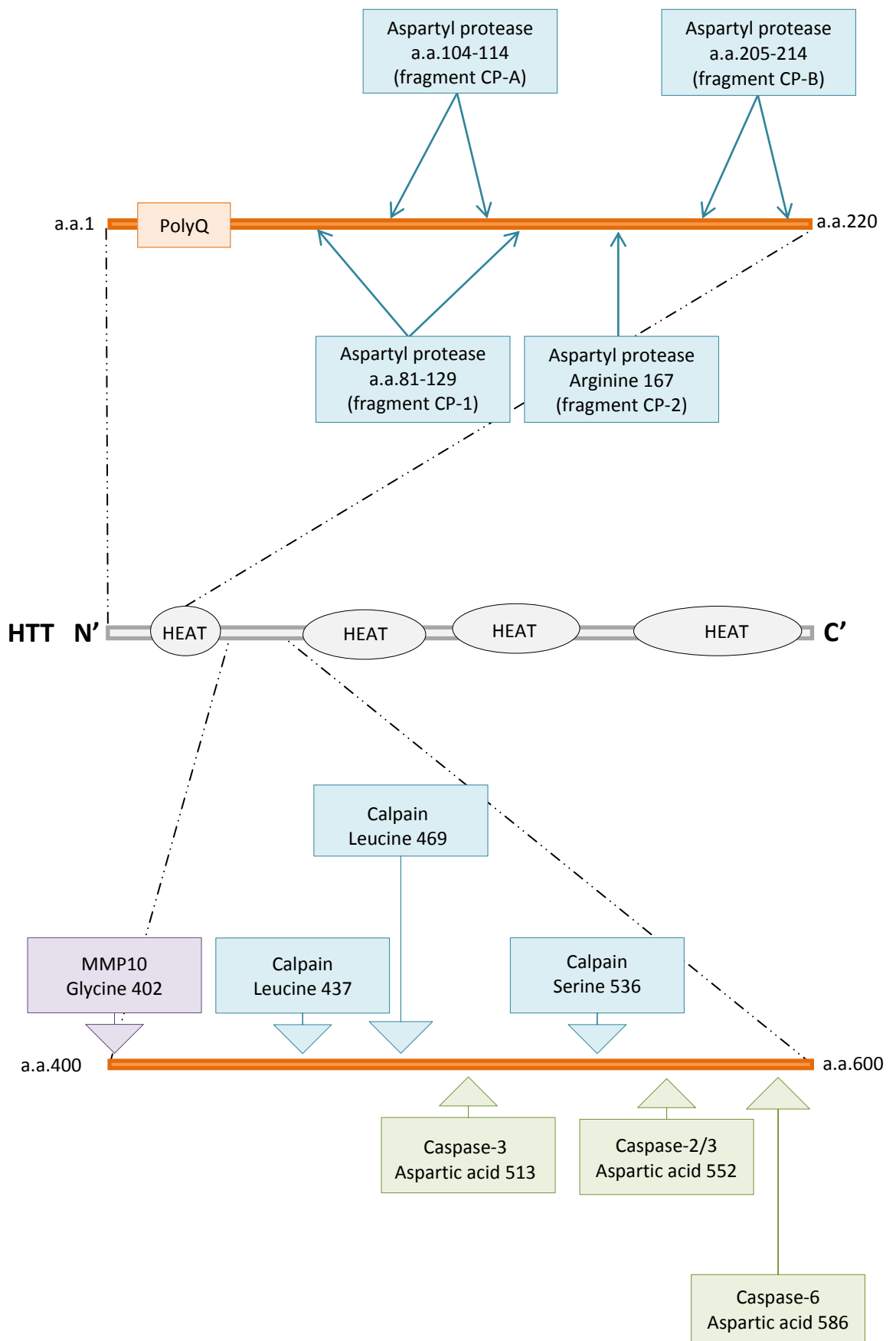
Figure 1.2 Simplified cartoon of cleavage sites on the HTT protein. a.a. = amino acid

HTT cleavage may also occur via the action of matrix metalloproteinases (MMPs); specifically, a cleavage site for MMP10 has been identified at amino acid 402 (J. P. Miller et al. 2010). MMP10 activity has been found to be increased in mouse models of HD, and the knock down of its activation reduced cell death (J. P. Miller et al. 2010). N-terminal fragments that are smaller than the predicted caspase, calpain and MMP cleavage products have also been identified in human HD brain, as well as in cell and mouse models, with the smallest fragment terminating at amino acid 90 (DiFiglia 1997; Ratovitski et al. 2009; Landles et al. 2010). The mechanism for the generation of these fragments has not yet been fully elucidated, however they may be a result of the action of aspartyl proteases (Lunkes et al. 2002; Kim et al. 2006), which may cleave HTT between amino acids 104-114, and 205-214 (Kim et al. 2006). This process has been found to be most efficient on smaller HTT fragments that have been previously cleaved by calpains, caspases and MMPs, rather than full length HTT (Tebbenkamp et al. 2012); this suggests that the proteolysis of HTT may be a series of sequential cleavage events (Lunkes et al. 2002; Ratovitski et al. 2009; Tebbenkamp et al. 2012). In contrast, only a single 180kDa N-terminal fragment of mHTT was detectable from human HD brain lysates when investigated by native gel electrophoresis (Sapp et al. 2012); therefore the extent and relevance of cleavage events in HD pathogenesis remains under debate.

1.4 Animal models of HD

The discovery of the HD gene has permitted the development of genetic models of HD, each with features that mimic the human disease. Although no single model is able to fully recapitulate human HD, they have provided invaluable insights into the both the developmental and degenerative mechanisms of the disease; for example, the characterisation and significance of NII formation, and the manipulation of *Htt* gene expression as a potential therapeutic target.

1.4.1 Transgenic and knock-in mouse models

Many mouse models of HD are now available, and are suited to different applications, depending on their patterns of neuropathology, motor abnormalities and disease progression. The models are generally grouped depending on their genetic manipulation; transgenic models were created using either truncated or full length HTT inserted randomly into the genome, whereas 'knock-in' models consist of a CAG expansion inserted into the mouse genome at the appropriate location on the *HTT* gene, which is expressed under the endogenous mouse promoter. Further details regarding the most commonly used mouse models of HD can be found in Table 1.3.

1.4.1.1 Behavioural phenotypes

Several tests and measures are used to assess the motor performance of HD mouse models, including gait abnormalities, basal activity, balance beam traversing time, swim speed, limb clasping following tail suspension, and latency to fall on the rotarod, which has proved to be one of the most robust measures of motor impairment in these models (Crook & Housman 2011).

	Background strain	Transgene	Promoter	CAG repeat length	Life span	Reference
N-Terminal transgenic models						
R6/2	CBA x C57Bl/6	Exon 1 human *HTT*	Human *HTT*	150	10-13 weeks	Mangiarini et al.1996; Carter et al. 1999
R6/1	CBA x C57Bl/6	Exon 1 human *HTT*	Human *HTT*	116	32-40 weeks	Mangiarini et al. 1996; Hodges et al. 2008
N171-82Q	C3H/HEJ x C57Bl/6	First 171 amino acids human *HTT*	Mouse prion promoter	82	16-22 weeks	Schilling et al. 1999; Schilling et al. 2004
Inducible models						
HD94	CBA x C57Bl/6	Chimeric human/mouse exon 1 *HTT*	TetO + tTA	94	Normal	Yamamoto et al. 2000
Inducible-148Q	C57BL/6	First 171 amino acids human *HTT*	PrP + tTA	148	28-40 weeks	Tanaka et al. 2006
Full-length transgenic models						
YAC72	FVB/N	Human *HTT*	Human *HTT*	72	Normal	Hodgson et al. 1999
YAC128	FVB/N	Human *HTT*	Human *HTT*	120	Normal	Slow et al. 2003
BACHD	FVB/N	Human *HTT*	Human *HTT*	97	Normal	Gray et al. 2008

Table 1.3 Continued on next page

Knock-in models						
Hdh^{Q72-80}	129Sv x C57Bl/6	Expanded CAG inserted in endogenous mouse *Htt*	Mouse *Htt*	72, 80	Normal	Shelbourne 1999
Hdh^{Q92}	CD1 × 129SvEv	Endogenous mouse *Htt* with chimeric human/mouse exon 1	Mouse *Htt*	90	Normal	Wheeler et al. 1999
Hdh^{Q94}	C57BL/6	Endogenous mouse *Htt* with chimeric human/mouse exon 1	Mouse *Htt*	94	Normal	Menalled et al. 2002
Hdh^{Q111}	CD1 × 129SvEv	Endogenous mouse *Htt* with chimeric human/mouse exon 1	Mouse *Htt*	109	Normal	Wheeler et al. 1999; Wheeler et al. 2002
Hdh^{Q140}	C57BL/6	Endogenous mouse *Htt* with chimeric human/mouse exon 1	Mouse *Htt*	140	Normal	Menalled et al. 2003
Hdh^{Q150}	129/Ola × C57BL/J6	Expanded CAG inserted in endogenous mouse *Htt*	Mouse *Htt*	150	Normal	Lin et al. 2001; Woodman et al. 2007
Hdh^{Q200}	C57BL/6J	Expanded CAG inserted in endogenous mouse *Htt*	Mouse *Htt*	200	Euthan-ised at 80 weeks	Heng et al. 2010

Table 1.3 Key features of the most commonly used mouse models of HD

1.4.1.1a Transgenic models

The transgenic N-terminal fragment mouse models develop overt behavioural abnormalities at an earlier age than the full length knock in models; the R6/2 mouse model exhibits deficits in rotarod performance by 6 weeks of age (Carter et al. 1999; Rattray et al. 2013), whereas the R6/1 and N171-82Q models develop deficits at 18 weeks and 3 months, respectively (Schilling et al. 2006; Hodges et al. 2008). Both R6 models develop a progressive motor phenotype, including choreiform movements, tremor, involuntary stereotyped movements, and handling induced seizures; these behaviours emerge at 9-11 weeks for the R6/2 mice, and 4-5 months for the R6/1 mice, followed by premature death at 10-16 weeks and 32-40 weeks, respectively

(Mangiarini et al. 1996; Rattray et al. 2013). N171-82Q mice also develop progressive motor abnormalities, such as loss of co-ordination, tremor, hypokinesis and abnormal gait from 3 months, and die prematurely after 16-22 weeks (Schilling et al. 1999; Schilling et al. 2004). Both inducible transgenic models, HD94 and Inducible 148Q, develop a progressive behavioural phenotype similar to the other transgenic models; this is apparent from 4 weeks with a mild clasping phenotype in HD94 mice (Yamamoto et al. 2000), and rotarod deficits and progressive ataxia in Inducible 148Q mice becoming apparent from 6 months (Tanaka et al. 2006). Despite a progressive tremor and hypoactivity in HD94 mice, these animals survive for a normal life span (Yamamoto et al. 2000). However, phenotypic progression is more severe in the Inducible 148Q mice, leading to premature death at 7-8 months (Tanaka et al. 2006).

YAC72, YAC128 and BACHD mouse models all contain a full length human HTT transgene; these mice exhibit similar behavioural abnormalities as the N-terminal transgenic models, but in contrast to the R6/2 mice, their onset is delayed. Motor abnormalities are not apparent in YAC72 mice until 9 months (Hodgson et al. 1999), and in YAC128 mice, mild deficits can be seen from 3 months (Slow 2003; Van Raamsdonk et al. 2005), although not all of these progressively worsen with time (Brooks, Jones, et al. 2012). A mild deficit in rotarod ability can be seen in BACHD mice from 1-2 months, but there is no continuous decline in performance until 28 weeks of age (Gray et al. 2008; Menalled et al. 2009). In addition to deficits in a standard battery of tests for motor function, these mice also display an initial hyperkinesia, followed by the development of hypokinesia (Hodgson et al. 1999; Slow 2003; Slow et al. 2005; Van Raamsdonk et al. 2005).

Increasingly, mouse models of HD are being assessed for cognitive and emotional abnormalities, such as procedural learning and anxiety behaviours, as in the human disease these subtle phenotypes often develop prior to any overt motor symptoms (Kirkwood et al. 2000; Ho et al. 2003; Holl et al. 2013). R6/2 mice have been found to have deficits in special memory from 4-5 weeks of age, as well as an increase in anxious behaviour from 8-10 weeks (Cowin et al. 2011). In addition, there is a gender effect in these mice for an aberrant startle response; female mice show reduced startle from 4 weeks of age, whereas male mice exhibit a loss of pre-pulse inhibition

(PPI) from 10 weeks (Cowin et al. 2011). R6/2 mice also have deficits in task reversal from 6 weeks, which develops into a more widespread deficit in learning by 10-11 weeks (Lione et al. 1999). R6/1 mice have been less thoroughly characterised, however they also exhibit deficits in procedural learning, a reduced startle response and PPI, as well as special memory impairments from 3 months (Cayzac et al. 2011; Brooks, Janghra, et al. 2012).

YAC128 mice also have impaired spatial memory from 8 months, as well as a learning deficiency; by 12 months they can no longer learn the rotarod task (Van Raamsdonk et al. 2005). They also exhibit perseveration during learning tasks (Slow 2003) and similar to both R6 models, have a reduced startle response and PPI from 12 months of age. BACHD mice have similar impairments with reversal learning and set shifting, and also have increased anxiety and an increased fear response during conditioning tasks (Abada et al. 2013).

<center>1.4.1.1b Knock-in models</center>

Knock-in mouse models tend to show a slower and more mildly progressive motor phenotype than transgenic models, and all have a normal life span, despite expressing CAG repeats much larger than those in the rapidly progressing transgenic models (Ferrante 2009). Models with repeats lower than 111 CAGs only exhibit very modest behavioural phenotypes; for example, Hdh^{Q72-80} mice have no reported motor abnormalities (Shelbourne 1999), and Hdh^{Q94} mice exhibit aberrant rearing behaviour at 2 months of age, followed by hypokinesia by 4-6 months (Menalled et al. 2002), but no other overt phenotypes. Hdh^{Q111} mice, however, develop a gait deficit by 24 months, consisting of a shortened stride and imprecise paw placement (Wheeler et al. 2002). However there are no observable differences in paw clasping behaviour, and there is only a very late impairment in rotarod performance in female mice at 100 weeks of age (Menalled et al. 2009).

In contrast, knock-in models exhibiting longer CAG repeats develop more overt behavioural abnormalities, although in comparison to transgenic models their onset is considerably later. Hdh^{Q140} mice have a similar behavioural phenotype to the Hdh^{Q94} model, although the expanded CAG repeat has hastened the age of onset; aberrant

rearing behaviour occurs at only 1 month of age, and hypokinesia occurs closer to 4 months (Menalled et al. 2003). In addition, these mice have uncoordinated gait and resting tremor from 20-26 months (Hickey et al. 2008), a progressive deficit in climbing ability from 1.5 months, and subtle balance and rotarod impairments from 4-6 months (Hickey et al. 2008). The Hdh^{Q150} model has an earlier onset of more severe observable motor impairments at 70 weeks, including rotarod deficits, balance impairments, and clasping behaviour from 40 weeks (Heng et al. 2007; Woodman et al. 2007; Brooks, Higgs, et al. 2012). Similar to the Hdh^{Q140} mice, a resting tremor and an unsteady gait is also apparent from 100 weeks, although a reduction in grip strength has also been reported at just 1.5 months in this model (Woodman et al. 2007). Finally, Hdh^{Q200} mice have the earliest onset and most severe phenotype of the knock-in models, but is currently one of the least thoroughly characterised; these mice display imbalance and poor motor co-ordination from 50 weeks, which progresses to deficits in gait by 60 weeks, and gross motor impairment by 80 weeks (Heng et al. 2010).

Due to their delayed and more subtle motor phenotypes, there is increasing interest in cognitive and emotional abnormalities in knock-in mice that may be apparent prior to motor symptom onset, and may be useful markers for disease progression and potential interventions. Long term spatial and recognition memory has been found to be impaired in Hdh^{Q111} mice at 8 months, which is considerably earlier than the appearance of any motor phenotype (Giralt et al. 2012). Consistent with several of the transgenic models, Hdh^{Q140} mice exhibit increased anxiety in the open field test, and increased freezing following fear conditioning tasks that occur from 1 month of age, as well as impaired motor learning (Hickey et al. 2008). Hdh^{Q150} and Hdh^{Q200} mice have not yet been as well characterised in their cognitive abilities, however Hdh^{Q150} mice display difficulty in set-shifting tasks (Brooks et al. 2006) and also have some spatial memory deficits (Brooks, Higgs, et al. 2012).

1.4.1.2 Neuropathology

1.4.1.2a Transgenic models

N-terminal transgenic mice display an earlier manifestation of neuropathological features in contrast to full length models. Brain atrophy is detectable in R6/2 mice from just 3 weeks using MRI (Zhang et al. 2010), and a 20% reduction in brain weight has been observed from a month of age (Mangiarini et al. 1996; Stack et al. 2005). It was initially suggested that this model also had a reduction in striatal volume caused by neuronal atrophy and death from 12 weeks (Stack et al. 2005), however more recent investigations reveal that rather than a loss in volume, growth of the striatum no longer occurs after 8 weeks, and neuronal loss is minimal (Rattray et al. 2013). HTT aggregates have been identified from postnatal day 1, which increase in both number and size throughout the entire brain during disease progression (Sathasivam et al. 1999; Meade et al. 2002; Yu et al. 2003; Stack et al. 2005; Rattray et al. 2013). The R6/1 model has a similar neuropathological phenotype that develops at a later time point; HTT nuclear inclusions are apparent from 9 weeks, and a reduction in brain volume is detectable from 18 weeks, including striatal atrophy (Naver et al. 2003). This atrophy has been attributed to cellular dysfunction rather than neuronal death (Yu et al. 2003). N171-82Q mice also share a similar pathology of striatal atrophy and ventricular enlargement, which was initially attributed to neuronal loss by 3 months (Yu et al. 2003; Gardian et al. 2005), however more recent reports propose that any neurodegeneration in this model is subtle, and atrophy is associated with neuronal dysfunction rather than apoptosis (Cheng et al. 2011). N171-82Q mice also have widespread neuronal HTT inclusions from 16 weeks that increase in size and number with disease progression (Schilling et al. 1999; Yu et al. 2003).

Neither inducible HD mouse model has been as thoroughly characterised as the N-terminal transgenic models, however both have mild to moderate entire brain atrophy, including a reduction in striatal volume and ventricular enlargement (Yamamoto et al. 2000; Tanaka et al. 2006). They also have widespread HTT nuclear inclusions, as well as evidence for some extranuclear aggregates in several brain regions (Yamamoto et al. 2000; Tanaka et al. 2006). YAC72 mice have a milder, more

specific neuropathological phenotype; at 12 months, there is striatal degeneration and the nuclear translocation of HTT in MSNs, and some rare microaggregates (Hodgson et al. 1999). YAC128 mice also do not develop dense and progressive HTT inclusions, although they have an increased presence of microaggregates at 12 months that increase in number over time (Slow 2003). In contrast to the YAC72 model, there is a reduction in both striatal and cortical volume by 12 months in YAC128 mice (Van Raamsdonk et al. 2007). Finally, the BACHD model exhibits a more severe neuropathological phenotype in comparison to the YAC mice; there is gross brain atrophy by 12 months, including significantly reduced cortical and striatal volume, which is due to neuronal dysfunction rather than death (Gray et al. 2008; Ferrante 2009). HTT inclusions are also apparent from 12 months, however these are mostly extranuclear and appear primarily in the cortex (Gray et al. 2008; Ferrante 2009).

1.4.1.2b Knock-in models

Despite their later onset and milder behavioural phenotypes, knock-in models develop several progressive neuropathological features that are present in transgenic models of HD. Hdh^{Q72-80} mice, despite no overt behavioural phenotype, develop neuropil HTT aggregates, and have a 10-15% reduction in brain weight by 4-6 months; however there is no evidence of reactive gliosis or neuronal loss (Shelbourne 1999). Similarly, Hdh^{Q94} mice exhibit no neuronal loss, although there are widely distributed microaggregates from 4-6 months, and some nuclear HTT inclusions by 18 months (Menalled et al. 2002; Hickey et al. 2008). Both Hdh^{Q92} and Hdh^{Q111} mice have a progressive nuclear phenotype that exhibits striatal specificity; HTT becomes increasingly localised in striatal neuronal nuclei by 6 weeks, which appears punctate and forms nuclear inclusions by 4 months in both models (Wheeler 2000; Bayram-Weston et al. 2012). There is also evidence of late onset neurodegeneration in the Hdh^{Q111} model (Wheeler et al. 2002).

In concordance with the association observed between CAG repeat length and motor phenotype severity in knock-in mouse models, there is also more severe and progressive neuropathology in models with longer CAG repeats. There is evidence for the formation of HTT aggregates from only 1 month in Hdh^{Q140} mice, which initially

form in the striatum and progressively become more widespread throughout the brain (Hickey et al. 2008). Striatal nuclear inclusions and neuropil aggregates are also apparent from 4 months, and spread to the cortex, nucleus accumbens, and olfactory tubercle (Menalled et al. 2003). By one year, there is substantial neuronal loss within the striatum (Menalled et al. 2003; Hickey et al. 2008). Progressive nuclear staining and nuclear inclusions have also been reported in Hdh^{Q150} striatum from 5 months (Woodman et al. 2007; Weiss et al. 2008; Bayram-Weston et al. 2012), accompanied by neuronal loss at 100 weeks, and a 40% loss in striatal volume by 23 months (Lin 2001; Yu et al. 2003; Tallaksen-Greene et al. 2005; Heng et al. 2007). Similarly, Hdh^{Q200} mice develop nuclear inclusions in the striatum and cortex by 20 weeks, although neuronal dysfunction rather than neuronal loss is reported (Heng et al. 2010). By 40-50 weeks, this model develops cytoplasmic and perinuclear HTT aggregates and exhibits a 40% reduction in cerebellar purkinje cells (Heng et al. 2010; Dougherty et al. 2013). By 80 weeks, there is substantial striatal and cortical astrogliosis (Heng et al. 2010).

1.4.2 Large animal models of HD

Large mammalian models are currently in development, including sheep (Jacobsen et al. 2010; Morton & Avanzo 2011), miniature pig (Uchida et al. 2001; Yang et al. 2010) and Rhesus macaque models (Yang et al. 2008). These are being developed with an aim to more faithfully reproduce human HD, as greater similarities in brain development and longer life spans in these animals allows for the more thorough investigation of the chronic effects of HD, as well as pre-clinical testing of new therapeutic compounds. In addition, it has been observed that species differences have a large impact on neuropathology; larger animals appear to be more susceptible to the toxicity of larger CAG repeats than rodents, and in some models, suffer a greater extent of neurodegeneration and neuronal apoptosis (Li & Li 2012).

1.5   The dynamic shuttling of HTT

Although HTT was initially considered to be a cytoplasmic protein (DiFiglia et al. 1995; Gutekunst et al. 1995), its nuclear presence has now been well characterised (Hilditch-Maguire et al. 2000; Trettel et al. 2000; Kegel et al. 2002; Truant 2003; Truant et al. 2007; Benn et al. 2008). HTT has been associated with a wide range of cellular functions, both within the cytoplasm and the nucleus; the dynamic shuttling between these compartments is therefore likely to be a mechanism by which the complex variety of HTT activities can be regulated (Truant 2003; Truant et al. 2007).

1.5.1 Subcellular localisation

HTT is primarily cytoplasmic in the majority of somatic cells, however within neurons, spermatocytes and lymphoblasts, its localisation is both nuclear and cytoplasmic (Hoogeveen et al. 1993), suggesting a differential role of HTT dependent on cell type that can be regulated by its localisation. HTT has been associated with a variety of organelles within the cytoplasm (De Rooij et al. 1996; DiFiglia 1997), such as the endoplasmic reticulum, Golgi body, the plasma membrane and cytoskeleton (Hilditch-Maguire et al. 2000; Ko et al. 2001; Atwal et al. 2007; Rockabrand et al. 2007). Within the cytoplasm, HTT is also associated with the regulation of vesicular transport; the palmitoylation of HTT targets it to membranes (Suopanki et al. 2006), and it is enriched in compartments containing vesicle associated proteins (DiFiglia et al. 1995), where it has been found to associate with vesicles and their interacting proteins (BlockGalarza et al. 1997; Qin et al. 2004; Atwal et al. 2007). Specifically, HTT may mediate the axonal transport of BDNF by mediating the interaction with vesicular motor proteins (Gauthier et al. 2004); a process which is disrupted in the presence of mHTT (Gunawardena et al. 2003). Furthermore, cytoplasmic HTT is thought to play a role in mediating protein-protein interactions (Bauer & Nukina 2009; Ehrnhoefer et al. 2011), as well as regulating gene expression; HTT sequesters repressor element 1-silencing transcription factor/neuron-restrictive silencing factor (REST/NRSF) in the cytoplasm, thus preventing its binding to the repressor element 1/neuron-restrictive silencing element (*RE1/NRSE*) on the promoter region of the *BDNF* gene, therefore ensuring *BDNF* expression (Zuccato et al. 2001; Zuccato et al. 2003; Zajac et al. 2010). HTT with

an expanded polyQ is unable to interact with REST/NRSF, and therefore *BDNF* expression is suppressed (Zuccato et al. 2003; Zuccato et al. 2010). Around 1900 *RE1/NRSE* sites have been identified on both mouse and human genomes (Bruce et al. 2004), suggesting that HTT is likely to be implicated in the expression of many genes other than BDNF.

Within cell nuclei, HTT has been found to localise to speckles, promyelocytic leukaemia (PML) bodies, and the nucleous (Hilditch-Maguire et al. 2000; Tao & Tartakoff 2001; Kegel et al. 2002), as well as associating with a variety of transcription factors and being able to target DNA directly; all of which are modified by the presence of the expanded polyQ repeat within mHTT (Boutell et al. 1999; McCampbell et al. 2000; Shimohata et al. 2000; Steffan et al. 2000; Dunah et al. 2002; Li et al. 2002; Kegel et al. 2002; Bae et al. 2005; Benn et al. 2008; Johnson et al. 2008). These interactions implicate HTT as having a necessary role in transcription and RNA processing within the nucleus, as well as in the assembly of nuclear matrix bound protein complexes (Kegel et al. 2002; Sun et al. 2007).

1.5.2 Nuclear import

HTT is present in cell nuclei in both truncated and full length forms (Hilditch-Maguire et al. 2000; Trettel et al. 2000; Kegel et al. 2002; Truant 2003; Truant et al. 2007; Benn et al. 2008), however the mechanism by which such a large protein is able to translocate between subcellular compartments has not yet been fully elucidated. Small proteins between 20-40kDa, such as truncated N-terminal fragments, are easily able to cross the nuclear pore by passive diffusion (Figure 1.3) (Truant 2003; Terry et al. 2007; Bauer & Nukina 2009), which may account for the global nuclear inclusion phenotype observed in N-terminal HD mouse models (Sathasivam et al. 1999; Schilling et al. 1999; Meade et al. 2002; Yu et al. 2003; Stack et al. 2005; Rattray et al. 2013).

However, this mechanism does not explain how longer epitopes of HTT may traverse the nuclear pore. Larger proteins must be accompanied through the nuclear pore via one of several transport pathways that require active diffusion; these pathways therefore exert stricter control of nuclear import and export than passive diffusion. Nuclear localisation signals (NLS) and nuclear export signals (NES) on a peptide act as

recognition sequences for an interaction with nuclear pore transporter molecules in order to regulate nuclear localisation via these pathways (Bessert et al. 1995; Desmond et al. 2013). It has been under debate whether HTT contains an endogenous NLS or not (Bessert et al. 1995; Xia 2003; Desmond et al. 2013). A consensus sequence for a typical NLS was initially identified between amino acids 1182-1190 on HTT, which when cloned into the cytoplasmic enzyme β-galactosidase, enhanced its nuclear localisation (Bessert et al. 1995). However, the NLS properties of this region were not replicated upon further investigation (Xia 2003). It has been proposed that the series of HEAT repeats on HTT may interact with the nuclear pore associated proteins, nucleoporins, which may mediate nuclear localisation (Suhr et al. 2001; Truant et al. 2007); the HEAT repeats on nuclear proteins importin-β and exportin have been shown to perform this function (Bayliss et al. 2002). In addition, mHTT nuclear inclusions sequester nucleoporins (Suhr et al. 2001), therefore suggesting that they may interact with either wild type or mutant HTT.

More recently, HTT has been associated with the karyopherin β2/transportin pathway (Desmond et al. 2012; Desmond et al. 2013). The three consensus components required for the formation of a karyopherin β2 –dependent proline tyrosine (PY)-NLS were identified between amino acids 174-207 of HTT, which may modulate the nuclear localisation of HTT (Desmond et al. 2013). The PY-NLS is typically unstructured, and forms the correct conformation upon binding to the HEAT-repeat rich region of karyopherin β2; the structure of the HTT PY-NLS does not adhere to the same mechanism utilised by other PY-NLS containing proteins, as the three consensus sequences are separated by a β-sheet structured region, which may provide a mechanism for regulating the action of the NLS in different cellular contexts (Desmond et al. 2013).

1.5.3 Nuclear export

A leucine-rich consensus sequence for a chromosome region maintenance 1 (CRM1) NES has been identified on the C-terminus end of HTT (Figure 1.3) (Xia 2003); as this region is often cleaved away during HTT proteolysis (Section 1.6.2), this may be a mechanism by which there is an enrichment of N-terminal HTT fragments present in

the nucleus compared to the cytoplasm (Wellington et al. 1998; Kim et al. 2003; Landles et al. 2010). The N-terminus of HTT has been found to bind to the nuclear pore protein translocated promoter region (TPR), which is associated with nuclear export, and this association declines in the presence of an expanded polyQ (Cornett et al. 2005). However, the association between HTT and TPR also diminished in the context of full length HTT (Cornett et al. 2005), therefore indicating that this may be a mechanism primarily for the nuclear export of truncated N-terminal fragments. In addition, post translational modifications of N-terminal HTT may reduce its association with the TPR, and therefore promote the nuclear localisation of phosphorylated HTT (Cornett et al. 2005).
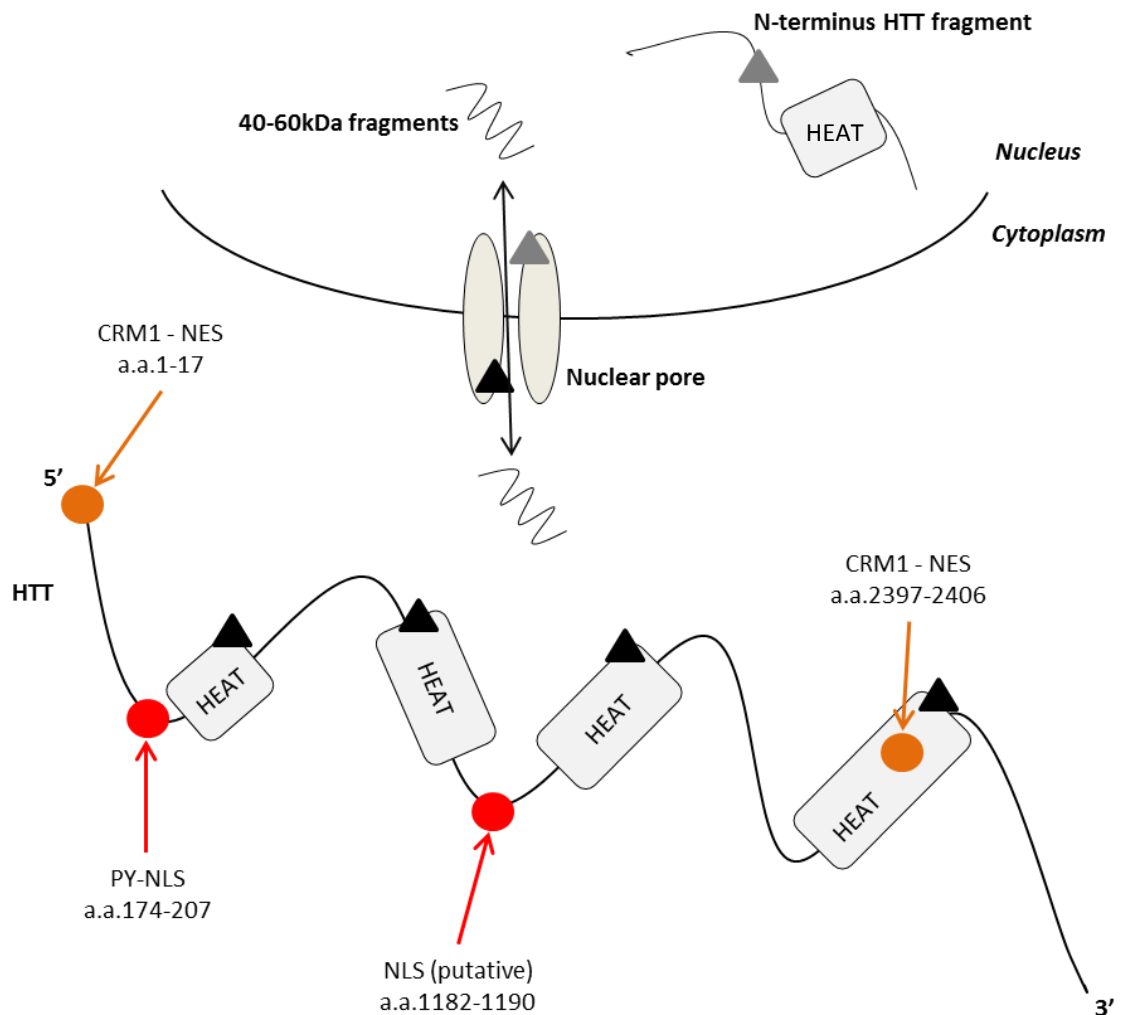
Figure 1.3 Cartoon representing the mechanisms of HTT subcellular localisation; small fragments can traverse the nuclear pore via passive diffusion. Grey triangles depict the interaction between nuclear pore- associated TPR proteins and N-terminus HTT. Black triangles represent the putative association between nucleoporins with HTT HEAT repeats. Red and orange circles depict NLS and NES sequences, respectively.

It has been suggested that amino acids 1-18 form an amphipathic alpha helical structure that act as a cytoplasmic retention signal, which targets HTT to the endoplasmic reticulum and vesicles; an association that can be disrupted by cellular stress or mutation of the region in order to alter its conformation, thus increasing the nuclear localisation of HTT (Atwal et al. 2007). As the structure of this region is thought to be disrupted in the presence of an expanded polyQ (Li et al. 2007; Długosz & Trylska 2011), this may be an additional mechanism for the increased nuclear localisation observed in HD models and human HD brain (DiFiglia 1997; Gomez-Tortosa et al. 2001). The first 17 amino acids of HTT have also been identified as a potential NES (Maiuri et al. 2013; Zheng et al. 2013); N17 of HTT is a leucine rich sequence, which is roughly a consensus sequence for exportin 1 and CRM1 mediated nuclear export (Maiuri et al. 2013; Zheng et al. 2013). By using mutations to leucines 4, 7 and 14, as well as to phenylalanine 11, to alter the NES sequence, the nuclear localisation of HTT was increased; however, alterations to other residues in this region had no effect (Zheng et al. 2013). In contrast, the phosphorylation of serines 13 (S13) and 16 (S16) have been found to reduce the association between HTT N17 and CRM1, possibly by altering the alpha-helical structure, and therefore increasing nuclear phosphorylated HTT epitopes (Maiuri et al. 2013).

1.6   Cellular signalling transduction pathways in HD

The expanded polyQ repeat within mHTT not only alters the regulation of its subcellular localisation, but may also initiate aberrant protein-protein interactions. In turn, this is likely to disrupt the complex balance between pro- and anti-apoptotic signalling transduction mechanisms that regulate cell growth and survival. Attention has therefore been given to the alterations of these pathways by mHTT, and the role they may play in HD pathogenesis; a depiction of the associations between several of these pathways can be found in Figure 4.1.

1.6.1 Anti-apoptotic and compensatory mechanisms

Anti-apoptotic pathways have been found to be important for prolonging neuronal survival during pathogenesis in HD models, as they may counter toxic metabolic changes elicited by mHTT (Ginés 2003). The most thoroughly characterised survival pathway in HD is the protein kinase B (AKT) pathway; baseline levels of AKT are relatively low in adult brain (Owada et al. 1997), however its activation rises following cellular stress and injury (Chong et al. 2005). AKT exerts its protective effects by phosphorylating and inactivating components of the cell death machinery, such as B-cell lymphoma-2 associated death promoter (BAD), caspase-9, forkhead box proteins (FOXOs) and inhibitor of kappa-β kinase (IKK) (Humbert et al. 2002; Humbert 2003).

The enhanced activation of AKT in HD models has been attributed to the reduced expression of its inhibitor, PH domain leucine-rich repeat protein phosphatase 1 (PHLPP1), which is suppressed in Hdh^{Q111}, R6/1, R6/2 and HD94 striata, as well as in human putamen (Saavedra et al. 2010). It has also been suggested that by interacting with growth factor receptor bound protein 2 (GRB2), mHTT may directly activate growth factor signalling cascades that are upstream of AKT activation, thus enhancing AKT phosphorylation (Liu et al. 1997). In contrast, the aberrant interaction between mHTT and GRB2 at the epidermal growth factor receptor (EGFR) and the receptor tyrosine kinase A (TRKA) has also been found to inhibit the downstream activation of AKT, mitogen activated protein kinase (MAPK) and c-jun N-terminal kinase (JNK) (Song et al. 2002). Therefore, although increasing AKT phosphorylation is a neuroprotective mechanism in HD pathogenesis, the nature of its activation in relation to mHTT requires further elucidation.

The activation of mitogen activated protein kinase kinase (MEK) and extracellular signal-regulated kinase (ERK) is required for BDNF-induced transcriptional regulation (Gokce et al. 2009), and as such, both are considered as pro-survival signalling pathways. In cell models of HD, compounds that inhibit cell death have been identified as acting via ERK phosphorylation (Varma et al. 2007; Scotter et al. 2010), and increasing ERK activity confers a protective effect by reducing the activation of caspase-3 (Apostol et al. 2006). However, in contrast to AKT activity, ERK

phosphorylation is consistently found to be either suppressed, which may increase cellular sensitivity to oxidative stress, or unchanged in models of HD (Apostol et al. 2006; Roze et al. 2008; Ginés et al. 2010; Taylor et al. 2013). This reduction is thought to be mediated by alterations in the upstream receptor tyrosine kinase B (TRKB); there is a reduction in the presence of TRKB receptors in HD models, as well as in human caudate (Ginés et al. 2006; Brito et al. 2013), which may be due to the inhibition of the retrograde transport of TRKB-containing vesicles as a result of aberrant interactions with mHTT (Liot et al. 2013). MEK has been less thoroughly investigated in the context of HD, however as it is upstream of ERK, it may be expected to regulate the protective effects of ERK activity in HD models. It has been found that MEK1 activation may enhance the phosphorylation of HTT (Schilling et al. 2006), which is generally considered to reduce mHTT toxicity (Bauer & Nukina 2009; Gu et al. 2009; Thompson et al. 2009; Warby et al. 2009; Atwal et al. 2011; Maiuri et al. 2013), and the overexpression of MEK1 in a PC12 model of HD enhanced ERK phosphorylation and reduced cell death (Apostol et al. 2006). However, in a *Drosophila* model of HD, MEK overexpression had no effect on survival (Iijima-ando et al. 2005).

1.6.2 Pro-apoptotic and inflammatory mechanisms

Hyperactivation of the two pro-apoptotic members of the MAPK family, JNK and P38 MAPK, has also been associated with HD (Taylor et al. 2013). The JNK pathway regulates transcription associated with the cell death response (Weston & Davis 2002), and can be activated by endoplasmic reticular stress; the stress response is initiated due to the accumulation of unfolded proteins, which leads to activation of apoptosis signal-regulating kinase 1 (ASK1) that induces JNK (Humbert 2003). Alternatively, JNK activation may be induced by the mixed lineage kinase 2 - MAP kinase kinase 7 - MAP kinase kinase 4 (MLK2-MKK7-MKK4) kinase cascade in response to growth factor signalling (Humbert 2003). The expanded polyQ has been suggested to enhance cell stress via activation of ASK1 (Nishitoh et al. 2002), and has been found to reduce the inhibitory association of wild type HTT with MLK2 (Humbert 2003), thus increasing JNK activation and supporting apoptosis. Increased JNK activation in response to mHTT has been noted in various cell and animal models of HD (Liu et al. 2000; Apostol et al. 2006; Perrin et al. 2009), where it has been found to enhance cellular toxicity and

increase the activation of caspase-3 (Apostol et al. 2006). P38 MAPK phosphorylation is increased in the striatum of R6/1, R6/2 and YAC128 mouse models of HD (Gianfriddo et al. 2004; Saavedra et al. 2011; Fan et al. 2012), and it has been suggested that its activity correlates with striatal damage (Gianfriddo et al. 2004). Additionally, suppressing P38 MAPK increases neuronal survival in a rat model, and primary neuronal model of HD (Wang et al. 2010; Taylor et al. 2013), implicating this kinase as a pro-apoptotic response to mHTT; however the co-ordination with other pro- and anti-apoptotic signalling networks will contribute towards determining cell fate.

Tumour suppressor protein 53 (P53) has also been associated with increased pro-apoptotic signalling in HD pathogenesis; P53 mediates tumour suppression by initiating cell cycle arrest, apoptosis and cellular senescence, and is increased in response to cellular stress (Chang et al. 2012). Levels of P53 are enhanced in HD patient lymphoblasts, N171-82Q mouse brain and in cell models of HD (Trettel et al. 2000; Bae et al. 2005); mHTT is also able to bind to P53 and has been shown to increase both its expression and nuclear localisation (Steffan et al. 2000). The aberrant regulation of P53 in models of HD is therefore a mechanism by which neuronal death is enhanced via pro-apoptotic signalling in response to mHTT.

The inhibitor of kappaB kinase beta/ nuclear factor kappa-light-chain-enhancer of activated B-cells (IKKβ/NFκβ) pathway is a prominent regulator of neuroinflammation, and its activation has been found to be increased both in models of HD, and in human HD patient serum and central nervous system (Khoshnan et al. 2004; Bjorkqvist et al. 2008; Khoshnan & Patterson 2011; Hsiao et al. 2013). Chronic elevation of IKKβ has been associated with increased neurodegeneration (Mattson 2006); one mechanism for this may be that an excessive inflammatory response in astrocytes confers additional damage to the adjacent neurons (Hsiao et al. 2013). Additionally, mHTT has been found to directly interact with the inhibitor of kappaB kinase gamma (IKKγ) subunit of IKKβ via the polyQ repeat and adjacent proline-rich region (Khoshnan et al. 2004). This interaction increases the activation of IKKβ, and subsequent activation of NFκβ (Khoshnan & Patterson 2011); in turn, activated IKKβ inactivates anti-apoptotic protein B-cell lymphoma – extra-large (BCL-XL) and activates caspase activity (Khoshnan et al. 2009). As well as promoting the expression of genes associated with

inflammation, NFκB activation may also promote AKT phosphorylation (Meng et al. 2002), which is compatible with the increased AKT phosphorylation observed in HD models, as described previously (Section 1.6.1).

IKKβ may also regulate HTT proteolysis, however the manner in which this occurs is under debate; increased IKKβ has been found to phosphorylate HTT on S13 and S16, which initiates HTT proteolysis and clearance by the proteasome and lysosome (Thompson et al. 2009). This may initially be a protective mechanism to enhance the clearance of mHTT, however with age related degradation of the proteasome system, this may lead to pathogenic accumulation of phosphorylated mHTT fragments (Thompson et al. 2009). In concordance with this, the reduction of IKKβ was found to prevent HTT proteolysis and increase cellular resistance to DNA damage, which improved neuronal survival (Khoshnan et al. 2009). Paradoxically, on another occasion the inhibition of IKKβ could also elicit the phosphorylation of HTT, which despite promoting proteolysis and targeting HTT to nuclear and subnuclear puncta, was neuroprotective (Atwal et al. 2011). Typically, the inhibition of IKKβ or NFκβ exerts neuroprotective effects in models of HD (Khoshnan et al. 2004; Khoshnan et al. 2009; Hsiao et al. 2013), implying that the enhanced IKKβ pathway in HD is likely to confer cellular toxicity. The paradoxical findings of HTT phosphorylation in response to IKKβ activation suggest that relationship between inflammatory kinases and the neuroprotective mechanisms of HTT phosphorylation are likely to be complex, and rely on cellular context and synergistic associations with multiple signal transduction pathways.

1.7   Gene expression in HD

Transcriptional dysregulation is one of the most central mechanisms contributing to HD pathogenesis (Ross et al. 2002; Zucker et al. 2005; Crocker et al. 2006; Crook & Housman 2011; Bowles et al. 2012; Seredenina & Luthi-Carter 2012), and is apparent from pre-symptomatic stages in mouse models of the disease (Crocker et al. 2006; Carnemolla et al. 2009; Becanovic et al. 2010), as well as in human HD embryonic stem cells (Feyeux et al. 2012) and in the blood of pre-symptomatic HD patients (Borovecki

et al. 2005). As such, there is currently a large volume of gene expression studies investigating the effect of mHTT- associated transcriptional dysregulation in a variety of HD models and tissues (Cha 2007; Seredenina & Luthi-Carter 2012).

1.7.1 Transcriptional profiles of HD and HD models

Despite variation in polyQ length, *HTT* gene dosage and expression context, there is a good correlation between the gene expression changes observed in post-mortem human HD caudate and mouse models of HD (Kuhn et al. 2007; Hodges et al. 2008), as well as with the immortalised embryonic striatal cell model (*StHdh*^{Q111}) of HD (Lee et al. 2007). The investigation of transcriptional dysregulation in human HD is limited to post-mortem caudate, which only allows for the transcriptional profiles of end-stage HD to be determined. However, the similarity of expression changes in mouse and cell models of the disease permits the characterisation of developmental mechanisms of dysregulation, and the exploration of potentially disease-modifying factors. The gene expression changes observed in different studies are reproducibly associated with similar biological pathways, including; neurotransmitter and neurotrophin receptors, transcription and chromatin remodelling, homeostasis, synaptic organisation, and regulation of metabolism (Luthi-Carter 2000; Hodges et al. 2006; Seredenina & Luthi-Carter 2012).

Although the downregulation of gene expression is most consistently observed in models of HD, upregulated genes are also present (Carnemolla et al. 2009; Crook & Housman 2011). However, the pattern of gene expression changes in response to mHTT is likely to be complex, and may not necessarily be stable over time; micro-RNA (miRNA) expression was initially upregulated in pre-symptomatic YAC128 mice, however at 12 months of age, miRNA expression was downregulated in comparison to control animals (Lee et al. 2011), which may reflect an initial compensatory mechanism for transcriptional control, followed by mHTT mediated disruption of miRNA regulation.

Additional autocompensatory mechanisms that serve to counter mHTT toxicity are also likely to be present in transcriptional profiles of HD and HD models, and the regulation of these genes aren't necessarily directly modulated by mHTT (Seredenina & Luthi-

Carter 2012). For example, the activity of the ETS-domain containing protein (ELK1) transcription factor has been found to be increased in mouse and cell models of HD , without any direct association with mHTT (Anglada-Huguet et al. 2012), and several ELK1 downstream target genes have also been observed to be dysregulated in these models (Spektor 2002; Roze et al. 2008). Consequently, inhibiting ELK1 activation or expression promoted cell death and enhanced caspase-3 cleavage (Anglada-Huguet et al. 2012). Therefore the transcriptional dysregulation observed in models of HD is unlikely to be universally due to direct mHTT interference with transcriptional machinery, so care must be taken when interpreting gene expression profiles.

1.7.2 Mechanisms of transcriptional dysregulation

Due to the extent of transcriptional dysregulation that is observed in HD, several different mechanisms have been identified by which mHTT may alter gene expression.

1.7.2.1 Protein-protein interactions

The sequestration of transcription factors (TFs) into mHTT aggregates is one of the most commonly described pathways for the alteration of transcriptional machinery; several TFs have been found to interact with mHTT neuronal aggregates, including CREB-binding protein (CBP), binding protein 300 (P300), P53, specificity protein 1 (SP1) and TATA-binding protein (TBP) (Kazantsev et al. 1999; Steffan et al. 2000; Nucifora et al. 2001). Sequestration into aggregates is predicted to prevent the normal associations of TFs with DNA, thus altering gene expression. The inhibition of positive regulators and loss of negative regulators of transcription mean that TF sequestration may lead to aberrant up- and down-regulations of gene expression. However, transcriptional dysregulation is observed in R6/2 neurons that do not contain intranuclear inclusions (Sadri-Vakili et al. 2006), and in $StHdh^{Q111}$ cells that do not form mHTT aggregates (Trettel et al. 2000); therefore TF sequestration is unlikely to be a major contributor to transcriptional dysregulation in models of HD.

Soluble mHTT has been found to interact abnormally with TFs in a manner that may modify gene expression patterns. For example, wild type HTT has been shown to interact with SP1, and this association is stronger with mHTT due to the expanded

polyQ repeat; (Shimohata et al. 2000; Dunah et al. 2002; Li et al. 2002). The association with mHTT inhibits SP1 binding to DNA in both pre-symptomatic and symptomatic post-mortem HD brain (Dunah et al. 2002), and has also been found to inhibit the interaction between SP1 and the general TF TFII130, therefore further altering transcriptional activation (Shimohata et al. 2000; Dunah et al. 2002). In addition to direct TF interactions, mHTT has also been found to inhibit TF activity by altering their clearance by the proteasome; CBP clearance is enhanced in the presence of mHTT, therefore reducing its availability for DNA binding (Cong et al. 2005), whereas in contrast, mHTT has been found to impair the clearance of β-catenin by aberrant interactions with its destruction complex (Godin et al. 2010). β-catenin accumulates in its phosphorylated form that marks it for proteasomal degradation, which results in increased cellular toxicity, but does not increase the expression of β-catenin target genes (Godin et al. 2010). Aberrant interactions with members of cellular kinase signal transduction pathways, as described previously (Section 1.6), may also be a mechanism by which mHTT alters the transcriptional regulation of downstream genes.

1.7.2.2 Chromatin remodelling

The architecture of chromatin significantly contributes to the regulation of transcription, and can be regulated by the post-translational modifications of histones. Histone marks have been found to be altered in several models of HD, including R6/2 and N171-82Q mice (Ferrante et al. 2003; Hockly et al. 2003; Gardian et al. 2005; Ryu et al. 2006; McFarland et al. 2012; Valor et al. 2013) and *StHdh*^{Q111} cells (Sadri-Vakili et al. 2007; Ng et al. 2013). Histone acetyltransferases, such as CBP, may be sequestered by mHTT, therefore reducing histone acetylation in models of HD (Seredenina & Luthi-Carter 2012). However, despite hundreds of hypoacetylated loci for histones H3 and H4 in the N171-82Q mouse model, very few genes with altered transcript levels showed significant changes in histone acetylation (Valor et al. 2013). There may therefore be little concordance between hypoacetylation and transcriptional dysregulation in HD (McFarland et al. 2012), and the two alterations may be independent manifestations of the effect of mHTT (Valor et al. 2013). However there was a small subset of genes where hypoacetylation of H3 –lysine 9 (K9) and H3-lysine 14 (K14) at the transcriptional start site was associated with transcriptional

dysregulation, and these genes were consistent between brain regions, mouse models and in HD patient tissue (Valor et al. 2013), and histone deacetylation inhibitors have proven to be neuroprotective (Ferrante et al. 2003; Hockly et al. 2003; Sadri-Vakili et al. 2007; Thomas et al. 2008; McFarland et al. 2012). Although the role of hypoacetylation in HD remains to be elucidated, additional epigenetic modifications are likely to contribute to the widespread transcriptional dysregulation in these models.

In contrast to acetylation, a large proportion of dysregulated genes have been associated with significant changes in methylation (Ng et al. 2013). Regions with a low cytosine-phosphate-guanine (CpG) content were particularly affected by increased DNA methylation, and were associated with activator protein 1 (AP1) and sex-determining region Y-box 2 (SOX2) TF activity (Ng et al. 2013). As DNA bound TFs can alter methylation patterns (Hogart et al. 2012; Stadler & Allis 2012), mHTT may alter histone methylation status by TF interactions; mHTT interacts with SET-domain, bifurcated 1 (SETDB1), a regulator of H3K9 trimethylation (Ryu et al. 2006). The activity of this methyltransferase is increased in human HD caudate and R6/2 brain (Ryu et al. 2006), and knocking down its expression reduces hypertrimethylation and ameliorates the R6/2 phenotype (Ryu et al. 2006). As methylation has been associated with a range of cognitive abilities, such as learning and memory (Liu et al. 2009; Day & Sweatt 2010), the modification of histone methylation may have significant implications for the daily functioning of HD patients.

1.7.2.3 Direct associations

In addition to the indirect modification of transcriptional regulation via sequestration and interactions with TFs, kinases, acetyltransferases and methyltransferases, mHTT can also bind directly to DNA in a manner that alters genomic DNA structure (Benn et al. 2008). mHTT has been identified as having increased DNA binding capacity in R6/2 striatum and in *StHdh*^{Q111} cells, having a higher binding occupancy at gene promoter regions than the wild type protein, and interfering with normal TF binding (Benn et al. 2008). Gene expression changes have also been observed in HTT-deficient cells

(Boudreau et al. 2009), therefore suggesting that HTT plays a normal, direct role in transcriptional control, which may be altered by the presence of mHTT.

1.8 Aims of this project

This project aims to investigate and characterise the mechanisms for transcriptional dysregulation associated with HTT localisation in the immortalised embryonic striatal cell model ($StHdh^{Q111}$) of HD. The model was derived from primary striatal neurons cultured from the Hdh^{Q111} knock-in mouse model of HD (Trettel et al. 2000); as such, wild type cells ($StHdh^{Q7/7}$) carry two alleles each containing 7 CAG repeats, and heterozygote ($StHdh^{Q7/111}$) and homozygote ($StHdh^{Q111/111}$) cells carry either one or two mutant alleles carrying 111 CAG repeats, respectively.

Since its development, the $StHdh^{Q111}$ cell line has been widely utilised. Comparisons between wild type and mutant cells have revealed phenotypes that mirror those also identified in mouse and human models of HD, such as mHTT mislocalisation (Trettel et al. 2000), transcriptional dysregulation (Benn et al. 2008; Saavedra et al. 2010), an augmented endoplasmic reticulum stress response (Trettel et al. 2000; Carnemolla et al. 2009), and altered kinase signalling (Ginés et al. 2003; Battaglia et al. 2011). The $StHdh^{Q111}$ cell model is therefore considered an appropriate model for the preliminary investigation of early cellular HD phenotypes.

By creating a dynamic model, it is possible to examine CAG repeat length-associated differential responses to cellular stimulation. This will be achieved by;

- Characterisation of the localisation of phosphorylated and non-phosphorylated N-terminal HTT epitopes in $StHdh^{Q111}$ cell lines prior to, and following stimulation with brain derived neurotrophic factor (BDNF), nerve growth factor (NGF) or epidermal growth factor (EGF),
- Identification of kinase signalling pathways elicited by growth factor stimulation, and of those that are aberrantly responding in the presence of mHTT,

- Inhibition of dysregulated kinase signalling pathways in order to determine the downstream effects on immediate-early gene transcription and HTT localisation,
- Analysis of differential gene expression changes following growth factor stimulation in order to determine additional signalling and transcriptional pathways that may be altered by mHTT,
- Replication of results from $StHdh^{Q111}$ cell lines in primary cell cultures from Hdh^{Q111} and Hdh^{Q150} E14 striata to determine whether any observed effects are model or CAG length specific.

Chapter 2:   Materials and methods

2.1 Materials

Addresses of all suppliers whose products were used in this study are listed below in alphabetical order:

Abcam plc, Cambridge, UK; **Affymetrix**, Santa Clara, California, USA; **Bioline reagents Ltd**, London, UK; **Bio-Rad laboratories Inc**, Hercules, California, USA; **Developmental Studies Hybridoma Bank**, Iowa City, Iowa, USA; **Fisher Scientific UK Ltd**, Loughborough, UK; **Jax®**, Bar Harbor, Maine, USA; **Leica Microsystems**, Wetzlar, Germany; **Life Technologies Corporation**, Carlsbad, California, USA; **Lorne Laboratories Ltd**, Reading, UK; **Merck Millipore**, Billerica, Massachusetts, USA; **New England Biolabs**, Hitchin, UK; **PAA laboratories**, Yeovil, UK; **Qiagen**, Manchester, UK; **Santa Cruz Biotechnology Inc**, Dallas, Texas, USA; **Sigma Aldrich Company Ltd**, Dorset, UK; **VWR international**, Lutterworth, UK.

2.1.2 Chemicals

All analytical grade chemicals were supplied by Sigma-Aldrich, unless otherwise stated.

2.1.3 Buffers and general reagents

Below are details of the buffers and reagents commonly used throughout this project, listed in alphabetical order:

Cell Lysis buffer
1 x Cell lysis buffer (New England Biolabs), containing:

20 mM Tris-Hydrochloride (Tris-HCl), pH 7.5

150 mM Sodium Chloride (NaCl)

1 mM Disodium-EDTA (Na_2EDTA)

1 mM Ethylene Glycol Tetraacetic Acid (*EGTA*)

1% Triton

2.5 mM Sodium Pyrophosphate ($Na_4P_2O_7$)

1 mM Beta-glycerophosphate (BGP)

1 mM Sodium Orthovanadate (Na$_3$VO$_4$)

1 µg/ml Leupeptin

1mM phenylmethanesulfonylfluoride (PMSF)

Distilled water (dH$_2$O)

DNA extraction buffer

1M Tris-HCl, pH8.0

0.5M Ethylenediaminetetraacetic acid (EDTA), pH8.0

10% Sodium Dodecyl Sulfate (SDS)

dH$_2$O

DNA Orange Loading Dye

70% dH2O

30% Glycerol

Orange G

Fractionation Buffer

250mM Sucrose

3mM Imidazole

1mM EDTA, pH8.0

1% Protease inhibitor

 dH$_2$O

PBS Tween (PBS-T)

1ml Tween®20 dissolved in 1L PBS.

Phosphate Buffered Saline (PBS)

Made by dissolving 5 PBS tablets in 1 litre dH$_2$O, giving a final yield of:

100nM phosphate buffer

27nM Potassium Chloride (KCl)

137nM NaCl, pH 7.4

Radioimmunoprecipitation assay (RIPA) buffer

Acquired ready-made, containing:

150nM NaCl

1.0% IGEPAL® CA-630

0.5% Sodium Deoxycholate

0.1% SDS

50 mM Trisaminomethane (Tris), pH8.0.

Tris/Borate/EDTA (TBE) buffer

44.5mM Tris

44.5mM Boric acid (H_3BO_3)

1mM EDTA, pH8.0

dH_2O

2.1.4 Cell lines

$StHdh^{Q7/7}$, $StHdh^{Q7/111}$ and $StHdh^{Q111/111}$ immortalised embryonic striatal cells were a kind gift from Marcy MacDonald (Molecular Neurogenetics Unit, Massachusetts General Hospital, Massachusetts, USA). The MW1 hybridoma cell line was provided by the Developmental Studies Hybridoma Bank, (University of Iowa, Iowa, USA).

2.1.5 Animals

Hdh^{Q150} mice bred on a C57/Bl6 background were obtained from Jax® (The Jackson laboratory, Bar Harbor, Maine, USA), and Hdh^{Q111} mice were from the Wheeler laboratory (Molecular Neurogenetics Unit, Massachusetts General Hospital, Massachusetts, USA). Both lines were housed under project licence PPL: 30/3036 on a 12 hour light-dark cycle from 6am to 6pm in a temperature controlled environment (20-22°C), with water freely available and environmental enrichment. The CAG repeat length in Hdh^{Q150} mice varied between 125-160 repeats, but was maintained at around 150. In Hdh^{Q111} mice, the repeat length ranged between 125-145, but was maintained at around 135. Timed mating was carried out by pairing heterozygote males and

females at 4pm, and leaving overnight until 9am, when they were then separated. Females were checked for plugs, and after 14 days the pregnant dams were killed by cervical dislocation, and the embryos were harvested for striatal dissections.

2.1.6 Cell culture

Penicillin-Streptomycin solution, Trypan Blue, Fetal Bovine Serum (FBS) for primary cell culture, and DMSO and the Nalgene® Mr.Frosty for cryogenic preservation of cell lines were all purchased from Sigma-Aldrich. FBS for immortalised and hybridoma cell lines was supplied by PAA, and the Trypsin for primary cell culture was purchased from Lorne Laboratories. T75 and T160 flasks and Nalgene cryovials were purchased from Fisher Scientific. All other culture media reagents were purchased from Life Technologies Incorporated.

2.1.7 Immunofluorescence materials

Chance Propper Ltd Blue Star glass microscopy slides, 6 well and 24 well plates were supplied by Fisher Scientific. 1cm and 24mm diameter coverslips were both purchased from VWR International Ltd. Poly-L-lysine and Poly-D-lysine for coating coverslips and Formalin to fix cells were all obtained from Sigma-Aldrich. For mounting coverslips, ProLong® Gold antifade reagent with DAPI was purchased from Life Technologies Incorporated.

2.1.8 Electrophoresis of proteins and protein transfer

SDS-PAGE gel electrophoresis was carried out in the XCell SureLock™Mini-Cell Electrophoresis system, and wet blotting was carried out in the XCell II Blot Module, both from Life Technologies Incorporated. Immobilon™-P Transfer membrane was purchased from Merck Millipore, and chromatography paper was from Fisher Scientific. The Precision Plus Protein™ molecular weight standard was supplied by BioRad, bovine serum albumen (BSA) was from Sigma Aldrich, and Marvel dried semi-skimmed milk was used as a blocking agent. All precast 4-12% NuPage® Bis-Tris gels and other protein electrophoresis and transfer materials were supplied by Life Technologies Incorporated.

2.1.9 Antibodies and labelling reagents

A table of all antibodies and labelling reagents used during this project can be found in Table 2.1, and details of the epitopes detected by the N-terminal antibodies against HTT and mHTT are depicted in Figure 2.1.

	Antibody	Source	IF dilution	WB dilution	Preferred blocking reagent	Supplier

Primaries

	Antibody	Source	IF dilution	WB dilution	Preferred blocking reagent	Supplier
Huntingtin	Mab2166	Mouse monoclonal	1:1000	1:1000	Milk	Millipore
	Ab109115	Rabbit polyclonal	1:100	1:1000	Milk	Abcam
	Ab675	Rabbit polyclonal	1:200	1:500	Milk	Covalab
	MW1	Mouse monoclonal hybridoma	-	1:1000	Milk	Developmental Studies Hybridoma Bank, University of Iowa
	Anti-pS13	Rabbit polyclonal	1:500	-	Milk	Kind gifts from Joan Steffan, University of California, Irvine, USA
	Anti-pS13S16	Rabbit polyclonal	1:1000	1:1000	Milk	
	N17	Rabbit polyclonal	1:250	1:5000	Milk	Kind gifts from Ray Truant, McMaster University, Canada
	N17 pS13S16	Rabbit polyclonal	1:250	1:5000	Milk	

	Antibody	Source	IF dilution	WB dilution	Preferred blocking reagent	Supplier
Cell Markers	Anti-MEK	Rabbit monoclonal	-	1:1000	BSA	New England Biolabs
	Anti-Lamin A/C	Mouse monoclonal	-	1:2000	Milk	New England Biolabs

	Antibody	Source	IF dilution	WB dilution	Preferred blocking reagent	Supplier
Receptors	Anti-EGFR	Rabbit monoclonal	1:50	1:1000	BSA	New England Biolabs
	Anti-TRKA	Rabbit monoclonal	1:100	-	Milk	Abcam

Table 2.1 Continued on next page

	Anti-TRKA	Rabbit monoclonal	-	1:1000	Milk	New England Biolabs
	Anti-TRKB	Rabbit polyclonal	1:100	1:100	Milk	Abcam
	Anti-P75 NTR	Rabbit polyclonal	1:500	1:500	Milk	Abcam

Loading Control	Anti-α-tubulin	Mouse monoclonal	-	1:10,000	Milk or BSA	Abcam

Striatal Cell markers	Anti-CTIP2	Rat monoclonal	1:500	-	BSA	Abcam
	Anti-DARPP-32	Rabbit polyclonal	1:200	-	BSA	Santa Cruz Biotechnology Inc

SMADs	SMAD1	Rabbit monoclonal	-	1:1000	Milk	New England Biolabs
	Phospho-SMAD1 (ser465)	Rabbit polyclonal	-	1:1000	Milk	Abcam
	Phospho-SMAD1/5 (ser463/465)	Rabbit monoclonal	-	1:1000	Milk	New England Biolabs
	SMAD2	Rabbit monoclonal	-	1:1000	Milk	New England Biolabs
	Phospho-SMAD2 (ser465/467)	Rabbit monoclonal	-	1:1000	Milk	New England Biolabs
	SMAD3	Rabbit monoclonal	-	1:1000	Milk	New England Biolabs
	Phospho-SMAD3 (ser423/425)	Rabbit monoclonal	-	1:1000	Milk	New England Biolabs
	SMAD4	Rabbit polyclonal	-	1:1000	Milk	New England Biolabs

Table 2.1 Continued on next page

SMAD5	Rabbit polyclonal	-	1:1000	Milk	New England Biolabs
Phospho-SMAD5 (ser463/465)	Rabbit monoclonal	-	1:500	Milk	Abcam
SMAD6	Rabbit polyclonal	-	1:1000	Milk	New England Biolabs
TGFBI	Goat polyclonal	-	1:1000	Milk	Abcam

Secondaries

Goat α Rabbit 568		1:100	-	Milk or BSA	Life Technologies Inc
Donkey α Mouse 488		1:100	-	Milk or BSA	Life Technologies Inc
Chicken α Rat 647		1:100	-	Milk or BSA	Life Technologies Inc
Goat α Mouse DyLight™ 800		-	1:20,000	Milk or BSA	Fisher Scientific
Rabbit α Goat 680		-	1:10,000	Milk	Life Technologies Inc
Goat α Rabbit 680		-	1:10,000	Milk or BSA	Life Technologies Inc
ProLong Gold Antifade with DAPI		1 drop	-	Milk or BSA	Life Technologies Inc

Table 2.1 Primary and secondary antibodies utilised throughout this project for both immunofluorescence (IF) and western blot (WB).
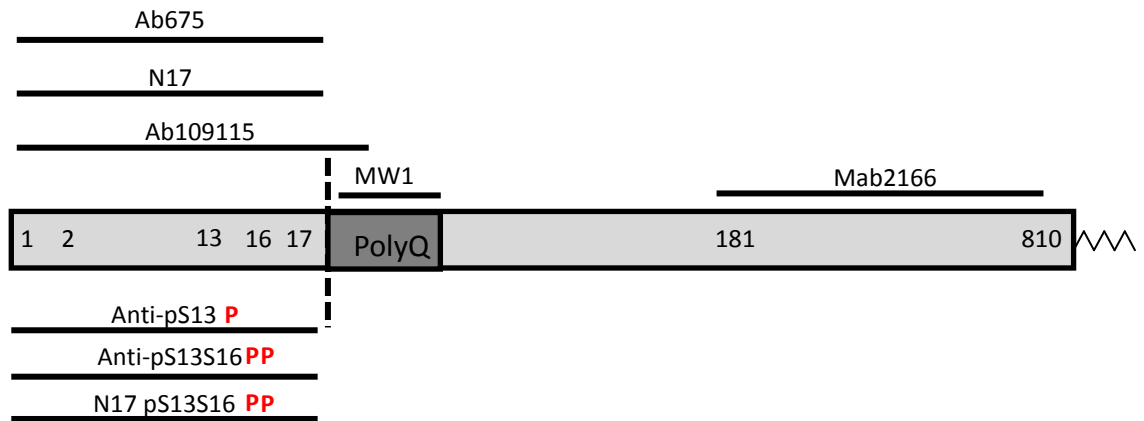
Figure 2.1 Cartoon of N-terminal Huntingtin, depicting the epitopes detected by the panel of anti-HTT primary antibodies used throughout this project. Red 'P' denotes a phosphorylation site at either serine 13 or 16.

2.1.10 Confocal microscopy

A Leica TCS SP5 confocal microscope was used to image all immunofluorescence experiments, using the Leica Suite Application Advanced Fluorescence 3 microscope software version 2.6.0 (copyright 1997-2011 Leica Microsystems CMS GmbH). Type F immersion oil was also from Leica.

2.1.11 ELISA kits

The following Cell Signalling Technology PathScan® Sandwich ELISA kits were all purchased from New England Biolabs:

Signalling Nodes Multi-Target kit, Cleaved PARP (Asp 214) kit, Phospho-BAD (Ser112) kit, Phospho-SAPK/JNK (Thr183/Tyr185) kit, Phospho-AKT (Ser473) kit, Phospho-MEK1 (Ser217/221) kit, Phospho-SMAD2 (ser 465/467), Total SMAD2, Total SMAD3 and Phospho-SMAD3 (Ser423/425).

2.1.12 General protein biochemistry materials

10cm round dishes used to grow cells for protein extraction, cell scrapers, lysing matrix D tubes and the 1ml glass Dounce homogeniser were all from Fisher Scientific, as was the protein assay kit for protein quantitation. Chromatography columns for

purification of antibodies from hybridoma cell lines were from BioRad, which used protein G sepharose beads from Sigma Aldrich. Ponceau S was also purchased from Sigma Aldrich, and SimplyBlue™ Safe Stain was from Life Technologies.

2.1.13 Oligonucleotides

Primers and assays for DNA and cDNA amplification were purchased from Life Technologies Incorporated. Details of the oligonucleotide sequences and identifications can be found in Table 2.2.

2.1.14 Preparation of nucleic acids

All reagents used for the extraction of RNA and DNA were purchased from Sigma Aldrich, with the exception of RNase*Zap®* and diethylpyrocarbonate (DEPC)-treated water, which were both from Life Technologies.

A

Gene	Forward 5'-3'	Reverse 5'-3'
Ubc	GAGTTCCGTCTGCTGTGTGA	CCTCCAGGGTGATGGTCTTA
C-fos	AGAAGGGGCAAAGTAGAGCA	GCAGCCATCTTATTCCGTTC
Egr1	CCTATGAGCACCTGACCACA	GGGATAACTCGTCTCCACCA
Ngfib	CAATGCTTCGTGTCAGCACT	TGGCGCTTTTCTGTACTGTG
Arc	GAGAGCTGAAAGGGTTGCAC	ACGTAGCCGTCCAAGTTGTT

B

Gene	Forward 5'-3'	Reverse 5'-3'
Htt	CCCATTCATTGCCTTGCT	GCGGCTGAGGGGGTTGA

Table 2.2 Continued on next page

C	Gene	ID
	18s	Mm03928990_g1
	Atf3	Mm00476032_m1
	Cdc42ep3	Mm00518245_m1
	Egr1	Mm00656724_m1
	Etv5	Mm00465816_m1
	Fgf2	Mm00433287_m1
	Fosl1	Mm04207958_m1
	Gadd45g	Mm01352550_g1
	Id3	Mm01188138_g1
	Junb	Mm04243546_s1
	Myc	Mm00487804_m1
	Ngf	Mm00443039_m1
	Rasa1	Mm00520858_m1
	Smad7	Mm00484742_m1
	Sox9	Mm00448840_m1

Gene	ID
Smad1	Mm00484723_m1
Smad3	Mm01170760_m1
Smad6	Mm00484738_m1
Smad9	Mm00649885_m1
Tgfb2	Mm00436955_m1
Tgfbr2	Mm00436977_m1
Tgfb3	Mm00436960_m1
Tgfbr3	Mm00803538_m1
Tgfbi	Mm00493634_m1
Smurf2	Mm03024086_m1
Csf1	Mm00432686_m1
Ctgf	Mm01192932_g1
Ereg	Mm00514794_m1
Rgs16	Mm00803317_m1
Ppargc1α	Mm01208835_m1

Table 2.2 Continued on next page

Usp43	Mm00620499_m1	*Nr4a2*	Mm00443060_m1
Rnd3	Mm00512162_m1	*Mybl1*	Mm00485327_m1
Id2	Mm00711781_m1	*Prl2c2*	Mm04208104_gH
Ccng2	Mm00432394_m1	*Gapdh*	Mm99999915_g1
Htt	Mm01213820_m1		

Table 2.2 Oligonucleotides designed and used for **A**. Sybr® Green qRTPCR, **B**. genotyping PCR and **C**. Identification codes for TaqMan® oligonucleotides used throughout this project.

2.1.15 Polymerase chain reaction reagents

The BioTaq™ DNA polymerase kit was purchased from Bioline, Proteinase K was from Life Technologies, and Betaine solution was provided by Sigma-Aldrich. All PCR reactions were carried out on a MJ research PTC-225 thermal cycler

2.1.16 Electrophoresis of DNA for Genotyping

Agarose was purchased from Sigma Aldrich, HyperLadder™50bp was from Bioline and Ethidium bromide was from Sigma Aldrich. All other materials and reagents were supplied by Life Technologies.

2.1.17 Quantitative reverse transcription polymerase chain reaction materials

All qRTPCR reagents and materials were from Life Technologies, although the RNeasy MinElute Cleanup Kit for purifying RNA extractions was purchased from Qiagen.

2.1.18 Small Interfering RNA reagents

Apart from cell culture reagents previously mentioned, all Dharmacon siRNA reagents were supplied by Fisher Scientific.

2.1.19 Microarray chips and analysis

Affymetrix GeneChip® Mouse Genome 430A 2.0 and Affymetrix GeneChip® Mouse Gene 1.0 ST arrays were utilised. Microarray data was analysed in the Partek® Genomics Suite™ 6.6$_{beta}$ (copyright 1993-2011 Partek Incorporated).

2.1.20 Growth factors and kinase inhibitors

EGF and NGF were purchased from Life Technologies, and BDNF was from Promega. Both AKT inhibitor VIII and MEK 1/2 inhibitor were supplied by Merck Millipore, and transforming growth factor-β 1 (TGFβ1) and 20mM citrate were from New England Biolabs.

2.2 Methods

2.2.1 General cell culture protocols

2.2.1.1 Maintenance of immortalised striatal cell lines

The *StHdh*^{Q111} cell line was derived from knock-in Hdh^{Q111} embryonic day 14 (E14) striatal cells by infection with the mouse adenovirus simian vacuolating 40 (SV40) large T antigen containing a temperature sensitive tsA58/U19 mutation (Trettel et al. 2000). *StHdh*$^{Q7/7}$, *StHdh*$^{Q7/111}$ and *StHdh*$^{Q111/111}$ cell lines were grown and maintained in high glucose Dulbecco's Modified Eagle Medium (DMEM) containing L-glutamine, sodium pyruvate, 1% Penicillin-Streptomycin solution, 1% 40mg/ml Geneticin and 10% FBS in T-75 flasks . These cells were grown in a humid environment at 33°C with 5% C0$_2$. Cells were split every 2-3 days. To passage adherent cells, monolayers were trypsinised in 2ml 0.25% Trypsin/EDTA for 5 minutes at 33°C. Flasks were then gently rocked to dislodge the cells, which were then resuspended in fresh complete medium and plated into new flasks.

2.2.1.2 Cell counting with a haemocytometer

To count cells for seeding onto coverslips or for cryogenic preservation, 10μl of cell suspension was applied to a haemocytometer. A haemocytometer is a modified glass

slide with two counting grids; each grid is made up of 9 squares, the volume of each square being $0.1mm^3$. Five of these squares are used for cell counting. The number of cells in each of the 5 squares is averaged to give the mean number of cells per $0.1mm^3$ (N). This is then used to determine the number of cells per 1ml suspension. The number of cells per $1cm^3$ is equal to N x 10^4.

2.2.1.3 Seeding immortalised striatal cell lines onto coverslips and culture dishes

To prepare a 6-well plate for seeding, 24mm diameter coverslips were washed in ethanol then left to dry in the wells of a 6-well plate. Cells were seeded at a concentration of $1x10^5$ per 1 ml on each coverslip. Each coverslip was then flooded with a further 1ml of complete media. For seeding into 10cm dishes, cells were trypsinised and resuspended into complete DMEM as previously described. A portion of the cell suspension was re-plated into a 10cm dish and flooded with 10ml complete DMEM. Cells were grown for 1-2 days before being serum starved overnight prior to processing.

2.2.1.4 Embryonic striatal microdissection

Pregnant mice were taken when at embryonic day 14 (E14), and killed by cervical dislocation. Both uterine horns were then removed and placed in Hank's balanced salt solution (BSS). The embryos were then removed and kept moist in a petri dish, also containing Hank's BSS. Individual embryos were moved to a separate petri dish, where they were killed by decapitation. All dissections were carried out using a dissection microscope with fibre optic light source and a transmitted light base. The brain was dissected by an incision at its base with a fine scalpel, the skin and meninges were peeled away with forceps, then the brain was freed by pinching at the base of the hind brain. The whole brain was then moved to an eyeglass well with a little Hank's BSS for striatal microdissection, while the rest of the body was kept and stored at -80°C.

In the eyeglass well, the brain was laid on its ventral surface. Using iridectomy scissors, a cut was made longitudinally through the medial cortex, which was then folded aside. This exposes the ganglionic eminence in the floor of the lateral ventricle. A superficial

cut was made either side of the ganglionic eminence, and then both lateral and medial sections of the striatum were removed and placed in DMEM/F-12 prior to processing. Figure 2.2 illustrates this process. The rest of the brain was kept and stored at -80°C.
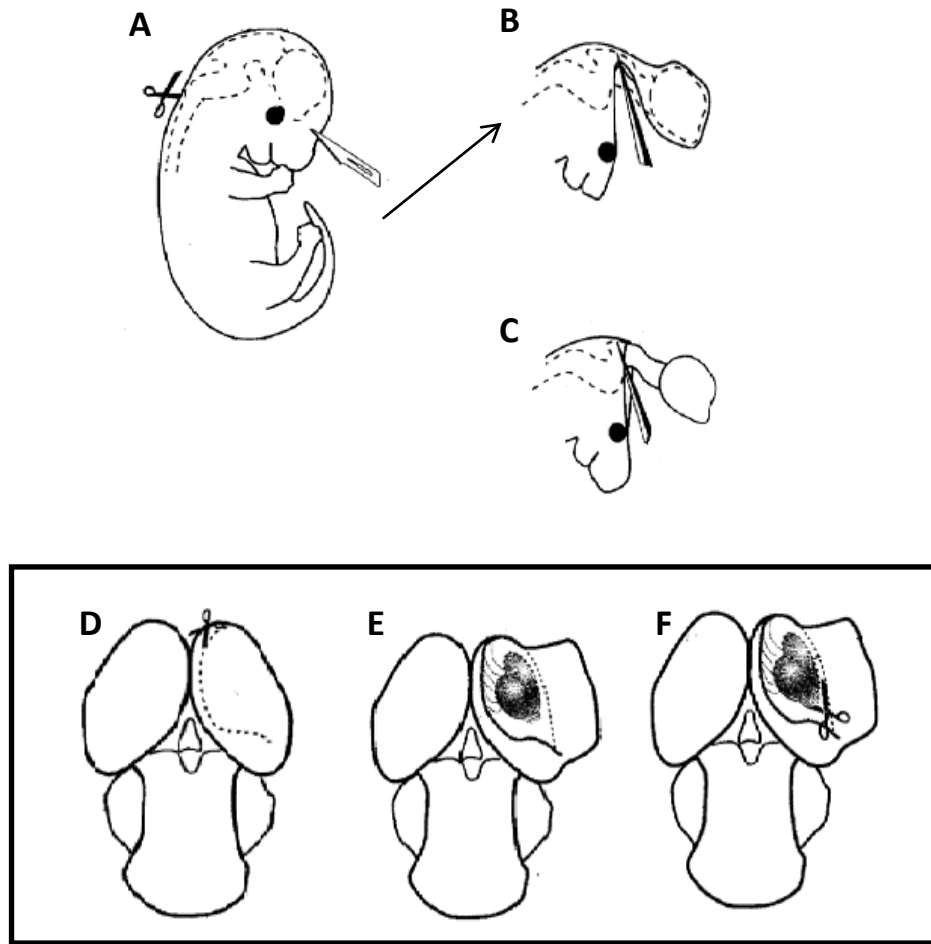
Figure 2.2 Microdissection of the ganglionic eminence from an E14 mouse embryo. **A.** The embryo is killed by decapitation, and **B-C.** the brain is dissected and removed. **D-F.** show the embryonic brain laying on its ventral surface. **D.** The medial cortex is cut to expose the ganglionic eminence **(E)**, which is then removed with microspring scissors **(F)**. Figure adapted from Dunnett & Bjorklund (1999).

2.2.1.5 Seeding primary striatal neurons from microdissections

To culture primary cells from Hdh^{Q111} and Hdh^{Q150} embryonic microdissections, each sample was washed in DMEM/F-12, then digested with 50µl 0.1 % Trypsin in 0.01% DNase in Hank's BSS, and incubated for 20 minutes at 37°C. Following trypsinisation, samples were incubated with an additional 150µl 0.01% DNAse in Hank's BSS for a further 5 minutes at 37°C. After this time, the supernatant was removed and the remaining sample was titrated 10-12 times with a pipette in 50µl DMEM/F-12 to create a cell suspension. Viable cells were identified using Trypan Blue and counted using a haemocytometer.

For immunofluorescence, primary cell suspensions were grown at 1×10^5 per well on 1cm diameter Poly-L-lysine treated coverslips in a 24 well plate. The entire cell suspension from each embryo was divided into two wells of a Poly-L-lysine treated 6-well plate for protein and RNA extraction experiments. To prepare coverslips for seeding, they were autoclaved then individually placed in wells. Coverslips and wells were then incubated for 1 hour with 100µg/ml Poly-L-lysine in dH$_2$O at room temperature. If the plates were being prepared for future use, they were then wrapped in cling film and stored at 4°C. Otherwise, they were washed three times with distilled water, and left to dry for 45 minutes in the culture hood with the UV light turned on. Cell suspensions were then pipetted directly on to the coverslips or into wells, and left to set down for 2-3 hours at 37°C. They were then flooded with complete DMEM/F-12, containing 1% antibiotic-antimycotic solution, 2% B-27 supplement, and 10% FBS, and grown in a humid environment at 37°C with 5% C0$_2$. Cells were fed with fresh complete DMEM/F-12 after 3 days, and were processed after 7 days.

2.2.1.6 Hybridoma cell culture

The MW1 hybridoma cell line was grown in T160 flasks with high glucose DMEM containing 1% Penicillin-Streptomycin solution and 20% FBS in a humid environment at 37°C with 5% CO$_2$. Hybridomas were passaged every 4 – 5 days by knocking the semi-adherent cells back into suspension within the flask. This suspension was then split into new T160 flasks and flooded with 50ml fresh complete DMEM.

2.2.1.7 Cryogenic preservation of cell lines

Following trypsinisation, cells were resuspended in complete media containing 10% DMSO at a concentration of 1-3 x 10^6 cells per 1ml and transferred to cryovials. The cryovials were placed in a Nalgene® Mr.Frosty containing isopropanol at -80°C. After 24 hours, the cryovials were either transferred to storage in liquid Nitrogen (-196°C), or kept at -80°C for short term storage. Cells were thawed for use by suspension in a water bath at 37°C for 90 seconds, before being transferred to complete DMEM, excluding Geneticin. The media was replaced the following day to ensure removal of any DMSO. After 2-3 days, Geneticin was added to the growth media, and cells were maintained as previously described (Section 2.2.1.1).

2.2.1.8 Sample preparation for immunofluorescence

Both primary and immortalised cells were prepared in the same manner for immunofluorescence. The media was removed from each well, and coverslips were then washed twice with sterile 1xPBS pH7.2, before being incubated with Formalin solution (containing 10% paraformaldehyde) for 20 minutes at room temperature. The Formalin solution was then removed, and the coverslips were washed a further three times with 1x PBS. Fixed cells were then stored in 1xPBS at 4°C until use.

2.2.1.9 Fluorescence microscopy

All coverslips were imaged on a Leica SP5 confocal microscope, using a x63 oil immersion objective lens. Images were captured with a 1024 x 1024 frame at a speed of 400Hz, a pinhole of 1 airy unit, with the line average and frame average both set at 4, and a 1.5x zoom. Table 2.3 displays the lasers and detection bandwidths for each photomultiplier tube (PMT) used for each secondary antibody. The level of smart gain for each antibody was kept at the same voltage across coverslips.

Secondary Antibody		AlexaFluor 488	AlexaFluor 568	AlexaFluor 647	DAPI
Laser		Argon (30%)	HeNe 543	HeNe 633	405 diode (UV)
Bandwidth	Start (nm)	510	550	640	411
	Finish (nm)	540	630	690	436

Table 2.3 Confocal microscopy settings used for imaging immunofluorescence experiments

2.2.1.10 Statistical analysis of confocal images

Images from confocal microscopy were analysed using the GNU Image Manipulation Program 2.6.11, Copyright 1995-2008. Images were initially converted to greyscale, and then the mean pixel intensities of particular cellular regions were determined. The ratio of intensity between the cytoplasm, perinuclear region and nucleus were then calculated for each individual cell in order to determine whether there was a change in protein localisation. An illustration of this process can be seen in Figure 2.3.

The resulting nuclear/cytoplasmic (N/C), nuclear/perinuclear (N/P) and perinuclear/cytoplasmic (P/C) ratios were then used for statistical analysis, using SPSS v.18 (SPSS Inc. Released 2009. PASW Statistics for Windows, Version 18.0. Chicago: SPSS Inc).
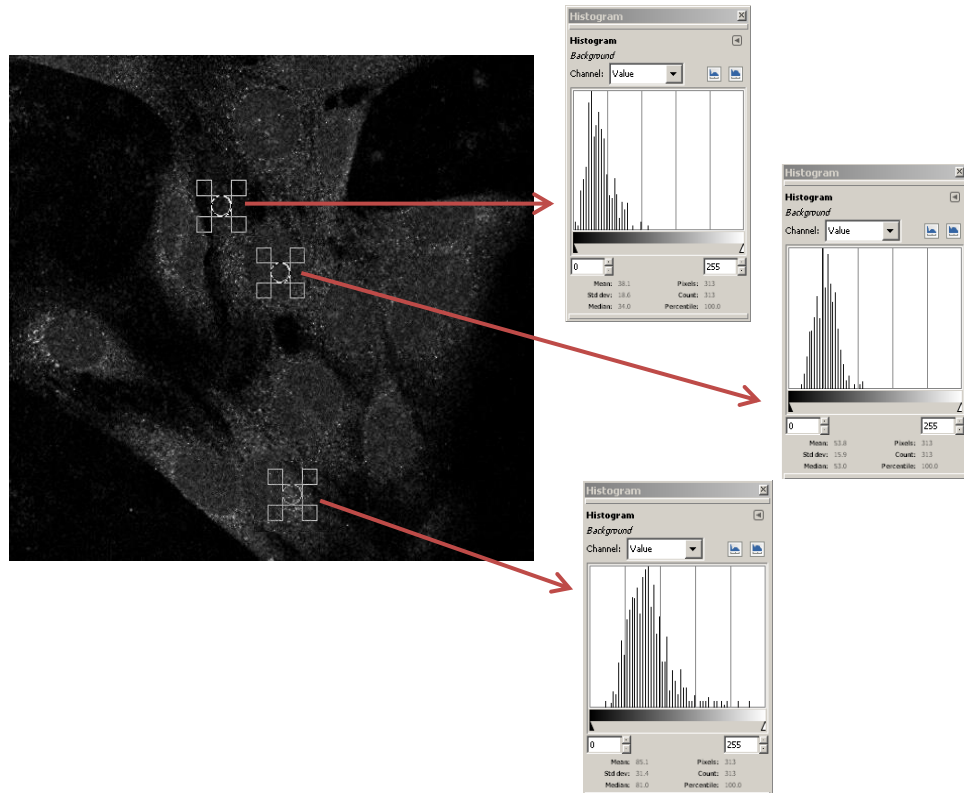
Figure 2.3 An example of immunofluorescence image quantification. For every cell, a circular region within the nucleus (N), perinuclear area (P) and cytoplasm (C) were selected, and a histogram displaying the mean pixel intensity for that region was given. Within each cell, an N/C, N/P and P/C pixel intensity ratio was calculated in order to control for variance in background staining across coverslips and images. This also allowed the determination of localisation change between these regions in response to treatment rather than intensity alterations for each region.

2.2.2 Protein biochemistry methods

2.2.2.1 Preparing protein lysates from immortalised striatal cells for ELISA

Immortalised cell lines were grown on 10cm culture dishes for 2 days in complete DMEM and then serum starved overnight prior to protein extraction. Cells were washed twice with 1xPBS, then incubated with 1xLysis Buffer (provided with the ELISA kits) containing 1mM phenylmethanesulfonylfluoride (PMSF) for 10 minutes on ice prior to scraping and collection into a 2ml tube. Lysates were briefly sonicated on ice then centrifuged for 10 minutes at 13,000xg at 4°C. The supernatant was retained as the protein lysate and the pellet was discarded.

2.2.2.2 Protein extraction from primary embryonic tissue and cells

Tissue was placed in a lysing matrix D tube along with cold RIPA buffer containing 1% protease inhibitor. The samples were then homogenised in a FastPrep® instrument for 20 seconds at a speed of 4.5 m/sec, then put straight back on ice. The lysate was then moved from the beads to a fresh tube, before being briefly sonicated on ice.

Protein was extracted from cultured primary striatal preparations in the same manner as described in Section 2.2.2.1.

2.2.2.3 Subcellular fractionations from immortalised striatal cell lines

Cells were seeded into 10cm culture dishes and grown for two days in complete DMEM and then serum starved overnight prior to subcellular fractionation. Cells were washed twice with 1xPBS before the addition of Fractionation Buffer (Section 2.1.3). Cells and buffer were then scraped into a 2ml tube and kept on ice for 10 minutes. Lysates were then subject to 30 strokes of a 1ml dounce homogeniser on ice. A portion of the resulting lysate was retained as a whole-cell fraction and was briefly sonicated on ice. The remaining lysate was centrifuged for 5 minutes at 500xg at 4°C. The supernatant was removed to a separate tube, and the pellet was resuspended in RIPA buffer, briefly sonicated on ice, and retained as the nuclear fraction. The supernatant was then centrifuged for a further 20 minutes at 10,000xg at 4°C. The new supernatant was retained as the cytoplasmic fraction, and the resulting pellet was discarded.

2.2.2.4 Antibody extraction and purification from hybridoma cell lines

The antibody supernatant was extracted from the hybridoma cell line by centrifuging the cell suspension in complete DMEM for 5 minutes at 500xg to pellet the cells. The supernatant was removed and either frozen for future use or purified on a chromatography column.

To purify the antibody supernatant, a chromatography column was loaded with 1ml Protein G Sepharose beads and washed with 1xPBS. The hybridoma supernatant was then loaded, collected, and re-loaded on to the column before washing with 1XPBS to remove any bed volume serum from the beads. To prevent the beads drying out

quickly, a frit disc was floated on the PBS while it was still in the column, and carefully pushed through the tube until it sat evenly 1mm above the beads.

Four eluates were collected from the column by loading volumes of IgG Elution Buffer to the column. Eluate 2 was the main antibody fraction. To store the column for future use, 10ml IgG Elution Buffer was added to the column and allowed to run through to waste, followed by a wash with 1xPBS, then 10ml 0.05% Sodium Azide in PBS. The column was then capped, wrapped in parafilm and stored at 4°C. Antibody concentrations were determined by Bradford Assay, and IgG bands were checked by subjecting the eluates to SDS-PAGE gel Electrophoresis for 1.5 hours at 150V on a NuPage® Bis-Tris 4-12% gel. The gel was then washed three times for 5 minutes with gentle agitation in dH_2O, and incubated for 1 hour in SimplyBlue^{TM} Safe Stain on a shaker. The gel was then washed for a further hour in dH_2O to reduce background staining, and was imaged on the Licor® Odyssey® quantitative fluorescent imaging system.

2.2.2.5 Protein quantification

Protein concentrations were determined by bicinchoninic acid assay (BCA)(based on a procedure described by Bradford (1976)), using the BCA protein assay kit from Thermo Fisher Scientific. 2 x 10μl replicates of each sample and of 9 Bovine Serum Albumin standards were added to a 96-well flat bottomed microwell plate. The wells were then flooded with 200μl working reagent solution (50:1, Reagent A:B), the plate was sealed and incubated for 30 minutes at 37°C. Following the incubation period, the plate was allowed to come to room temperature, and the absorbance was measured at 562nm in a BioTek® μQuant™ microplate spectrophotometer.

2.2.2.6 Acetone precipitation of protein

Acetone precipitation was performed when the protein concentration in cell lysates was low. Acetone was first cooled to -20°C, then 4x volume of the sample was added to each lysate. Samples were then vortexed and incubated at -20°C for 1 hour. They were then centrifuged for 10 minutes at 14,000xg at 4°C. The supernatant was discarded, and the pellets left to dry at room temperature for 30 minutes. After drying,

pellets were resuspended in a smaller volume of RIPA buffer, and protein quantification was repeated.

2.2.2.7 SDS-PAGE gel electrophoresis

Sodium dodecyl sulphate - polyacrylamide gel electrophoresis (SDS-PAGE) was carried out using the XCell SureLock™Mini-Cell Electrophoresis system. Pre-cast mini (8cm x 8cm) Novex® NuPage® gels were used with a 4-12% polyacrylamide gradient, in order to optimise the separation between wild type and polyglutamine expanded huntingtin bands. These gels are Bis-Tris-HCl buffered (pH6.4) and were designed to be used for denaturing gel electrophoresis.

20µg protein was loaded per lane, unless otherwise stated. Protein samples were denatured by heating for 10 minutes at 70°C with NuPage® 4x lithium dodecyl sulphate (LDS) sample buffer and NuPage® 10x sample reducing agent. Electrophoresis was carried out in 1x NuPage® 3-(N-morpholino)propanesulfonic acid (MOPS) SDS running buffer (50mM MOPS, 50mM Tris base, 0.1% SDS, 1mM EDTA) containing 1ml NuPage® antioxidant in order to maintain reducing conditions. Electrophoresis was carried out at 150V for 2 hours, until the tracking dye ran off the bottom of the gel. Precision Plus Protein™ standard from Bio-Rad was used as the molecular weight marker.

2.2.2.8 Western blotting

Resolved proteins in NuPage® gels were blotted onto an Immobilon-P polyvinylidene difluoride (PVDF) membrane. Prior to transfer in the XCell II Blot Module, the PVDF membrane (8.5 x 7.5cm) was wet in methanol and rinsed with dH$_2$O. The PVDF membrane, two sheets of chromatography paper (8.5 x 7.5cm) and 6 blotting sponges were then soaked in 1x NuPage® Transfer buffer (25mM Bicine, 25mM Bis-Tris, 1mM EDTA), with 0.01% SDS added in order to aid the blotting of larger proteins by maintaining reducing conditions. Methanol was not added as this strips SDS from proteins and aids the transfer of smaller proteins only. Transfer of higher molecular weight proteins was found to be increased with 0% methanol during optimisation of this protocol (Section 2.2.2.9). The blot was assembled as illustrated in Figure 2.4. The

inner chamber was flooded with transfer buffer, and the outer chamber was filled with dH$_2$O.
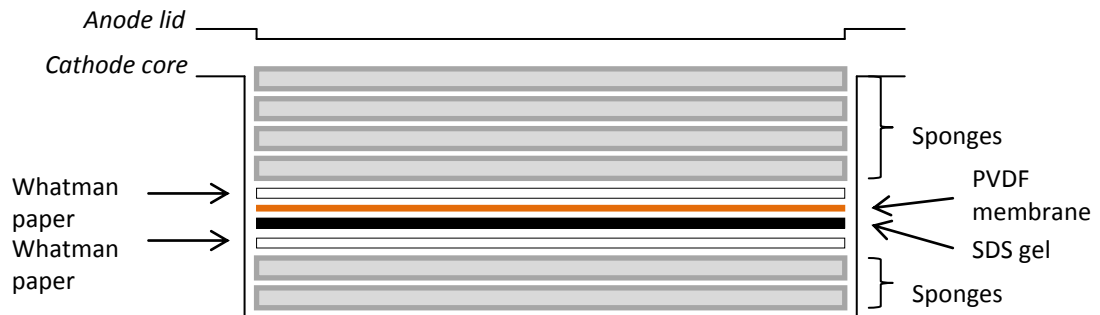
Figure 2.4 Blot assembly. The SDS gel and PVDF membrane are sandwiched between two sheets of chromatography paper and several sponges, all soaked in NuPage® Transfer buffer with 0.01% SDS.

For the detection of high molecular weight proteins, gels were blotted at 15V overnight, and kept at 4°C to prevent overheating; otherwise, blotting was carried out at 30V for 1 hour at room temperature. Blots were then dissembled, and the membrane was blocked in either 5% Marvel dried milk powder in PBS-T or 5% BSA in PBS-T, depending on supplier recommendations for each antibody, for 30 minutes at room temperature on a shaker, or overnight at 4°C. Primary antibodies were diluted in the appropriate blocking buffer (Table 2.1), and incubated either for 1 hour at room temperature, or overnight at 4°C on a roller. Unbound antibody was then removed by 3 x 5 minute washes with PBS-T and 1 x 5 minute wash with PBS. The secondary antibody was then diluted in the same buffer used for the primary antibody, and was incubated with the membrane for 1 hour at room temperature on a roller before being washed as detailed above. Protein bands were imaged on the Licor® Odyssey® quantitative fluorescent imaging system.

In order to strip away previously bound antibodies from blots, membranes were incubated for 15 minutes at room temperature in Restore™ Plus Western Blot Stripping Buffer, followed by another 15 minutes incubation with Restore™ Western

Blot Stripping Buffer, and a 5 minute wash in PBS, all with gentle shaking. Membranes were then re-blocked and probed with a new antibody as previously described.

2.2.2.9 Optimisation of blotting technique

As HTT and mHTT are high molecular weight proteins, optimisation of the blotting protocol was carried out to improve protein transfer onto the PVDF membrane. This included varying methanol and SDS concentrations in the transfer buffer, as well as varying the voltage and length of time for which the blotting occurred. To test protein transfer efficiency, following blotting the PVDF membrane was washed twice for 5 minutes with dH_2O at room temperature. To visualise the protein that had been blotted to the PVDF, the membrane was then incubated with Ponceau S solution for 1 hour at room temperature on a shaker. After this time, the solution was discarded and the membrane was given 3 x 5 minute washes in dH_2O.

To visualise the protein that remained on the gel following blotting, the gel was initially given 3 x 5 minute washes with dH_2O, followed by incubation for 1 hour with SimplyBlue™ SafeStain at room temperature on a shaker, then a 1 hour wash in dH_2O for an hour on the shaker. The gel was then imaged on the Licor® Odyssey® quantitative fluorescent imaging system.

2.2.2.10 ELISA protocol

Following the protein extraction protocol outlined in Section 2.2.2.1, lysates were diluted in the diluent buffer provided with the ELISA kit (Section 2.1.11) to the required protein concentration. The ELISA protocol was then carried out according to manufacturer's instructions, and absorbance was read on a Biotek® µQuant™ microplate spectrophotometer at 450nm.

2.2.2.11 Immunofluorescence

To permeabilise cells, fixed coverslips were first incubated with 1% Triton x-100 in 1xPBS for 30 minutes on a shaker at room temperature, and were then washed 3 times with PBS to ensure the detergent was fully removed. Cells were then blocked with 1% (w/v) BSA in PBS for 30 minutes on a shaker at room temperature. After this time, the

BSA solution was removed and the primary antibody at the relevant dilution (Table 2.1) was applied. Coverslips were then either incubated for 1 hour at 37°C, or overnight at 4°C with the primary antibody, depending on supplier recommendations.

The primary antibody was then removed, and coverslips were washed with PBS for 3 x 10 minutes, followed by a 30 minute wash on a shaker at room temperature. Cells were then incubated with the relevant secondary antibody (Table 2.1) for 1 hour at 37°C, while covered in tin foil to block out light. The wash process was then repeated. Coverslips were then mounted onto glass microscope slides using a drop of ProLong® Gold antifade reagent with DAPI. Coverslips were stored in the dark at 4°C for 24 hours to allow the mountant to dry and the DAPI to develop, before sealing with clear nail varnish and imaging.

To control for non-specific binding of the secondary antibodies, secondary-only controls were carried out on both immortalised $StHdh^{Q111}$ embryonic striatal cell lines, and primary Hdh^{Q111} and Hdh^{Q150} embryonic cell cultures (Figure 2.5).
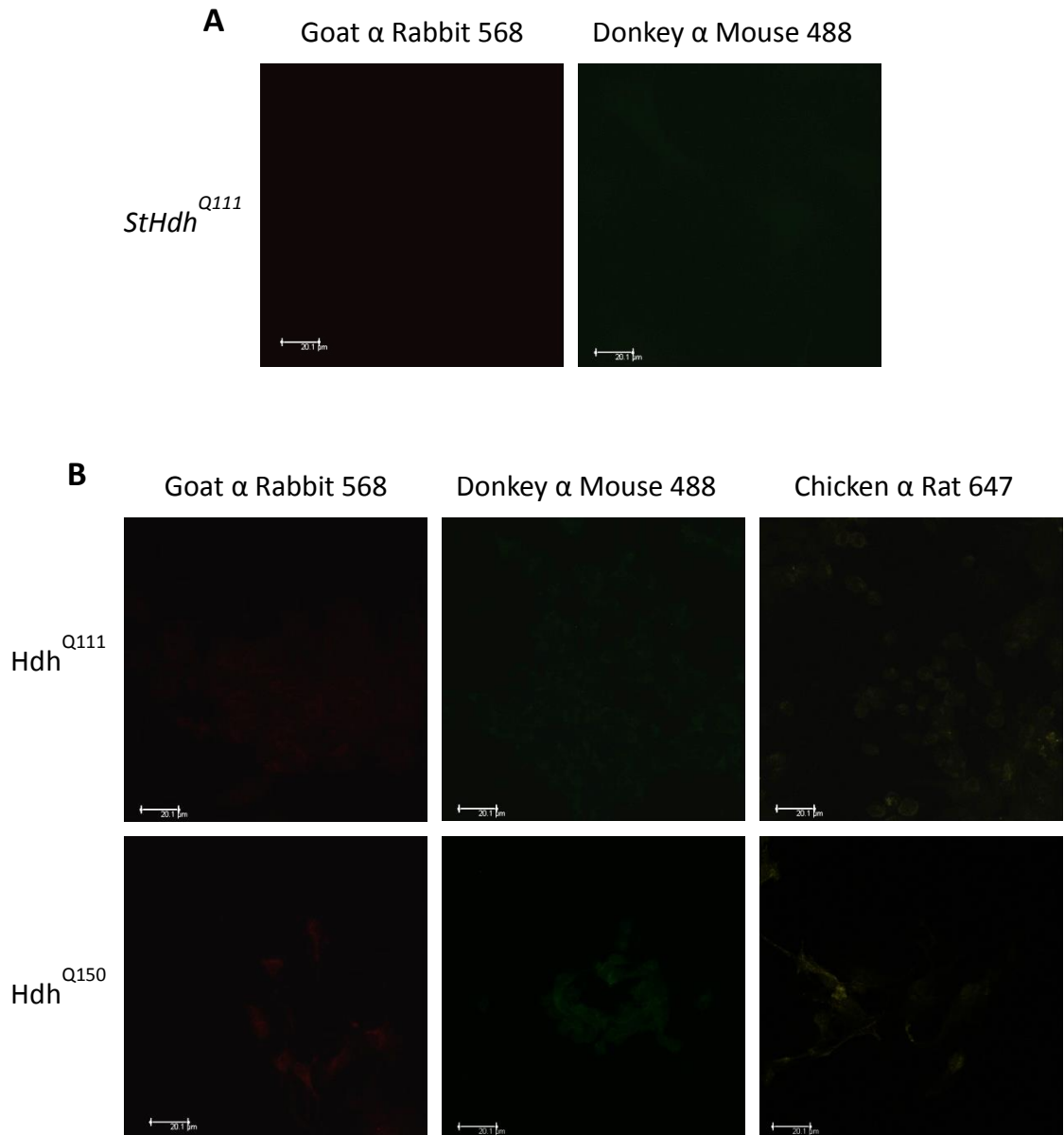
Figure 2.5 AlexaFluor secondary antibody-only immunofluorescence controls for **A**. *StHdh*^{Q111} cell lines and **B.** primary embryonic Hdh^{Q111} and Hdh^{Q150} cell cultures. Cells were treated in the same manner as previously described (Section 2.2.2.11) with the exclusion of the primary antibody incubation stage. Coverslips were then imaged in the same manner as previously described (Section 2.2.1.9).

2.2.3 Nucleic acid manipulation techniques

2.2.3.1 Phenol/chloroform RNA extraction

For total RNA extraction, both immortalised and primary cells were grown in 6 well plates. Media was removed, and the cells were washed twice with PBS. All surfaces were treated with RNase*ZAP®* to destroy RNases. The cells were then lysed and dissociated from the wells by the addition of TRIzol® (a phenol and guanidine isothiocyanate solution), and were then transferred to a centrifuge tube, and left to incubate at room temperature for 5 minutes. Chloroform was added to each sample, and was vortexed for 15 seconds to mix the solutions.

The samples were then spun at 12,000xg for 15 minutes at 4°C in a Beckman Coulter Avanti J-E centrifuge. The resulting upper aqueous phase was then transferred to a fresh 2ml eppendorf. To precipitate the RNA, isopropanol was added and gently shaken into the sample by hand, then left to precipitate at room temperature for 10 minutes. To pellet the RNA, samples were then spun at 12,000xg for 10 minutes at 4°C in a Biofuge. The supernatant was then gently removed and the pellet was washed with 75% ethanol, made with nuclease free water. To re-pellet the RNA, it was spun again at 9,500xg for 10 minutes at 4°C. This wash step was repeated again, and all of the remaining supernatant was removed and discarded. To aid with drying the pellets, tubes were kept in a 45°C oven for 15 minutes.

Following this, the remaining pellets were resuspended in 100µl diethylpyrocarbonate DEPC-treated water by vortexing, heating at 65°C on a block for 5 minutes, and then vortexing again.

2.2.3.2 Purification of RNA samples

Resuspended RNA samples were purified by silica membrane spin columns, by using the RNeasy MinElute Cleanup kit (Section 2.1.13) according to manufacturer's instructions.

To degrade any DNA contaminants in the RNA samples, they were treated with TURBO™DNase according to manufacturer's instructions. The resulting purified RNA was then stored at -80°C.

A

	C-fos	Egr-1	Ngfib	Arc
R2	0.99	0.98	0.99	0.99
Slope	-3.37	-3.06	-3.38	-3.36
Efficiency (%)	98.18	112.38	97.81	98.35

B

	18s	Atf3	Cdc42ep3	Egr1	Etv5	Fgf2	Fosl1	Gadd45g	Id3	Junb	Myc	Ngf	Rasa1	Smad7	Sox9
R2	0.99	0.99	1	0.99	0.98	0.99	0.99	0.97	0.99	0.98	0.99	0.99	1	0.98	1
Slope	-3	-3.62	-3.11	-3.46	-2.93	-3.22	-3.01	-3.11	-3.93	-3.52	-3.65	-3.66	-3.16	-3.05	-3.35
Efficiency (%)	115.52	88.78	109.52	94.69	119.31	104.23	114.93	109.82	79.66	92.36	87.94	87.56	107.36	112.5	98.88

C

	Csf1	Ctgf	Ereg	Rgs16	Ppargc1α	Nr4a2	Rnd3	Id2	Ccng2	Mybl1	Prl2c2
R2	1	1	0.96	0.96	0.98	0.99	0.95	1	0.99	0.97	0.93
Slope	-3.35	-3.31	-2.81	-3.15	-3.21	-3.47	-2.99	-3.4	-2.95	-2.68	-2.45
Efficiency (%)	98.8	100.6	126.7	107.9	104.8	94.1	115.9	96.9	118.1	136.3	156.4

D

	Smad1	Smad3	Smad6	Smad9	Tgfb2	Tgfbr2	Tgfb3	Tgfbr3	Tgfbi	Smurf2
R2	0.99	1	1	0.95	1	1	1	0.94	0.99	0.99
Slope	-3.89	-3.65	-3.32	-2.86	-3.58	-3.45	-3.41	-3.49	-4.66	-3.38
Efficiency (%)	80.8	87.9	100.3	123.8	90.4	94.8	96.4	93.4	63.8	97.6

Table 2.4 Tables displaying the qRTPCR efficiencies for **A**. Sybr® Green primers, **B-C**. TaqMan® assays supporting the **B**. EGF and **C**. NGF microarrays, and **D**. *Smad* genes. *Usp43* was not highly expressed enough in *StHdh*^{Q111} cells to determine an efficiency value.

2.2.3.3 Quantitation of nucleic acids

Both DNA and RNA were quantified on a Nanodrop spectrophotometer, and the 260/280 and 260/230 ratios were utilised as a rough determination of nucleic acid quality.

2.2.3.4 Quantitative reverse-transcription polymerase chain reaction

Both SYBR® Green and TaqMan® qRTPCR technologies were used in this project in a two-step protocol. For both methods, 1µg RNA per sample underwent reverse transcription (RT) using the High Capacity RNA-to-cDNA™ kit from Life Technologies, according to manufacturer's instructions. This concentration of RNA was determined by carrying out an RT reaction efficiency curve. This was done by performing the reaction with 250ng, 500ng and 1µg RNA, followed by qPCR using an example primer pair. If the RT reaction is efficient, the threshold cycle (C_t) values will decrease with increased RNA load.

Similarly, amplification efficiencies were determined for every primer pair for SYBR® Green and TaqMan® assays by loading a serial dilution of cDNA into the qRTPCR reaction. If the reaction is efficient, there will be a linear relationship between the concentration of cDNA put into the reaction, and the resulting C_t value. The R^2 and slope of this relationship were then identified from the Sequence Detection Systems (SDS) Version 2.3 programme (copyright 2005, Applied Biosystems), and the PCR efficiency can be determined from these (see formulae below). Probe efficiencies relevant to this project can be found in Table 2.4.

Efficiency:

$$((10^{(-1/slope)}) -1) \times 100$$

For SYBR® Green qRTPCR, the resulting cDNA from the RT reaction was diluted 1:5 with nuclease free water before use. A mastermix was created for each primer pair that was to be used (Table 2.2), which per 20µl sample, consisted of:

10µl   SYBR® Green
0.6µl   each oligonucleotide primer at 100µM concentration

4.8µl   nuclease free water

4µl   cDNA template

The mastermix and cDNA samples were loaded into Fast Optical 96 well plates, and sealed with optical adhesive film. The plate was then briefly centrifuged at 10,000xg before being loaded into the Applied Biosystems 7900HT Real Time PCR machine. The thermal cycler protocol was as follows:

Stage 1

95°C   10 minutes   (Initialisation)

Stage 2 (x40 cycles)

95°C   15 seconds   (Denaturation)

55°C   1 minute   (Annealing/extension)

Stage 3 (Dissociation curve)

95°C   15 seconds   (following gradual ramp)

A thermal ramp was included at the end of the cycle in order to create a dissociation curve to determine the specificity of cDNA amplification to each particular primer pair. In order to ensure there was no contamination of samples at each stage of the 2-step process, each plate also included an RT- control (where no RT reaction was carried out), a water RT control (where the RT reaction was performed, but with no RNA template), and a No Template control (where cDNA was replaced with dH_2O).

For Taqman® qRTPCR, 200ng of cDNA template was loaded into each reaction, and made up to a total volume of 9µl with nuclease free water. This was added to a mastermix of 10µl Taqman® Fast Advanced master mix and 1µl of the relevant Taqman® gene expression assay per well, which was then loaded into Fast Optical 96 well plates, then sealed with optical adhesive film. The plate was then briefly centrifuged at 10,000xg before being loaded into the Applied Biosystems 7900HT Real Time PCR machine. The thermal cycler protocol was as follows:

Stage 1

50°C   2 minutes   (UNG activation)

95°C   20 seconds   (Polymerase activation)

Stage 2 (x40 cycles)

95°C   1 second   (Denaturation)

60°C   20 seconds   (Annealing/extension)

All qRTPCR protocols were controlled and analysed by Sequence Detection Systems (SDS) Version 2.3 programme from Applied Biosystems. Taqman® data were also analysed using SDS RQ Manager Version 1.2, also by Applied Biosystems.

2.2.3.5 DNA extraction from primary tissue

For the purpose of genotyping, the remaining mouse embryo brain was digested overnight in a shaking incubator at 40°C in DNA extraction buffer (Section 2.1.3), plus 10μl Proteinase K per sample. The next day, 6M Sodium Chloride was added, the samples vortexed and centrifuged for 10 minutes at 13,000xg. The resulting supernatant was retained and the pellet discarded. To precipitate the DNA, Isopropanol was added to the supernatant, and put in a -80°C freezer for 15 minutes. Samples were centrifuged again at 13,000xg for 10 minutes to pellet the DNA, and the supernatant discarded.

The pellet was then washed in 70% ethanol, and centrifuged again to remove all the remaining ethanol. The pellet was then placed on a heating block at 80°C for 2 minutes, and then resuspended in nuclease free water at room temperature for an hour. The DNA was then quantified as described in Section 2.2.3.3.

2.2.3.6 Genotyping polymerase chain reaction

Reactions were performed in a 25μl final volume, containing 5M Betaine, 50mM Magnesium Chloride ($MgCl_2$), 10mM deoxyribonucleotide triphosphate (dNTP) mix, ammonium (NH_4) reaction buffer, 100μM each forward and reverse primers (Table 2.2), and BioTaq™ DNA polymerase, with 50ng DNA per reaction. PCR reactions were all performed with the following protocol:

Stage 1

94°C   5 minutes   (Initialisation)

Stage 2 (x 34)

94°C   30 seconds   (Denaturation)

50°C   30 seconds   (Annealing)

72°C   3 minutes   (Extension)

Stage 3

72°C   5 minutes   (Final extension)

Completed reactions were then stored at 4°C until use.

2.2.3.7 Oligonucleotide primer design

Primers used for SYBR® Green qRTPCR were designed over gene exon boundaries using the program Primer 3 (V.0.4.0), which is available on the internet (http://frodo.wi.mit.edu/). All primers were synthesised to a scale of 25nM, and were provided in a desalted lyophilised form, and were then resuspended to a 100µM stock solution using nuclease free water, and then stored at -20°C. TaqMan® gene expression assays were pre-designed by Life Technologies.

2.2.3.8 Agarose gel electrophoresis of DNA

PCR products were run on 1% agarose gels made with TBE; agarose was dissolved in TBE buffer by heating in a microwave, and was then cooled before adding 3µl ethidium bromide. The liquid was poured into a mould and allowed to set for at least 30 minutes.

Following PCR amplification, 6µl of DNA orange loading dye was added to each PCR product and gently mixed by pipetting. HyperLadder™50bp was loaded into the first and last lanes of each gel, and 15µl of PCR product containing loading dye was loaded into each lane. The gels were electrophoresed at 100V for 1 hour, before being visualised using a 3UV™ Transilluminator and imaged on the UVP AutoChemi™ BioImaging system, where it was then analysed in Labworks Image Acquisition and Analysis Software version 4.5.0 (copyright 1996-2003, Media Cybernetics Inc).

2.2.3.9 Microarray

Microarray experiments were kindly carried out by Megan Musson in Cardiff University's Central Biotechnology Services (CBS) department.

2.2.3.10 siRNA transfection for antibody validation

ON-TARGET*plus* SMARTpool siRNA oligonucleotides were purchased at 5nmol, and were resuspended into a stock solution of 20µM by mixing with 250µl 1 x siRNA buffer (diluted from 5x stock solution with nuclease free water) on a shaker for 30 minutes at room temperature. siRNA experiments were carried out with a final siRNA concentration of 25nM, with 1µl DharmaFECT transfection reagent no.1 per well (using a 6 well plate). Details of the siRNA oligonucleotides and the relevant TaqMan® primer efficiencies can be found in Table 2.5.

To prepare the siRNA for transfection, 20µM stock siRNA was first diluted to a 5µM working solution using 1x siRNA buffer. 10µl/well was then gently mixed with 190µl/well serum free media, and left to incubate at room temperature for 5 minutes. 1µl/well DharmaFECT transfection reagent was mixed with 199µl serum free media in a separate tube and also incubated for 5 minutes at room temperature. Following the incubation time, 200µl/well of the DharmaFECT media was transferred to the siRNA media, mixed gently and incubated for 20 minutes at room temperature. 1600µl/well of antibiotic free media was then added to the transfection media and mixed; this was now the complete transfection reagent. Old media was removed from the cells and replaced with 2ml of the appropriate transfection reagent.

StHdh$^{Q7/7}$ cells were seeded at 0.25x10^5/well, and *StHdh*$^{Q7/111}$ and *StHdh*$^{Q111/111}$ cells were seeded at 0.5x10^5/well in 6 well plates in 5% FBS antibiotic free media. For RNA analysis, siRNA was applied 24 hours after seeding, and RNA was extracted following 48 hours of incubation. For protein analysis, siRNA was applied 24 hours after seeding, applied again 48 hours later, and either protein lysates were extracted or cells were fixed after a further 48 hours.

A

Huntingtin	
Target sequence	**Exon**
GAACGUACCCAGUUUGAAA	60
AUACAGAUGUGUGGAGUAA	62-63
GGCCUUACCUGGUGAAUCU	5-6
GAAUGGUGCUCCUCGAAGU	5

B

Gapdh	
Target sequence	**Exon**
GUGUGAACCACGAGAAAUA	1
GGAGAAACCUGCCAAGUAU	1
UCAAGAAGGUGGUGAAGCA	1
UGGUGAAGCAGGCAUCUGA	1

C

	Huntingtin	Gapdh
R^2	0.96	1
Slope	-2.91	-3.66
Efficiency (%)	120.6	87.7

Table 2.5 ON-TARGET*plus* SMARTpool siRNA target sequences for mouse **A.** *Htt* and **B.** *Gapdh*. Each siRNA that was utilised consisted of a pool of four separate oligonucleotides for increased gene coverage. **C**. TaqMan® probe efficiencies for the primers used to assess siRNA knockdown.

2.2.4 Growth factor stimulation and pathway inhibition

2.2.4.1 Growth factors

EGF, NGF and BDNF were reconstituted and diluted to a stock solution of 100μg/ml in PBS and stored at -20°C. TGFβ1 was also reconstituted to a stock solution of 100μg/ml, but in 20mM citrate, pH 3.0, and stored at -20°C. 24 hours prior to growth factor treatment, the present media was removed from the cell cultures and replaced with the same volume of serum free media. The following day, the appropriate growth factor was diluted to 100ng/ml in fresh serum free media; the previous serum free media was removed from the cells and replaced with the growth factor media for the appropriate length of time before subsequent processing.

2.2.4.2 Kinase inhibition

AKT inhibitor VIII was reconstituted in DMSO to a stock solution of 0.1mM, and MEK 1/2 inhibitor was initially reconstituted in DMSO, before being diluted to a 0.05mM stock solution in serum free media. Aliquots of both inhibitors were stored at -20°C. Cells were serum starved for 24 hours (as described in Section 2.2.4.1) prior to treatment with either kinase inhibitor. Each inhibitor was diluted to the appropriate concentration in serum free media, and was incubated with the cells for 2 hours prior to EGF stimulation. Serum free media containing the equivalent volume of just DMSO was used as a control. EGF was diluted to 100ng/ml in fresh serum free media that also contained the appropriate concentration of each kinase inhibitor or DMSO before incubation with the cells.

Chapter 3:   The localisation and phosphorylation of huntingtin in immortalised murine knock-in embryonic striatal cell lines

3.1 Introduction

Early immunofluorescence studies detected the localisation of the HTT protein as primarily cytoplasmic (DiFiglia et al. 1995; Gutekunst et al. 1995), and nuclear localisation was thought to be indicative of a pathogenic process of mHTT (Reddy et al. 1999). Specifically, HTT has been found to localise with the endoplasmic reticulum and presynaptic vesicles (Atwal et al. 2007), as well as the Golgi body, dendritic plasma membrane and cytoskeleton (Ko et al. 2001; Rockabrand et al. 2007). However, it is now accepted that both HTT and mHTT localise to nuclei in cell and mouse models of HD, as well as in human HD brain (De Rooij et al. 1996; Hilditch-Maguire et al. 2000; Trettel et al. 2000; Wheeler 2000; Ko et al. 2001; Tao & Tartakoff 2001; Kegel et al. 2002; Truant 2003; Benn et al. 2008).

HTT is thought to perform several necessary roles within the nucleus (Hilditch-Maguire et al. 2000; Trettel et al. 2000; Kegel et al. 2002; Benn et al. 2008), and as such, shuttling dynamically between the cytoplasm and the nucleus may be a means by which its function is regulated (Truant 2003; Truant et al. 2007), although the mechanism by which this occurs is not fully understood. Full length HTT has been found to be present in cell nuclei (De Rooij et al. 1996; Dorsman et al. 1999; Trettel et al. 2000; Kegel et al. 2002), although to a lesser extent than in the cytoplasm; however there is an enrichment of N-terminal fragments of HTT in the nucleus compared to the cytoplasm (Hilditch-Maguire et al. 2000; Tao & Tartakoff 2001; Kegel et al. 2002). These fragments may be created by proteolytic cleavage of HTT by caspases (Bauer & Nukina 2009); in the case of mHTT, N-terminal fragments containing the expanded polyglutamine repeat are able to translocate to the nucleus (Hackam et al. 1998), where their presence may be detrimental due to aggregation and aberrant function. However, in YAC128 mice resistant to HTT cleavage by caspase-6, there was delayed nuclear localisation of HTT, as there were fewer small fragments available for passive diffusion across the nuclear pore (Graham, Slow, et al. 2006).

The majority of HTT and mHTT N-terminal fragments have had the putative C-terminal NES cleaved away (Wellington et al. 1998; Kim et al. 2003; Xia 2003; Landles et al. 2010), which may explain why a larger proportion of truncated HTT and mHTT remain in cell nuclei. Mutations of the first 17 amino acids, including the presence of an expanded polyglutamine repeat, may impair the cytoplasmic retention signal activity of this region by altering its structure, and impair the CRM1 dependent NES, thus leading to increased nuclear localisation of HTT (Steffan et al. 2004; Cornett et al. 2005; Atwal et al. 2007; Rockabrand et al. 2007; Gu et al. 2009; Maiuri et al. 2013).

There is some uncertainty over how full length HTT and mHTT are able to localise to the nucleus, given how large the protein is. In addition to the potential NLS sites identified on HTT (Bessert et al. 1995; Xia 2003; Truant et al. 2007; Desmond et al. 2013), the HTT protein may also require an exogenous NLS in order to traverse the nuclear pore, and this mechanism may be specific to cortical and striatal neurons (Truant 2003; Truant et al. 2007). Indeed, there are several HTT-interacting proteins, including transcription factors that may act as potential chaperones (Li et al. 1995; Faber et al. 1998). The presence and activation of these chaperone proteins have also been identified as a moderating factor of nuclear inclusion formation and toxicity of mHTT in *Drosophila*, yeast and mammalian models of HD (Ferrigno & Silver 2000).

Post-translational modification of HTT by phosphorylation has been identified as a mechanism by which the subcellular localisation of HTT may be regulated. For example, phosphorylation of S421 can inhibit proteolytic cleavage and reduce the amount of HTT transported to the nucleus (Bauer & Nukina 2009; Warby et al. 2009); as such, phosphorylation of S421 has a protective effect in models of HD by reducing the levels of nuclear toxic fragments available. Phosphorylation of both S13 and S16 have also been found to influence HTT cellular localisation (Gu et al. 2009; Thompson et al. 2009; Atwal et al. 2011; Havel et al. 2011). Phosphomimetic mutations of both S13 and S16 to aspartate have been found to increase the nuclear localisation of full length and fragmented HTT and mHTT in immortalised murine embryonic striatal cells (Thompson et al. 2009) as well as in a bacterial artificial chromosome mouse model (BACHD) of HD containing 97 glutamine repeats (Gu et al. 2009). In both models, this modification was found to be protective by enhancing clearance of the mutant protein

(Thompson et al. 2009), and by preventing aggregate formation and neurodegeneration (Gu et al. 2009). In the BACHD model, it was suggested that phosphorylation of S16 was more important for the nuclear localisation of HTT, as a phosphomimetic mutation of S16 had effects similar to that of a double mutant; whereas mutation of S13 alone did not elicit the same protection (Gu et al. 2009). Atwal et al. 2011 also found that phosphomimetic mutation of S16 alone increased the nuclear localisation of HTT in immortalised striatal neurons, but mutation of S13 did not.

Havel et al. 2011 proposed that phosphorylation of S16 is key for generating N-terminal fragments of HTT that localise to the nucleus, but rather than this being a protective effect, they found that it enhanced the formation of nuclear aggregates in primary rat striatal neurons transfected with N-terminal mHTT containing 143 glutamine repeats. It was also found that phosphorylated mHTT in the nucleus was less able to interact with the nuclear pore complex protein TPR, which is implicated in the nuclear export of HTT, as well as other proteins (Bangs et al. 1998; Frosst et al. 2002; Cornett et al. 2005). In addition, phosphomimetic mutations of HTT S13 and S16 reduced the interaction of HTT with the nuclear export factor CRM1, thus retaining it in the nucleus (Maiuri et al. 2013). Smaller fragments of phosphorylated HTT and mHTT may therefore translocate to the nucleus via passive diffusion, but phosphorylated forms of mHTT are less able to leave the nucleus and therefore gradually accumulate over time and may form aggregates.

The phosphorylation of S13 and S16 may influence the shuttling of HTT and mHTT between cellular compartments, but whether this is a protective effect or not is still unknown. However, if increased phosphorylation and nuclear localisation of mHTT is initially protective, gradual nuclear accumulation is likely to be damaging. Striatal cells from knock-in Hdh^{Q140} mice showed increased staining for phosphorylated S16 compared to wild type (WT) cells at 6 months of age, and this increased further by 24 months of age (Havel et al. 2011). However, immortalised murine embryonic striatal neurons carrying an expanded polyglutamine repeat have been found to be hypophosphorylated on these two serines (Atwal et al. 2011). mHTT has been identified as being phosphorylated less efficiently than wild type HTT (Thompson et al.

2009), so these results may reflect the transient nature of phosphorylation in early, non-symptomatic stages of disease prior to gradual accumulation of this modification on mHTT due to a reduced ability to translocate between cellular compartments.

HTT and its phosphorylation have been implicated in various neurotrophin associated signalling pathways; for example, the phosphorylation of HTT has been related to the activity of various cellular kinases such as IKK, AKT and casein kinase 2 (CK2), which can influence the phosphorylation of S13 and S16, and subsequently the localisation of HTT (Thompson et al. 2009; Atwal et al. 2011; Khoshnan & Patterson 2011; Desmond et al. 2013). Here, we aim to characterise the localisation and phosphorylation of HTT and mHTT epitopes in the $StHdh^{Q111}$ immortalised murine embryonic striatal cell model of HD in response to stimulation with a panel of different growth factors, in order to determine whether HTT localisation may be regulated by kinase signalling pathway activation, and if this is disrupted in the context of mHTT.

3.2 Identifying the appropriate growth factor receptors

The presence of the appropriate growth factor receptors in $StHdh^{Q7/7}$, $StHdh^{Q7/111}$ and $StHdh^{Q111/111}$ cell lines was checked to ensure that these cells were capable of responding to stimulation with either BDNF, NGF or EGF.

3.2.1 The TRKB receptor

The receptor for BDNF, TRKB, was found to be present in $StHdh^{Q7/7}$, $StHdh^{Q7/111}$ and $StHdh^{Q111/111}$ cells (Figure 3.1). It appeared to be localised in the same manner between genotypes, and although quantification of its detection by western blot suggested slightly lower levels of TRKB in $StHdh^{Q7/111}$ and $StHdh^{Q111/111}$ cells, this was not statistically significant ($p > 0.05$).
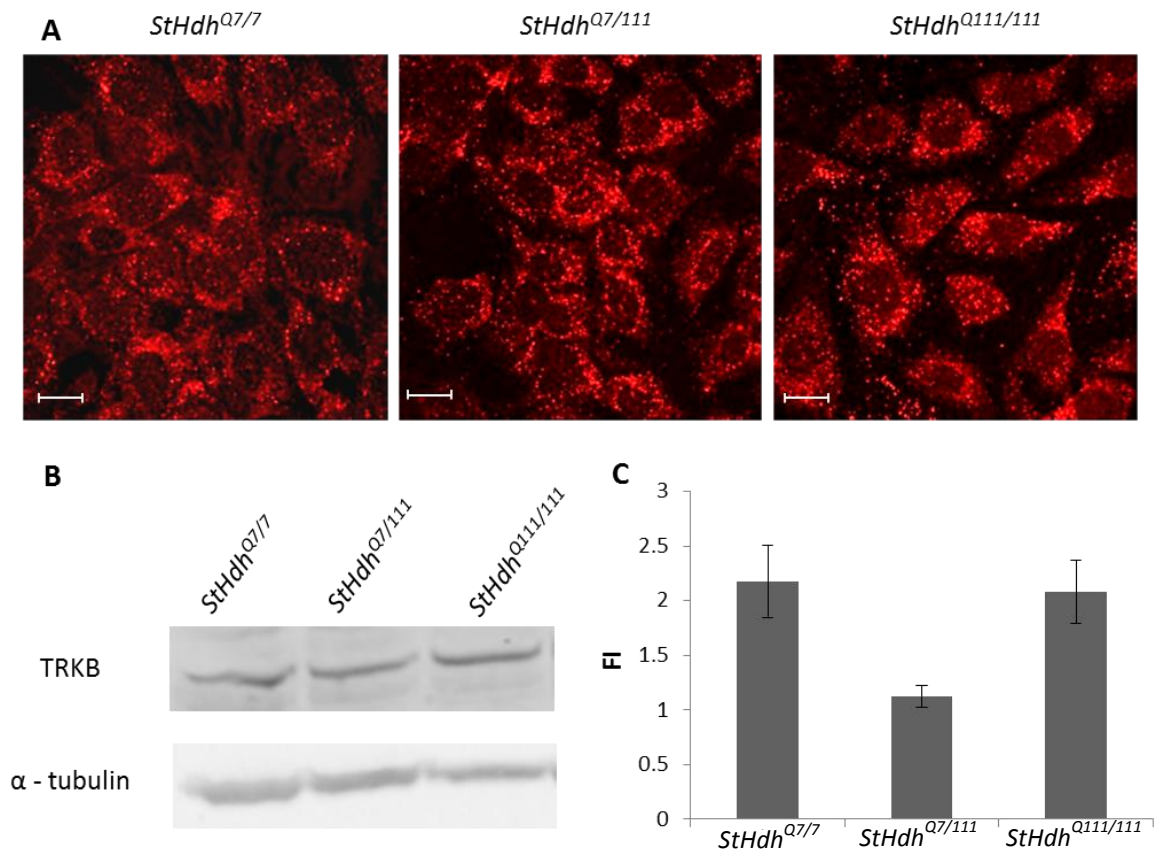
Figure 3.1 A. Immunofluorescence images of $StHdh^{Q7/7}$, $StHdh^{Q7/111}$ and $StHdh^{Q111/111}$ cells, stained using an Anti-TRKB antibody. Scale bar = 20µm. **B.** Western blot indicating similar expression of the TRKB protein in all three cell lines using the same antibody as in *A*. (TRKB 92kDa, α-tubulin 50kDa). **C**. Licor Odyssey quantification of fluorescence intensity (FI) of *B*; TRKB normalised to α-tubulin loading control. There are no significant differences in the levels of the TRKB receptor between $StHdh^{Q7/7}$, $StHdh^{Q7/111}$ and $StHdh^{Q111/111}$ cells (Error bars = SEM, n=3).

3.2.2 The TRKA and P75 NTR receptors

NGF stimulates both TRKA and the low affinity P75 neurotrophin receptor (P75 NTR). Both NGF receptors were found to be present in all three genotypes (Figure 3.2); there were no apparent differences in localisation by immunofluorescence for P75 NTR, although for the TRKA receptor, the localisation is slightly more diffuse in $StHdh^{Q7/111}$ and $StHdh^{Q111/111}$ cells compared to $StHdh^{Q7/7}$ cells, and isn't detected in such large clusters. However, there is no significant difference in the detection of each receptor by western blot between genotypes.

85
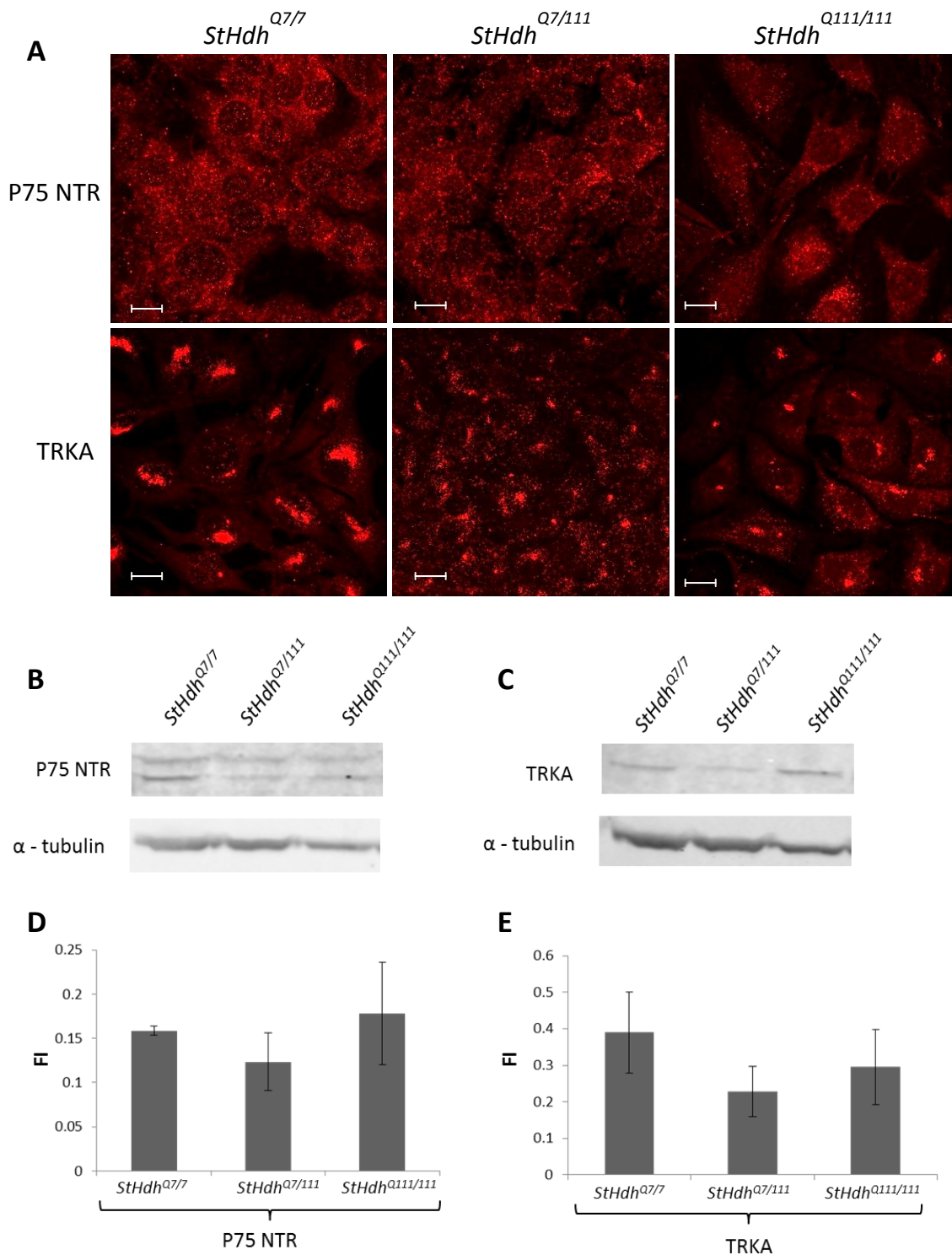
Figure 3.2 A. Immunofluorescence images of *StHdh*$^{Q7/7}$, *StHdh*$^{Q7/111}$ and *StHdh*$^{Q111/111}$ cells, stained using antibodies against P75 NTR and TRKA. Scale bar = 20μm. **B-C.** Western blots indicating similar expression of the P75 NTR (60-75kDa) and TRKA (140kDa) proteins in all three cell lines using the same antibody as in *A*, using α-tubulin (50kDa) as a loading control. **D-E**. Licor Odyssey quantification of *B* and *C*, normalising receptor fluorescence intensity (FI) levels to α-tubulin loading control; there are no significant differences in the levels of the P75 NTR or TRKA receptors between *StHdh*$^{Q7/7}$, *StHdh*$^{Q7/111}$ and *StHdh*$^{Q111/111}$ cells (Error bars = SEM, n=3).

3.2.3 The EGF receptor

The EGFR was found to be present in *StHdh*$^{Q7/7}$, *StHdh*$^{Q7/111}$ and *StHdh*$^{Q111/111}$ cells, and there were no differences in its subcellular localisation between genotypes, as identified by immunofluorescence and western blot (Figure 3.3), which has been observed previously in the same cell line (Ginés et al. 2010).
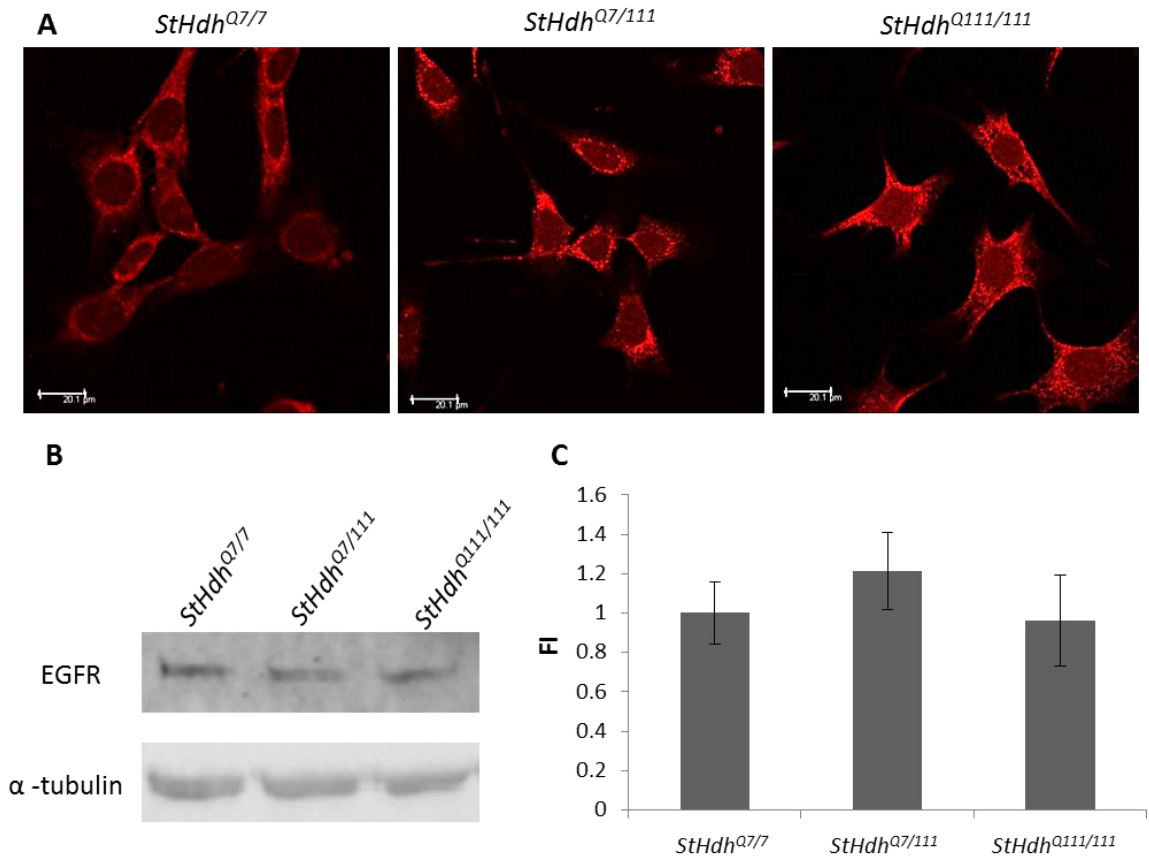
Figure 3.3 A. Immunofluorescence images of *StHdh*$^{Q7/7}$, *StHdh*$^{Q7/111}$ and *StHdh*$^{Q111/111}$ cells, stained using an Anti-EGFR antibody. Scale bar = 20µm **B.** Western blot indicating similar expression of the EGFR protein (175kDa) in all three cell lines using the same antibody as in *A*, and α-tubulin (50kDa) as a loading control. **C.** Licor Odyssey quantification of fluorescence intensity (FI) of *B* normalised to loading control; there are no significant differences in the levels of EGFR between *StHdh*$^{Q7/7}$, *StHdh*$^{Q7/111}$ and *StHdh*$^{Q111/111}$ cells (Error bars = SEM, n=3).

3.3 Localisation of HTT epitopes in response to growth factor stimulation

StHdh$^{Q7/7}$, *StHdh*$^{Q7/111}$ and *StHdh*$^{Q111/111}$ cells were stimulated with one of three growth factors at 100ng/ml for 0, 5, 15 and 30 minutes following overnight serum starvation, before being fixed and probed with a panel of antibodies against different HTT epitopes. A summary of these antibodies can be found in Table 2.1 and Figure 2.1.

3.3.2 Characterisation of HTT N-terminal antibodies

The specificity of several antibodies against N-terminal HTT utilised in these experiments was validated by knocking down the expression of *Htt* in *StHdh*$^{Q7/7}$, *StHdh*$^{Q7/111}$ and *StHdh*$^{Q111/111}$ cells.

3.3.2.1 Gene expression

The expression of *Htt* was analysed by qRTPCR in response to incubation with *Htt* siRNA, in comparison to incubation with *Gapdh* siRNA, non-coding siRNA and transfection reagent only controls. Further details of the protocol and the siRNA oligonucleotides utilised can be found in Section 2.2.3.11 and Table 2.5. There was a significant reduction in *Htt* expression in *StHdh*$^{Q7/7}$ cells (Figure 3.4) following 48 hours of incubation with 25nM *Htt* siRNA as compared to all three control conditions (all $p<0.025$).

Gapdh control siRNA was able to significantly reduce the expression of *Gapdh* in these cells compared to all other conditions (all $p<0.001$) without significantly reducing *Htt* expression. The relative quantification (RQ) score for *Htt* expression in *StHdh*$^{Q7/111}$ and *StHdh*$^{Q111/111}$ cells was lower than the control conditions, although due to high variability, possibly due to the mutant expansion, and low statistical power, this difference did not reach significance for individual control conditions. However, there is a trend that *Htt* is being knocked down in these cells, as the expression of *Htt* is significantly lower following *Htt* siRNA treatment in *StHdh*$^{Q7/111}$ cells when the control conditions are pooled ($p=0.038$), and there is a trend towards a significant difference in *StHdh*$^{Q111/111}$ cells ($P=0.069$). Conversely, *Gapdh* expression was significantly reduced compared to all controls in *StHdh*$^{Q7/111}$ cells ($p<0.001$) and compared to the non-coding

siRNA control in *StHdh*$^{Q111/111}$ cells (p=0.028), indicating that these cells are capable of being transfected with the same efficiency as *StHdh*$^{Q7/7}$ cells.
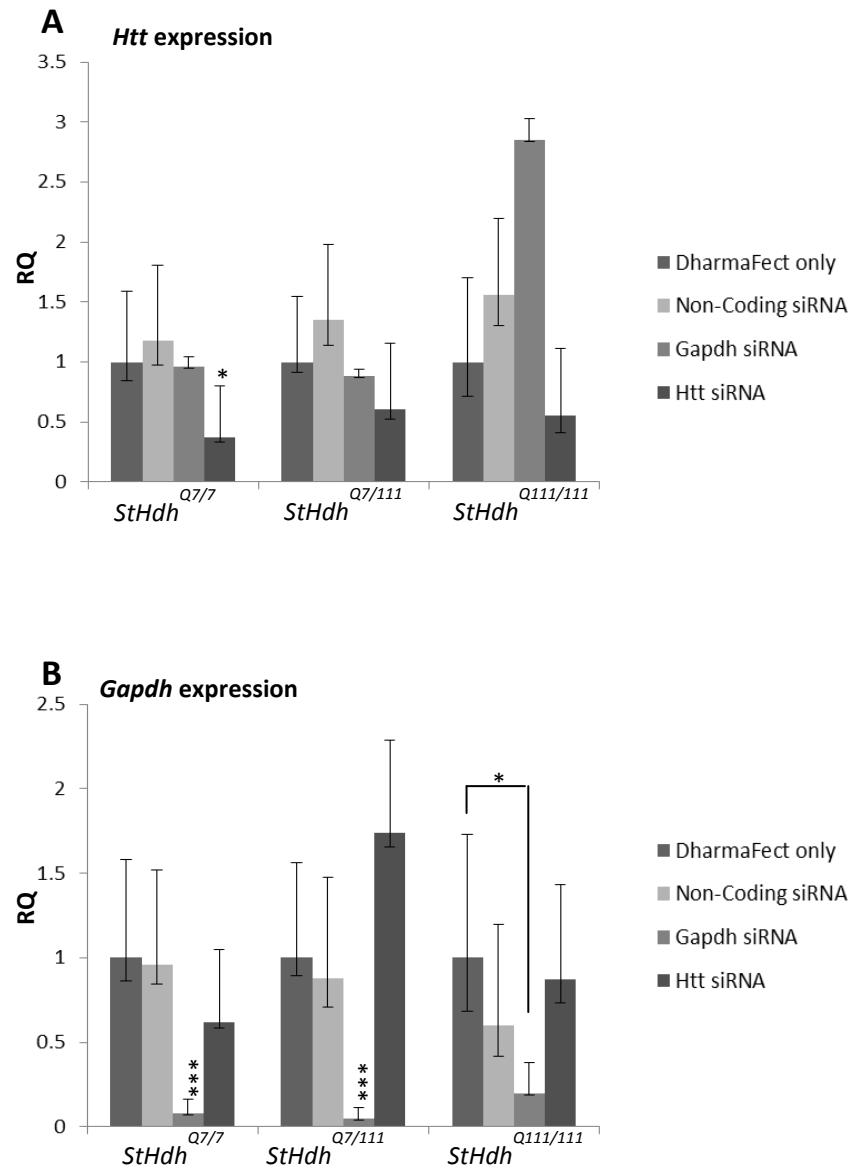
Figure 3.4 A. qRTPCR relative quantification (RQ) values representing the expression of *Htt* in *StHdh*$^{Q7/7}$, *StHdh*$^{Q7/111}$ and *StHdh*$^{Q111/111}$ cells when treated with either the DharmaFECT transfection reagent alone, a non-coding siRNA, *Gapdh* siRNA, or *Htt* siRNA for 48 hours prior to RNA extraction. **B**. The expression of *Gapdh* under the same conditions. Differences in cycle threshold (C_t) values were statistically analysed by genotype individually using a one-way ANOVA and post-hoc Tukey tests (Error bars = SEM, n=3). '*' indicates a significant difference to DharmaFect only control.

*p<0.05   **p<0.01   ***p<0.001

3.3.2.2 Western blot analysis

In order to validate whether the high molecular weight ~350kDa band on western blot analyses detected by our panel of anti-HTT antibodies was in fact the HTT protein, cells were incubated for 48 hours with the appropriate siRNA or control oligonucleotides, followed by another 48 hour incubation with fresh oligonucleotides prior to collection of protein lysates. The extension of the siRNA protocol was due to the longer degradation time of proteins compared to mRNAs. The experiment was carried out with triplicate samples, and after the initial detection, each blotted membrane was stripped and re-probed with the panel of HTT antibodies.

There was a visible reduction in the strength of the high molecular weight band in all three genotypes following *Htt* siRNA treatment compared to the control conditions (Figure 3.5), however due to noise and a lack of power, quantification of the HTT band intensity was not significantly different to quantification of the transfection reagent only control. Despite this, qualitatively, *Htt* siRNA treatment reduces the strength of the high molecular weight band detected by all anti-HTT antibodies, and therefore these antibodies are likely to be picking up full length HTT by western blot. The concentration of the protein lysate for *StHdh*$^{Q7/7}$ cells treated with *Htt* siRNA was lower than the other lysates, and as such less could be loaded onto the gel, however normalisation to the α-tubulin loading control reveals that there is still a relative reduction in the strength of detection of the HTT band.
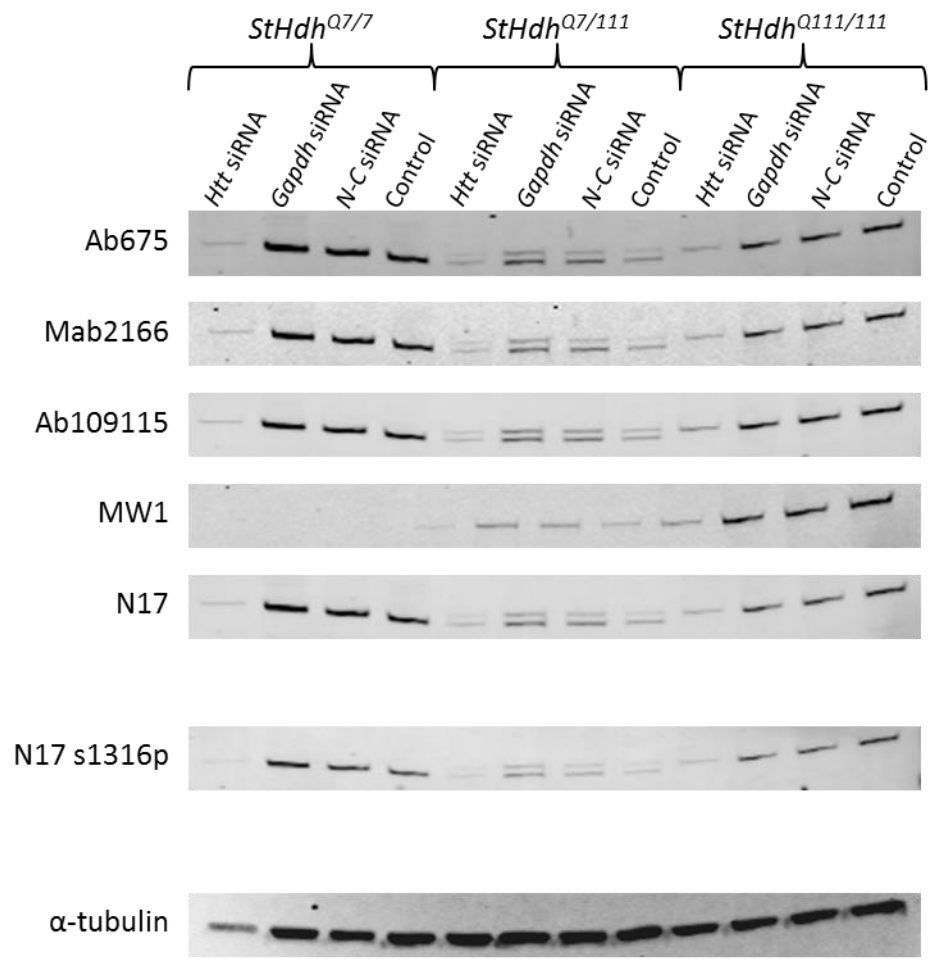
Figure 3.5 Continued on next page
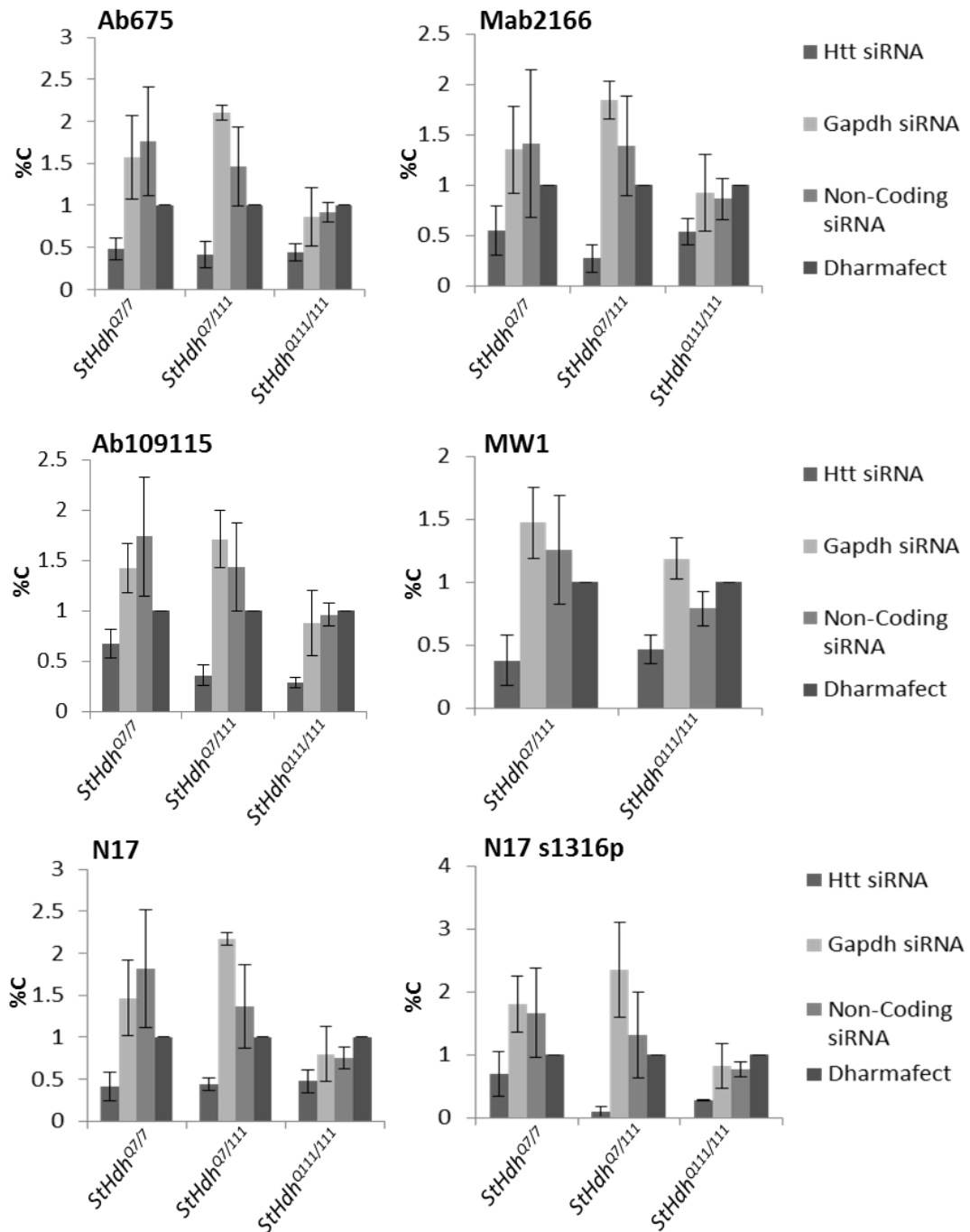
Figure 3.5 A. Western blots of *StHdh*$^{Q7/7}$, *StHdh*$^{Q7/111}$ and *StHdh*$^{Q111/111}$ cells treated with either 25nM *Htt* siRNA, 25nM *Gapdh* siRNA, 25nM non-coding (N-C) siRNA or transfection reagent only control for 48 hours, followed by a second 48 hour incubation with the same treatment. Blots were double-probed for Ab675 and Mab2166 before being stripped and re-probed sequentially with the rest of the panel of N-terminal HTT antibodies, and α-tubulin as a loading control. **B.** Licor Odyssey quantification of fluorescence intensities in *A*. Intensities were normalised to α-tubulin loading control, then expressed as a percentage of the transfection-only control intensity (%C) (Error bars = SEM, n=3).

3.3.2.3 Immunofluorescence

As there was no effect on the expression of *Htt* or presence of its protein product when cells were treated with *Gapdh* or non-coding siRNA oligonucleotides, only the transfection reagent control was used for the immunofluorescence experiments in order to preserve antibody stocks. For all antibodies investigated, there was little visible reduction of signal in *StHdh*$^{Q7/7}$ cells that had been treated with *Htt* siRNA compared to the transfection reagent only control (Figure 3.6). However, there was a visible reduction when looking at Ab109115, N17 and N17 s1316p; this is particularly evident for the two non-phosphorylated HTT antibodies, where there is a visible reduction in the detection of nuclear HTT. There is a larger apparent difference in *StHdh*$^{Q7/111}$ and *StHdh*$^{Q111/111}$ cells for all antibodies when *Htt* is knocked down; similar to *StHdh*$^{Q7/7}$ cells, the most obvious difference is the reduction of a nuclear signal. It has previously been observed that the expression of the mutant HTT protein is lower than the wild type protein (Gutekunst et al. 1995; Persichetti et al. 1996; J. Miller et al. 2010; Pouladi et al. 2010), and that this may be due to reduced stability (Sapp et al. 2012) and a shorter half-life of mHTT (J. Miller et al. 2010); both of which may contribute to a greater reduction in HTT detection following siRNA treatment in *StHdh*$^{Q7/111}$ and *StHdh*$^{Q111/111}$ cells compared to *StHdh*$^{Q7/7}$ line.

The knock down of *Htt* in these cells appears to have also had an effect on cell morphology, particularly in *StHdh*$^{Q7/111}$ and *StHdh*$^{Q111/111}$ cells; qualitatively, cell soma became considerably smaller, and there was a reduction in cell number. Whether this was due to increased cell death or was a suppression of growth was not investigated as this was not the primary aim of this experiment. However, as it has been previously noted that in the developing cortical neuroepithelium, knocking out *Htt* disturbs cell migration and proliferation, and increases cell death (Tong et al. 2011), it is not unexpected that reducing *Htt* expression in an embryonic striatal cell model has detrimental effects on cell survival.

A

$StHdh^{Q7/7}$

	DharmaFECT only	*Htt* siRNA
Ab675		
Mab2166		
Ab109115		
N17		
N17 s1316p		

Figure 3.6 Continued on next page

B

$StHdh^{Q7/111}$

DharmaFECT only   *Htt* siRNA

Ab675

Mab2166

Ab109115

N17

N17 s1316p
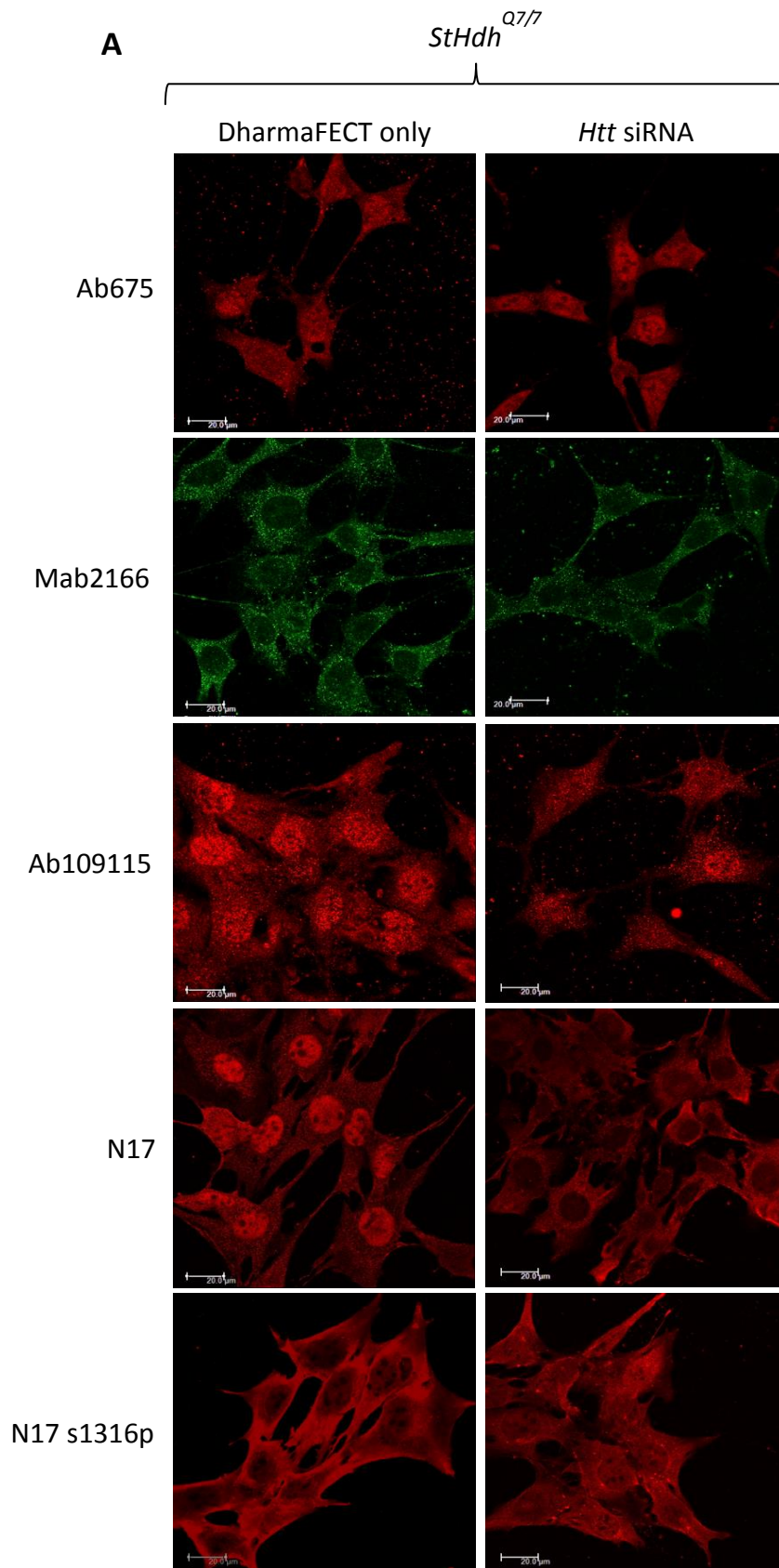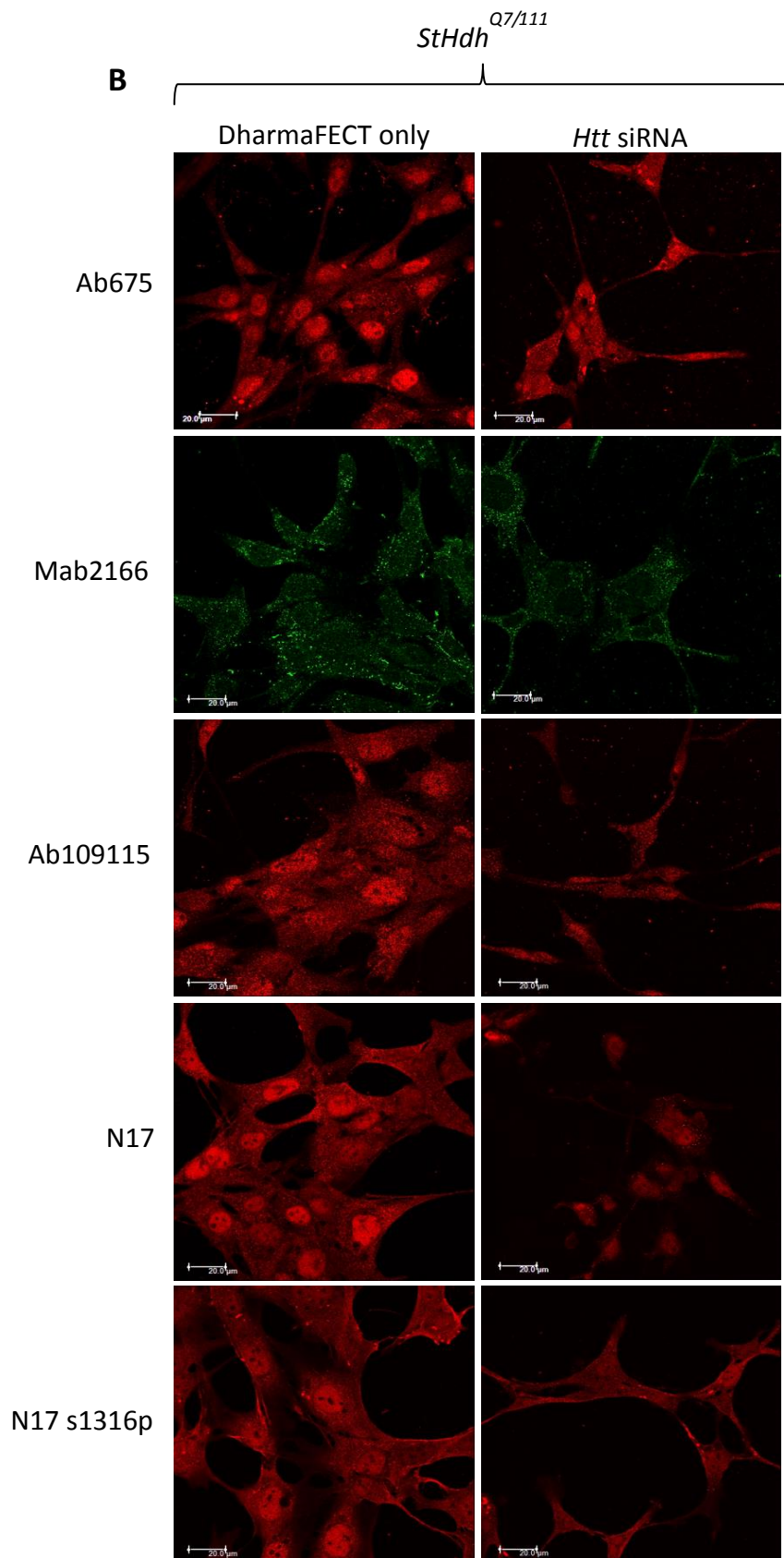
Figure 3.6 Continued on next page
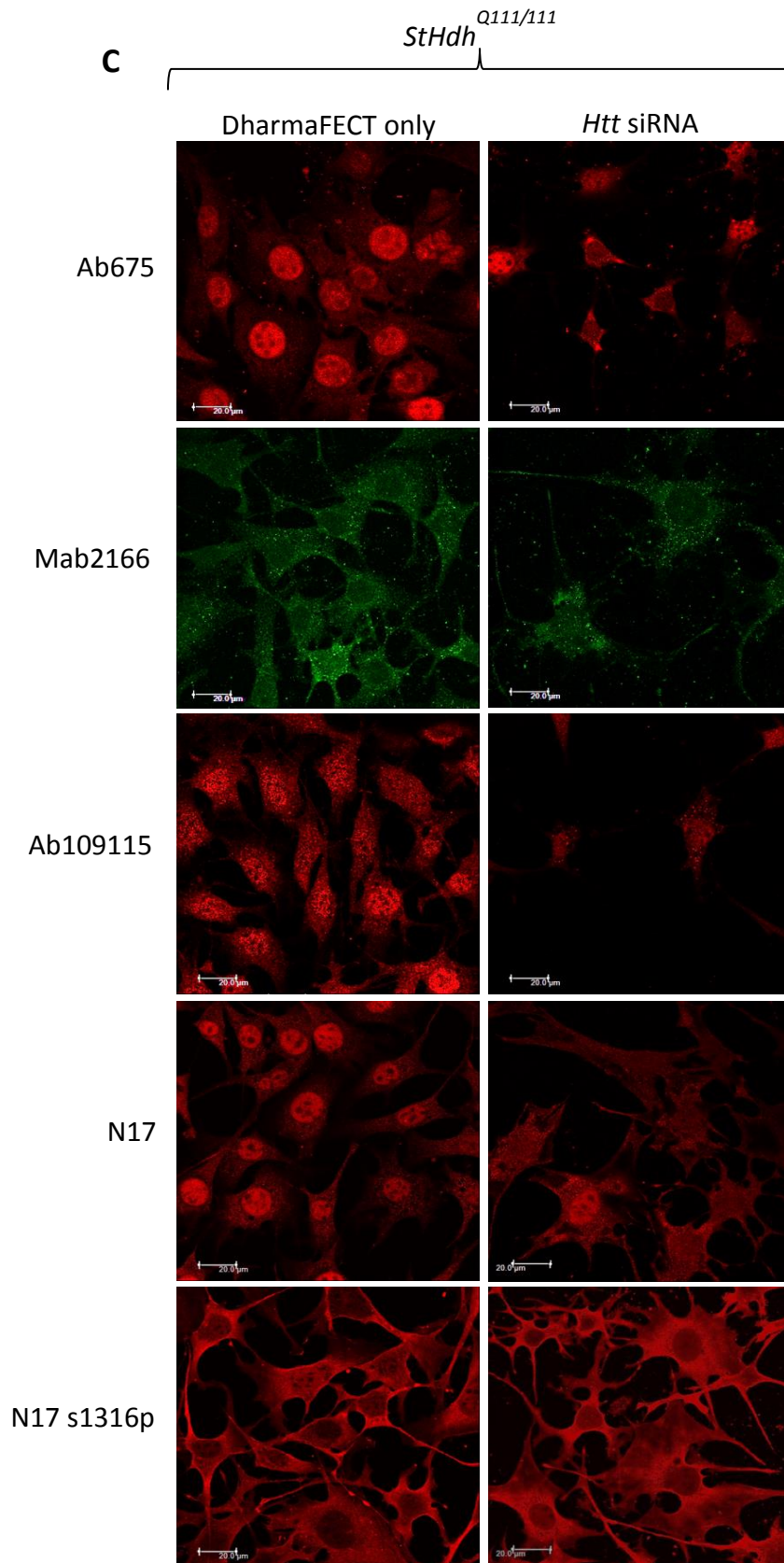
Figure 3.6. Immunofluorescence images of **A.** *StHdh*$^{Q7/7}$, **B**. *StHdh*$^{Q7/111}$ and **C**. *StHdh*$^{Q111/111}$ cells treated with either 25nM *Htt* siRNA or transfection reagent-only for 48 hours followed by a second 48 hour incubation with the same treatment, then probed with a panel of N-terminal HTT antibodies. Scale bar = 20μm.

Despite the knock down of the HTT protein not being entirely successful, we have shown evidence that suggests each of the N-terminal HTT antibodies that were analysed are likely to be detecting the HTT protein, particularly in cell nuclei. However, the extent of any non-specific binding could not be assessed due to incomplete protein knock down. Several other models may have been particularly useful for anti-HTT antibody validation, such as HTT knock-out mouse neural stem cell lines (Conforti et al. 2013) and conditional *Htt* null mutation mouse fibroblast cells (Zhang et al. 2008; Dragatsis et al. 2000). However, these were not available to us, and as they were not derived from the same mouse model utilised here, may have had the extra confound of additional or alternative HTT epitopes that are not apparent in *StHdh*^{Q111} cell lines when using the same antibodies.

3.3.3 Immunostaining with antibody 675

3.3.3.1 BDNF stimulation

At baseline, the N-terminal epitope of HTT as detected by Ab675 is primarily cytoplasmic in *StHdh*$^{Q7/7}$ cells, although it becomes increasingly nuclear with increased mHTT load (Figures 3.7 and 3.8). Statistical analysis of quantitative measures (for further details, see Section 2.2.1.10 and Figure 2.3) of the nuclear/cytoplasmic (N/C) pixel intensity ratio showed that there was a significant main effect of cell type (F (2, 664) = 22.56, p<0.001) and time of growth factor stimulation (F (3, 664) = 19.79, p<0.001) on the localisation of HTT epitopes, as well as a significant interaction between the two (F (6, 664) = 2.27, p=0.035). Simple main effects analysis showed that *StHdh*$^{Q7/7}$ had significantly lower N/C intensity ratios than both the *StHdh*$^{Q7/111}$ and *StHdh*$^{Q111/111}$ cell lines (P<0.001), which did not differ from each other (P=0.17). Post-hoc Tukey HSD tests revealed that following 5 minutes of BDNF stimulation, there was a significant reduction in the nuclear/cytoplasmic (N/C) intensity ratio for all three cell lines (*StHdh*$^{Q7/7}$ p=0.011*, StHdh*$^{Q7/111}$ p=0.044, *StHdh*$^{Q111/111}$ p<0.001); the effect of which was persistent for up to 30 minutes of stimulation (*StHdh*$^{Q7/7}$ p=0.011, *StHdh*$^{Q7/111}$ p<0.001, *StHdh*$^{Q111/111}$ p<0.001). In *StHdh*$^{Q7/7}$ cells, there was also a significant reduction in the nuclear/perinuclear (N/P) ratio (F (3,664) = 16.78, p<0.001) and perinuclear/cytoplasmic (P/C) ratio following BDNF stimulation (F (3,664) = 19.72,

p<0.001), both of which significantly interacted with cell type (N/P $F_{(6,664)}$ = 10.88, p<0.001, N/C $F_{(6,664)}$ = 3.03, p=0.006). This suggests that there is reduction of the N-terminal epitope of HTT and mHTT in the nucleus and a concordant increase in the cytoplasm following BDNF stimulation, but that this effect is influenced by cell type.

In both *StHdh*$^{Q7/111}$ and *StHdh*$^{Q111/111}$ cells, there was a significant reduction in the N/P ratio for N-terminal HTT and mHTT epitopes over time. In *StHdh*$^{Q7/111}$ cells, there is significant reduction in the N/P ratio by 30mins (Tukey HSD p<0.001), but no difference in the P/C ratio (p=0.076), suggesting that although there may be some movement out of the nucleus, there doesn't appear to be relocalisation to the cytoplasm. In contrast, *StHdh*$^{Q111/111}$ cells show reduced N/C and P/C ratios after only 5 minutes (p<0.001), but there is no significant change in the N/P ratio itself at any time point (p>0.05).
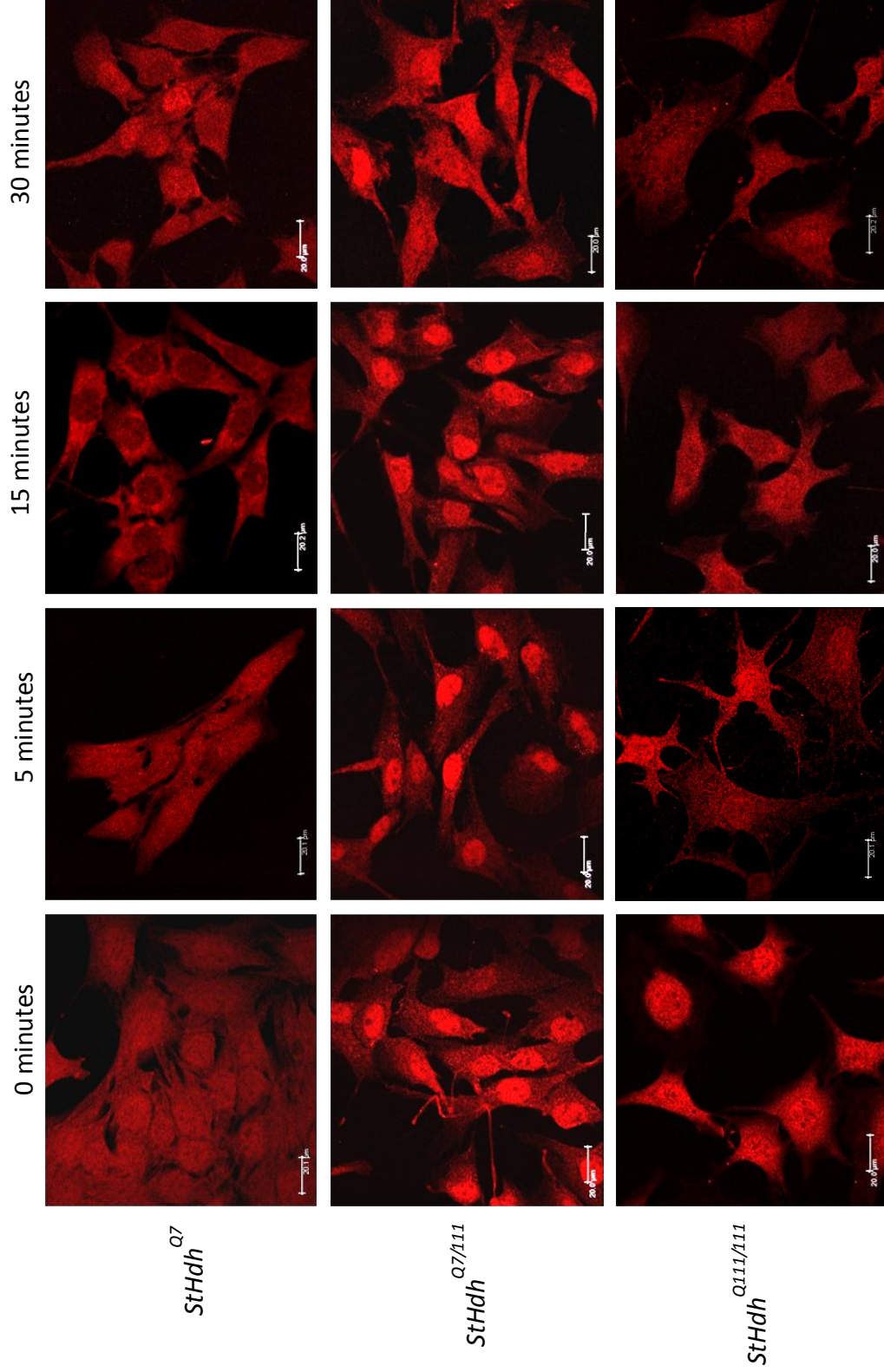
Figure 3.7 Subcellular localisation of an N-terminal epitope of HTT and mHTT in *StHdh*[Q7], *StHdh*[Q7/111] and *StHdh*[Q111/111] cell lines. Cells were fixed following 0, 5, 15 and 30 minutes of stimulation with 100ng/ml BDNF, labelled with Ab675 against amino acids 1-17 of HTT then analysed by confocal microscopy (see Sections 2.2.1.8 and 2.2.1.9 for further details). Scale bar = 20μm
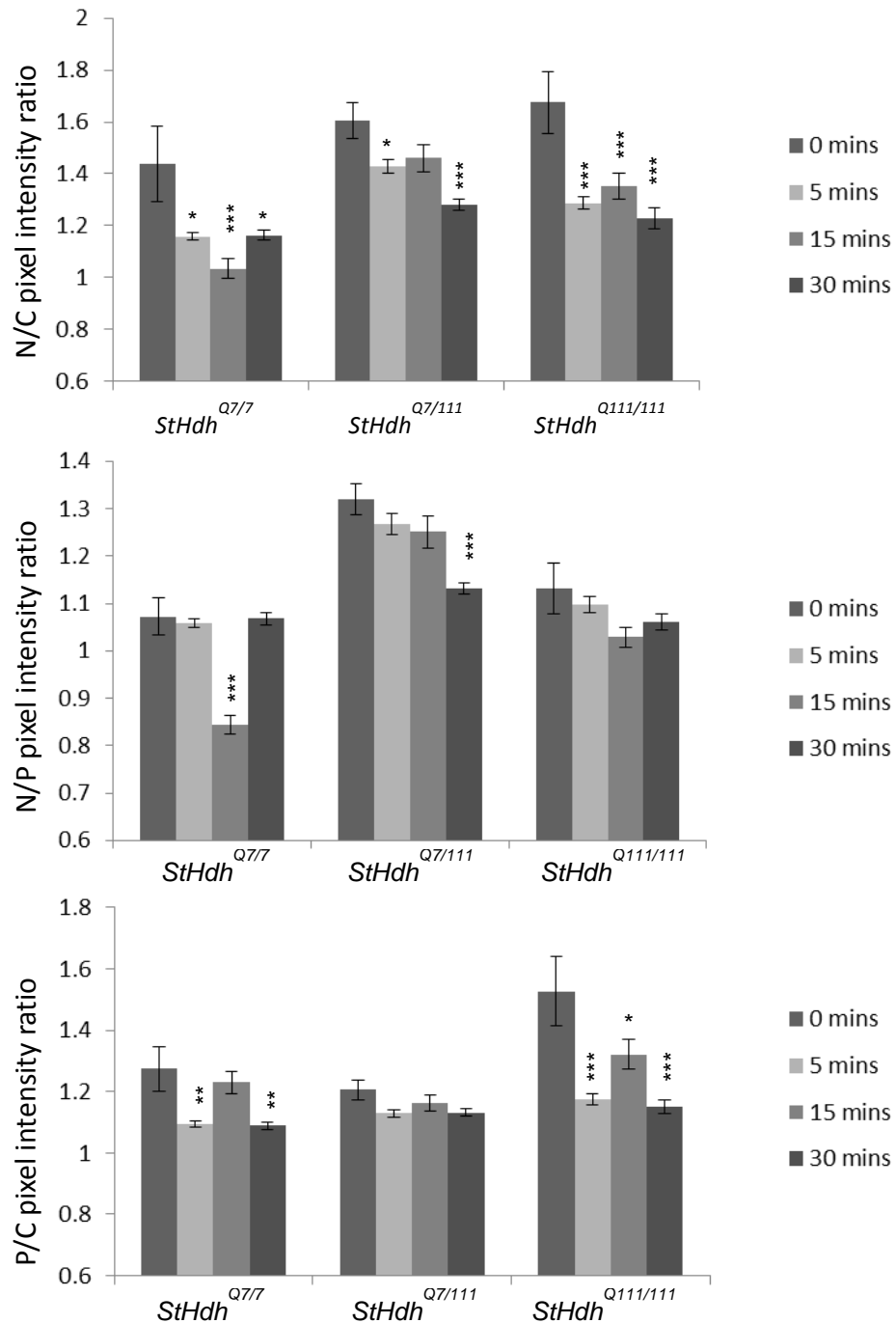
Figure 3.8 Quantitative analysis of immunofluorescence images in Figure 3.7. Nuclear/Cytoplasmic (N/C), Nuclear/Perinuclear (N/P) and Perinuclear/Cytoplasmic (P/C) mean pixel intensity ratios for $StHdh^{Q7/7}$, $StHdh^{Q7/111}$ and $StHdh^{Q111/111}$ cells following 0, 5, 15 and 30 minutes of stimulation with 100ng/ml BDNF. Mean pixel intensities were calculated from confocal microscopy images using GNU Image Manipulator (further details of the analysis can be found in Section 2.2.1.10). All images were randomised and analysed blind to genotype and length of time stimulated with BDNF. Each condition consisted of 9 confocal microscopy images taken from 3 separate coverslips. A two-way ANOVA was carried out for main effects analysis, followed by planned one way ANOVAs and post-hoc Tukey tests. Error bars = SEM

* p<0.05   ** p<0.01   *** p<0.001

3.3.3.2 NGF stimulation

In contrast to BDNF stimulation, NGF stimulation of immortalised embryonic cell lines prompted a significant nuclear increase of the N-terminal HTT epitope ($F_{(3,826)} = 5.38$, $p=0.001$), but there was also a significant interaction between length of stimulation and cell type ($F_{(6,826)} = 12.50$, $p<0.001$) (Figures 3.9 & 3.10). This occurs as early as after 5 minutes in $StHdh^{Q7/7}$ cells ($p=0.039$), although the effect is delayed to 30 and 15 minutes in both the $StHdh^{Q7/111}$ and $StHdh^{Q111/111}$ cell lines, respectively ($StHdh^{Q7/111}$ 30mins $p<0.001$, $StHdh^{Q111/111}$ 15mins $p=0.002$). Statistical analysis of the N/P ratio for $StHdh^{Q7/7}$ and $StHdh^{Q7/111}$ cells shows a significant reduction by 15 minutes, when the N/P intensity ratio returns to baseline following the 5 minute increase ($StHdh^{Q7/7}$ $p<0.001$, $StHdh^{Q7/111}$ $p<0.001$). There is no significant change in the P/C ratio for any genotype at these times, suggesting that detection of HTT epitopes is changing largely between the nucleus and the perinuclear region rather than between the nucleus and cytoplasm. However, $StHdh^{Q111/111}$ cells show a significant increase in the P/C ratio following NGF stimulation by 15 minutes ($p=0.002$), with no significant N/P change, suggesting that the N-terminal epitope of mHTT may be recruited from the cytoplasm, and becomes condensed in the nuclear and perinuclear regions of the cell.

Figure 3.9 Subcellular localisation of an N-terminal epitope of HTT and mHTT in *StHdh*^Q7/7, *StHdh*^Q7/11 and *StHdh*^Q111/11 cell lines. Cells were fixed following 0, 5, 15 and 30 minutes of stimulation with 100ng/ml NGF, labelled with Ab675 against amino acids 1-17 of HTT, then analysed by confocal microscopy (see Sections 2.2.1.8 and 2.2.1.9 for further details). Scale bar = 20μm
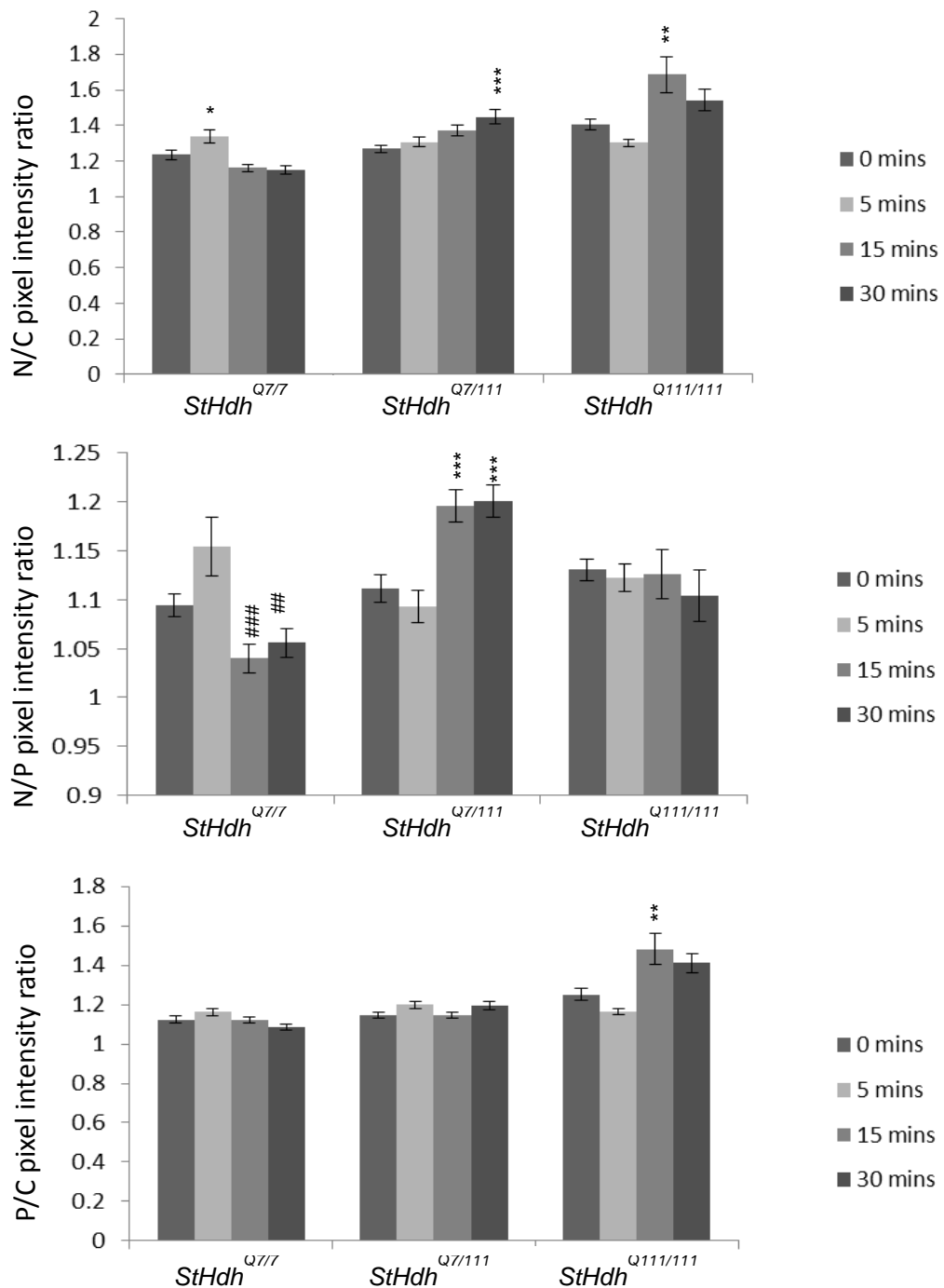
Figure 3.10 Quantitative analysis of immunofluorescence images in Figure 3.9. Nuclear/Cytoplasmic (N/C), Nuclear/Perinuclear (N/P) and Perinuclear/Cytoplasmic (P/C) mean pixel intensity ratios for $StHdh^{Q7/7}$, $StHdh^{Q7/111}$ and $StHdh^{Q111/111}$ cells following 0, 5, 15 and 30 minutes of stimulation with 100ng/ml NGF. Mean pixel intensities were calculated from confocal microscopy images using GNU Image Manipulator (further details of the analysis can be found in Section 2.2.1.10). All images were randomised and analysed blind to genotype and length of time stimulated with NGF. Each condition consisted of 9 confocal microscopy images taken from 3 separate coverslips. A two-way ANOVA was carried out for main effects analysis, followed by planned one way ANOVAs and post-hoc Tukey tests. Error bars = SEM.

* Denotes a significant difference from 0mins

\# Denotes a significant difference from 5mins

* p<0.05   ** p<0.01   *** p<0.001

3.3.3.3 EGF stimulation

Although there is a significant effect of both time (F (3,797) = 6.15, p<0.001) and cell type (F (2, 797) = 77.25, p<0.001) on the N/C ratio following EGF stimulation there was no significant interaction (F (6,797) = 0.38, p=0.89). However, the interaction was significant for the N/P ratio (F (6, 797) = 6.42, p<0.001). Similar to BDNF stimulation, EGF prompted a reduction of the N-terminal epitope of HTT in the nucleus by 5 minutes of stimulation in both $StHdh^{Q7/7}$ and $StHdh^{Q7/111}$ cell lines (p=0.021, p=0.001 respectively), although the effect is not persistent beyond this time point (Figure 3.11 & 3.12). There was a trend towards the same effect in the $StHdh^{Q111/111}$ cells, although this was not significant (p=0.702). Analogous to the effect seen following NGF, there were significant differences in the N/P ratio for the $StHdh^{Q7/7}$ and $StHdh^{Q7/111}$ cell lines by 5 minutes (p=0.021, p=0.001 respectively), but there was no significant change in the P/C ratio at any time point. $StHdh^{Q111/111}$ cells don't show any significant differences in N/C or N/P pixel intensity ratios over time, suggesting reduced movement of the N-terminal epitope of mHTT in response to EGF. However, there is a statistically significant increase of the P/C ratio at 30 minutes following a non-significant trend away from the perinuclear region at 5 minutes (p=0.023).
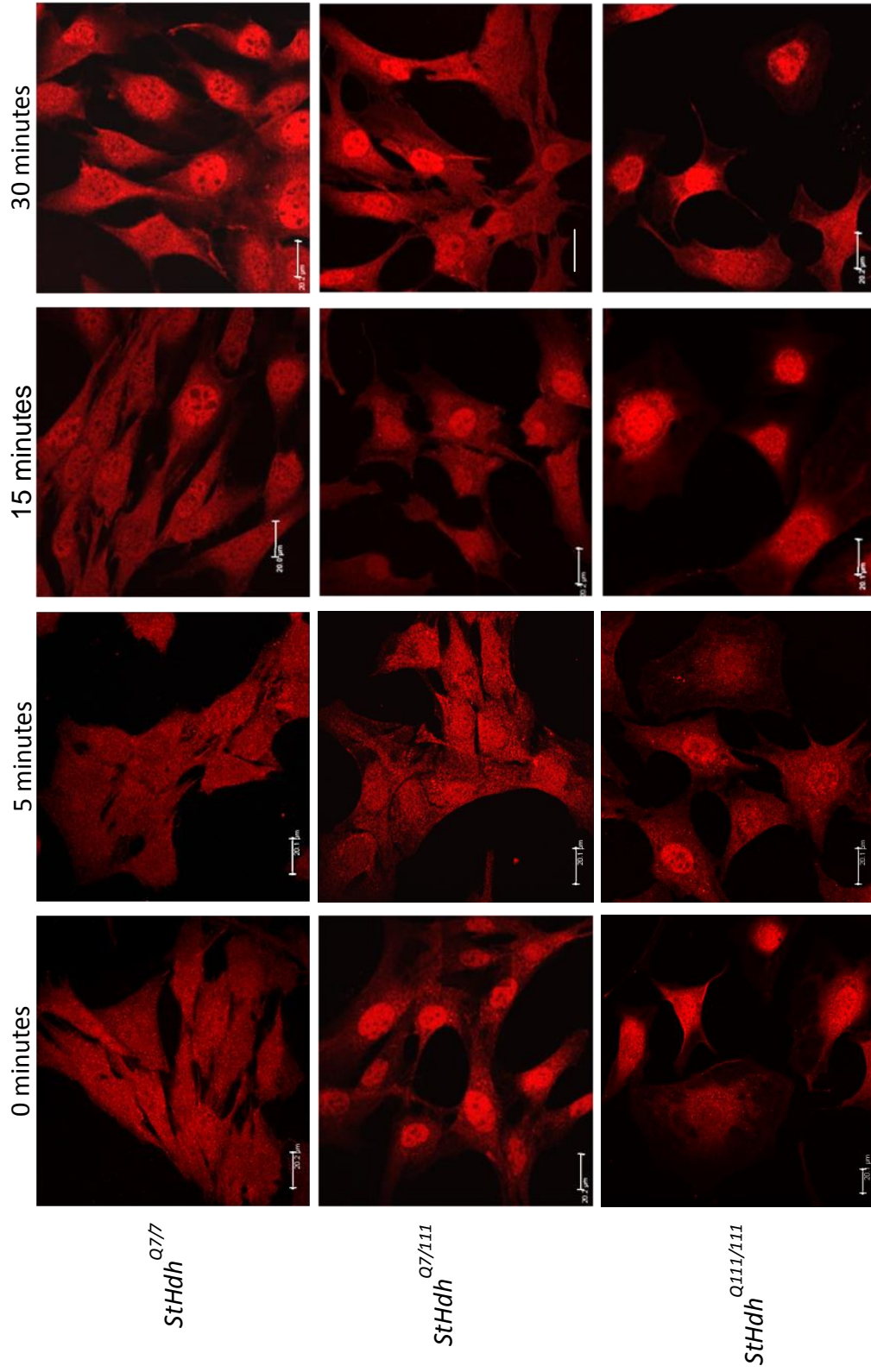
Figure 3.11 Subcellular localisation of an N-terminal epitope of HTT and mHTT in *StHdh*$^{Q7/7}$, *StHdh*$^{Q7/111}$ and *StHdh*$^{Q111/111}$ cell lines. Cells were fixed following 0, 5, 15 and 30 minutes of stimulation with 100ng/ml EGF, labelled with Ab675 against amino acids 1-17 of HTT, then analysed by confocal microscopy (see Sections 2.2.1.8 and 2.2.1.9 for further details). Scale bar = 20μm
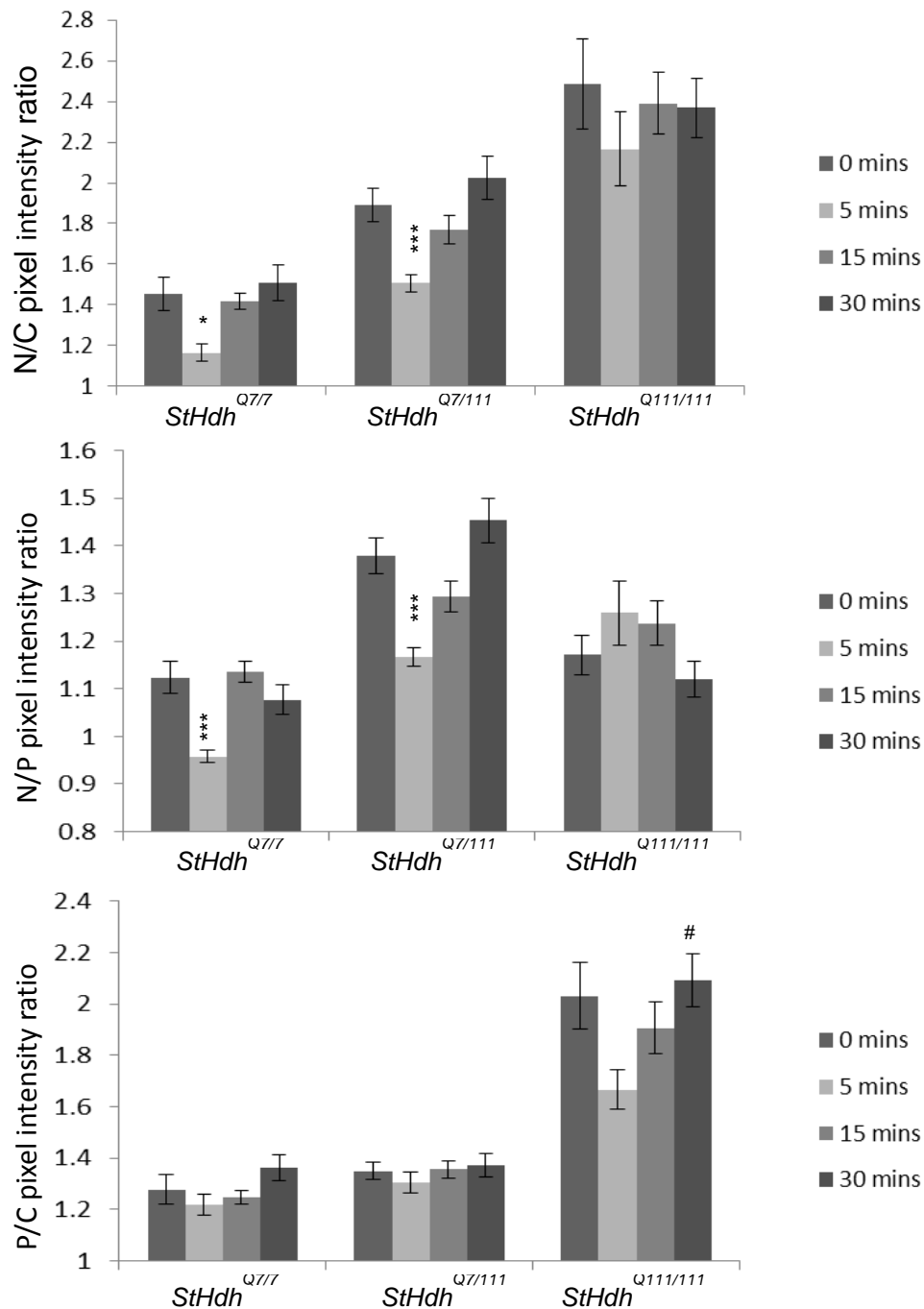
Figure 3.12 Quantitative analysis of immunofluorescence images in Figure 3.11. Nuclear/Cytoplasmic (N/C), Nuclear/Perinuclear (N/P) and Perinuclear/Cytoplasmic (P/C) mean pixel intensity ratios for $StHdh^{Q7/7}$, $StHdh^{Q7/111}$ and $StHdh^{Q111/111}$ cells following 0, 5, 15 and 30 minutes of stimulation with 100ng/ml EGF. Mean pixel intensities were calculated from confocal microscopy images using GNU Image Manipulator (further details of the analysis can be found in Section 2.2.1.10). All images were randomised and analysed blind to genotype and length of time stimulated with EGF. Each condition consisted of 9 confocal microscopy images taken from 3 separate coverslips. A two-way ANOVA was carried out for main effects analysis, followed by planned one way ANOVAs and post-hoc Tukey tests. Error bars = SEM.

* Denotes a significant difference from 0mins

# Denotes a significant difference from 5mins

* p<0.05   ** p<0.01   *** p<0.001

3.3.4 Immunostaining with Mab2166

Like Ab675, Mab2166 also detects an N-terminal epitope of HTT and mHTT, although it has been raised against amino acids 181-810, which are located downstream of the polyglutamine expansion. It shows a different pattern of localisation at baseline than Ab675, as it is primarily perinuclear, particularly in the $StHdh^{Q7/7}$ cells. Similar to Ab675, as the genetic load of mHTT increases, this epitope becomes more densely nuclear and perinuclear in its localisation (Figures 3.13 and 3.14).

3.3.4.1 BDNF stimulation

Similar to the effect observed with Ab675, there is a significant interaction between cell line and length of growth factor stimulation in the N/C ratio (F (6, 688) = 7.18, p<0.001). In both $StHdh^{Q7/7}$ and $StHdh^{Q7/111}$ cells, there is also a significant reduction in the N/C ratio ($StHdh^{Q7/7}$ p= 0.003, $StHdh^{Q7/111}$ p=0.03), although this is observed at 15 minutes of stimulation rather than 5. In contrast, there is no significant effect in the $StHdh^{Q111/111}$ cells in the N/C ratio (p >0.05), although the N/P ratio suggests an increase in nuclear mHTT compared to the perinuclear area in these cells, and in $StHdh^{Q7/7}$ cells as early as 5 minutes following stimulation (both p<0.001). $StHdh^{Q7/7}$ then have a significant increase in both the N/C (p=0.007) and N/P (p<0.001) ratios at 30 minutes, indicating a return of this epitope to the nucleus above baseline levels. The majority of significant alterations in pixel intensity lie within N/C and N/P ratios, while the P/C ratio shows no significant effects in either the $StHdh^{Q7/111}$ or $StHdh^{Q111/111}$ cell lines (p>0.05). However in $StHdh^{Q7/7}$ cells, the pattern of the P/C ratio reflects the possible movement of HTT between the cytoplasm and perinuclear area.
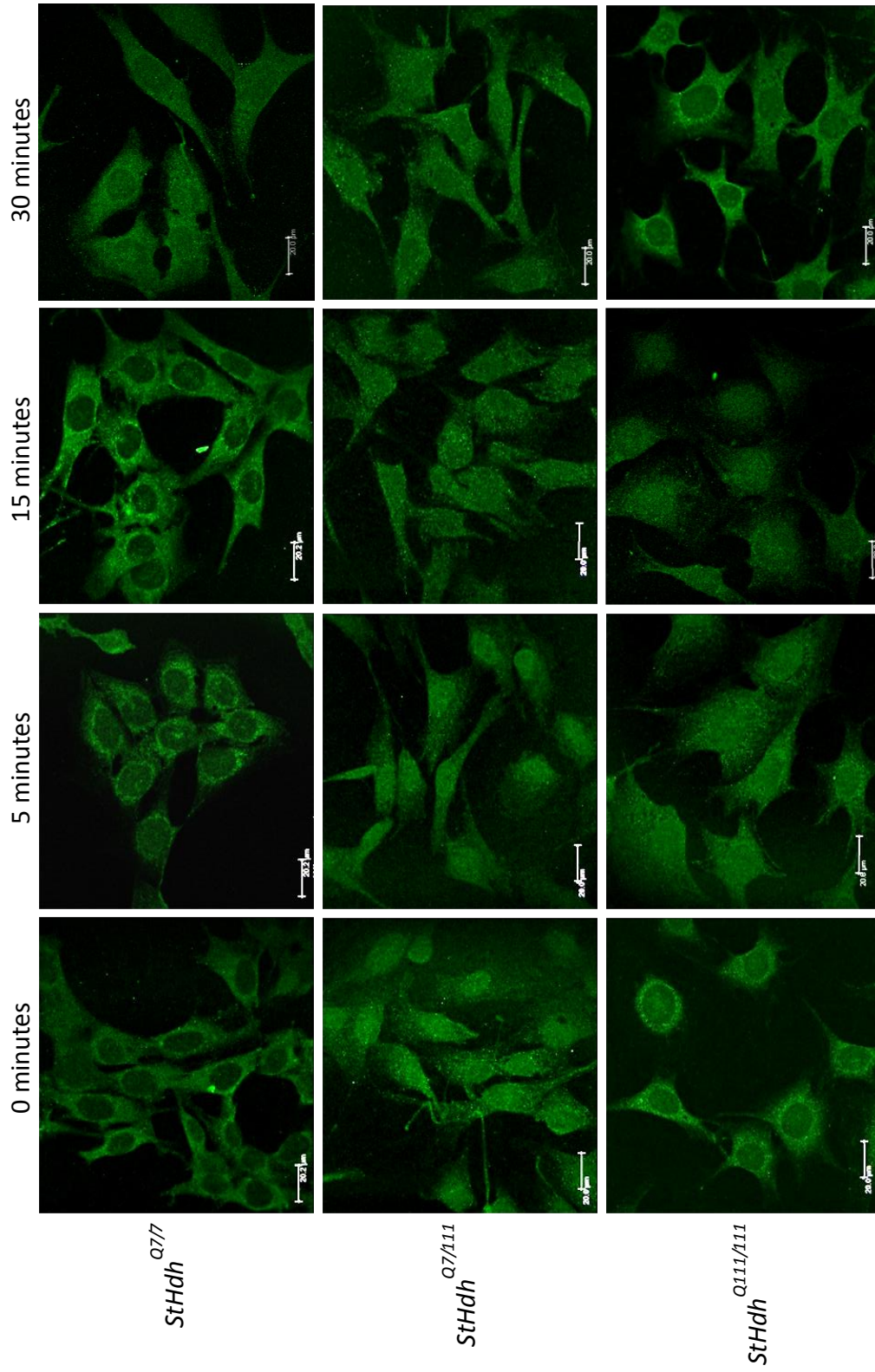
Figure 3.13 Subcellular localisation of an N-terminal epitope of HTT and mHTT in *StHdh*^Q7/7, *StHdh*^Q7/111 and *StHdh*^Q111/111 cell lines. Cells were fixed following 0, 5, 15 and 30 minutes of stimulation with 100ng/ml BDNF, labelled with Mab2166 against amino acids 181-810 of HTT, then analysed by confocal microscopy (see Sections 2.2.1.8 and 2.2.1.9 for further details). Scale bar = 20μm
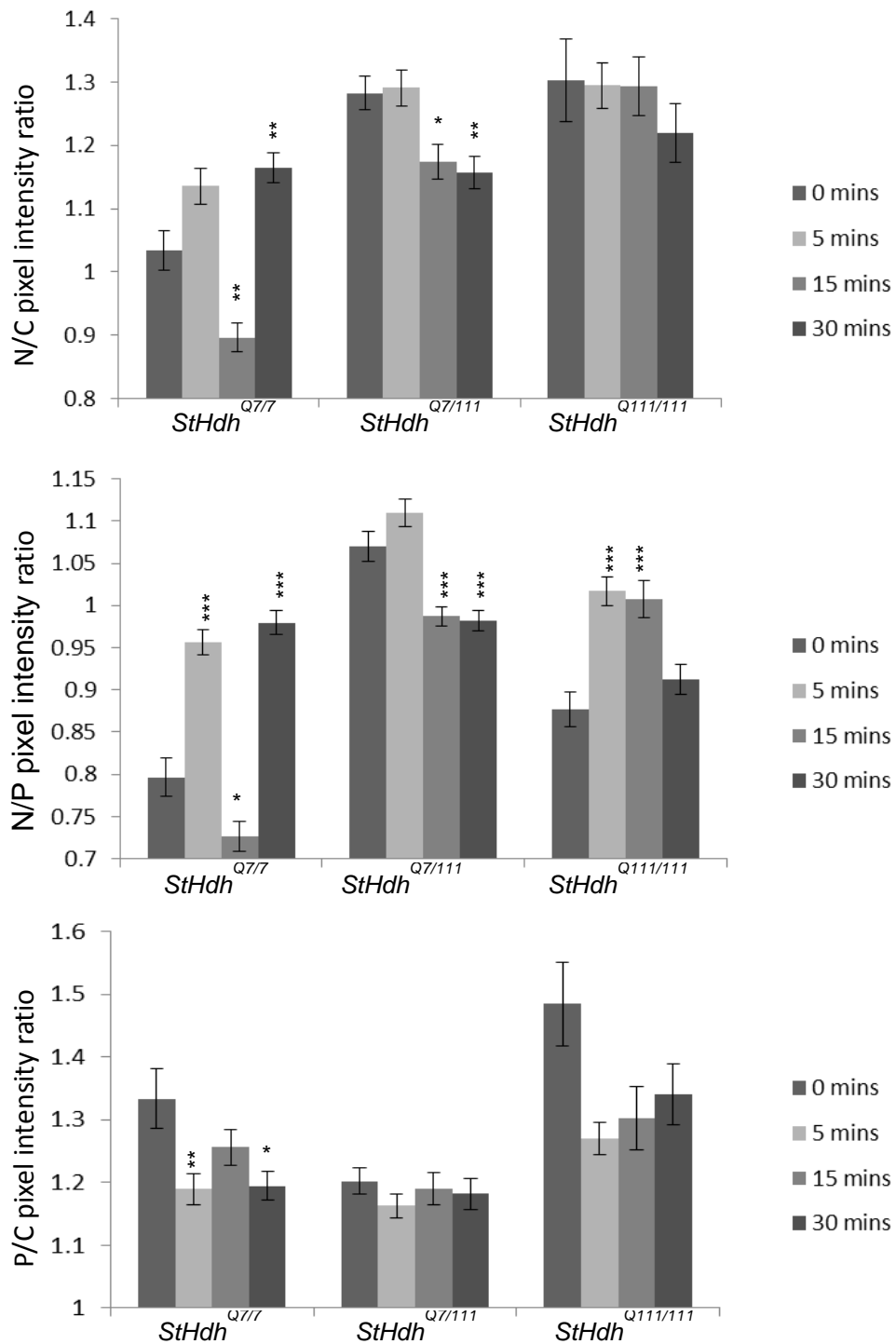
Figure 3.14 Quantitative analysis of immunofluorescence images in Figure 3.13. Nuclear/Cytoplasmic (N/C), Nuclear/Perinuclear (N/P) and Perinuclear/Cytoplasmic (P/C) mean pixel intensity ratios for $StHdh^{Q7/7}$, $StHdh^{Q7/111}$ and $StHdh^{Q111/111}$ cells following 0, 5, 15 and 30 minutes of stimulation with 100ng/ml BDNF. Mean pixel intensities were calculated from confocal microscopy images using GNU Image Manipulator (further details of the analysis can be found in Section 2.2.1.10). All images were randomised and analysed blind to genotype and length of time stimulated with BDNF. Each condition consisted of 9 confocal microscopy images taken from 3 separate coverslips. A two-way ANOVA was carried out for main effects analysis, followed by planned one way ANOVAs and post-hoc Tukey tests. Error bars = SEM

* p<0.05   ** p<0.01   *** p<0.001

3.3.4.2 NGF stimulation

Mab2166 detects a nuclear increase of HTT and mHTT following NGF stimulation, although this effect is statistically significant in the N/P ratio ($F_{(3, 757)} = 23.85$, $p<0.001$), not in the N/C ratio ($F_{(3,757)} = 2.54$, $p= 0.056$) (Figures 3.15 & 3.16). Post-hoc Tukey HSD tests indicate that for $StHdh^{Q7/7}$ and $StHdh^{Q7/111}$ cells, this increase in nuclear intensity occurs at 15 minutes ($StHdh^{Q7/7}$ $p<0.001$, $StHdh^{Q7/111}$ $p<0.001$). Analysis of the individual intensity ratios suggests that these changes could be due to relocalisation of HTT and mHTT between the perinuclear region and the nucleus, rather than movement between the cytoplasm and nucleus. Interestingly, $StHdh^{Q111/111}$ cells indicate the opposite effect; there is a reduction of the N/P ratio from 15 minutes of NGF stimulation ($p=0.005$). The $StHdh^{Q7/7}$ cells show the formation of discrete nuclear foci of N-terminal HTT at 15 minutes following NGF stimulation, which is not observed in either the $StHdh^{Q7/111}$ or $StHdh^{Q111/111}$ cell lines.
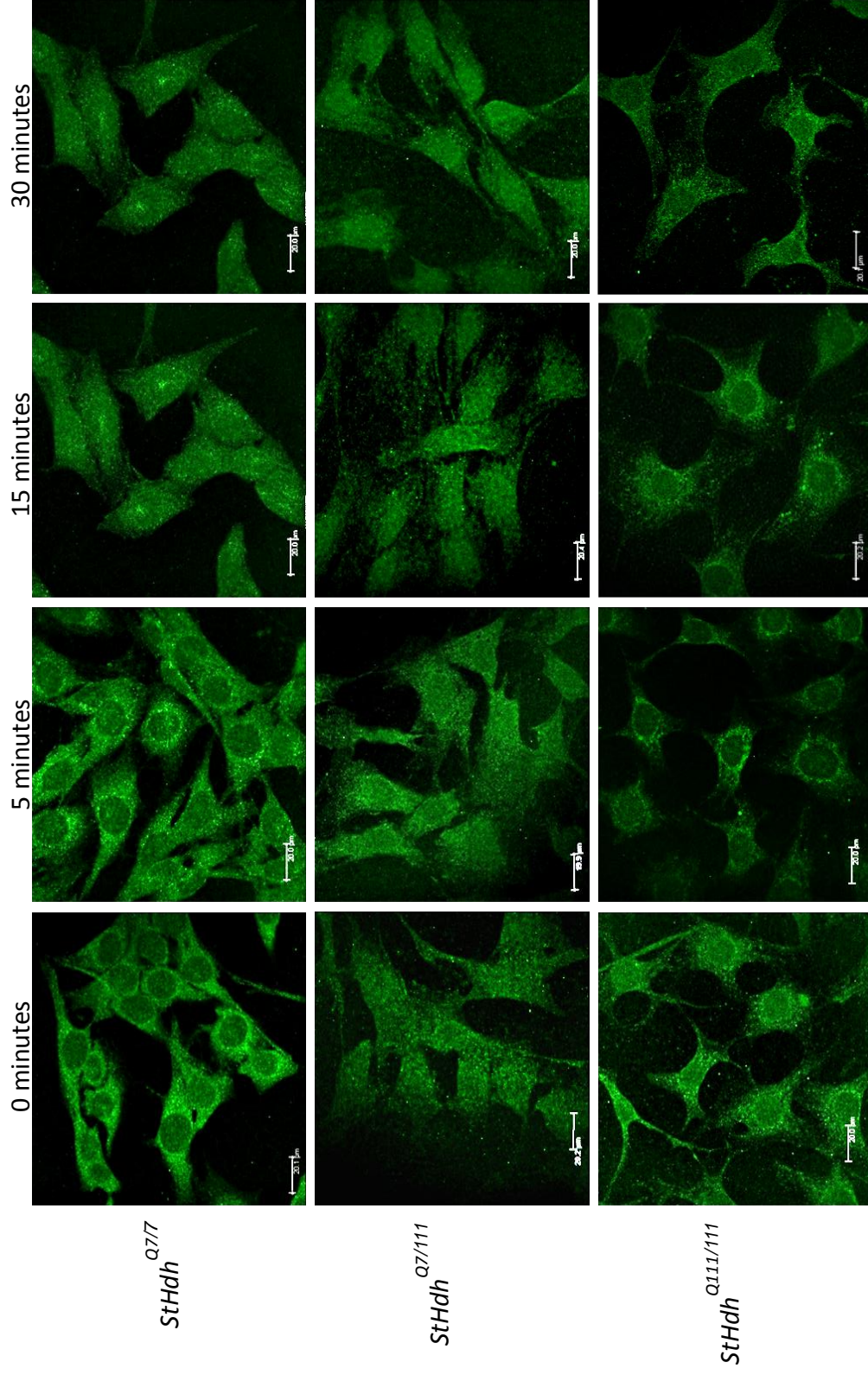
Figure 3.15 Subcellular localisation of an N-terminal epitope of HTT and mHTT in *StHdh*$^{Q7/7}$, *StHdh*$^{Q7/111}$ and *StHdh*$^{Q111/111}$ cell lines. Cells were fixed following 0, 5, 15 and 30 minutes of stimulation with 100ng/ml NGF, labelled with Mab2166 against amino acids 181-810 of HTT, then analysed by confocal microscopy (see Sections 2.2.1.8 and 2.2.1.9 for further details). Scale bar = 20µm
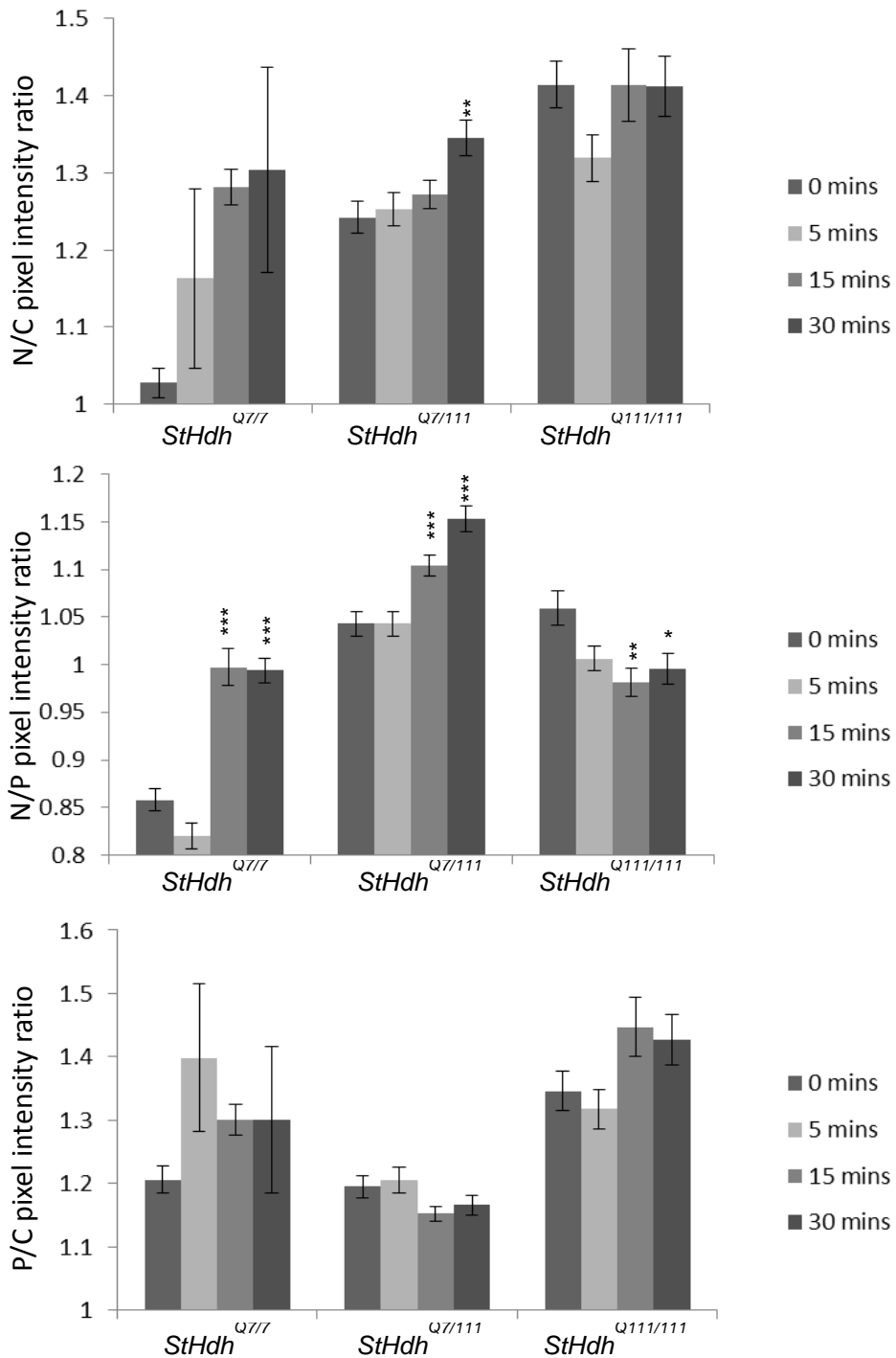
Figure 3.16 Quantitative analysis of immunofluorescence images in Figure 3.15. Nuclear/Cytoplasmic (N/C), Nuclear/Perinuclear (N/P) and Perinuclear/Cytoplasmic (P/C) mean pixel intensity ratios for $StHdh^{Q7/7}$, $StHdh^{Q7/111}$ and $StHdh^{Q111/111}$ cells following 0, 5, 15 and 30 minutes of stimulation with 100ng/ml NGF. Mean pixel intensities were calculated from confocal microscopy images using GNU Image Manipulator (further details of the analysis can be found in Section 2.2.1.10). All images were randomised and analysed blind to genotype and length of time stimulated with NGF. Each condition consisted of 9 confocal microscopy images taken from 3 separate coverslips. A two-way ANOVA was carried out for main effects analysis, followed by planned one way ANOVAs and post-hoc Tukey tests. Error bars = SEM.

* $p<0.05$ ** $p<0.01$ *** $p<0.001$

3.3.4.3 EGF stimulation

Mab2166 shows the same pattern of localisation following EGF stimulation in all three cell lines as Ab675 (Figures 3.17 & 3.18). For the N/C ratio, there was a significant effect of cell type ($F_{(2, 847)} = 46.93$, $p<0.001$) and growth factor stimulation ($F_{(3,847)} = 26.43$, $p<0.001$), but there was no interaction between the two ($F_{(6, 847)} = 1.37$, $p=0.225$). However, there was no longer a significant interaction in the N/P ratio as there was previously ($F_{(6, 847)} = 1.56$, $p=0.16$), which is likely due to the N/P ratio in *StHdh*$^{Q111/111}$ cells now reaching significance by 5 minutes of EGF stimulation ($p<0.001$). Again, significant effects are predominantly found between the nuclear and perinuclear regions, although the same pattern of movement within the cell is reflected in the P/C ratio. This reaches significance at 30 minutes of stimulation in *StHdh*$^{Q7/7}$ cells ($p=0.009$), and at 5 minutes in the *StHdh*$^{Q7/111}$ cells ($p=0.044$).

3.3.5 Immunostaining with other N-terminal HTT antibodies

In order to more thoroughly characterise the localisation of HTT and mHTT, as well as support the results from Ab675 and Mab2166, both another rabbit polyclonal antibody created in a different lab against the same epitope as Ab675 (N17), and a commercial equivalent of Ab675 (Ab109115) that was raised against a slighter longer epitope of HTT (amino acids 1-30), were also utilised. Only EGF stimulation was selected to be followed up using these antibodies, as it produced the most consistent results and clear effect of genotype.

In concordance with Ab675, there was a similar pattern of HTT localisation following EGF stimulation when cells were immunostained with Ab109115; details of these results can be found in Appendix I. There was not enough of the N17 antibody available to immunostain sufficient cell numbers for quantification and statistical analysis. However, in comparison with the other N-terminal antibodies, there was no effect of EGF stimulation on the localisation of HTT epitopes detected by N17 in any of the genotypes; further details and images from this experiment can be found in Appendix II. A comparison of the differential effects of growth factor stimulation on the nuclear localisation of HTT detected by the panel of N-terminal HTT antibodies can be found in Table 3.1.
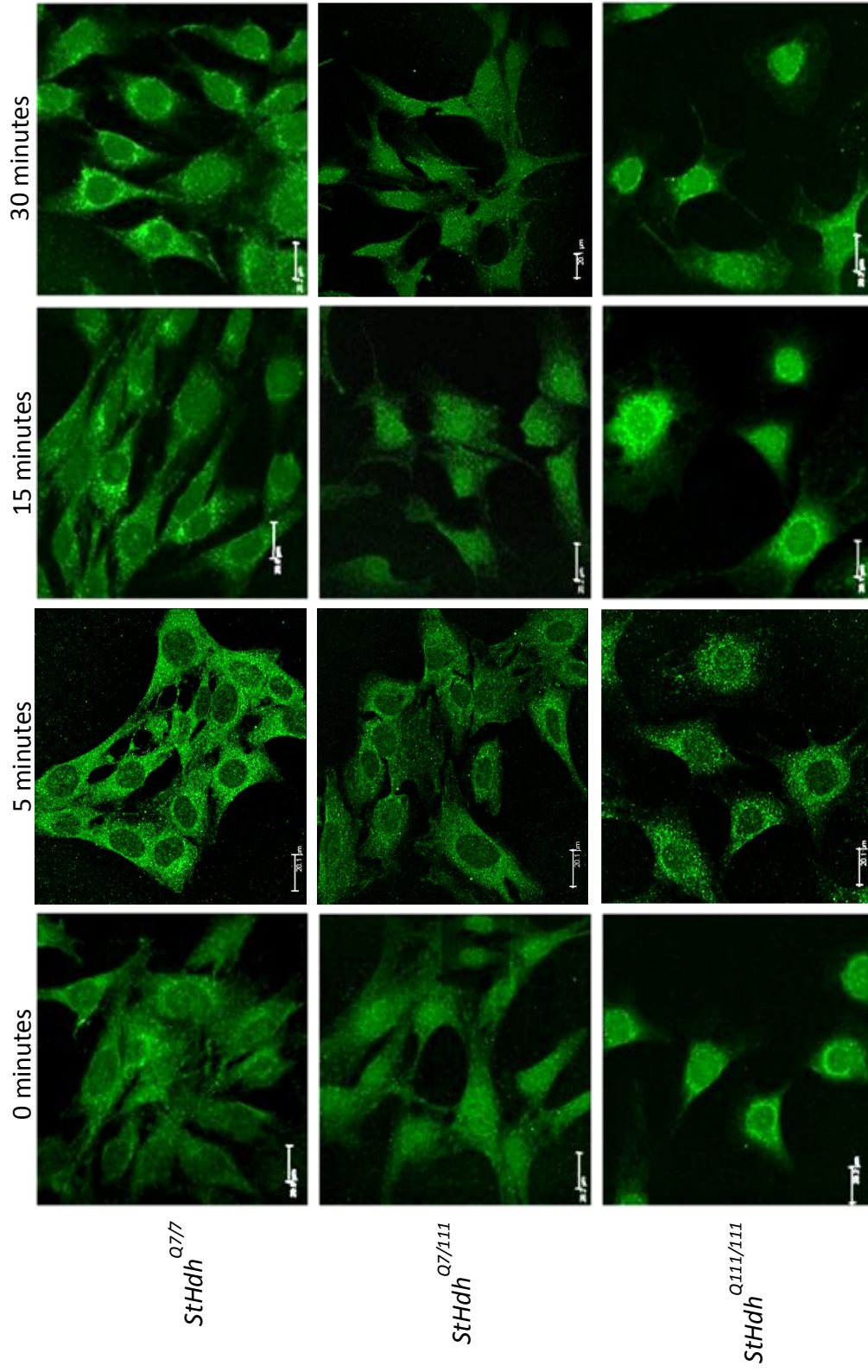
Figure 3.17 Subcellular localisation of an N-terminal epitope of HTT and mHTT in *StHdh*$^{Q7/7}$, *StHdh*$^{Q7/111}$ and *StHdh*$^{Q111/111}$ cell lines. Cells were fixed following 0, 5, 15 and 30 minutes of stimulation with 100ng/ml EGF, labelled with Mab2166 against amino acids 181-810 of HTT, then analysed by confocal microscopy (see Sections 2.2.1.8 and 2.2.1.9 for further details). Scale bar = 20µm
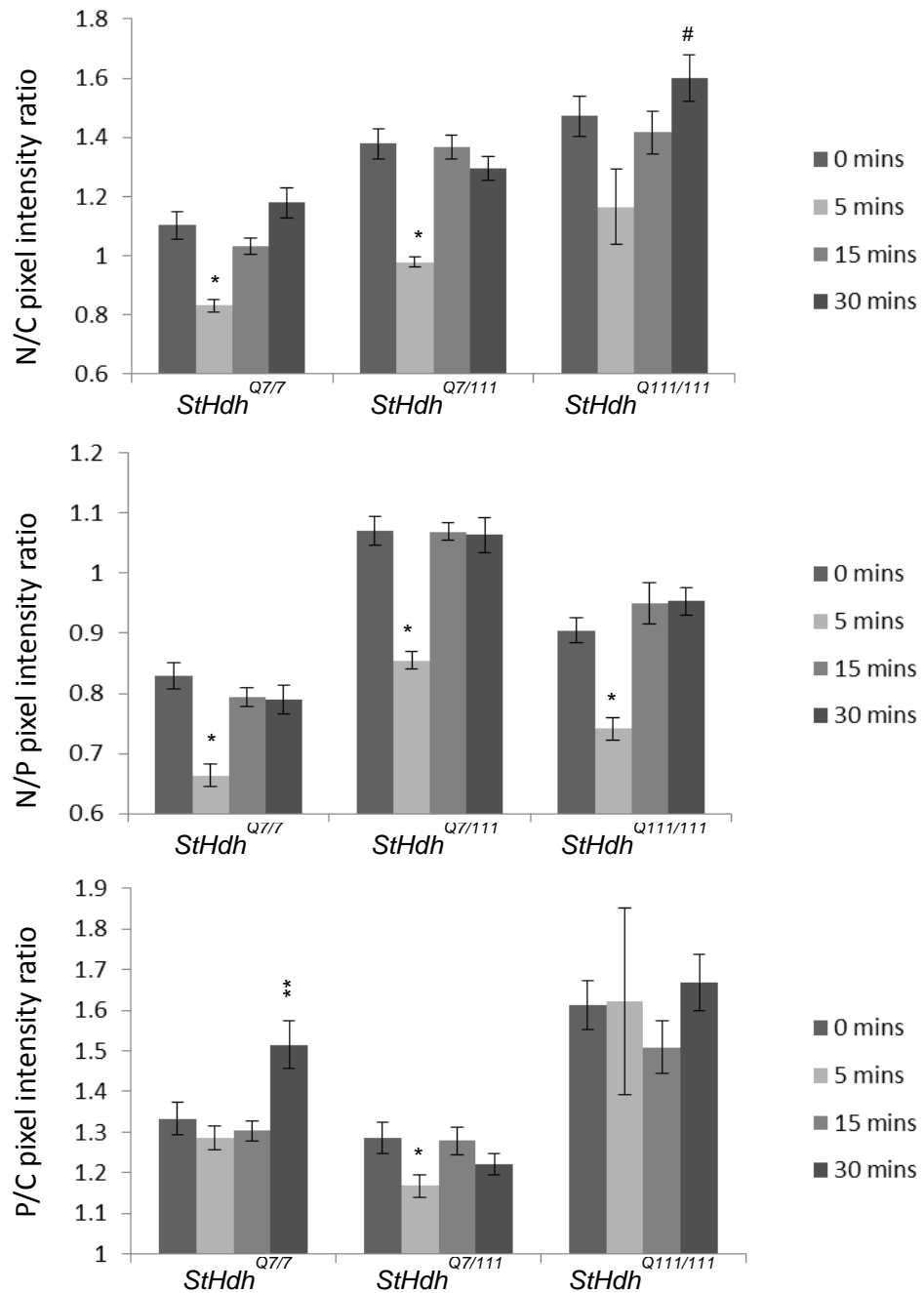
Figure 3.18 Quantitative analysis of immunofluorescence images in Figure 3.17. Nuclear/Cytoplasmic (N/C), Nuclear/Perinuclear (N/P) and Perinuclear/Cytoplasmic (P/C) mean pixel intensity ratios for $StHdh^{Q7/7}$, $StHdh^{Q7/111}$ and $StHdh^{Q111/111}$ cells following 0, 5, 15 and 30 minutes of stimulation with 100ng/ml EGF. Mean pixel intensities were calculated from confocal microscopy images using GNU Image Manipulator (further details of the analysis can be found in Section 2.2.1.10). All images were randomised and analysed blind to genotype and length of time stimulated with EGF. Each condition consisted of 9 confocal microscopy images taken from 3 separate coverslips. A two-way ANOVA was carried out for main effects analysis, followed by planned one way ANOVAs and post-hoc Tukey tests. Error bars = SEM.

* Denotes a significant difference from 0mins

# Denotes a significant difference from 5mins

* p<0.05   ** p<0.01   *** p<0.001

Antibody	BDNF			NGF			EGF		
	$StHdh^{Q7/7}$	$StHdh^{Q7/111}$	$StHdh^{Q111/111}$	$StHdh^{Q7/7}$	$StHdh^{Q7/111}$	$StHdh^{Q111/111}$	$StHdh^{Q7/7}$	$StHdh^{Q7/111}$	$StHdh^{Q111/111}$
Ab675	↓ 5 mins	↓ 5 mins	↓ 5 mins	↑ 5 mins	↑15 mins	↑ 15 mins	↓ 5 mins	↓ 5 mins	X
Mab2166	↓15 mins	↓15 mins	↑ 5 mins	↑15 mins	↑15 mins	↓ 15 mins	↓ 5 mins	↓ 5 mins	↓ 5 mins
Ab109115	-	-	-	-	-	-	↓15 mins	↓ 5 mins	X
N17	-	-	-	-	-	-	X	X	X

Table 3.1 A summary of the comparison of apparent HTT nuclear localisation in response to BDNF, NGF and EGF stimulation in $StHdh^{Q7/7}$, $StHdh^{Q7/111}$ and $StHdh^{Q111/111}$ cells as detected by a panel of N-terminal HTT antibodies. '↓' indicates a reduction in nuclear staining intensity and '↑' indicates an increase at the time point of growth factor stimulation that is stated. 'X' represents no change in HTT nuclear localisation at any time point.

3.3.6 Using subcellular fractionation to determine cellular localisation of HTT epitopes

In order to further investigate the subcellular localisation of HTT and mHTT, protein extraction and subcellular fractionation were performed following growth factor stimulation, and were followed by SDS-PAGE gel electrophoresis and western blotting (for further details, see Section 2.2.2.3). Nuclear fractions were confirmed by the presence of nuclear protein Lamin A/C, and cytoplasmic fractions were confirmed by the presence of MEK. In addition to Ab109115 and Mab2166, blots were also probed with MW1; a mouse monoclonal antibody that only detects mHTT. Ab675 and N17 were also used to visualise full length HTT on these blots, but due to limited antibody availability, these were not able to be replicated and quantified.

All five antibodies detected full length HTT and mHTT in both nuclear and cytoplasmic fractions (example blots and quantifications following BDNF and EGF stimulation can be found in Figures 3.19 - 3.21. The remaining blots can be found in Appendix III). Lysates from $StHdh^{Q111/111}$ cells showed fainter bands as compared to both $StHdh^{Q7/7}$ and $StHdh^{Q7/111}$ cell lysates when detected by the four N-terminal antibodies, Ab675, Ab109115, Mab2166 and N17. This may be partly due to a lower affinity of these antibodies to the mutant protein, as there was strong detection of mHTT when the blots were probed with MW1. However, the larger protein may fail to blot as efficiently as wild type HTT, or this may reflect a reduction in mHTT protein levels, as has been observed in other HD models (Gutekunst et al. 1995; Persichetti et al. 1996; J. Miller et al. 2010; Pouladi et al. 2010).

Following stimulation with any of the three growth factors, there was no change in the quantification of full length HTT or mHTT between nuclear and cytoplasmic fractions with any of the antibodies used for detection.
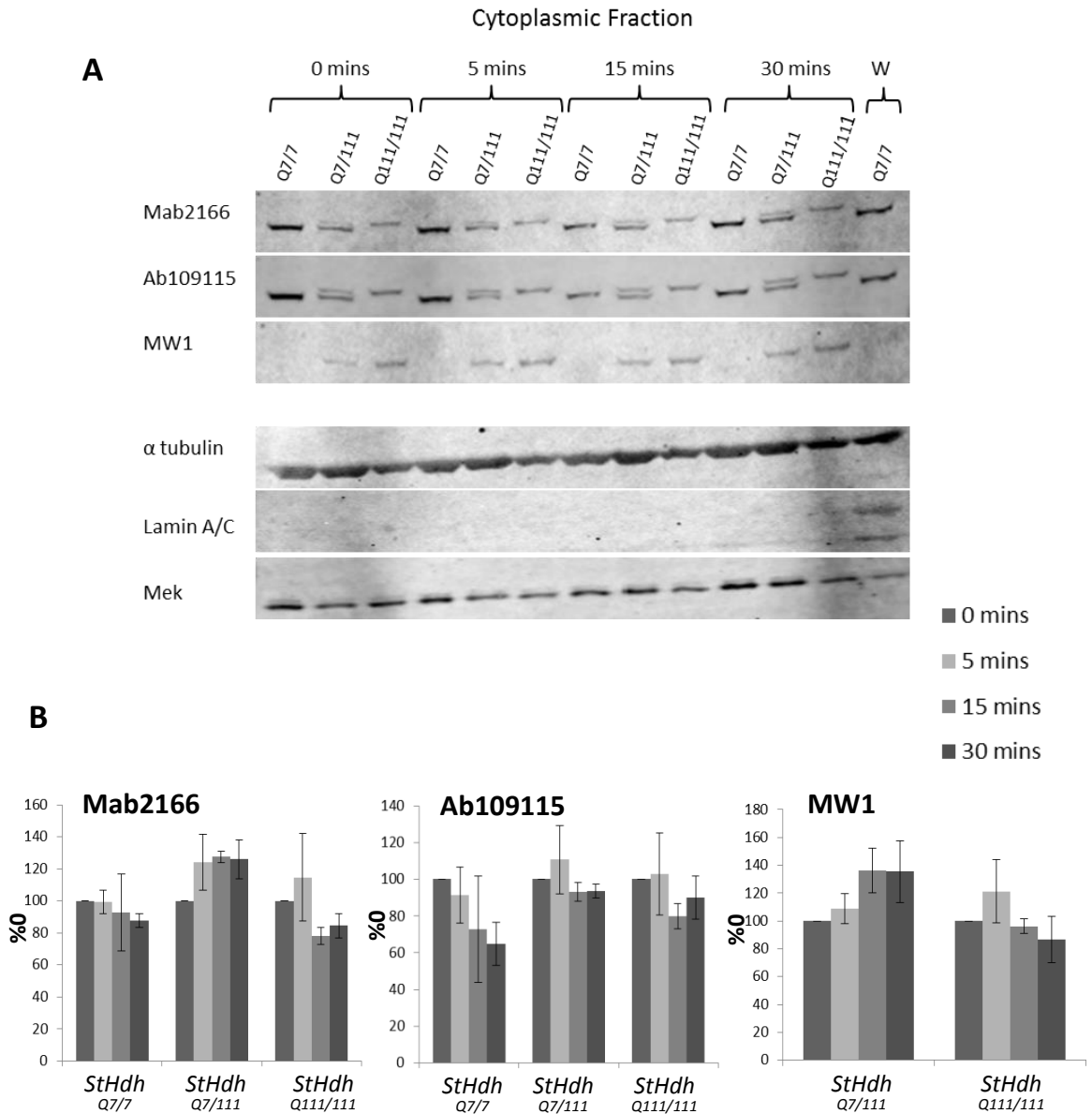
Figure 3.19 A. Western blots of cytoplasmic fractions of *StHdh*^{Q7/7}, *StHdh*^{Q7/111} and *StHdh*^{Q111/111} cells stimulated with 100ng/ml BDNF for 0, 5, 15 and 30 minutes before cell lysis and subcellular fractionation (see Section 2.2.2.3 for more details), and a whole cell lysate control (W). Blots were probed with Mab2166, stripped and re-probed with Ab109115, followed by MW1. Fractions were normalised to α-tubulin loading control, and purity of the fraction was assessed by the presence of cytoplasmic marker MEK (40kDa) and lack of the nuclear marker Lamin A/C (70-75kDa). **B.** Licor Odyssey quantification of fluorescence intensities (FI) in *A* normalised to the loading control, and expressed as a percentage of 0 mins BDNF stimulation (%0). Percentages were analysed by genotype individually using a one way ANOVA due to differences in band intensity between cell types, followed by post-hoc Tukey tests. (Error bars = SEM, n=3).
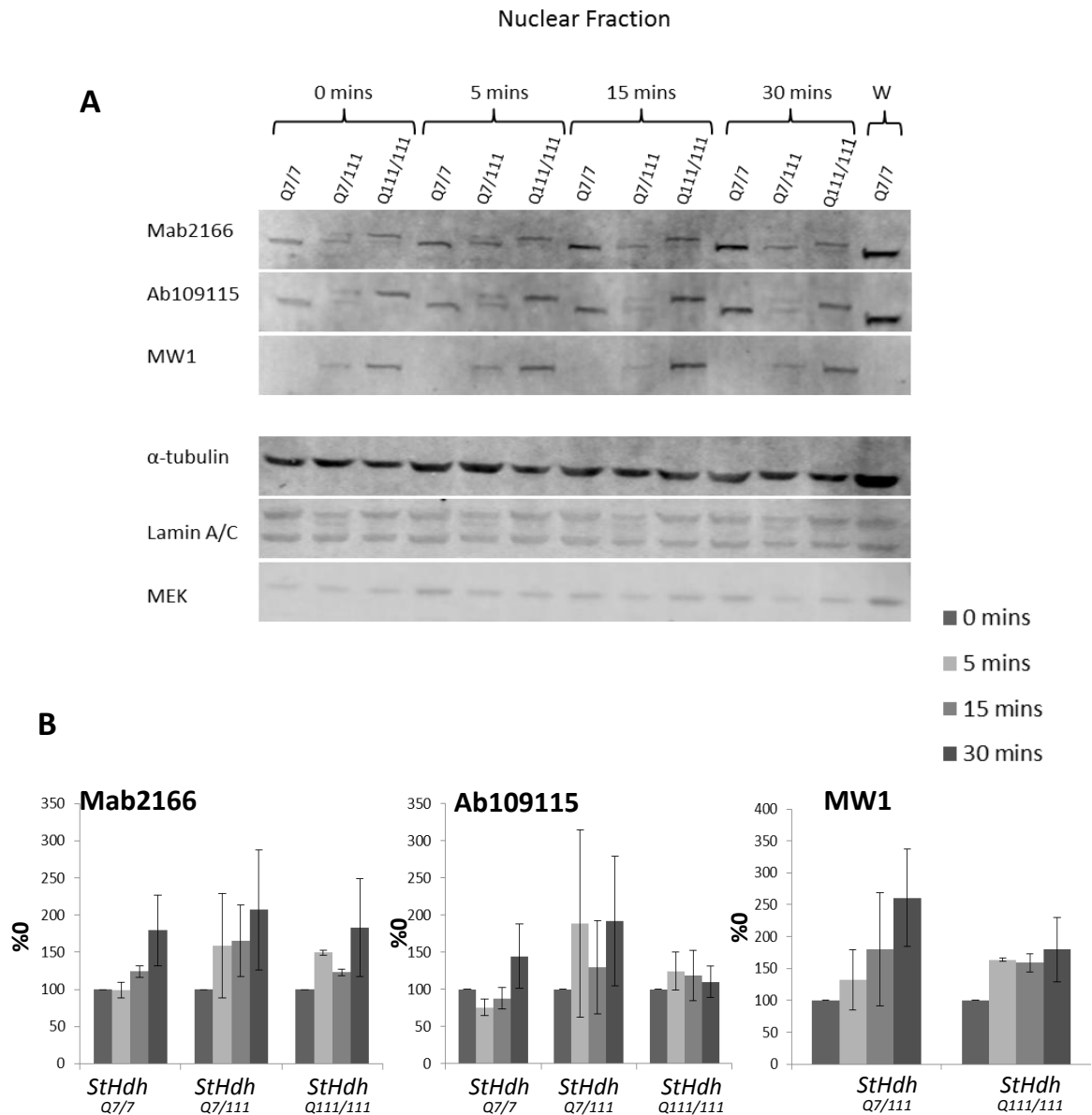
Figure 3.20 A. Western blots of nuclear fractions of *StHdh*$^{Q7/7}$, *StHdh*$^{Q7/111}$ and *StHdh*$^{Q111/111}$ cells stimulated with 100ng/ml BDNF for 0, 5, 15 and 30 minutes before cell lysis and subcellular fractionation (see Section 2.2.2.3 for more details), and a whole cell lysate control (W). Blots were probed with Mab2166, stripped and re-probed with Ab109115, followed by MW1. Fractions were normalised to α-tubulin loading control, and purity of the fraction was assessed by the presence of nuclear marker Lamin A/C (70-75kDa) and lack of the cytoplasmic marker MEK (40kDa). **B.** Licor Odyssey quantification of fluorescence intensities (FI) in *A* normalised to the loading control, and expressed as a percentage of 0 mins BDNF stimulation (%0). Percentages were analysed by genotype individually using a one way ANOVA due to differences in band intensity between cell types, followed by post-hoc Tukey tests (Error bars = SEM, n=3).
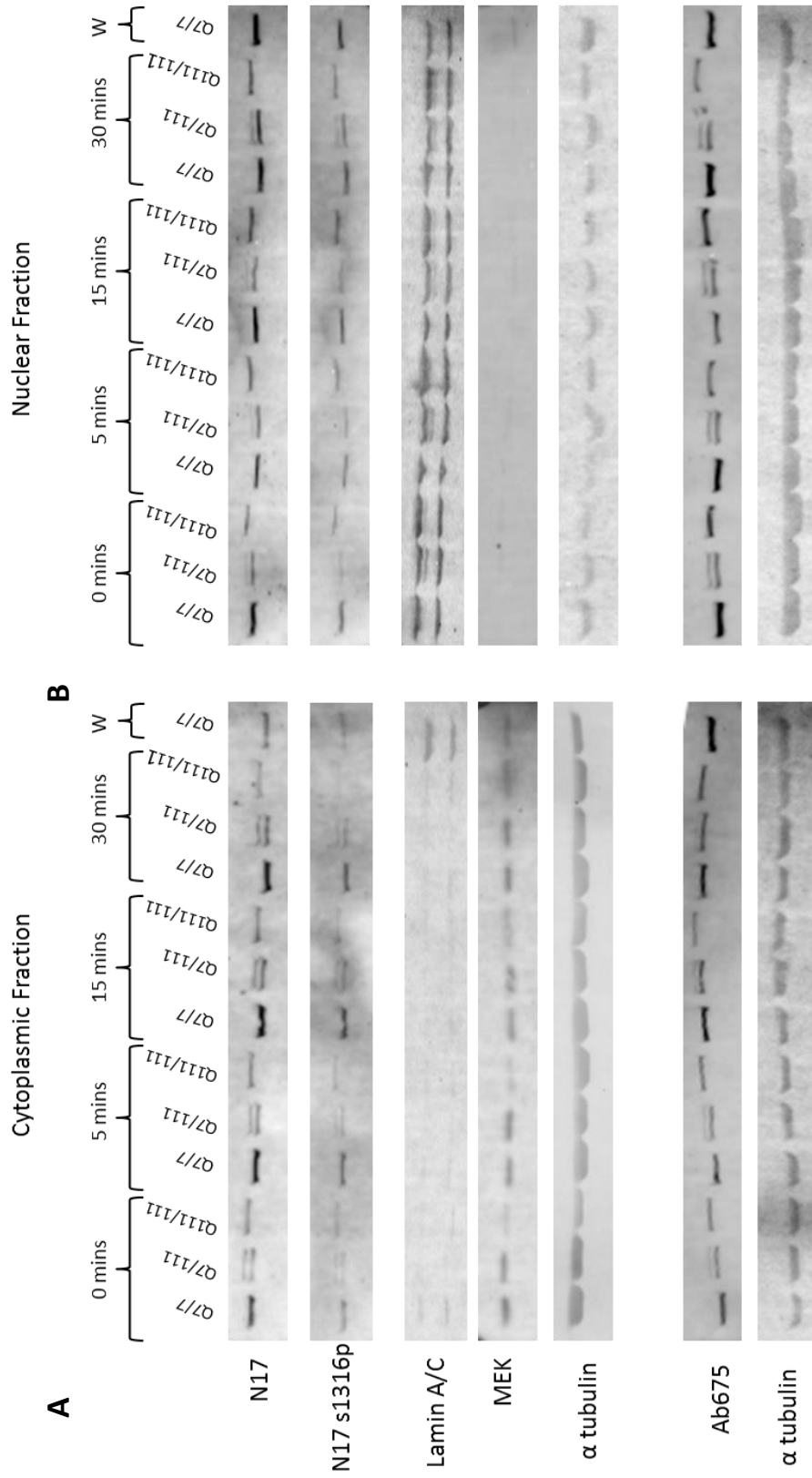
Figure 3.21 A. Western blots of cytoplasmic fractions of *StHdh*$^{Q7/7}$, *StHdh*$^{Q7/11}$ and *StHdh*$^{Q111/111}$ cells stimulated with 100ng/ml EGF for 0, 5, 15 and 30 minutes before cell lysis and subcellular fractionation (see Section 2.2.2.3 for more details), and a whole cell lysate control (W). Blots were probed with N17, stripped and re-probed with N17 s1316p. Fractions were normalised to α-tubulin loading control, and purity of the fraction was assessed by the presence of cytoplasmic marker MEK and lack of the nuclear marker Lamin A/C. A separate blot using the same lysates was probed with Ab675. **B**. Nuclear fractions treated as described in *A*. Nuclear fractions were assessed by the presence of nuclear marker Lamin A/C and a lack of cytoplasmic marker MEK.

3.4 The localisation of phosphorylated HTT in response to growth factor stimulation

Anti-S13p and Anti-S1316p were both kind gifts from Joan Steffan (University of California, Irvine, USA), and were raised against the first 17 amino acids of HTT, including phosphorylation on either serine 13 (Anti-S13p) or both serines 13 and 16 (Anti-S1316p). A similar antibody, N17 s1316p, which was raised in Ray Truant's laboratory against the same immunogen, was also utilised to support the changes in the localisation of the double phosphorylated epitope of HTT identified with the Anti-S1316p antibody following EGF stimulation.

3.4.1 Immunostaining with anti-phosphorylated S13 antibody

3.4.1.1 BDNF stimulation

HTT phosphorylated on S13 is detected predominantly in the cytoplasm of $StHdh^{Q7/7}$ cells, although there is denser accumulation around the perinucleus (Figures 3.22 & 3.23). With increasing mHTT load, there is a higher nuclear presence of phosphorylated HTT, and stronger staining of perinuclear regions. Contrary to previous reports that mHTT is hypophosphorylated in these cells (Atwal et al. 2011), there is no indication of reduced S13 phosphorylation in this case.

Following BDNF stimulation, there is a significant effect of cell type in the N/C ratio ($F_{(2, 681)} = 16.28$, $p<0.001$) and of time stimulated ($F_{(3, 681)} = 72.38$, $p<0.001$), as well as a significant interaction between the two ($F_{(6, 681)} = 6.69$, $p<0.001$). Simple main effects analysis shows that significant changes in the N/C ratio are at 5 minutes ($p<0.001$) and 30 minutes ($p<0.001$) of BDNF stimulation, and that localisation of phosphorylated S13 HTT in $StHdh^{Q7/7}$ cells differs significantly from $StHdh^{Q111/111}$ cells ($p<0.001$), but not $StHdh^{Q7/111}$ cells ($p=0.089$). Post-hoc analysis of the N/C ratio shows that BDNF stimulation led to a nuclear increase of phosphorylated S13 HTT in $StHdh^{Q7/7}$ and $StHdh^{Q111/111}$ cell lines. This occurred twice; once at 5 minutes (both $p<0.001$), and again at 30 minutes (both $p<0.001$), however there was a significant decrease in the N/C ratio at 15 minutes of stimulation in the $StHdh^{Q7/111}$ cell lines ($p<0.001$). The effect seen in the N/C ratio is mirrored in the N/P ratio. However, although there is a

significant effect of cell type in the P/C ratio (F (2, 681) = 24.58, p<0.001), there is no effect of BDNF stimulation (F (3, 681) = 2.28, p=0.078).

3.4.1.2 NGF stimulation

There was a significant effect of cell type (F (2, 755) = 97.75, p<0.001) and of NGF stimulation (F (3, 755) = 21.66, p<0.001) on the N/C ratio of HTT and mHTT phosphorylated on S13 (Figures 3.24 & 3.25), as well as a significant interaction between the two (F (6, 755) = 3.03, p=0.006). Tukey HSD tests show that there was a significant reduction in the N/C ratio at 15 minutes for $StHdh^{Q7/7}$ cells (p<0.001). In $StHdh^{Q7/111}$ cells, however, there was a significant increase in the N/C ratio at 5 minutes of stimulation (p<0.001), which was followed by a return to baseline. There was no significant effect of NGF stimulation on the N/C ratio of $StHdh^{Q111/111}$ cells. The N/P ratio of $StHdh^{Q7/7}$ cells mirrors the effect seen in the N/C ratio; there is a reduction at 5 minutes (p=0.018), which is persistent for the full 30 minutes of stimulation (15 and 30 minutes, p<0.001). This effect is also seen in the N/P ratio for $StHdh^{Q111/111}$ cells, although the reduction becomes significant at 15 minutes (P=0.001). Again, there is a significant increase in this ratio for the $StHdh^{Q7/111}$ cells, which is significant at 30 minutes (p=0.038). Despite a significant main effect of cell type (F (2, 755) = 73.31, p<0.001) and NGF stimulation (F (3, 755) = 5.18, p=0.002) in the P/C ratio, there is only a small significant increase in the P/C ratio for $StHdh^{Q7/7}$ cells at 5 minutes (p=0.029), but no other significant post-hoc effects. To summarise, NGF stimulation appears to elicit a movement of nuclear S13 phosphorylated epitopes of HTT in $StHdh^{Q7/7}$ and $StHdh^{Q111/111}$ cells to the perinuclear region. Interestingly, it prompts a nuclear increase of this HTT epitope in $StHdh^{Q7/111}$ cells, although the effect remains primarily between the nuclear and perinuclear areas.
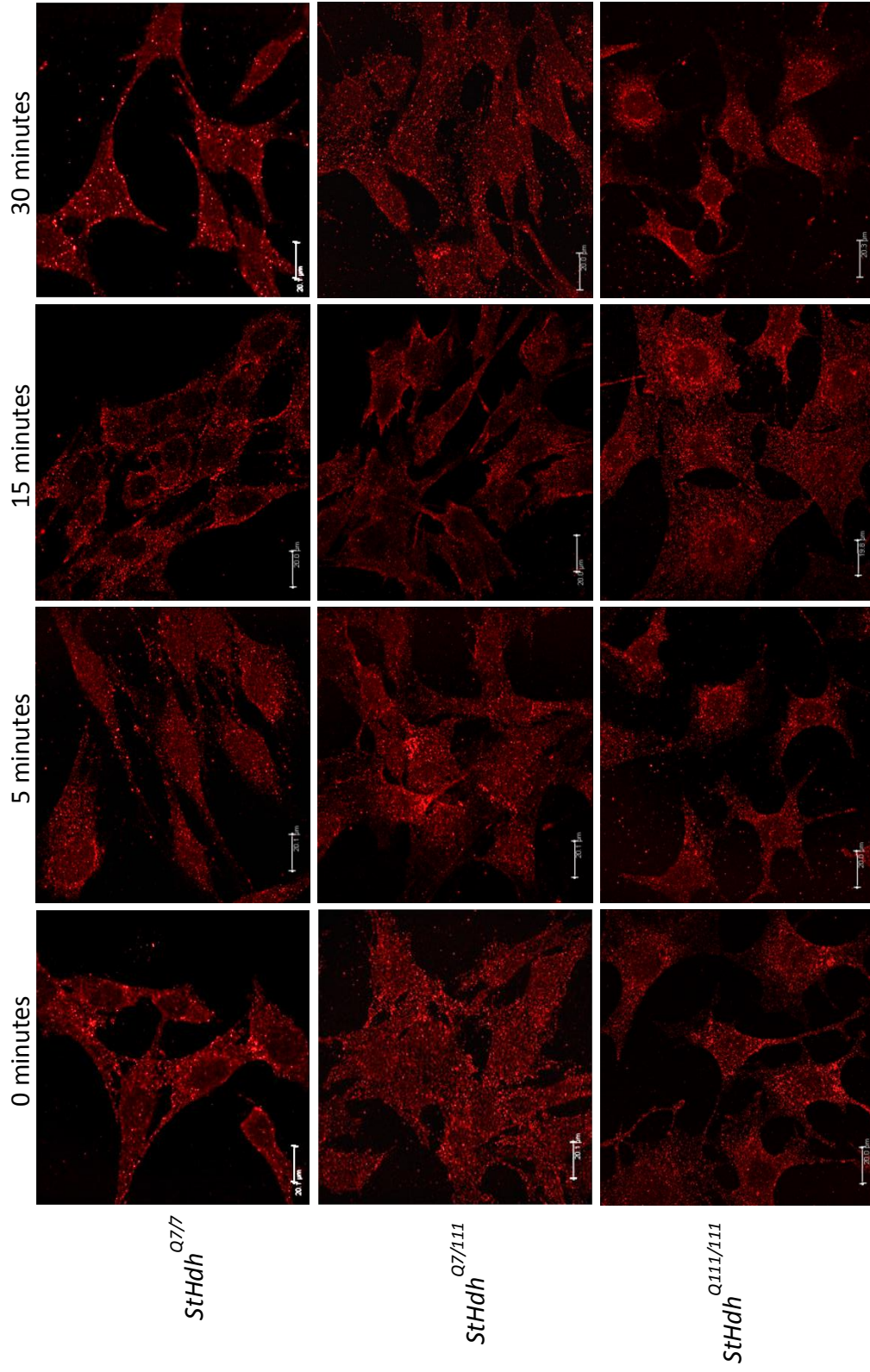
Figure 3.22 Subcellular localisation of an N-terminal epitope of HTT and mHTT phosphorylated on serine 13 in *StHdh*^Q7/7^, *StHdh*^Q7/11^ and *StHdh*^Q111/111^ cell lines. Cells were fixed following 0, 5, 15 and 30 minutes of stimulation with 100ng/ml BDNF, labelled with Anti-S13p, then analysed by confocal microscopy (see Sections 2.2.1.8 and 2.2.1.9 for further details). Scale bar = 20μm
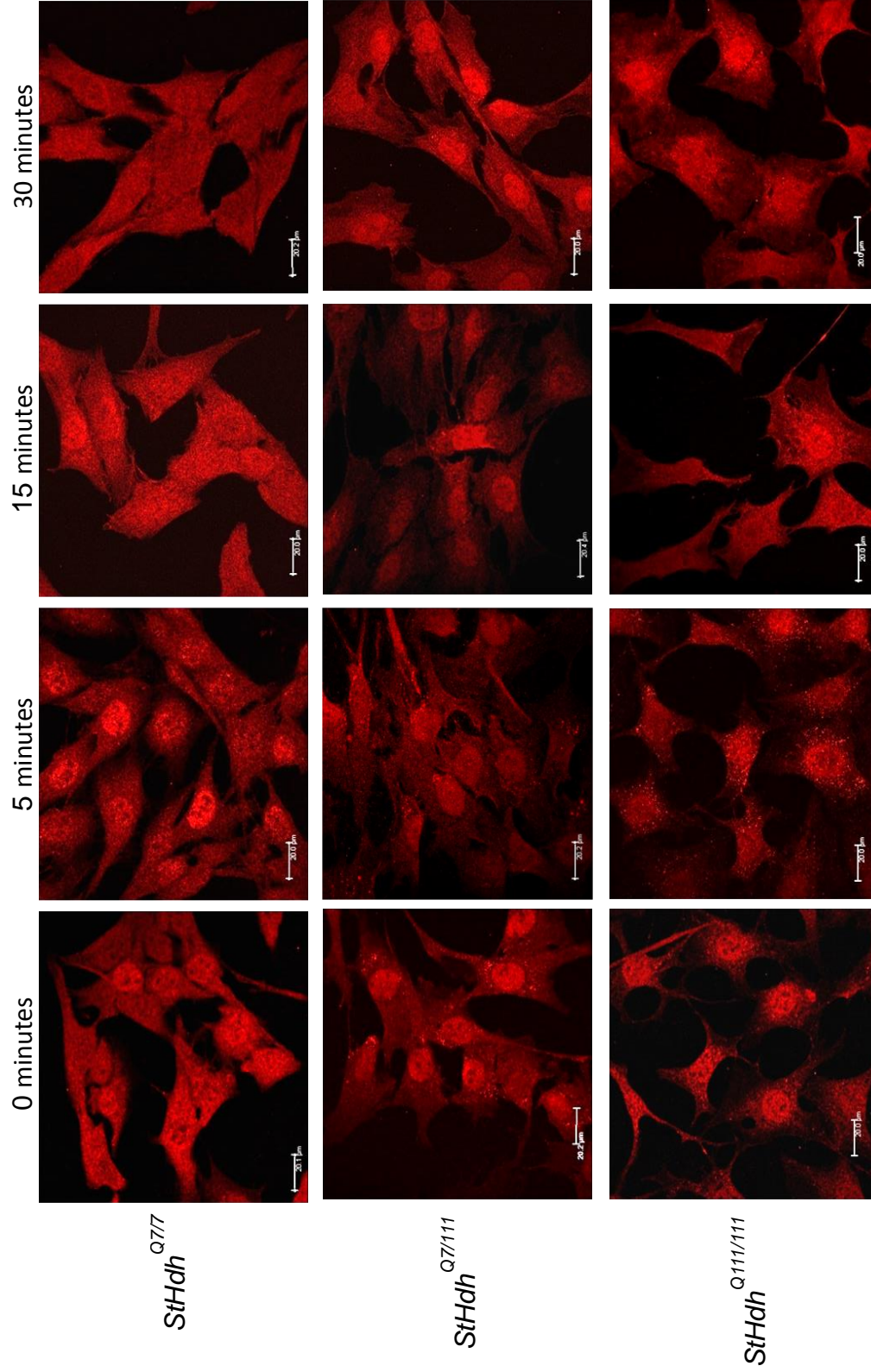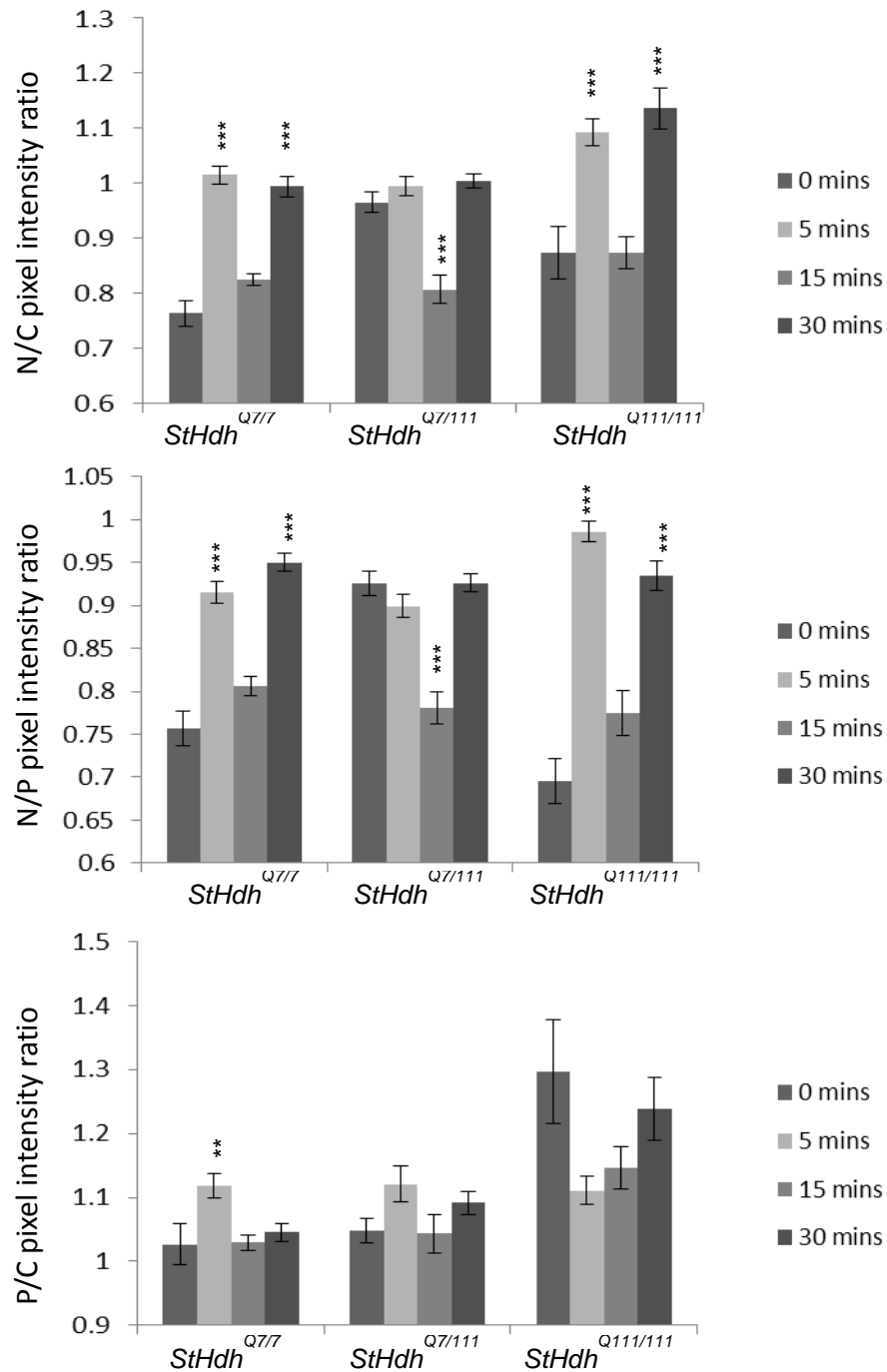
Figure 3.23 Quantitative analysis of immunofluorescence images in Figure 3.22. Nuclear/Cytoplasmic (N/C), Nuclear/Perinuclear (N/P) and Perinuclear/Cytoplasmic (P/C) mean pixel intensity ratios for $StHdh^{Q7/7}$, $StHdh^{Q7/111}$ and $StHdh^{Q111/111}$ cells following 0, 5, 15 and 30 minutes of stimulation with 100ng/ml BDNF. Mean pixel intensities were calculated from confocal microscopy images using GNU Image Manipulator (further details of the analysis can be found in Section 2.2.1.10). All images were randomised and analysed blind to genotype and length of time stimulated with BDNF. Each condition consisted of 9 confocal microscopy images taken from 3 separate coverslips. A two-way ANOVA was carried out for main effects analysis, followed by planned one way ANOVAs and post-hoc Tukey tests. Error bars = SEM

* p<0.05   ** p<0.01   *** p<0.001

Figure 3.24 Subcellular localisation of an N-terminal epitope of HTT and mHTT phosphorylated on serine 13 in *StHdh*^Q7/7^, *StHdh*^Q7/11^ and *StHdh*^Q111/111^ cell lines. Cells were fixed following 0, 5, 15 and 30 minutes of stimulation with 100ng/ml NGF, labelled with Anti-S13p, then analysed by confocal microscopy (see Sections 2.2.1.8 and 2.2.1.9 for further details). Scale bar = 20µm
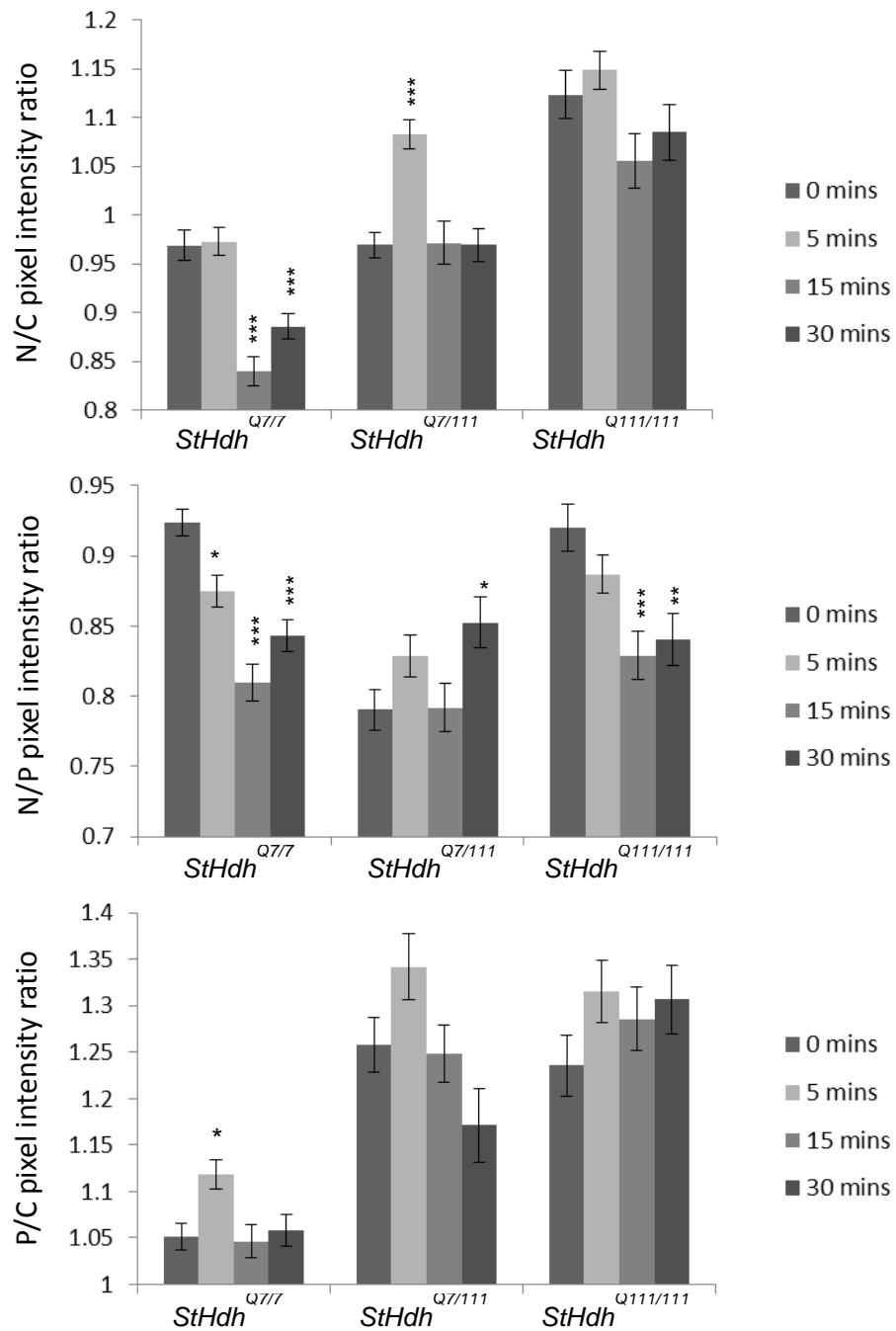
Figure 3.25 Quantitative analysis of immunofluorescence images in Figure 3.24. Nuclear/Cytoplasmic (N/C), Nuclear/Perinuclear (N/P) and Perinuclear/Cytoplasmic (P/C) mean pixel intensity ratios for $StHdh^{Q7/7}$, $StHdh^{Q7/111}$ and $StHdh^{Q111/111}$ cells following 0, 5, 15 and 30 minutes of stimulation with 100ng/ml NGF. Mean pixel intensities were calculated from confocal microscopy images using GNU Image Manipulator (further details of the analysis can be found in Section 2.2.1.10). All images were randomised and analysed blind to genotype and length of time stimulated with NGF. Each condition consisted of 9 confocal microscopy images taken from 3 separate coverslips. A two-way ANOVA was carried out for main effects analysis, followed by planned one way ANOVAs and post-hoc Tukey tests. Error bars = SEM.

* p<0.05   ** p<0.01   *** p<0.001

3.4.1.3 EGF stimulation

There was again a significant main effect of cell type in the N/C ratio ($F_{(2, 673)} = 9.08$, $p < 0.001$), but there was not a significant effect of time of EGF stimulation ($F_{(3, 673)} = 2.42$, $p = 0.065$) (Figures 3.26 & 3.27). However, there was a significant interaction between the two ($F_{(6, 673)} = 7.38$), $p < 0.001$). Simple main effects analysis showed that significant differences in the N/C ratio lay between the *StHdh*$^{Q7/7}$ and *StHdh*$^{Q111/111}$ cells ($p < 0.001$) rather than the *StHdh*$^{Q7/111}$ cells ($p = 0.944$). Tukey HSD post-hoc tests reveal that there is a significant reduction in the N/C ratio in both *StHdh*$^{Q7/7}$ and *StHdh*$^{Q7/111}$ cells, which is significant at 5 minutes ($p < 0.001$) and at 15 minutes ($p < 0.001$), respectively, suggesting a reduction of S13 phosphorylated HTT epitopes in the nucleus. In contrast, there is a significant increase in the N/C ratio in *StHdh*$^{Q111/111}$ cells at 15 minutes of EGF stimulation ($p = 0.008$). The increase in nuclear staining for S13 phosphorylated mHTT in these cells appears in discrete foci in some of these cells rather than in the diffuse pattern previously seen. Analysis of the N/P ratio shows that there was no effect of cell type ($F_{(2, 673)} = 1.36$, $p = 0.258$), but there was a significant effect of EGF stimulation over time ($F_{(3, 673)} = 11.08$, $p < 0.001$), and a significant interaction between the two ($F_{(6, 673)} = 10.62$, $p < 0.001$). Post-hoc analysis shows that there is no significant difference from baseline in *StHdh*$^{Q7/7}$ cells in this ratio, but both the *StHdh*$^{Q7/111}$ and *StHdh*$^{Q111/111}$ cells show a significant increase following 5 minutes of EGF stimulation (*StHdh*$^{Q7/111}$ $p < 0.000$, *StHdh*$^{Q111/111}$ $p < 0.031$), which was followed by a significant reduction in the N/P ratio below baseline by 15 minutes in *StHdh*$^{Q7/111}$ cells ($p = 0.002$). The P/C ratio for both *StHdh*$^{Q7/7}$ and *StHdh*$^{Q111/111}$ cell lines reflect the pattern of nuclear and perinuclear S13 phosphorylated HTT and mHTT observed in the N/C and N/P ratios, although there are no significant effects in the *StHdh*$^{Q7/111}$ cells.
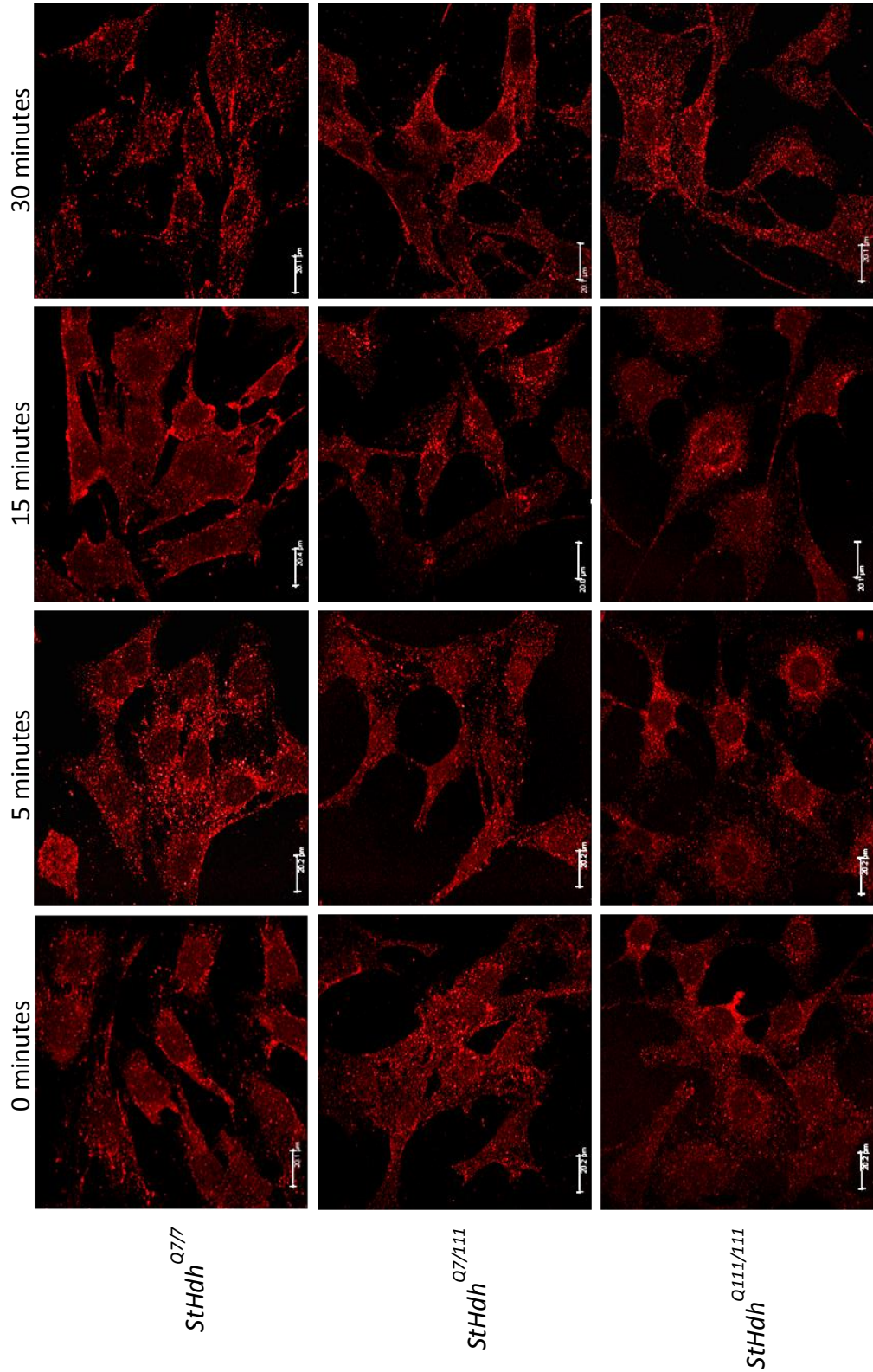
Figure 3.26 Subcellular localisation of an N-terminal epitope of HTT and mHTT phosphorylated on serine 13 in *StHdh*$^{Q7/7}$, *StHdh*$^{Q7/111}$ and *StHdh*$^{Q111/111}$ cell lines. Cells were fixed following 0, 5, 15 and 30 minutes of stimulation with 100ng/ml EGF, labelled with Anti-S13p, then analysed by confocal microscopy (see Sections 2.2.1.8 and 2.2.1.9 for further details). Scale bar = 20µm
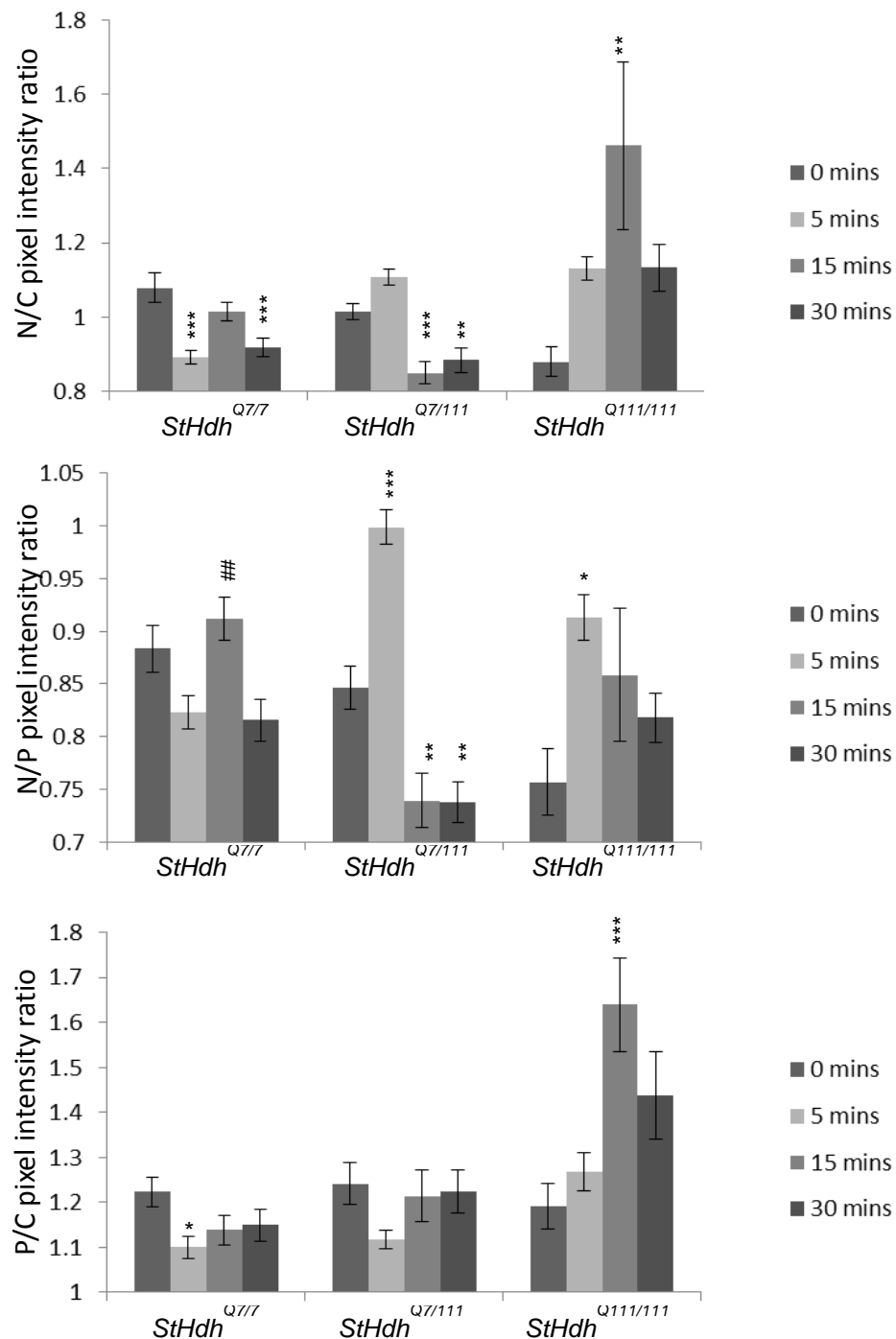
Figure 3.27 Quantitative analysis of immunofluorescence images in Figure 3.26. Nuclear/Cytoplasmic (N/C), Nuclear/Perinuclear (N/P) and Perinuclear/Cytoplasmic (P/C) mean pixel intensity ratios for $StHdh^{Q7/7}$, $StHdh^{Q7/111}$ and $StHdh^{Q111/111}$ cells following 0, 5, 15 and 30 minutes of stimulation with 100ng/ml EGF. Mean pixel intensities were calculated from confocal microscopy images using GNU Image Manipulator (further details of the analysis can be found in Section 2.2.1.10). All images were randomised and analysed blind to genotype and length of time stimulated with EGF. Each condition consisted of 9 confocal microscopy images taken from 3 separate coverslips. A two-way ANOVA was carried out for main effects analysis, followed by planned one way ANOVAs and post-hoc Tukey tests. Error bars = SEM. * Denotes a significant difference from 0mins, # Denotes a significant difference from 5mins. * $p<0.05$ ** $p<0.01$ *** $p<0.001$

3.4.2 Immunostaining with anti-phosphorylated s1316 antibody

3.4.2.1 BDNF stimulation

Similar to previously observed patterns of localisation in this chapter, the epitope of HTT detected by the anti-phosphorylated s1316p antibody was more nuclear with increased mutant HTT load (Figures 3.28 & 3.29). This is reflected in the significant main effects of cell type found for the N/C (F (2, 661) = 9409.292, p<0.001), N/P (F (2, 661) = 43.22, p<0.001) and P/C ratios (F (2, 661) = 27.84, p<0.001). For the N/C and P/C ratios, there were significant simple main effects between all three genotypes (p<0.01), however for the N/P ratio, there was a significant difference between *StHdh*$^{Q7/7}$ cells and both *StHdh*$^{Q7/111}$ (p<0.001) and *StHdh*$^{Q111/111}$ cells (p<0.001), but there was no difference between the *StHdh*$^{Q7/111}$ and *StHdh*$^{Q111/111}$ lines (p>0.05). This suggests that when mHTT is present, there is mislocalisation of phosphorylated mHTT to nuclear and perinuclear areas, regardless of the extent of mHTT load.

There was no significant effect of BDNF stimulation in the N/C ratio (p=0.08) or in the P/C ratio (p=0.333) across all three genotypes, and post-hoc analyses of the genotypes individually support this finding (p>0.05 in all cases). There was, however, a significant effect of BDNF in the N/P ratio (F (3, 661) = 7.04, p<0.001); simple main effects analysis indicated that this was due to a reduction in this epitope of HTT in the nucleus and a perinuclear increase after 30 minutes of stimulation (p<0.05). Post-hoc analysis reveals that this is due to a significant reduction in nuclear phosphorylated HTT at 30 minutes in the *StHdh*$^{Q7/7}$ (p<0.001) and *StHdh*$^{Q7/111}$ (p<0.01) cells only; there was no effect of BDNF stimulation in *StHdh*$^{Q111/111}$ cells (p=0.286). Similar to the HTT epitope phosphorylated on S13 alone, there was an increase in the nuclear presence of the double phosphorylated epitope at 5 minutes in both *StHdh*$^{Q7/7}$ and *StHdh*$^{Q7/111}$ cells, although this does not reach significance, and does not appear again at 30 minutes. The localisation of this epitope of HTT following BDNF stimulation shows a slightly delayed pattern to the non-phosphorylated epitopes; previously it was observed that there was a reduction in nuclear HTT at 15 minutes (Sections 3.3.3.1 & 3.3.4.1), but in this case the reduction is only apparent at 30 minutes.
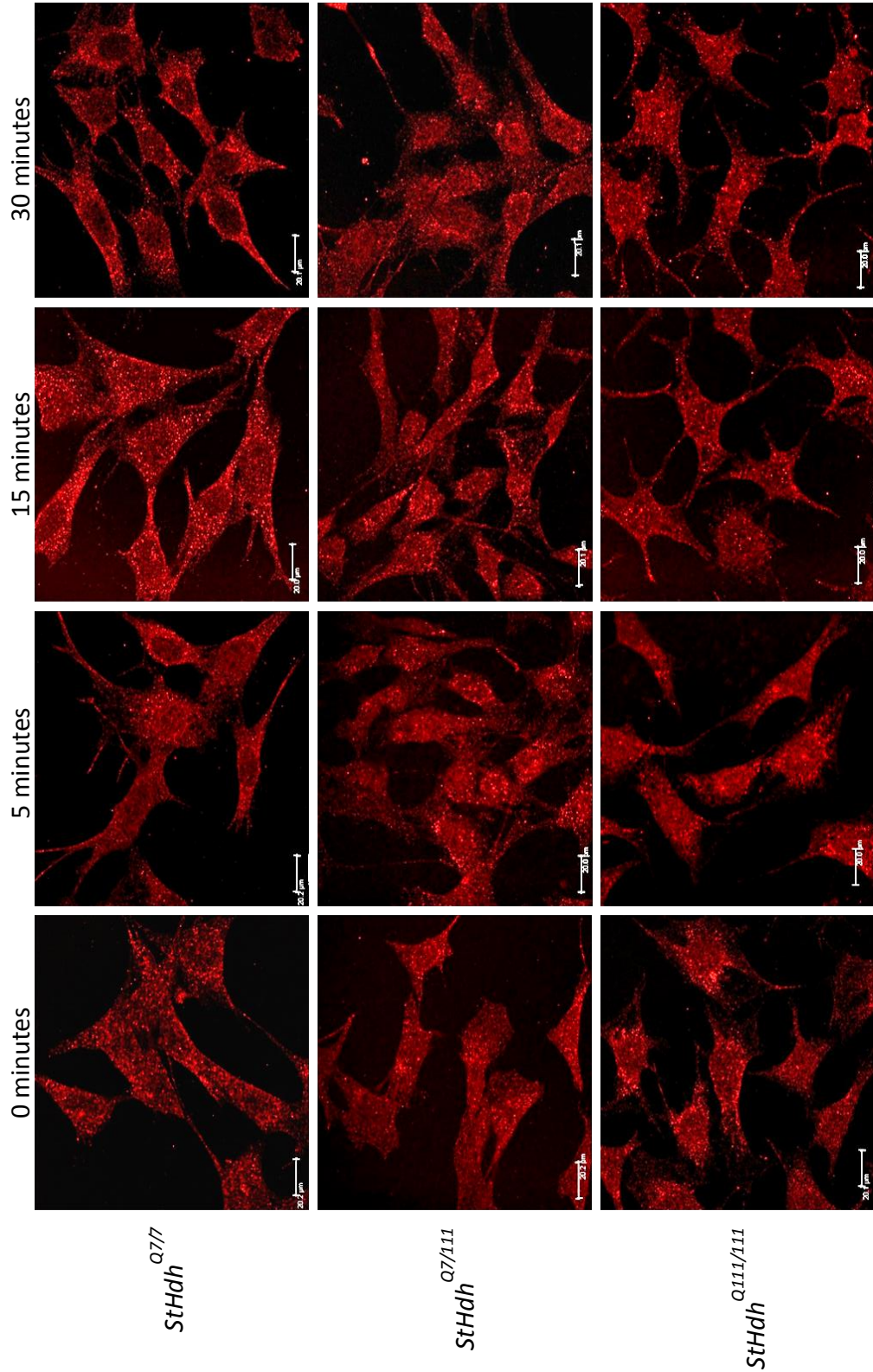
Figure 3.28 Subcellular localisation of an N-terminal epitope of HTT and mHTT phosphorylated on serines 13 and 16 in $StHdh^{Q7/7}$, $StHdh^{Q7/11}$ and $StHdh^{Q111/111}$ cell lines. Cells were fixed following 0, 5, 15 and 30 minutes of stimulation with 100ng/ml BDNF, labelled with Anti-S1316p, then analysed by confocal microscopy (see Sections 2.2.1.8 and 2.2.1.9 for further details). Scale bar = 20µm

131
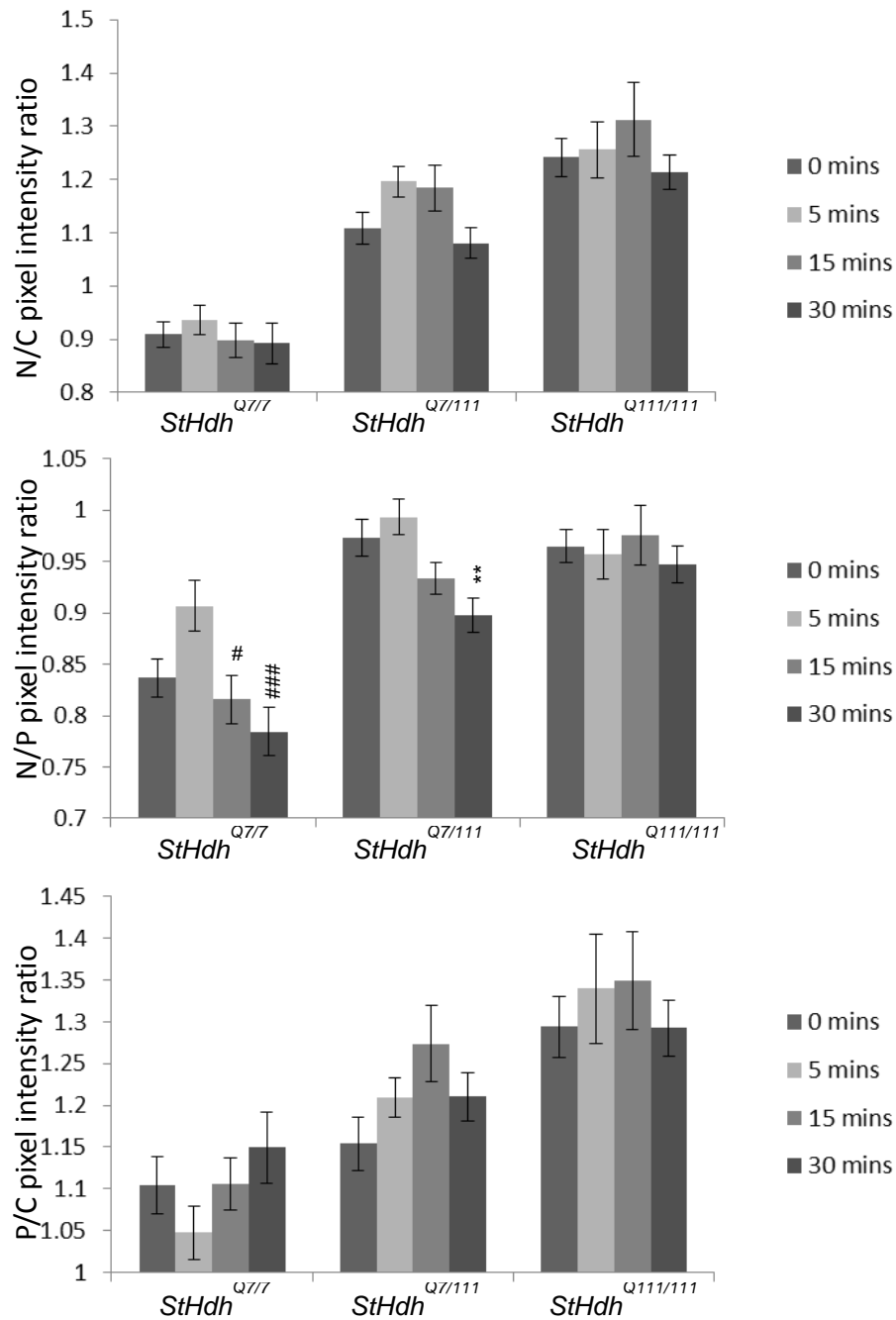
Figure 3.29 Quantitative analysis of immunofluorescence images in Figure 3.28. Nuclear/Cytoplasmic (N/C), Nuclear/Perinuclear (N/P) and Perinuclear/Cytoplasmic (P/C) mean pixel intensity ratios for $StHdh^{Q7/7}$, $StHdh^{Q7/111}$ and $StHdh^{Q111/111}$ cells following 0, 5, 15 and 30 minutes of stimulation with 100ng/ml BDNF. Mean pixel intensities were calculated from confocal microscopy images using GNU Image Manipulator (further details of the analysis can be found in Section 2.2.1.10). All images were randomised and analysed blind to genotype and length of time stimulated with BDNF. Each condition consisted of 9 confocal microscopy images taken from 3 separate coverslips. A two-way ANOVA was carried out for main effects analysis, followed by planned one way ANOVAs and post-hoc Tukey tests. Error bars = SEM

* Denotes a significant difference from 0mins
# Denotes a significant difference from 5mins
* p<0.05   ** p<0.01   *** p<0.001

3.4.2.2 NGF stimulation

There was again a significant main effect of genotype in the N/C (F (3,655) = 27, p<0.001), N/P (F (3, 655) = 15.69, p<0.001) and P/C ratios (F (3, 655) = 10.75, p<0.001), as well as a significant effect of time of NGF stimulation for all three ratios (p<0.003). Similar to the findings following BDNF stimulation, simple main effects analysis showed significant differences between *StHdh*$^{Q7/7}$ cells and both *StHdh*$^{Q7/111}$ and *StHdh*$^{Q111/111}$ cells (p<0.002) for all three ratios, but no significant differences in localisation of the double phosphorylated HTT epitope were found between *StHdh*$^{Q7/111}$ and *StHdh*$^{Q111/111}$ cells (Figures 3.30 & 3.31). In all three ratios, there was also a significant interaction between genotype and time of NGF stimulation (N/C p=0.027, N/P p=0.028, P/C p=0.018).

Post hoc analyses reveal that in *StHdh*$^{Q7/7}$ cells following NGF stimulation, there is an increase in the perinuclear localisation of the double phosphorylated epitope of HTT at 15 minutes, which is reflected in the N/P ratio (p=0.006). There is also a reduction in the N/C ratio at 15 minutes, as well as an increase in the P/C ratio from 5 minutes of stimulation, suggesting movement out of the nucleus into a perinuclear ring, although these don't reach significance due to larger variability than was seen in the N/P ratio. By 30 minutes, the localisation of this epitope had returned to baseline. This is the same pattern that was observed with the single phospho-S13 epitope, although the nuclear reduction persisted up to 30 minutes (Section 3.4.1.2). Double phosphorylation of both S13 and S16 may therefore be more variable and transitory in response to NGF stimulation compared to the phosphorylation of S13 alone.

StHdh$^{Q7/111}$ cells, although exhibiting a significantly different phospho-S13S16 HTT localisation to *StHdh*$^{Q7/7}$ cells, show a similar response to NGF. There is a significant reduction in the N/P ratio at 15 minutes (p=0.001) in these cells, as well as a reduction in the N/C ratio at the same time point, which is significantly lower than at 5 minutes of NGF stimulation (p=0.024). However, both ratios remain consistently higher than in *StHdh*$^{Q7/7}$ cells, reflecting the increased nuclear and perinuclear localisation of previously investigated HTT epitopes in the presence of mHTT. There is an unexpected increase in the P/C ratio in *StHdh*$^{Q7/111}$ cells at 30 minutes (p=0.004), and the N/P ratio

does not quite return to baseline by this time point as it did in *StHdh*$^{Q7/7}$ cells. It is therefore possible that although there is the same pattern of response to NGF in *StHdh*$^{Q7/111}$ cells as in wild type cells, the increased perinuclear localisation of this phosphorylated epitope is more persistent. This pattern is quite different to the effect seen with the single phospho-S13 antibody, which had a significant nuclear increase at 5 minutes in these cells (Section 3.4.1.2). This may be due to the phosphorylation of S13 occurring prior to the phosphorylation of S16 (Thompson 2009); the latter event promoting perinuclear, rather than nuclear, localisation of this epitope.

Perhaps surprisingly, *StHdh*$^{Q111/111}$ cells show a similar response to NGF stimulation in both the N/C and N/P ratios. In both cases, there is a significant nuclear reduction at 15 minutes of stimulation (p<0.001), although similar to the effect seen in *StHdh*$^{Q7/111}$ cells, this effect is persistent for up to 30 minutes in the N/P ratio (p=0.001), suggesting a reduced capacity for mHTT to return to its baseline localisation. There is also an increase in the P/C ratio at 30 minutes that supports increased perinuclear localisation of this epitope, although this is only significantly different from 5 minutes of NGF stimulation (p=0.012). This is the same pattern that was observed with the single phospho-S13 antibody, which suggests that the localisation of both phosphorylated epitopes is very similar following NGF stimulation
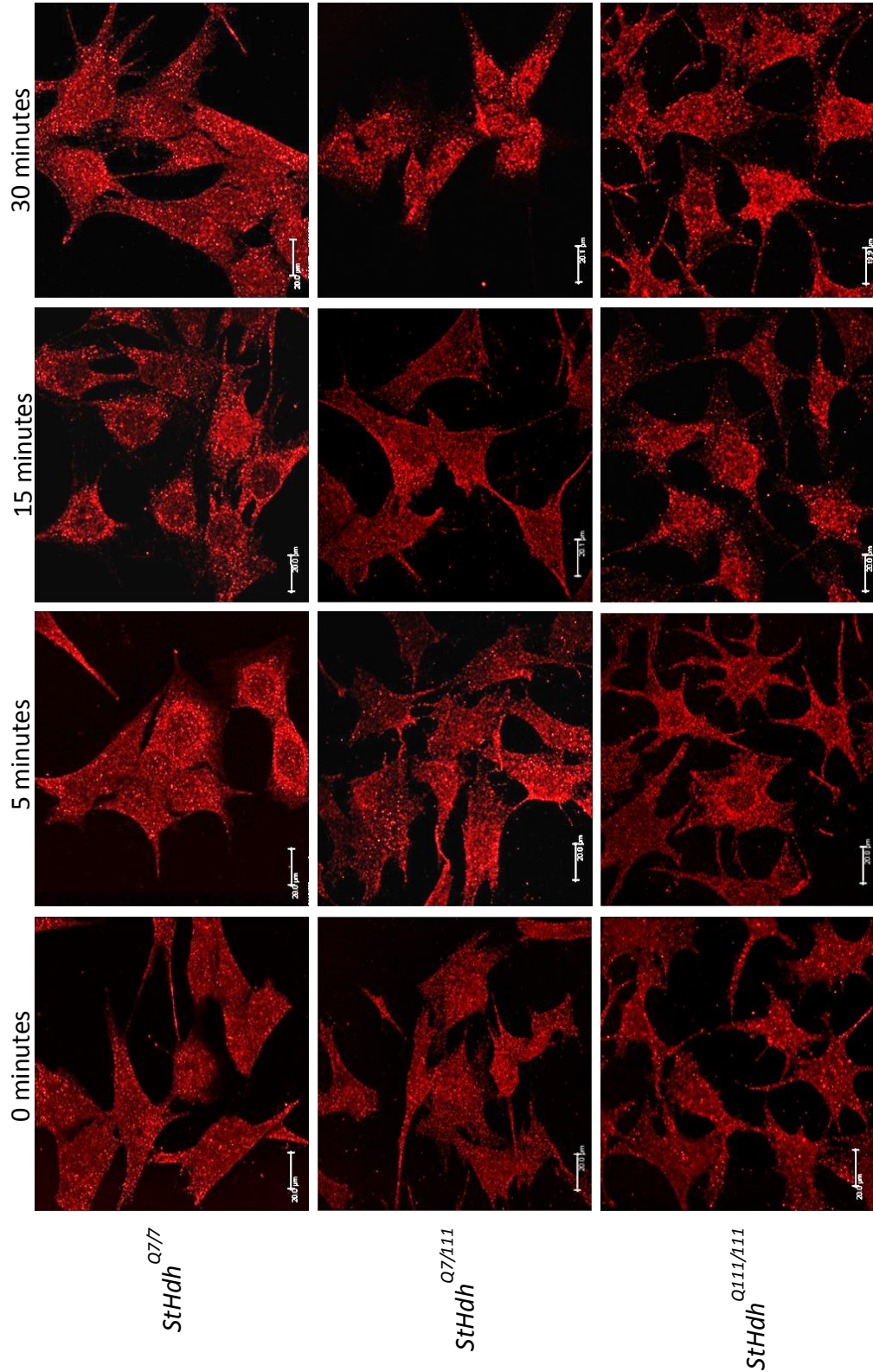
Figure 3.30 Subcellular localisation of an N-terminal epitope of HTT and mHTT phosphorylated on serines 13 and 16 in *StHdh*^{Q7/7}, *StHdh*^{Q7/11} and *StHdh*^{Q111/111} cell lines. Cells were fixed following 0, 5, 15 and 30 minutes of stimulation with 100ng/ml NGF, labelled with Anti-S1316p, then analysed by confocal microscopy (see Sections 2.2.1.8 and 2.2.1.9 for further details). Scale bar = 20μm
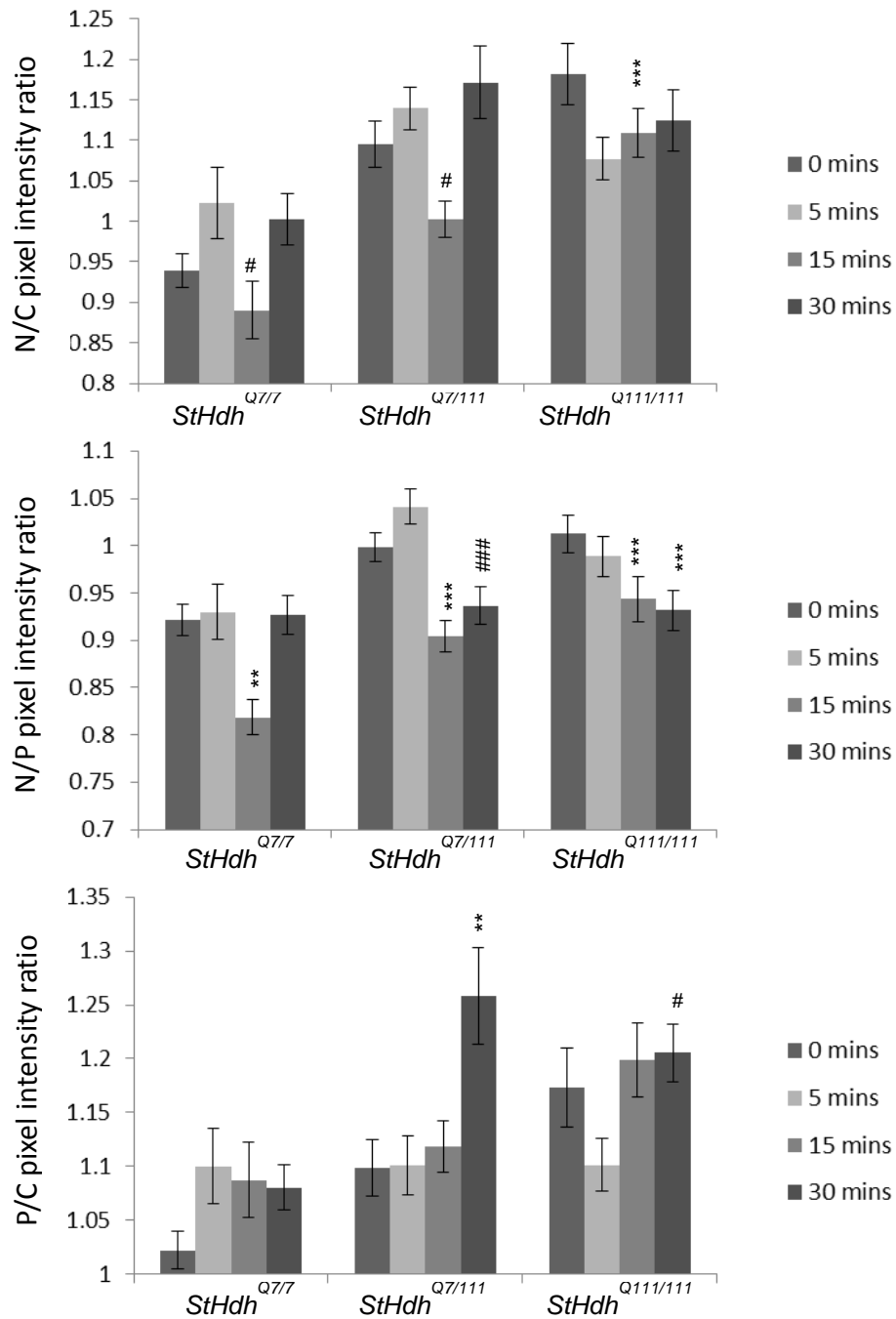
Figure 3.31 Quantitative analysis of immunofluorescence images in Figure 3.30. Nuclear/Cytoplasmic (N/C), Nuclear/Perinuclear (N/P) and Perinuclear/Cytoplasmic (P/C) mean pixel intensity ratios for $StHdh^{Q7/7}$, $StHdh^{Q7/111}$ and $StHdh^{Q111/111}$ cells following 0, 5, 15 and 30 minutes of stimulation with 100ng/ml NGF. Mean pixel intensities were calculated from confocal microscopy images using GNU Image Manipulator (further details of the analysis can be found in Section 2.2.1.10). All images were randomised and analysed blind to genotype and length of time stimulated with NGF. Each condition consisted of 9 confocal microscopy images taken from 3 separate coverslips. A two-way ANOVA was carried out for main effects analysis, followed by planned one way ANOVAs and post-hoc Tukey tests. Error bars = SEM.

* Denotes a significant difference from 0mins

# Denotes a significant difference from 5mins

* $p<0.05$ ** $p<0.01$ *** $p<0.001$

3.4.2.3 EGF stimulation

There was a significant main effect of genotype for the N/C ($F_{(2, 723)}$ = 51.7, $p<0.001$), N/P ($F_{(2, 723)}$ = 27.19, $p<0.00$) and P/C ($F_{(2,723)}$ = 19.59, $p<0.001$) following EGF stimulation (Figures 3.32 & 3.33). However, unlike the observations following BDNF and NGF stimulation, simple main effects analysis showed a significant difference between all three genotypes for all three ratios ($p<0.008$). There was only a main effect of time for the N/C and P/C ratios ($F_{(3, 723)}$ =6.36, $p<0.001$, $F_{(3, 723)}$=8.59, $p<0.001$, respectively), with no effect of EGF stimulation in the N/P ratio. All three ratios showed a significant genotype x EGF stimulation interaction (all $p<0.01$).

In $StHdh^{Q7/7}$ cells, there was an increase in nuclear HTT at 15 minutes, which appeared as focal loci in the centre of the nucleus and persisted up to 30 minutes of stimulation, which was reflected as a significant increase in the N/C ratio ($p=0.001$. There was also a significant increase in the P/C ratio at both 15 and 30 minutes ($p=0.004$, $p=0.041$ respectively), although there is not a visible increase in perinuclear localisation as seen following BDNF and NGF stimulation (Sections 3.4.2.1 & 3.4.2.2). This may reflect reduced cytoplasmic localisation of this epitope due to recruitment to the nucleus. In $StHdh^{Q7/111}$ cells, no significant effects were observed at any time point, although as previously noted for other antibodies investigated in this chapter, localisation of this epitope of HTT was more nuclear than in $StHdh^{Q7/7}$ cells. The lack of effect seen in these cells may be due to a suppressed response to EGF stimulation, or large variability in the localisation of phosphorylated HTT in these cells. $StHdh^{Q111/111}$ cells show a large increase in the N/C ($p=0.006$) and P/C ($p<0.001$) ratios at 30 minutes. This is due to formation of discrete loci of this epitope of HTT being detected in the nucleus, rather than a generalised nuclear increase. These are similar to the loci seen in $StHdh^{Q7/7}$ cells, although they are not formed as early or to the same extent.

These findings are contrary to those observed with the single phospho-S13 antibody, where there was a reduction in nuclear detection in both $StHdh^{Q7/7}$ and $StHdh^{Q7/111}$ cells, but an increase in the $StHdh^{Q111/111}$ (Section 3.4.1.3). This may be due to differing regulatory effects of phosphorylation of either S13 alone or both S13 and S16 together. This also demonstrates that the phosphorylation of HTT does not have a

single universal response to growth factor stimulation, but differences in signalling pathways may modulate its phosphorylation and localisation, which therefore lead to alternate downstream cellular effects.
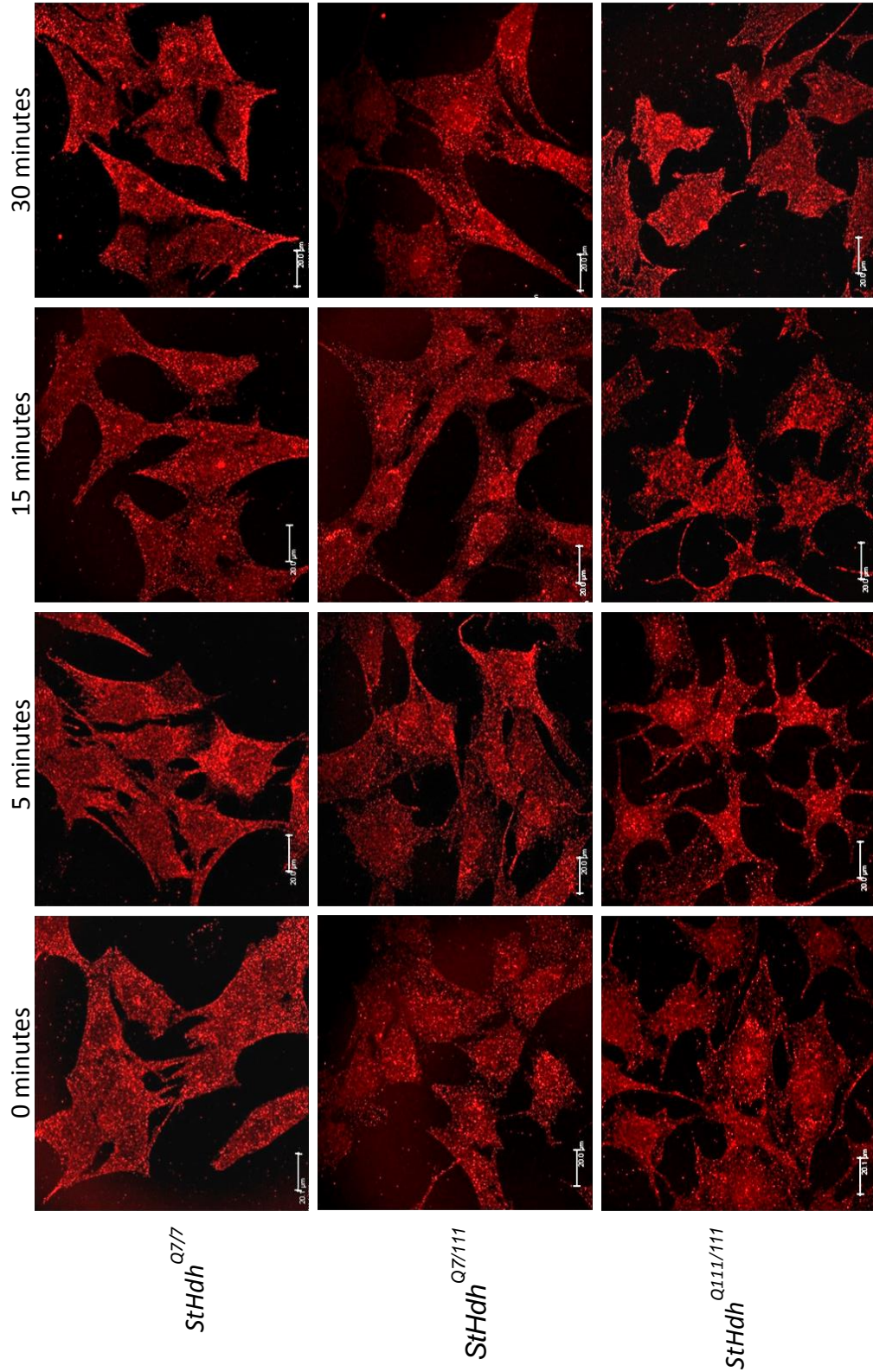
Figure 3.32 Subcellular localisation of an N-terminal epitope of HTT and mHTT phosphorylated on serines 13 and 16 in *StHdh*$^{Q7/7}$, *StHdh*$^{Q7/11}$ and *StHdh*$^{Q111/111}$ cell lines. Cells were fixed following 0, 5, 15 and 30 minutes of stimulation with 100ng/ml EGF, labelled with Anti-S1316p, then analysed by confocal microscopy (see Sections 2.2.1.8 and 2.2.1.9 for further details). Scale bar = 20µm
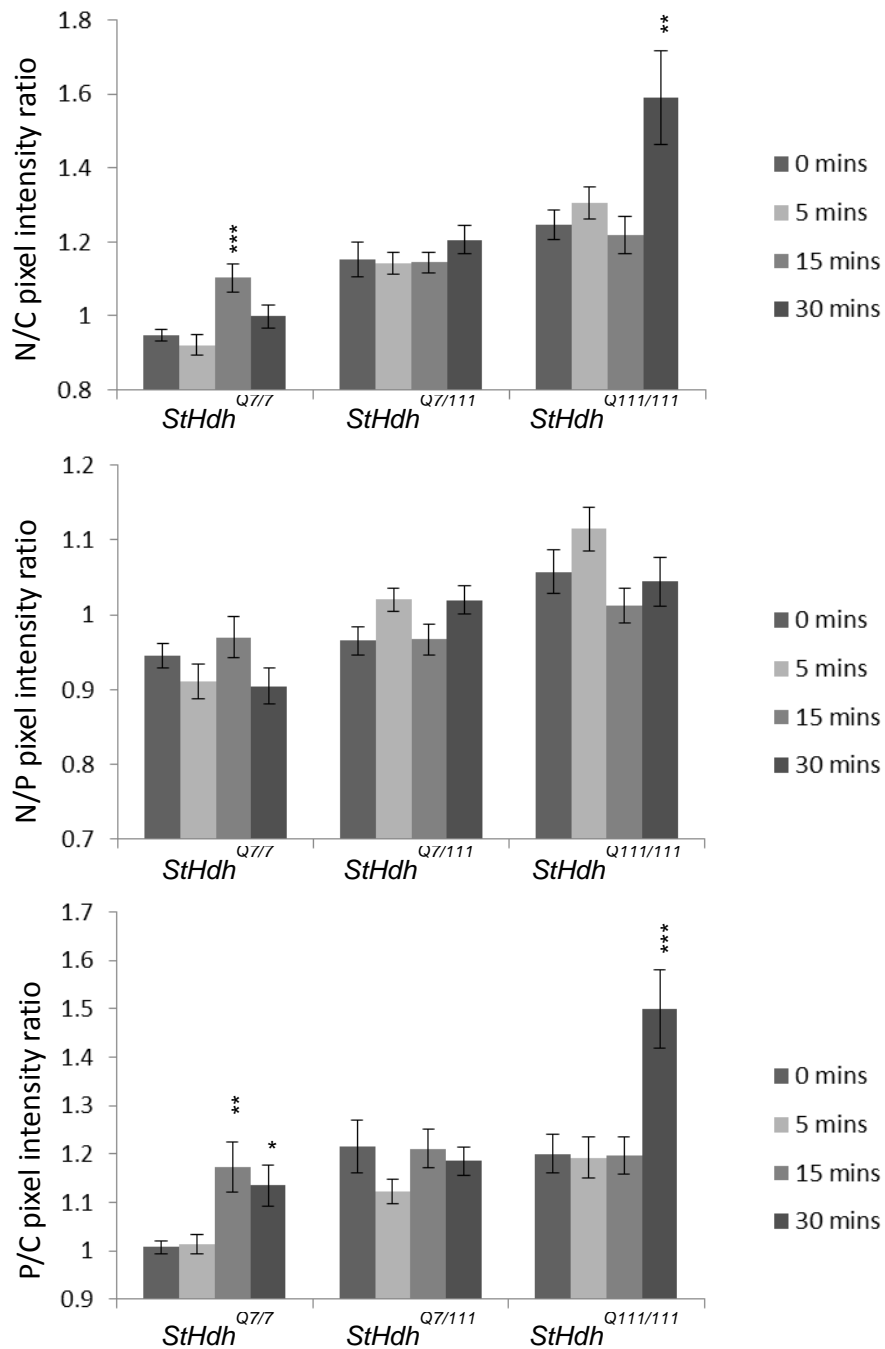
Figure 3.33 Quantitative analysis of immunofluorescence images in Figure 3.32. Nuclear/Cytoplasmic (N/C), Nuclear/Perinuclear (N/P) and Perinuclear/Cytoplasmic (P/C) mean pixel intensity ratios for $StHdh^{Q7/7}$, $StHdh^{Q7/111}$ and $StHdh^{Q111/111}$ cells following 0, 5, 15 and 30 minutes of stimulation with 100ng/ml EGF. Mean pixel intensities were calculated from confocal microscopy images using GNU Image Manipulator (further details of the analysis can be found in Section 2.2.1.10). All images were randomised and analysed blind to genotype and length of time stimulated with EGF. Each condition consisted of 9 confocal microscopy images taken from 3 separate coverslips. A two-way ANOVA was carried out for main effects analysis, followed by planned one way ANOVAs and post-hoc Tukey tests. Error bars = SEM.

* $p<0.05$ \ \ \ \ \ ** $p<0.01$ \ \ \ \ \ *** $p<0.001$

3.4.3 Immunostaining with the N17 s1316p antibody

As it was not possible to validate the anti-phosphorylated s1316 antibody, another antibody that was raised against a similar immunogen but produced in a different laboratory was also tested. However, cells were only probed with this antibody following EGF stimulation.

Immunostaining with the N17 s1316p antibody showed a similar localisation of HTT as immunostaining with the previous anti-phosphorylated s1316 antibody (Section 3.4.2). As with the other antibodies analysed, there is increasing nuclear intensity with mHTT load (Figure 3.34 & 3.35). This is reflected in the significant main effect of genotype for all three ratios (N/C $F_{(2, 983)}$ =6.323, p=0.002, N/P $F_{(2, 983)}$ =33.193, p<0.001, P/C $F_{(2,983)}$ = 29.655, p<0.001). There is also a significant effect of EGF stimulation in all three ratios (all p<0.006), and a significant genotype x EGF interaction (all p<0.003). However, contrary to the previous anti-phosphorylated s1316 antibody (Section 3.4.2.3), for both the N/C and P/C ratios, there was no effect between $StHdh^{Q7/7}$ and $StHdh^{Q7/111}$ cells, but there was a significant difference between both of these genotypes and the $StHdh^{Q111/111}$ cells (p<0.003). This suggests that with this antibody, $StHdh^{Q7/111}$ cells appear more similar to $StHdh^{Q7/7}$ cells than their homozygote counterparts, despite the mutant gene. However, in the N/P ratio, there is a significant difference between all three genotypes (p<0.001), thus indicating there is still a discernible effect of genotype on the localisation of phosphorylated HTT.

There is increased nuclear detection of phosphorylated HTT in $StHdh^{Q7/7}$ cells after 15 minutes of stimulation with EGF (N/C p=0.006, N/P p<0.001), which persisted up to 30 minutes of stimulation. This is the same as the effect observed with the previous anti-phosphorylated s1316 antibody (Section 3.4.2.3), although in this case, no discrete loci are detected, and nuclear staining is more diffuse. In $StHdh^{Q7/111}$ cells, however, the pattern of localisation differed to the previous antibody. Using the N17 s1316p antibody, there was a significant reduction in the detection of nuclear HTT at 5 minutes (N/C p=0.001) and 30 minutes (N/C p<0.001), while there was a return to the N/C baseline at 15 minutes, and an increase in the N/P ratio at the same time point (p=0.029). $StHdh^{Q111/111}$ cells showed the same pattern of localisation in response to

EGF stimulation as *StHdh*$^{Q7/111}$ cells, although due to higher variability, none of the time points reached significance. This increased variability and altered pattern of localisation in both *StHdh*$^{Q7/111}$ and *StHdh*$^{Q111/111}$ cell lines may be due to the expanded polyQ preventing stable phosphorylation of serines 13 and 16, which as a consequence, alters the localisation of this epitope of HTT.

As a similar pattern of localisation is observed in the *StHdh*$^{Q7/7}$ cells using both phospho-antibodies, it is likely that both antibodies are detecting phosphorylated HTT. However, the differences in the pattern of nuclear staining, and the response to EGF in *StHdh*$^{Q7/111}$ and *StHdh*$^{Q111/111}$ cells suggests that different epitopes of phosphorylated HTT are possibly being detected. A summary of the pattern of phosphorylated HTT nuclear localisation in response to stimulation with different growth factors can be seen in Table 3.2.

3.4.4 Characterising the cellular localisation of phosphorylated epitopes of HTT by subcellular fractionation

Consistent with the findings from western blots probed with non-phosphorylated N-terminal HTT antibodies in Section 3.3.6, there was no apparent change in the cytoplasmic or nuclear localisation of phosphorylated HTT as detected by N17 s1316p (Figure 3.21). Unfortunately, the other two phospho-antibodies were not available for this experiment, and there was only one replicate of each blot probed with N17 s1316p, so quantification was not possible. However, as described previously (Section 3.3.6), this method may not be the most sensitive way to characterise transient changes in protein localisation.
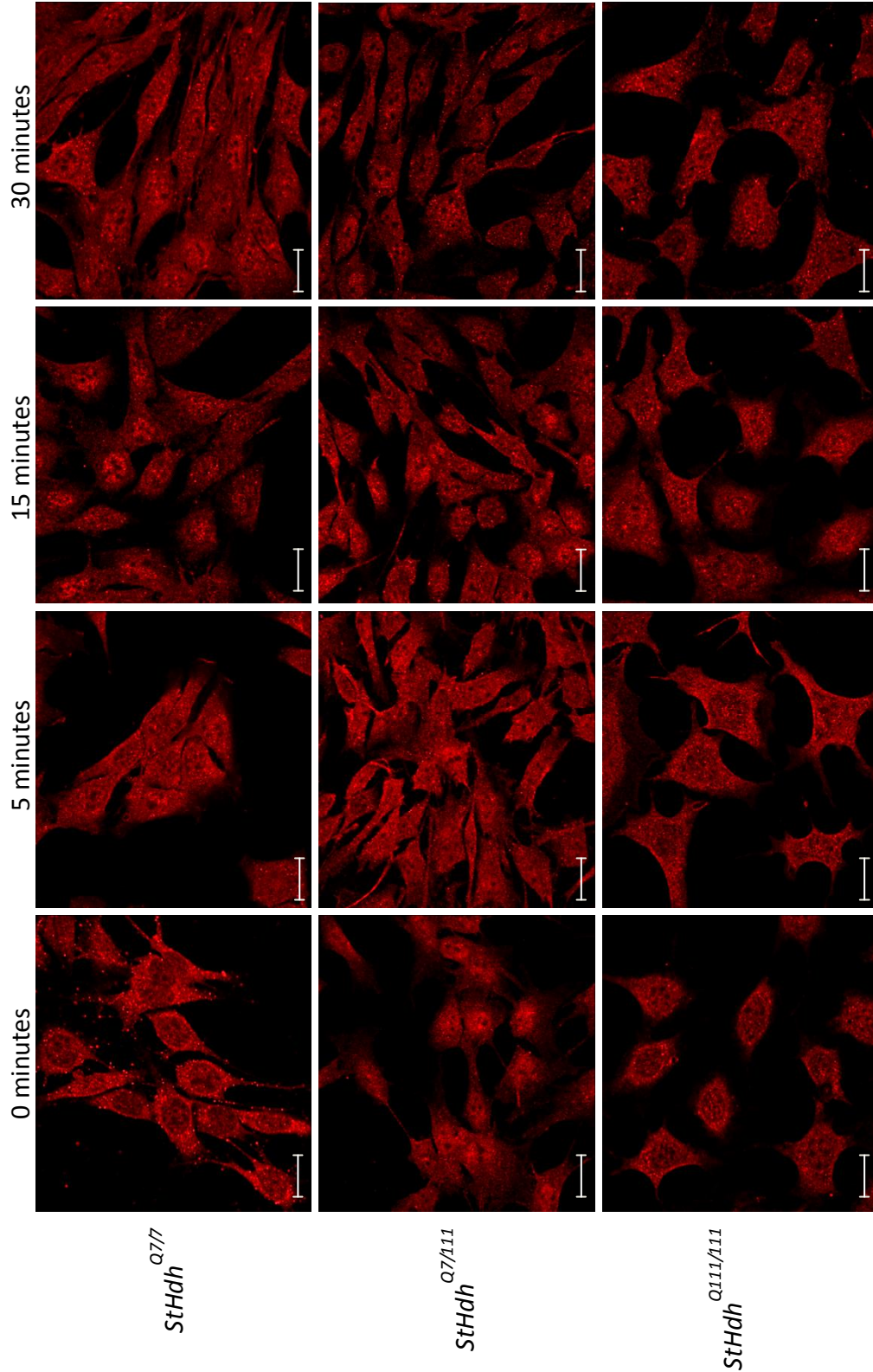
Figure 3.34 Subcellular localisation of an N-terminal epitope of HTT and mHTT phosphorylated on serines 13 and 16 in $StHdh^{Q7/7}$, $StHdh^{Q7/11}$ and $StHdh^{Q111/11}$ cell lines using an alternative antibody to Anti-S1316p. Cells were fixed following 0, 5, 15 and 30 minutes of stimulation with 100ng/ml EGF, labelled with N17 s1316p against amino acids 1-17 of HTT with phosphorylation on S13 and S16, then analysed by confocal microscopy (see Sections 2.2.1.8 and 2.2.1.9 for further details). Scale bar = 20μm

143
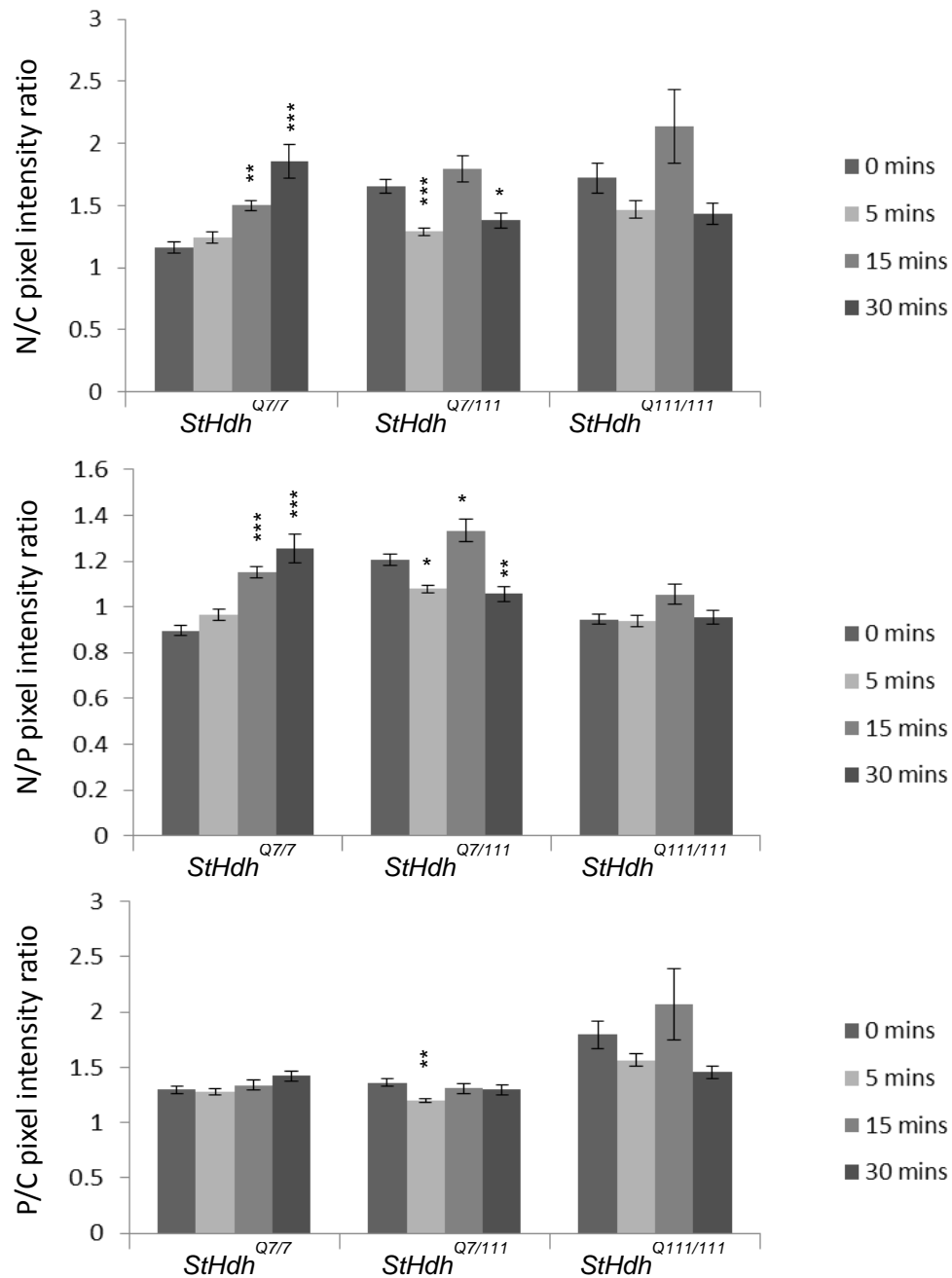
Figure 3.35 Quantitative analysis of immunofluorescence images in Figure 3.34. Nuclear/Cytoplasmic (N/C), Nuclear/Perinuclear (N/P) and Perinuclear/Cytoplasmic (P/C) mean pixel intensity ratios for $StHdh^{Q7/7}$, $StHdh^{Q7/111}$ and $StHdh^{Q111/111}$ cells following 0, 5, 15 and 30 minutes of stimulation with 100ng/ml EGF. Mean pixel intensities were calculated from confocal microscopy images using GNU Image Manipulator (further details of the analysis can be found in Section 2.2.1.10). All images were randomised and analysed blind to genotype and length of time stimulated with EGF. Each condition consisted of 9 confocal microscopy images taken from 3 separate coverslips. A two-way ANOVA was carried out for main effects analysis, followed by planned one way ANOVAs and post-hoc Tukey tests. Error bars = SEM.

* p<0.05   ** p<0.01   *** p<0.001

Antibody	BDNF			NGF			EGF		
	$StHdh^{Q7/7}$	$StHdh^{Q7/111}$	$StHdh^{Q111/111}$	$StHdh^{Q7/7}$	$StHdh^{Q7/111}$	$StHdh^{Q111/111}$	$StHdh^{Q7/7}$	$StHdh^{Q7/111}$	$StHdh^{Q111/111}$
S13p	↑5 & 30mins	↓ 15 mins	↑5 & 30mins	↓ 5 mins	← 5 mins	→ 15 mins	→ 5 mins	← 5 mins ↓15 mins	← 5 mins
S1316p	↓ 30 mins	↓ 30 mins	X	↓ 15 mins	↓ 15 mins	↓ 15 mins	← 15 mins	X	← 30 mins
N17 s1316p	-	-	-	-	-	-	← 15 mins	→ 5 mins	X

Table 3.2 A summary of the comparison of apparent phosphorylated HTT nuclear localisation in response to BDNF, NGF and EGF stimulation in $StHdh^{Q7/7}$, $StHdh^{Q7/111}$ and $StHdh^{Q111/111}$ cells as detected by a panel of Anti-phosphorylated N-terminal HTT antibodies. '↓' indicates a reduction in nuclear staining intensity and '↑' indicates an increase at the time point of growth factor stimulation that is stated. 'X' represents no change in HTT nuclear localisation at any time point.

3.5 Discussion

3.5.1 N-terminal HTT localisation

We demonstrate an apparent differential subcellular localisation of HTT and mHTT using a panel of several antibodies against N-terminal epitopes of HTT following growth factor stimulation, suggesting that the regulation of HTT localisation may be downstream of kinase signalling pathways. As different batches of polyclonal antibody stocks can exhibit variability in detection, which can alter the apparent localisation of HTT, this experiment therefore focused on the pattern of subcellular ratio changes rather than absolute fluorescence intensities. The presence of HTT in the nucleus is increased in the context of the expanded polyQ; a phenotype that has been previously described in this cell model (Trettel et al. 2000; Truant 2003; Atwal et al. 2007; Atwal et al. 2011) and in other models of HD (Hoogeveen et al. 1993; Dorsman et al. 1999; Hilditch-Maguire et al. 2000; Wheeler 2000; Kegel et al. 2002; Wheeler et al. 2002; Rockabrand et al. 2007; Seong et al. 2010). By using a panel of different antibodies, we have also observed that the detection of HTT localisation is modulated by the epitope against which the antibody was raised; Ab675 and N17 were both raised against amino acids 1-17, and they both demonstrate a strong nuclear presence. In contrast, Ab109115 was raised against a longer epitope of amino acids 1-30, and Mab2166 was raised against an epitope downstream of the polyQ repeat. Their pattern of detection appears considerably less nuclear than the amino acid 1-17 antibodies, suggesting that these antibodies may be detecting either a different epitope or a different conformation of HTT in these cells. Short N-terminal fragments of HTT have been identified as being enriched in cell nuclei (Hilditch-Maguire et al. 2000; Tao & Tartakoff 2001; Kegel et al. 2002), and aberrant splicing and subsequent translation of exon 1 of mHTT has been found in the Hdh^{Q150} mouse model (Sathasivam et al. 2013), thus more short N-terminal mHTT fragments may be aberrantly available in the presence of the expanded polyQ. Therefore the difference in localisation between Ab109115 and Mab2166 compared to the amino acid 1-17 antibodies may reflect the increased presence of shorter HTT fragments in the nuclei of these cells, and the increased nuclear intensity in *StHdh$^{Q7/111}$* and *StHdh$^{Q111/111}$* cells may reflect increased availability of this epitope.

Mab2166 and Ab109115 detect primarily perinuclear and cytoplasmic forms of HTT and mHTT, although in *StHdh*$^{Q7/111}$ and *StHdh*$^{Q111/111}$ cells, there is also a stronger nuclear presence. This may be a more open conformation of mHTT in cell nuclei due to the polyQ expansion leaving N-terminal epitopes more accessible (Wheeler 2000), it may be increased nuclear accumulation of mHTT (Truant 2003; Cornett et al. 2005; Atwal et al. 2007; Truant et al. 2007; Benn et al. 2008; Bauer & Nukina 2009) or there could be increased non-specific binding in mHTT carrying cells. HTT is thought to play a role in the formation of perinuclear organelles, such as mitochondria, the Golgi complex and the endoplasmic reticulum (Hilditch-Maguire et al. 2000), which may explain the clustering of detection of these epitopes to this region. Distinct versions of full length HTT have also been identified as being differentially localised between the nucleus and cytoplasm, which alter epitope accessibility and can create different patterns of antibody reactivity (Trettel et al. 2000; Wheeler 2000). Typically, the nuclear forms of full length HTT were found to be 'amino-terminal accessible,' whereas internal portions of the protein were inaccessible, and cytoplasmic forms that associated with membrane organelles close to the nucleus were 'internal accessible' (Trettel et al. 2000; Wheeler 2000). Therefore all of the antibodies investigated here may be detecting full length HTT, but the pattern of localisation that is elicited may be dependent upon HTT conformation; amino acid 1-17 antibodies Ab675 and N17 may be more able to detect amino accessible forms present in the nucleus, but Ab109115 and MW1 may be more sensitive to the internal accessible form present in the cytoplasm and associated with perinuclear organelles.

3.5.2 BDNF stimulation

The different epitopes of HTT in *StHdh*^{Q111} cell lines exhibited differential responses to stimulation with each growth factor. Following BDNF stimulation, there was a dramatic reduction in nuclear HTT, as detected by both Ab675 and Mab2166, although this effect was more variable when visualising the epitope probed by Mab2166. Furthermore, this effect was suppressed in the presence of the polyQ repeat; although there was still a reduction of nuclear HTT in both *StHdh*$^{Q7/111}$ and *StHdh*$^{Q111/111}$ cells following BDNF stimulation, it occurred to a lesser extent and at a later time point, suggesting that the response to BDNF stimulation is impaired in mutant cell types,

despite similar levels of the TRKB receptor between genotypes. This is perhaps unsurprising, as a loss of BDNF signalling in models of HD and in human HD brain have been well characterised (Canals et al. 2001; Reilly 2001; Zuccato et al. 2003; Baquet et al. 2004; Canals et al. 2004; Zuccato & Cattaneo 2007). As well as a reduction in BDNF available to striatal cells from cortical afferent inputs (Ferrer et al. 2000; Zuccato et al. 2001; Gauthier et al. 2004; Strand et al. 2007), one mechanism that may contribute to reduced BDNF responsive signalling in HD models may be the impairment of retrograde transport of TRKB containing vesicles in response to BDNF activation (Liot et al. 2013). In the Hdh^{Q111} mouse model of HD, it was found that HTT co-localises with these vesicles, and upon BDNF stimulation, aids their binding to microtubules for transport from the dendrites to the cell body, but that this process was impaired due to the mutant polyQ repeat (Liot et al. 2013). Therefore, it is possible that the localisation of HTT in response to BDNF stimulation in *StHdh$^{Q7/111}$* and *StHdh$^{Q111/111}$* cells may be a result of impaired TRKB trafficking and activation, despite a lack of impairment in its expression.

This suppressed response to BDNF stimulation has been observed previously; BDNF-mediated phosphorylation of ERK1/2 was found to be diminished in the same cell line, and although stimulation with BDNF protected *StHdh$^{Q7/7}$* cells from oxidative stress, it failed to exert the same protection in cells carrying mHTT (Ginés et al. 2010). Similarly, in primary cell cultures from R6/1 and Hdh^{Q111} mice, BDNF stimulation also failed to protect against N-methyl-D-aspartate (NMDA) excitotoxicity (Brito et al. 2013). Despite this, BDNF is generally considered a protective factor, as its overexpression prevents striatal neuron loss and motor dysfunction in the YAC128 model (Xie et al. 2010), and it can block polyQ mediated cell death in an in vitro model of HD (Saudou et al. 1998). Its expression was also enhanced in response to voluntary running in R6/1 hippocampus, which delayed motor symptom onset (Zajac et al. 2010).

The localisation of HTT may be altered in response to BDNF stimulation, as BDNF is a major regulator of excitatory pathways, which may elicit transcriptional activity as well as synaptic transmission and plasticity (Soulé et al. 2006). It has been postulated that HTT acts as a TF, and its activity is regulated by its localisation (Truant 2003; Truant et al. 2007). For example, the expression of *Bdnf* is regulated by HTT localisation; HTT

sequesters the *Bdnf* expression repressors NRSF/REST in the cytoplasm, therefore allowing the expression of *Bdnf* (Zuccato et al. 2001). However, mislocalisation of mHTT to cell nuclei and aberrant protein interactions due to the expanded polyQ prevent this sequestration, and *Bdnf* expression is suppressed (Zuccato et al. 2003). REST also regulates other genes associated with growth factors, neurotransmitters and vesicular trafficking (Zuccato & Cattaneo 2007), the transcription of which were recently found to be dysregulated in primary cells from Hdh^{Q109} mice; a phenotype that was rescued with REST knock-down (Soldati et al. 2013). Therefore, movement of HTT into the cytoplasm following BDNF stimulation may be a mechanism by which REST is further sequestered by HTT in order to enhance transcriptional activity, but this cytoplasmic localisation in response to stimulation is aberrant in *StHdh*$^{Q7/111}$ and *StHdh*$^{Q111/111}$ cells, thus contributing to disrupted transcriptional regulation.

3.5.3 NGF stimulation

NGF stimulation elicited the opposite response in *StHdh*^{Q111} cell lines compared with BDNF stimulation, and there was a clear difference in the detection and localisation of different HTT epitopes. NGF stimulation led to an increase in nuclear HTT in *StHdh*$^{Q7/7}$ cells, which appeared at 5 minutes and was diffuse when probed with Ab675, but demonstrated aggregated foci from 15 minutes of stimulation when visualised with Mab2166. NGF is required for neuronal survival, growth and maintenance of neuronal function (Allen et al. 2013), and as such is associated with mechanisms such as transcription, neurite outgrowth and differentiation (Song et al. 2002; Humbert 2003; Chen et al. 2012). However, NGF has been found to be reduced in HD patient plasma (Tasset et al. 2012), and phosphorylation of its receptor, TRKA, was suppressed in PC12 cells carrying mHTT (Song et al. 2002). Similarly, in PC12 cell models of HD, MAPK and JNK signalling pathways in response to NGF stimulation have previously been found to be suppressed (Humbert 2003), plus NGF-mediated neurite outgrowth is blocked (Song et al. 2002). These effects are thought to be due to either an aberrant interaction between mHTT and TRKA (Song et al. 2002), or interference with huntingtin associated protein 1 (HAP1), a stabiliser for TRKA activation (Rong et al. 2006).This suggests that as well as levels of endogenous NGF being lowered due to the presence of mHTT, the sensitivity of cells in HD models may also be suppressed due to interference at the

receptor. This is observed here in the $StHdh^{Q7/111}$ and $StHdh^{Q111/111}$ cell lines; similar to the effect seen following BDNF stimulation, there is still an effect of NGF stimulation on these cells, but it is delayed to a later time point compared with the $StHdh^{Q7/7}$ cells. In addition, $StHdh^{Q111/111}$ cells exhibit a much more variable localisation of the HTT epitope detected by Mab2166, and neither mHTT line exhibit the nuclear foci that develop in $StHdh^{Q7/7}$ cells, suggesting aberrant activity of HTT in these cells.

N-terminal HTT has been found to aggregate in the perinuclear region prior to translocation to the nucleus, particularly in response to cellular stress (Sawa et al. 2005). The epitope of HTT labelled with Mab2166 exhibits a strong perinuclear signal in $StHdh^{Q7/7}$ cells, and this may have primed the transport of this epitope into the nucleus following NGF stimulation, whereas $StHdh^{Q7/111}$ and $StHdh^{Q111/111}$ cells already demonstrate increased nuclear presence of this epitope, so increased nuclear translocation in response to NGF stimulation may be less efficient. It remains to be elucidated what the nuclear foci seen in $StHdh^{Q7/7}$ cells are, but it is possible that they appear within the cell nucleoli; it has previously been observed that invaginations of the nuclear membrane can make contact with the nucleolus (Fricker et al. 1997), providing a potential mechanism for entry of N-terminal HTT to the nucleus. Association with the nucleolus may implicate HTT in ribosomal synthesis, which has been found to be dysregulated in models of HD (Trettel et al. 2000; Kegel et al. 2002) and can be modulated by NGF stimulation (Angelastro et al. 2002). In addition, the internal-accessible epitope of HTT that we postulate may be detected by Mab2166 in these cells, and is associated with perinuclear organelles, has also been identified in the nucleolus (Trettel et al. 2000).

Alternatively, HTT has also been associated with subnuclear speckles and promyelocytic leukaemia (PML) bodies, where it may play a role in transcription and RNA processing (Kegel et al. 2002). This suggests that stimulation with NGF may be eliciting transcriptional activity, and the localisation of HTT is modulated in response (Kegel et al. 2002). The lack of foci formation in $StHdh^{Q7/111}$ and $StHdh^{Q111/111}$ cells suggests that there may be dysregulation of normal HTT nuclear processes in these cells in response to stimulation with NGF due to mislocalisation of the mutant protein and disorganisation of nuclear structures.

The differences in localisation and time of response between Ab675 and Mab2166 may reflect a change in HTT conformation within the nucleus, thus allowing for differential antibody detection. For example, the diffuse nuclear filling with Ab675 is less apparent at 15 minutes of NGF stimulation, which is when the Mab2166 labelled foci appear. However, the perinuclear labelling with Mab2166 also disappears at this time point, which may be more indicative of a change in localisation rather than change in conformation.

There have been mixed reports as to whether enhancing NGF availability in affected striatal cells is beneficial in models of HD. Bone marrow mesenchymal stem cells overexpressing NGF had little therapeutic effect when transplanted into YAC128 striata (Dey et al. 2010), although enhanced NGF via an astrocytic NGF enhancer proved to be protective against neuronal death in response to the mitochondrial toxin 3-nitropropionic acid (3-NP) (Almeida et al. 2010; Chen et al. 2012). However, if cells carrying mHTT have a suppressed response to stimulation by NGF, as observed here, then a more efficacious therapeutic target may be the TRKA receptor, or downstream targets associated with nuclear processes.

3.5.4 EGF stimulation

EGF stimulation is known to elicit the transcription of immediate-early genes (Lin et al. 2001; Cabodi et al. 2009), and is associated with a range of essential cellular functions such as development, differentiation and survival (Liévens et al. 2008), and is implicated in the inflammatory and immune response (Cabodi et al. 2009). It has also been suggested that the EGFR may act as a transcriptional regulator itself (Lin et al. 2001); therefore incubating $StHdh^{Q111}$ cell lines with EGF is likely to elicit a transcriptional response. Stimulation of $StHdh^{Q7/7}$ cells with EGF led to a reduction in nuclear HTT for three of the N-terminal antibodies utilised, although alterations in localisation remained primarily between the nucleus and perinuclear regions of the cell, rather than diffusing out into the cytoplasm. This change in localisation may be a mechanism by which to regulate the transcriptional response that occurs following EGF stimulation. Similar to the effect seen following stimulation with either BDNF or NGF, there was a suppressed response to EGF in both $StHdh^{Q7/111}$ and $StHdh^{Q111/111}$

cells, which would be consistent with transcriptional dysregulation seen in models of HD (Ross et al. 2002; Zucker et al. 2005; Crocker et al. 2006; Crook & Housman 2011).

How the localisation of HTT may be regulating the transcriptional response to growth factor stimulation remains to be elucidated. However, HTT has previously been found to associate with the EGFR via its SRC-homology 3 (SH3) domain, and in turn this can regulate the RAS-dependent signalling pathway by competitive inhibition of Ras GTPase activating protein (RasGAP*); mechanisms that have both been found to be disrupted by an extended polyQ repeat (Liu et al. 1997; Song et al. 2002). A reduction in nuclear HTT may therefore reflect localisation with the EGFR and downstream kinases that regulate transcription in response to EGF stimulation. However, there have been mixed findings with regards to the effect of mHTT on the activation of the downstream kinase ERK 1/2. In some models, EGF-mediated activation of ERK 1/2 is suppressed in the presence of mHTT (Song et al. 2002; Liévens et al. 2008; Melone et al. 2013), although in *StHdh*$^{Q111/111}$ cells, ERK 1/2 activation by EGF stimulation was not found to differ from *StHdh*$^{Q7/7}$ cells (Ginés et al. 2010).

Alternatively, as HTT is known to localise to the Golgi and endosomes (Pal et al. 2006; del Toro et al. 2009), it may be playing a role in the recycling and degradation of the EGFR following stimulation with EGF, thus its increased perinuclear localisation may reflect translocation to the Golgi body and late endosomes in order to process the EGFR, or to assist with its nuclear localisation. Indeed, delayed EGFR degradation and altered trafficking has been observed in human HD fibroblasts (Melone et al. 2013). Of course, the role of HTT on the downstream effects of EGF may be more direct; HTT is able to bind directly to DNA and chromatin in order to act as a transcription factor (Benn et al. 2008), or can bind to other transcription factors to regulate their activity (Bauer & Nukina 2009). Therefore the reduction in nuclear HTT that is observed following EGF stimulation may be reflective of this process, and may be either a true change in localisation, or a conformational change that alters the availability of the N-terminal epitope. Evidence for the latter may be the effect of EGF on the epitope detected by the N17 antibody; this was much more nuclear than the other N-terminal antibodies, and showed no response to EGF stimulation. As there was a reduction in its signal following *Htt* siRNA treatment, it is unlikely that N17 is detecting entirely non-

specific products. Therefore it may be detecting an alternative epitope of HTT that remains detectable despite a potential change in HTT conformation.

3.5.5 Western blot analysis of HTT subcellular localisation

Western blot analysis also provided support that there may not necessarily be changes in the localisation of HTT following growth factor stimulation, as none of the three growth factors or five antibodies utilised elicited any visible change in the presence of full length HTT in either nuclear or cytoplasmic fractions. The lack of localisation change identified by western blot may indicate that there is a conformational change in nuclear HTT in response to growth factor stimulation rather than a translocation. In contrast, this may be a methodological issue, in that the process by which subcellular fractionation was carried out is not sensitive enough to retain the transient alterations in HTT localisation observed by immunofluorescence.

3.5.6 HTT shuttling mechanisms

Despite sharing some downstream kinase signalling pathways, each growth factor had a separate effect on the localisation of HTT; this may be due to be different interactions of HTT with each growth factor receptor, but also to the different kinetics of activation in response to each growth factor. For example, NGF stimulation elicits sustained activation of MAPK in PC12 cells, whereas EGF stimulation elicits only transient activation (Ji et al. 2010). In addition, it has been found previously that only BDNF-mediated ERK 1/2 activation was suppressed in $StHdh^{Q111/111}$ cells, but EGF-mediated ERK 1/2 activation showed no difference to $StHdh^{Q7/7}$ cells (Ginés et al. 2010), suggesting that upstream mediators alter the effect of different stimuli on shared signalling pathways. These alterations in signalling kinetics and mediators appear to be enough to regulate the localisation and/or the conformation of HTT in order to mediate different cellular functions, the natures of which are yet to be elucidated.

Various mechanisms have been described that can explain the ability of full length HTT to shuttle between the nucleus and cytoplasm, as it is too large to passively diffuse across the nuclear pore (Terry et al. 2007). For example, the ability of the first 17

amino acids to act as a cytoplasmic retention signal (Xia 2003), including the CRM1-dependent NES (Maiuri et al. 2013), both act to target HTT to the cytoplasm. In addition, several HEAT repeats along HTT have been described as being similar to other nuclear import factors (Atwal et al. 2007; Truant et al. 2007), and an NLS that binds to nuclear import receptors importin beta 1 and transportin has been identified between amino acid residues 174 - 207, which can be activated by cellular stress (Desmond et al. 2012; Desmond et al. 2013). The availability of these sequences in the different conformations of HTT, as well as binding to exogenous chaperones to traverse the nuclear pore (Li et al. 1995; Faber et al. 1998; Ferrigno & Silver 2000; Truant et al. 2007) may be a mechanism by which growth factor stimulation can alter the localisation of HTT. It has also been observed that the phosphorylation of HTT can alter the action of its NES and NLS sequences, and can regulate its subcellular localisation (Gu et al. 2009; Thompson et al. 2009; Atwal et al. 2011; Havel et al. 2011; Maiuri et al. 2013).

3.5.7 The localisation of phosphorylated HTT

We therefore also investigated the localisation of phosphorylated epitopes of HTT both prior to, and in response to growth factor stimulation. As observed for non-phosphorylated N-terminal epitopes of HTT, there was increased nuclear and perinuclear localisation at baseline in $StHdh^{Q7/111}$ and $StHdh^{Q111/111}$ cells, and there were differential growth factor effects on the localisation of phosphorylated HTT. Following BDNF stimulation, there was initially a reduction in nuclear HTT phosphorylated on S13, followed by a nuclear increase again and a subsequent second reduction in $StHdh^{Q7/7}$ cells. $StHdh^{Q7/111}$ and $StHdh^{Q111/111}$ cells showed a similar pattern of response, but this was much more variable. There was the same pattern of localisation as detected by Ab675 and Mab2166, suggesting that the alterations in subcellular HTT detection following BDNF may be due to alterations in its localisation rather than a conformational change. In contrast, there was little effect of BDNF stimulation on the localisation of the double S1316 phosphorylated epitope in any genotype; therefore the pathways activated by BDNF stimulation may be capable of S13 phosphorylation, but do not elicit S16 phosphorylation.

In contrast, there is a reduction in the detection of nuclear single S13 and double S1316 phosphorylated HTT epitopes following NGF stimulation in $StHdh^{Q7/7}$ cells. However, this is also more variable for $StHdh^{Q7/111}$ and $StHdh^{Q111/111}$ cell types, suggesting dysregulation in the control of mHTT localisation and phosphorylation. The phosphorylation of HTT on S13 and S16 tends to be associated with increased nuclear localisation of HTT (Atwal et al. 2007; Thompson et al. 2009; Atwal et al. 2011; Havel et al. 2011; Desmond et al. 2013; Maiuri et al. 2013), suggesting that NGF stimulation is either not having an effect on the phosphorylation of HTT on S13 or S16, or it is dephosphorylating these epitopes. The pattern of localisation is similar to that detected by Ab675, but is the opposite of that displayed by Mab2166; nuclear foci are detected by Mab2166 at the same 15 minute time point following NGF stimulation when a reduction in nuclear phosphorylated epitopes occurs. Therefore, this may be indicative of a conformational change in nuclear HTT that reduces the ability of anti-phosphorylated S13 and S1316 antibodies to detect HTT; the detection of HTT by the phosphorylated S13 antibody has been found to alter detection by Mab2166 before (Wheeler 2000; Thompson et al. 2009; Di Pardo et al. 2012).

Following EGF stimulation, there was a reduction in phosphorylated S13 apparent in cell nuclei in $StHdh^{Q7/7}$ and $StHdh^{Q7/111}$ cells, but an increase in $StHdh^{Q111/111}$ cells. In contrast, there was an increase in the double phosphorylated epitope in the nuclei of $StHdh^{Q7/7}$ cells for both anti-phosphorylated S1316 HTT antibodies that were analysed, but there was a more variable response in $StHdh^{Q7/111}$ and $StHdh^{Q111/111}$ cells. This suggests that EGF stimulation may elicit the phosphorylation of both S13 and S16, but that the double phosphorylation event is more relevant to the nuclear localisation of HTT; an effect that has been described previously (Gu et al. 2009; Atwal et al. 2011; Havel et al. 2011). This effect is in contrast to the localisation of HTT detected by Ab675, Mab2166 and Ab109115 following EGF stimulation, where there was a reduction in nuclear HTT. Therefore, these results may reflect either an alteration in HTT conformation; i.e the phosphorylation of HTT epitopes in the nucleus reduces the binding capacity of non-phosphorylated N-terminal antibodies, or there is a bidirectional shuttling of HTT epitopes between the nucleus and perinuclear region dependent upon phosphorylation status. Phosphorylation at S13 and S16 can reduce

the interaction of HTT with the nuclear export factors CRM1 (Maiuri et al. 2013) and TPR (Cornett et al. 2005), therefore non-phosphorylated epitopes could still be capable of leaving cell nuclei at the same time as phosphorylated epitopes are imported. The S1316 phosphorylated epitopes form nuclear speckles in *StHdh*$^{Q7/7}$ cells following 15 minutes of EGF stimulation, which may be areas associated with transcription; Atwal et al. 2011 previously noted that phosphorylation on these two serines in response to stress targeted full length HTT to chromatin subregions of the nucleus in *StHdh*^{Q111} cell lines.

3.5.8 The role of phosphorylated HTT subcellular localisation

All three growth factors investigated altered the detection of the subcellular localisation of phosphorylated HTT epitopes, however whether this is due to nuclear-cytoplasmic shuttling, changes in conformation within cellular compartments, or a more complex combination of these two processes remains to be elucidated. However, different patterns of responses in combination with our findings from non-phosphorylated N-terminal epitope antibodies suggests that different stimulations are likely to be eliciting different processes. The majority of the localisation changes occurred between the nucleus and the perinucleus, rather than any large alterations within the cytoplasm. This is consistent with perinuclear aggregation of HTT prior to nuclear translocation (Sawa et al. 2005), and the role of phosphorylation in the subcellular shuttling of HTT (Atwal et al. 2007; Thompson et al. 2009; Atwal et al. 2011; Ehrnhoefer et al. 2011; Greiner & Yang 2011; Havel et al. 2011; Khoshnan & Patterson 2011; Desmond et al. 2013; Maiuri et al. 2013).

The nuclear localisation of HTT is thought to be able to alter gene expression (Zoghbi & Orr 2000; Kegel et al. 2002) and can also affect nuclear organisation and function (Sun et al. 2007), and the phosphorylation of HTT is one mechanism by which this may be regulated (Holmberg et al. 2002; Ehrnhoefer et al. 2011). Phosphorylation at S13 and S16 is known to be a protective mechanism, despite inducing an increase in nuclear HTT, which is typically associated with enhanced toxicity (Gu et al. 2009; Thompson et al. 2009; Atwal et al. 2011; Khoshnan & Patterson 2011; Di Pardo et al. 2012; Mishra et al. 2012). Typically, alterations in the phosphorylation of HTT have been investigated in

cells and mouse models carrying the mutant protein, and have looked at alterations in aggregation pathology and clearance of mHTT via the ubiquitin proteasome system (Gu et al. 2009; Thompson et al. 2009; Di Pardo et al. 2012). However, we have identified that the localisation and phosphorylation of endogenous wild type HTT can be altered by growth factor stimulation, and therefore nuclear translocation of phosphorylated epitopes may be a mechanism by which cell signalling responses are regulated, as well having a role as a protective mechanism following cell stress and for modifying mHTT toxicity (Gu et al. 2009; Thompson et al. 2009; Atwal et al. 2011; Mishra et al. 2012; Di Pardo et al. 2012). However, it was observed that alterations in localisation and phosphorylation in response to growth factor stimulation are suppressed in the cell lines carrying mHTT, suggesting there may be polyQ dependent hypophosphorylation of mHTT, as has previously been identified in these cells and other models of HD (Thompson et al. 2009; Atwal et al. 2011). Whether this is due to interference in kinase signalling pathways upstream of HTT phosphorylation or to less efficient phosphorylation of mHTT due to physical disruption from the expanded polyQ remains to be elucidated.

3.5.9 Other post-translational modifications of HTT

There are many other post-translational modifications of HTT that may also be occurring in response to growth factor stimulation, and that may also modulate the localisation of HTT. One of the most well characterised phosphorylation sites on HTT is at S421, which has been associated with the regulation of proteolysis and clearance (Warby et al. 2009), as well as BDNF vesicle transport (Gauthier et al. 2004; Zala et al. 2008), and can be elicited by AKT or serine/threonine protein kinase (SGK) activity (Warby et al. 2005; Zala et al. 2008; Bauer & Nukina 2009; Warby et al. 2009). In accordance with the phosphorylation of S13 and S16, S421 phosphorylation has also been found to be protective in models of HD (Warby et al. 2005; Zala et al. 2008; Bauer & Nukina 2009; Warby et al. 2009), but in contrast to S13 and S16, has been found to reduce the nuclear localisation of HTT (Bauer & Nukina 2009; Warby et al. 2009). We were unfortunately unable to utilise an anti-phosphorylated S421 antibody in this experiment, however it may have provided additional information on the regulation of HTT localisation; for example, when a nuclear reduction in HTT was observed, such as

following BDNF and EGF stimulation, it would have been informative to investigate whether this may have been relocalisation of HTT epitopes towards the cytoplasm to aid with vesicular transport.

HTT is also phosphorylated on Threonine 3 (T3) in a polyQ dependent manner (Aiken et al. 2009), with mHTT being hypophosphorylated. T3 phosphorylation is considered to be neuroprotective by regulating the secondary structure of N-terminal HTT, thus altering its availability for further modification and clearance (Aiken et al. 2009); therefore the baseline phosphorylation of T3 in this model may be modulating the phosphorylation responses to growth factor stimulation. In addition, it has been postulated that phosphorylation at S13 and S16 may interact with nearby ubiquitination and small ubiquitin like modifier (SUMO)-ylation sites on lysines 6 (K6), 9 (K9) and 15 (K15) (Steffan et al. 2004; Ehrnhoefer et al. 2011). Ubiquitin and SUMO modifiers compete for these sites (Steffan et al. 2004), and tend to have opposing effects on the toxicity of mHTT in HD models; ubiquitination has been associated with increasing mHTT clearance and therefore reducing toxicity (Kalchman et al. 1996; Steffan et al. 2004; Jana et al. 2005), whereas SUMOylation stabilises the mHTT protein, thereby increasing its nuclear localisation and worsening transcriptional dysregulation, thus enhancing toxicity (Steffan et al. 2004). As most SUMO modifiers are in the nucleus (Steffan et al. 2004), this may contribute to the reduced export of nuclear forms of mHTT in $StHdh^{Q7/111}$ and $StHdh^{Q111/111}$ cells following growth factor stimulation. There are also several acetylation and palmitoylation sites on HTT (Pennuto et al. 2009; Ehrnhoefer et al. 2011), but these have not been directly associated with the shuttling of HTT between cellular compartments, although any post-translational modifications of HTT are likely to affect its regulation in response to cellular stimulation. Proteolytic cleavage of HTT by caspases and calpains are a modification of HTT that can alter its subcellular localisation due to the exclusion of NES or NLS sequences on the protein, and the generation of small fragments that can passively diffuse across the nuclear pore (Wellington et al. 1998; Toneff et al. 2002; Kim et al. 2003; Terry et al. 2007; Bauer & Nukina 2009; Landles et al. 2010; Ehrnhoefer et al. 2011). However, analysis of HTT localisation by subcellular fractionation and western blot did not reveal any HTT fragments smaller than the full

length protein (examples of full blots can be found in Appendix IV), indicating that either proteolytic cleavage of HTT does not occur in the *StHdh*^{Q111} cell model of HTT, the abundance of cleaved fragments was too low for detection, or the method by which fractionation occurred was too harsh in order to retain the integrity of cleaved products. Regardless of the mechanism, we were unable to assess the contribution of cleaved HTT products to our localisation and phosphorylation observations.

3.5.10 Conclusion

In conclusion, different growth factors elicit differential subcellular localisation and phosphorylation of N-terminal epitopes of HTT, which may be due to different signalling pathways and kinetics downstream of the growth factor receptors. This process is suppressed in cells carrying the mutant protein, although it remains to be determined at what stage of the cell signalling process this disruption occurs, i.e. at the receptor, during kinase phosphorylation, or at mHTT itself. Post-translational modifications and the shuttling of HTT between cellular compartments are both associated with the regulation of its function (Truant 2003; Truant et al. 2007), such as the control of gene expression (Atwal et al. 2011), regulating protein-protein interactions (Bauer & Nukina 2009; Ehrnhoefer et al. 2011) and interactions with organelles (Hilditch-Maguire et al. 2000; Kegel et al. 2002; Tao & Tartakoff 2001; Atwal et al. 2007). However, investigation of these processes is confounded by the ability of HTT to undergo dramatic conformational switches (Seong et al. 2010), particularly following post-translational modifications such as phosphorylation (Aiken et al. 2009; Gu et al. 2009; Atwal et al. 2011; Mishra et al. 2012) that alter its binding capacity to N-terminal antibodies. As such, we were unable to determine whether the alterations in localisation and phosphorylation of HTT that we observe were due to changes in either its conformation or nuclear translocation in response to growth factor stimulation. However, by comparing results from the localisation patterns of several different antibodies, a mechanism can be hypothesised; this appears to differ between growth factors, with BDNF perhaps eliciting translocation, NGF leading to a conformation change, and both events occurring following EGF stimulation (a summary can be found in Table 3.3). The investigation of the identity of the nuclear foci that co-localised with

HTT in response to growth factor stimulation would have been advantageous; however, there was not the opportunity within this project.

Although validation of the antibodies used by siRNA was not unequivocally successful, the antibodies used to detect N-terminal HTT tend to show the same pattern of localisation and response to stimulation that suggests they are detecting similar proteins, likely to be HTT-related. It is therefore reasonable to infer that our immunofluorescence findings are not heavily confounded by non-specific binding. Despite demonstrating differential HTT localisation and phosphorylation responses due to genotype and growth factor stimulation, we have not yet elucidated what signalling pathways may be leading to these responses. Therefore we next aimed to discover which signalling pathways were most relevant to our panel of growth factors in this cell line, and whether aberrant upstream activity may be responsible for the altered mHTT localisation and phosphorylation responses.

	N-terminal antibodies		Phospho-antibodies		Potential mechanism
GF	$StHdh^{Q7/7}$	$StHdh^{Q111/111}$	$StHdh^{Q7/7}$	$StHdh^{Q111/111}$	
BDNF	↓	↑/↓	↓	X /↑	HTT translocation
NGF	↑	↑/↓	↓	↓	Conformation change
EGF	↓	X /↓	↑/↓	↑	Translocation & conformation change

Table 3.3 A comparison of the general effects of growth factor (GF) stimulation on the apparent nuclear localisation of HTT and phosphorylated HTT epitopes in $StHdh^{Q7/7}$ and $StHdh^{Q111/111}$ cells. Arrows indicate an increase or decrease in the intensity of nuclear HTT detection, and a cross indicates no observable change. Where more than one direction is present, findings were mixed between antibodies. The presence of an expanded CAG repeat in $StHdh^{Q111/111}$ cells inhibited the HTT localisation and phosphorylation responses to GF stimulation. A comparison of non-phosphorylated and phosphorylated HTT localisation patterns allows for conclusions about the potential mechanisms underlying the differential observable effects for each GF to be drawn.

Chapter 4:   Characterisation of the signalling pathways induced by growth factor stimulation in immortalised embryonic striatal cells

4.1 Introduction

Patients with HD have been reported as having a low incidence of tumour formation, as well as a lower glucose metabolism (Kuwert et al. 1990; Grafton et al. 1992), suggesting that growth factor responsive kinase pathways may play a role in the pathogenic mechanism of the disease. A cartoon depicting several of the overlapping signalling pathways investigated in this chapter can be found in Figure 4.1. The EGFR is involved with cell development, differentiation and survival (Liévens et al. 2008), and its signalling complex has been found to interact with both HTT and mHTT (Liu et al. 1997; Song et al. 2002; Apostol et al. 2006; Liévens et al. 2008). Specifically, the proline rich motifs in HTT appear to associate with SH3 domain-containing molecules within the EGFR complex, and this association is strengthened with EGFR stimulation (Liu et al. 1997). It is unknown exactly what role HTT may have at the EGFR, but it may regulate the consequent RAS-dependent pathway by competitive inhibition (Liu et al. 1997).

There have been inconsistent findings regarding the effect of mHTT at the EGFR and the consequences for downstream signalling. It has generally been found that mHTT attenuates signalling pathways downstream of the EGFR by its association with GRB2 (Liu et al. 1997; Song et al. 2002), and as a result, activation of AKT and ERK is antagonised (Song et al. 2002; Humbert 2003). However, this effect may be model specific; attenuated AKT and ERK were identified in PC12 cells expressing the mutant protein (Song et al. 2002; Humbert 2003), in *Drosophila* (Liévens et al. 2008), and in R6/1 hippocampus (Ransome & Hannan 2013). In contrast, increased AKT phosphorylation has been identified in the $StHdh^{Q111}$ immortalised cell line of HD (Ginés et al. 2003; Kong et al. 2009; Atwal et al. 2011), in Hdh^{Q111} mice (Ginés et al. 2003), and in the striata of R6/1 mice (Saavedra et al. 2010). Conversely, in YAC128 and R6/2 mice, no difference in active AKT was found between wild type and mutant mice (Warby et al. 2005; Xie et al. 2010).

GRB2 has also been implicated with the NGF-responsive TRKA receptor; subsequently, phosphorylation of this receptor was found to be repressed in PC12 cells expressing mHTT (Song et al. 2002). The NGF pathway shares several of the same signalling pathways as EGF downstream of stimulation of its receptor, such as MAPK (Torcia et al. 2001; Rosini et al. 2004; Ji et al. 2010) and AKT (Rong et al. 2002). Regulation of the MEK/ERK cascade is also thought to mediate the effect of NGF on neurite outgrowth (Levkovitz & Baraban 2002). In the presence of mHTT, the phosphorylation and activation of these pathways following NGF stimulation have been found to be substantially suppressed (Song et al. 2002; Humbert 2003; Rong et al. 2006) despite evidence that suggests the level of NGF secretion does not change with overexpression of mHTT (Zuccato et al. 2001). This suggests that in the context of NGF signalling, the mutant protein may be exerting its effects at the TRKA receptor rather than disrupting NGF itself.

The P75 NTR also acts as a receptor for NGF stimulation, but in contrast to evidence that suggests downregulation of TRKA activity in HD models, *P75 ntr* mRNA was found to be significantly increased in the caudate of human HD brain (Zuccato et al. 2008), as well as in Hdh^{Q111} and R6/1 mouse striata (Brito et al. 2013). In addition to regulating the NGF response, the P75 NTR also modulates TRKB activity (Brito et al. 2013), which has consistently been identified as being downregulated in mouse models of HD, as well as in human HD brain (Ginés et al. 2006; Brito et al. 2013). Reduced BDNF in HD models and human HD brain is also a well characterised phenotype (Baquet et al. 2004; Xie et al. 2010; Zajac et al. 2010), which is thought to be due to reduced transcription of the *Bdnf* gene in response to aberrant regulation of NRSF/REST signalling (Zuccato et al. 2001; Zuccato et al. 2003; Zajac et al. 2010), coupled with reduced BDNF vesicle transport efficiency (Gunawardena et al. 2003). The BDNF signalling pathway also overlaps with both NGF and EGF pathways; specifically, BDNF is known to activate the MAPK (Altar et al. 2004; Ji et al. 2010) and AKT pathways (Kaplan & Miller 2000). A reduction in MAPK activation has been observed in the *StHdh^{Q111}* immortalised cell line following BDNF stimulation, but there was no difference in the effect on the downstream AKT pathway (Ginés et al. 2010). It was therefore suggested that despite reduced levels of the TRKB receptor, a diminished presence and binding of

adaptor proteins may be an additional mechanism that leads to dysregulation of kinase signalling (Ginés et al. 2010). Inhibition of MEK also abrogated the protective effect of BDNF stimulation in *StHdh^Q111* cells, implicating this pathway as a downstream modulator of BDNF activity (Ginés et al. 2010). However, despite substantial disruptions identified at the receptors of various growth factors, mHTT may also be exerting an effect on signalling cascades downstream of growth factor receptors.

HTT and mHTT have been implicated in MAPK signalling pathways; HTT binds to the SH3 domain of MLK2, which prevents activation of the pro-apoptotic JNK pathway. However, in PC12 cells, mHTT is unable to bind to MLK2, therefore increasing activation of the JNK pathway that leads to cell death (Humbert 2003). However, similar to the lack of consensus over AKT activation, there have been mixed findings about the effect of mHTT on MAPK signalling pathways. For example, an 80-90% reduction in MAPK and JNK activation has been reported in PC12 cells (Song et al. 2002), but an increase in sustained ERK activation and alterations in the genes associated with this pathway have also been identified in the same cell line (Apostol et al. 2006). Unfortunately, there has so far been little work investigating the role of P38 MAPK signalling in HD mouse models and immortalised cell lines.

The effect of HTT and mHTT on growth factor signalling pathways has implications for the regulation of transcription; both the AKT pathway and MAPKs are known to play a role in transcription, either by direct regulation or through the phosphorylation of other proteins (Lin et al. 2001; Apostol et al. 2006; Cabodi et al. 2009; Kong et al. 2009; Ro et al. 2010). Therefore it is possible that mHTT may disrupt transcriptional regulation via interruption of growth factor signalling pathways. AKT can directly phosphorylate HTT on S421 (Humbert 2003) and potentially on S13 and S16 (Thompson et al. 2009), which may affect mHTT toxicity by modulating its localisation, and therefore regulation of transcription. The overall phosphorylation of HTT has also been found to be repressed by inhibiting MEK1 activation in 293T cells expressing either 23Q or 148Q (Schilling et al. 2006), suggesting a role of MEK stimulation in the phosphorylation of HTT and mHTT. The effect of disrupted growth factor signalling pathways may therefore alter the phosphorylation of HTT and mHTT, and may also be an indirect mechanism by which transcription is dysregulated in models of HD.

Here, we aim to identify the signalling pathways that are aberrantly controlled in the $StHdh^{Q111}$ cell model of HD in response to a panel of growth factors, and to ascertain whether these pathways are likely to influence the transcription of a panel of immediate-early (IE) genes we have identified as being differentially expressed between genotypes in response to growth factor stimulation. We also aim to determine whether AKT and MEK activity in these cells may be regulating the phosphorylation and nuclear localisation of HTT, and if this may be a mechanism for transcriptional regulation in response to EGF stimulation.
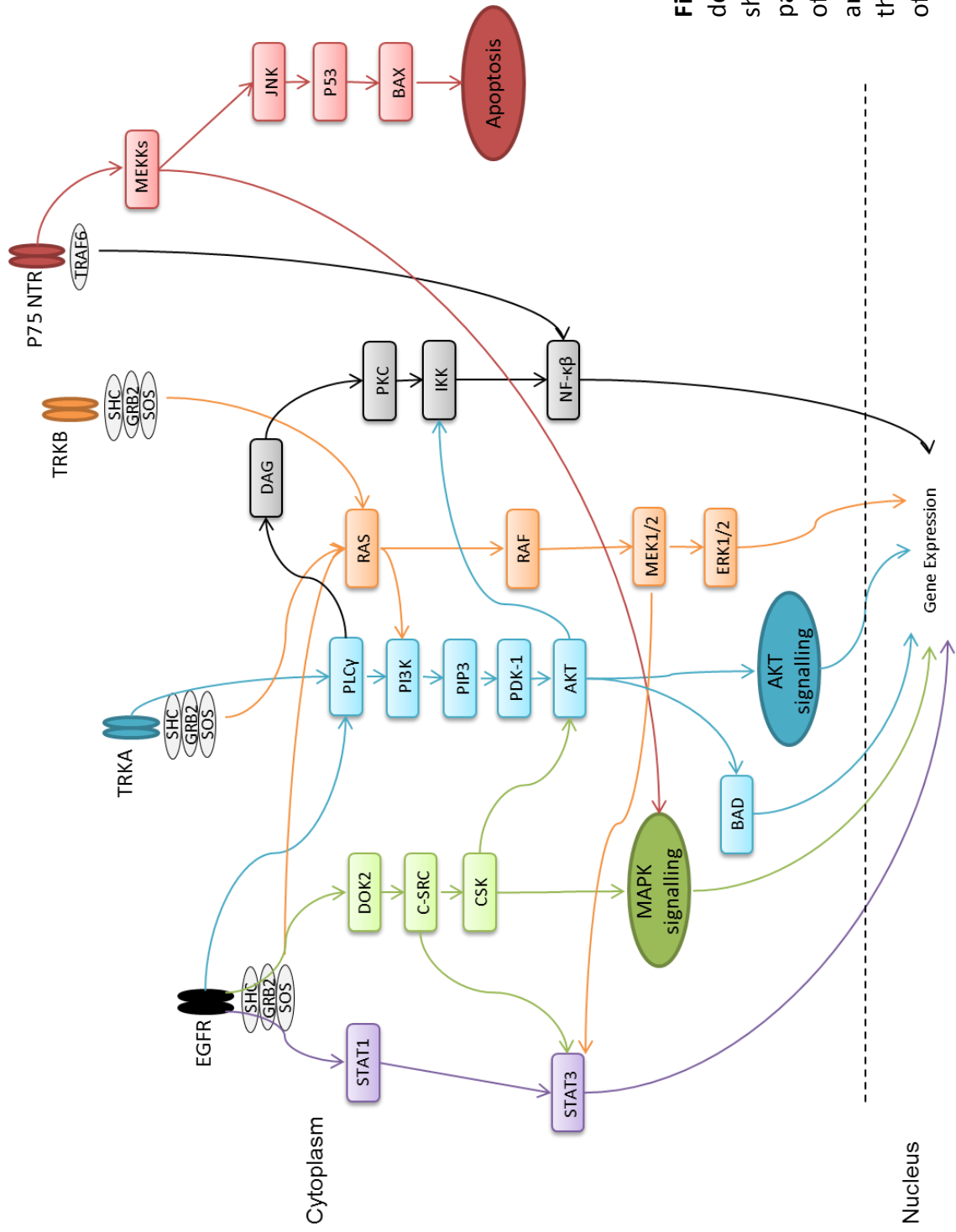
Figure 4.1 A cartoon depicting some of the shared kinase signalling pathways downstream of EGFR, TRKA, TRKB and P75 NTR activation that result in the control of gene expression.

4.2 Signalling pathways downstream of BDNF receptor stimulation

A panel of sandwich ELISA assays was used to investigate the activity within several kinase signalling pathways in *StHdh^{Q111}* cell lines (see Section 2.2.2.10 for further details). In addition to investigating common cellular signalling pathways, three apoptosis-associated signalling markers were also examined; markers of cell stress have previously been identified as being enhanced in models of HD (Liu et al. 1997; Trettel et al. 2000; Humbert 2003; Bae et al. 2005; Apostol et al. 2006; Carnemolla et al. 2009), and dysregulation within these pathways may therefore be an additional mechanism contributing to gene expression changes in the *StHdh^{Q111}* cell model of HD.

4.2.1 Cell signalling pathways

There was a significant interaction effect of BDNF stimulation on the level of AKT1 phosphorylated on serine 473 in *StHdh^{Q111}* cells (Figure 4.2) ($F_{(1, 12)}$ = 10.79, p=0.006). Simple main effects analysis showed that there was no effect of BDNF in *StHdh$^{Q7/7}$* cells (p=0.798), but there was a small reduction in *StHdh$^{Q111/111}$* cells (p=0.013); this reduction lead to a significant difference in the extent of phosphorylated AKT1 change following EGF stimulation between genotypes ($t_{(6)}$ =7.312, p<0.001). However, there were significantly higher levels of phosphorylated AKT1 detected in *StHdh$^{Q111/111}$* cells at baseline compared to *StHdh$^{Q7/7}$* cells (p<0.001), as well as following BDNF stimulation (P= 0.004).

There was also a significant difference in the level of MEK1 phosphorylated on serines 217/221 between *StHdh$^{Q7/7}$* and *StHdh$^{Q111/111}$* cells at baseline (p<0.001) and following BDNF treatment (P< 0.001) (Figure 4.2). Overall, there was a significant effect of both cell type ($F_{(1, 12)}$ = 121.6, p<0.001) and BDNF stimulation ($F_{(1, 12)}$ = 27.23, p<0.001) on the level of phosphorylated MEK1, but there was no significant interaction between the two (P=0.185). Both cell types showed increased phosphorylated MEK1 following BDNF stimulation, but this was only significant in *StHdh$^{Q7/7}$* cells (P=0.003).

P38 MAPK phosphorylated on threonine 180 and tyrosine 182 was not different between genotypes (P=0.115), and there was no effect of BDNF stimulation (P=0.501), plus there was no significant interaction between the two (P=0.523) (Figure 4.2). There

was also no effect of BDNF on phosphorylated signal transducer and activator of transcription 3 (STAT3) (tyrosine 705) (P=0.844), but there was a significant effect of genotype (F (1, 12) = 25.5, p<0.001). Simple main effects analysis showed that this was due to increased phosphorylated STAT3 in *StHdh*$^{Q111/111}$ cells at baseline compared to *Sthdh*$^{Q7/7}$ (P=0.006). BDNF stimulation also had no effect on NFκβ p65, phosphorylated on serine 536 (P=0.152).
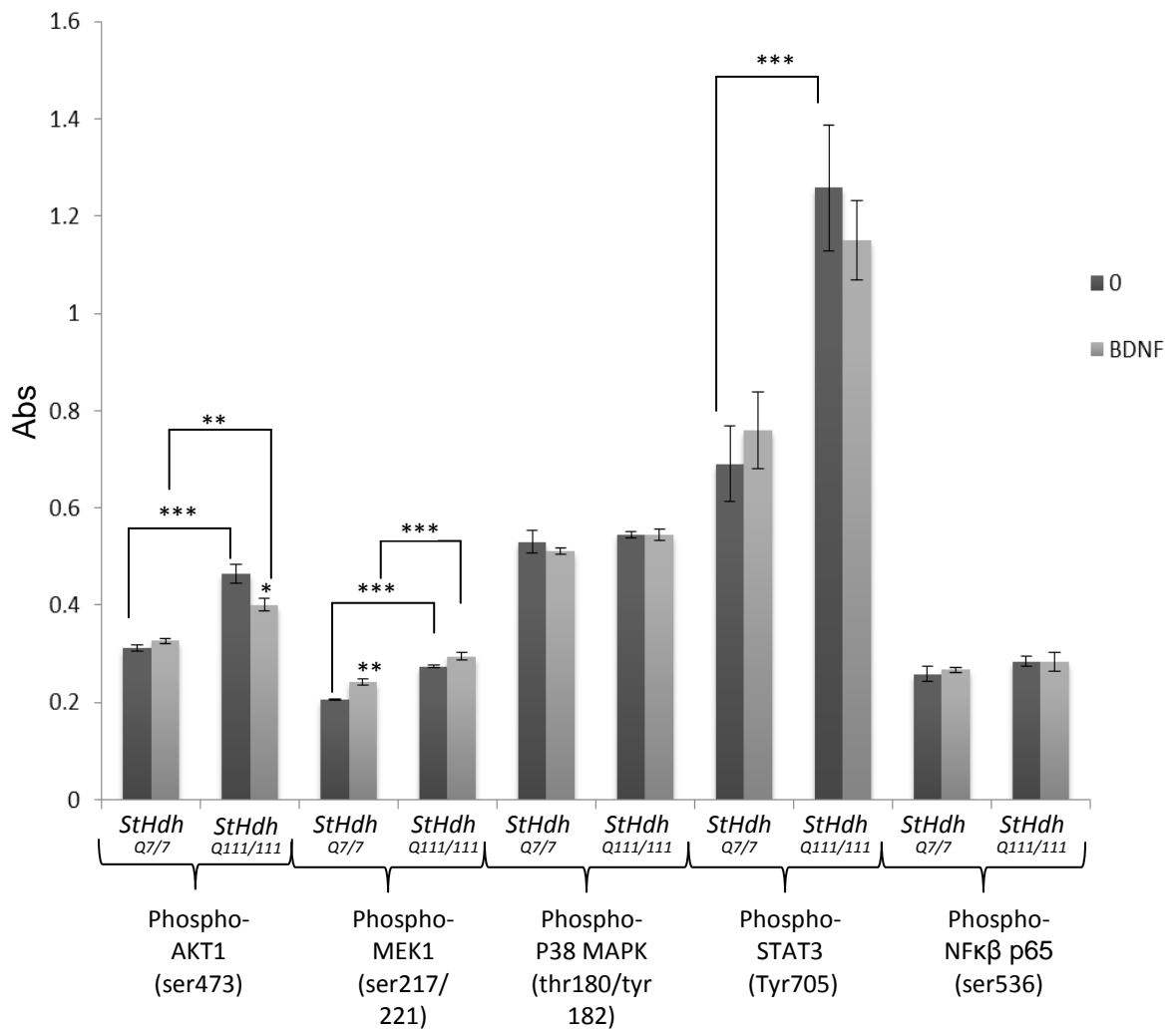
Figure 4.2 Mean absorbance (Abs) read at 450nm following a sandwich ELISA protocol for the detection of a panel of cell signalling markers in *StHdh*$^{Q7/7}$ and *StHdh*$^{Q111/111}$ cells at 0 and 10 minutes of 100ng/ml BDNF stimulation. Absorbance values were statistically analysed by two-way ANOVAs for main effects analysis, followed by a priori one-way ANOVAs to determine simple main effects and post-hoc Tukey tests. Differences between the extent of phosphorylation change following growth factor stimulation were determined by subtracting the absorbance values from 0 mins from 10 mins for each genotype, and were submitted to independent-samples T-tests for analysis. (Error bars = SEM, n=4).
* P<0.05   **P<0.01   ***P<0.001

4.2.2 Apoptotic pathways

To investigate whether different responses to BDNF stimulation between genotypes were a result of differing apoptotic pathways, a series of further sandwich ELISA assays were performed on typical cell death signalling markers (Figure 4.3).
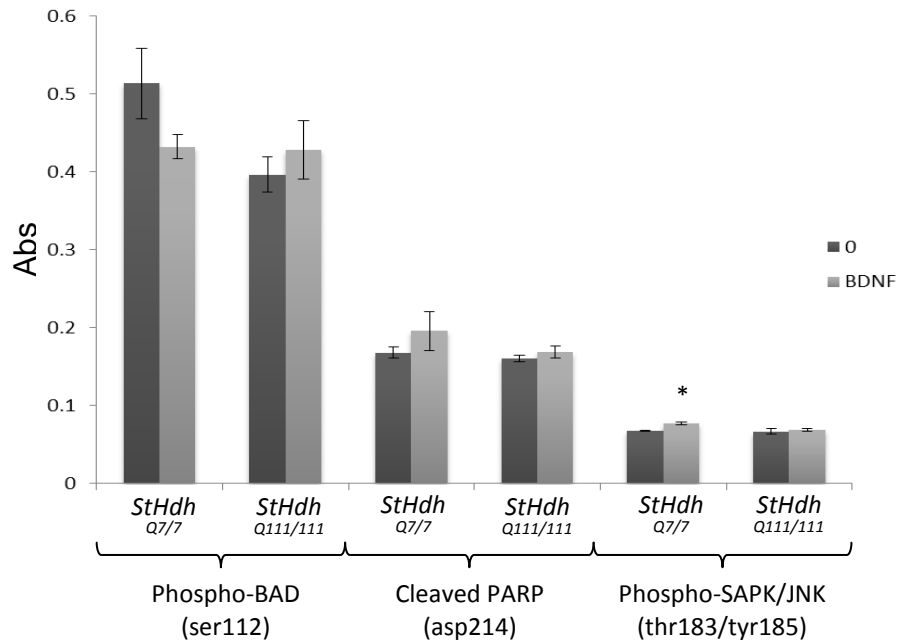
Figure 4.3 Mean absorbance read at 450nm following sandwich ELISA protocol for a panel of cellular apoptotic markers in $StHdh^{Q7/7}$ and $StHdh^{Q111/111}$ cells following 0 and 10 minutes 100ng/ml BDNF stimulation. Absorbance values were statistically analysed by two-way ANOVAs for main effects analysis, followed by a priori one-way ANOVAs to determine simple main effects and post-hoc Tukey tests. Differences between the extent of phosphorylation change following growth factor stimulation were determined by subtracting the absorbance values from 0 mins from 10 mins for each genotype, and were submitted to independent-samples T-tests for analysis. (Error bars = SEM, n=4).
* P<0.05   **P<0.01   ***P<0.001

There was no effect of either genotype or BDNF on the levels of phosphorylated BAD (serine 112) (P= 0.098 and P=0.463, respectively), or cleaved Poly (ADP-ribose) polymerase (PARP) (aspartate 214) (genotype p= 0.229, BDNF p= 0.217), and there were no significant baseline differences between $StHdh^{Q7/7}$ and $StHdh^{Q111/111}$ cells for either of these markers (phosphorylated BAD p= 0.125, cleaved PARP p= 0.979).

However, there was a significant effect of BDNF stimulation on phosphorylated stress activated kinase (SAPK)/JNK (threonine 183/tyrosine 185) (F (1, 12) = 7.59, p= 0.017), although there was no effect of genotype (p= 0.063) and no significant interaction between the two (p=0.139). Post Hoc Tukey tests revealed that the effect of BDNF was in *StHdh*$^{Q7/7}$ cells only, where it initiated a slight increase in phosphorylated SAPK/JNK (P= 0.042), but there was no effect in *StHdh*$^{Q111/111}$ cells.

4.3 Signalling pathways downstream of NGF receptor stimulation

4.3.1 Cell signalling pathways

There were no significant effects of NGF on any of the cell signalling markers that were tested (Figure 4.4). However, the differences found previously between *StHdh*$^{Q7/7}$ and *StHdh*$^{Q111/111}$ cells at baseline were replicated in these samples. There was a significant effect of genotype for phosphorylated AKT1 (F (1, 12) = 71.57, p< 0.001), phosphorylated MEK1 (F (1, 12) = 52.23), p< 0.001) and phosphorylated STAT3 (F (1, 12) = 29.5, p< 0.001), but no interaction with NGF stimulation in any case (p> 0.05). These differences were found to be significant between the genotypes at both baseline and following NGF stimulation.

There was a significant main effect of genotype for phosphorylated P38 MAPK (F (1, 12) = 20.96, p= 0.001), but simple main effects analysis showed that there was no significant difference between the genotypes at baseline (p= 0.68). The effect was found to be from a small, yet significant difference (p= 0.008) between genotypes following NGF stimulation due to a non-significant increase in P38 MAPK phosphorylation in *StHdh*$^{Q7/7}$ cells. However, there was no significant genotype x NGF interaction (p= 0.303). This was also the case for phosphorylated NFκβ; there was a significant effect of genotype (F (1, 12) = 14, p= 0.003), which was found to be from an increase in *StHdh*$^{Q7/7}$ cells following NGF stimulation (p= 0.014) rather than a difference between genotypes at baseline (p= 0.552).
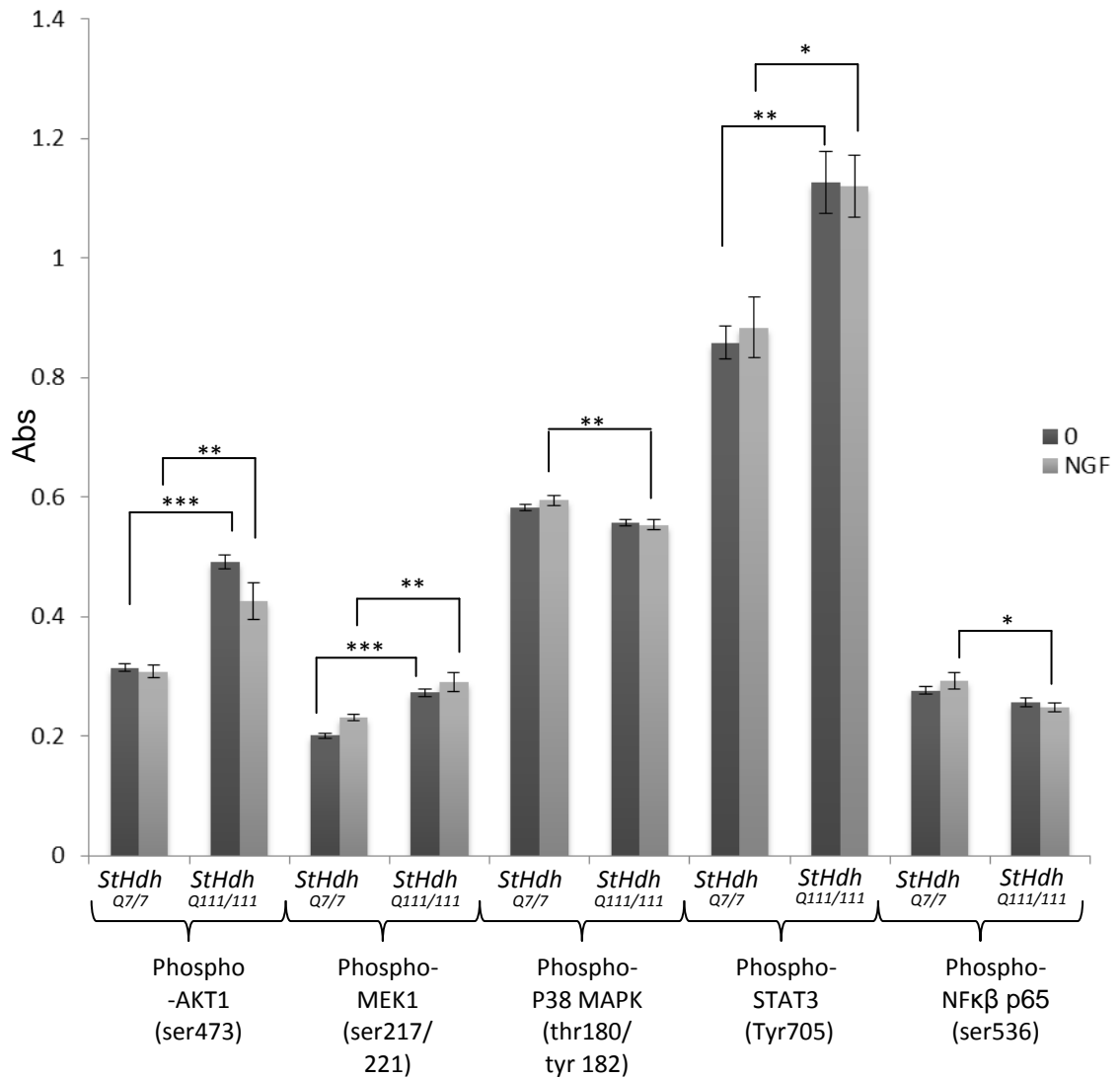
Figure 4.4 Mean absorbance (Abs) read at 450nm following a sandwich ELISA protocol for the detection of a panel of cell signalling markers in $StHdh^{Q7/7}$ and $StHdh^{Q111/111}$ cells at 0 and 10 minutes of 100ng/ml NGF stimulation. Absorbance values were statistically analysed by two-way ANOVAs for main effects analysis, followed by a priori one-way ANOVAs to determine simple main effects and post-hoc Tukey tests. Differences between the extent of phosphorylation change following growth factor stimulation were determined by subtracting the absorbance values from 0 mins from 10 mins for each genotype, and were submitted to independent-samples T-tests for analysis. (Error bars = SEM, n=4).

* P<0.05   **P<0.01   ***P<0.001

4.3.2 Apoptotic pathways

In contrast to previous findings when looking at BDNF stimulation, there was a significant effect of genotype when looking at phosphorylated BAD in these samples ($F_{(1, 12)} = 30.86$, $p < 0.001$); this difference was due to significantly decreased phosphorylated BAD in $StHdh^{Q111/111}$ cells at baseline ($p = 0.019$) and following NGF stimulation ($p = 0.009$). However, the BDNF samples also showed a reduction in phosphorylated BAD in $StHdh^{Q111/111}$ cells, but this failed to reach significance. There was no significant effect of NGF stimulation or a significant interaction with genotype ($P = 0.33$ and $P = 0.48$, respectively) (Figure 4.5).

Cleaved PARP also showed a significant effect of genotype ($F_{(1, 12)} = 19.33$, $P = 0.001$), but no significant effect of NGF ($P = 0.179$) or a significant interaction ($P = 0.345$). Similar to the pattern of activation described in section 4.2.1 following BDNF stimulation, simple main effects analysis shows that the observed genotype effect is due to a slight increase in cleaved PARP in $StHdh^{Q7/7}$ cells following NGF stimulation, causing a significant difference between genotypes ($P = 0.012$). Finally, there was a significant effect of genotype for phosphorylated SAPK/JNK ($F_{(1, 12)} = 8.84$, $p = 0.012$), but this effect failed to remain significant when looking at the simple main effect of genotype at baseline ($P = 0.295$) or following NGF stimulation ($P = 0.142$). There was also no effect of NGF stimulation ($P = 0.06$) or a significant genotype x NGF interaction ($P = 0.736$).
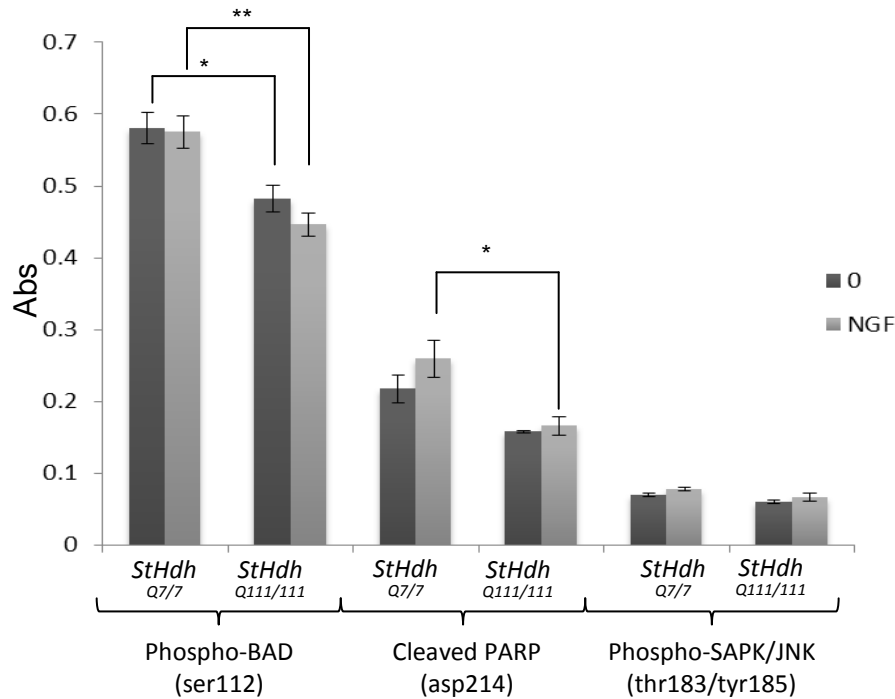
Figure 4.5 Mean absorbance read at 450nm following sandwich ELISA protocol for a panel of cellular apoptotic markers in $StHdh^{Q7/7}$ and $StHdh^{Q111/111}$ cells following 0 and 10 minutes 100ng/ml NGF stimulation. Absorbance values were statistically analysed by two-way ANOVAs for main effects analysis, followed by a priori one-way ANOVAs to determine simple main effects and post-hoc Tukey tests. Differences between the extent of phosphorylation change following growth factor stimulation were determined by subtracting the absorbance values from 0 mins from 10 mins for each genotype, and were submitted to independent-samples T-tests for analysis. (Error bars = SEM, n=4).
* P<0.05   **P<0.01   ***P<0.001

4.4 Signalling pathways downstream of EGF receptor stimulation

4.4.1 Cell signalling pathways

EGF stimulation appears to have had the most striking effect on the activated kinases investigated in these cell lines compared to both NGF and BDNF stimulation. For phosphorylated AKT1, there was a significant effect of genotype (F (1, 12) = 12.75, p= 0.004), EGF (F (1, 12) = 756.23, p<0.001), and a significant interaction between the two (F (1,12) = 5.8, p= 0.033). Although the difference between genotypes that was previously observed at baseline was not replicated here, the level of phosphorylated AKT1 following EGF stimulation was significantly higher in $StHdh^{Q111/111}$ cells than in

172

StHdh$^{Q7/7}$ cells (P= 0.006), thus supporting the notion that there is increased active AKT1 in these cells. In this case, there is a significant increase in phosphorylated AKT1 for both *StHdh*$^{Q7/7}$ (P<0.001) and *StHdh*$^{Q111/111}$ cells (P<0.001), but this response is augmented in the latter cell type (t(6) = -2.465, p=0.049) (Figure 4.6).

The same pattern is observed for phosphorylated MEK1; there is a significant effect of genotype (F (1,12) = 98, p<0.001), EGF (F (1,12) = 3082.28, p<0.001), and a significant interaction between the two (F (1,12) = 81.33, p<0.001). However, although both genotypes have increased phosphorylated MEK1 following EGF stimulation (both p<0.001), the effect is suppressed in *StHdh*$^{Q111/111}$ cells (t(6) = 8.107, p<0.001), which have significantly lower phosphorylated MEK1 following EGF than *StHdh*$^{Q7/7}$ cells (p<0.001). Contrary to previous observations (Sections 4.2.1 & 4.3.1), there was no significant difference between genotypes at baseline in these samples.

In accordance with previous findings, there was a significant effect of genotype for phosphorylated STAT3 (F (1, 12) = 759.78, p<0.001), which was due to increased levels in *StHdh*$^{Q111/111}$ cells at baseline (p<0.001) and following EGF stimulation (p<0.001). There was also a significant effect of EGF (F (1, 12) = 33.75, p<0.001) and a significant interaction (F (1, 12) = 43.03, p<0.001), both due to a large increase in phosphorylated STAT3 in *StHdh*$^{Q111/111}$ cells following EGF stimulation (p<0.001), but no effect in *StHdh*$^{Q7/7}$ cells. The difference in the extent of phosphorylation change following EGF stimulation was therefore significantly higher in *StHdh*$^{Q111/111}$ cells (t(6) = -12.821, p<0.001). The same pattern was observed for phosphorylated P38 MAPK.

Finally, there was a significant effect of genotype for phosphorylated NFκβ (F (1, 12) = 6.43, p= 0.026), which was due to higher activation in *StHdh*$^{Q111/111}$ cells at baseline (P= 0.012). Previously, this had not reached significance; however there was a trend towards this in Section 4.2.1 (BDNF stimulation). This difference disappeared following EGF stimulation due to a small, non-significant reduction in *StHdh*$^{Q111/111}$ cells. There was no effect of EGF stimulation (P= 0.347) on phosphorylated NFκβ, however there was a significant genotype x EGF interaction (F (1, 12) = 8.07, p= 0.015).
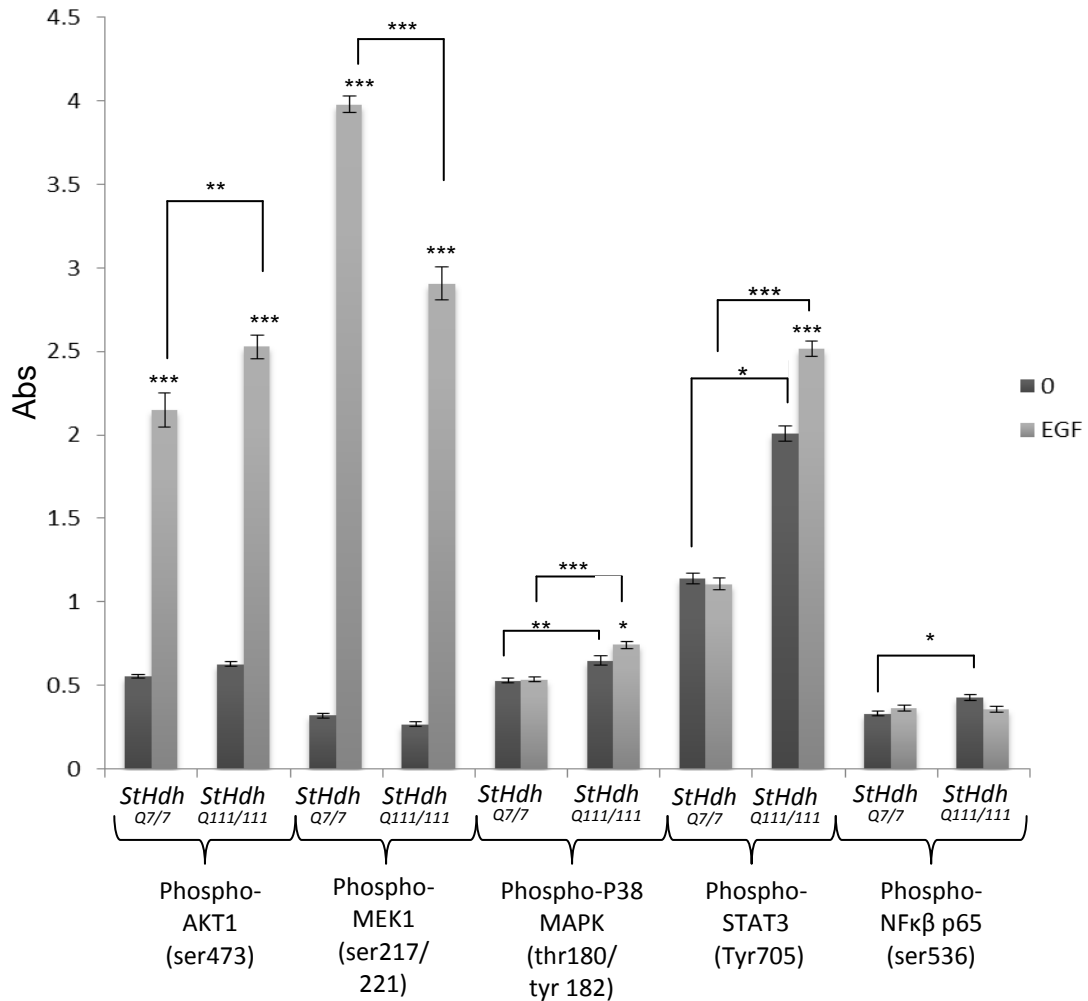
Figure 4.6 Mean absorbance (Abs) read at 450nm following a sandwich ELISA protocol for the detection of a panel of cell signalling markers in $StHdh^{Q7/7}$ and $StHdh^{Q111/111}$ cells at 0 and 10 minutes of 100ng/ml EGF stimulation. Absorbance values were statistically analysed by two-way ANOVAs for main effects analysis, followed by a priori one-way ANOVAs to determine simple main effects and post-hoc Tukey tests. Differences between the extent of phosphorylation change following growth factor stimulation were determined by subtracting the absorbance values from 0 mins from 10 mins for each genotype, and were submitted to independent-samples T-tests for analysis. (Error bars = SEM, n=4).
* P<0.05   **P<0.01   ***P<0.001

4.4.2 Apoptotic pathways

In contrast with BDNF and NGF stimulation, there was a significant effect of EGF on phosphorylated BAD in both cell lines (Figure 4.7) (F (1, 12) = 111.62, p<0.001), as levels of phosphorylated BAD increased in both $StHdh^{Q7/7}$ (P= 0.002) and $StHdh^{Q111/111}$ (P<0.001) cells. However, there was also a significant interaction with genotype (F (1,

12) = 10.98, p= 0.008), as phosphorylation was enhanced in $StHdh^{Q111/111}$ cells (p<0.001), which was to a significantly larger extent than in $StHdh^{Q7/7}$ cells (t(4) = -3.81, p=0.019). In contrast to the BDNF and NGF results reported here, there was no difference at baseline between genotypes (P= 0.194).

There was no effect of genotype, EGF, or an interaction between the two for either cleaved PARP or phosphorylated SAPK/JNK (P>0.05).
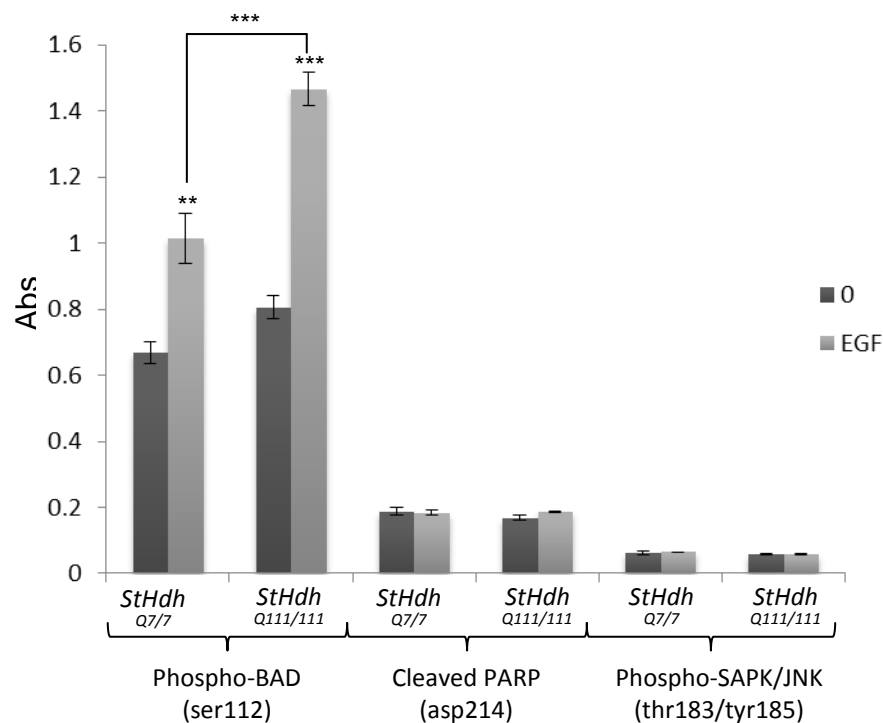
Figure 4.7 Mean absorbance read at 450nm following sandwich ELISA protocol for a panel of cellular apoptotic markers in $StHdh^{Q7/7}$ and $StHdh^{Q111/111}$ cells following 0 and 10 minutes 100ng/ml EGF stimulation. Absorbance values were statistically analysed by two-way ANOVAs for main effects analysis, followed by a priori one-way ANOVAs to determine simple main effects and post-hoc Tukey tests. Differences between the extent of phosphorylation change following growth factor stimulation were determined by subtracting the absorbance values from 0 mins from 10 mins for each genotype, and were submitted to independent-samples T-tests for analysis. (Error bars = SEM, n=4).
* P<0.05   **P<0.01   ***P<0.001

4.5 Inhibition of EGF signalling pathways

As EGF stimulation elicited the greatest response in *StHdh^{Q111}* cells, we utilised this growth factor in order to further investigate aberrant cell signalling pathways due to the presence of mHTT. EGF had the largest effect on AKT1 and MEK1 phosphorylation in a differential manner between genotypes, so these pathways were chosen for further investigation.

4.5.1 AKT inhibition

4.5.1.1 Inhibitor concentration

AKT inhibitor VIII is a reversible quinoxaline compound that can selectively inhibit the phosphorylation of AKT1 and 2; its structure and mode of action are described in Figure 4.8. In order to determine the optimum concentration of AKT inhibitor VIII required to efficiently inhibit phosphorylated AKT1 in *StHdh^{Q111}* cells, a concentration curve experiment was carried out (Figure 4.9).

Although 250nM of AKT inhibitor VIII reduced the level of phosphorylated AKT1 measured by ELISA assay to levels that were comparable to baseline in *StHdh$^{Q7/7}$* cells (p= 0.054), phosphorylated AKT1 in both *StHdh$^{Q7/111}$* and *StHdh$^{Q111/111}$* cells, remained significantly higher than baseline (P<0.001, P=0.004 respectively). At 500nM of inhibitor, although there was still significantly more phosphorylated AKT1 in *StHdh$^{Q7/111}$* cells than at baseline (p= 0.006), it was still significantly lower than when the cells were stimulated with EGF without any inhibitor present (p<0.001). At this molarity, levels in *StHdh$^{Q111/111}$* cells were brought back down to baseline (p= 0.124), and in *StHdh$^{Q7/7}$* cells AKT1 phosphorylation was slightly suppressed below baseline levels (p= 0.041). There was no significant effect of AKT inhibitor VIII on the activation of MEK1, suggesting that this compound is targeting a separate pathway. It was therefore decided that 500nM AKT inhibitor VIII would be used for the following experiments.
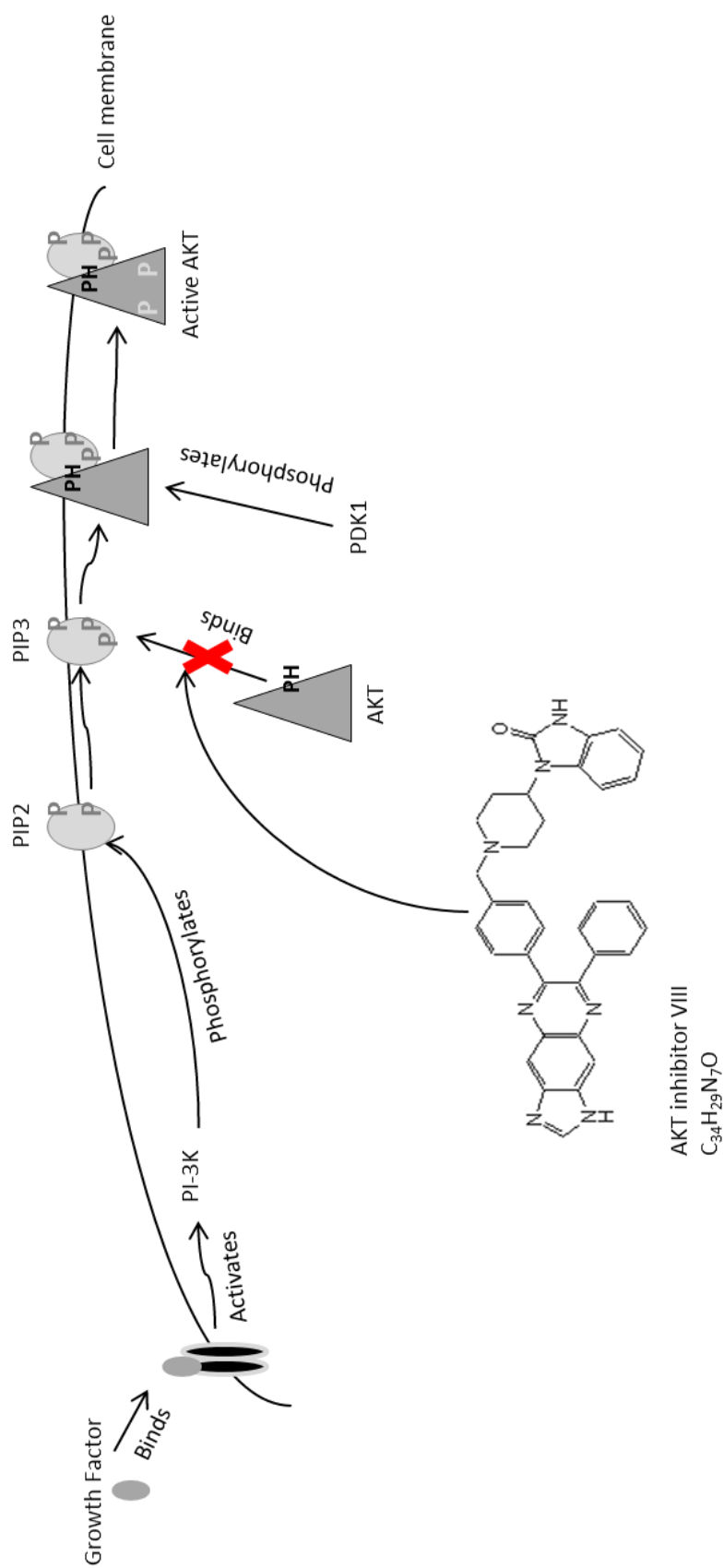
Figure 4.8 Simplified cartoon depicting the activation of AKT and its inhibition by AKT inhibitor VIII. Growth factor binding to a receptor tyrosine kinase activates PI-3K, which phosphorylates PIP2, creating PIP3. AKT is then anchored to PIP3 through its PH-domain. This allows activation of AKT by phosphorylation of its tyrosine and serine residues by PDK1. AKT inhibitor VIII is PH-domain specific, so prevents AKT binding to PIP3, thus inhibiting AKT activation.
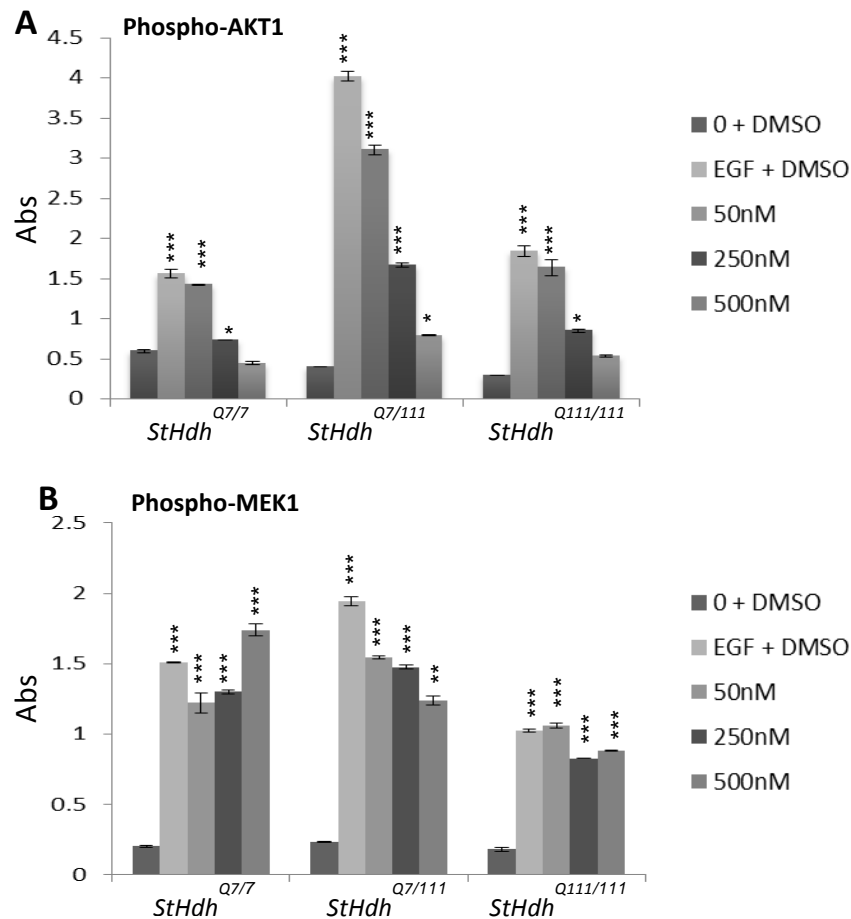
Figure 4.9 Mean absorbance read at 450nm following a sandwich ELISA protocol in $StHdh^{Q111}$ cells to determination the optimum concentration of AKT inhibitor VIII in order to prevent phosphorylation of AKT1 on serine 473 following 5 minutes stimulation with 100ng/ml EGF. The inhibitor was tested at 50, 250 and 500nM, prepared in DMSO solution for 2 hours prior to EGF stimulation. Inhibitor-free time points included the equivalent volume of DMSO in the media for the same length of time prior to EGF stimulation and sample collection. **A**. Effect of AKT inhibitor VIII on the phosphorylation of AKT1 (serine 473). **B.** Effect of AKT Inhibitor VIII on the phosphorylation of MEK1 (serines 217/221). Absorbance values were statistically analysed by two-way ANOVAs for main effects analysis, followed by a priori one-way ANOVAs to determine simple main effects and post-hoc Tukey tests. (Error bars = SEM, n=3).

*p<0.05   ** p<0.01   ***p<0.001

4.5.1.2 Localisation of HTT and mHTT following EGF stimulation when AKT is inhibited

To investigate whether AKT signalling following EGF stimulation may play a role in the control of HTT and mHTT localisation, $StHdh^{Q7/7}$, $StHdh^{Q7/111}$ and $StHdh^{Q111/111}$ cells were serum starved overnight, then cells were treated with either DMSO or AKT inhibitor VIII for 2 hours prior to stimulation with EGF for 0, 5, 15 and 30 minutes. The cells were then fixed, stained, imaged and analysed in the same manner as described in Chapter 3.

4.5.1.2a Ab109115

Once fixed, the cells were double stained with HTT N-terminal antibodies Ab109115 and Mab2166. It was previously found that the nuclear detection of HTT decreased in $StHdh^{Q7/7}$ cells for both of these antibodies following EGF stimulation when no inhibitor was present, but there was a slight increase in nuclear detection in $StHdh^{Q111/111}$ cells (Sections 3.3.4.3 & 3.3.5).

When AKT activation was inhibited during stimulation with EGF, there was a significant increase in the N/C ratio after 5 ($p=0.014$) and 15 minutes ($p=0.03$) in $StHdh^{Q7/7}$ cells, which was also apparent in the N/P ratio at 15 minutes ($p<0.001$), indicating an increase in detection of this epitope of HTT in the nucleus (Figures 4.10 and 4.11). There is also a significant reduction in the P/C ratio from 15 minutes of EGF stimulation ($p=0.016$), which supports the relocalisation of HTT from the perinuclear area into the nucleus. The increase in nuclear HTT appears in a speckled pattern rather than as a diffuse stain, and is most apparent at 5 minutes of stimulation. In comparison, when $StHdh^{Q7/7}$ cells are stimulated with EGF for 5 minutes without AKT inhibition, there is no difference in the localisation of HTT.

In $StHdh^{Q111/111}$ cells, there was the converse effect of inhibiting AKT activation by EGF stimulation. In Chapter 3, there was very little effect of EGF stimulation on the localisation of mHTT in these cells. However, when AKT was inhibited, there was a significant reduction in nuclear mHTT at all three time points when looking at the N/P ratio ($p<0.001$ in all cases). The reduction was also apparent in the N/C ratio, but this

did not reach significance. There was also an increase in the P/C ratio at 5 minutes, which would mirror movement of mHTT from the nucleus into the perinucleus, but this did not reach significance due to high variability among cells. When AKT was not inhibited, EGF stimulation had no effect on the localisation of mHTT in these cells. This suggests that HTT and mHTT may interact very differently with the AKT pathway in a manner that may regulate its localisation. There was no effect of AKT inhibition or EGF stimulation on the detection of this epitope of HTT in $StHdh^{Q7/111}$ cells at any time point in the N/C, N/P or P/C ratios; it is possible that this reflects the opposing effects of AKT inhibition on HTT and mHTT, both of which are present in these cells.
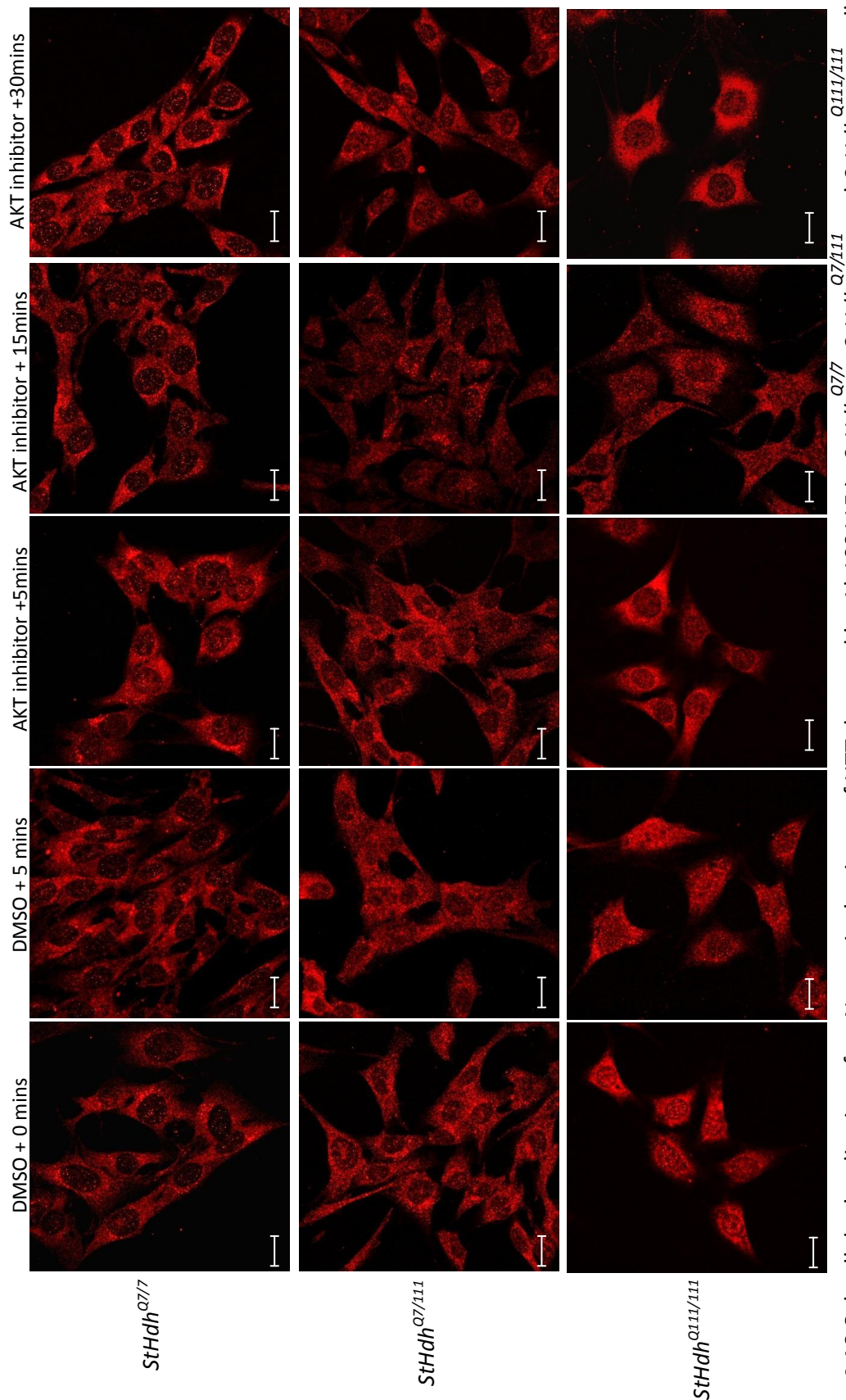
Figure 4.10 Subcellular localisation of an N-terminal epitope of HTT detected by Ab109115 in *StHdh*^Q7/7^, *StHdh*^Q7/11^ and *StHdh*^Q111/111^ cells. All genotypes were serum starved overnight before being treated for 0, 5, 15 and 30 minutes with 100ng/ml EGF after either 2 hours incubation with 500nM AKT inhibitor VIII, or media containing the equivalent volume of DMSO (see Sections 2.2.4.1 & 2.2.4.2). Cells were then analysed by confocal microscopy (see Sections 2.2.1.8 & 2.2.1.9 for further details). Scale bar = 20μm
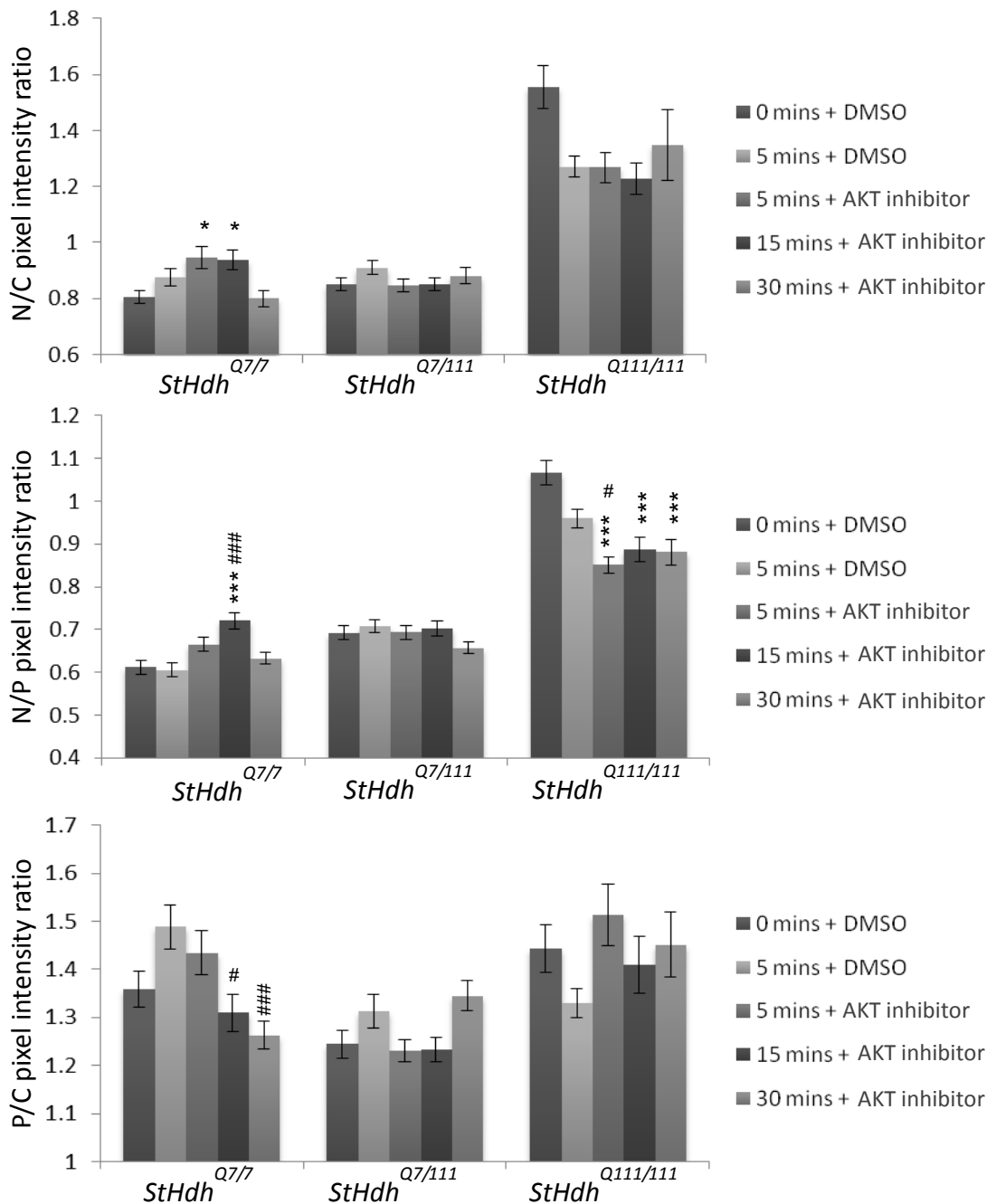
Figure 4.11 Quantitative analysis of immunofluorescence images in Figure 4.10. Nuclear/Cytoplasmic, Nuclear/Perinuclear and Perinuclear/Cytoplasmic mean pixel intensity ratios for $StHdh^{Q7/7}$, $StHdh^{Q7/111}$ and $StHdh^{Q111/111}$ cells following 0, 5, 15 and 30 minutes of stimulation with 100ng/ml EGF following 2 hours incubation with either 500nM AKT inhibitor VIII or the equivalent volume of DMSO. Mean pixel intensities were calculated from confocal microscopy images using GNU Image Manipulator (further details of the analysis can be found in Section 2.2.1.10). All images were randomised and analysed blind to genotype, AKT inhibition and length of time stimulated with EGF. Each condition consisted of 9 confocal microscopy images taken from 3 separate coverslips. A two-way ANOVA was carried out for main effects analysis, followed by planned one-way ANOVAs and post-hoc Tukey tests. Error bars = SEM

* Denotes difference from 0. # Denotes difference from 5 mins + DMSO

*p<0.05, ** p<0.01, *** p<0.001

4.5.1.2b Mab2166

StHdh^{Q111} cells stained with Ab109115 were double-labelled with Mab2166, however as this antibody detects a different epitope of HTT, the patterns of localisation differed slightly. In *StHdh*$^{Q7/7}$ cells, there was still a significant increase in the nuclear detection of HTT at 5 minutes of EGF stimulation when AKT was inhibited, which was most apparent in the N/P ratio (p=0.001), but was also present in the N/C ratio (p=0.026). However, this did not persist beyond 5 minutes (Figures 4.12 & 4.13). The epitope of HTT that was detected in the nucleus by Mab2166 was more diffuse and subtle than the epitope detected by Ab109115. There was no difference in the P/C ratio in *StHdh*$^{Q7/7}$ cells, although there was a trend towards a perinuclear accumulation of this epitope, which may reflect the movement of nuclear HTT out of the nucleus following its initial increase at 5 minutes.

In contrast to Ab109115, there was a significant increase in the N/P ratio for *StHdh*$^{Q7/111}$ cells from 5 minutes of EGF stimulation when AKT was inhibited (p<0.001) as compared to both 0 and 5 minutes of EGF stimulation without inhibition. The N/P ratio decreased by 15 minutes, but remained significantly higher than the non-inhibited 5 minute time point for the entire 30 minutes of stimulation (p<0.001). There was no significant effect in the N/C ratio, but there was a decrease in the P/C ratio at 5 minutes (p=0.03), which is concordant with an increased N/P ratio. Taken together, this suggests that any movement of HTT in this model occurs mostly between the nuclear and perinuclear regions of the cell, which is consistent with previous findings (Section 3.3.4.3). These findings also suggest that although the effect is smaller, for this epitope of HTT the *StHdh*$^{Q7/111}$ cells respond more similarly to *StHdh*$^{Q7/7}$ cells than the *StHdh*$^{Q111/111}$ cells.

The epitope of mHTT detected by Mab2166 appears to be less responsive to the effect of AKT inhibition in *StHdh*$^{Q111/111}$ cells than the epitope detected by Ab109115, however the N/P ratio is still significantly reduced at 15 minutes (p<0.001), indicating a reduction in nuclear mHTT. In contrast, both the N/C and P/C ratios are significantly increased at 30 minutes (p=0.015, p=0.004 respectively), which isn't apparent with Ab109115. In addition to the likely detection of alternate mHTT epitopes by these two

antibodies, this effect may be due to a delayed response of potentially longer mHTT epitopes to AKT inhibition in these cells, or may be a homeostatic reaction in response to the prior reduction in nuclear mHTT.
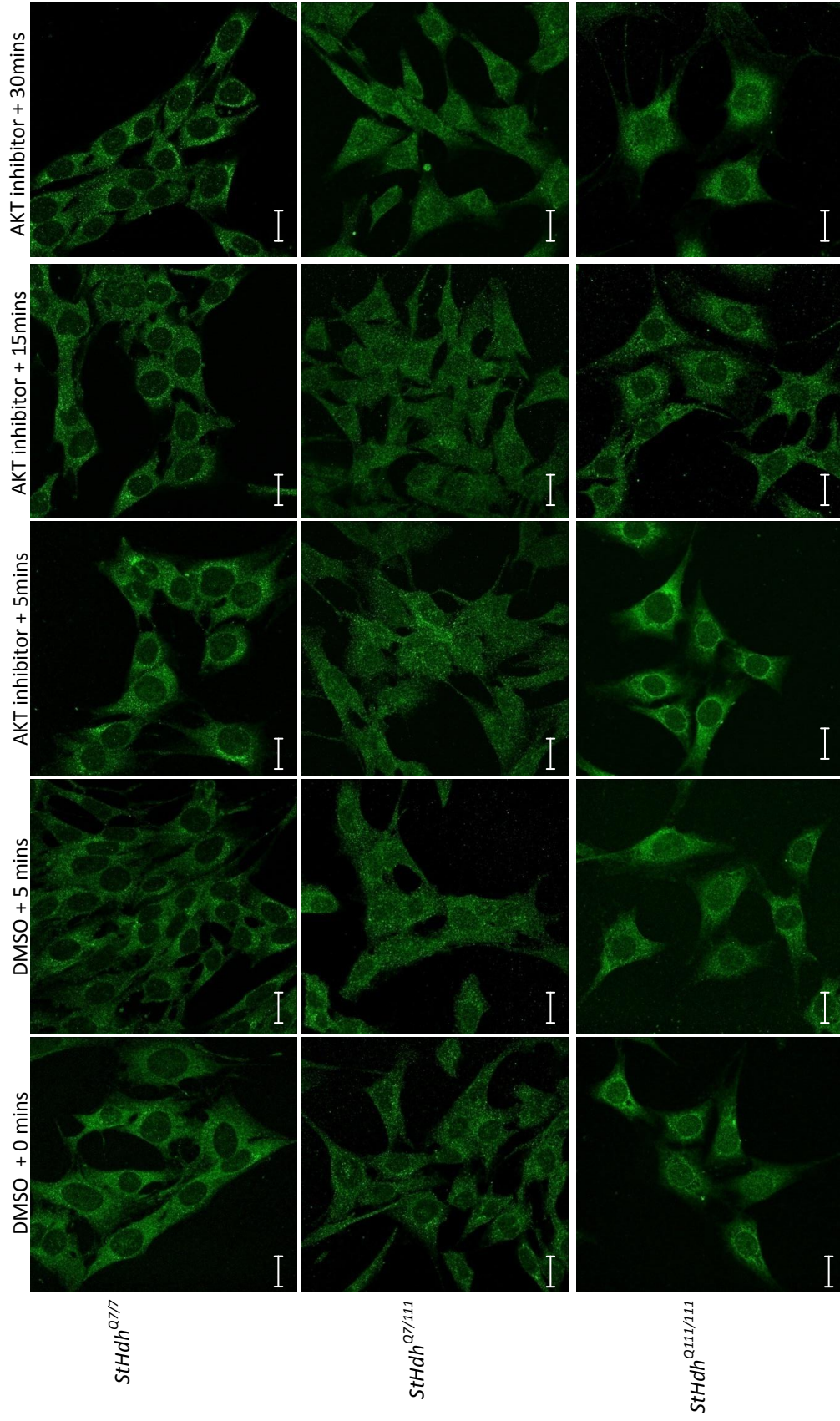
Figure 4.12 Subcellular localisation of an N-terminal epitope of HTT detected by Mab2166 in $StHdh^{Q7/7}$, $StHdh^{Q7/111}$ and $StHdh^{Q111/111}$ cells. All genotypes were serum starved overnight before being treated for 0, 5, 15 and 30 minutes with 100ng/ml EGF after either 2 hours incubation with 500nM AKT inhibitor VIII, or media containing the equivalent volume of DMSO (see Sections 2.2.4.1 & 2.2.4.2). Cells were then analysed by confocal microscopy (see Sections 2.2.1.8 & 2.2.1.9 for further details). Scale bar = 20μm
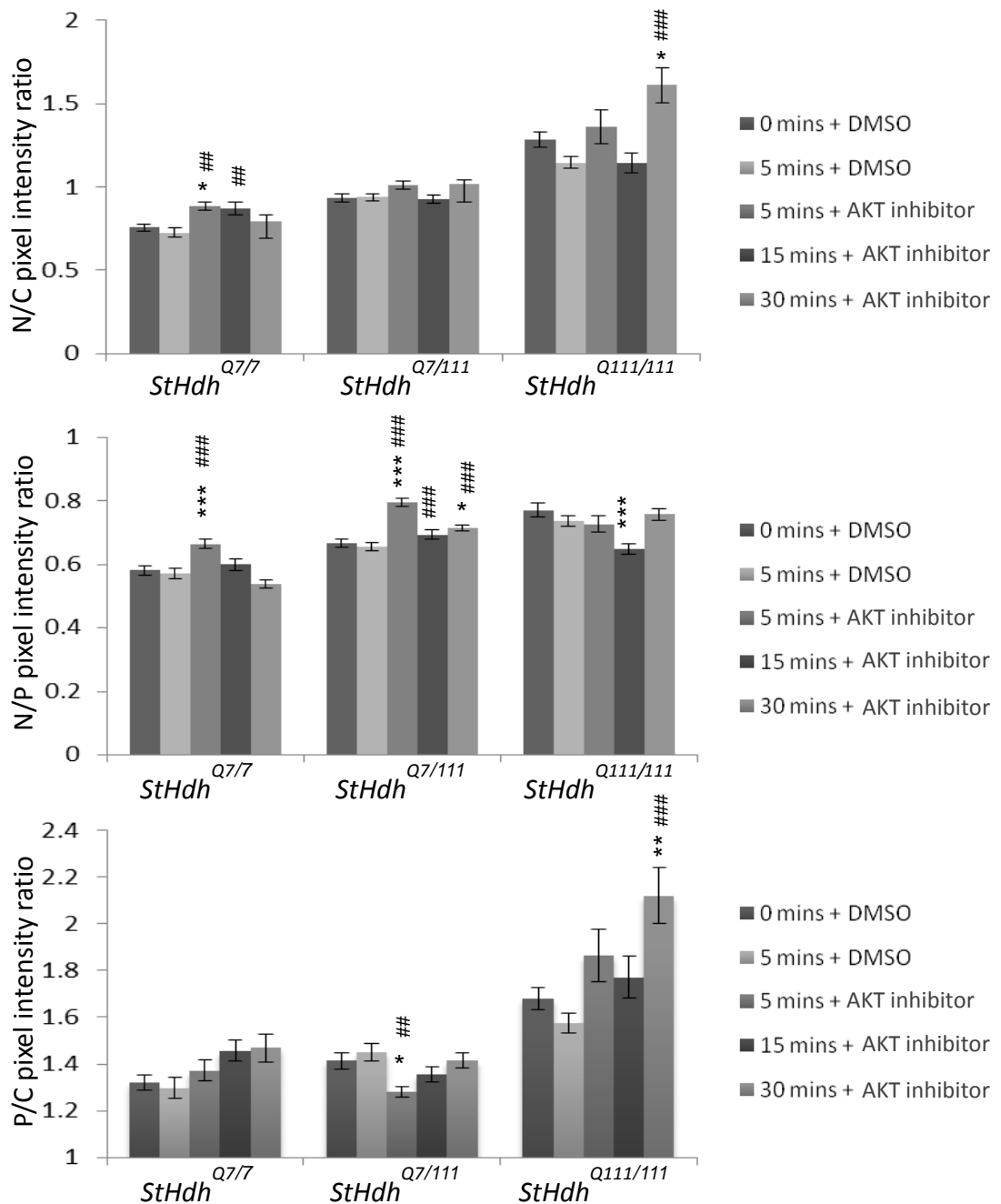
Figure 4.13 Quantitative analysis of immunofluorescence images in Figure 4.12. Nuclear/Cytoplasmic, Nuclear/Perinuclear and Perinuclear/Cytoplasmic mean pixel intensity ratios for $StHdh^{Q7/7}$, $StHdh^{Q7/111}$ and $StHdh^{Q111/111}$ cells following 0, 5, 15 and 30 minutes of stimulation with 100ng/ml EGF following 2 hours incubation with either 500nM AKT inhibitor VIII or the equivalent volume of DMSO. Mean pixel intensities were calculated from confocal microscopy images using GNU Image Manipulator (further details of the analysis can be found in Section 2.2.1.10). All images were randomised and analysed blind to genotype, AKT inhibition and length of time stimulated with EGF. Each condition consisted of 9 confocal microscopy images taken from 3 separate coverslips. . A two-way ANOVA was carried out for main effects analysis, followed by planned one-way ANOVAs and post-hoc Tukey tests. Error bars = SEM

* Denotes difference from 0. # Denotes difference from 5 mins + DMSO

*p<0.05, ** p<0.01, *** p<0.001

4.5.1.2c Ab675 and N17

In order to determine the reproducibility of these findings, the experiment was repeated and cells were labelled with either Ab675 or N17; both N-terminal HTT antibodies that detect a similar epitope to Ab109115. In Chapter 3, cells stained with Ab675 exhibited the same pattern of response following EGF stimulation as those stained with Ab109115, but there was no effect of EGF on the epitope detected by N17. In contrast to the previous experiment, these images were not quantitatively analysed.

Ab675 detected a similar pattern of localisation as Ab109115 when AKT activity was inhibited (Figure 4.14); there is a visible increase in nuclear staining in $StHdh^{Q7/7}$ cells following incubation with the AKT inhibitor, and a contrasting reduction in nuclear detection in $StHdh^{Q111/111}$ cells from 5 to 15 minutes of EGF stimulation is also seen. $StHdh^{Q7/111}$ cells exhibit less of an effect, as they did with Ab109115, supporting a gene dosage effect. However, there is a slight reduction in nuclear HTT from 15 minutes, suggesting that in terms of the response of this epitope to inhibited AKT activity, they may be more similar to $StHdh^{Q111/111}$ cells than $StHdh^{Q7/7}$.

In general, the N17 antibody supported the results from the previous N-terminal antibodies, however consistent with the different pattern of detection in Chapter 3 following EGF stimulation, the findings also differed slightly when AKT was inhibited. In $StHdh^{Q7/7}$ cells, there was again an increase in the detection of nuclear HTT that was apparent from 5 minutes of stimulation (Figure 4.15). However, there was also a visible reduction in the nuclei of $StHdh^{Q111/111}$ cells, but this did not occur until 15 minutes of stimulation, and did not persist up to 30 minutes. Similarly, $StHdh^{Q7/111}$ cells also had a reduction in detection of nuclear HTT at 15 minutes, which was more like the detection by Ab675, but in contrast to Mab2166. This suggests that generally the localisation response of HTT and mHTT to EGF stimulation when AKT is inhibited is reproducible and similar between different epitopes of HTT; inhibiting AKT in $StHdh^{Q7/7}$ cells prompts localisation of HTT towards the nucleus, whereas it elicits a reduction of mHTT in $StHdh^{Q111/111}$ cells. The findings in $StHdh^{Q7/111}$ are a lot more variable, most likely due to a gene dosage effect and the expression of both HTT and mHTT epitopes.
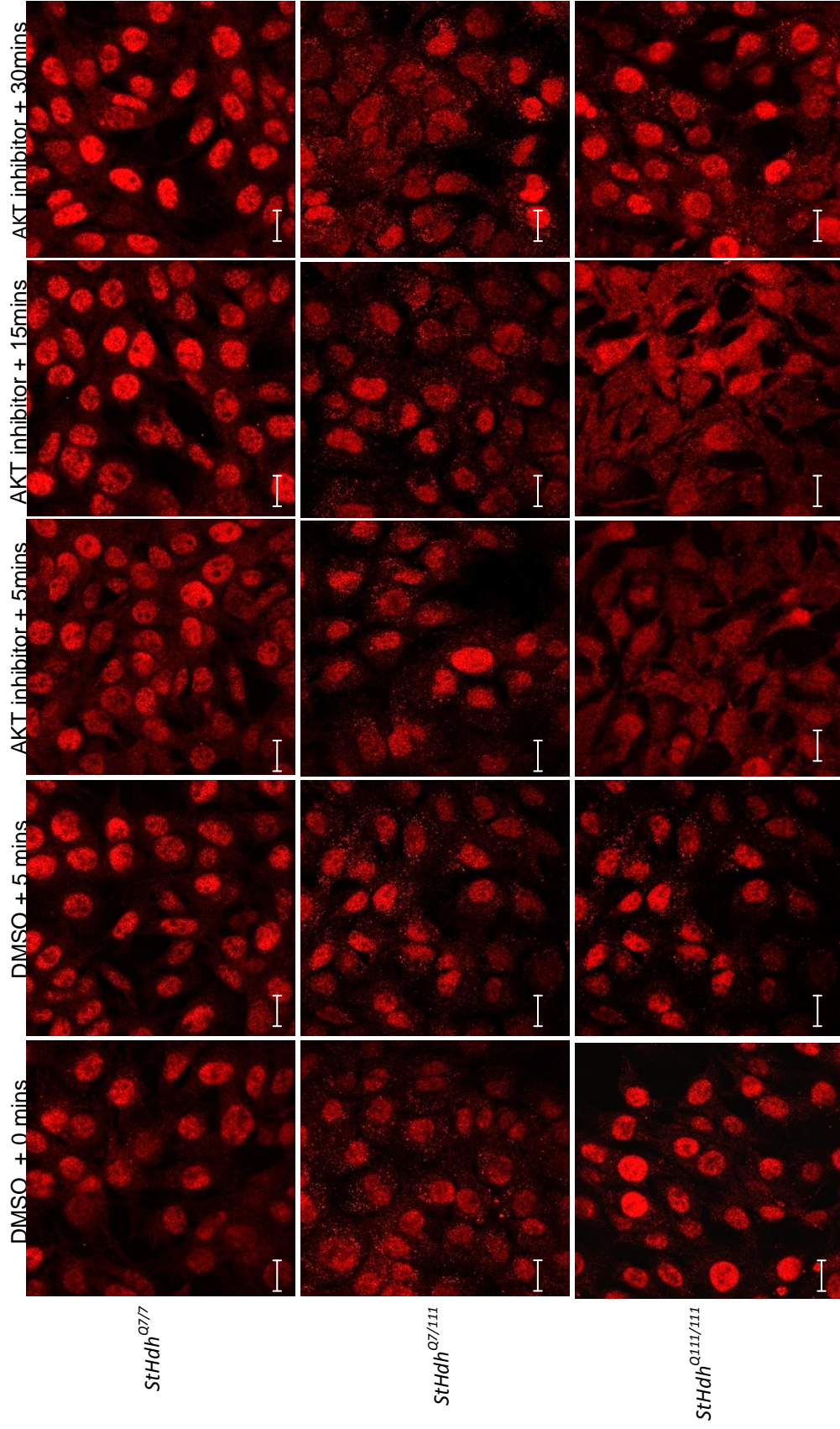
Figure 4.14 Subcellular localisation of an N-terminal epitope of HTT detected by Ab675 in *StHdh*$^{Q7/7}$, *StHdh*$^{Q7/111}$ and *StHdh*$^{Q111/111}$ cells. All genotypes were serum starved overnight before being treated for 0, 5, 15 and 30 minutes with 100ng/ml EGF after either 2 hours incubation with 500nM AKT inhibitor VIII, or media containing the equivalent volume of DMSO (see Sections 2.2.4.1 & 2.2.4.2). Cells were then analysed by confocal microscopy (see Sections 2.2.1.8 & 2.2.1.9 for further details). Scale bar = 20μm
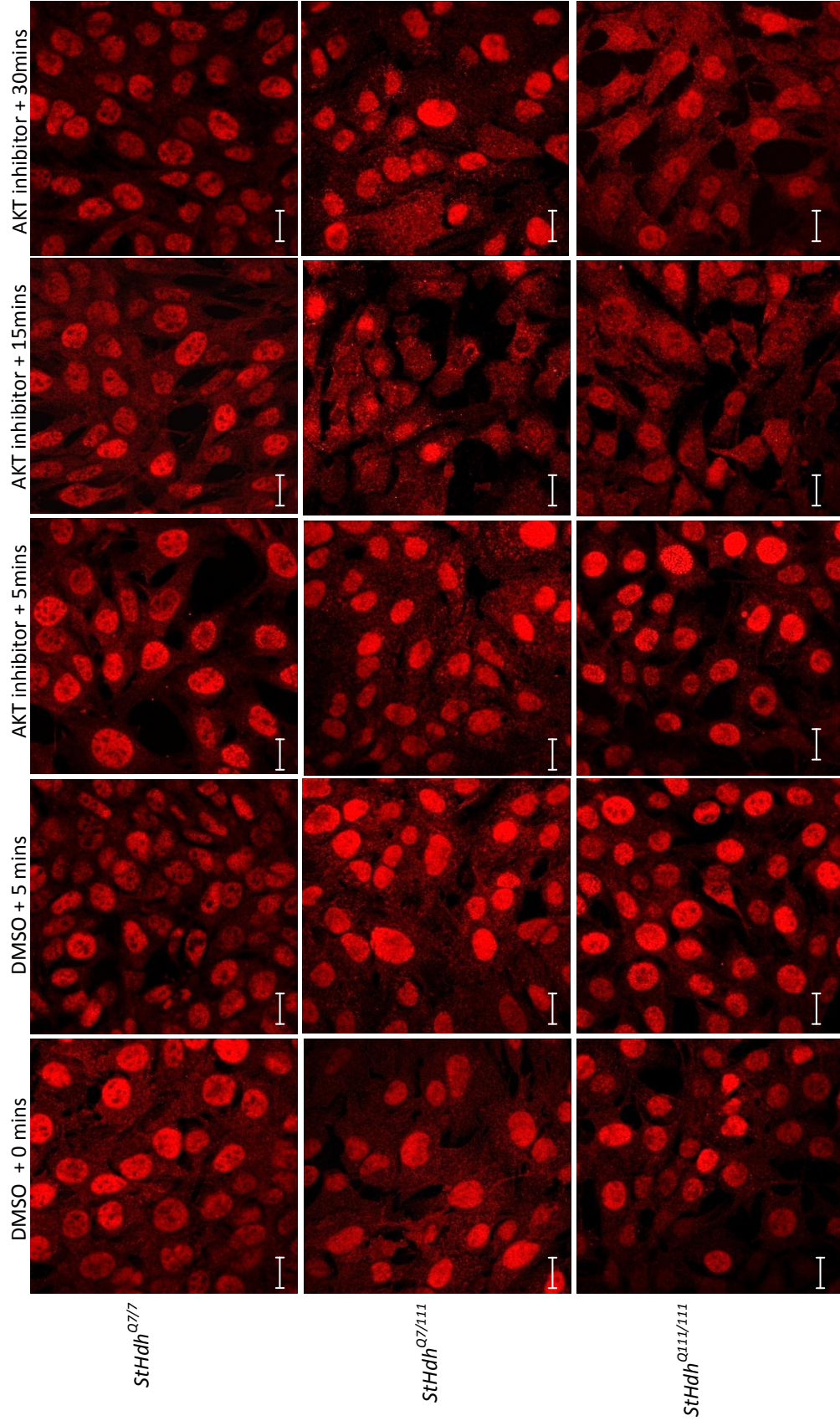
Figure 4.15 Subcellular localisation of an N-terminal epitope of HTT detected by N17 in *StHdh*$^{Q7/7}$, *StHdh*$^{Q7/111}$ and *StHdh*$^{Q111/111}$ cells. All genotypes were serum starved overnight before being treated for 0, 5, 15 and 30 minutes with 100ng/ml EGF after either 2 hours incubation with 500nM AKT inhibitor VIII, or media containing the equivalent volume of DMSO (see Sections 2.2.4.1 & 2.2.4.2). Cells were then analysed by confocal microscopy (see Sections 2.2.1.8 & 2.2.1.9 for further details). Scale bar = 20µm

4.5.1.3 Localisation of phosphorylated HTT epitopes following EGF stimulation when AKT is inhibited.

The same experiment was repeated, and cells were labelled with the N17 S1316p phospho-antibody. This was the only remaining phospho-antibody available, so we were unable to look at the effect on S13 phosphorylation alone or compare double phosphorylation antibodies. In this instance, $StHdh^{Q7/111}$ cells were not utilised as the staining and imaging was of insufficient quality.

There was a significant nuclear increase of phosphorylated HTT in $StHdh^{Q7/7}$ cells at 5 minutes of stimulation with EGF when AKT was inhibited ($p<0.001$ in both N/C and N/P ratios), compared to no significant change at 5 minutes when AKT phosphorylation was not inhibited. This effect appeared to fluctuate; at 15 minutes the amount of phosphorylated HTT detected in the nucleus returned to baseline, but there was again a significant increase in both N/C and N/P ratios ($p<0.05$) at 30 minutes (Figures 4.16 and 4.17). An increase in these ratios was also apparent in the previous chapter when these cells were stimulated with EGF, although this did not become significant until after 15 minutes of stimulation, and the effect persisted. It may therefore be possible that by inhibiting AKT activation downstream of EGF stimulation, the stability of HTT phosphorylation is reduced.

Despite this epitope of phosphorylated mHTT already being primarily nuclear in $StHdh^{Q111/111}$ cells at baseline, inhibition of AKT lead to a significant increase of its nuclear presence in these cells by 5 minutes of EGF stimulation, although this was only apparent in the N/P ratio ($p<0.001$), and persisted for 15 minutes ($p<0.001$) until a return to baseline by 30 minutes of stimulation. In contrast to previous observations (Section 3.4.3), there was initially more nuclear phosphorylated mHTT in this experiment at baseline, and there was a significant increase in the N/P ratio at 5 minutes of stimulation with EGF without AKT inhibition ($p=0.01$), whereas there was no effect of EGF in the prior experiment. This may be due to the addition of DMSO to the media in this instance, or could reflect that the phosphorylation of mHTT may be more unstable and transient in comparison to wild type HTT.

Figure 4.16 Subcellular localisation of an N-terminal epitope of HTT phosphorylated on serines 13 and 16, detected by N17 s1316p in *StHdh*$^{Q7/7}$ and *StHdh*$^{Q111/111}$ cells. All genotypes were serum starved overnight before being treated for 0, 5, 15 and 30 minutes with 100ng/ml EGF after either 2 hours incubation with 500nM AKT inhibitor VIII, or media containing the equivalent volume of DMSO (see Sections 2.2.4.1 & 2.2.4.2). Cells were then analysed by confocal microscopy (see Sections 2.2.1.8 & 2.2.1.9 for further details). Scale bar = 20μm
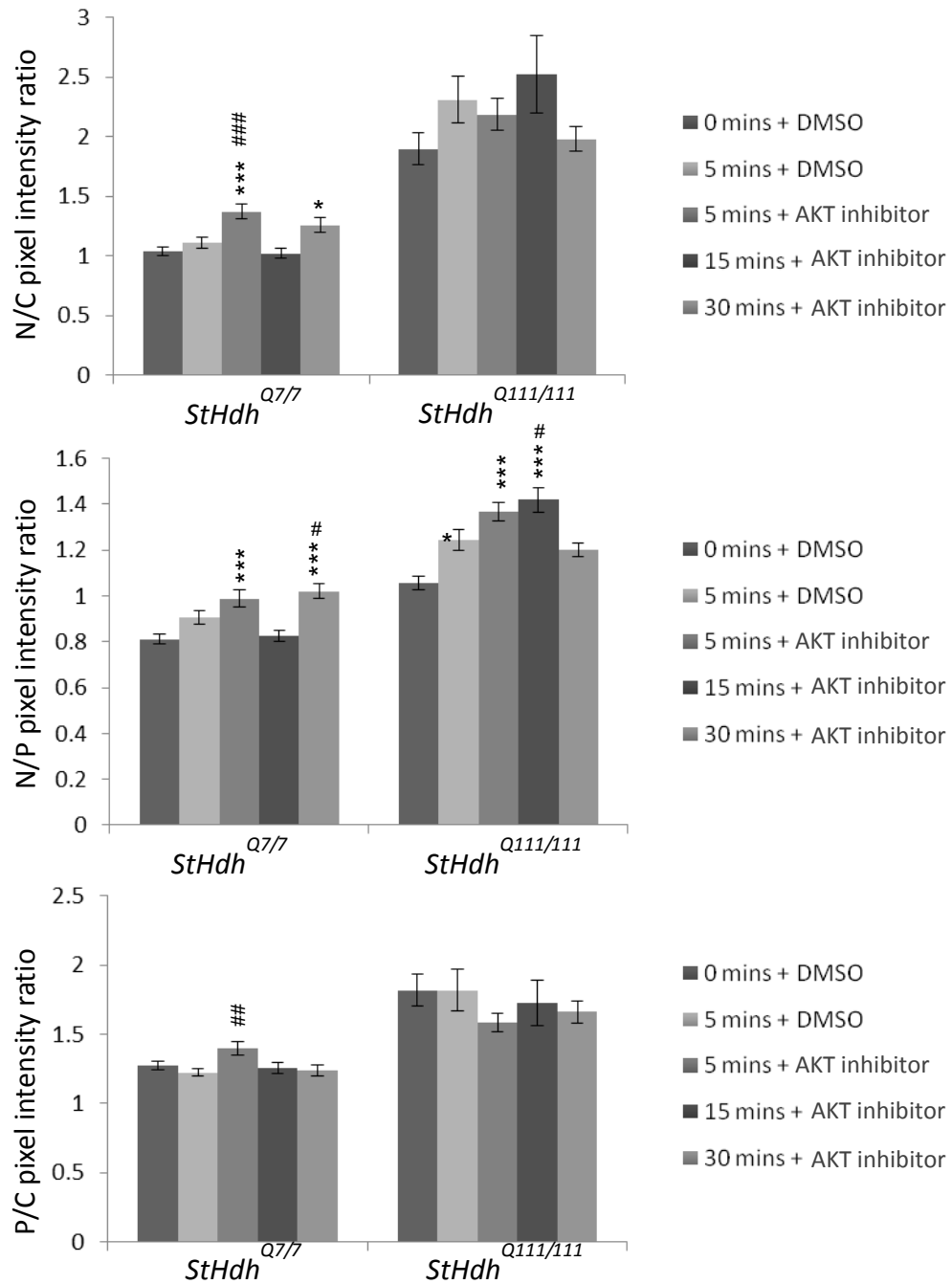
Figure 4.17 Quantitative analysis of immunofluorescence images in Figure 4.16. Nuclear/Cytoplasmic, Nuclear/Perinuclear and Perinuclear/Cytoplasmic mean pixel intensity ratios for *StHdh*$^{Q7/7}$ and *StHdh*$^{Q111/111}$ cells following 0, 5, 15 and 30 minutes of stimulation with 100ng/ml EGF following 2 hours incubation with either 500nM AKT inhibitor VIII or the equivalent volume of DMSO. Mean pixel intensities were calculated from confocal microscopy images using GNU Image Manipulator (further details of the analysis can be found in Section 2.2.1.10). All images were randomised and analysed blind to genotype, AKT inhibition and length of time stimulated with EGF. Each condition consisted of 9 confocal microscopy images taken from 3 separate coverslips. A two-way ANOVA was carried out for main effects analysis, followed by planned one-way ANOVAs and post-hoc Tukey tests. Error bars = SEM

* Denotes difference from 0. # Denotes difference from 5 mins + DMSO

*p<0.05, ** p<0.01, *** p<0.001

4.5.1.4 Immediate-early gene expression changes

In order to determine whether the AKT signalling pathway is relevant to gene expression changes in these cells, both due to disruption by mHTT and in response to EGF stimulation, qRTPCR on a selection of IE genes was carried out following AKT inhibition. This panel of genes was selected as they have been identified as being downstream of growth factor signalling pathways, particularly AKT and/or MEK pathways (Cosgaya & Aranda 1999; Levkovitz & Baraban 2002; Fuentes et al. 2008; Cabodi et al. 2009; Gokce et al. 2009; Ji et al. 2010; Liot et al. 2013). Generally, the transcriptional response of IE genes in *StHdh*$^{Q111/111}$ cells was more sensitive to EGF stimulation, which elicited much larger gene expression fold changes than in *StHdh*$^{Q7/7}$ cells. Therefore, there was a stronger ability for kinase inhibition to have a significant effect on IE gene expression (Figure 4.18).

There was no difference in the level of *C-fos* expression between *StHdh*$^{Q7/7}$ and *StHdh*$^{Q111/111}$ cells, and although EGF stimulation reduced the expression in both genotypes, this did not reach significance. AKT inhibition did not have any significant effect on the expression of *C-fos* following EGF stimulation in either genotype.

There was a significant increase in *Egr1* expression in response to EGF stimulation in both *StHdh*$^{Q7/7}$ and *StHdh*$^{Q111/111}$ cells (F (3, 24) = 17.95, p<0.001), the effect of which was augmented in the *StHdh*$^{Q111/111}$ cell line (p<0.001) as compared to the *StHdh*$^{Q7/7}$s (p= 0.035). In the *StHdh*$^{Q7/7}$ cells, there was no effect of AKT inhibition on *Egr1* expression (p= 0.82), and its expression remained significantly increased compared to 0 minutes EGF (p= 0.029). In *StHdh*$^{Q111/111}$ cells, there was a reduction of *Egr1* expression following AKT inhibition, although this did not reach significance (p= 0.167), and in parallel with *StHdh*$^{Q7/7}$ cells, expression remained significantly higher than at 0 minutes EGF (p= 0.002).

Similarly, for the expression of *Arc*, there was a significant increase following EGF stimulation when looking at the main effect of treatment (p = 0.004). However in post-hoc Tukey HSD testing, this increase of expression failed to reach significance in *StHdh*$^{Q7/7}$ cells (p= 0.507), but was highly significant due to a larger response in *StHdh*$^{Q111/111}$ cells, thus providing more signal compared to background noise (p=

0.001). Although there was a reduction in *Arc* expression due to AKT inhibition in the *StHdh*[Q111/111] cells, this was not significant (p= 0.636), and there was no effect in *StHdh*[Q7/7] cells.

Finally, EGF stimulation elicited a significant increase in *Ngfib* expression in both genotypes ($F_{(3, 24)}$ = 8.07, p= 0.001). AKT inhibition led to a slight decrease in *Ngfib* expression in both cases; although this was not a significant reduction compared to EGF stimulation alone, expression was no longer significantly higher than baseline (p>0.05). Therefore for this panel of IE genes, stimulation of the AKT pathway is not likely to be the main contributor to gene expression regulation, despite regulatory effects on the localisation and phosphorylation of HTT.
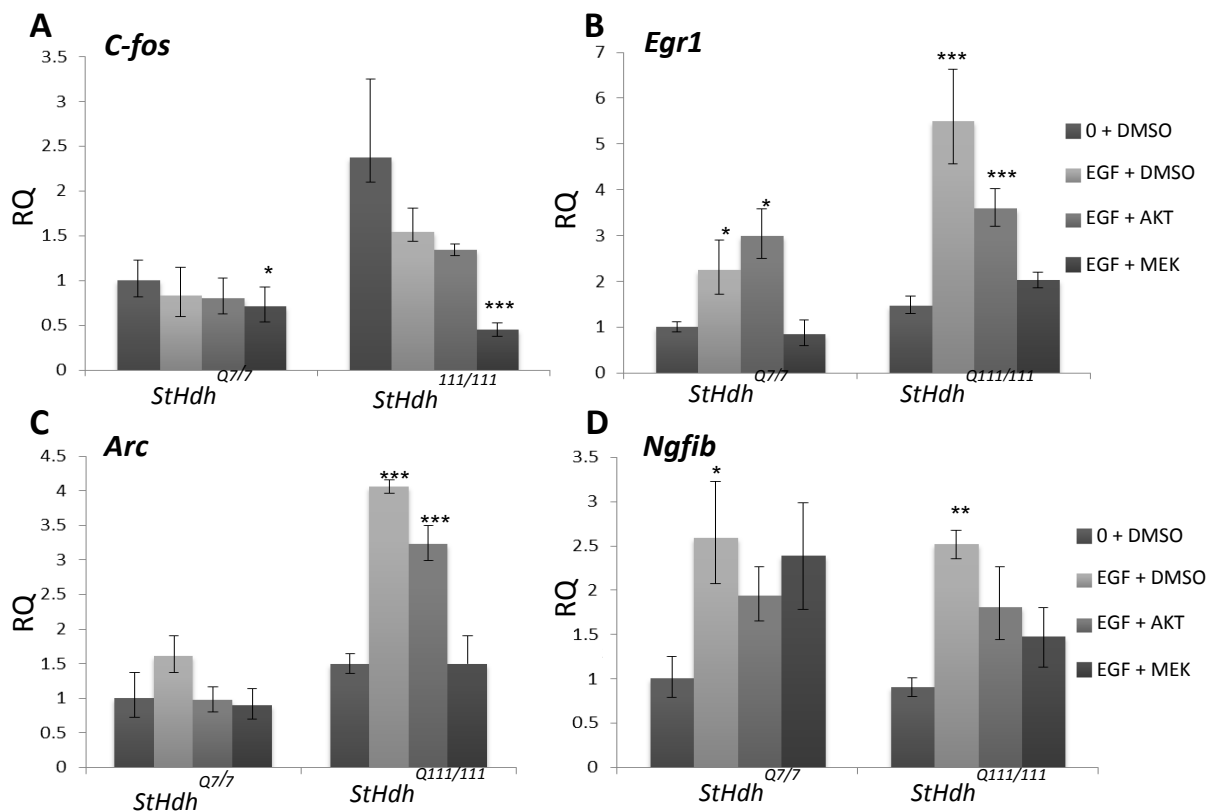
Figure 4.18 Relative quantitation (RQ) values representing gene expression fold changes in *StHdh*[Q7/7] and *StHdh*[Q111/111] cells following inhibition with either 500nM AKT inhibitor VIII, 1uM MEK 1⁄2 inhibitor or the equivalent volume of DMSO, followed by 0 or 2 hours of 100ng/ml EGF stimulation for **A.** *C-fos,* **B**. *Egr1* **C**. *Arc* and **D**. *Ngfib*. Statistical analysis was conducted on ΔC_t values using a two-way ANOVA followed by post-hoc Tukey tests. (Error bars = SEM, n = 5)
'*' denotes a significant difference from 0.
* p<0.05   ** p<0.01   ***p<0.001

4.5.2 MEK 1/2 inhibition

4.5.2.1 Inhibitor concentration

MEK 1/2 inhibitor is a vinylogous cyanamide that is a potent inhibitor of MEK1 and 2; its structure and mode of action are described in Figure 4.19. A concentration curve experiment was carried out for this inhibitor (Figure 4.20); all three concentrations of the inhibitor significantly reduced phosphorylated MEK1 as compared to stimulation with EGF with no inhibitor present ($p < 0.001$ in all cases). However, even at the highest concentration, this inhibitor failed to reduce levels of activated MEK1 to the equivalent of baseline. At all concentrations of MEK 1/2 inhibitor that were tested, there was no significant reduction in phosphorylated AKT1, indicating that these inhibitors are targeting different cellular signalling pathways. As the largest reduction of phosphorylated MEK1 was at 1μM of inhibitor, this concentration was used for the following experiments.
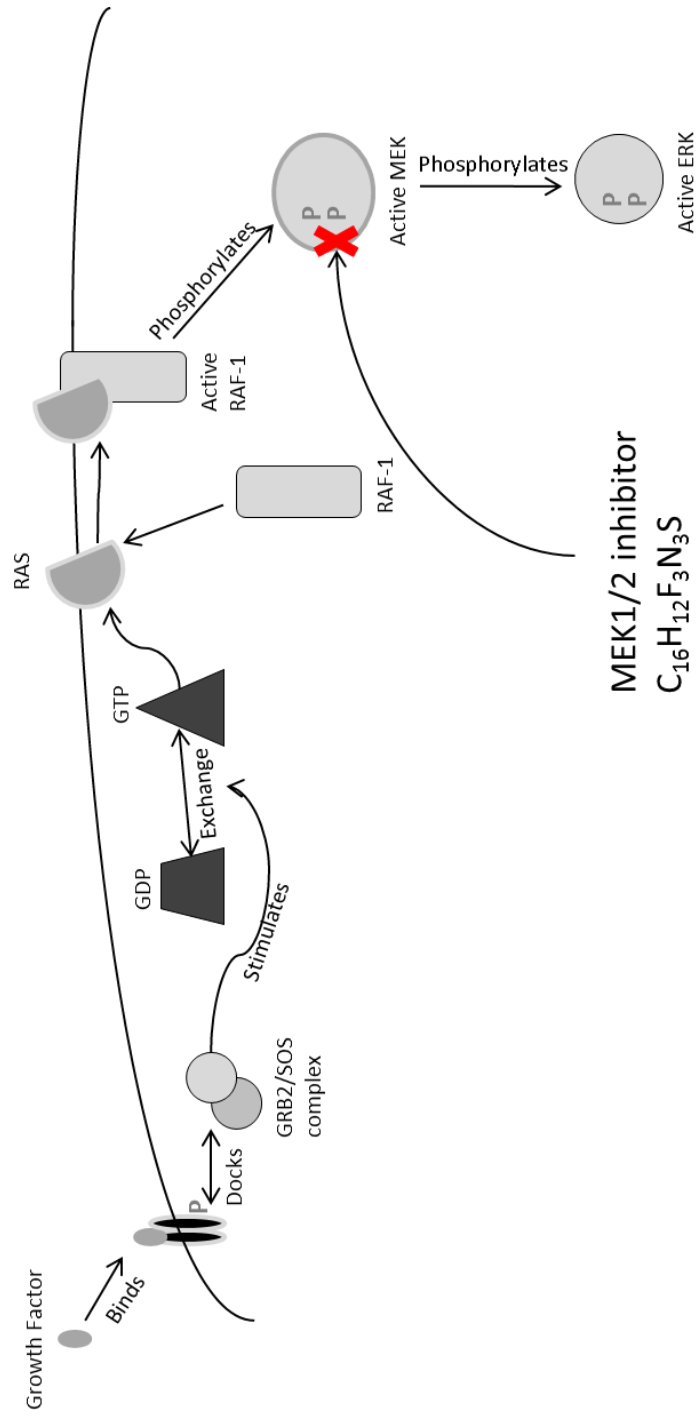
Figure 4.19 Simplified cartoon depicting growth factor stimulated activation of the MEK/ERK pathway. The GRB2/SOS complex docks with the phosphotyrosine kinase receptor, and stimulates the exchange of guanosine diphosphate (GDP) for guanosine triphosphate (GTP). This prompts a conformation change in RAS, which recruits RAF-1 from the cytoplasm to the cell membrane, leading to its phosphorylation and activation. Active RAF-1 then phosphorylates and activates MEK, which in turn phosphorylates and activates ERK. MEK 1/2 inhibitor is a non-competitive inhibitor of MEK, thus preventing its phosphorylation and further activation of ERK.
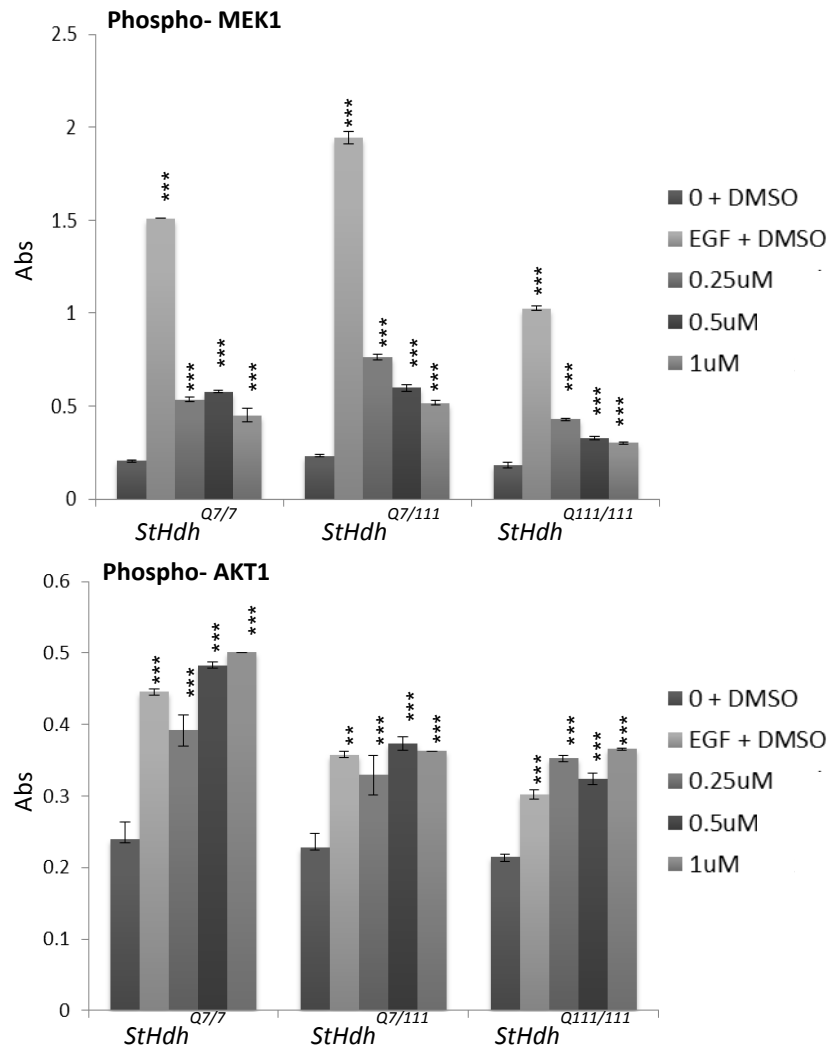
Figure 4.20 Mean absorbance (Abs) read at 450nm following sandwich ELISA protocol in *StHdh*^Q111 cells to determination the optimum concentration of MEK 1/2 inhibitor in order to prevent phosphorylation of MEK1 on serines 217/221 following 5 minutes stimulation with 100ng/ml EGF. The inhibitor was tested at 0.25, 0.5 and 1μM, prepared in DMSO solution for 2 hours prior to EGF stimulation. Inhibitor-free time points included the equivalent volume of DMSO in the media for the same length of time prior to EGF stimulation and sample collection. **A**. The effect of MEK 1/2 inhibitor on phosphorylated MEK1. **B**. The effect of MEK 1/2 inhibitor on phosphorylated AKT1 (serine 473). (Error bars = SEM, n=3).

'*' denotes a significant difference from 0.

* p<0.05   ** p<0.01   ***p<0.001

4.5.2.2 Localisation of HTT and mHTT following EGF stimulation when MEK 1/2 is inhibited

This series of experiments was carried out at the same time as the AKT inhibition experiments in Section 4.5.1.2, and therefore share the same baseline '0 mins + DMSO' and '5 mins + DMSO' time points. They were treated in the same manner as previously described, but with the use of 1µM MEK 1/2 inhibitor for 2 hours prior to stimulation with 100ng/ml EGF.

4.5.2.2a Ab109115

MEK inhibition appears to have had a similar effect on the localisation of the HTT epitope detected by Ab109115 as AKT inhibition, although the effect is more pronounced and less persistent with time (Figures 4.21 and 4.22). In $StHdh^{Q7/7}$ cells, there was a significant increase in the N/C and P/C ratios at 5 minutes of EGF stimulation when MEK was inhibited ($p<0.001$ and $p=0.043$, respectively). Similar to the observations following AKT inhibition, this did not present as a diffuse nuclear stain, but appeared as particular foci within nuclei (Figure 5.20). There was also an increase in the P/C ratio at this time point, suggesting movement from the entire cell towards the nucleus rather than shuttling between the nucleus and perinucleus, but this did not reach significance. In contrast to AKT inhibition, the effect did not persist past 5 minutes. However, there was a second significant increase in the N/P ratio ($p=0.007$) and a reduction in the P/C ratio ($p=0.012$) at 30 minutes; there was no visible nuclear increase in the immunofluorescent images, so this may be reflecting a reduction of HTT that had accumulated in the perinuclear region back towards the cytoplasm.

When MEK was inhibited, $StHdh^{Q111/111}$ cells had a dramatic reduction in the detection of nuclear mHTT at 5 minutes after stimulation with EGF; this was apparent in both the N/C ($p<0.001$) and N/P ($p<0.001$) ratios. However, despite this reduction, there were still discrete foci of mHTT that remained in the nuclei of some of these cells. As $StHdh^{Q111/111}$ cells do not form aggregates of mHTT, the function of these discrete foci requires elucidation; they may represent the interaction of mHTT with areas of transcription, or may be a result of impaired nuclear-cytoplasmic trafficking in these

cells. Similar to the effect in $StHdh^{Q7/7}$ cells, the reduction in nuclear mHTT was not persistent in $StHdh^{Q111/111}$ cells, and returned to baseline by 15-30 minutes of EGF stimulation.

Similar to Ab109115 detection following AKT inhibition in $StHdh^{Q7/111}$ cells, there was very little effect of MEK inhibition in these cells. There was a slight nuclear increase at 5 minutes when MEK was inhibited in the N/C ratio (p=0.003), which reflects the nuclear increase observed in $StHdh^{Q7/7}$ cells. However, as previously noted, this lack of effect may be due to the balancing of opposing effects of inhibition on HTT and mHTT.
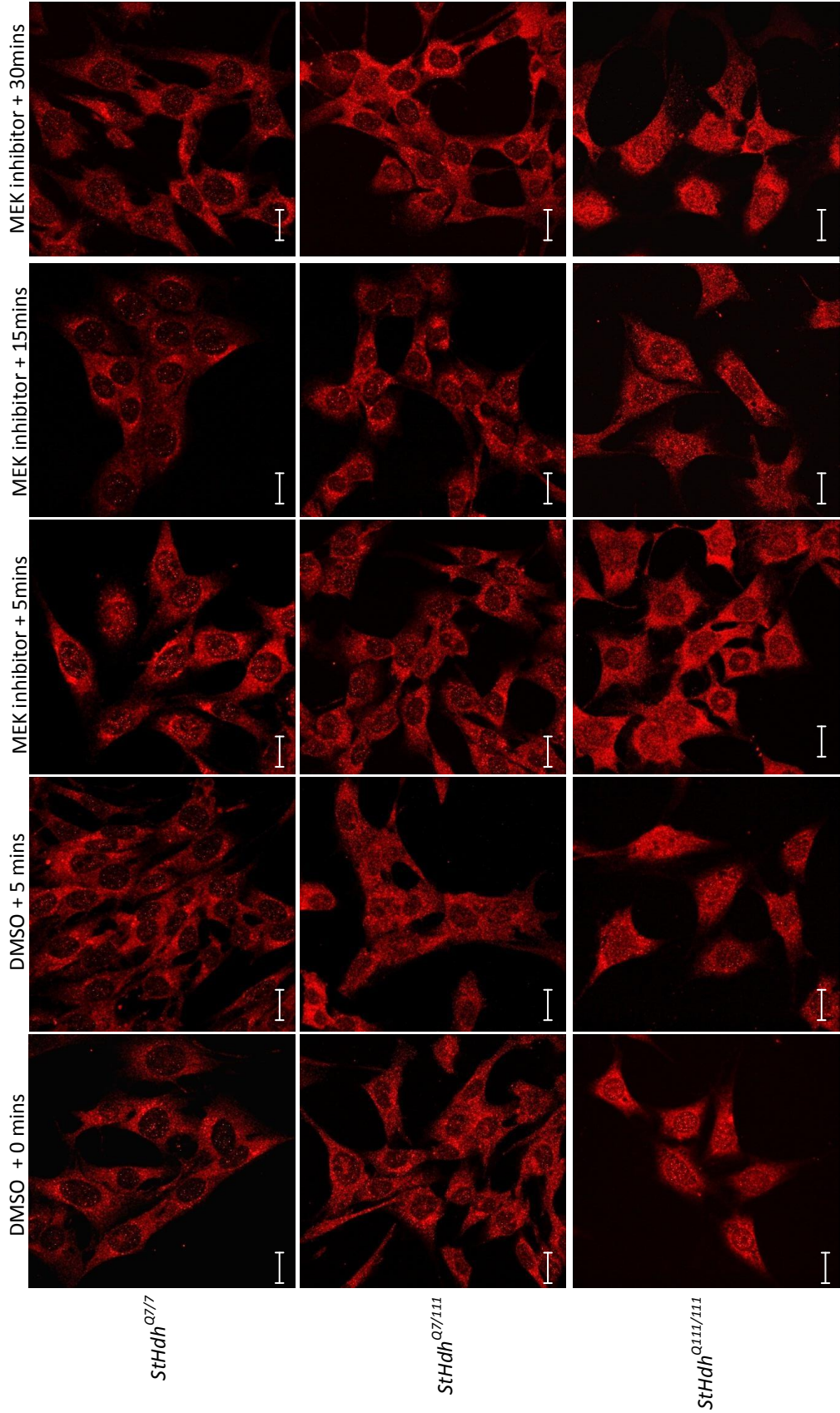
Figure 4.21 Subcellular localisation of an N-terminal epitope of HTT detected by Ab109115 in *StHdh*$^{Q7/7}$, *StHdh*$^{Q7/111}$ and *StHdh*$^{Q111/111}$ cells. All genotypes were serum starved overnight before being treated for 0, 5, 15 and 30 minutes with 100ng/ml EGF after either 2 hours incubation with 1μM MEK 1/2 inhibitor, or media containing the equivalent volume of DMSO (see Sections 2.2.4.1 & 2.2.4.2). Cells were then analysed by confocal microscopy (see Sections 2.2.1.8 & 2.2.1.9 for further details). Scale bar = 20μm
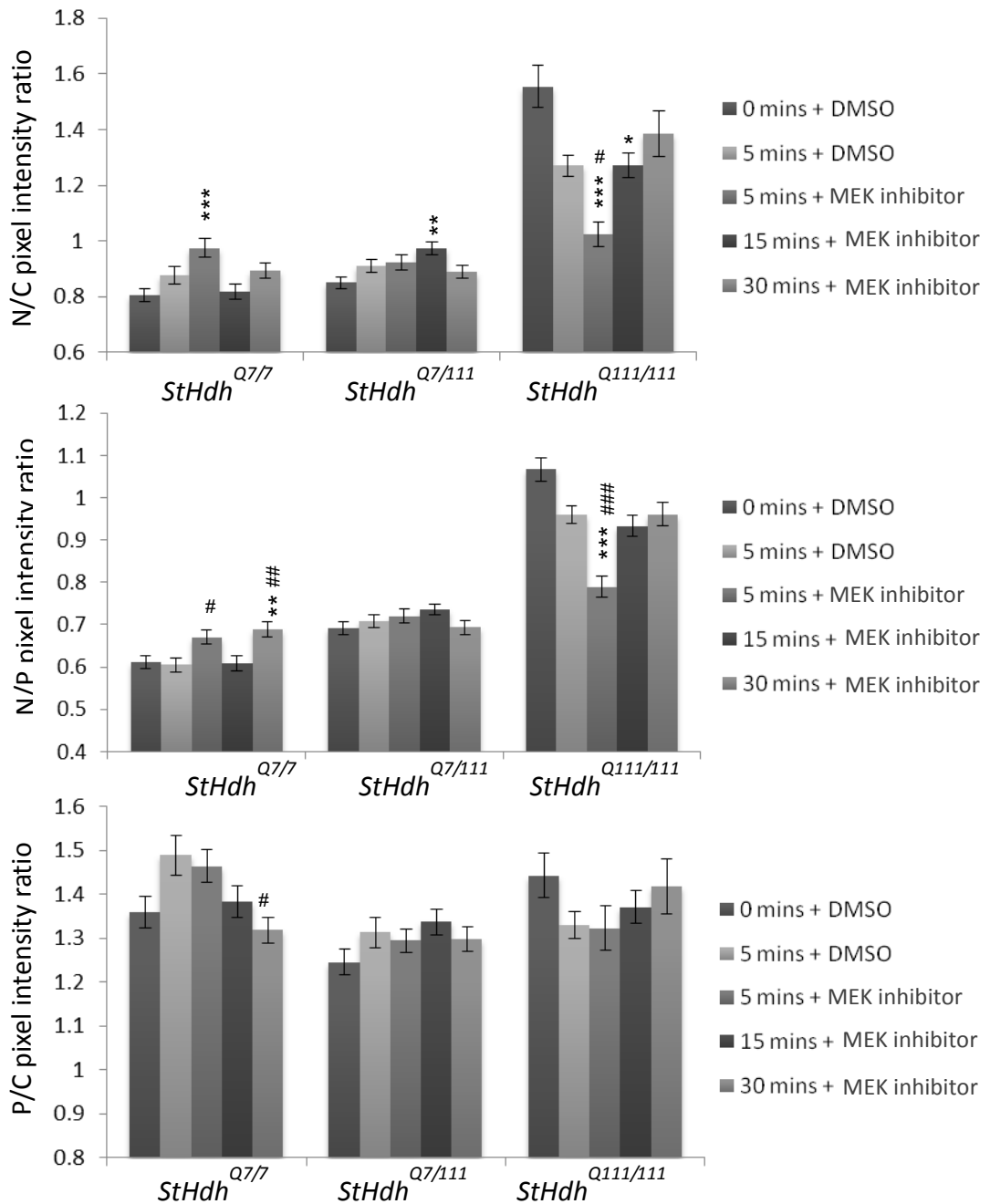
Figure 4.22 Quantitative analysis of immunofluorescence images in Figure 4.21. Nuclear/Cytoplasmic, Nuclear/Perinuclear and Perinuclear/Cytoplasmic mean pixel intensity ratios for $StHdh^{Q7/7}$, $StHdh^{Q7/111}$ and $StHdh^{Q111/111}$ cells following 0, 5, 15 and 30 minutes of stimulation with 100ng/ml EGF following 2 hours incubation with either 1µM MEK1/2 inhibitor or the equivalent volume of DMSO. Mean pixel intensities were calculated from confocal microscopy images using GNU Image Manipulator (further details of the analysis can be found in Section 2.2.1.10). All images were randomised and analysed blind to genotype, MEK inhibition and length of time stimulated with EGF. Each condition consisted of 9 confocal microscopy images taken from 3 separate coverslips. A two-way ANOVA was carried out for main effects analysis, followed by planned one-way ANOVAs and post-hoc Tukey tests. Error bars = SEM
* Denotes difference from 0. # Denotes difference from 5 mins + DMSO
*$p<0.05$, ** $p<0.01$, *** $p<0.001$

4.5.2.2b Mab2166

StHdh$^{Q7/7}$, *StHdh*$^{Q7/111}$ and *StHdh*$^{Q111/111}$ cells that were stained with Ab109115 were also double labelled with Mab2166. There was the same increase in the N/C and N/P ratios at 5 minutes of stimulation when MEK was inhibited in *StHdh*$^{Q7/7}$ cells (p=0.008 and p<0.001, respectively), but this was followed by a significant reduction in the N/P ratio below baseline at 15 and 30 minutes of stimulation (both p=0.002), and a consequent increase in the P/C ratio that reached significance at 30 minutes (p=0.015) (Figures 4.23 and 4.24). Due to the more transient nature of the effect of MEK inhibition on HTT localisation, this may be an effect of the movement of this epitope of HTT that accumulated in the nucleus back out into the perinuclear area. As has previously been observed when labelling these cells with Mab2166, the increase in nuclear detection is more diffuse than the Ab109115 signal, which may be reflective of the detection of different HTT epitopes, which are nevertheless responding in a similar manner.

StHdh$^{Q111/111}$ cells stained with Mab2166 show the same pattern of effect as Ab109115; there was a significant reduction in both the N/C and N/P ratios from 5 minutes of EGF stimulation when MEK was inhibited (N/C p=0.032, N/P p<0.001), although no localised foci were left behind in the nucleus as previously seen; this may be due to Mab2166 detecting potentially longer N-terminal epitope than Ab109115, suggesting the foci that are seen with Ab109115 may include shorter fragments of mHTT. The nuclear reduction is still apparent at 15 minutes in *StHdh*$^{Q111/111}$ cells, but the ratios return to baseline by 30 minutes.

In contrast to detection by Ab109115, there was a significant increase in the N/C (p<0.001) and N/P (p<0.001) ratios for *StHdh*$^{Q7/111}$ cells from 5 minutes of EGF stimulation when MEK was inhibited. In concordance with the data following AKT inhibition, this suggests that this epitope of HTT behaves more similarly to the epitope detected in *StHdh*$^{Q7/7}$ cells than mHTT in *StHdh*$^{Q111/111}$ cells. However, the effect appears to be less transient in *StHdh*$^{Q7/111}$ cells than the other two genotypes, as nuclear detection of this epitope remained higher than baseline at both 15 and 30 minutes of stimulation (p<0.001 for both N/C and N/P ratios for both time points).
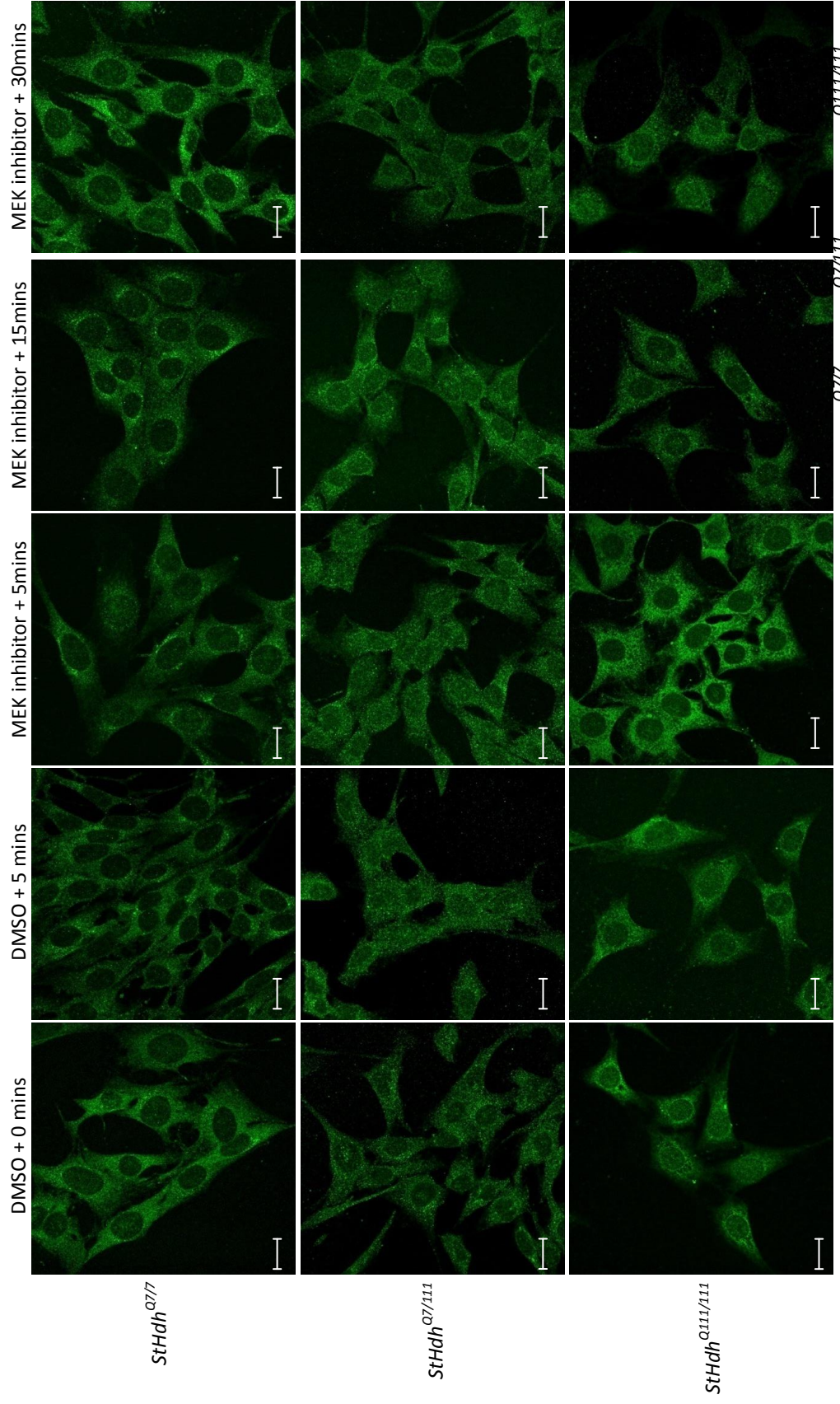
Figure 4.23 Subcellular localisation of an N-terminal epitope of HTT detected by Mab2166 in $StHdh^{Q7/7}$, $StHdh^{Q7/111}$ and $StHdh^{Q111/111}$ cells. All genotypes were serum starved overnight before being treated for 0, 5, 15 and 30 minutes with 100ng/ml EGF after either 2 hours incubation with 1µM MEK1/2 inhibitor, or media containing the equivalent volume of DMSO (see Sections 2.2.4.1 & 2.2.4.2). Cells were then analysed by confocal microscopy (see Sections 2.2.1.8 & 2.2.1.9 for further details). Scale bar = 20µm
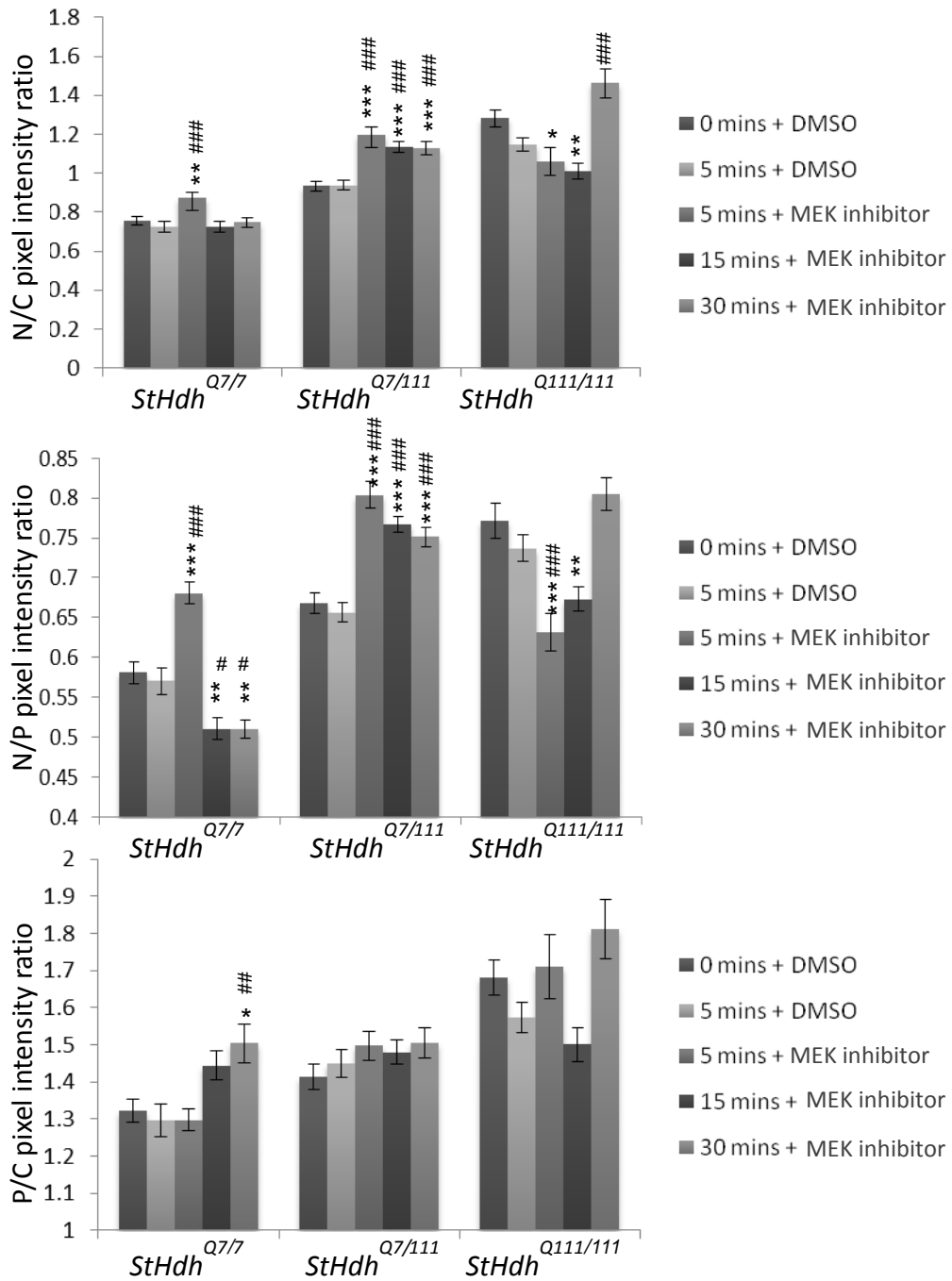
Figure 4.24 Quantitative analysis of immunofluorescence images in Figure 4.23. Nuclear/Cytoplasmic, Nuclear/Perinuclear and Perinuclear/Cytoplasmic mean pixel intensity ratios for *StHdh*[Q7/7], *StHdh*[Q7/111] and *StHdh*[Q111/111] cells following 0, 5, 15 and 30 minutes of stimulation with 100ng/ml EGF following 2 hours incubation with either 1μM MEK 1/2 inhibitor or the equivalent volume of DMSO. Mean pixel intensities were calculated from confocal microscopy images using GNU Image Manipulator (further details of the analysis can be found in Section 2.2.1.10). All images were randomised and analysed blind to genotype, MEK inhibition and length of time stimulated with EGF. Each condition consisted of 9 confocal microscopy images taken from 3 separate coverslips. A two-way ANOVA was carried out for main effects analysis, followed by planned one-way ANOVAs and post-hoc Tukey tests. Error bars = SEM

* Denotes difference from 0. # Denotes difference from 5 mins + DMSO

*$p<0.05$, ** $p<0.01$, *** $p<0.001$

4.5.2.2c Ab675 and N17

Cells labelled with Ab675 appear to support the effects of MEK inhibition in *StHdh*^{Q111} cells labelled with the other N-terminal antibodies Ab109115 and Mab2166 (Figure 4.25). Although HTT localisation appears much more nuclear in all three genotypes, there is a small increase in nuclear intensity in both *StHdh*$^{Q7/7}$ and *StHdh*$^{Q7/111}$ cells following EGF stimulation when the MEK 1/2 inhibitor is applied. In addition, there is also a dramatic reduction of this epitope of mHTT detected in the majority of *StHdh*$^{Q111/111}$ nuclei from 5 minutes of stimulation that returns to baseline by 30 minutes, which is concordant with the findings from the other N-terminal antibodies used here.

There is a similar effect when looking at the N17 antibody; there is little difference in *StHdh*$^{Q7/7}$ and *StHdh*$^{Q7/111}$ cells over time, however there is a noticeable reduction in nuclear mHTT detected by this antibody in *StHdh*$^{Q111/111}$ cells, although there is not complete emptying of nuclei as seen when using Ab675 (Figure 4.26). Overall, four different HTT N-terminal antibodies that each detect slightly different epitopes of HTT and mHTT exhibit the same response to EGF stimulation on the localisation of HTT when MEK is inhibited in *StHdh*^{Q111} cells.
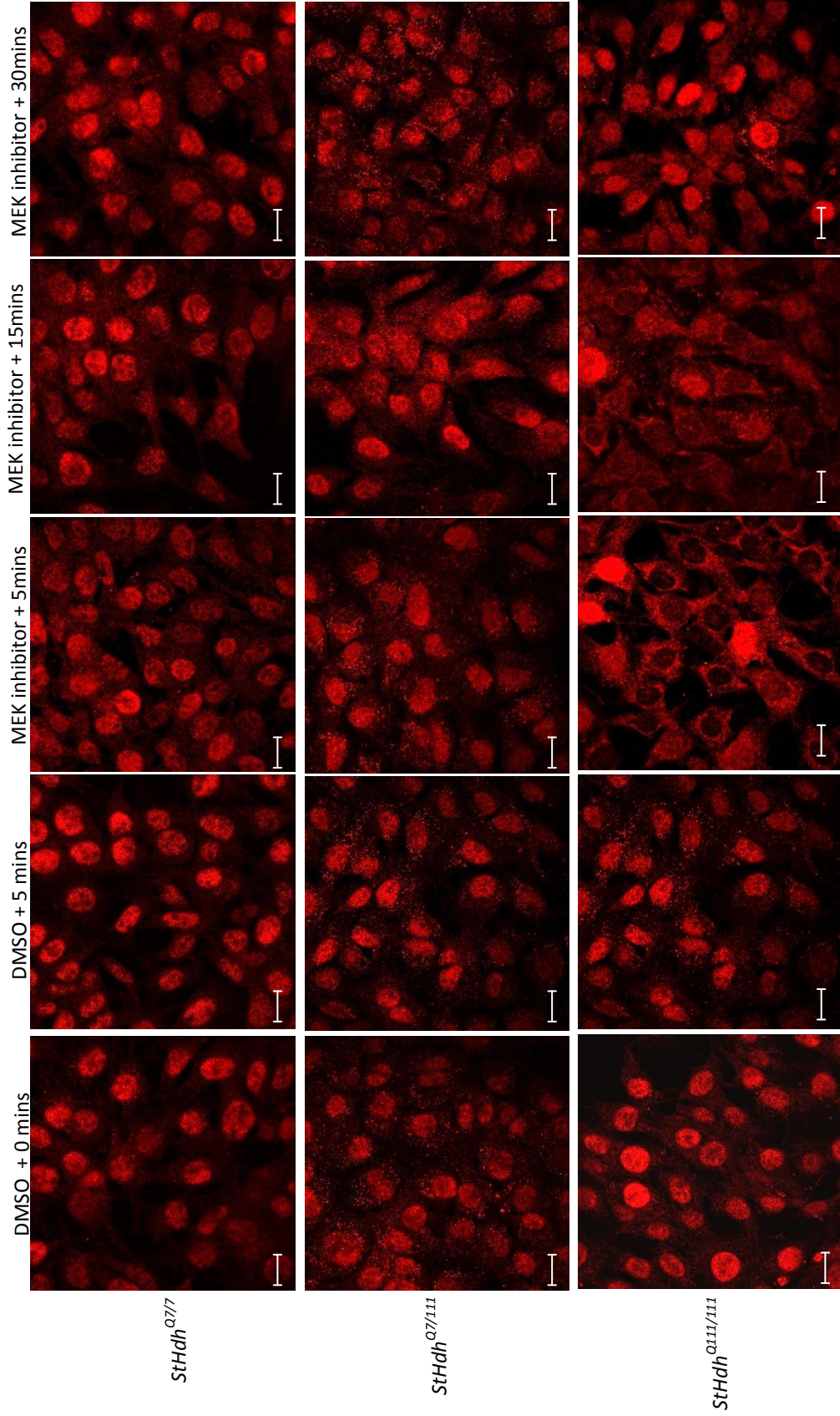
Figure 4.25 Subcellular localisation of an N-terminal epitope of HTT detected by Ab675 in *StHdh*$^{Q7/7}$, *StHdh*$^{Q7/111}$ and *StHdh*$^{Q111/111}$ cells. All genotypes were serum starved overnight before being treated for 0, 5, 15 and 30 minutes with 100ng/ml EGF after either 2 hours incubation with 1µM MEK 1/2 inhibitor, or media containing the equivalent volume of DMSO (see Sections 2.2.4.1 & 2.2.4.2). Cells were then analysed by confocal microscopy (see Sections 2.2.1.8 & 2.2.1.9 for further details). Scale bar = 20µm
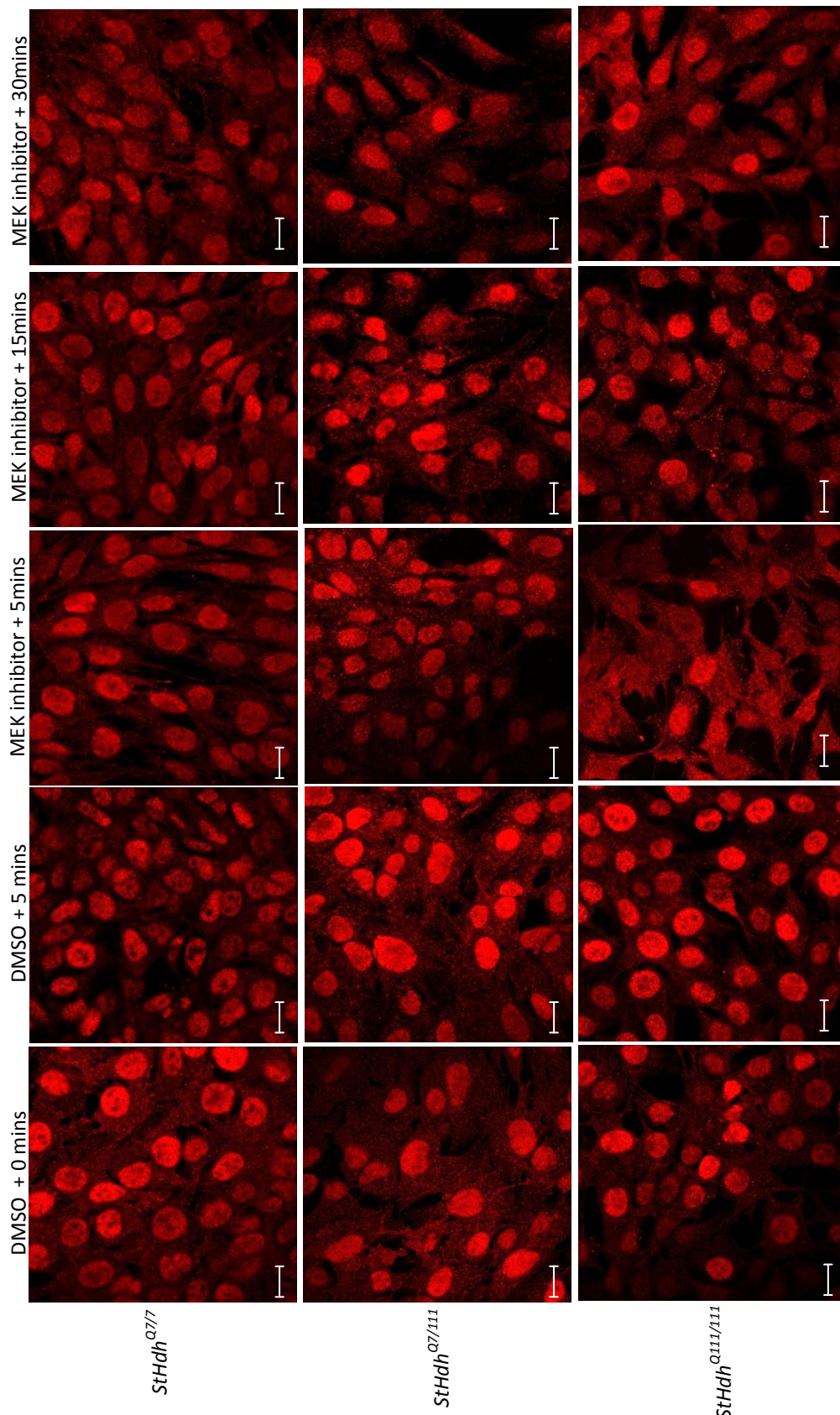
Figure 4.26 Subcellular localisation of an N-terminal epitope of HTT detected by N17 in *StHdh*$^{Q7/7}$, *StHdh*$^{Q7/111}$ and *StHdh*$^{Q111/111}$ cells. All genotypes were serum starved overnight before being treated for 0, 5, 15 and 30 minutes with 100ng/ml EGF after either 2 hours incubation with 1μM MEK 1/2 inhibitor, or media containing the equivalent volume of DMSO (see Sections 2.2.4.1 & 2.2.4.2). Cells were then analysed by confocal microscopy (see Sections 2.2.1.8 & 2.2.1.9 for further details). Scale bar = 20μm
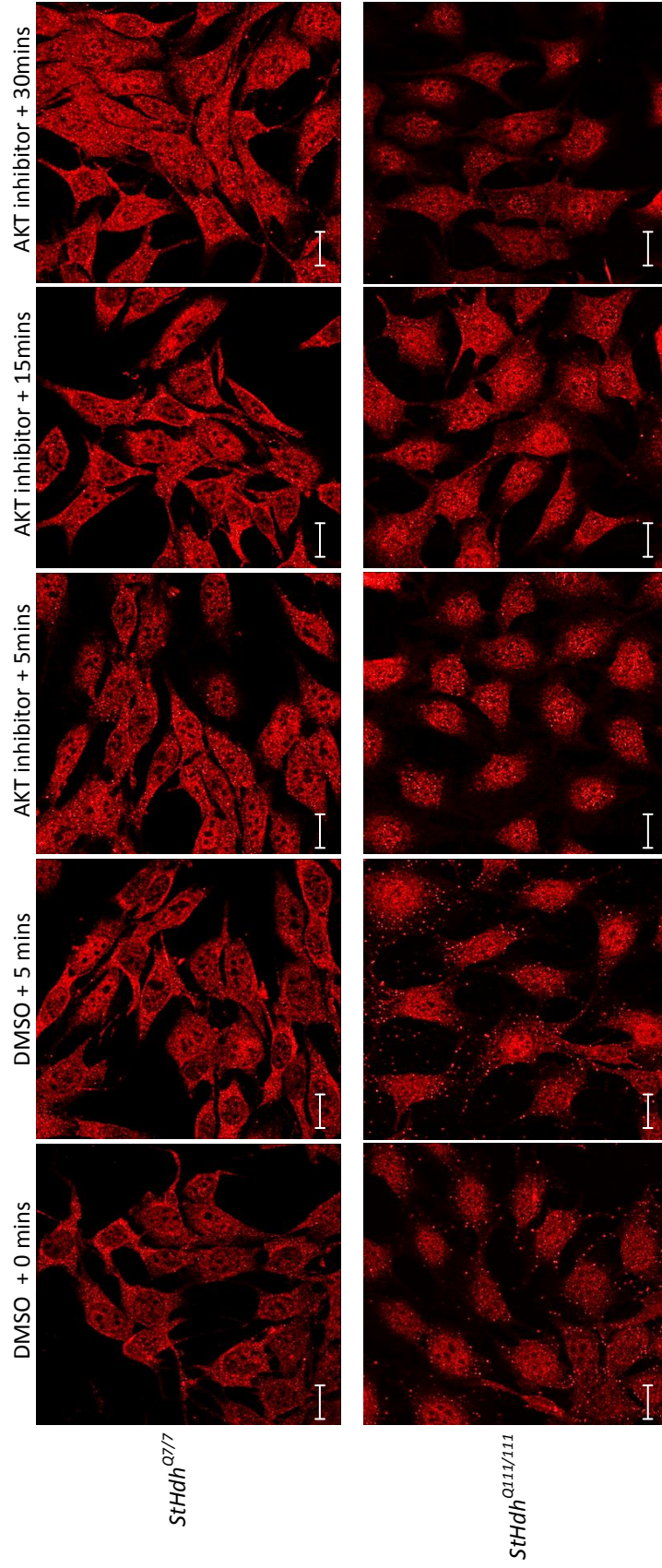
4.5.2.3 Localisation of phosphorylated HTT epitopes following EGF stimulation when MEK 1/2 is inhibited.

As this experiment was carried out at the same time as the AKT inhibition experiment, the quality of $StHdh^{Q7/111}$ cell staining with the N17 s1316p was also too poor for inclusion, so only $StHdh^{Q7/7}$ and $StHdh^{Q111/111}$ cells are reported here.

MEK inhibition had a similar effect on the localisation of phosphorylated HTT in $StHdh^{Q7/7}$ cells as AKT inhibition did (Figures 4.27 and 4.28). There was also a significant increase in nuclear detection at 5 minutes of stimulation when MEK was inhibited (both N/C and N/P ratios $p<0.001$). However, in contrast to AKT inhibition and to non-phospho-antibodies following MEK inhibition, this effect remained more stable for the entire 30 minutes; the N/P ratio remained significantly higher than baseline at both 15 ($p<0.001$) and 30 minutes ($p=0.005$) of EGF stimulation. There was no significant effect in the P/C ratio, indicating that relocalisation of this epitope of phosphorylated HTT occurs mostly between the nucleus and perinucleus.

After an initial increase in nuclear phosphorylated mHTT in $StHdh^{Q111/111}$ cells following EGF stimulation, inhibiting MEK led to a small reduction in nuclear detection. However, this doesn't reach significance until 30 minutes in the N/C ratio ($p=0.02$), but the reduction is visible in the immunofluorescence images. This reduction is not apparent in every cell, which may account for the lack of any quantifiable differences. The reduction of nuclear phospho-HTT following MEK inhibition in $StHdh^{Q111/111}$ cells is in contrast to the effect of AKT inhibition; this may be due to different mechanisms downstream of either signalling pathway having differential interactions with mHTT.
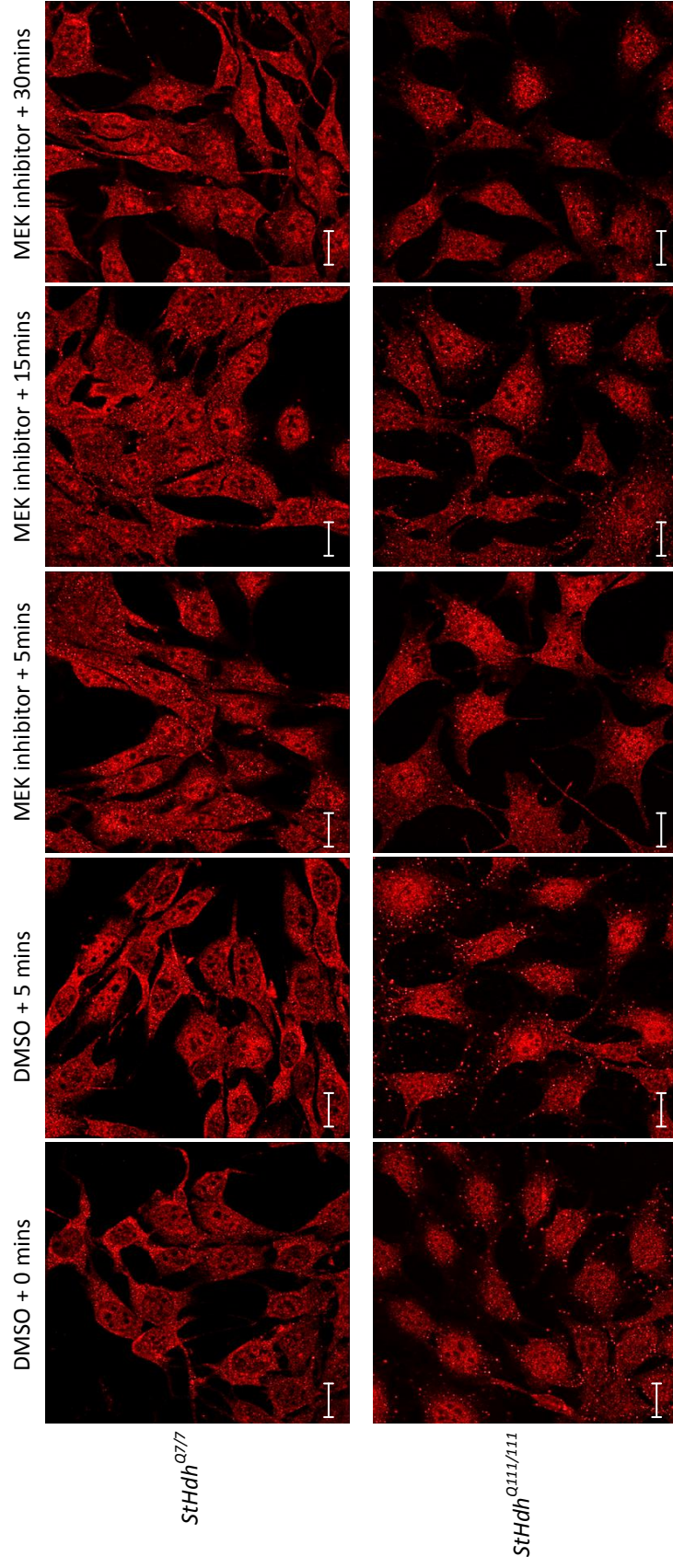
Figure 4.27 Subcellular localisation of an N-terminal epitope of HTT phosphorylated on serines 13 and 16, detected by N17 s1316p in **A**. *StHdh*^Q7/7 and **B**. *StHdh*^Q111/111 cells. All genotypes were serum starved overnight before being treated for 0, 5, 15 and 30 minutes with 100ng/ml EGF after either 2 hours incubation with 1µM MEK 1/2 inhibitor, or media containing the equivalent volume of DMSO (see Sections 2.2.1.8 & 2.2.1.9 for further details). Cells were then analysed by confocal microscopy (see Sections 2.2.4.1 & 2.2.4.2). Scale bar = 20µm
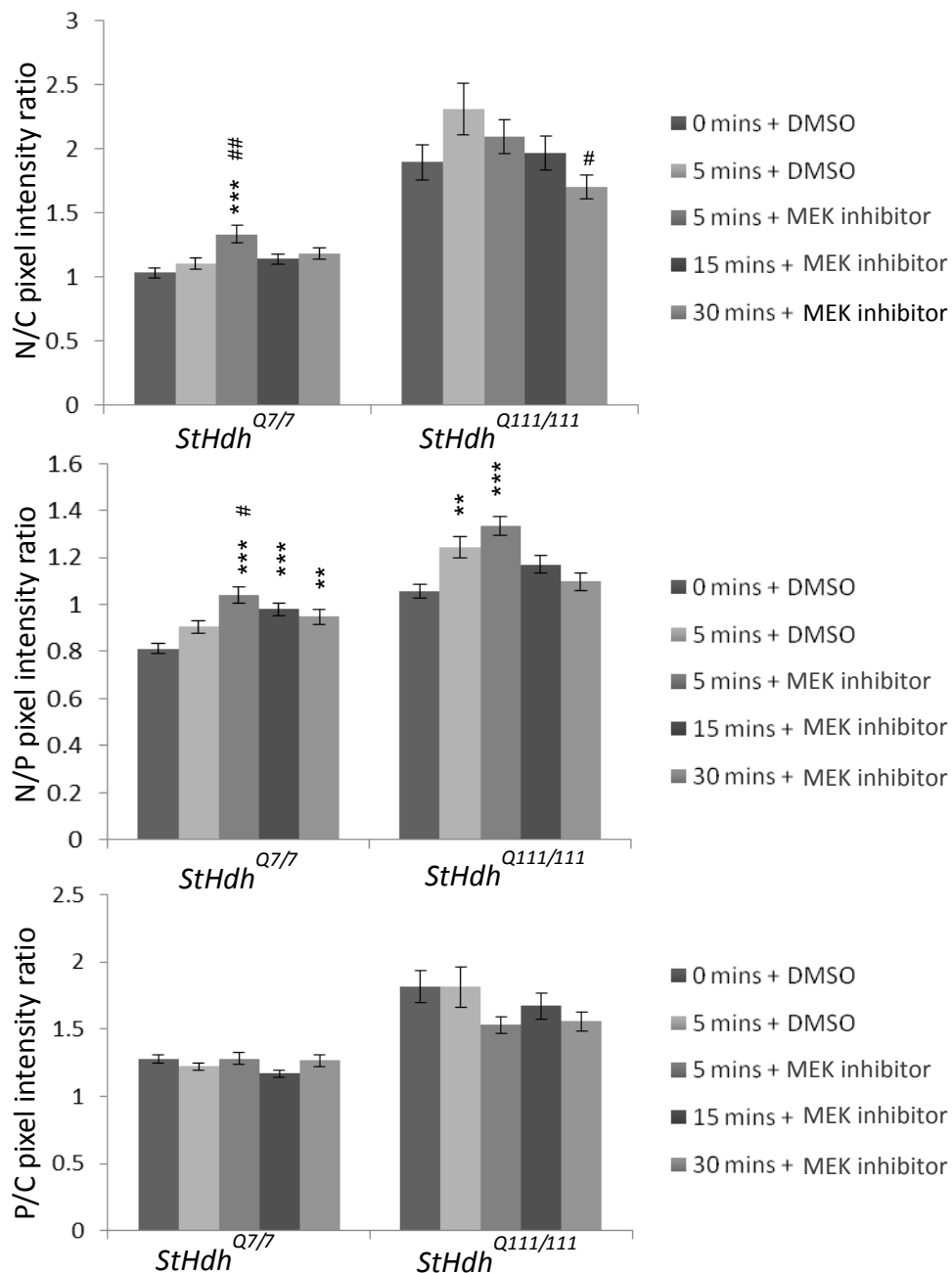
Figure 4.28 Quantitative analysis of immunofluorescence images in Figure 4.27. Nuclear/Cytoplasmic, Nuclear/Perinuclear and Perinuclear/Cytoplasmic mean pixel intensity ratios for $StHdh^{Q7/7}$ and $StHdh^{Q111/111}$ cells following 0, 5, 15 and 30 minutes of stimulation with 100ng/ml EGF following 2 hours incubation with either 1µM MEK ½ inhibitor or the equivalent volume of DMSO. Mean pixel intensities were calculated from confocal microscopy images using GNU Image Manipulator (further details of the analysis can be found in Section 2.2.1.10). All images were randomised and analysed blind to genotype, MEK inhibition and length of time stimulated with EGF. Each condition consisted of 9 confocal microscopy images taken from 3 separate coverslips. A two-way ANOVA was carried out for main effects analysis, followed by planned one-way ANOVAs and post-hoc Tukey tests. Error bars = SEM

* Denotes difference from 0. # Denotes difference from 5 mins + DMSO

*p<0.05, ** p<0.01, *** p<0.001

MEK inhibition experiments were carried out in parallel with AKT inhibition, and therefore share the same baseline; as such, the data have been presented together (Figure 4.18). Inhibition of MEK 1/2 phosphorylation had a greater effect on IE gene expression than AKT inhibition, although similar to the patterns of IE gene expression following AKT inhibition, there was again a larger response in $StHdh^{Q111/111}$ cells compared to $StHdh^{Q7/7}$.

MEK inhibition amplified the effect of EGF on *C-fos* by reducing its expression below baseline in both $StHdh^{Q7/7}$ (p= 0.015) and $StHdh^{Q111/111}$ cells (p< 0.001), and further below the level of expression following EGF stimulation ($StHdh^{Q7/7}$ p= 0.44, $StHdh^{Q111/111}$ p= 0.004). There was a strong effect of MEK inhibition on the expression of *Egr1*; in both genotypes, the increased expression due to EGF stimulation was inhibited, so that the resulting level of expression was not different from baseline.

There was no effect of MEK inhibition on *Arc* expression in $StHdh^{Q7/7}$ cells, although this is likely due to the lack of initial EGF effect. However, the increase in expression that was observed in $StHdh^{Q111/111}$ cells following EGF stimulation did not occur when MEK activity was inhibited. A similar pattern occurred for expression of *Ngfib*; there was little effect of EGF or MEK inhibition in $StHdh^{Q7/7}$ cells, but MEK inhibition suppressed the EGF-associated increase of *Ngfib* expression in $StHdh^{Q111/111}$ cells.

4.6 Discussion

We demonstrate that several kinase signalling pathways activated by growth factor stimulation are dysregulated in cells carrying mHTT, and that AKT and MEK signalling in particular may regulate both the localisation of HTT and downstream transcriptional control.

A panel of ELISA assays exposed differences in kinase signalling activity between $StHdh^{Q7/7}$ and $StHdh^{Q111/111}$ cells both prior to, and following growth factor stimulation. There were consistent baseline differences in phosphorylated AKT1, MEK1 and STAT3;

all of which were found to be at an increased concentration in $StHdh^{Q111/111}$ cells. Enhanced AKT activity has been identified in this cell line previously (Ginés et al. 2003; Kong et al. 2009; Atwal et al. 2011), as well as in a neural stem cell model of HD (Ritch et al. 2012), which may reflect a neuroprotective response to mHTT in these cells (Chong et al. 2005). Incubation with EGF elicited a substantial increase in AKT1 stimulation in both $StHdh^{Q7/7}$ and $StHdh^{Q111/111}$ cells, which was significantly larger in $StHdh^{Q111/111}$ cells. This suggests that as well as an increase in baseline AKT activity, these cells are also more sensitive to stimulation of this pathway. However, there was no effect of NGF stimulation in either genotype, and BDNF elicited a small, but significant reduction in phosphorylated AKT1 in $StHdh^{Q111/111}$ cells. This is surprising, as neural stem cells expressing mHTT have been found to be hyper-responsive to BDNF stimulation, though this was following an hour of stimulation (Ritch et al. 2012).

Increased AKT activation is likely to be a neuroprotective, compensatory response; it has been suggested that in these cells it counteracts the early excitotoxic effects of mHTT (Ginés et al. 2003), and increasing AKT activity reduced neurotoxicity in a *Drosophila* model of HD (Liévens et al. 2008), in addition to reducing the number of intranuclear inclusions formed in striatal cells expressing mHTT (Humbert et al. 2002). The neuroprotective effects of AKT activity are likely to also be exerted through its phosphorylation of HTT on S421 (Humbert et al. 2002; Humbert 2003), which has been found to reduce the toxicity of mHTT and the nuclear accumulation of toxic mHTT fragments, as well as restoring axonal transport (Liévens et al. 2008; Zala et al. 2008; Pineda et al. 2009; Pennuto et al. 2009; Warby et al. 2009). Despite the aberrant interaction between mHTT and GRB2 at the EGFR (Liu et al. 1997; Song et al. 2002), $StHdh^{Q111/111}$ cells are still able to respond more sensitively than $StHdh^{Q7/7}$ cells to EGF stimulation, suggesting that there may be an additional mechanism by which EGF exerts its effects in the presence of mHTT. For example, EGF is known to play a synergistic role with other growth factor signalling pathways, such as the transforming growth factor-beta (TGFβ) pathway (Kang et al. 2012; Song et al. 2012), which may therefore be more strongly involved in EGF signalling pathways in the context of mHTT disruption. mHTT-associated dysregulation at the level of the EGFR may also not be sufficient to suppress the normal effect of EGF stimulation, or it is possible that the

previously identified aberrant interaction of mHTT with GRB2 (Liu et al. 1997; Song et al. 2002) does not occur in this cell model.

There is currently less information available regarding the role of MEK1 signalling in models of HD, however its activation has previously been found to be reduced in *StHdh^Q111* cells (Ginés et al. 2010). In contrast, we found an increased basal level of phosphorylated MEK1 in *StHdh^Q111/111* cells, but its response to both EGF and BDNF stimulation was supressed in contrast to *StHdh^Q7/7* cells, thus providing some support for the current literature. It has been reported that HTT can be phosphorylated by MEK1 activation (Schilling et al. 2006), although the implications for this mechanism are yet to be elucidated. However, it could be hypothesised that as HTT phosphorylation by AKT is protective (Thompson et al. 2009; Warby et al. 2009), phosphorylation by MEK1 may confer a similar role. For example, a constitutively active form of MEK1 was found to be protective against cell death in a mHTT expressing PC12 model of HD (Apostol et al. 2006), although in a *Drosophila* model of HD, the induction of MEK1 activity was found to provide no protection against polyQ induced lethality (Iijima-ando et al. 2005). ERK1/2 activity has been found to be neuroprotective in models of HD (Apostol et al. 2006; Saavedra et al. 2011) and as it lies downstream of MEK1, it could be inferred that its action is representative of MEK1 activity. In *StHdh^Q111/111* cells, despite an initial baseline increase in MEK1 phosphorylation, which would be consistent with a protective compensatory mechanism, further activation of MEK1 is less efficient following EGF stimulation, which may be indicative of mHTT interference at the EGFR.

Although there was little effect of growth factor stimulation on phosphorylated STAT3 in this cell model, increased baseline phospho-STAT3 was consistently identified in *StHdh^Q111/111* cells. Increased expression and activation of STAT3 has also been found from embryonic day 12.5 in the striata of Hdh^Q111 mice, where it is likely to play a role in brain maturation (Molero et al. 2009). As the immortalised cell model was derived from these mice, it is unsurprising that the same hyper-activation was seen, and this may be a marker of very early aberrant neuronal development in HD. Conversely, no increase in STAT3 mRNA or activity was identified in neural stem cells carrying mHTT (Ritch et al. 2012), so differences in its activation may be developmental stage-specific.

STAT3 phosphorylation was found to be suppressed in a MEK1 knock out cell model, suggesting that there may be a regulatory interaction between these two pathways (Li et al. 2012); as MEK1 activity shows evidence of being enhanced in these $StHdh^{Q111/111}$ cells, this may be a mechanism by which STAT3 phosphorylation is also boosted. Following EGF stimulation, STAT3 phosphorylation increased in $StHdh^{Q111/111}$ cells only, supporting the potential for increased sensitivity in this pathway, which is likely to have downstream effects on transcriptional regulation.

There were mixed observations for the presence of phosphorylated BAD; in the initial BDNF experiment, there was no difference between the genotypes, although there was a trend towards a reduction in $StHdh^{Q111/111}$ cells. In the following experiment, the reduction of BAD activation in $StHdh^{Q111/111}$ cells reached significance. BAD is a pro-apoptotic signalling kinase, but its activation by phosphorylation inactivates it and promotes neuronal survival (Datta et al. 1997; Zala et al. 2008). Reduced activation of BAD is therefore consistent with cellular stress due to the presence of mHTT. However, as BAD has been found to be phosphorylated in response to the activation of AKT (Zala et al. 2008), it could be anticipated that due to higher levels of AKT activation in $StHdh^{Q111/111}$ cells, BAD phosphorylation would also be increased in these cells. The variation in basal levels of BAD phosphorylation may reflect a general dysregulation of this pathway as opposed to a blanket reduction in its activity. Following EGF stimulation, although there were no baseline differences in the levels of BAD phosphorylation, there was a significant increase in both genotypes that was augmented in $StHdh^{Q111/111}$ cells. This was in parallel to hyperphosphorylation of AKT in these cells, so this may be part of a sensitive pro-survival compensatory mechanism in response to EGF stimulation.

The phosphorylation of P38 MAPK has previously been seen in several models of HD; although in general the activity of the MAPK signalling family has been found to be reduced in the presence of mHTT (Song et al. 2002; Humbert 2003; Rong et al. 2006), increased induction of both JNK and P38 MAPKs have also been found in models of HD. For example, there is increased P38 MAPK activity in R6/1 striata from 20 weeks of age (Saavedra et al. 2011), and in 10-11 week old R6/2 mice (Gianfriddo et al. 2004). It has also been observed in YAC128 striata from only 1 month of age (Fan et al. 2012).

Whether increased activation of P38 MAPK is protective or not remains under debate. Gianfriddo et al. 2004 suggested that the rise in P38 MAPK correlated with striatal damage, and may therefore play a role in apoptosis and reducing neuronal survival. Reducing P38 MAPK activation has also been found to improve neuronal survival in a rat model of HD (Wang et al. 2010) and in primary neuronal cultures expressing a mHTT fragment (Taylor et al. 2013). However, it has also been argued that P38 MAPK activation has the potential to be neuroprotective; in R6 mouse models, the lack of neuronal loss has been attributed to the anti-apoptotic effects of increased P38 MAPK and AKT activity (Mangiarini et al. 1996; Taylor et al. 2013). These pro- or anti-apoptotic properties of P38 MAPK may be dependent on the activation of downstream substrates. In the *StHdh^{Q111}* cell line, we also identified increased P38 MAPK activity in *StHdh$^{Q111/111}$* cells, but this only reached significance in the final experiment utilising EGF stimulation. This may be due to a lack of statistical power, or could be a result of instability in P38 MAPK phosphorylation, or biological variation resulting from cell passage number. However, following EGF stimulation, there was a significant increase in P38 MAPK phosphorylation in *StHdh$^{Q111/111}$* cells, whereas there was no effect in *StHdh$^{Q7/7}$* cells. This supports the current literature, as well as the evidence for increased sensitivity of several kinase signalling pathways to growth factor stimulation that has been observed here.

There was no effect of growth factor stimulation on cleaved PARP, phosphorylated NFκβ or phosphorylated SAPK/JNK, and any genotypic differences were minor and variable between the three growth factor experiments, thus making it difficult to draw any conclusion about their role in this model of HD. Increased cleaved PARP has been previously identified in this cell line, and is thought to potentiate caspase-3 activity (Kong et al. 2009), but we did not replicate this effect. Similarly, SAPK/JNK activation is usually found to be increased in models of HD, including PC12 cells (Apostol et al. 2006), YAC128 striata (Fan et al. 2012) and R6/1 striata (Taylor et al. 2013), but despite the increase in P38 MAPK observed in *StHdh$^{Q111/111}$* cells, there was no effect for phosphorylated SAPK/JNK. The lack of phosphorylation following growth factor application may be due to the short period of stimulation, and a longer incubation time may be required to see any differential effects. Finally, although NFκβ activity has

been identified as being increased in the central nervous system of R6/2 mice (Khoshnan & Patterson 2011), no differences in its activity were previously found in the same immortalised striatal cell model, although in $StHdh^{Q111/111}$ cells, NFκβ did show increased responsiveness to stimulation by its activator, interleukin-1β (IL-1β) (Khoshnan et al. 2004). Although we also found no difference in basal NFκβ activation in these cells, none of the growth factors utilised had any effect. This is likely to be due to the length of stimulation not being sufficient to alter its activation, as NFκβ has been found to be downstream of AKT phosphorylation (Humbert 2003), so should be induced in this model.

The transcription of IE genes is typically activated by growth factors, and so their expression could be expected to be affected by dysregulation in upstream kinase signalling pathways, as observed in this cell line. There was no difference in the expression of *C-fos* between genotypes, although there was a trend towards higher expression in $StHdh^{Q111/111}$ cells, which is unsurprising, as *C-fos* is associated with the stress response and survival (Zhang et al. 2002). However, the expression of *C-fos* in both R6/2 and Hdh^{Q111} mice has been found to be downregulated (Luthi-Carter 2000; Roze et al. 2008; Liot et al. 2013). In R6/2 mouse striatal neurons, this was correlated with the hyperactivation of ERK (Roze et al. 2008), whereas the opposite was found in Hdh^{Q111} striatal cells (Liot et al. 2013). There was no effect of EGF stimulation on the expression of *C-fos* in this cell model, despite *C-fos* previously being associated with activation of the EGFR (Haugwitz et al. 2006; Fuentes et al. 2008). This may be due to the length of time that cells were stimulated for; mRNA was collected following 2 hours of EGF stimulation, which may have been too long to detect an increase in *C-fos* activity; *C-fos* expression has previously been found to be increased immediately following EGF stimulation in smooth muscle A-10 cell lines, but this effect was maximal following only 30 minutes, and was no longer detectable by 1 hour of stimulation (Fuentes et al. 2008). Therefore *C-fos* expression may be too fast and transient to have been detected in this experiment.

There was no observable effect of AKT inhibition on *C-fos* expression, although if the transient expression increase of *C-fos* in response to EGF stimulation occurred earlier than 2 hours, then any effect of AKT inhibition would also have been missed. Despite

this, there was a reduction in *C-fos* expression below baseline levels in both *StHdh*$^{Q7/7}$ and *StHdh*$^{Q111/111}$ cells when MEK was inhibited, which occurred to a larger extent in *StHdh*$^{Q111/111}$ cells. This suggests that *C-fos* expression in these cells may be downstream of MEK/ERK signalling, as has been previously suggested (Roze et al. 2008; Liot et al. 2013), although the nature of this association remains to be elucidated. However, it has been previously noted that *C-fos* expression is able to be induced independent of both MEK and ERK activation (Fuentes et al. 2008), suggesting that *C-fos* expression may be downstream of several signalling pathways, and thus the role of mHTT on its expression is unlikely to be via a single mechanism.

Baseline expression of *Egr1* was similar between genotypes, but there was an enhanced response to EGF stimulation in *StHdh*$^{Q111/111}$ cells. AKT inhibition had no effect on the expression of *Egr1* in either cell type, although there was a trend towards a reduction in *StHdh*$^{Q111/111}$ cells. In contrast, MEK inhibition completely suppressed the effects of EGF stimulation on the expression of *Egr1*. *Egr1* is a marker of cellular signal transduction and controls the regulation of transcription (Tsai et al. 2000). It has been found to be induced by stimulation at the EGFR, and has been associated with both AKT and MEK signalling pathways; It was previously found to be dependent on the silencing of its transcriptional repressor forkhead box protein 01 (FOXO1) by activated AKT (Cabodi et al. 2009), and both inhibitors of phosphatidylinositide 3-kinase (PI3K) and MEK have been found to suppress its activity in response to growth factor stimulation (Fuentes et al. 2008; Gokce et al. 2009). In *StHdh*^{Q111} cells, the MEK signalling pathway appears to be more relevant for the control of *Egr1* expression. However, as MEK activation is slightly suppressed in *StHdh*$^{Q111/111}$ cells following EGF stimulation, it may be a synergism between MEK signalling and AKT hyperactivation that elicits the larger expression response in these cells. There have been mixed findings regarding *Egr1* expression in models of HD; it has been identified as a commonly downregulated gene in R6/2 mice (Luthi-Carter 2000; Macgibbon et al. 2002; Spektor 2002; Yamanaka et al. 2010), however in a PC12 cell model expressing a 103 polyQ repeat, the expression of *Egr1* was increased x2.4 fold (Apostol et al. 2006). Both the R6/2 and PC12 models of HD contain only an N-terminal transgene of *Htt*, whereas the *StHdh*^{Q111} cell line is a full length *Htt* knock-in model. This may therefore

have consequences on the involvement of mHTT in aberrant cell signalling and downstream control of gene expression. However, aberrant splicing of *Htt* exon 1 has been identified in a full length knock in model of HD (Hdh^{Q150} mouse model), which creates a short N-terminal transcript of HTT (Sathasivam et al. 2013). This shorter transcript may therefore contribute to HD pathogenesis in the same manner as it does in N-terminal transgenic models, and so the abundance and accumulation of the pathogenic protein over time may also be contributing to differences in observed gene expression changes. In addition, these models all looked at the expression of *Egr1* at baseline without any cellular input, whereas this dynamic model illustrates the importance of taking into account cellular kinase pathway reactivity when assessing transcriptional changes in HD models.

Arc and *Ngfib* have been less thoroughly characterised than *C-fos* and *Egr1*, however the induction of both has been found to be downstream of common cell signalling pathways, such as following EGF stimulation (Cosgaya & Aranda 1999; Gokce et al. 2009; Ji et al. 2010). The ARC protein has been found to be increased in R6/2 cortex and hippocampus, and was also found to associate with mHTT nuclear aggregates (Maheshwari et al. 2012), suggesting that expression of the *Arc* gene may also be increased in this model. We found that although levels of *Arc* expression were similar at baseline in *StHdh*$^{Q7/7}$ and *StHdh*$^{Q111/111}$ cells, the pattern of activation following EGF was similar to that seen for *Egr1* expression; there was an enhanced transcriptional response in *StHdh*$^{Q111/111}$ cells, which is consistent with the finding that there may be accumulation of the ARC protein in models of HD (Maheshwari et al. 2012). We also find that *Arc* expression is downstream of MEK signalling in these cells, as inhibition of AKT had no effect on its expression. This is also consistent with a previous finding that MEK inhibition can diminish *Arc* expression in response to BDNF in rat striatal cells (Gokce et al. 2009). It is currently unknown what the significance of increased *Arc* expression may be in the context of HD, although its association with glutamate receptor activity may mean it plays a role in synaptic dysfunction (Maheshwari et al. 2012).

Finally, no significant difference in *Ngfib* expression was observed in these cells, and EGF elicited a similar response of *Ngfib* expression in both *StHdh*$^{Q7/7}$ and *StHdh*$^{Q111/111}$

cells. This was more effectively suppressed by MEK inhibition, although preventing AKT activation also reduced its expression so it was no longer significantly higher than baseline. Therefore, for the panel of IE genes investigated here, it appears that MEK dependent signalling is more relevant for the control of their expression following EGF stimulation than AKT signalling, although hyperphosphorylation of the AKT pathway in $StHdh^{Q111/111}$ cells may be a mechanism by which the transcriptional response of these genes is augmented.

Inhibition of both AKT and MEK activation had an effect on the localisation of HTT and mHTT in $StHdh^{Q111}$ cells following EGF stimulation; both elicited an increase in nuclear HTT in $StHdh^{Q7/7}$ cells, as detected by all four N-terminal HTT antibodies. It is therefore likely that the localisation of N-terminal fragments of HTT is able to be regulated by AKT and MEK activity. Increased nuclear localisation of HTT is usually considered to be pathogenic, and is typically associated with transcriptional repression (Reddy et al. 1999; Crook & Housman 2011), so in $StHdh^{Q7/7}$ cells following AKT and MEK inhibition, this may be a mechanism for the suppression of IE gene expression. Arguably, this effect is enhanced following MEK inhibition, as the extent of nuclear filling in $StHdh^{Q7/7}$ cells is greater, and for the three primary antibodies that detect amino acids 1-17, there appears to be aggregation of HTT to discrete nuclear foci, which have the potential to be specific loci of transcription (Osborne et al. 2004). Mab2166 does not show such a large nuclear increase in signal as the other N-terminal antibodies do, and this may be due to detection of a different epitope of HTT, as the amino acid sequence contributing to the epitope is further down the HTT protein. The nuclear HTT that is observed in $StHdh^{Q7/7}$ cells following EGF may therefore be a smaller N-terminal epitope of HTT that is capable of moving across the nuclear membrane by passive diffusion (Hackam et al. 1998; Truant 2003; Bauer & Nukina 2009), or it may be associating with chaperone-acting TFs that allow HTT to traverse the nuclear pore (Li et al. 1995; Faber et al. 1998) in order to regulate transcription. In addition, the non-classical proline-tyrosine NLS that has been identified on the N-terminus of HTT may be altering the nuclear localisation of HTT by mechanisms of active diffusion (Desmond et al. 2012; Desmond et al. 2013).

Conversely, AKT and MEK inhibition in $StHdh^{Q111/111}$ cells elicit the opposite effect, as there is a dramatic reduction in nuclear mHTT following treatment with EGF when these kinase pathways are suppressed. This suggests that the expanded polyQ in these cells is capable of modifying the normal interaction of mHTT with elements downstream of kinase signalling pathways, which then alters its activity. Following MEK inhibition, although there is a reduction in nuclear mHTT detected using Ab109115, the same nuclear foci are apparent as in the $StHdh^{Q7/7}$ cells that could also be areas of transcription. Unfortunately, there was not the opportunity to specifically investigate what these foci could be. The same reduction in nuclear HTT is seen in $StHdh^{Q7/7}$ cells following EGF stimulation when there is no other treatment (see Chapter 3), which may suggest that when hyperactivation of the MEK and AKT pathways is prevented, $StHdh^{Q111/111}$ cells look more like $StHdh^{Q7/7}$ cells. There is little change in $StHdh^{Q7/111}$ cells when either MEK or AKT activities are inhibited, which may be an indication of a gene dosage effect; as both HTT and mHTT appear to have converse responses to inhibition of these pathways, it could be expected that these balance each other out, resulting in an apparent lack of effect. However, when looking at Mab2166, these cells more closely resemble their wild type counterparts, which may be a reflection of the different epitope of HTT that is being detected with this antibody. This may have implications for the mechanism of signalling dysregulation in human HD, as the majority of patients are heterozygous for the mutant gene. As these cells are an embryonic model, and some dysfunction is already apparent, it may be the case that heterozygosity confers a longer developmental period, after which a gene dosage effect is no longer apparent. These results implicate MEK and AKT signalling as important modulators of mHTT localisation and transcriptional function, although the mechanism for how this occurs remains unknown. As both have been identified as being able to phosphorylate HTT (Humbert 2003; Schilling et al. 2006; Thompson et al. 2009), we also looked at the effect of kinase pathway inhibition on the localisation of HTT and mHTT phosphorylated on S13 and S16.

The nuclear localisation of phosphorylated epitopes of HTT and mHTT increased in the context of both AKT and MEK inhibition following EGF stimulation. For $StHdh^{Q7/7}$ cells, the same pattern occurred following EGF stimulation with no kinase inhibition,

however there was previously no effect in $StHdh^{Q111/111}$ cells (see Chapter 3). Similar to non-phosphorylated epitopes of mHTT detected by the other N-terminal antibodies, the inhibition of AKT and MEK signalling in $StHdh^{Q111/111}$ cells prompts mHTT to behave more similarly to wild type HTT following EGF stimulation. Although MEK inhibition had a larger effect on the nuclear localisation of phosphorylated HTT epitopes than AKT inhibition, AKT inhibition appeared to have a longer lasting effect, as was also the case for non-phosphorylated epitopes. However, the localisation of phosphorylated HTT did not remain consistent in $StHdh^{Q7/7}$ cells when AKT was inhibited; there was an initial increase at 5 minutes, followed by a reduction before another peak. This may indicate that AKT activation is required for the stability of HTT phosphorylation, and therefore disruption of this pathway in $StHdh^{Q111/111}$ cells may elicit aberrant control of this mechanism. Interestingly, there is an increase in phosphorylated mHTT in the nuclei of $StHdh^{Q111/111}$ cells following AKT and MEK inhibition, but the non-phosphorylated epitopes show a substantial reduction. This could be an indication that the antibodies are picking up entirely different epitopes of HTT, and there is a nuclear increase of phosphorylated mHTT while non-phosphorylated mHTT reduces, or there may be a conformational change in the protein that prevents it being detected by N-terminal antibodies following its phosphorylation.

In conclusion, by using a dynamic model, we have identified several kinase signalling pathways that show aberrant activity in $StHdh^{Q111/111}$ cells following stimulation with BDNF, NGF and EGF, which includes hyperphosphorylation as well as suppression of activity. We have shown that two of these pathways; AKT and MEK, are both important in the regulation of IE genes in both $StHdh^{Q7/7}$ and $StHdh^{Q111/111}$ cells, but that MEK signalling may be a more relevant pathway for their transcriptional control (see Table 4.1 for a summary). However, as MEK activity is suppressed in $StHdh^{Q111/111}$ cells, but IE gene expression is enhanced, it is likely that a synergistic mechanism between several dysregulated pathways in $StHdh^{Q111/111}$ cells contribute to aberrant transcriptional control. In addition, both AKT and MEK activity modulate the localisation of N-terminal epitopes of HTT and mHTT, suggesting that control of HTT localisation is downstream of both these pathways. MEK inhibition had the greatest magnitude of effect, although this was more transient than AKT inhibition, and

inhibition of either pathway led to the localisation of mHTT in $StHdh^{Q111/111}$ cells more closely resembling HTT localisation in $StHdh^{Q7/7}$ cells. Therefore the increased activity in these kinase pathways may be a mechanism for the increased nuclear localisation of mHTT seen in $StHdh^{Q111/111}$ cells and other models of HD. Activity in the AKT pathway may be a more important requirement for the localisation and stability of HTT phosphorylation than MEK activity, as the nuclear increase of phosphorylated HTT that occurs following EGF stimulation (see Chapter 3) still occurred following MEK inhibition, but occurred to a lesser extent than when AKT was inhibited. Therefore integration of both pathways may be required for the regulation of HTT localisation and phosphorylation, which in turn may be a mechanism for transcriptional control downstream of growth factor signalling. MEK and AKT signalling may also have effects on other post-translational modifications of HTT, which may alter epitope availability for antibody binding, as well as HTT localisation; a discussion of this can be found in Section 3.5.9. Inhibiting both pathways concurrently would be of interest to determine the extent to which synergism between the two modulate the localisation and phosphorylation of HTT, and consequent transcriptional control. Unfortunately there was not the opportunity to conduct this experiment within the time frame of this project.

A

GF	AKT1		MEK1		P38 MAPK		STAT3		NFKβ P65		BAD		PARP		SAPK/JNK	
	$StHdh^{Q7/7}$	$StHdh^{Q111/111}$	$StHdh^{Q7/7}$	$StHdh^{Q111/111}$	$StHdh^{Q7/7}$	$StHdh^{Q111/111}$	$StHdh^{Q7/7}$	$StHdh^{Q111/111}$	$StHdh^{Q7/7}$	$StHdh^{Q111/111}$	$StHdh^{Q7/7}$	$StHdh^{Q111/111}$	$StHdh^{Q7/7}$	$StHdh^{Q111/111}$	$StHdh^{Q7/7}$	$StHdh^{Q111/111}$
BDNF	X	↓ (red)	↑ (green)	X	X	X	X	X	X	X	X	X	X	X	↑ (green)	X
NGF	X	X	X	X	X	X	X	X	X	X	X	X	X	X	X	X
EGF	↑	↑ (red)	↑ (green)	↑	X	↑ (red)	X	↑ (red)	X	X	↑	↑ (red)	X	X	X	X

B

Non-phospho HTT

	EGF alone	AKT inhibitor	MEK inhibitor
$StHdh^{Q7/7}$	↓	↑	↑
$StHdh^{Q7/111}$	↓	X	X
$StHdh^{Q111/111}$	X	↓	↓

Phospho HTT

	EGF alone	AKT inhibitor	MEK inhibitor
$StHdh^{Q7/7}$	↑	↑	↑
$StHdh^{Q7/111}$	-	-	-
$StHdh^{Q111/111}$	X	↑	↑

Table 4.1 A. Summary of the effects of BDNF, NGF and EGF on the activation of a panel of cell signalling kinases. Arrows indicate the direction of effect following growth factor (GF) stimulation; red arrows indicate a larger magnitude of effect in $StHdh^{Q111/111}$ cells, and green arrows indicate a larger magnitude of effect in $StHdh^{Q7/7}$ cells. Crosses represent no significant change from baseline. **B.** A comparison of the effect of EGF stimulation alone (Chapter 3) and EGF coupled with kinase inhibition on the intensity of HTT and phosphorylated HTT nuclear detection.

Chapter 5: Comparing differential gene expression changes in an immortalised cell model of HD in response to either NGF or EGF stimulation.

5.1 Introduction

It has been suggested that the increased nuclear localisation of mHTT may interfere with gene expression (Zoghbi & Orr 2000; Bauer & Nukina 2009), and that its presence can disrupt the organisation and function of the cell nucleus itself (Sun et al. 2007). Several mechanisms have been identified by which mHTT may disrupt gene expression; for example, several TFs have been found to interact with the polyglutamine expansion in the mHTT protein (Kazantsev et al. 1999; Shimohata et al. 2000; Steffan et al. 2000; Nucifora et al. 2001; Dunah et al. 2002; Li et al. 2002), which can compromise TF activity by altering their binding ability, or by sequestration into mHTT aggregates (Crook & Housman 2011). mHTT is also able to bind directly to DNA and modulate chromatin structure (Benn et al. 2008; McFarland et al. 2012; Seredenina & Luthi-Carter 2012; Ng et al. 2013; Valor et al. 2013).

The majority of transcriptional changes observed in post-mortem human HD caudate and in mouse models of HD are downregulations (Crook & Housman 2011), which may be reflective of the reduction in TF activity due to mHTT. There is good correlation in the pattern of gene expression changes when mHTT is present, not only between mouse models of HD, but also between models and post-mortem human HD brain. A meta-analysis of seven mouse models and human HD caudate indicated that the transcriptional changes observed in mouse models were similar to those identified in human HD (Kuhn et al. 2007). In addition, although the N-terminal HTT models, such as the R6/1 and R6/2 mice showed a more rapid progression of transcriptional changes, which develop by 6-12 weeks of age, the profiles of the slower developing full-length HTT models, such as CHL2$^{Q150/Q150}$, Hdh$^{Q92/Q92}$ and YAC128 mice, develop similar transcriptional profiles to their N-terminal counterparts by 15-24 months, which are also comparable to human HD brain (Kuhn et al. 2007). Several other studies comparing the transcriptional profiles of HD mouse models have reached similar conclusions (Strand et al. 2007; Hodges et al. 2008; Carnemolla et al. 2009; Mazarei et

al. 2010), and there is generally good concordance between different gene expression microarray platforms (Crocker et al. 2006; Becanovic et al. 2010). This suggests that mouse models of HD recapitulate the gene expression changes that occur in human HD caudate, and are therefore a useful tool when investigating gene expression. In addition, as transgenic mice containing only the pathogenic N-terminal of mHTT display a similar pattern of gene expression to the knock in full length models and human caudate, it is likely that it is the N-terminal polyglutamine repeat that is responsible for alterations in gene expression; whether these changes are entirely pathogenic or may also play a compensatory role is yet to be elucidated.

Mouse and cell models of HD allow the investigation of early, pre-symptomatic striatal gene expression changes that are not possible to determine from human HD brain. These models indicate that transcriptional dysregulation is identifiable from an early age; for example, the expression of several genes associated with RNA regulation were found to be disrupted in 3 month old YAC128 mouse striata (Becanovic et al. 2010), and genes associated with transcription, translation, protein synthesis and calcium homeostasis were altered in R6/2 mice from only 10 weeks of age (Crocker et al. 2006). In addition, the increased expression of regulator of ribosome synthesis *(Rrs1)*, has been identified as an early event in Hdh$^{Q111/Q111}$ mice (15 weeks of age), as well as in *StHdh$^{Q111/Q111}$* cells, due to endoplasmic reticular stress (Fossale et al. 2002; Carnemolla et al. 2009). Increased expression of *Rrs1* was also identified in post-mortem human HD caudate (Carnemolla et al. 2009). As well as there being concordance in gene expression between HD mouse models and human brain, *StHdh$^{Q111/111}$* cells have also been found to share similar changes in gene expression to human HD caudate (Lee et al. 2007), suggesting that in addition to mouse models, these cells are also a relevant model of early transcriptional dysregulation in HD.

Growth factor signalling can induce the activation of pathways responsible for the regulation of gene expression. Both NGF and EGF are known to increase the activity of AKT and MAPKs (Humbert 2003), which can either modulate gene expression directly, or via activation of transcriptional regulators such as EGR1 (Cabodi et al. 2009), AP1 (Liu et al. 2011) and NFkβ (Kyriakis & Avruch 2001). Both NGF and EGF have also been found to interact with the transforming growth factor-beta (TGFβ) pathway in both a

synergistic and antagonistic manner (Lutz et al. 2004; Caja et al. 2011; Jin et al. 2011; Kang et al. 2012). The TGFβ pathway is a versatile regulator of cell growth, proliferation and apoptosis, and is upstream of the core regulatory mothers against decapentaplegic- homologue (SMAD) family of TFs (Massague 2003; Massague 2005). A cartoon depicting the mechanism of SMAD TF activity can be found in Figure 5.1.
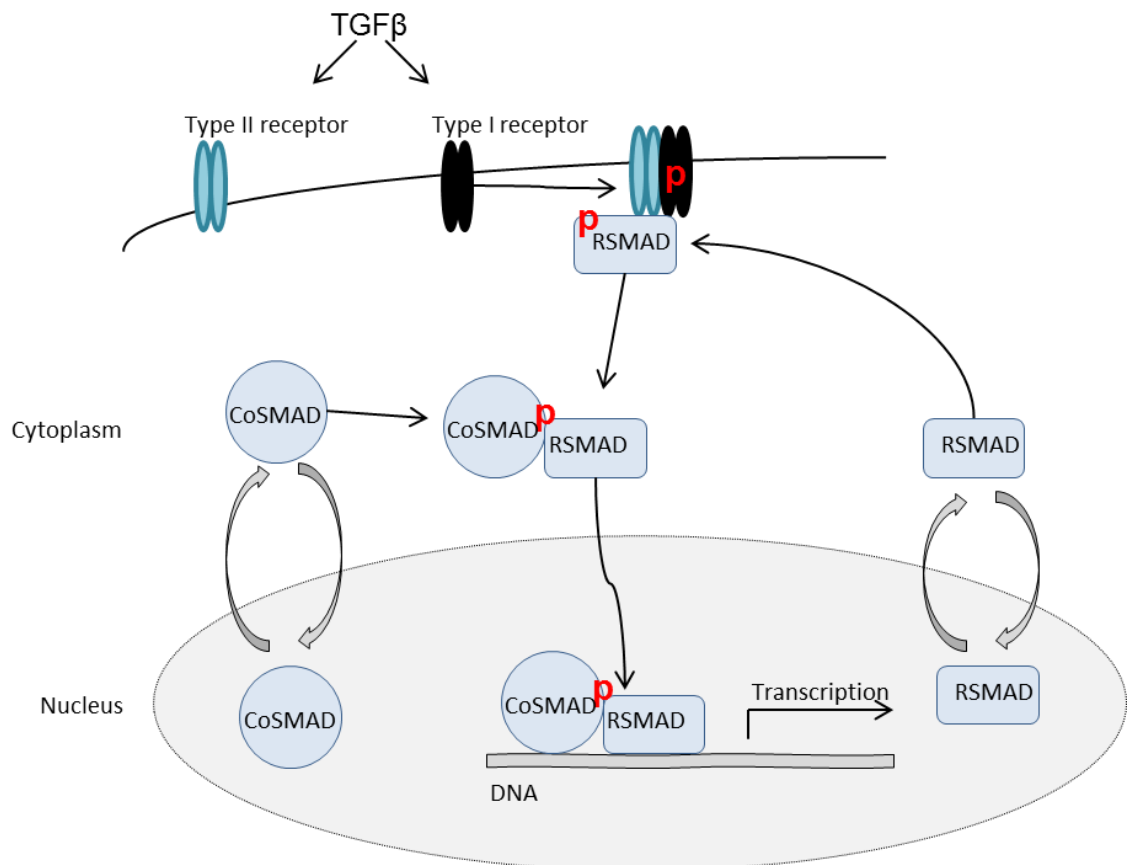
Figure 5.1 Simplified cartoon depicting the basic mechanism of SMAD TF signalling in the TGFβ pathway. TGFβ stimulates its Type I and Type II receptors, creating a hetero-tetrameric receptor complex. Here, the Type II receptor phosphorylates the Type I receptor, which then allows the phosphorylation of receptor-regulated SMADs (RSMADs). The RSMADs are SMADs1-3, 5 and 8, and are constantly shuttling between the nucleus and cytoplasm until anchor proteins recruit them to the active Type I receptor. Phosphorylated RSMADs can bind to the common-mediator SMAD (CoSMAD). The CoSMAD is SMAD4, which is also consistently shuttling between nuclear and cytoplasmic compartments. The resulting RSMAD-CoSMAD complex then localises to the nucleus, where it may either bind directly to DNA to stimulate transcription, or will incorporate DNA binding cofactors. The process can be repressed by the activation of the inhibitory SMADs 6 and 7 in a self-regulatory manner (Massague 2003, 2005). A red 'P' indicates target phosphorylation.

Details of how mHTT may disrupt growth factor signalling, and consequently downstream changes in gene expression, were detailed in the previous chapter, and several IE genes were identified as being differentially regulated in $StHdh^{Q111/111}$ cells in response to EGF stimulation. In this chapter, microarray analysis is utilised to investigate global differential gene expression changes between $StHdh^{Q7/7}$, $StHdh^{Q7/111}$ and $StHdh^{Q111/111}$ cells in response to growth factor stimulation. This creates a dynamic model that allows the identification of additional signalling and transcriptional pathways that may be dysregulated due to the presence and mislocalisation of mHTT downstream of kinase signal transduction, which would not ordinarily be evident without cellular stimulation.

5.2 Microarray experiment

The EGF experiment used a 3x2 design, which included $StHdh^{Q7/7}$, $StHdh^{Q7/111}$ and $StHdh^{Q111/111}$ cells stimulated with 100ng/ml EGF for either 0 or 2 hours, before RNA extraction and purification (n= 5 replicates run on individual chips for each group). This experiment utilised the Affymetrix GeneChip® Mouse Gene 1.0 ST array system, which contains oligonucleotide probes in multiple exons of a gene in order to give whole transcript expression information. Each array consists of 770,000 probes to cover 28,000 genes.

The NGF experiment was a 2x2 design; $StHdh^{Q7/7}$ and $StHdh^{Q111/111}$ cells were stimulated with 100ng/ml NGF for either 0 or 2 hours, and were processed in the same manner as the EGF samples (n= 4 replicates run on individual chips for each group). These samples were run on Affymetrix GeneChip® Mouse Genome 430A 2.0 arrays, which contain multiple probes for each transcript in order to increase accuracy and reliability. Each array chip has 22,600 probe sets that cover 14,000 genes.

All samples used in microarray experiments had an RNA integrity number (RIN) of 10. Analysis of microarray data was carried out in Partek® Genomics Suite™ unless otherwise stated.

5.2.1 Quality control metrics

Both the NGF and EGF microarray experiments were analysed in the same manner. The raw data underwent quantile normalisation to log base 2, and median polish probeset summarisation. There was no adjustment for GC content or probe sequence, and robust multi-array average (RMA) background correction was applied.

5.2.1.1 EGF

Principal components analysis (PCA) was carried out as an initial exploratory analysis of the gene expression data as a whole. PCA mapping of the EGF microarray data indicates that the main source of variance in gene expression is attributable to genotype, and stimulation with EGF is the second source of variance (Figure 5.2). However, it is evident from the PCA map that the *StHdh*$^{Q7/7}$ cells are overall more responsive to EGF stimulation than *StHdh*$^{Q111/111}$ cells, whereas *StHdh*$^{Q7/111}$ cells fall in between the two.

Unsupervised hierarchical clustering of genes with a significant interaction term following ANOVA analysis (see section 5.2.2) was carried out in Partek to visualise the grouping of differentially expressed genes, the results of which can be seen in Figure 5.3, presented as a Euclidean distance heat map. It is evident from this figure that *StHdh*$^{Q7/7}$ and *StHdh*$^{Q7/111}$ cells cluster more closely together than with *StHdh*$^{Q111/111}$ cells in terms of their gene expression profiles. Cells stimulated with EGF also cluster more closely to their control counterparts than to the other EGF stimulated genotypes. This reflects the PCA, in that it indicates that growth factor stimulation can distinguish the samples within each genotype, and that each genotype is responding to EGF stimulation in a differential manner.
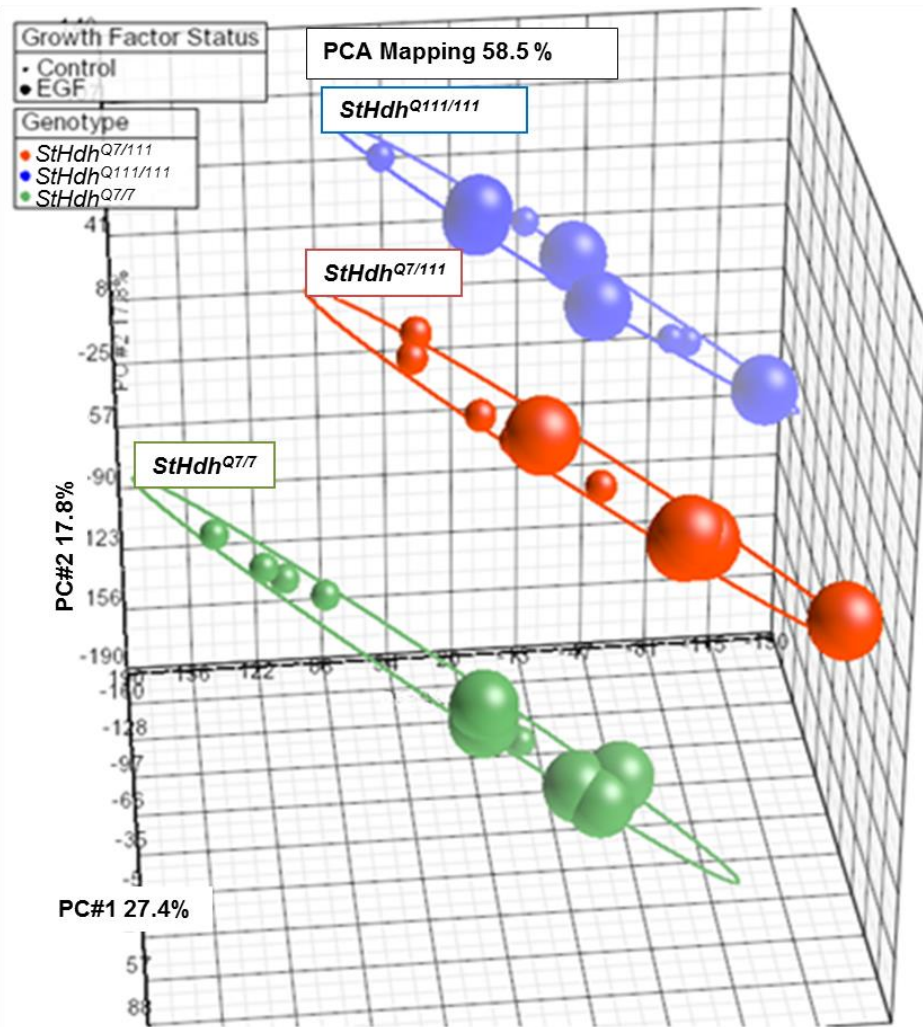
Figure 5.2 PCA of EGF microarray data. Genotype is the main principle component, which accounts for 27.4% of the variance in gene expression. EGF stimulation is the second principle component, and accounts for 17.8% of the variance. Each genotype clusters together, but there is clear separation between 0 and 2 hours EGF stimulation in *StHdh*^{Q7/7} cells. This separation reduces in the *StHdh*^{Q7/111} cells, and is not apparent in the *StHdh*^{Q111/111} cells.
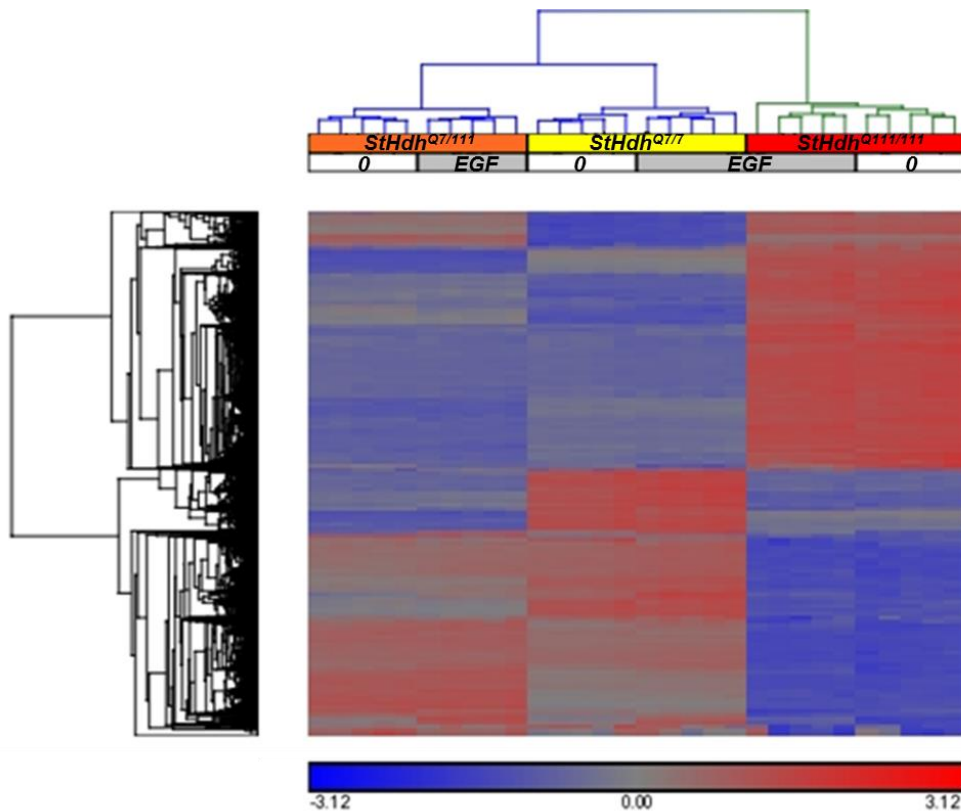
Figure 5.3 Heat map representing unsupervised hierarchical clustering of interaction data from the EGF microarray experiment. The data was transformed so that the mean expression value for each gene was 0, with a standard deviation of 1. Blue depicts a reduction in gene expression, and red depicts an increase. Grey indicates no change. The more closely clustered each category is, the more common their gene expression profiles. $StHdh^{Q7/111}$ cells (orange) have more similar gene expression profiles to $StHdh^{Q7/7}$ cells (yellow) than $StHdh^{Q111/111}$ cells (red). The smaller effect of EGF on gene expression compared to genotype is also evident from this map. Each genotype clusters closer to its own control following 2 hours of 100ng/ml EGF stimulation.

5.2.1.2 NGF

The PCA of the NGF data also showed a very clear separation of gene expression profiles between $StHdh^{Q7/7}$ and $StHdh^{Q111/111}$ cell types. Genotype was again the main source of variance, with NGF stimulation being the second (Figure 5.4). However, in contrast to the responses to EGF, there is a greater effect of NGF on gene expression in $StHdh^{Q111/111}$ cells, and a much smaller effect in $StHdh^{Q7/7}$.
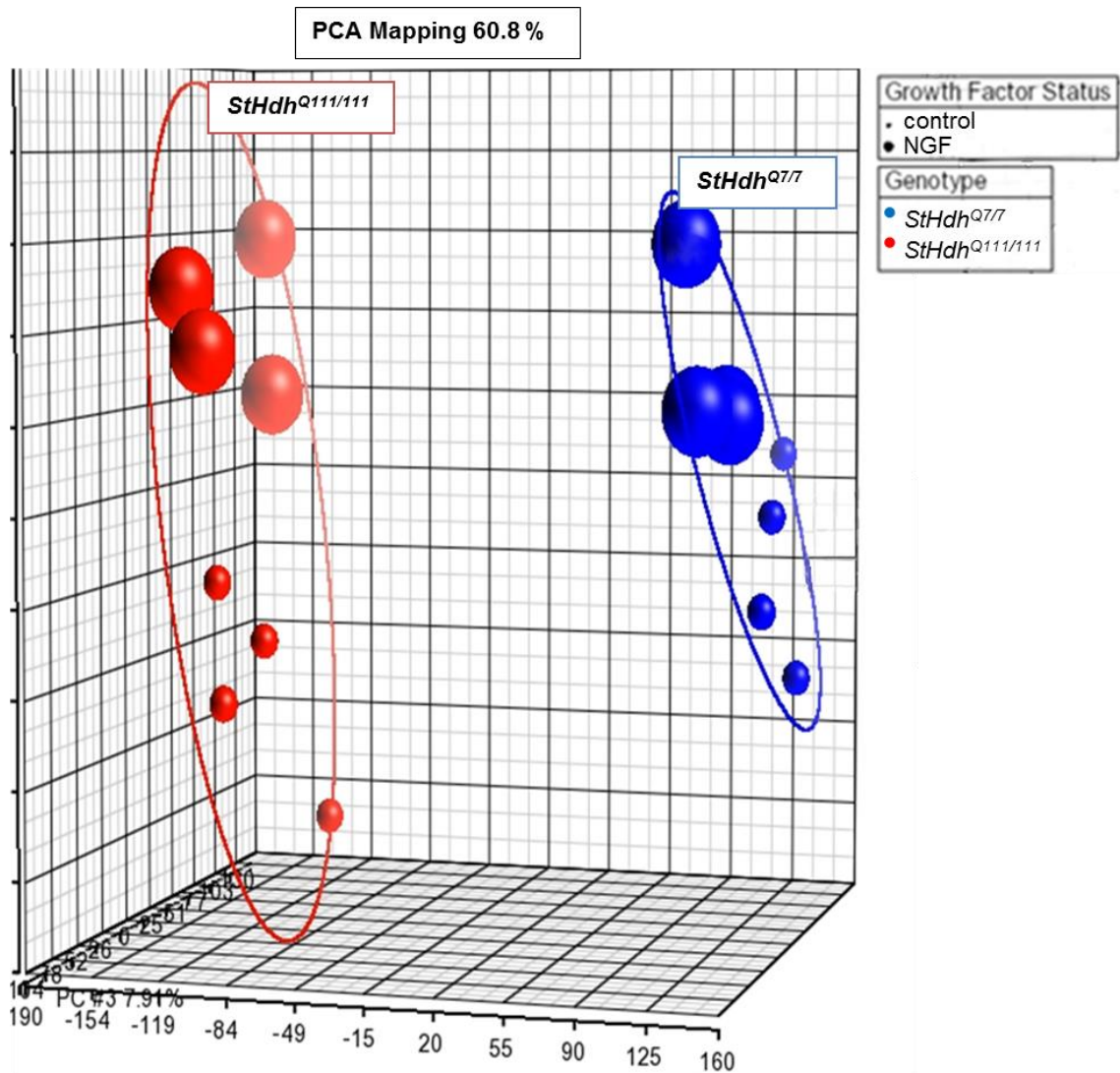
Figure 5.4 PCA of NGF microarray data. Genotype is the main principle component, which accounts for 43.2% of the variance in gene expression. NGF stimulation is the second principle component, and accounts for 29.74% of the variance. Each genotype clusters together, but there is clear separation between 0 and 2 hours NGF stimulation in *StHdh*$^{Q111/111}$ cells. This separation is reduced in the *StHdh*$^{Q7/7}$ cells, suggesting an augmented gene expression response to NGF in cells containing mHTT.

Hierarchical clustering was performed in the same manner as following EGF stimulation. Comparison of the two expression analyses shows that at baseline, there is a similar pattern of differential gene expression between the two experiments. As seen in the PCA for the NGF microarray data, there is clear separation between the genotypes (Figure 5.5); NGF stimulated cells cluster closer to the control of the same

genotype, which is the same pattern observed following EGF. However, in contrast to EGF stimulated cells, the NGF heat map illustrates that there is a greater extent of gene expression change in NGF treated $StHdh^{Q111/111}$ cells as compared to $StHdh^{Q7/7}$ cells.
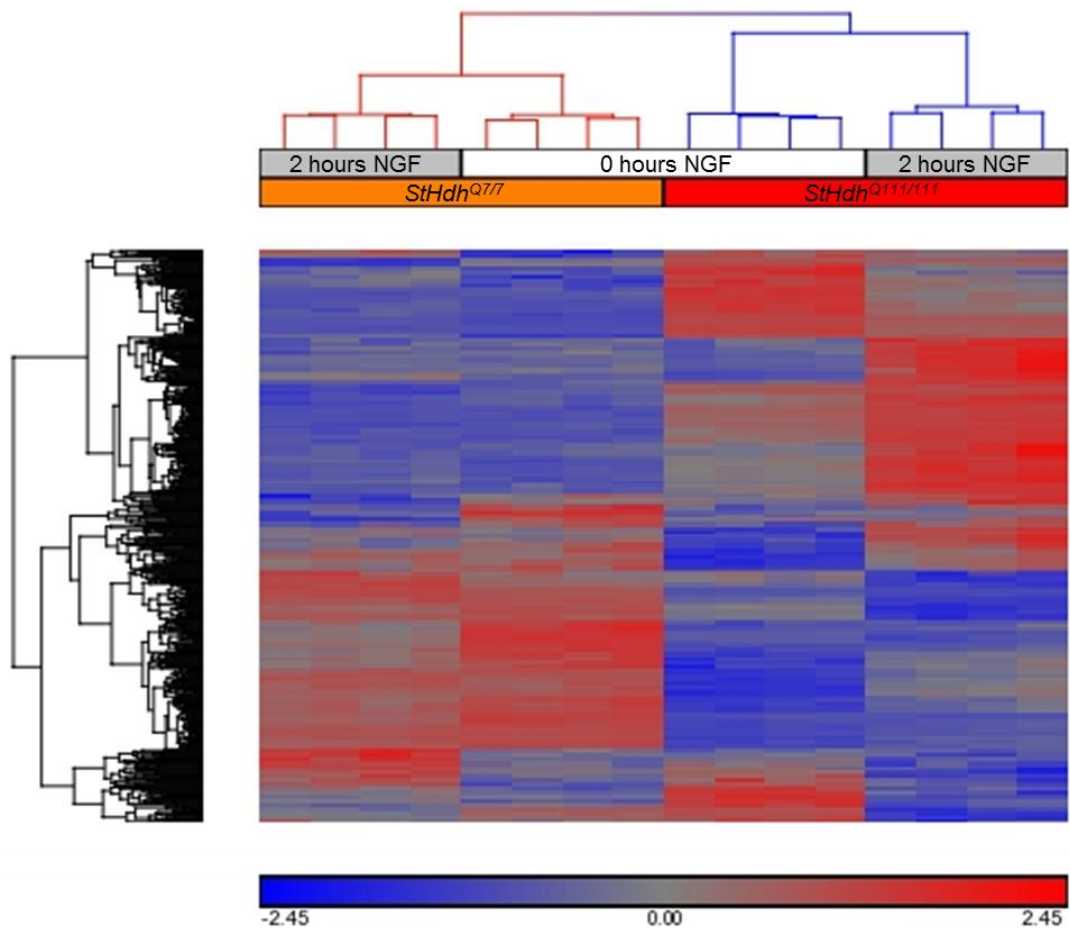
Figure 5.5 Heat map representing unsupervised hierarchical clustering of interaction data from the NGF microarray experiment. The data was transformed so that the mean expression value for each gene was 0, with a standard deviation of 1. Blue depicts a reduction in gene expression, and red depicts an increase. Grey indicates no change.

5.2.2 Differential gene expression

The data from both EGF and NGF microarrays were analysed separately, but in the same manner. All gene expression data were analysed by a 2-way ANOVA with an interaction term, plus individual contrasts to identify simple main effects. The focus for the following stages of analysis was on the differences between $StHdh^{Q7/7}$ and

StHdh$^{Q111/111}$ cell lines only, as this is where the largest differences were expected to lie. The following lists of significantly differentially expressed genes were then created from the resulting data with the parameters described below:

- *StHdh$^{Q7/7}$* 0 hours vs. *StHdh$^{Q111/111}$* 0 hours   Fold change >2 - <-2
                                                      False discovery rate (FDR) 0.05

- *StHdh$^{Q7/7}$* 0 hours vs. *StHdh$^{Q7/7}$* 2 hours   Fold change >1.5 - <-1.5, FDR 0.05

- *StHdh$^{Q111/111}$* 0 hours vs. *StHdh$^{Q111/111}$* 2 hours   Fold change >1.5 - <-1.5, FDR 0.05

- Interaction   Fold change >2 - <-2, FDR 0.05

5.2.2.1 Differentially expressed genes at baseline

For the EGF experiment, there were 1394 significantly differentially expressed genes between *StHdh$^{Q7/7}$* and *StHdh$^{Q111/111}$* cells at baseline, whereas for the NGF experiment, this figure was much higher at 3201. The magnitude of the largest fold change in both experiments was drastically different, the largest in the EGF experiment being +59, and +496 for the NGF experiment. As this large fold change in the NGF microarray experiment was between *StHdh$^{Q111/111}$* cells and *StHdh$^{Q7/7}$* cells at baseline, it is unlikely to be an effect of an enhanced response to NGF stimulation compared to EGF stimulation. Histograms representing the frequency of particular fold change occurrences between *StHdh$^{Q7/7}$* and *StHdh$^{Q111/111}$* cells at baseline (Figure 5.6) indicate that there are slightly varied distributions between EGF and NGF microarrays; accordingly, the variance of the EGF baseline data was 4.71, whereas the variance for the NGF array was much broader at 41.97, which may be a result of the smaller sample size utilised in the NGF experiment. However, it may also be due to the nature of the different Affymetrix chips used between experiments, or a result of different batches of cells used at different times. In addition, although the NGF baseline data has a skewness close to a normal distribution (-1.44) the EGF data is skewed further towards the upregulated expression of genes in *StHdh$^{Q111/111}$* cells, although two downregulated genes with large fold changes give the data a skewness value of -16.49. Nevertheless, despite these variance and expression differences, similar gene ontology (GO) categories were identified from the most significant genes in both groups (Section

5.2.3), suggesting a degree of homogeneity between the baseline expression profiles of the two experiments.
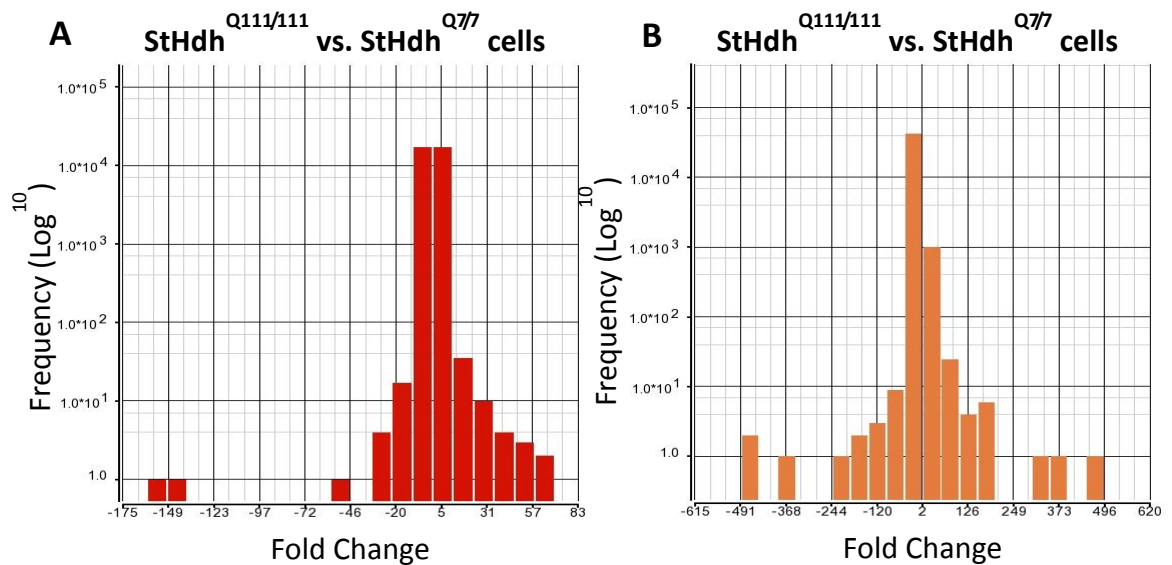
Figure 5.6 Histograms of the frequency of the magnitude of gene expression fold changes between *StHdh*$^{Q7/7}$ and *StHdh*$^{Q111/111}$ cells at baseline in **A.** EGF and **B.** NGF microarray datasets. The NGF data exhibits a distribution closer to normal (skew = -1.437), but large positive and negative fold changes gives rise to a high kurtosis value (2866.68). Although the EGF data is less widely spread (kurtosis = 1582.17), two large negative fold changes give the data substantial skew (-16.49). Fold changes are indicative of the level of *StHdh*$^{Q111/111}$ gene expression in comparison to *StHdh*$^{Q7/7}$ gene expression.

5.2.2.2 Differentially expressed genes following growth factor stimulation

Both growth factors had roughly equal effects on the magnitude of expression fold changes, with the majority of genes being up or downregulated by a fold change of x2. Gene expression changes following growth factor stimulation also exhibited a similar distribution between genotypes (Figure 5.7).

The differential effects of the two growth factors on the different genotypes were also reflected in the gene lists. Following EGF stimulation, where there was a greater effect in *StHdh*$^{Q7/7}$ cells, where there were 391 significantly differentially expressed genes, whereas there were only 171 following NGF stimulation. In contrast, there were only

254 differentially expressed genes in *StHdh*$^{Q111/111}$ cells following EGF stimulation, but 418 following NGF stimulation.

Despite the larger effect of NGF stimulation in *StHdh*$^{Q111/111}$ cells compared to *StHdh*$^{Q7/7}$, there were only 576 genes that had a significant genotype x growth factor interaction effect, whereas there were 2687 that reached significance for an interaction following EGF stimulation. This is likely to be a combinatory effect of the responses to the different growth factors, as well as the different chips used; there are twice as many genes detected on the chips used in the EGF experiment.
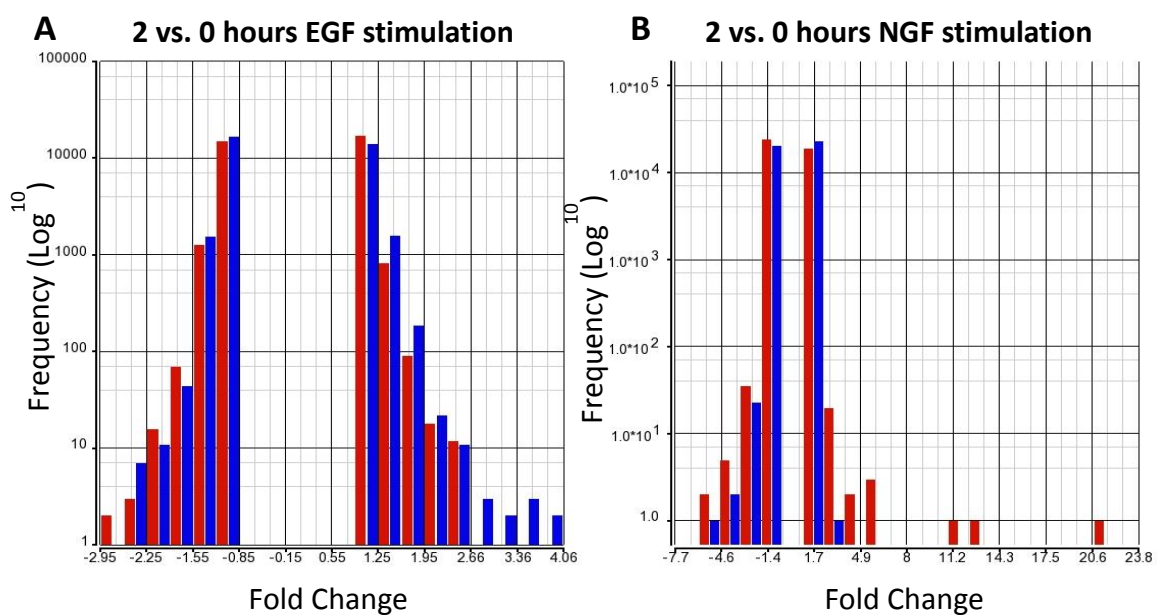
Figure 5.7 Histograms of the frequency of the magnitude of gene expression fold changes between 0 and 2 hours stimulation with **A.** EGF or **B.** NGF for both *StHdh*$^{Q7/7}$ (blue) and *StHdh*$^{Q111/111}$ *(*red) cells. Both *StHdh*$^{Q7/7}$ and *StHdh*$^{Q111/111}$ cells exhibit similar distributions of gene expression fold changes in response to either growth factor, and the majority of changes cluster between -4 and +4. Neither data set deviates markedly from the normal distribution;
NGF skew = -0.11 (*StHdh*$^{Q7/7}$), 0.5 (*StHdh*$^{Q111/111}$) & NGF kurtosis = -1.92 (*StHdh*$^{Q7/7}$), 2.8 (*StHdh*$^{Q111/111}$).
EGF skew = -0.17 (*StHdh*$^{Q7/7}$), -0.09 (*StHdh*$^{Q111/111}$) & EGF kurtosis = -1.9 (*StHdh*$^{Q7/7}$), -1.93 (*StHdh*$^{Q111/111}$).
More *StHdh*$^{Q7/7}$ cells have larger positive fold changes following EGF stimulation than *StHdh*$^{Q111/111}$ cells, which is concordant with the PCA data (Figure 5.2). In opposition, *StHdh*$^{Q111/111}$ cells exhibit more genes with higher fold changes than *StHdh*$^{Q7/7}$ cells following NGF stimulation, which is also concordant with the PCA data (Figure 5.4).

5.2.3 Pathway analysis

Either the entire gene list, or the top 500 most significant genes from each gene list were put through pathway analyses enriched for the GO categories, using the web based gene set analysis toolkit program, WebGestalt V2 (Http://bioinfo.vanderbilt.edu/webgestalt/) (Zhang et al. 2005; Wang et al. 2013). This program uses a hypergeometric statistical method, plus the Benjamini & Hochberg multiple test adjustment (Benjamini & Hochberg 1995). The minimum number of genes required for a category to be considered was set to 2, and the top 10 most significant biological categories were investigated further.

5.2.3.1 Baseline differences

The top 10 most significant biological GO categories and their associated p-values for genes differentially expressed between genotypes at baseline can be seen in Table 5.1. Seven of the top categories overlap with those identified from the equivalent gene list from the NGF microarray experiment, despite differences in the magnitude of fold changes. Of the 138 genes that were part of the top 10 GO categories in the EGF data, 91 of these genes were also in the list of genes that were differentially expressed between genotypes at baseline in the NGF data. However, hypergeometric testing revealed that the probability of this overlap was not significantly different to chance (p (x=138) = 2.35). However, the similarities in GO categories still suggest that there may be some homogeneity and reproducibility between different batches of these cells, and across different microarray chips on the Affymetrix platform. The identified GO categories are largely associated with development, which is likely to be due to the derivation of this cell line from embryonic striatal cells that are not yet fully differentiated into adult neurons.

GO Category	P-value	
	EGF	NGF
System development	1.2×10^{13}	5.2×10^{9}
Anatomical structure development	3.2×10^{13}	5.2×10^{9}
Multicellular organismal development	3.2×10^{13}	2.7×10^{8}
Developmental Process	9.5×10^{13}	1.4×10^{8}
Anatomical structure morphogenesis	1.7×10^{12}	1.4×10^{8}
Organ development	1.6×10^{10}	1.8×10^{7}
Organ morphogenesis	4.7×10^{9}	1.6×10^{7}
Biological adhesion	7.3×10^{8}	-
Cell adhesion	7.3×10^{8}	-
Nervous system development	2.5×10^{6}	-
Positive regulation of biological process	-	1.4×10^{7}
Positive regulation of cellular process	-	7.3×10^{7}
Vasculature development	-	8.6×10^{7}

Table 5.1 Comparison of the top 10 significant biological GO categories identified by WebGestalt pathway analysis for genes differentially expressed between *StHdh*$^{Q7/7}$ and *StHdh*$^{Q111/111}$ cells at baseline in both EGF and NGF microarray experiments.

5.2.3.2 EGF microarray

5.2.3.2a Pathways implicated following EGF stimulation

Despite substantial differences in gene expression profiles both at baseline and following EGF stimulation, pathway analyses of this data suggested very similar GO categories as being implicated following EGF stimulation in both *StHdh*$^{Q7/7}$ and *StHdh*$^{Q111/111}$ cell lines (Table 5.2). Although some of the identified pathways were associated with developmental processes, the majority of the top 10 pathways were related to transcription and transcriptional control. This suggests that EGF stimulation in both cell lines initiates expression changes in genes that may regulate transcriptional pathways.

GO Category	P-value		
	$StHdh^{Q7/7}$	$StHdh^{Q111/111}$	Interaction
Regulation of nitrogen compound metabolic process	2.1×10^{7}	1.2×10^{7}	
Regulation of RNA metabolic process	2.0×10^{7}	1.3×10^{7}	
RNA biosynthetic process	2.0×10^{7}	1.3×10^{7}	
Regulation of transcription, DNA dependent	2.0×10^{7}	1.3×10^{7}	
Regulation of transcription from RNA polymerase II	2.0×10^{7}	1.1×10^{7}	
Transcription, DNA dependent	2.0×10^{7}	1.3×10^{8}	
Transcription	2.0×10^{7}	1.3×10^{8}	2×10^{11}
Anatomical structure development	2.0×10^{7}	1.1×10^{7}	1.3×10^{9}
System development	2.0×10^{7}	1.4×10^{7}	
Regulation of nucleobase, nucleoside, nucleotide and nucleic acid metabolic process	2.0×10^{7}		
Regulation of developmental processes		1.0×10^{7}	
Developmental process			1.8×10^{12}
Multicellular organismal development			1.8×10^{12}
Regulation of cellular metabolic process			7.8×10^{12}
Regulation of metabolic process			5.7×10^{11}
Blood vessel development			2.8×10^{10}
Vasculature development			3.7×10^{10}
Regulation of transcription			5.3×10^{10}
Organ morphogenesis			5.3×10^{10}

Table 5.2 Comparison of the top 10 significant biological GO categories identified by WebGestalt pathway analysis for genes differentially expressed following 2 hours 100ng/ml EGF stimulation for $StHdh^{Q7/7}$ and $StHdh^{Q111/111}$ cells, as well as for genes with a significant genotype x growth factor interaction.

5.2.3.2b Pathways implicated in the EGF x genotype interaction

The top 10 biological GO pathways identified from the EGF x genotype interaction analysis reflects both the differences between these cells found at baseline, and following EGF stimulation (Table 5.2). The majority of the pathways are part of various developmental processes, and this is likely to be a reflection of genotype as the main source of variance. However, the 'Transcription' and 'Regulation of transcription' pathways remain highly significant when looking at the interaction effect, indicating that there are significant differential effects between $StHdh^{Q7/7}$ and $StHdh^{Q111/111}$ cell lines in pathways that may exert some transcriptional control.

5.2.3.2c Selecting genes to follow up

In order to create a smaller list of genes to take forward for further analysis, the genes that were in the two GO categories associated with transcription from the interaction analysis were cross-referenced with the genes that had a significant effect of EGF in either $StHdh^{Q7/7}$ or $StHdh^{Q111/111}$ cells. Therefore the genes in the resulting list should have the strongest differential expression effects, as well as a strong effect of EGF. This means the observed effects in these genes are less likely to be by chance, and are most likely to be associated with differences in transcriptional pathways between $StHdh^{Q7/7}$ and $StHdh^{Q111/111}$ cells. This reduced list of genes was then further split into three separate lists, depending on the direction of effect; these lists can be found in Table 5.3. By looking at genes whose expression is changed by EGF stimulation in $StHdh^{Q7/7}$ cells only, it should be possible to elucidate the signalling pathways that are generally activated by EGF. In contrast, genes that have an augmented response to EGF in the $StHdh^{Q111/111}$ cells are of interest, as the majority of gene expression changes observed in this cell line and other HD models are downregulations (Crook & Housman 2011) so the genes that are more sensitive to modification of expression may be indicative of aberrant signalling pathways in cells that contain mHTT.

Effect of EGF in *StHdh*^{Q7/7} only		
Gene Name	Gene Symbol	Ref Sequence
Aryl hydrocarbon receptor nuclear translocator-like	*Arntl* ↑	NM_007489
Fibroblast growth factor 2	*Fgf2* ↑	NM_008006
Forkhead box C2	*Foxc2* ↑	NM_013519
Human immunodeficiency virus type I enhancer binding protein 1	*Hivep1* ↑	NM_007772
Jun oncogene	*Jun* ↑	NM_010591
Jun-B oncogene	*Junb* ↑	NM_008416
KDM1 lysine (K)-specific demethylase 6B	*Kdm6b* ↑	NM_001017426
Kruppel-like factor 5	*Klf5* ↑	NM_009769
Myelocytomatosis oncogene	*Myc* ↑	NM_010849
MAD homolog 7 (Drosophila)	*Smad7* ↑	NM_001042660
SRY-box containing gene 9	*Sox9* ↑	NM_011448
Sprouty homolog 2 (*Drosophila*)	*Spry2* ↑	NM_011897
TEA domain family member 4	*Tead4* ↑	NM_011567
Teashirt zinc finger family member 1	Tshz1 ↑	NM_001081300

Effect of EGF in both genotypes, enhanced in *StHdh*^{Q111/111}		
Gene Name	Gene Symbol	Ref Sequence
Activating transcription factor 3	*Atf3* ↑	NM_007498
B-cell CLL/lymphoma 6, member B	*Bcl6b* ↑	NM_007528
Basic helix-loop-helix family, member e40	*Bhlhe40* ↑	NM_011498
Early growth response 1	*Egr1* ↑	NM_007913
Ets variant gene 5	*Etv5* ↑	NM_023794
Fos-like antigen 1	*Fosl1* ↑	NM_010235
High mobility group AT-hook 2	*Hmga2* ↑	NM_010441
Inhibitor of DNA binding 3	*Id3* ↓	NM_008321
Interferon regulatory factor 2 binding protein 2	*Irf2bp2* ↑	NM_001164598
Nuclear receptor subfamily 4, group A, member 3	*Nr4a3* ↑	NM_015743

Table 5.3 Continued on next page

Effect of EGF in *StHdh* $^{Q111/111}$ only		
Gene Name	Gene Symbol	Ref Sequence
Biregional cell adhesion molecule-related/down-regulated by oncogenes	*Boc* ↓	NM_172506
CDC42 effector protein (Rho GTPase binding) 3	*Cdc42ep3* ↓	NM_026514
Growth arrest and DNA-damage-inducible, gamma interacting protein	*Gadd45g* ↓	NM_183358
Nerve growth factor	*Ngf* ↑	NM_013609
RAS p21 protein activator 1	*Rasa1* ↑	NM_145452

Table 5.3 Gene lists created by cross-referencing the top genes with a significant genotype x EGF interaction with the top genes with a significant effect of EGF in GO category transcription related pathways. Arrows indicate the direction of expression change following EGF stimulation.

5.2.3.3 NGF microarray

5.2.3.3a Pathways implicated following NGF stimulation

In contrast to EGF stimulation, NGF stimulation of *StHdh*$^{Q7/7}$ and *StHdh*$^{Q111/111}$ cells lead to the identification of almost entirely different pathways, with only one overlapping GO category between the genotypes (Table 5.4). In *StHdh*$^{Q7/7}$ cells, these were largely regulatory pathways associated with cell growth and metabolic activity. The GO categories identified in *StHdh*$^{Q111/111}$ cells were more similar to the categories identified following EGF stimulation than to *StHdh*$^{Q7/7}$ cells following NGF stimulation; three of the categories were associated with transcriptional pathways, and the others were regulatory or developmental categories. The implication of more transcriptional-related pathways in *StHdh*$^{Q111/111}$ cells following NGF stimulation may partly explain why the extent of gene expression changes is greater in these cells than in *StHdh*$^{Q7/7}$ cells.

5.2.3.3b Pathways implicated in the NGF x genotype interaction

The pathways implicated in the NGF x genotype interaction partially overlap with those identified following EGF stimulation, such as 'Regulation of metabolic processes' and 'Regulation of transcription' (Table 5.4). This similarity may be due to the overlapping effects of EGF and NGF on *StHdh*$^{Q111/111}$ cells. However, by looking at the PCA analyses

for both data sets, it is likely that although similar pathways are involved in these cell lines following both EGF and NGF stimulation, the nature of the effect is likely to be different. For all the genes with a significant gene expression change in $StHdh^{Q7/7}$ cells following EGF stimulation, only 14.6% of those were downregulations, whereas following NGF stimulation, this figure was 49.7%. On the other hand, in $StHdh^{Q111/111}$ cells, the percentage of downregulated genes following both NGF and EGF stimulation stayed roughly similar (35% and 40%, respectively), suggesting that the response of $StHdh^{Q111/111}$ cells to growth factor stimulation may be less specific to particular compounds than in $StHdh^{Q7/7}$ cells.

<div align="center">5.2.3.3c Selecting genes to follow up</div>

More focused gene lists were created in the same manner as described previously (Section 5.2.3.2c), and can be found in Table 5.5. From these lists, there were 5 genes that also appeared on the EGF lists. These can be seen in Table 5.6, where the magnitude and direction of their expression changes following growth factor stimulation are also detailed. The hypergeometric probability of this overlap was calculated as p(x=5) = 0.04, thus suggesting that both NGF and EGF are likely to be stimulating similar gene expression pathways, but in a differential manner.

GO Category	P-value		
	$StHdh^{Q7/7}$	$StHdh^{Q111/111}$	Interaction
Regulation of cellular process	5.2×10^7		8.6×10^7
Regulation of cellular metabolic process	5.2×10^7		1.1×10^6
Regulation of metabolic process	1.0×10^6		1.1×10^6
Regulation of biological process	2.0×10^6	3.9×10^7	2.1×10^6
Biological regulation	3.9×10^6		
Regulation of protein kinase activity	1.1×10^5		
Regulation of kinase activity	1.2×10^5		
Regulation of transferase activity	1.3×10^5		
Regulation of cell proliferation	2.5×10^5		
Negative regulation of cellular process	3.0×10^5		
Organ development		6.2×10^8	
Organ morphogenesis		6.2×10^8	
Anatomical structure morphogenesis		1.2×10^7	
Regulation of transcription, DNA dependent		2.4×10^7	2.2×10^6
Regulation of RNA metabolic process		3.2×10^7	2.1×10^6
System development		4.0×10^7	
RNA biosynthetic process		4.0×10^7	
Transcription, DNA dependent		4.0×10^7	2.5×10^6
Tube morphogenesis			2.1×10^6
Regulation of primary metabolic process			2.2×10^6
Regulation of nitrogen compound metabolic process			2.4×10^6

Table 5.4 Comparison of the top 10 significant biological GO categories identified by WebGestalt pathway analysis for genes differentially expressed between $StHdh^{Q7/7}$ and $StHdh^{Q111/111}$ cells, as well as for genes with a significant genotype x growth factor interaction following 2 hours 100ng/ml NGF stimulation.

	Effect of NGF in *StHdh*$^{Q111/111}$ only	
Gene Name	Gene Symbol	Ref Sequence
A disintegrin-like and metallopeptidase (reprolysin type) with thrombospondin type 1 motif 5	*Adamts5* ↓	NM_011782
Aryl-hydrocarbon receptor	*Ahr* ↓	NM_013464
ADP-ribosylation factor-like 4C	*Arl4c* ↓	NM_177305
Activating transcription factor 3	*Atf3* ↑	NM_007498
BTB and CNC homology 1	*Bach1* ↑	NM_007520
BCL2-like 11 (apoptosis facilitator)	*Bcl2l1* ↑	NM_009754
Bone morphogenetic protein 4	*Bmp4* ↓	NM_007554
CDC42 effector protein (Rho GTPase binding) 3	*Cdc42ep3* ↓	NM_026514
cAMP responsive element modulator	*Crem* ↑	NM_001110850
Chromobox homolog 4 (Drosophila Pc class)	*Cxb4* ↑	NM_007625
DNA-damage-inducible transcript 4	*Ddit4* ↑	NM_029083
E26 avian leukemia oncogene 2, 3' domain	*Ets2* ↑	NM_011809
Forkhead box A1	*Foxa1* ↑	NM_008259
Frizzled homolog 8 (Drosophila)	*Fzd8* ↓	NM_008058
Growth arrest and DNA-damage-inducible 45 gamma	*Gadd45g* ↓	NM_011817
GRP1 (general receptor for phosphoinositides 1)-associated scaffold protein	*Grasp* ↑	NM_019518
Homeobox A2	*Hoxa2* ↑	NM_010451
Homeobox A5	*Hoxa5* ↑	NM_010453
Insulin-like growth factor binding protein 3	*Igfbp3* ↑	NM_008343
Jumonji, AT rich interactive domain 2	*Jarid2* ↑	NM_021878
Ajuba	*Jub* ↓	NM_010590
Max interacting protein 1	*Mxi1* ↑	NM_001008542
Nuclear receptor subfamily 4, group A, member 1	*Nr4a1* ↑	NM_010444
Nuclear receptor subfamily 4, group A, member 2	*Nr4a2* ↑	NM_001139509
Paired box gene 9	*Pax9* ↑	NM_011041
Pyruvate dehydrogenase kinase, isoenzyme 4	*Pdk4* ↑	NM_013743
Peroxisome proliferative activated receptor, gamma, coactivator 1 alpha	*Ppargc1a* ↑	NM_008904
Prostaglandin F receptor	*Ptgfr* ↑	NM_008966
Parathyroid hormone-like peptide	*Pthlh* ↑	NM_008970
Protein tyrosine phosphatase 4a1	*Ptp4a1* ↑	NM_011200
Receptor (calcitonin) activity modifying protein 3	*Ramp3* ↑	NM_019511
Regulator of G-protein signaling 2	*Rgs2* ↑	NM_009061

Table 5.5 Continued on next page

Gene Name	Gene Symbol		Ref Sequence
Rho family GTPase 3	*Rnd3*	↓	NM_028810
Sex comb on midleg homolog 1	*Scmh1*	↓	NM_001159630
Salt inducible kinase 1	*Sik1*	↑	NM_010831
Suppressor of cytokine signaling 3	*Socs3*	↓	NM_007707
Thrombospondin 1	*Thbs1*	↓	NM_011580
Toll-like receptor 2	*Tlr2*	↑	NM_011905
TSC22 domain family, member 3	*Tsc22d3*	↑	NM_001077364
Twist homolog 1 (Drosophila)	*Twist1*	↓	NM_011658
Vitamin D receptor	*Vdr*	↑	NM_009504
Vascular endothelial growth factor A	*Vegfa*	↑	NM_001025250

Effect of NGF in *StHdh* Q7/7 only			
Gene Name	Gene Symbol		Ref Sequence
Cyclin G2	*Ccng2*	↑	NM_007635
Cyclin-dependent kinase inhibitor 1A (P21)	*Cdkn1a*	↓	NM_007669
Carcinoembryonic antigen-related cell adhesion molecule 1	*Ceacam1*	↓	NM_001039185
Fos-like antigen 1	*Fosl1*	↓	NM_010235
Inhibitor of DNA binding 2	*Id2*	↓	NM_010496
Kit ligand	*Kitl*	↑	NM_013598
Myeloblastosis oncogene-like 1	*Mybl1*	↓	NM_008651
Nuclear factor, interleukin 3, regulated	*Nfil3*	↓	NM_017373
Prolactin family 2, subfamily c, member 2	*Prl2c2*	↑	NM_011118
Prostaglandin E receptor 4 (subtype EP4)	*Ptger4*	↓	NM_001136079
Regulating synaptic membrane exocytosis 2	*Rims2*	↓	NM_053271

Effect of NGF in both genotypes, enhanced in *StHdh* Q111/111			
Gene Name	Gene Symbol		Ref Sequence
Connective tissue growth factor	*Ctgf*	↓	NM_010217
Colony stimulating factor 1 (macrophage)	*Csf1*	↓	NM_001113529
Cysteine rich protein 61	*Cyr61*	↓	NM_010516
Prostaglandin-endoperoxide synthase 2	*Ptgs2*	↑	NM_011198

Table 5.5 Gene lists created by cross-referencing the top genes with a significant genotype x NGF interaction with the top genes with a significant effect of NGF in GO category transcription related pathways. Arrows indicate the direction of expression change following EGF stimulation

Gene	EGF		NGF	
	$StHdh^{Q7/7}$	$StHdh^{Q111/111}$	$StHdh^{Q7/7}$	$StHdh^{Q111/111}$
Arntl	↑1.64	↑1.13	↓ 1.14	↑1.36
Atf3	↑1.56	↑1.99	↓ 1.14	↑2.87
Fosl1	↑2.23	↑2.54	↓ 2.14	↓1.26
Hivep1	↑1.51	↑1.41	↓ 1.03	↑1.48
Tshz1	↑1.74	↑1.38	↑1.05	↑1.47

Table 5.6 The genes that appear on the reduced gene lists for both EGF and NGF stimulation. Direction of expression change following growth factor stimulation is indicated by arrows, alongside the fold change.

5.2.4 Gene expression validation

Gene expression changes were validated by qRTPCR. A selection of genes from each list in Tables 5.3 and 5.5 were chosen for validation.

5.2.4.1 EGF

Reverse transcribed RNA from the same samples used for the microarray experiment were used for expression validation by qRTPCR. Eight out of 15 genes tested were fully confirmed, and four showed the same pattern of expression, but did not reach statistical significance. This is likely due to the small sample of only 5 replicates, and the small magnitude of expression changes following EGF stimulation. Only three of the 15 genes tested were not validated. A summary of these results can be seen in Table 5.7. On this occasion, *Egr1* was one of the genes that were unable to be validated; however the same pattern of expression as was seen in the microarray was previously identified when using an alternative qRTPCR assay in a previous experiment (Chapter 4, Figure 4.9), so it was not excluded from further analysis.

Genes with higher response in *StHdh*[Q111/111] cells following EGF stimulation

Gene	Genotype	Microarray		qRTPCR		Confirmed?
		Fold change	P-value	RQ value ratio	P-value	
Id3	*StHdh*[Q7/7]	-1.75	1.8×10^{11}	0.3	0.001	✓
	StHdh[Q7/111]	-1.68	2.5×10^{10}	0.51	0.035	
	StHdh[Q111/111]	-2.18	3.6×10^{14}	0.21	0.001	
Atf3	*StHdh*[Q7/7]	1.56	2.2×10^{8}	1.86	-	✓
	StHdh[Q7/111]	1.37	1.2×10^{5}	3.84	0.003	
	StHdh[Q111/111]	1.98	1.0×10^{11}	3.26	0.058	
Egr1	*StHdh*[Q7/7]	1.54	9.2×10^{13}	1.37	-	χ
	StHdh[Q7/111]	1.28	1.8×10^{7}	1.21	-	
	StHdh[Q111/111]	1.56	1.2×10^{12}	1.25	-	
Fosl1	*StHdh*[Q7/7]	2.23	1.6×10^{22}	3.36	0.002	✓
	StHdh[Q7/111]	2.5	1.4×10^{23}	5.61	0.001	
	StHdh[Q111/111]	2.54	1.2×10^{23}	3.37	0.001	
Etv5	*StHdh*[Q7/7]	1.52	3.7×10^{11}	0.69	-	χ
	StHdh[Q7/111]	1.35	6.4×10^{8}	0.95	-	
	StHdh[Q111/111]	1.74	2.4×10^{13}	1.34	-	

Table 5.7 Continued on next page

Genes with higher response in *StHdh*$^{Q7/7}$ cells following EGF stimulation

Gene	Genotype	Microarray		qRTPCR		Confirmed?
		Fold change	P-value	RQ value ratio	P-value	
Smad7	*StHdh*$^{Q7/7}$	1.69	3.0×10^{16}	1.53	-	≈
	StHdh$^{Q7/111}$	1.16	2.7×10^{5}	0.88	-	
	StHdh$^{Q111/111}$	1.15	5.1×10^{5}	0.37	-	
Fgf2	*StHdh*$^{Q7/7}$	1.82	1.4×10^{14}	1.53	-	≈
	StHdh$^{Q7/111}$	1.28	4.9×10^{9}	2.07	-	
	StHdh$^{Q111/111}$	1.4	7.1×10^{9}	1.4	-	
Myc	*StHdh*$^{Q7/7}$	1.64	2.0×10^{14}	2	-	≈
	StHdh$^{Q7/111}$	1.9	9.6×10^{17}	3.17	0.024	
	StHdh$^{Q111/111}$	1.01	-	0.48	-	
Sox9	*StHdh*$^{Q7/7}$	2.16	4.7×10^{23}	2.3	0.029	✓
	StHdh$^{Q7/111}$	1.2	1.2×10^{6}	0.97	-	
	StHdh$^{Q111/111}$	-1.04	-	0.74	-	
Junb	*StHdh*$^{Q7/7}$	1.52	4.3×10^{12}	1.5	-	✗
	StHdh$^{Q7/111}$	1.36	7.9×10^{9}	2.56	-	
	StHdh$^{Q111/111}$	1.21	1.3×10^{5}	1.78	-	

Table 5.7 Continued on next page

Genes responsive only in *StHdh*[Q111/111] cells following EGF stimulation

Gene	Genotype	Microarray		qRTPCR		Confirmed?
		Fold change	P-value	RQ value ratio	P-value	
Gadd45g	*StHdh*[Q7/7]	-1.24	1.9×10^{5}	1.14	-	✓
	StHdh[Q7/111]	-2.48	4.0×10^{18}	0.55	-	
	StHdh[Q111/111]	-1.89	1.7×10^{14}	0.65	0.006	
Cdc42ep3	*StHdh*[Q7/7]	-1.3	1.7×10^{10}	0.74	-	✓
	StHdh[Q7/111]	-1.5	3.6×10^{14}	0.68	-	
	StHdh[Q111/111]	-1.94	8.7×10^{19}	0.36	0.001	
Ngf	*StHdh*[Q7/7]	1.17	1.2×10^{5}	0.74	-	≈
	StHdh[Q7/111]	1.57	9.3×10^{14}	1.7	-	
	StHdh[Q111/111]	2.01	3.7×10^{18}	1.26	-	
Rasa1	*StHdh*[Q7/7]	1.23	2.12×10^{8}	1.22	-	✓
	StHdh[Q7/111]	1.20	4.2×10^{7}	1.4	0.01	
	StHdh[Q111/111]	1.53	1.1×10^{14}	1.96	0.09	

Table 5.7 Continued on next page

Genes with no significant change
following EGF stimulation

Gene	Genotype	Microarray		qRTPCR		Confirmed?
		Fold change	P-value	RQ value ratio	P-value	
Usp43	$StHdh^{Q7/7}$	-1.1	-	0.87	-	
	$StHdh^{Q7/111}$	-1.06	-	1.28	-	✓
	$StHdh^{Q111/111}$	1.01	-	0.64	-	

Table 5.7 Validation of differentially expressed genes by qRTPCR, as identified by microarray analyses. The microarray gene expression fold change data from $StHdh^{Q111/111}$, $StHdh^{Q7/111}$ and $StHdh^{Q7/7}$ cells following 2 hours 100ng/ml EGF stimulation are given with their associated p-values. In comparison is the ratio of the qRTPCR RQ value following EGF stimulation with the baseline RQ value, and the associated p-value. qRTPCR data was analysed using a two-way ANOVA followed by post-hoc Tukey tests. A '✓' indicates that the gene was validated, non-validated genes are noted with a '✗,' and genes that showed the same pattern of expression as the microarray data but did not reach significance following qRTPCR analysis are given a '≈.' n=5.

5.2.4.2 NGF

To validate the NGF microarray data, qRTPCR was carried out on different cDNA samples than those used in the microarray experiment. However, nine of the 14 genes investigated were confirmed, three showed the same pattern of expression but did not reach statistical significance, and only 2 were unable to be validated. A summary can be found in Table 5.8.

5.2.5 Comparison of gene functions

As our primary interest is the aberrant control of transcriptional processes in response to growth factor stimulation, only the gene lists from the EGF microarray analyses were taken forward for further investigation as these were more strongly associated with transcriptional regulation for both $StHdh^{Q7/7}$ and $StHdh^{Q111/111}$ cell lines. In addition, the expression of Ngf was found to be altered in $StHdh^{Q111/111}$ cells in the EGF

experiment, so this may prove to be a confounding factor when considering the NGF microarray data.

A literature search was performed in order to determine if any of the identified lists of genes had any processes or functions in common. The genes that had a larger expression change in *StHdh*$^{Q7/7}$ cells were implicated in a range of signalling pathways, including P38 MAPK, AKT, MEK and TGFβ. 14 out of the 15 genes identified as having a larger effect following EGF stimulation in *StHdh*$^{Q111/111}$ cells have also been implicated in or associated with the TGFβ pathway and its downstream family of SMAD transcription factors. From this we inferred that the altered expression patterns of these genes may indicate enhanced activity in this pathway (for details, see Section 5.4).

Genes with higher response in *StHdh*$^{Q111/111}$ cells following NGF stimulation

Gene	Genotype	Microarray		qRTPCR		Confirmed?
		Fold change	P-value	RQ value ratio	P-value	
Csf1	*StHdh*$^{Q7/7}$	-1.7	2.6×10^{12}	0.56	0.015	✓
	StHdh$^{Q111/111}$	-2.1	3.2×10^{14}	0.57	0.016	
Ctgf	*StHdh*$^{Q7/7}$	-1.7	3.4×10^{6}	0.42	-	✓
	StHdh$^{Q111/111}$	-3.6	1.4×10^{10}	0.07	0	

Table 5.8 Continued on next page

Genes with higher response in *StHdh*[Q7/7] cells following NGF stimulation

Gene	Genotype	Microarray		qRTPCR		Confirmed?
		Fold change	P-value	RQ value ratio	P-value	
Ereg	*StHdh*[Q7/7]	-3	4.0×10^{6}	0.43	0.003	✓
	StHdh[Q111/111]	1.82	0.0012	1	-	
Rgs16	*StHdh*[Q7/7]	-3	7.2×10^{9}	0.26	0.006	✓
	StHdh[Q111/111]	-1.2	-	-	-	

Genes responsive only in *StHdh*[Q111/111] cells following NGF stimulation

Gene	Genotype	Microarray		qRTPCR		Confirmed?
		Fold change	P-value	RQ value ratio	P-value	
Atf3	*StHdh*[Q7/7]	-1.14	-	1.51	-	✓
	StHdh[Q111/111]	2.9	8.5×10^{5}	2.1	0.057	
Ppargc1α	*StHdh*[Q7/7]	1.1	-	1.43	-	✓
	StHdh[Q111/111]	2.4	3.0×10^{7}	2.29	0.041	
Nr4a2	*StHdh*[Q7/7]	1.24	-	2.13	-	✓
	StHdh[Q111/111]	11.9	4.2×10^{11}	6.18	0	
Cdc42ep3	*StHdh*[Q7/7]	-1.06	-	0.67	-	✓
	StHdh[Q111/111]	-1.8	2.5×10^{9}	0.44	0	
Rnd3	*StHdh*[Q7/7]	-1.34	7.6×10^{6}	0.79	-	≈
	StHdh[Q111/111]	-2.4	4.5×10^{11}	0.7	-	

Table 5.8 Continued on next page

Genes responsive only in *StHdh*$^{Q7/7}$ cells following NGF stimulation

Gene	Genotype	Microarray		qRTPCR		Confirmed?
		Fold change	P-value	RQ value ratio	P-value	
Fosl1	*StHdh*$^{Q7/7}$	-2.1	2.8×10^{8}	0.75	-	≈
	StHdh$^{Q111/111}$	-1.26	0.001	0.67	-	
Id2	*StHdh*$^{Q7/7}$	-1.9	1.2×10^{4}	1.52	-	✗
	StHdh$^{Q111/111}$	1.21	-	2.05	-	
Ccng2	*StHdh*$^{Q7/7}$	2.3	8.4×10^{11}	2.73	0.004	✓
	StHdh$^{Q111/111}$	1.42	1.4×10^{6}	1.6	-	
Mybl1	*StHdh*$^{Q7/7}$	-1.9	1.5×10^{6}	0.68	-	≈
	StHdh$^{Q111/111}$	-1.28	0.006	1	-	
Prl2c2	*StHdh*$^{Q7/7}$	1.5	2.0×10^{8}	0.76	-	✗
	StHdh$^{Q111/111}$	1.08	0.04	2.46	0.026	

Table 5.8 Validation of differentially expressed genes by qRTPCR, as identified by microarray analyses. The microarray gene expression fold change data from *StHdh*$^{Q111/111}$ and *StHdh*$^{Q7/7}$ cells following 2 hours 100ng/ml NGF stimulation are given with their associated p-values. In comparison is the ratio of the qRTPCR RQ value following EGF stimulation with the baseline RQ value, and the associated p-value. qRTPCR data was analysed using a two-way ANOVA followed by post-hoc Tukey tests. A '✓' indicates that the gene was validated, non-validated genes are noted with a '✗,' and genes that showed the same pattern of expression as the microarray data but did not reach significance following qRTPCR analysis are given a '≈.' n=5.

5.2.6 Promoter region analysis

Analysis of promoter regions was carried out in the Genomatix Software Suite v2.6 (www.genomatix.de). This program compares the promoter regions of a given list of genes (500 base pairs upstream of the first transcription start site (TSS) and 100 base pairs downstream of the last TSS), and analyses them for potential TF binding sites that all of the promoter regions may have in common, by using literature searches and sequence analysis. The gene lists identified in Table 5.3 were entered into the program and analysed for each group separately.

All of the genes identified in the three lists from the EGF experiment shared two putative TF binding sites; early growth response factors (EGRFs) and SP1s (Figure 5.8). These were the only common binding sites for those genes that showed a larger expression change in $StHdh^{Q7/7}$ cells only. However, there were six additional potential common TF binding sites in the promoter regions of the genes with a larger expression change in $StHdh^{Q111/111}$ cells. For those genes that were only responsive to EGF stimulation in $StHdh^{Q111/111}$ cells, there were 3 potential TF binding sites in common with the previous list, and a further 15 common TF binding sites in their promoter regions. However, this gene list was much smaller than the others, and so it would be more likely for all genes to share common factors. A summary of common putative TF binding sites and their associated p-values can be found in Table 5.9.

Due to the implication of SMADs and TGFβ signalling during a comparison of gene functions in Section 5.2.5, the presence of SMAD TF binding sites in the promoter regions of the gene lists was also analysed. It was found that there were no SMAD TF binding sites on the promoters of any genes that had a stronger response to EGF in $StHdh^{Q7/7}$ cells. However, there were 6 genes from the remaining two lists combined that did have putative SMAD TF binding sites; these were *Bhlhe40, Fosl1, Id3, Nr4a2, Boc* and *Ngf* (Figure 5.9), which was significantly higher than chance, as calculated by Genomatix (p=0.01). The hypergeometric distribution probability of these genes containing a SMAD promoter binding site when $StHdh^{Q7/7}$-associated genes did not was also significant at p(x=6) = 0.01.
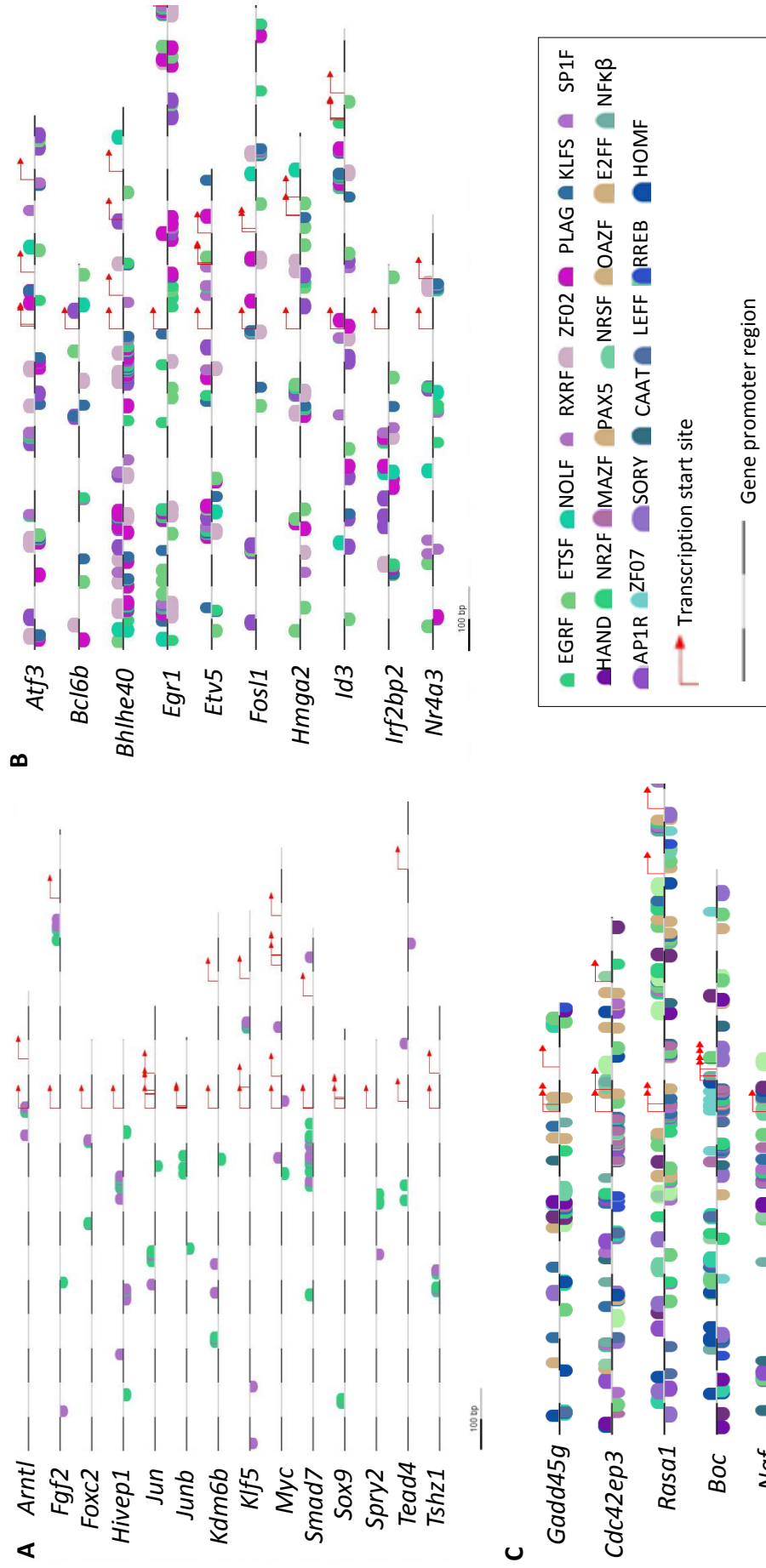
Figure 5.8 Common putative TF binding sites on the promoter regions of genes in the lists detailed in Table 5.9. Each colour represents a different TF, the details of which can be found in Table 5.3. **A.** Genes with a change in expression following EGF stimulation in $StHdh^{Q7/7}$ cells only. **B.** Genes with a change in expression in both genotypes following EGF stimulation, but with a higher response in $StHdh^{Q111/111}$ cells. **C.** Genes with a change in expression following EGF stimulation in $StHdh^{Q111/111}$ cells only.

TF name	TF symbol	StHdh$^{Q7/7}$ only	Larger change in StHdh$^{Q111/111}$	StHdh$^{Q111/111}$ only
Early growth response factor	EGRF	P<0.001	P=0.001	p-=0.02
Stimulating proteins	SP1	P=0.01	P=0.003	P=0.03
E-twenty six factors	ETSF	-	P=0.03	P=0.04
Neuron-specific-olfactory factor	NOLF	-	P<0.001	-
RXR heterodimer binding sites	RXRF	-	P=0.03	P>0.05
C2H2 zinc finger transcription factors 2	ZF02	-	P=0.003	-
Pleiomorphic adenoma gene	PLAG	-	P=0.001	-
Krüppel-like factors	KLFS	-	P=0.03	P>0.05
Twist subfamily of class B bHLH transcription factors	HAND	-	-	P>0.05
Nuclear receptor subfamily 2 factors	NR2F	-	-	P>0.05
MYC-associated zinc finger protein	MAZF	-	-	P=0.01
Paired box protein 5 binding sites	PAX5	-	-	P=0.04
Neuron-restrictive silencer factor	NRSF	-	-	P=0.01
Oligoadenylate synthetase	OAZF	-	-	P<0.001
E2F-homolog cell cycle regulators	E2FF	-	-	P=0.04
Nuclear factor kappa B/c-rel	NFKB	-	-	P=0.02
MAF and AP1 related factors	AP1R	-	-	P>0.05
C2H2 zinc finger transcription factors 7	ZF07	-	-	P=0.002
SOX/SRY-sex/testis determining and related HMG box factors	SORY	-	-	P>0.05
CCAAT binding factors	CAAT	-	-	P=0.04
Lymphoid enhancer factor-1/T-cell factor family	LEFF	-	-	P>0.05
Ras-responsive element binding protein	RREB	-	-	P=0.003
Homeodomain transcription factors	HOMF	-	-	P>0.05

Table 5.9 TF families identified from the promoter region analysis described in Section 5.2.6, which are common to all genes in each of the three lists detailed in Table 5.3. P-values represent the probability to obtain an equal or greater number of sequences that all contain a binding site in their promoter region for each defined TF in a randomly drawn sample of the same size as the number of input sequences. P-values were calculated by the Genomatix Software Suite v2.6 (www.genomatix.de).
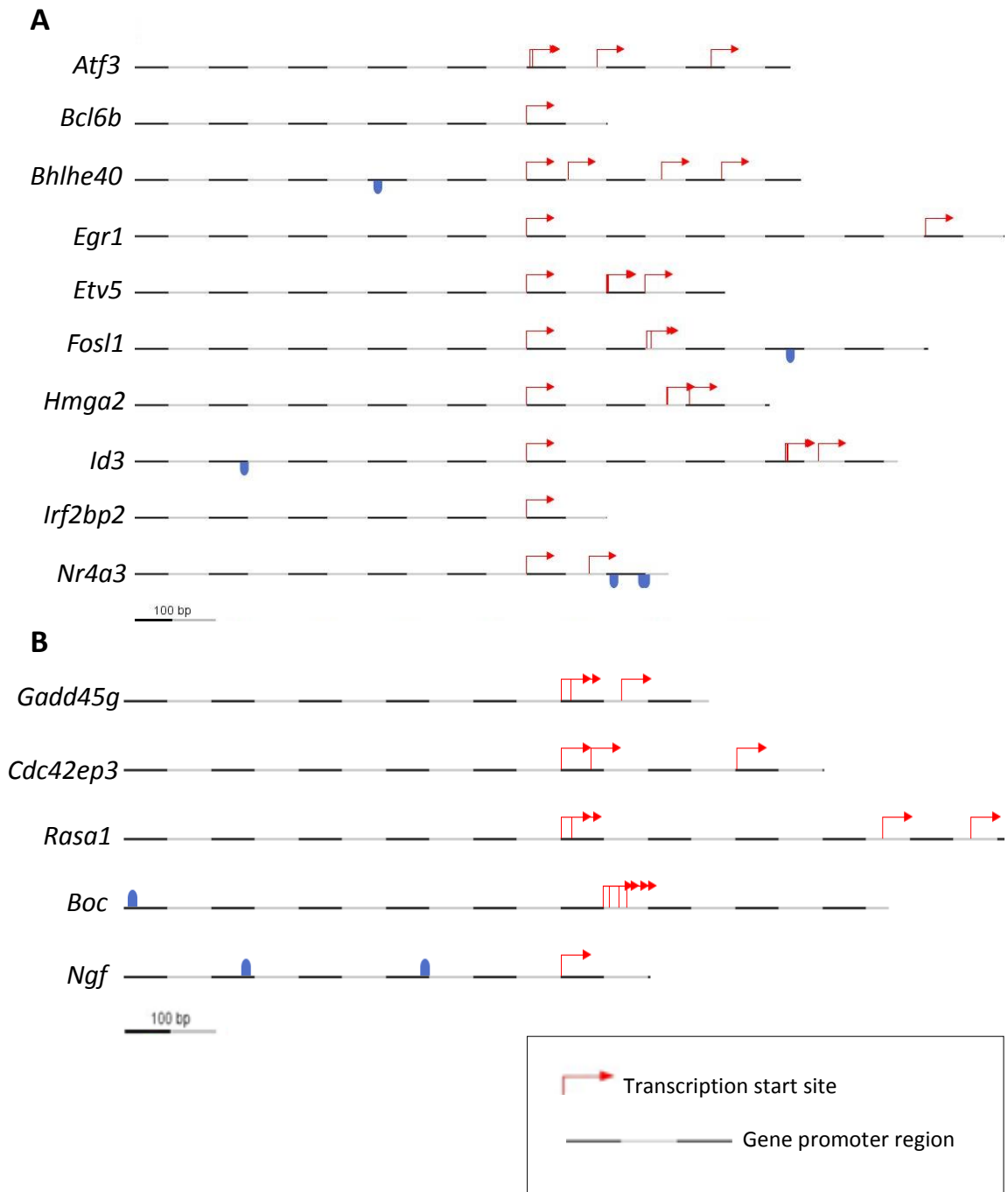
Figure 5.9 Putative SMAD transcription factor binding sites (represented by blue cylinders) on the promoter regions of genes that **A.** showed a larger gene expression response to EGF stimulation in *StHdh*^Q111/111 cells compared to *StHdh*^Q7/7 cells, and **B.** had a transcriptional response in *StHdh*^Q111/111 only.

5.3 Investigating TGFβ and SMAD activity

As SMADs may be playing a role in transcriptional control following EGF stimulation, validation of the microarray data for *Smad* gene expression was carried out.

5.3.1 Gene expression

Following EGF microarray analysis, *Smads 3, 6* and *9* had significantly higher expression in *StHdh$^{Q111/111}$* cells at baseline compared to *StHdh$^{Q7/7}$* cells (Table 5.10). In addition, there was also significantly higher expression of *Smurf2*, and some of the *Tgfβ* related genes (summarised in Table 5.10). There was also small, but significant, downregulation of some of the other *Smad*, *Smurf* and *Tgfβ*-related genes, suggesting aberrant control of this pathway.

qRTPCR analysis was carried out on the same samples used in the EGF microarray and previous validation experiments in order to confirm expression patterns of *Smad* and *Smad*-related genes that were identified as being more highly expressed in *StHdh$^{Q111/111}$* cells (Figure 5.10). *Smad3* was significantly more highly expressed in *StHdh$^{Q111/111}$* cells than in both *StHdh$^{Q7/7}$* (p<0.001) and *StHdh$^{Q7/111}$* (p=0.001) cell lines, although there was no effect of EGF stimulation on its expression. There was the same effect for *Smad6* expression (both p<0.003), although EGF stimulation significantly downregulated its expression in both *StHdh$^{Q7/7}$* (p=0.004) and *StHdh$^{Q111/111}$* (p=0.023) cells. Similarly, *Smad9* expression was also higher in *StHdh$^{Q111/111}$* cells than in both other genotypes (both p<0.009), but its expression was significantly lower than *StHdh$^{Q7/7}$* in *StHdh$^{Q7/111}$* cells (p<0.001). There was only a significant effect of EGF in *StHdh$^{Q111/111}$* cells (p=0.03), where expression dropped to similar levels as in *StHdh$^{Q7/7}$* cells at baseline.

Gene symbol	Gene name	Difference in fold change between $StHdh^{Q111/111}$ and $StHdh^{Q7/7}$ cells at baseline	P-value
Smad1	Mothers against decapentaplegic homolog 1	-1	0.45
Smad3	Mothers against decapentaplegic homolog 3	1.27	1.2×10^{12}
Smad6	Mothers against decapentaplegic homolog 6	1.6	3.3×10^{15}
Smad9	Mothers against decapentaplegic homolog 9	1.8	3.2×10^{14}
Smurf2	Smad specific E3 ubiquitin protein ligase 2	1.74	2.1×10^{13}
Tgfβ1	Transforming growth factor beta 1	-1.5	2.4×10^{14}
Tgfβr1	TGF-β receptor 1	-1.2	1.6×10^{5}
Tgfβ2	Transforming growth factor beta 2	1.5	1.2×10^{14}
Tgfβr2	TGF-β receptor 2	3	5.2×10^{33}
Tgfβ3	Transforming growth factor beta 3	3	1.2×10^{25}
Tgfβr3	TGF-β receptor 3	6	2.1×10^{27}
Tgfβi	TGF-β induced protein	11.4	2.1×10^{30}

Table 5.10 Expression differences of *Smad, Tgfβ* and related genes between *StHdh*$^{Q111/111}$ and *StHdh*$^{Q7/7}$ cells identified from the microarray experiment detailed in section 5.2 at 0 minutes EGF stimulation.
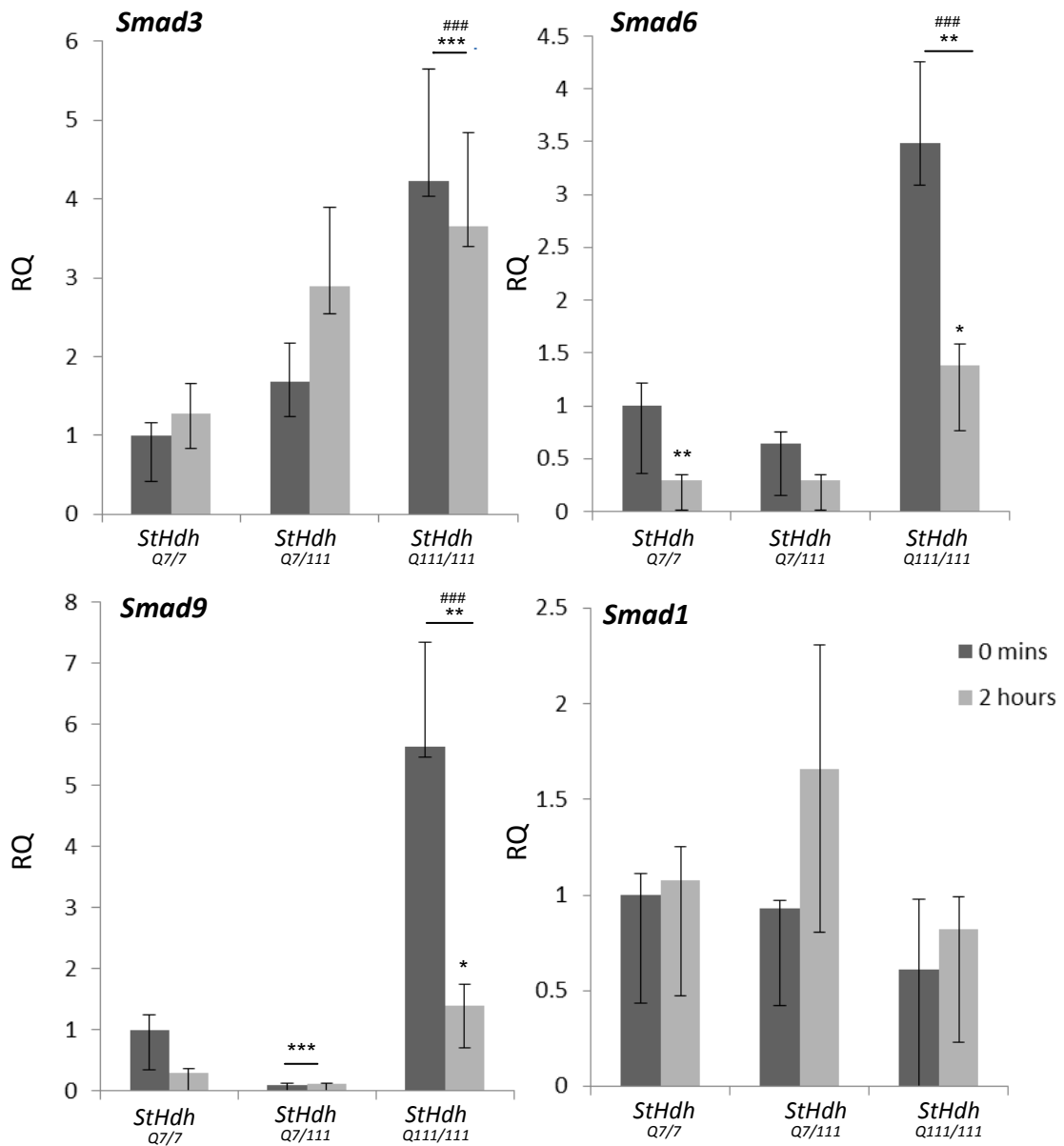
Figure 5.10 Relative quantification (RQ) values of selected *Smad* genes following qRTPCR to confirm microarray data from *StHdh*$^{Q7/7}$, *StHdh*$^{Q7/111}$ and *StHdh*$^{Q111/111}$ cells prior to, and following 2 hours of 100ng/ml EGF stimulation. Statistical analysis was carried out on ΔC_t values, and analysed using a two-way ANOVA, followed by post-hoc Tukey tests. (Error bars = SEM, n=5).

* Denotes a significant difference from *StHdh*$^{Q7/7}$ cells,

\# Denotes a significant difference from *StHdh*$^{Q7/111}$ cells.

* p<0.05   ** p<0.01   *** p<0.001

Tgfβ2, *Tgfβr2*, *Tgfβ3* and *Smurf2* expression patterns identified in the microarray analysis were not able to be confirmed by qRTPCR, and there was no significant effect of EGF stimulation on their expression. However, EGF-stimulated *StHdh*$^{Q7/111}$ and *StHdh*$^{Q111/111}$ cells showed higher expression of *Tgfβr2* (both p<0.001), and *StHdh*$^{Q7/111}$ cells displayed higher *Tgfβ3* expression (p<0.001) compared to *StHdh*$^{Q7/7}$ cells, indicating a trend towards increased expression of these genes in the presence of mHTT. *Tgfβr3* and *Tgfβi* both showed much higher expression in *StHdh*$^{Q111/111}$ cells compared to both other genotypes (p<0.003), and there was no effect of EGF stimulation. However, similar to the effect seen for *Smad9*, the expression of both *Tgfβr3* and *Tgfβi* was significantly lower in *StHdh*$^{Q7/111}$ cells compared to *StHdh*$^{Q7/7}$ (p<0.003) (Figure 5.11). *Smad1* was identified from the microarray data as not showing any difference between genotypes, and no effect of EGF stimulation. This was validated by qRTPCR in these cells, as there was no significant difference between genotypes or following EGF stimulation (p>0.05).
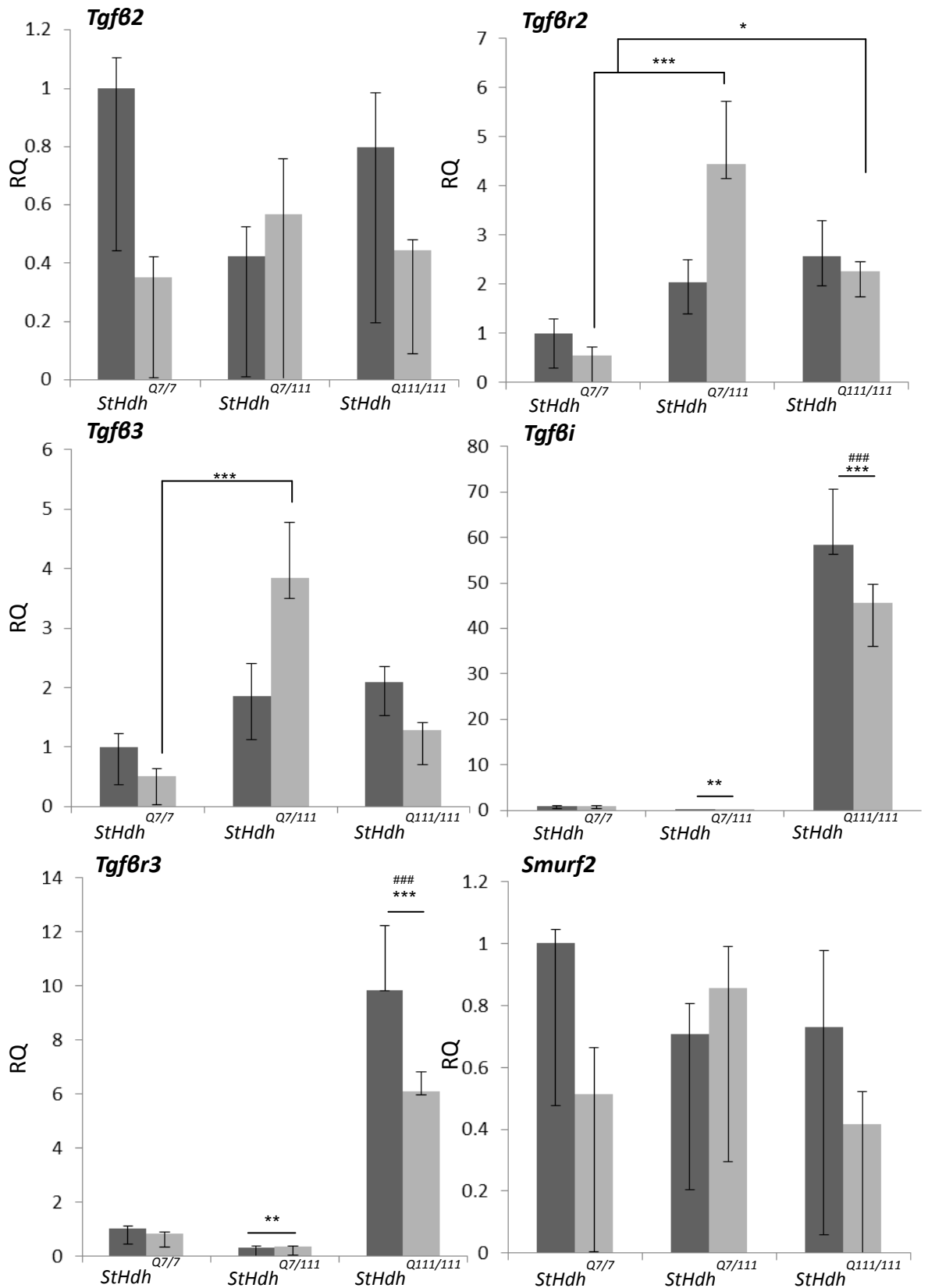
Figure 5.11 Relative quantification (RQ) values of selected *Tgfβ*-related genes following qRTPCR to confirm microarray data from *StHdh*$^{Q7/7}$, *StHdh*$^{Q7/111}$ and *StHdh*$^{Q111/111}$ cells prior to (dark grey bars), and following 2 hours (light grey bars) of 100ng/ml EGF stimulation. Statistical analysis was carried out on ΔC_t values, and analysed using a two-way ANOVA, followed by post-hoc Tukey tests. (Error bars = SEM, n=5).

*Denotes a significant difference from *StHdh*$^{Q7/7}$ cells, # Denotes a significant difference from *StHdh*$^{Q7/111}$ cells.   *p<0.05   ** p<0.01   ***p<0.001

5.3.2 Protein analysis

Western blots and ELISA assays were carried out in order to determine if the increased expression of *Smad* genes was also identifiable in the proteome, and if there was an effect of mHTT on their activation by phosphorylation. As SMAD2 and SMAD3 have been more thoroughly characterised than the other SMADs, ELISA assays were only available for these two proteins. All cells were stimulated with 100ng/ml TGFβ for either 0 or 30 minutes after being serum starved overnight.

5.3.2.1 SMAD2

Smad2 was not identified as having differential expression between genotypes from the microarray analysis, however investigation by ELISA revealed that there was reduced total SMAD2 protein in *StHdh*$^{Q111/111}$ cells in comparison to *StHdh*$^{Q7/7}$ (p=0.017) cells, and *StHdh*$^{Q7/111}$ cells lay between these two (Figure 5.12). Cells were stimulated with TGFβ in order to phosphorylate the SMAD proteins in order to determine if there was an effect of mHTT on their activity. As expected, there was no effect of TGFβ stimulation on total SMAD2, however there were significant increases in SMAD2 phosphorylated on serines 465/467 in both *StHdh*$^{Q7/7}$ (p=0.013) and *StHdh*$^{Q7/111}$ (p<0.001) cell lines following treatment with TGFβ. In contrast, there was no significant increase in SMAD2 phosphorylation in *StHdh*$^{Q111/111}$ cells following TGFβ stimulation, although the level of phosphorylation did not differ from the other genotypes at baseline (Figure 5.12).

Despite the lack of effect in *StHdh*$^{Q111/111}$ cells, *StHdh*$^{Q7/111}$ cells showed a strong response to TGFβ stimulation, as the level of phospho-SMAD2 detected following TGFβ treatment was significantly higher than in the *StHdh*$^{Q7/7}$ cells (p=0.023), despite no difference in their baseline. This suggests that despite the presence of mHTT, there may be increased sensitivity to TGFβ stimulation in these cells, which is reversed with increased *mHtt* gene dosage. As the level of total SMAD2 was reduced in *StHdh*$^{Q111/111}$ cells, the ratio of phosphorylated SMAD2 to total SMAD2 was also calculated in order to determine if phosphorylation was hindered or if it reflected reduced total protein. The ratio of phosphorylated to total SMAD2 was still significantly lower in *StHdh*$^{Q111/111}$

cells following TGFβ stimulation, suggesting that SMAD2 activation is inhibited in these cells.
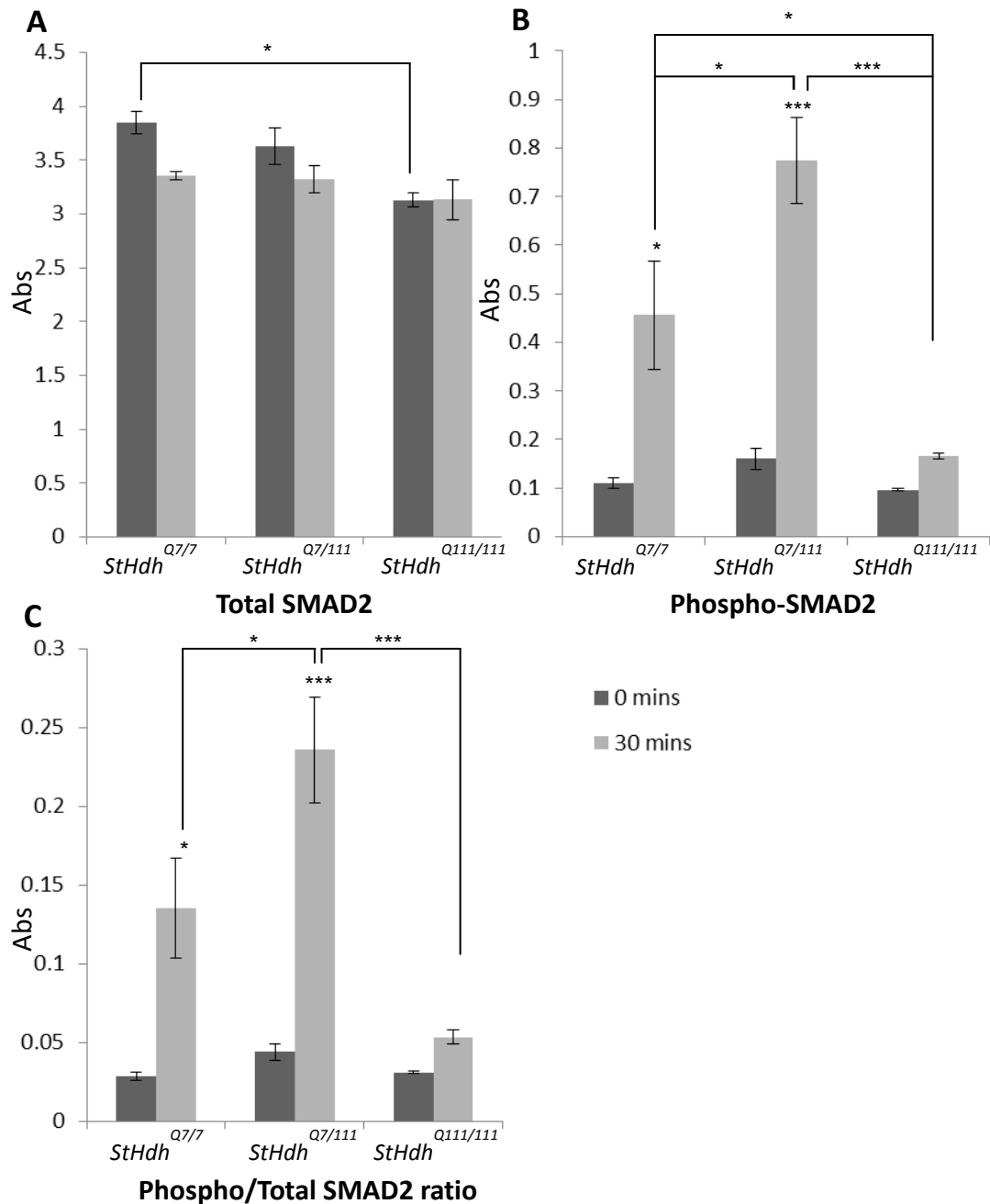
Figure 5.12 Mean absorbance (Abs) read at 450nm following a sandwich ELISA protocol in *StHdh*^Q7/7^, *StHdh*^Q7/111^ and *StHdh*^Q111/111^ cells following 0 and 30mins stimulation with TGFβ for **A**. total SMAD2, **B**. SMAD2 phosphorylated on serines 465/467, and **C**. Ratio of phosphorylated to total SMAD2 mean absorbance. Statistical analysis was carried out by using a two-way ANOVA followed by post-hoc Tukey tests (Error bars = SEM, n=3).
* p<0.05   **p<0.01   ***p<0.001

Western blots confirmed the ELISA results (Figure 5.13); there was significantly less total SMAD2 in *StHdh*$^{Q111/111}$ cells compared to *StHdh*$^{Q7/7}$ (p=0.013), and there was no effect of TGFβ stimulation. In addition, there were significantly increased levels of phosphorylated SMAD2 in both the *StHdh*$^{Q7/7}$ and *StHdh*$^{Q7/111}$ cells following stimulation with TGFβ (both p=0.002). However, the larger response in *StHdh*$^{Q7/111}$ cells was not found by western blot, with the phosphorylation of SMAD2 not being significantly different to *StHdh*$^{Q7/7}$ cells. There was a detectable increase in phospho-SMAD2 in *StHdh*$^{Q111/111}$ cells following growth factor treatment, but this does not reach significance, and is significantly lower than the level of phosphorylation in both *StHdh*$^{Q7/7}$ and *StHdh*$^{Q7/111}$ cells (p<0.01). Analysis of the phosphorylated to total SMAD2 ratio also yielded the same results as the ELISA assay. Taken together, these results suggest that not only is there a reduction in available SMAD2 in *StHdh*$^{Q111/111}$ cells despite no observable reduction in gene expression, but its activation by phosphorylation is also inhibited in these cells.
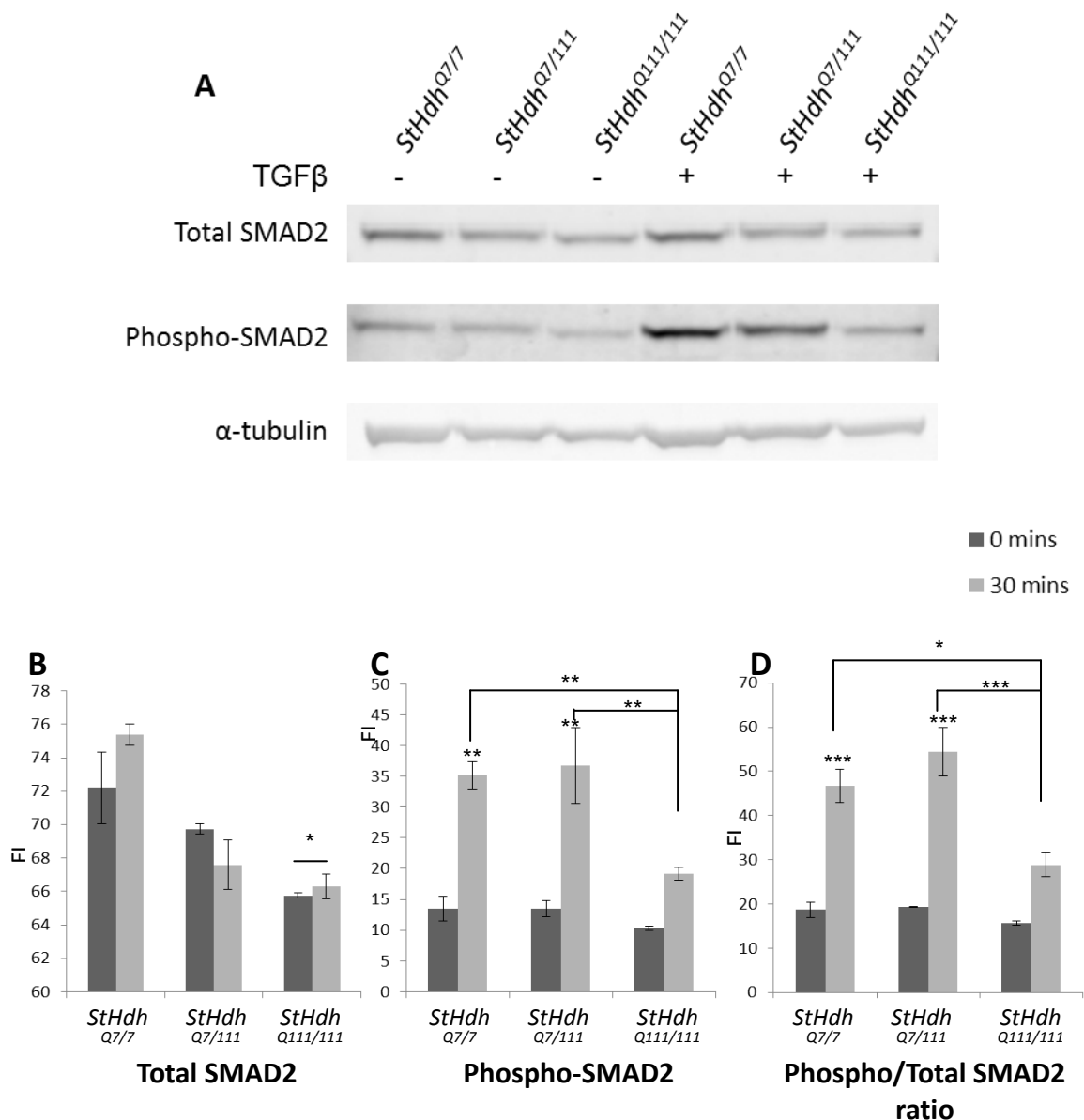
Figure 5.13 A. Western blot analysis of $StHdh^{Q7/7}$, $StHdh^{Q7/111}$ and $StHdh^{Q111/111}$ cells at 0 and 30 minutes of stimulation with 100ng/ml TGFβ. The membrane was probed with an antibody against total SMAD2, with α-tubulin utilised as a loading control. The membrane was then stripped (see section 2.2.2.8) and reprobed with an antibody against SMAD2 phosphorylated on serines 465/467. **B-D.** Quantification of the fluorescence intensity (FI) of *A* using the Licor Odyssey quantitative fluorescent imaging system, with SMAD antibodies normalised to the loading control. Statistical analysis was carried out by using a two-way ANOVA followed by post-hoc Tukey tests (Error bars = SEM, n=3).

*p<0.05   **p<0.01   ***p<0.001

Smad3 was found to have significantly increased expression in *StHdh*$^{Q111/111}$ cells (Section 5.3.1). However, analysis of the SMAD3 protein by ELISA assay showed that there was a significant reduction in total SMAD3 in both *StHdh*$^{Q7/111}$ (p<0.001) and *StHdh*$^{Q111/111}$ (p=0.001) cells compared to *StHdh*$^{Q7/7}$ cells; this reduction was roughly equal in both heterozygote and homozygote cells carrying mHTT (Figure 5.14). Unexpectedly, there was also a significant reduction in total SMAD3 following TGFβ stimulation in *StHdh*$^{Q7/7}$ cells (p=0.01), although it is possible that this is an artefact of reduced antibody binding due to phosphorylation of the targeted epitope. This reduction was also observed in the remaining two genotypes, but did not reach significance.

TGFβ stimulation significantly increased the detection of SMAD3 phosphorylated on serines 423/425 in all three genotypes (*StHdh*$^{Q7/7}$ p<0.001, *StHdh*$^{Q7/111}$ p<0.001, *StHdh*$^{Q111/111}$ p=0.005) (Figure 5.14). However, the extent of phosphorylation was lowered with mHTT load; the level of phospho-SMAD3 at baseline was not significantly different between genotypes, however once stimulated with TGFβ, significantly more phospho-SMAD3 was detected in *StHdh*$^{Q7/7}$ cells than in both *StHdh*$^{Q7/111}$ and *StHdh*$^{Q111/111}$ cells (p<0.001), but *StHdh*$^{Q7/111}$ cells still had significantly higher levels of phosphorylation than *StHdh*$^{Q111/111}$ cells (p<0.001). A ratio of phosphorylated to total SMAD3 was calculated, and this revealed that although there is reduced phosphorylation of SMAD3 in *StHdh*$^{Q7/111}$ cells, the ratio of this to total SMAD3 is not significantly different to *StHdh*$^{Q7/7}$ cells (p>0.05). However, the ratio of phosphorylated to total SMAD3 in *StHdh*$^{Q111/111}$ cells was significantly lower than both *StHdh*$^{Q7/7}$ and *StHdh*$^{Q7/111}$ cell lines (both p<0.001). This suggests that although there is less available SMAD3 in *StHdh*$^{Q7/111}$ cells, it is still phosphorylated to the same extent as in *StHdh*$^{Q7/7}$ cells following TGFβ stimulation, but in *StHdh*$^{Q111/111}$ cells, as well as there being less SMAD3 present in the cell, the capacity for its phosphorylation is also reduced.
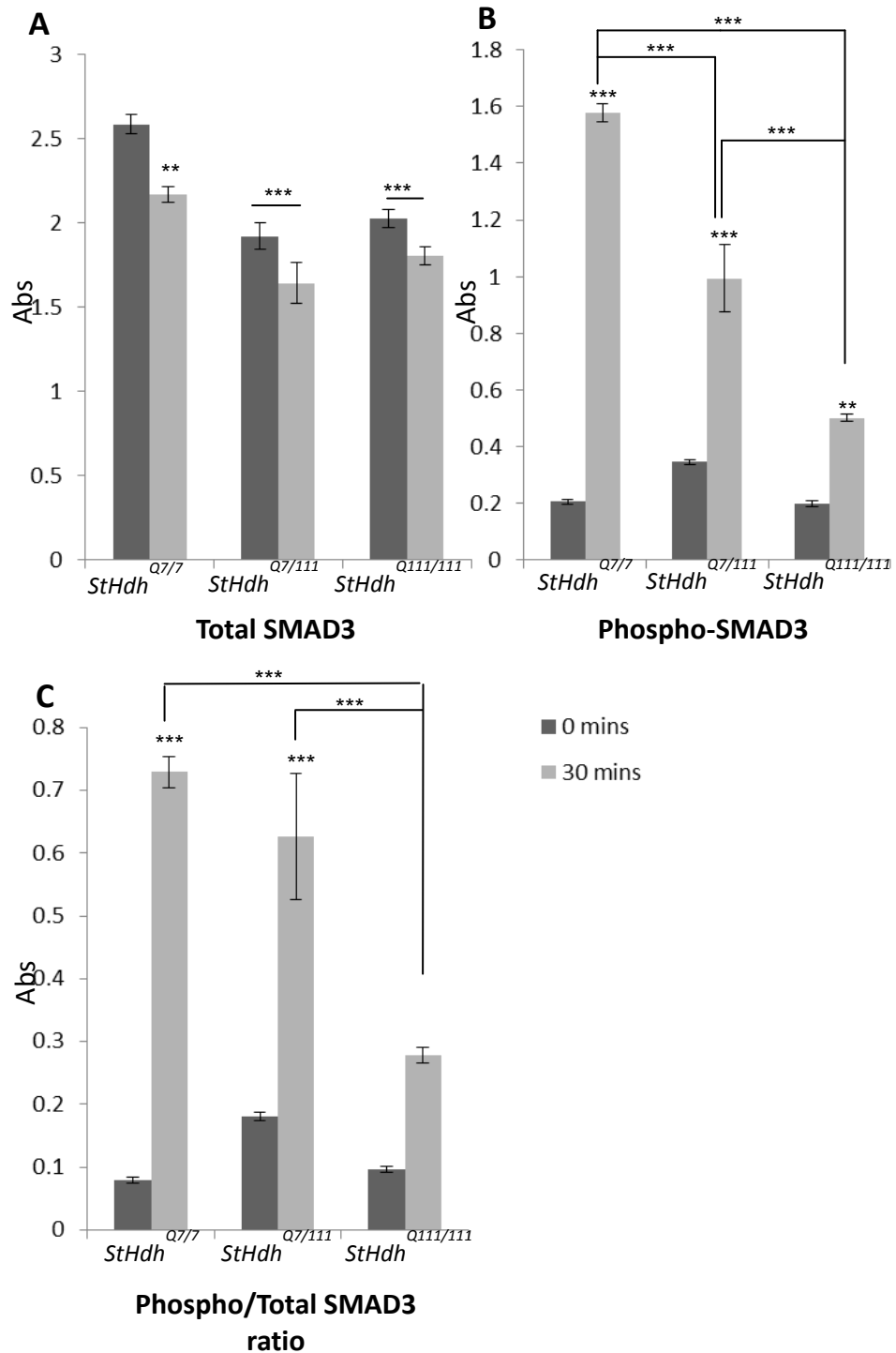
Figure 5.14 Mean absorbance (Abs) read at 450nm following a sandwich ELISA protocol in *StHdh*^Q7/7^, *StHdh*^Q7/111^ and *StHdh*^Q111/111^ cells following 0 and 30mins stimulation with TGFβ for **A**. total SMAD3, **B**. SMAD3 phosphorylated on serines 423/425, and **C**. Ratio of phosphorylated to total SMAD3 mean absorbance. Statistical analysis was carried out by using a two-way ANOVA followed by post-hoc Tukey tests (Error bars = SEM, n=3).

* p<0.05   **p<0.01   ***p<0.001

Analysis of SMAD3 and its phosphorylation yielded different results when investigated by western blot (Figure 5.15). It appeared that there was more total SMAD3 detected in $StHdh^{Q111/111}$ cells both before, and following TGFβ stimulation, which is reflective of the gene expression results (Section 5.3.1). However, this difference does not reach significance due to large variability in imaging quality between replicates.

As was observed in the ELISA, there was no significant difference between genotypes in the amount of phosphorylated SMAD3 at baseline. In addition, there was only a significant increase in the amount of phospho-SMAD3 detected in $StHdh^{Q7/111}$ (p=0.008) and $StHdh^{Q111/111}$ cells (p=0.001) following TGFβ stimulation. There was an increase in $StHdh^{Q7/7}$ cells, but this did not reach significance, and it remained significantly lower than the level detected in $StHdh^{Q111/111}$ cells (p=0.03). However, when the ratio of phosphorylated to total SMAD3 was investigated, there were no significant differences between genotypes. This suggests that the observed increase in phosphorylated SMAD3 in $StHdh^{Q7/111}$ and $StHdh^{Q111/111}$ cells may not be due to an increased sensitivity to activation, but due to the increased amount of total SMAD3 available to be phosphorylated, although $StHdh^{Q7/111}$ cells appear perhaps more sensitive to stimulation than both other genotypes. However, why the western blot data is so dramatically different to the ELISA data is yet to be elucidated, as the antibodies used for both techniques were the same. However, these western blots are normalised to an α-tubulin loading control, whereas the ELISAs are not, so it is possible that the difference in these findings could be reflective of this. The denaturing process in preparation for SDS-PAGE gel electrophoresis may also alter the binding capacity of the antibody, thus altering the evident levels of SMAD3 and phosphorylated SMAD3.
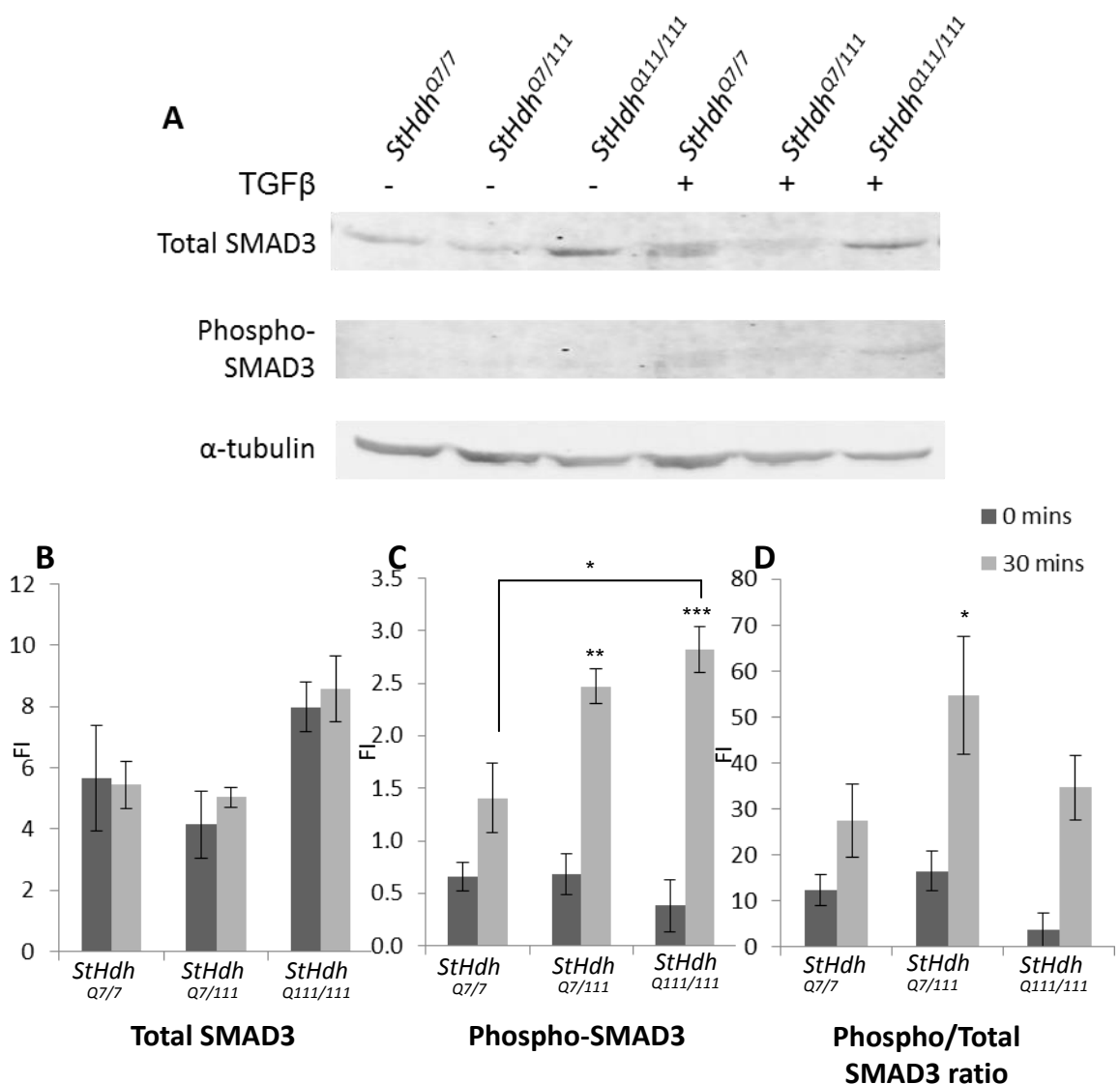
Figure 5.15 A. Western blot analysis of $StHdh^{Q7/7}$, $StHdh^{Q7/111}$ and $StHdh^{Q111/111}$ cells at 0 and 30 minutes of stimulation with 100ng/ml TGFβ. The membrane was probed with an antibody against total SMAD3, with α-tubulin utilised as a loading control. The membrane was then stripped (see section 2.2.2.8) and reprobed with an antibody against SMAD3 phosphorylated on serines 423/425. **B-D.** Quantification of the fluorescence intensity (FI) of *A* using the Licor Odyssey quantitative fluorescent imaging system, with SMAD antibodies normalised to the loading control. Statistical analysis was carried out by using a two-way ANOVA followed by post-hoc Tukey tests (Error bars = SEM, n=3).

*p<0.05   **p<0.01   ***p<0.001

5.3.2.3 Other SMAD TFs and TGFβI

The following SMAD proteins and TGFβI were only investigated by western blot, as the appropriate ELISA kits were not available.

There was no effect of TGFβ on SMAD1 in all three genotypes, however there was a small reduction in $StHdh^{Q7/111}$ cells compared to $StHdh^{Q7/7}$ cells, which only just reaches significance (p=0.046) (Figure 5.16). However, there is no significant difference between the levels of SMAD1 detected in $StHdh^{Q111/111}$ cells and either $StHdh^{Q7/7}$ or $StHdh^{Q7/111}$ cells, which is reflective of the qRTPCR and microarray findings on gene expression (Section 5.3.1). Two antibodies were available for the detection of phosphorylated SMAD1; one was specific to SMAD1 phosphorylation (serine 465), and one that detected both phosphorylated SMAD1 and 5 (serines 463/465). There were no significant differences in the level of phosphorylated SMAD1 detected with either antibody between all three genotypes, and there was also no change in the level of phosphorylation following stimulation with TGFβ. This is not unexpected, as although SMAD1 is part of the TGFβ signalling pathway, it is mainly a substrate for bone morphogenetic protein (BMP) members of the TGFβ family (Massague 2005).

SMAD5 was significantly reduced in $StHdh^{Q111/111}$ cell lines in comparison to both $StHdh^{Q7/7}$ (p=0.015) and $StHdh^{Q7/111}$ cells (p<0.001), although significantly more was detected in $StHdh^{Q7/111}$ cells compared to wild type (p=0.032) (Figure 5.17). As expected, there was no difference in total SMAD5 following stimulation with TGFβ in any of the genotypes. However, TGFβ treatment did significantly increase SMAD5 phosphorylated on serines 463/465 in $StHdh^{Q7/7}$ and $StHdh^{Q7/111}$ cells (both p<0.003). There was an observable increase in phosphorylated SMAD5 in the $StHdh^{Q111/111}$ cells, but surprisingly this did not reach significance. When looking at the phosphorylated to total SMAD5 ratio, it initially appears that SMAD5 in $StHdh^{Q111/111}$ cells is actually hyperphosphorylated both prior to, and following TGFβ stimulation than its $StHdh^{Q7/7}$ and $StHdh^{Q7/111}$ counterparts. Although these differences don't reach significance, this may suggest that although there is reduced total SMAD5 in cells homozygote for mHTT, its phosphorylation capabilities are equal, and potentially larger, than in $StHdh^{Q7/7}$ and $StHdh^{Q7/111}$ cells.
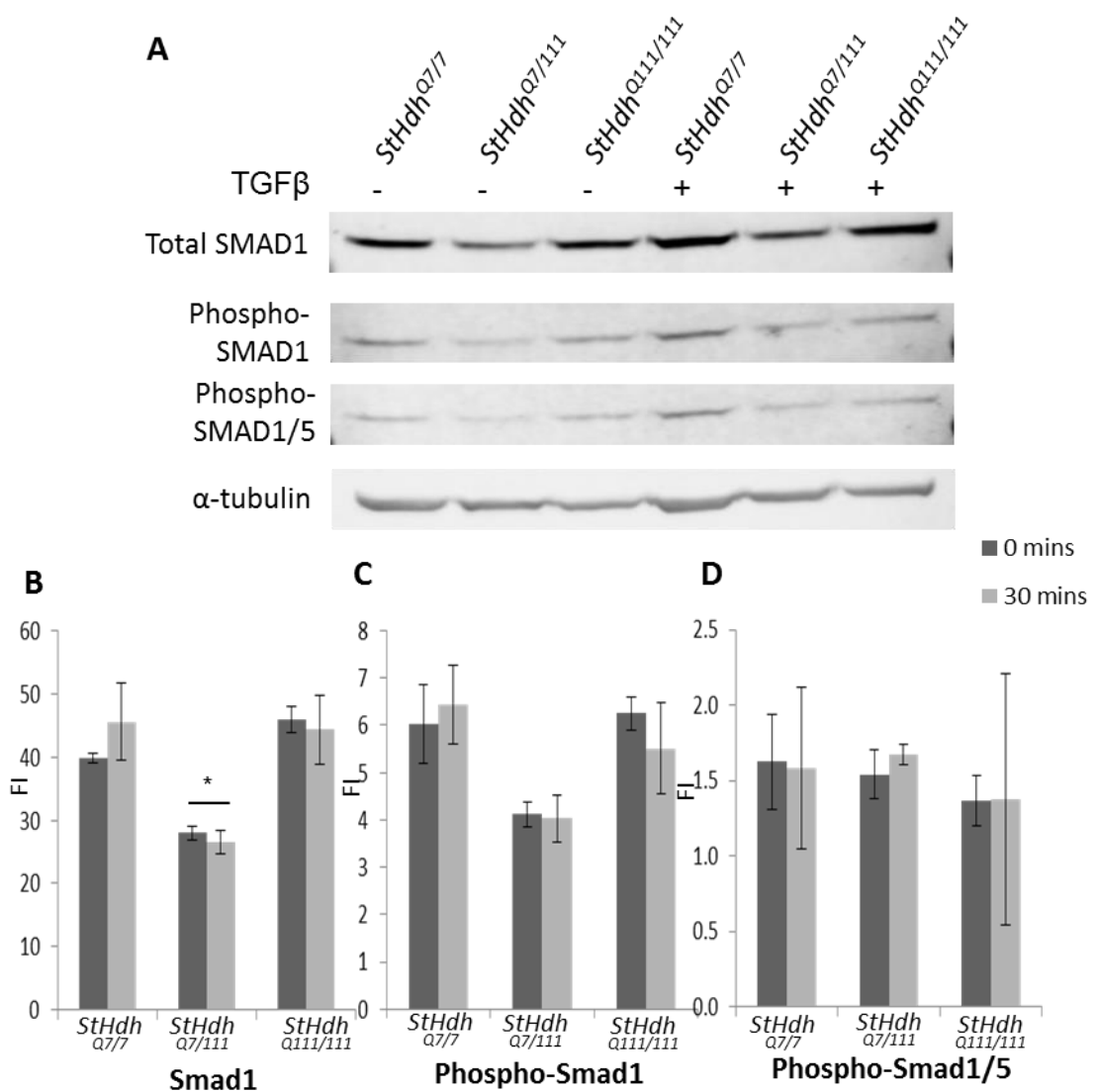
Figure 5.16 A. Western blot analysis of *StHdh*$^{Q7/7}$, *StHdh*$^{Q7/111}$ and *StHdh*$^{Q111/111}$ cells at 0 and 30 minutes of stimulation with100ng/ml TGFβ. The membrane was probed with an antibody against total SMAD1, with α-tubulin utilised as a loading control. The membrane was then stripped (see section 2.2.2.8) and reprobed with an antibody against SMAD1 phosphorylated on serine 465, then again with an antibody against phosphorylated SMAD1/5 (serines 463/465). **B-D.** Quantification of the fluorescence intensity (FI) of *A* using the Licor Odyssey quantitative fluorescent imaging system, with SMAD antibodies normalised to the loading control. Statistical analysis was carried out by using a two-way ANOVA followed by post-hoc Tukey tests (Error bars = SEM, n=3).

*p<0.05   **p<0.01   ***p<0.001
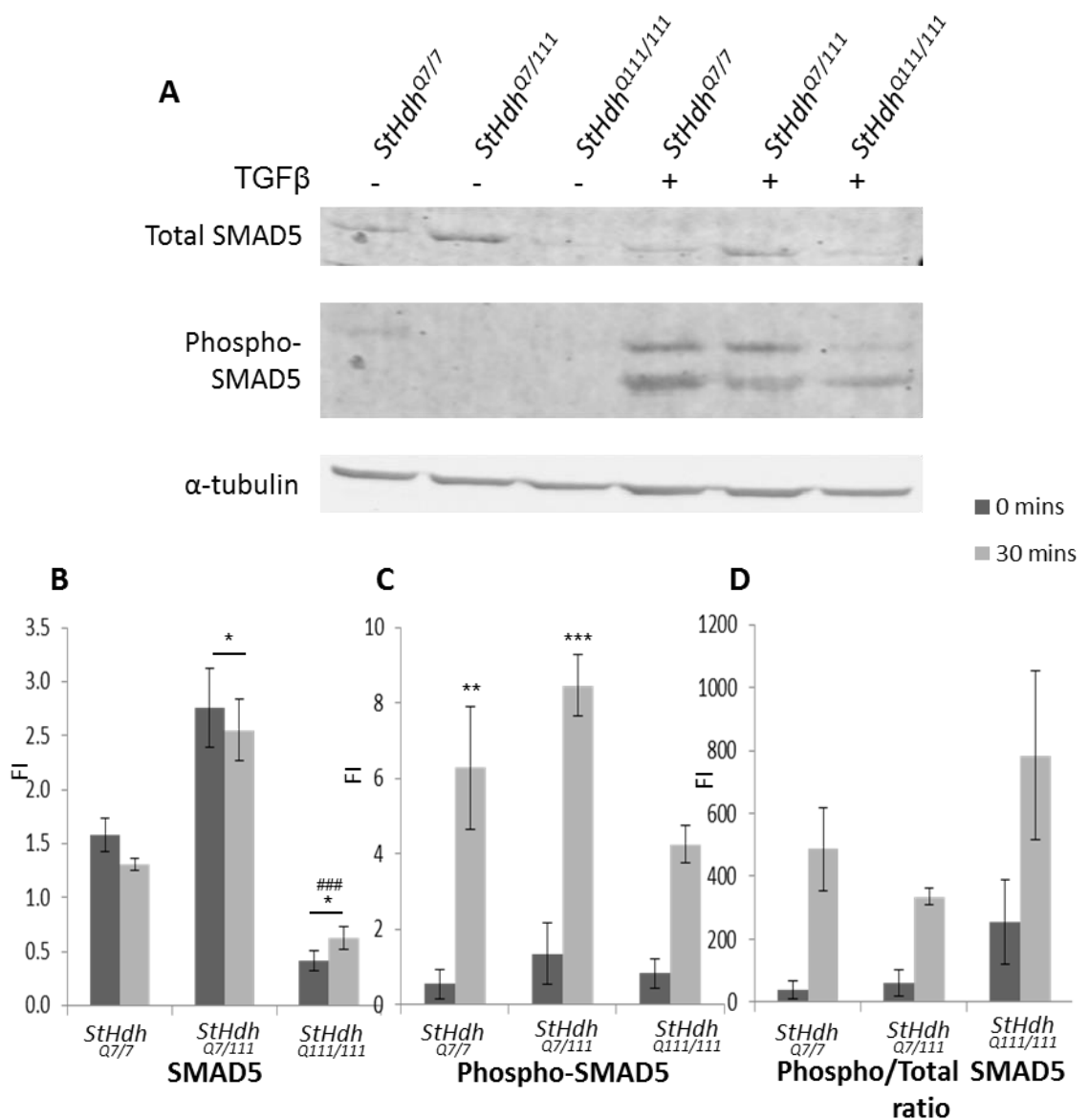
Figure 5.17 A. Western blot analysis of *StHdh*$^{Q7/7}$, *StHdh*$^{Q7/111}$ and *StHdh*$^{Q111/111}$ cells at 0 and 30 minutes of stimulation with100ng/ml TGFβ. The membrane was probed with an antibody against total SMAD5, with α-tubulin utilised as a loading control. The membrane was then stripped (see section 2.2.2.8) and reprobed with an antibody against SMAD5 phosphorylated on serines 463⁄465. **B-D.** Quantification of the fluorescence intensity (FI) of *A* using the Licor Odyssey quantitative fluorescent imaging system, with SMAD antibodies normalised to the loading control. Statistical analysis was carried out by using a two-way ANOVA followed by post-hoc Tukey tests (Error bars = SEM, n=3).

*p<0.05   **p<0.01   ***p<0.001

Phospho-specific antibodies were not available for SMAD4 and SMAD6, so only the total protein could be investigated during this project. Although there was increased SMAD4 in *StHdh*$^{Q111/111}$ cells at 0mins TGFβ stimulation, this did not quite reach significance (*StHdh*$^{Q7/7}$ p=0.067, *StHdh*$^{Q7/111}$ p=0.052). There was also no effect of TGFβ on the detection of total SMAD4 (Figure 5.18). In contrast to the gene expression data in Section 5.3.1, there were no differences between the genotypes for the detection of SMAD6, and there was also no significant effect of TGFβ stimulation (Figure 5.18).

Due to such large overexpression in *StHdh*$^{Q111/111}$ cells identified earlier (Section 5.3.1), TGFβI was also investigated. Although there was a visible increase in the TBFβI protein in *StHdh*$^{Q111/111}$ cells (Figure 5.19), due to variability between replicates and high levels of noise in the data, this did not reach significance from *StHdh*$^{Q7/7}$ cells, although it was significantly higher than in *StHdh*$^{Q7/111}$ cells (p=0.003). There was no effect of TGFβ stimulation on the level of TGFβI in any of the genotypes. Although not fully reaching significance, the trend towards higher levels of TGFβI detection in *StHdh*$^{Q111/111}$ cells, coupled with the gene expression data, suggest that this may still be a potentially interesting target in the TGFβ pathway to follow up.
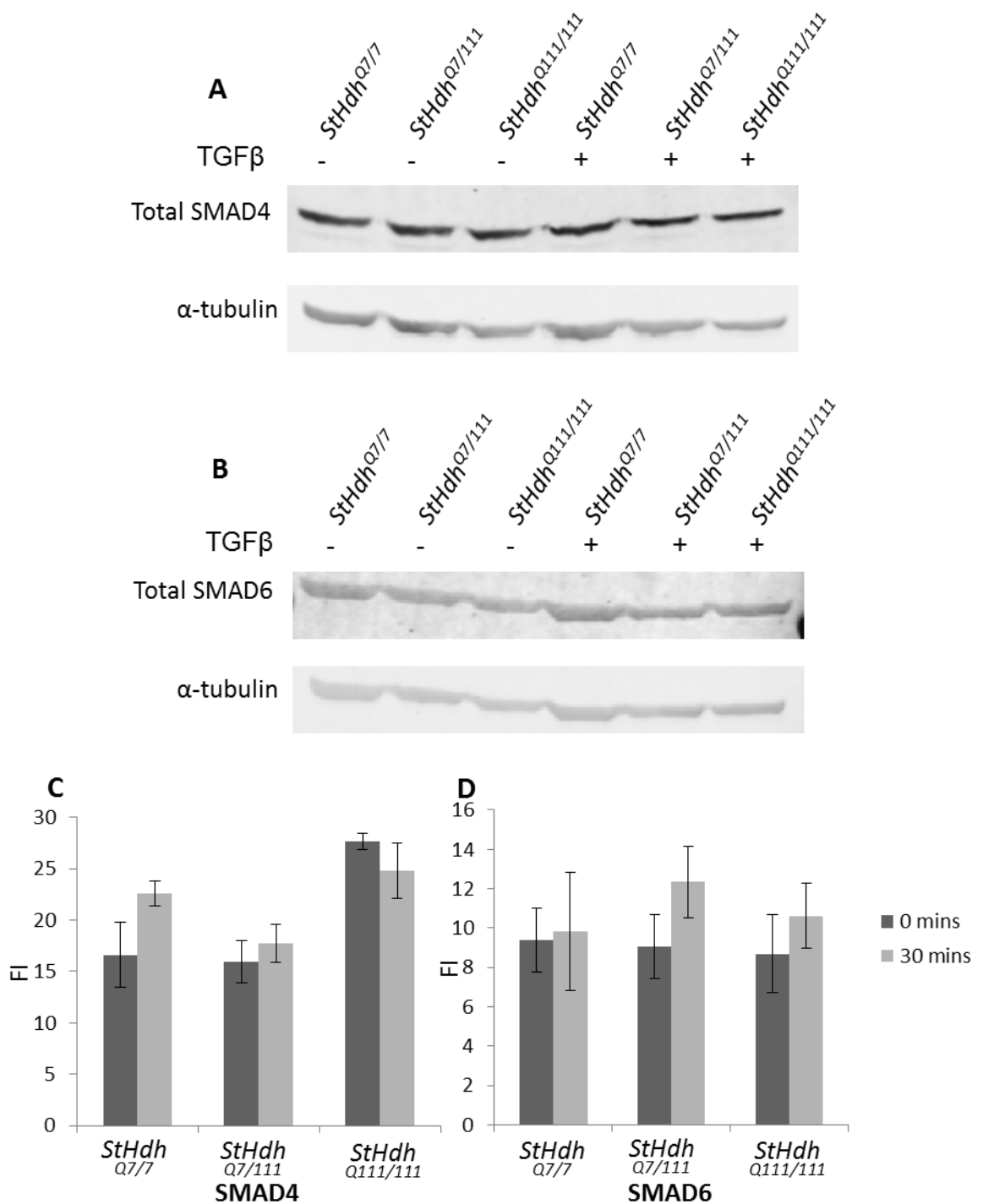
Figure 5.18 A. Western blot analysis of *StHdh*$^{Q7/7}$, *StHdh*$^{Q7/111}$ and *StHdh*$^{Q111/111}$ cells at 0 and 30 minutes of stimulation with100ng/ml TGFβ. The membrane was probed with an antibody against total SMAD4, with α-tubulin utilised as a loading control. **B**. Western blot analysis of *StHdh*$^{Q7/7}$, *StHdh*$^{Q7/111}$ and *StHdh*$^{Q111/111}$ cells at 0 and 30 minutes of stimulation with 100ng/ml TGFβ. The membrane was probed with an antibody against total SMAD6, with α-tubulin utilised as a loading control **C-D.** Quantification of fluorescence intensities (FI) in *A* and *B* using the Licor Odyssey quantitative fluorescent imaging system, with SMAD antibodies normalised to the loading control. Statistical analysis was carried out by using a two-way ANOVA followed by post-hoc Tukey tests (Error bars = SEM, n=3).

A

	StHdh^Q7/7	StHdh^Q7/111	StHdh^Q111/111	StHdh^Q7/7	StHdh^Q7/111	StHdh^Q111/111
TGFβ	−	−	−	+	+	+

TGFβI

α-tubulin

B

TGFβI
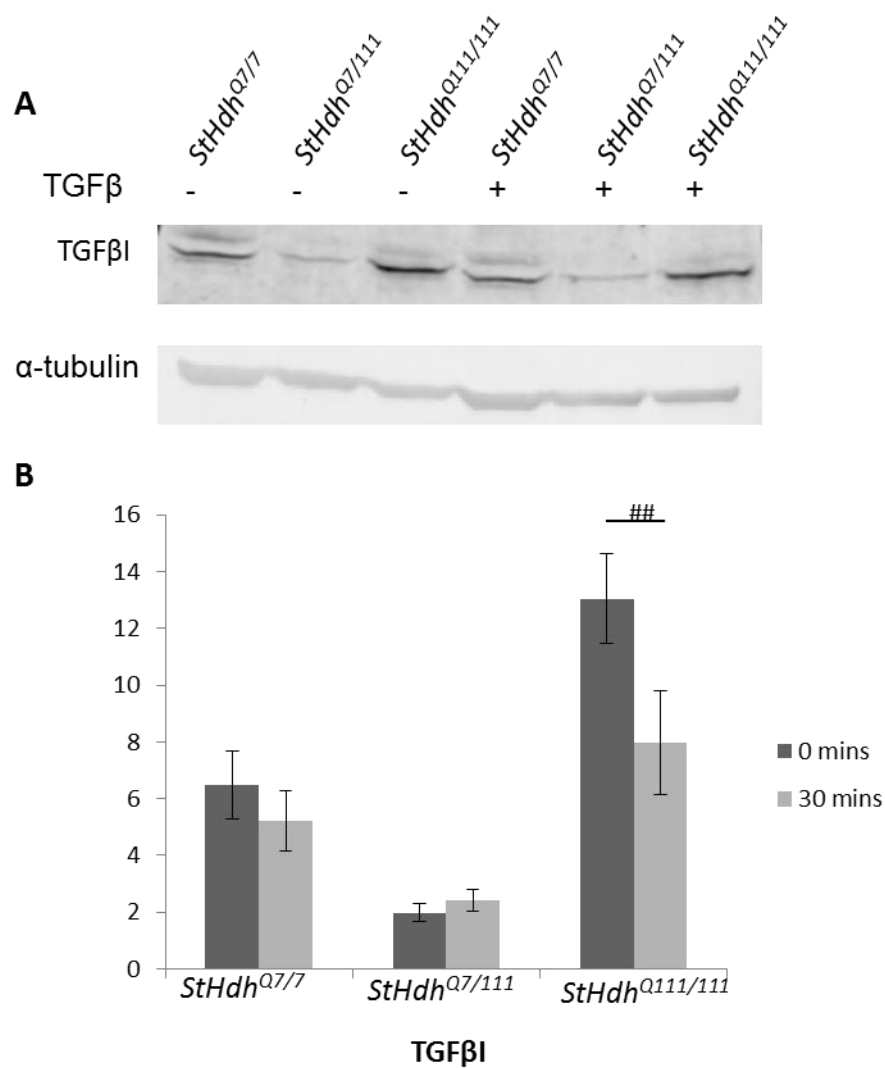
Figure 5.19 A. Western blot analysis of *StHdh*$^{Q7/7}$, *StHdh*$^{Q7/111}$ and *StHdh*$^{Q111/111}$ cells at 0 and 30 minutes of stimulation with 100ng/ml TGFβ. The membrane initially probed with total SMAD6 was stripped and reprobed with an antibody against TGFβI **B.** Quantification of the fluorescence intensities (FI) of *A* using the Licor Odyssey quantitative fluorescent imaging system, with the TGFβI antibody normalised to the loading control. Statistical analysis was carried out by using a two-way ANOVA followed by post-hoc Tukey tests (Error bars = SEM, n=3).

'#' Denotes a significant difference from *StHdh*$^{Q7/111}$ cells.

#p<0.05   ##p<0.01   ###p<0.001

5.4 Discussion

We have used a dynamic model to investigate the differential transcriptional effects of growth factor stimulation in an immortalised embryonic striatal cell model of HD. The comparison of microarray data from both EGF and NGF experiments at baseline suggests that the expression changes between genotypes remain relatively homogenous and robust between different batches of cells, and the use of different Affymetrix chips provide a degree of reproducibility. The top GO categories that were associated with these baseline differences were mostly developmental pathways, which are likely to be reflective of the embryonic nature of this cell model. As such, the focus of further analyses was on genes that were associated with transcriptional related pathways, and those that were differentially affected between the genotypes following growth factor stimulation.

StHdh$^{Q7/7}$ cells responded differently to EGF and NGF stimulation in terms of their gene expression response. Despite both growth factors sharing similar downstream kinase signalling pathways, such as AKT, MEK and P38 MAPK (Song et al. 2002; Humbert 2003; Yang et al. 2007; Cabodi et al. 2009; Ji et al. 2010), their subsequent gene expression profiles differed. NGF stimulation elicited the expression of genes that were associated with the regulation of cellular and metabolic processes, which may be reflective of NGF's association with promoting neurite outgrowth and cellular proliferation (Pang et al. 1995; Levkovitz & Baraban 2002; Song et al. 2002). On the other hand, EGF has been more closely linked with transcriptional control (Liévens et al. 2008), and the EGFR itself has been identified as a potential TF (Lin et al. 2001). In addition, in HeLa cells, 46 different transcriptional regulators were identified as being phosphorylated within 20 minutes of EGF stimulation (Olsen et al. 2006), thus implicating this as a key pathway for the control of gene expression. EGF and NGF may therefore be stimulating similar cellular signalling responses but in a differential manner; it has been suggested that the downstream kinetics of kinase signalling pathways in response to growth factor stimulation may be the mechanism for differentiation between signals that would otherwise share similar cellular responses (Ji et al. 2010). Alternatively,

both NGF and EGF may be stimulating separate downstream signalling pathways that are then differentially modified by the presence of mHTT.

$StHdh^{Q111/111}$ cells do not appear to exhibit such distinct responses to EGF and NGF stimulation as $StHdh^{Q7/7}$ cells do. In both cases, several of the top 10 GO categories identified from pathway analysis were associated with the regulation of transcription. This may explain why we observed a greater transcriptional response in $StHdh^{Q111/111}$ cells compared to the $StHdh^{Q7/7}$ cells following NGF stimulation, despite evidence suggesting that cellular responses to NGF are suppressed in cells containing mHTT (Song et al. 2002; Humbert 2003), and that activation of its receptor TRKA is disrupted by mHTT associated mechanisms (Rong et al. 2006). The kinase activation data from the previous chapter suggests that $StHdh^{Q111}$ cell lines do not show the same phosphorylation response in kinase pathways, such as AKT, MEK and P38 MAPK following NGF stimulation as they do following EGF (Figures 4.3-4.6). Therefore, it is possible that there are distinct mechanisms by which the transcriptional response occurs in response to varying growth factor stimulation. For example, NGF stimulation of PC12 cells leads to sustained activation of Map kinase kinase (MAPKK), which consequently activates MAPK, whereas EGF stimulation initiates a more rapid phosphorylation response that decays after 60 minutes (Traverse et al. 1992). In addition, both growth factors have differential effects on the translocation of MAPK to the nucleus; this only occurs following NGF (Traverse et al. 1992), and may be a mechanism by which transcriptional control differs between two pathways that share similar upstream kinases. The differential responses that distinguish the cellular reactions to different stimuli may be aberrantly regulated in the presence of mHTT, resulting in a homogeneous response when alternate growth factors are presented. As NGF stimulation elicited considerable gene expression changes, and is known to upregulate the expression of similar IE genes to EGF stimulation (Cosgaya & Aranda 1999), the lack of an observed phosphorylation response following NGF stimulation in the previous chapter may be an artefact of only investigating one time point of growth factor stimulation. Therefore to more fully elucidate the upstream kinase signalling pathways involved in transcriptional dysregulation in the $StHdh^{Q111}$ model of HD, a more thorough characterisation of kinase phosphorylation kinetics would be required.

Comparing the lists of differentially expressed genes between genotypes following EGF stimulation was used as a method to identify potentially aberrant pathway signalling in *StHdh*$^{Q111/111}$ cells. The genes that had significantly increased expression following EGF stimulation in *StHdh*$^{Q7/7}$ cells are known to encode proteins that perform a range of functions and belong to several different classes of TFs. For example, HIVEP1, KLF5 and TSHZ1 are all members of the zinc finger family of TFs that are associated with functions as broad as embryonic stem cell (ESC) pluripotency, cell growth and differentiation, and soft palate development in mice (Ghaleb et al. 2005; Yao et al. 2006; Coré et al. 2007; Guo et al. 2009; Bourillot & Savatier 2010). *Klf5* expression has also previously been found to be dependent on EGFR stimulation, and is downstream of MEK/ERK signalling (Yang et al. 2007). KDM6B is a histone demethylase; this family of TFs is thought to activate gene expression by removing histone H3 lysine 27 trimethylation marks from chromatin, which are repressive to transcription (Ramadoss et al. 2012).

Other genes identified from this analysis, such as *Jun* and *Junb*, encode proteins that have roles as both transcription activators and repressors, and are IE genes that form part of the early growth response (Finch et al. 2002; Cabodi et al. 2009). They also form a complex with members of the FOS and ATF TF families to create the activator protein 1 (AP1), which is a well-known transcriptional regulator, the composition of which can determine differential specificity of DNA binding in order to control gene expression (Shaulian & Karin 2002; Eferl & Wagner 2003). As members of both the ATF and FOS families (*Atf3* and *Fosl1*) were identified in this study as being dysregulated in *StHdh*$^{Q111/111}$ cells in response to EGF stimulation, the altered formation of the AP1 complex may be a mechanism for transcriptional dysregulation in this cell model. In addition, both *Jun* and *Junb* were identified as having reduced expression in R6/2 mouse striata at 10-11 weeks of age (Spektor 2002), which supports the differential expression pattern following EGF stimulation observed here, and may also indicate dysregulation of the AP1 complex. Interestingly, a putative binding site for AP1 has also been identified in the *Htt* gene promoter region (Wang et al. 2012), the disruption of which may be a mechanism for the alterations in *Htt* expression that has been

observed in several models of HD (Gutekunst et al. 1995; Persichetti et al. 1996; J. Miller et al. 2010; Pouladi et al. 2010).

Several of the remaining genes have also been identified in other models of HD as having altered expression; *Sox9* is a member of the high mobility group box TF family, and is most commonly associated with male sexual development, as well as tumour progression (Song et al. 2013). However, it has been found to be increased x0.9 fold in post mortem HD human cortex and caudate (Hodges et al. 2006). In this data, *Sox9* was also found to be significantly increased in *StHdh*$^{Q111/111}$ cells at baseline (fold change x2.4), although following EGF stimulation, its expression is reduced x1 fold. In contrast, in *StHdh*$^{Q7/7}$ cells, *Sox9* expression increases x2.16 fold following EGF stimulation. This suggests some concordance between the gene expression profiles of this cell model and human HD brain (as has previously been noted, Crook & Housman 2011), but also highlights the importance of using a dynamic model in order to draw conclusions about aberrant cell signalling from gene expression data. In addition, *Fgf2* is a powerful activator of MEK/ERK signalling, and is associated with cellular proliferation (Ishii et al. 2012; Li et al. 2012). It was identified as being increased x1 fold in human HD cortex and caudate (Hodges et al. 2006), although this was not replicated in the current model. *Tead4* is a transcriptional enhancer, and has been found to have reduced expression in R6/2 mice at 8 weeks of age compared to their wild type littermates, but the correct level of expression can be restored with a combination treatment of tacrine, maclobemide and creatine (Morton et al. 2005). Although this difference was not apparent prior to EGF stimulation in this model, its transcriptional response to stimulation was suppressed in *StHdh*$^{Q111/111}$ cells compared to *StHdh*$^{Q7/7}$s. This suggests that interference with transcriptional control is apparent from as early as the embryonic stages of development in HD.

Finally, *Arntl* is a basic helix loop helix (BHLH) TF associated with circadian rhythm (Reppert & Weaver 2002), and has been identified as being typically dysregulated in models of HD (Seredenina & Luthi-Carter 2012). Its expression was found to be reduced x1.38 fold in symptomatic R6/2 mice (Crocker et al. 2006), although no significant difference was found in the baseline expression of *Arntl* in these cells; this

may be due to the difference in the developmental stage of each model. However, we did find a suppressed response of *Arntl* expression to growth factor stimulation in *StHdh*$^{Q111/111}$ cells, which may be an early indicator of progressive downregulation of this gene. The implication of *Arntl* dysregulation in HD is of particular interest, as disruption in circadian rhythm is a key clinical feature of HD in humans, and has been identified in mouse models of the disease (Morton et al. 2005; Pallier et al. 2007; Fedele et al. 2010; Morton 2013).

The genes that were identified as having a stronger transcriptional response in *StHdh*$^{Q111/111}$ cells also represented a diverse range of functions, predominantly cellular survival and proliferation. However, the majority of genes on these lists are responsive to TGFβ stimulation, and several have direct associations with SMAD TFs. For example, the HMGA2 protein regulates a feed forward mechanism of gene transcription via a direct interaction with SMADs 3 and 4 (Thuault et al. 2008). *Irf2bp2* encodes a muscle enriched TF (Teng et al. 2011) that has been found to be a TGFβ responsive gene (Koinuma et al. 2009), as has *Cdc42ep3* and *Gadd45g* (Zawel et al. 2002; Lim et al. 2005; Gomis et al. 2006), the second of which also mediates the activation of P38 MAPK (Johnen et al. 2013). *Gadd45* was also found to be increased x2.7 fold in an inducible PC12 model carrying an N-terminal fragment of mHTT (Apostol et al. 2006), which is similar to the x2.45 fold change difference between genotypes observed in this cell model. *Gadd45g* was downregulated in response to EGF stimulation; however as a negative regulator of cell growth, downregulation following growth factor stimulation is consistent with the predicted growth response. As well as having a putative SMAD TF binding site on its promoter, NGF is a mediator of SMAD activity, and specifically can enhance the activity of SMAD3 by promoting its complex formation with SMAD4 (Lutz et al. 2004). Therefore the enhanced NGF expression observed in response to EGF stimulation in *StHdh*$^{Q111/111}$ cells may be consistent with heightened SMAD activity in this model. In addition, an increased SMAD activity response in these cells may explain why there was a much larger transcriptional reaction in *StHdh*$^{Q111/111}$ cells compared to *StHdh*$^{Q7/7}$ cells following NGF stimulation.

Bhlhe40 codes for a BHLH transcriptional repressor that can be induced by TGFβ (Ehata

et al. 2007; Hsiao et al. 2009), which is consistent with our identification of a putative SMAD TF binding site in its promoter region. EGR1 has been found to have a physical and functional interaction with SMAD3, which is an association that stimulates transcription (Fortin & Bernard 2010). Its increase in expression may be in response to increased P38 MAPK or AKT signalling, as identified in the previous chapter. Increased expression of *Egr1* was also observed in an inducible PC12 model of HD (Liang et al. 2009), although other studies have consistently identified a downregulation of this gene in other models of HD (Luthi-Carter 2000; Spektor 2002; Morton et al. 2005; Crocker et al. 2006). No differences in *Egr1* expression at baseline were identified in this study, so it is possible that this discrepancy is a result of the different stages of phenotypic development between these models. However, lower baseline expression does not exclude the potential for increased sensitivity to stimulation.

There is currently no literature linking FOSL1 to either SMAD or TGF-β activity, however as previously noted, it is known to dimerize with JUN or ATF proteins in order to form the AP1 TF complex (Shaulian & Karin 2002; Eferl & Wagner 2003). Combined with a potential SMAD TF binding site within its promoter region, it may be indirectly associated with aberrant TGFβ signalling. Increased expression of *Fosl1* was also found in the same inducible N-terminal mHTT PC12 cell model of HD that found increased *Egr1* expression (Liang et al. 2009). The same authors also found a substantial increase in *Atf3* expression (x24.6 fold), and suggested that this was a protective effect, as knock down of this gene increased mHTT toxicity (Liang et al. 2009). We did not identify *Atf3* as being different between genotypes at baseline; however regulation of its expression was more sensitive in *StHdh*$^{Q111/111}$ cells. *Atf3* is downstream of P38 MAPK (Kang et al. 2003; Lu et al. 2007), and is known to be induced following cellular stress (Hai et al. 2010). It is a transcriptional repressor (Chen et al. 1994; Hai et al. 2010), and as a result its overexpression suppresses cell growth (Fan et al. 2002) and induces apoptosis by increasing caspase activity (Mashima et al. 2001). Therefore, the effects of its overexpression in this and other models of HD are coherent with observable phenotypes caused by the mHTT protein. ATF3 is a common target of TGFβ signalling, and is activated specifically by SMAD3 (Kang et al. 2003), suggesting that there may be enhanced SMAD3 activity in *StHdh*$^{Q111/111}$ cells in order to drive increased

ATF3 activity. This was supported in the gene expression data, but the evidence for increased SMAD3 protein phosphorylation and activity in these cells still requires elucidation.

The ATF3/SMAD3 complex is part of the regulatory machinery that controls *Id3* expression; *Id3* was identified here as having a putative SMAD TF binding site in its promoter region, and the extent of its downregulation in response to EGF stimulation was larger in *StHdh*$^{Q111/111}$ cells. *Id3* is known to be mediated by the EGFR via the activation of SMAD5, which is phosphorylated by increased AKT activity (Jin et al. 2011), and is downregulated by TGFβ stimulation (Kang et al. 2003). It has already been demonstrated that there is an increased AKT response in *StHdh*$^{Q111/111}$ cells (see previous chapter), which is concordant with an exaggerated response in downstream gene expression. In this cell model, although there was no difference in SMAD5 gene expression, there was reduced SMAD5 protein in *StHdh*$^{Q111/111}$ cells, but a trend towards its hyperphosphorylation; this may be in part due to the increased AKT response in these cells, although more thorough investigation is required to clarify this relationship. The pattern of *Id3* expression is also consistent with *Bcl6b* expression in this model, as the latter is downstream of activated MEK (Ishii et al. 2012), which is phosphorylated in response to EGF stimulation (see previous chapter), and contains an *Id3* repressive element (Jin et al. 2011).

As a suppressor of RAS function, the increased expression of *Rasa1* in *StHdh*$^{Q111/111}$ cells is consistent with previous findings that RAS/MAPK/ERK signalling is impaired in this cell model (Ginés et al. 2010), and that its expression was found to be increased x1.7 fold in an inducible N-terminal HTT PC12 cell model of HD (Apostol et al. 2006). Its protein, RASGAP, is also known to interact with HTT through its SH3 domain, and this interaction is mediated through stimulation of the EGFR (Liu et al. 1997). The RAS/MAPK and TGFβ pathways interact in both a co-operative and antagonistic manner (Massague 2003); for example, RAS hyperactivity is able to inhibit the function of SMADs1, 2 and 3 (Kretzschmar et al. 1997; Calonge & Massagué 1999). Therefore increased *Rasa1* expression and the consequent suppression of RAS could be expected to promote enhanced SMAD activity.

The association of the TGFβ pathway and SMAD signalling is not exclusive to the genes that elicit a stronger response in *StHdh*$^{Q111/111}$ cells; several of the genes identified from the *StHdh*$^{Q7/7}$ list have also been implicated with this pathway, although in contrast to the panel of genes just discussed, these are primarily negatively regulated by increased TGFβ and SMAD activity. For example, *Myc* is commonly downregulated in response to TGFβ in diverse cell types (Alexandrow & Moses 1995), and *Sox9* expression is enhanced in the context of repressed TGFβ activity (Song et al. 2013). *Spry2* has also been found to mediate the crosstalk between EGF and TGFβ pathways; its activation is increased by stimulation of the EGFR, where it then propagates the signal by preventing degradation of the EGFR. TGFβ suppresses the transcription of *Spry2*, therefore degrading its protein and suppressing EGFR activation (Ding et al. 2007). Consequently, its expression in *StHdh*$^{Q111/111}$ cells could be expected to be reduced if there is enhanced activity in the TGFβ pathway, which would also be consistent with their generally suppressed response of transcription following EGF stimulation. Finally, *Smad7* expression was also enhanced in *StHdh*$^{Q7/7}$ cells following EGF stimulation; *Smad7* is an inhibitor of TGFβ and SMAD signalling by competitively interacting with the type 1 TGFβ receptor (Blanchette et al. 2001) and interfering with SMAD-SMAD interactions (Massague 2005). It is also expressed in response to EGF stimulation in order to act as a negative regulator of the pathway (Kim et al. 2012); in the context of this experiment, *Smad7* may be enhanced following EGF stimulation in order to mediate the response of *StHdh*$^{Q7/7}$ cells, but in *StHdh*$^{Q111/111}$ cells, lower expression and potentially lower activity of its protein may be permissive of enhanced TGFβ pathway activity, and consequently prevents normal regulation of cell signalling pathways.

Despite having different roles in specific signalling pathways, all of the genes identified as having differential responses to EGF between genotypes share two potential TF family binding sites on their promoter regions, suggesting that these are likely to be the main regulatory elements controlling their expression. The first of these is the early growth response factor family (EGRF), of which one of the *StHdh*$^{Q111/111}$ upregulated genes, *Egr1*, is a member. The function of *Egr1* has already been discussed, but its increased availability in *StHdh*$^{Q111/111}$ cells in response to growth factor stimulation may

be a mechanism by which the expression change of genes in these cells is enhanced. The implication of the SP1 family of TFs in the expression of this panel of genes is also of particular interest, as SP1 has been found to bind to the HTT protein, with a higher affinity to mHTT (Dunah et al. 2002; Li et al. 2002; Hu et al. 2004), and is also able to regulate the transcription of *Htt* itself (Wang et al. 2012). The potential role of SP1 in HD is still under debate; increased expression of it has been observed in 15 week old R6/1 mice, where there was also an increase in its DNA binding capacity (Hu et al. 2004), but in human HD brain this was found to be impaired, which was coupled with the downregulation of a variety of SP1-regulated genes (Luthi-Carter et al. 2002; Chen-Plotkin et al. 2006). Whether SP1 has the capacity to be neuroprotective remains to be elucidated; the overexpression and the suppression of *Sp1* have both separately been found to be neuroprotective (Li et al. 2002; Qiu et al. 2006), which suggests that an additional regulatory element may be involved in its effects in HD. Although SP1 is a major TF in neuronal cells (Ross 2002), increased *Sp1* expression is consistent with gene expression changes seen here in the same manner as increased *Egr1* expression, and the probability of the presence of its binding site in the promoter regions of all of the identified genes was found to be significantly unlikely to be due to chance. Alterations in the broad activity of SP1 as a neuronal TF may also be a mechanism by which global transcriptional dysregulation occurs in HD, and also may explain some of the specific susceptibility of neuronal cells to mHTT insult.

The potential roles of the additional TF binding sites on the promoter regions of genes with enhanced expression change following EGF stimulation in *StHdh*$^{Q111/111}$ cells is currently unclear, as they are all associated with a range of different functions and signalling pathways. The increased number of TFs in common may simply be due to chance, as a shorter gene list is more likely to have more common elements due to reduced specificity. Alternatively, being downstream of several kinase signalling pathways, they may reflect enhanced activity of these pathways (as observed in the previous chapter), therefore promoting a broader range of TF activity in *StHdh*$^{Q111/111}$ cells. The presence of SMAD TF binding sites in the promoter regions of *StHdh*$^{Q111/111}$ related genes is also of interest, as it supports the hypothesis that SMAD activity may be augmented in these cell types, and this may be a mechanism for the enhanced

expression response of these genes.

Gene expression data suggested that several members of the TGFβ pathway are drastically upregulated in *StHdh*^{*Q111/111*} cells, and as already discussed, this increased activity would be concordant with the pattern of gene expression changes observed following EGF stimulation in both *StHdh*^{*Q7/7*} and *StHdh*^{*Q111/111*} cells. In order to investigate this further, we used a panel of antibodies against several SMAD proteins to determine if the observed increases in gene expression were reflected in protein levels and their activation. As SMAD9 is one of the least researched members of the SMAD TF family, no antibody was available to investigate its activity. A comparison between the *Smad* gene expression data and SMAD protein data can be found in Table 5.11. Increased expression of the *Smad6* gene was not reflected in the level of total SMAD6 protein; this may be due to a reduced capacity of *StHdh*^{*Q111/111*} cells to translate mRNA into protein, meaning that increased expression of this gene is a compensatory response required for normal protein availability. It also was not possible to investigate SMAD6 phosphorylation in this project, so it remains to be elucidated whether its activity is altered in *StHdh*^{*Q111/111*} cells. SMAD6 is an inhibitory member of the TGFβ pathway (Park 2005) that acts by competing with SMAD4 for SMAD1 binding (Massague 2005), so it could be expected that its activity will be suppressed in these cells. However, its activity is more closely associated with the BMP pathway (Massagué 1998; Massague 2005), so the significance of its overexpression in this cell model remains unclear.

In contrast, there were some mixed results for the activity of SMAD3; the expression of the gene was found to be substantially higher in *StHdh*^{*Q111/111*} cells, and there was suggestion from western blot data that this also translated into increased presence of the protein and its phosphorylation. Several of the genes that had an augmented response in *StHdh*^{*Q111/111*} cells are known to be regulated by SMAD3 activity, such as *Atf3* (Kang et al. 2003), *Egr1* (Fortin & Bernard 2010) and *Ngf* (Lutz et al. 2004). Increased expression and phosphorylation of SMAD3 may therefore be a mechanism for some of the transcriptional dysregulation apparent in this cell model of HD. However, the ELISA data elicited opposing results regarding both total and

phosphorylated SMAD3, so its exact role in transcriptional control in *StHdh*$^{Q111/111}$ cells requires further investigation. There is also a trend towards increased SMAD4 protein in *StHdh*$^{Q111/111}$ cells, although this did not reach significance. However as SMAD3 is required to form a complex with SMAD4 in order to localise to the nucleus and to bind with DNA (Massague 2005), increased SMAD4 would be required to accommodate the increased activation of SMAD3.

	Gene Expression		Western Blot		ELISA	
	Microarray (Fold change)	qRTPCR (RQ Ratio)	Total protein (FI ratio)	Phospho-protein (FI ratio)	Total protein (Abs ratio)	Phospho-protein (Abs ratio)
SMAD1	ND	ND	ND	ND	-	-
SMAD2	-1.20 ↓	-	0.9 ↓	0.54 ↓	0.8 ↓	0.4 ↓
SMAD3	1.27 ↑	4.2 ↑	1.4 ↑	2 ↑	0.78 ↓	0.3 ↓
SMAD4	-1.03 ↓	-	ND	-	-	-
SMAD5	-1.15 ↓	-	0.3 ↓	0.7 ↓	-	-
SMAD6	1.60 ↑	3.5 ↑	ND	-	-	-
SMAD7	-1.30 ↓	0.58 ↓	-	-	-	-
SMAD9	1.80 ↑	5.6 ↑	-	-	-	-

Table 5.11 A summary of all *Smad* gene expression and SMAD protein comparison data between *StHdh*$^{Q111/111}$ and *StHdh*$^{Q7/7}$ cells. Arrows indicate the level of gene expression or protein concentration in *StHdh*$^{Q111/111}$ cells compared to *StHdh*$^{Q7/7}$ cells (↑ = higher, ↓ = lower). RQ = relative quantification, FI = fluorescence intensity, Abs = absorbance at 450nm.

Both *Smad2* and *Smad5* showed no difference between genotypes in terms of their gene expression in the microarray analysis, however both total and phosphorylated SMADs2 and 5 were present at lower levels in *StHdh*$^{Q111/111}$ cells compared to the *StHdh*$^{Q7/7}$s, indicating suppression of the TGFβ pathway. This is not entirely incompatible with the SMAD3 hypothesis, as TGFβ signalling is a very broad mechanism, and the different SMAD proteins are likely to regulate different subsets of genes; the suppression of this arm of the pathway may be an additional mechanism for some of the transcriptional downregulations commonly seen in models of HD (Crook & Housman 2011). Finally, *Tgfbi* is a key gene associated with corneal dystrophy (El

Kochairi et al. 2006), but there is currently no data on its role in TGFβ signalling in brain, or in the context of neurodegeneration, so any potential contribution it may have to transcriptional control in neurons remains to be seen.

There is currently limited evidence for the implication of TGFβ and SMAD signalling in the progression of HD; TGFβ1 is reduced in the peripheral blood of asymptomatic HD patients, and its presence had an inverse correlation with CAG repeat length (Battaglia et al. 2011). YAC128 and R6/2 mice also had reduced TGFβ1 in the cortex, but there was a slight increase in its presence in the striata of symptomatic mice, which was thought to be indicative of an inflammatory response in astrocytes and glial cells (Battaglia et al. 2011). In contrast, human HD induced pluripotent stem cells (iPSCs) were found to have an upregulation of the TGFβ pathway, which could be restored to normal levels by replacement of the expanded CAG repeat with a CAG repeat of non-pathogenic length (An et al. 2012). In addition, increased TGFβ signalling has been identified in the hippocampus of a transgenic rat model of HD as well as in the R6/2 mouse model, where it has an inverse effect on neural stem cell proliferation (Kandasamy et al. 2010). Currently, there is no evidence for the association of SMAD proteins with either HTT or mHTT. However, evidence is slowly mounting that supports dysregulation of this pathway in models of HD, suggesting that it could be a potentially interesting new target for research and therapeutics.

In conclusion, we have identified differential gene expression responses to growth factor stimulation in *StHdh*^{Q111} cell lines, and have identified novel signalling pathways that may be implicated in HD-associated transcriptional dysregulation. This study also supports the plethora of other work identifying general transcriptional dysregulation in various models of HD, and in human HD striata (Crook & Housman 2011), as well as replicating some specific gene expression changes. By using an immortalised embryonic striatal cell model, we also demonstrate that transcriptional dysregulation is a very early event in the development of the HD phenotype. However, we have also highlighted the usefulness of utilising a dynamic model in order to investigate the effects of aberrant kinase signalling on downstream gene expression, which is particularly informative when considering altered mechanisms of transcriptional

regulation in models of HD. In this cell model, we have identified a panel of genes that exhibit an altered pattern of expression in response to EGF stimulation, the nature of which were consistent with the kinase activation responses identified in Chapter 4. This implied that there may be potentially aberrant control of TGFβ and SMAD signalling pathways in the presence of mHTT, which may prove to be a novel mechanism for the transcriptional dysregulation observed in this, and other models of HD. There is currently only modest support for the involvement of these pathways in HD, however when pooling the vast kinase signalling and transcriptional regulation data with these findings, it appears that this pathway may prove to be an interesting and worthwhile target for further investigation.

Chapter 6: Recapitulating the effects of EGF stimulation on huntingtin localisation, kinase signalling pathways and transcriptional control in primary embryonic striatal cells from the Hdh^Q111 and Hdh^Q150 mouse models of HD.

6.1 Introduction

The Hdh^{Q111} and Hdh^{Q150} knock in mouse models are genetic recapitulations of HD, and as such have been thoroughly characterised and investigated (Wheeler 1999; Wheeler 2000; Fossale et al. 2002; Ginés 2003; Carnemolla et al. 2009; Menalled et al. 2009; Molero et al. 2009; Saavedra et al. 2010; Fossale et al. 2011). The Hdh^{Q111} mouse model consists of a human/mouse chimeric exon 1 of the *Htt* gene carrying an expanded CAG repeat that ranges between 97-114 CAGs, which is under the endogenous murine promoter (Wheeler 2000; Menalled et al. 2009).

Despite the late onset of motor abnormalities in this model, Hdh$^{Q111/111}$ mice show progressive striatal abnormalities that predate any overt behavioural symptomology. These abnormalities can occur from a few months of age (Ginés et al. 2006); from 6 weeks of age, a weak nuclear stain of mHTT can be detected in striatal cell nuclei (Wheeler 2000; Fossale et al. 2002), which progressively increases over time until a punctate nuclear signal is detectable by only 4.5 months (Wheeler 2000; Wheeler et al. 2002). Strong nuclear reactivity and dark nuclear puncta are apparent from 10-15 months in Hdh$^{Q111/111}$ mice (Wheeler 2000; Wheeler et al. 2002), which still predates development of the motor phenotype by around a year (Fossale et al. 2002). However, correlating with the appearance of nuclear puncta, there has been suggestion of some subtle reduction in the startle response in these mice at 52 weeks (Menalled et al. 2009), which is consistent with the finding of subtle differences in cognition in human HD patients prior to motor symptom onset (Hahn-Barma et al. 1998; Lawrence et al. 1998; Berrios et al. 2002; Snowden et al. 2002). In concordance, the genetically similar Hdh^{Q92} mouse model exhibits impairments in operant conditioning learning tasks and deficits in visuomotor responding from 4-5 months old (Trueman et al. 2007; Trueman, Dunnett, et al. 2012; Trueman, Jones, et al. 2012). Also in accordance with the human

HD phenotype, Hdh$^{Q111/111}$ mice show a significant reduction in body weight by 28 weeks (Menalled et al. 2009; van der Burg et al. 2009).

Although increased nuclear HTT is associated with the pathogenesis of HD (DiFiglia 1997; Gutekunst et al. 1999), there are also earlier neuronal changes that can be detected in Hdh$^{Q111/111}$ mice that occur prior to nuclear accumulation and aggregation of the mutant protein (Fossale et al. 2002; Ginés et al. 2003; Carnemolla et al. 2009; Molero et al. 2009; Fossale et al. 2011). For example, gene expression changes have been found to occur in Hdh$^{Q111/111}$ mice from 3-10 weeks, and in striatal neurons these changes have been associated with pathways such as the regulation of RNA metabolism and transcriptional/translational control (Fossale et al. 2011). Increased *Rrs1* expression can be identified from only 3 weeks in Hdh$^{Q111/111}$ mouse striatum; a phenotype that worsens with age (Fossale et al. 2002), and several ER-stress associated markers have been found to have increased expression from only 15 weeks (Carnemolla et al. 2009), suggesting that prior to both overt motor symptoms and neuropathology, mHTT is able to elicit cellular dysregulation from a very early age in these mice.

Neuronal dysfunction in Hdh$^{Q111/111}$ mice has also been identified in embryonic striatal primordia. For example, genes associated with embryonic brain maturation were more highly expressed between E13.5 and E15.5 in Hdh$^{Q111/111}$ mice (Molero et al. 2009), and there were deficits in neurogenesis, such as a delayed exit of the cell cycle. This was hypothesised to be due to either abnormal phase lengthening or transient arrest of the cell cycle (Molero et al. 2009). Together, these may alter striatal neuronal homeostasis and confer increased susceptibility to future insult by mHTT presence. This also suggests that mHTT is altering striatal neuronal activity prior to birth, and other dysfunctional processes that may also occur at this time point may help explain the specificity of striatal degeneration in HD, and the progression of the disease over time.

The Hdh^{Q150} mouse model of HD is genetically similar to the Hdh^{Q111} model; however it does not have a chimeric exon 1, but rather consists of an expanded CAG fragment containing 150 CAG repeats knocked into the mouse *Htt* gene (Lin 2001). Despite their genetic similarities, the Hdh^{Q150} model shows a more severe and progressive

phenotype (Lin 2001; Heng et al. 2007; Woodman et al. 2007). The original Hdh^{Q150} model was maintained on a mixed 129/Ola x C57Bl/J6 mouse strain background; in contrast to Hdh^{Q111/111} mice, these mice exhibited clasping behaviour, rotarod deficits and motor disturbances from 25-40 weeks in homozygote mice, and 40-65 weeks of age in heterozygotes (Lin 2001). These mice also suffered seizures from 25 weeks (Lin 2001), but subsequent cohorts with altered background strains removed the seizure phenotype and delayed the progression of motor symptoms (Heng et al. 2007; Woodman et al. 2007; Brooks, Higgs, et al. 2012). In Hdh^{Q150} models with an increased percentage of C57Bl/J6 lineage or a replacement of 129/Ola with a CBA background, motor abnormalities occurred later from 70-100 weeks (Heng et al. 2007; Woodman et al. 2007; Brooks, Higgs, et al. 2012), which is more comparable with the Hdh^{Q111} phenotype.

In accordance with cognitive deficits being found to precede motor abnormalities in Hdh^{Q111} mice, a similar phenotype has also been uncovered in the Hdh^{Q150} model. Hdh^{Q150} mice perform less well in a set-shifting task from 24 weeks, which consists of mice being required to switch previously learned cue-reward associations (Brooks et al. 2006); a cognitive phenotype also observed in human HD patients (Lawrence et al. 1998). Hdh^{Q150} mice also had an increased latency to finding a hidden platform in the Morris water maze task from 4 months old, due to a reduced ability to efficiently navigate (Brooks, Higgs, et al. 2012).

The Hdh^{Q150} model also develops neuropathological features prior to motor and cognitive abnormality onset (Woodman et al. 2007; Weiss et al. 2008; Bayram-Weston et al. 2012), although to date, earlier neuronal dysfunction in this model has not yet been investigated. The transcriptional profile of 15-22 month old Hdh^{Q150/150} mice has been found to correlate well with human HD caudate as well as with other transgenic mouse models of HD (Kuhn et al. 2007), although earlier developmental time points have not yet been investigated. However, as transcriptional changes are concordant between mouse models of HD, this suggests that the nature of the changes may be mechanistically similar, and therefore early transcriptional changes may also exist in Hdh^{Q150/150} mice.

Similarities between the immortalised $StHdh^{Q111}$ and Hdh^{Q111} mouse models have been observed previously; both have been found to have decreased cyclic adenosine monophosphate (cAMP) responsive element-mediated gene transcription (Ginés 2003), and display markers of the endoplasmic reticulum stress response (Carnemolla et al. 2009). In addition, increased AKT activation has also been identified in both models; a phenotype that is present prior to overt motor abnormalities (Ginés et al. 2003; Saavedra et al. 2010). In this chapter, we aim to replicate the localisation, signalling and transcriptional data that was observed in the $StHdh^{Q111}$ cell model in Chapters 3-5 in primary striatal cells from E14 Hdh^{Q111} mice in order to determine whether our findings were a result of the nature of the immortalised cell model, or if the presence of mHTT can elicit early embryonic changes in striatal neurons. In addition, where possible, we have aimed to repeat the experiments in primary E14 Hdh^{Q150} striatal cells to determine if the results may be generalizable to longer polyQ length models of HD.

6.2 The effect of EGF stimulation on the localisation of N-terminal HTT epitopes in primary Hdh^{Q111} striatal cells

Striatal cells were dissected from E14 Hdh^{Q111} and Hdh^{Q150} mouse model embryos, the details of which can be found in Section 2.2.1.4. In order to confirm the presence of striatal cells in primary cell cultures, a typical selection of cells was immunostained with antibodies against striatal cell markers dopamine- and cAMP-regulated neuronal phosphoprotein (DARPP-32) and CTIP2 (Figure 6.1), both of which have been identified as being expressed specifically in medium spiny neurons, and are commonly used markers in the current literature (Slow 2003; Carri et al. 2013; Taylor et al. 2013). The proportion of striatal to non-striatal cells was then determined (Table 6.1). The majority of cells present in dissections were labelled with striatal markers, and therefore the following experiments were considered to reflect the characterisation of a striatal cell population. In the images that have been presented representing CTIP2 and DARPP-32 co-localisation, the $Hdh^{Q111/111}$ cells are considerably smaller than the $Hdh^{Q150/150}$ cells. This may be due to the number of surviving cells in culture;

Hdh^{Q111/111} cells were more densely plated on this occasion due to reduced cell death. In addition, these experiments were separated by a large period of time, and therefore variance in batches of serum and media, as well as any uncontrollable environmental changes during dissection and culture may have contributed to different cellular morphologies. However, in both cell lines, the localisation of both DARPP-32 and CTIP2 is predominantly nuclear.
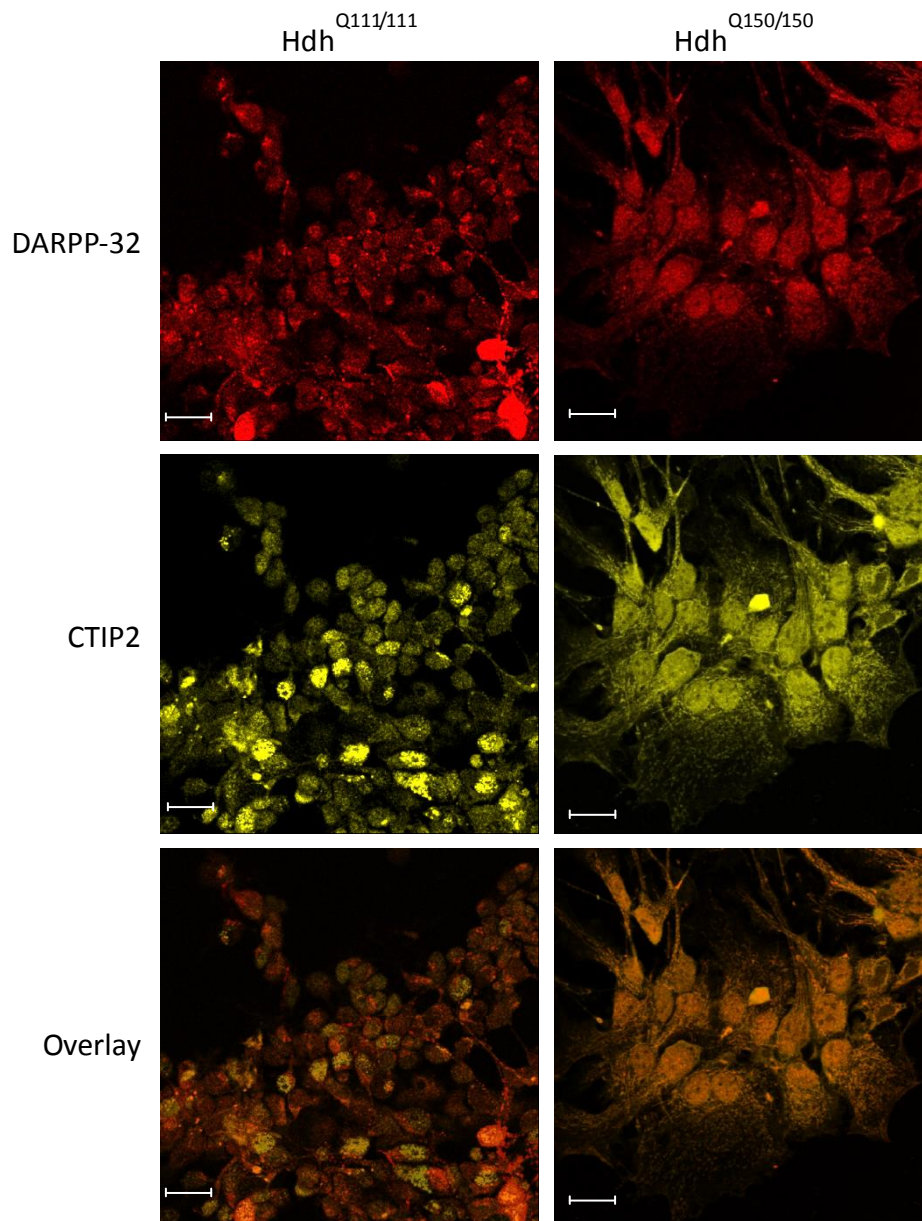
Figure 6.1 The co-localisation of striatal cell markers DARPP-32 and CTIP2 in primary E14 striatal cells cultured from Hdh$^{Q111/111}$ and Hdh$^{Q150/150}$ mice. Scale bar = 20μm.

	Total no. cells	No. cells negative for striatal markers	% Striatal cells
Hdh^{Q111}	891	55	93.83
Hdh^{Q150}	202	7	96.53

Table 6.1 The percentage of cells immunostained with striatal cell markers DARPP-32 and CTIP2 from a selection of primary cells dissected from E14 striata of Hdh^{Q111} and Hdh^{Q150} HD knock in mice. Cell numbers were counted from 3 fields of view selected at random on 4 individual coverslips representing at least one coverslip from each genotype. The majority of cells were stained with the appropriate markers, suggesting that dissected cell populations represented mouse striatal primordia.

6.2.1 Confirming the presence of the EGFR in Hdh^{Q111} cells

Immunofluorescence analysis revealed that the EGFR was present and had the same subcellular localisation in primary striatal cells from all three genotypes; Hdh$^{Q7/7}$, Hdh$^{Q7/111}$ and Hdh$^{Q111/111}$ (Figure 6.2). Western blot analysis suggests that there may be a trend towards reduced levels of the EGFR in Hdh$^{Q7/111}$ and Hdh$^{Q111/111}$ cells, although this difference does not reach significance.
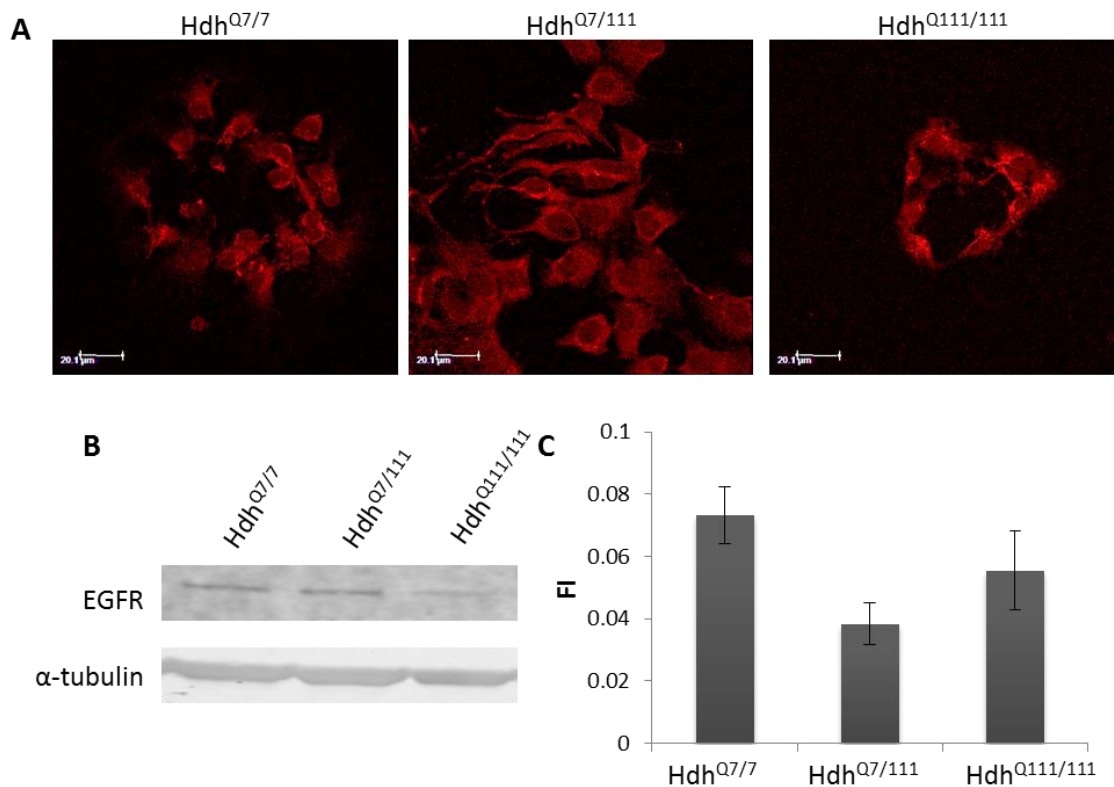
Figure 6.2 A. Immunofluorescence images of primary E14 striatal cells from the Hdh^{Q111} mouse model of HD immunostained for the EGFR. Scale bar = 20µm **B**. Western blot identifying EGFR expression in $Hdh^{Q7/7}$, $Hdh^{Q7/111}$ and $Hdh^{Q111/111}$ primary embryonic striatal cells. **C.** Licor Odyssey quantification of fluorescence intensity (FI) in *B*; EGFR is normalised to α-tubulin loading control. (Error bars = SEM, n=3)

6.2.2 Immunostaining with Ab109115 and Mab2166

Primary striatal cells were double labelled with Ab109115 and Mab2166, and were analysed blind to genotype and time of EGF stimulation in the same manner as previously described (Section 2.2.1.10).

6.2.2.1 Ab109115

Ab109115 displayed a similar localisation of HTT in primary embryonic striatal cells as in *StHdh*^{Q111} cell lines (Section 3.3.5); it was primarily perinuclear in all three

genotypes, although this appeared to be more densely stained in Hdh$^{Q111/111}$ cells, despite no apparent increase in nuclear localisation (Figures 6.3 & 6.4). Main effects analysis revealed that there was a significant effect of time of EGF stimulation on the N/C ratio in Hdh^{Q111} primary embryonic striatal cells (F (3, 571) = 3.526, p=0.015), but only a trend towards a significant effect of genotype (p=0.059), and no significant interaction between the two (p>0.05). Simple main effects revealed that there were no significant differences between individual genotypes for the N/C ratio, and the significant effect of EGF stimulation came from a significant difference between 5 and 30 minutes (p=0.013), and a trend towards a difference between 0 and 30 minutes of stimulation (p=0.091). Post-hoc Tukey tests revealed that there was no difference in the N/C ratio for either Hdh$^{Q7/111}$ and Hdh$^{Q111/111}$ cells, however there was a significant difference in Hdh$^{Q7/7}$ cells between 5 and 30 minutes (p=0.004) and 15 and 30 minutes (p=0.05). These differences arise due to a slight reduction in nuclear HTT in Hdh$^{Q7/7}$ cells at 5 minutes of EGF stimulation, and an increase in nuclear HTT at 30 minutes. However, this is not seen in cells carrying mHTT, suggesting a suppressed response to EGF stimulation.

There was a significant main effect of genotype when analysing the N/P ratio (F (2, 571) = 12.744, p<0.001), although there was no effect of EGF stimulation, or an interaction between the two. Across time points, the N/P ratio was significantly different between Hdh$^{Q7/7}$ and Hdh$^{Q111/111}$ cells (p<0.001) and between Hdh$^{Q7/111}$ and Hdh$^{Q111/111}$ cells (p=0.012), but there was no difference between Hdh$^{Q7/7}$ and Hdh$^{Q7/111}$ cells, indicating that for the localisation of nuclear and perinuclear HTT, heterozygote cell types are more similar to wild type cells than Hdh$^{Q111/111}$ cells, perhaps suggesting a gene dosage effect. Similar to the N/C ratio analyses, there was no effect of EGF stimulation on the N/P ratio for Hdh$^{Q7/111}$ or Hdh$^{Q111/111}$ cells; however, there was a significant reduction in the N/P ratio in Hdh$^{Q7/7}$ cells at 5 minutes of stimulation (p=0.017). There was also a significant difference between 5 and 30 minutes of EGF stimulation (p<0.000), which reflects the increase in nuclear HTT that was also observed in the N/C ratio. In contrast, there was no significant effect of the P/C ratio at any time of EGF stimulation, or for any genotype.
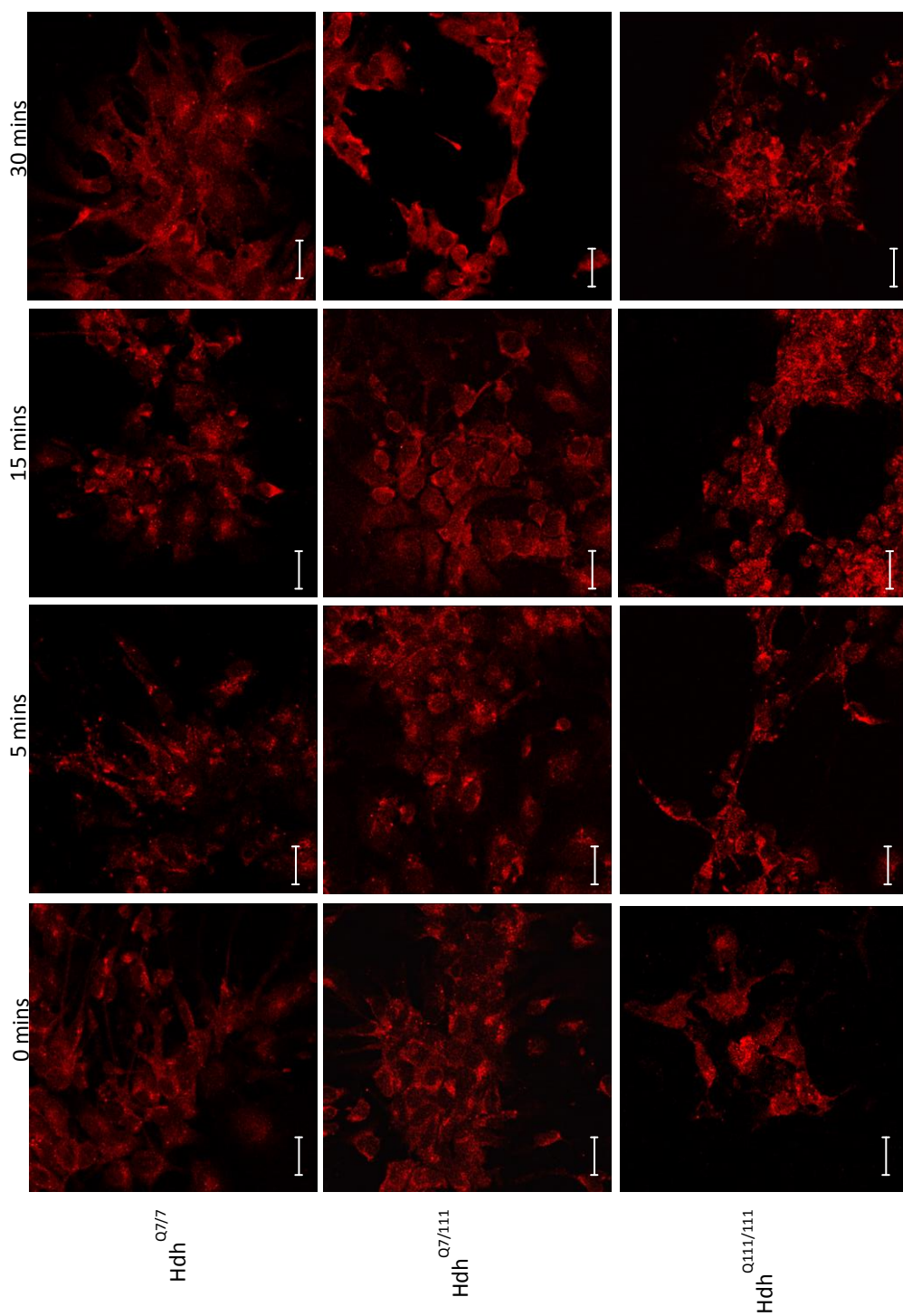
Figure 6.3 Subcellular localisation of an N-terminal epitope of HTT and mHTT in Hdh$^{Q7/7}$, Hdh$^{Q7/111}$ and Hdh$^{Q111/111}$ E14 primary striatal cell cultures. Cells were fixed following 0, 5, 15 and 30 minutes of stimulation with 100ng/ml EGF, labelled with Ab109115 against amino acids 1-30 of HTT, then analysed by confocal microscopy (see Sections 2.2.1.8 and 2.2.1.9 for further details). Scale bar = 20µm
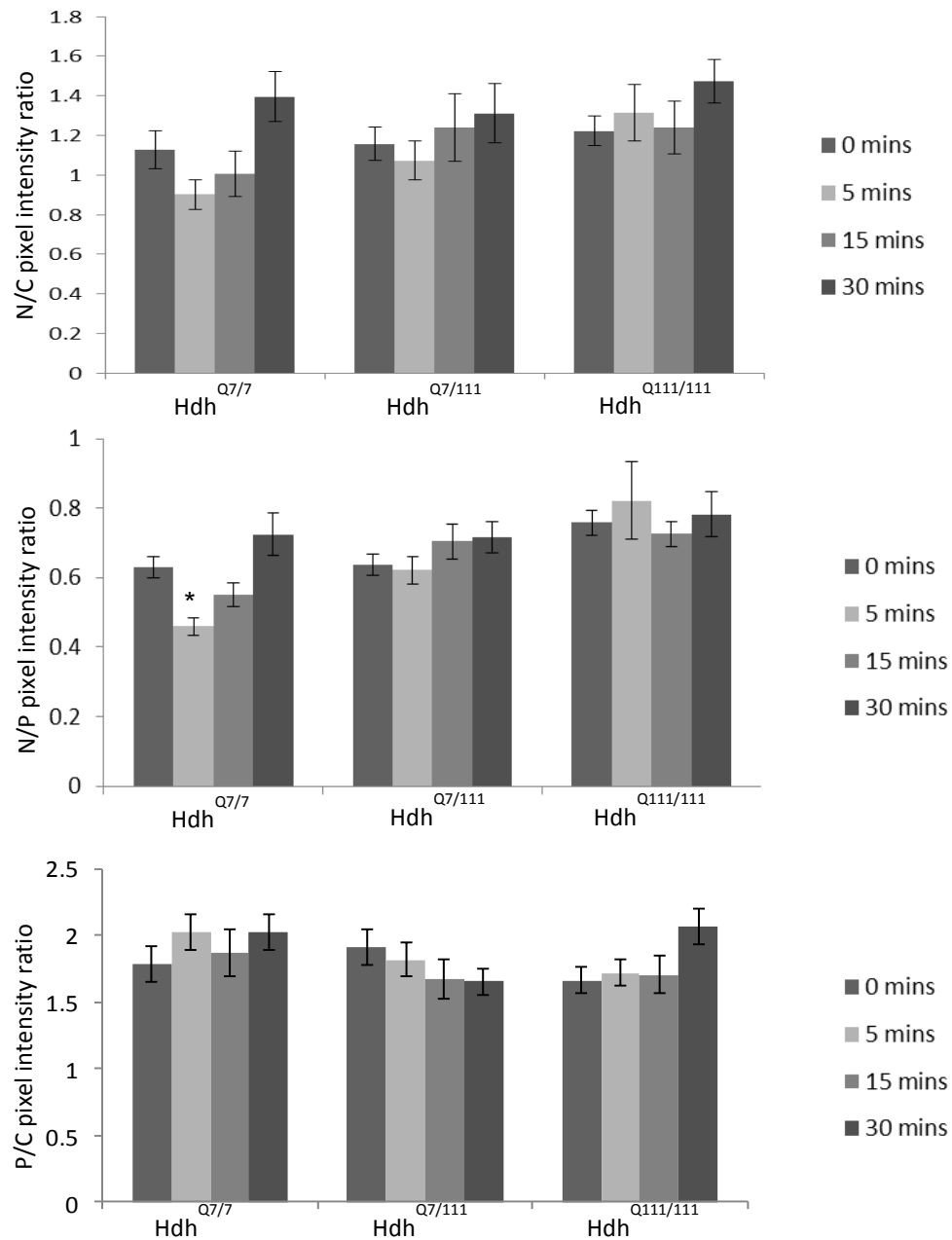
Figure 6.4 Quantitative analysis of immunofluorescence images in Figure 6.3. Nuclear/Cytoplasmic (N/C), Nuclear/Perinuclear (N/P) and Perinuclear/Cytoplasmic (P/C) mean pixel intensity ratios for $Hdh^{Q7/7}$, $Hdh^{Q7/111}$ and $Hdh^{Q111/111}$ primary embryonic striatal cells following 0, 5, 15 and 30 minutes of stimulation with 100ng/ml EGF. Mean pixel intensities were calculated from confocal microscopy images using GNU Image Manipulator (further details of the analysis can be found in Section 2.2.1.10). All images were randomised and analysed blind to genotype and length of time stimulated with EGF. Each condition consisted of 1 confocal microscopy image taken from 4-5 separate embryos of each genotype. A two-way ANOVA was carried out for main effects analysis, followed by planned one way ANOVAs and post-hoc Tukey tests. Error bars = SEM

* p<0.05   ** p<0.01   *** p<0.001

6.2.2.2 Mab2166

The localisation of the HTT epitope detected by Mab2166 was primarily perinuclear in Hdh$^{Q7/7}$, Hdh$^{Q7/111}$ and Hdh$^{Q111/111}$ cells, as observed in immortalised striatal cell lines (Section 3.3.4.3), and was less present in the cytoplasm and cell processes in Hdh$^{Q111/111}$ cells (Figures 6.5 & 6.6). An overlay of both Ab109115 and Mab2166 can be found in Figure 6.7. There was a significant effect of genotype in the N/C ratio (F (2, 668) = 3.879, p=0.021), which simple main effects analysis revealed to be due to a significantly higher N/C ratio over time in Hdh$^{Q7/111}$ compared to Hdh$^{Q111/111}$ cells (p=0.016). Post-hoc Tukey tests indicate a significant reduction in the N/C ratio in Hdh$^{Q7/7}$ cells after 5 minutes of EGF stimulation (p=0.025), but there were no significant effects for either mHTT genotypes.

In concordance with the epitope of HTT detected by Ab109115, the majority of significant effects of EGF stimulation and genotype were apparent in the N/P ratio for Mab2166. There was a significant main effect of EGF (F (3, 668) = 2.676, p=0.046), and although the genotype effect failed to reach significance, there was a significant interaction with EGF stimulation (F (6, 668) = 3.004, p=0.007). This was due to a significant reduction in the N/P ratio in Hdh$^{Q7/7}$ cells after 5 minutes (p=0.004) and 15 minutes (p=0.002) of EGF stimulation, but no effects in either Hdh$^{Q7/111}$ or Hdh$^{Q111/111}$ cells, suggesting an inhibited response of HTT localisation in the presence of mHTT. Similar to Ab109115, there was no significant main effect of either genotype or EGF stimulation in the P/C ratio.

Figure 6.5 Subcellular localisation of an N-terminal epitope of HTT and mHTT in Hdh$^{Q7/7}$, Hdh$^{Q7/111}$ and Hdh$^{Q111/111}$ E14 primary striatal cell cultures. Cells were fixed following 0, 5, 15 and 30 minutes of stimulation with 100ng/ml EGF, labelled with Mab2166 against amino acids 181-810 of HTT, then analysed by confocal microscopy (see Sections 2.2.1.8 and 2.2.1.9 for further details). Scale bar = 20µm
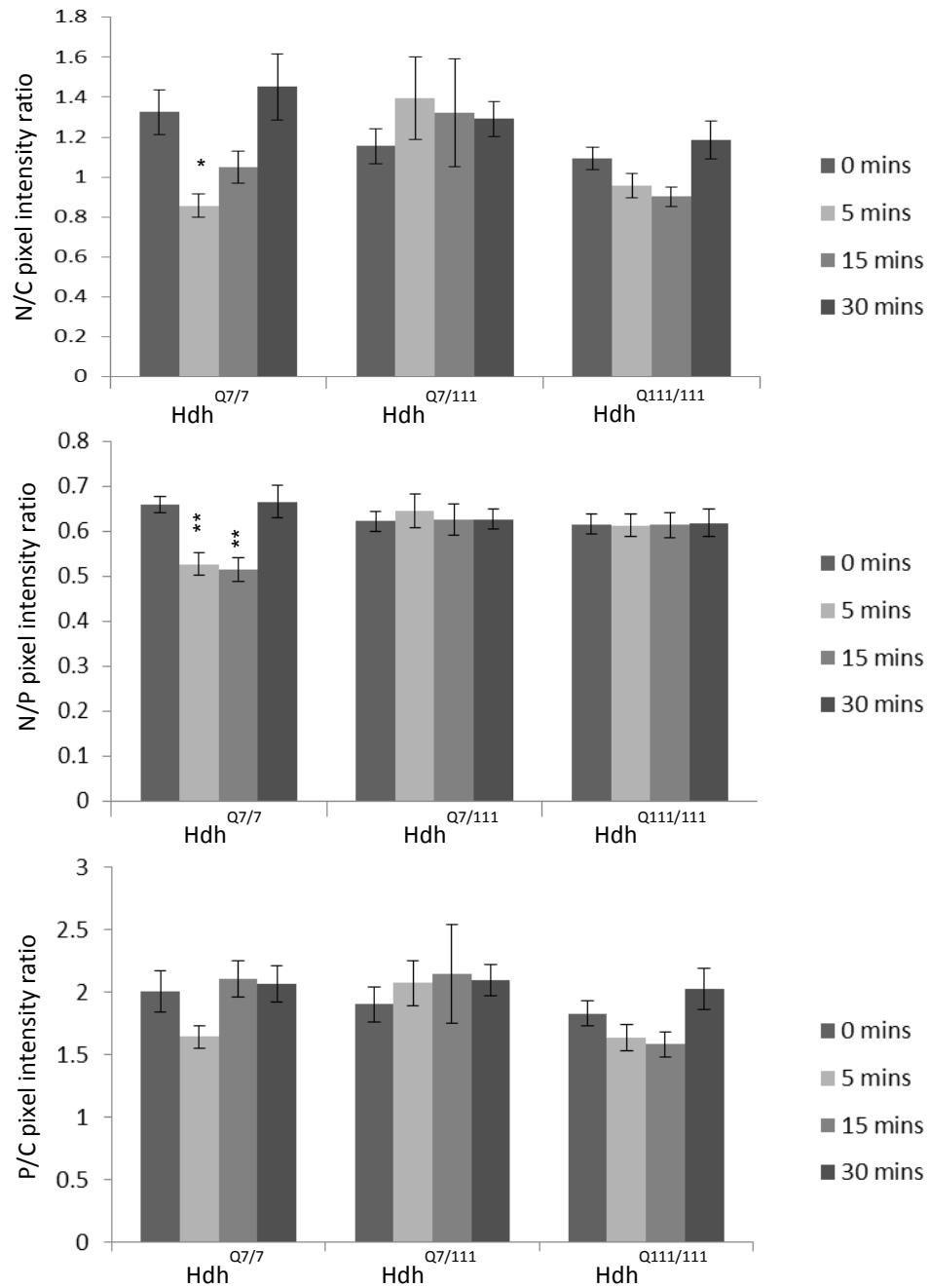
Figure 6.6 Quantitative analysis of immunofluorescence images in Figure 6.5. Nuclear/Cytoplasmic (N/C), Nuclear/Perinuclear (N/P) and Perinuclear/Cytoplasmic (P/C) mean pixel intensity ratios for $Hdh^{Q7/7}$, $Hdh^{Q7/111}$ and $Hdh^{Q111/111}$ primary embryonic striatal cells following 0, 5, 15 and 30 minutes of stimulation with 100ng/ml EGF. Mean pixel intensities were calculated from confocal microscopy images using GNU Image Manipulator (further details of the analysis can be found in Section 2.2.1.10). All images were randomised and analysed blind to genotype and length of time stimulated with EGF. Each condition consisted of 1 confocal microscopy images taken from 4-5 separate coverslips. A two-way ANOVA was carried out for main effects analysis, followed by planned one way ANOVAs and post-hoc Tukey tests. Error bars = SEM

* p<0.05   ** p<0.01   *** p<0.001

Figure 6.7 Overlay of Ab109115 (Figure 6.3) and Mab2166 (Figure 6.5) in Hdh$^{Q7/7}$, Hdh$^{Q7/111}$ and Hdh$^{Q111/111}$ E14 primary striatal cell cultures following 0, 5, 15 and 30 minutes of stimulation with 100ng/ml EGF. Scale bar = 20µm

6.2.3 Supporting HTT localisation results using additional N-terminal antibody, N17

As antibody stocks of both Ab675 and N17 were low and the number of available Hdh^{Q111} embryos was restricted, it was not possible to immunostain sufficient numbers of coverslips for statistical analysis. However, enough reagents were available to identify if there may be a qualitative trend towards similar patterns of HTT localisation as detected by amino acid 1-17 antibodies in Hdh^{Q111} cells as in *StHdh^{Q111}* cell lines.

Consistent with previous observations when using Ab675 and N17, HTT localisation is more nuclear than when it is detected with either Ab109115 or Mab2166 (Section 3.3.5). Examples of the detection of the localisation of HTT by Ab675 can be found in Appendix V. In contrast, there is no obvious effect of EGF stimulation on the epitope of HTT detected by N17 (Figure 6.8), but there was stronger nuclear detection with increased mHTT load at 0 minutes. Despite the lack of effect, this is in accordance with the findings in *StHdh^{Q111}* cell lines following EGF stimulation when HTT was detected by N17 (Appendix II).
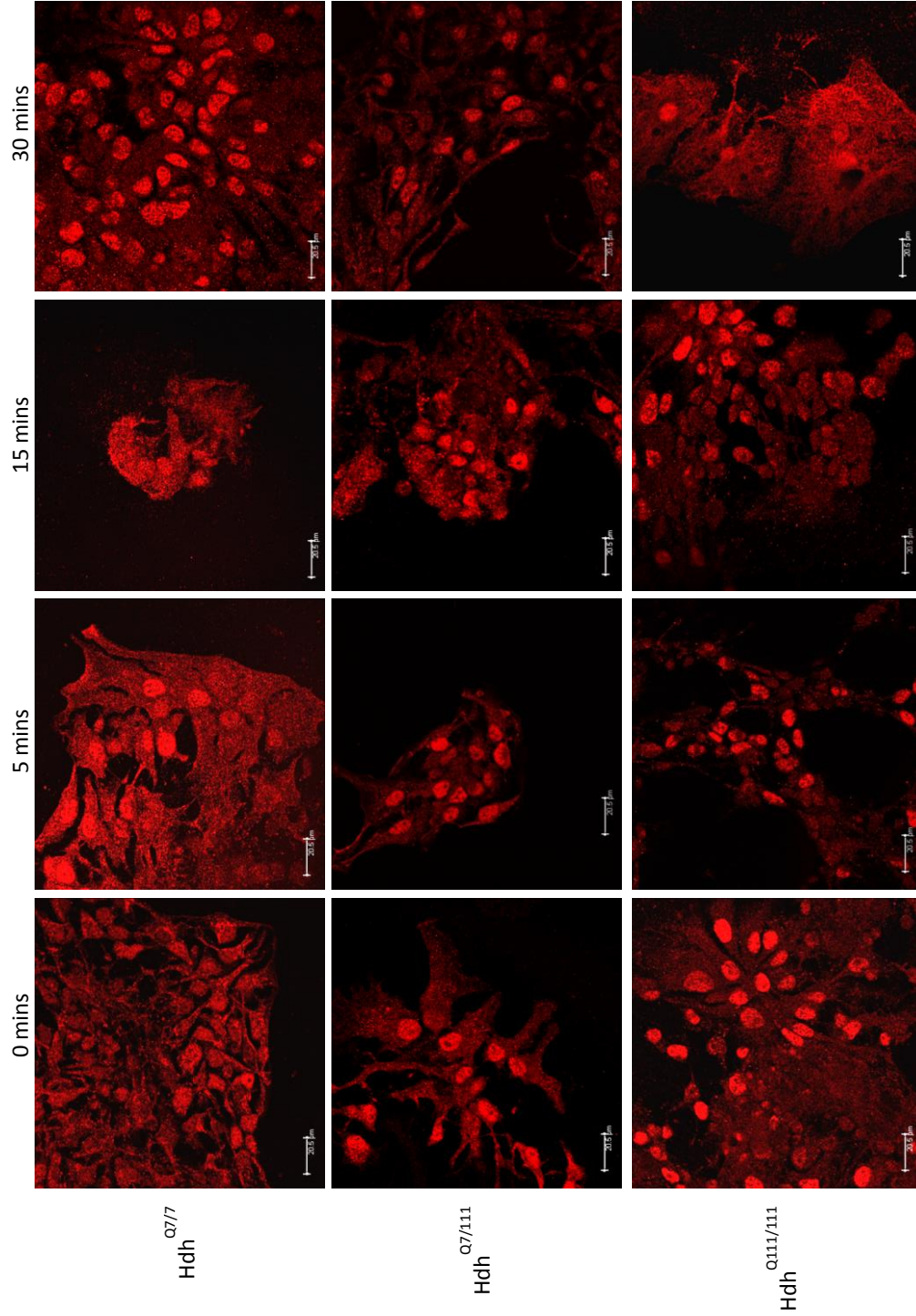
Figure 6.8 Subcellular localisation of an N-terminal epitope of HTT and mHTT in Hdh$^{Q7/7}$, Hdh$^{Q7/111}$ and Hdh$^{Q111/111}$ E14 primary striatal cell cultures. Cells were fixed following 0, 5, 15 and 30 minutes of stimulation with 100ng/ml EGF, labelled with N17 against amino acids 1-17 of HTT, then analysed by confocal microscopy (see Sections 2.2.1.8 and 2.2.1.9 for further details). Scale bar = 20μm

6.3 The effect of EGF stimulation on the localisation of N-terminal HTT epitopes in primary Hdh^{Q150} cells

In order to determine whether alterations in HTT localisation in response to EGF stimulation only occurred in cells derived from the Hdh^{Q111} mouse model, the localisation experiments were repeated in primary embryonic striatal cell cultures from E14 Hdh^{Q150} mice.

6.3.1 Confirming the presence of the EGFR

Hdh$^{Q7/7}$, Hdh$^{Q7/150}$ and Hdh$^{Q150/150}$ cells were immunostained for the EGFR in order to determine if all three genotypes expressed the receptor to the same extent (Figure 6.9). All cells expressed the EGFR and there were no qualitative differences between genotypes. This was confirmed by western blot; there was no significant difference in the quantification of EGFR expression by this method.
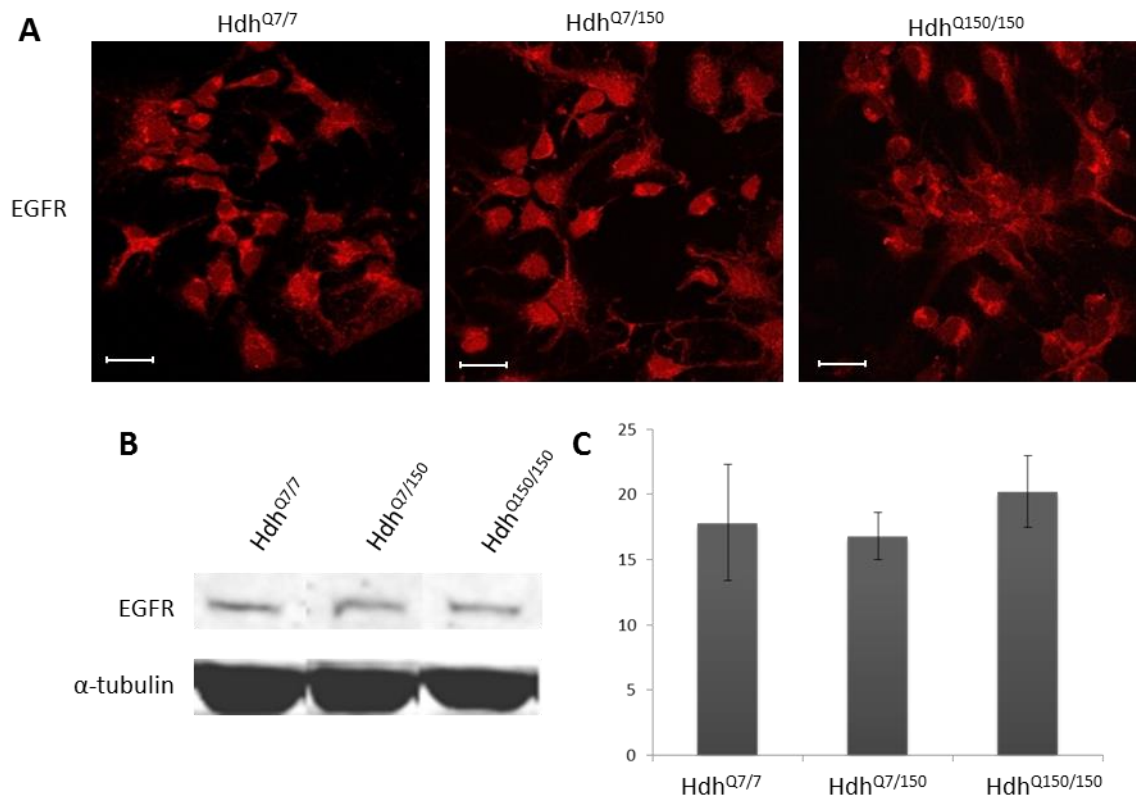
Figure 6.9 A. Immunofluorescence images of primary E14 striatal cells from the Hdh^{Q150} mouse model of HD immunostained for the EGFR. Scale bar = 20µm **B**. Western blot identifying EGFR expression in Hdh$^{Q7/7}$, Hdh$^{Q7/150}$ and Hdh$^{Q150/150}$ primary embryonic striatal cells. **C.** Licor Odyssey quantification of fluorescence intensity (FI) in *B*; EGFR is normalised to α-tubulin loading control. (Error bars = SEM, n=3)

6.3.2 Immunostaining with Ab109115 and Mab2166

Hdh^{Q150} cells were treated in the same manner as described in section 6.2.2.

6.3.2.1 Ab109115

The HTT epitope detected by Ab109115 had a primarily perinuclear localisation in Hdh$^{Q7/7}$ cells from the Hdh^{Q150} model (Figures 6.10 & 6.11), in accordance with previous observations in wild type cells from the Hdh^{Q111} mouse model and *StHdh$^{Q7/7}$* cells (Sections 3.3.5 & 6.2.2.1). However, in both Hdh$^{Q7/150}$ and Hdh$^{Q150/150}$ cells, detection of this epitope of HTT was more nuclear than in models expressing a shorter

polyQ repeat. This is reflected in the significant main effect of cell type in N/C ($F_{(2, 772)}$ = 7.966, p<0.001), N/P ($F_{(2, 772)}$ = 46.492, p<0.001) and P/C ratios ($F_{(2, 772)}$ = 23.831, p<0.001). There were also significant differences in the simple main effects between individual genotypes for all three ratios (all p<0.017), with the exception of between Hdh$^{Q7/150}$ and Hdh$^{Q150/150}$ cells in the N/C ratio; this suggests that although there may be a gene dosage effect in the localisation of HTT as measured by N/P and P/C ratios, the increased nuclear localisation is a dominant effect of the expanded polyQ.

There was a main effect of EGF stimulation in the N/C ratio ($F_{(3, 772)}$ = 22.779, p<0.001), however there was no interaction with genotype. This is due to all three genotypes exhibiting a significant increase in nuclear HTT and a reduction in cytoplasmic HTT (Hdh$^{Q7/7}$ (p=0.001), Hdh$^{Q7/150}$ (p=0.005) and Hdh$^{Q150/150}$ (p<0.001)) by 30 minutes of EGF stimulation. There was also a significant main effect of EGF stimulation in the N/P ratio ($F_{(3, 772)}$ = 23.961, p<0.001), and a significant interaction with genotype ($F_{(6, 772)}$ = 2.717, p=0.013). Post-hoc Tukey tests revealed that this is due to differential patterns of HTT localisation following EGF stimulation in the N/P ratio; at 5 minutes of stimulation, there was a significant reduction of nuclear HTT in Hdh$^{Q7/7}$ cells (p=0.031), as has been observed previously following EGF stimulation (Sections 3.3.5 & 6.2.2.1). In contrast, this does not occur in cells carrying mHTT, but there is a significant increase in nuclear HTT compared to the perinucleus by 30 minutes in both Hdh$^{Q7/150}$ and Hdh$^{Q150/150}$ cells. Finally, despite a significant main effect of EGF stimulation ($F_{(3, 772)}$ = 3.02, p=0.029) and a significant EGF x genotype interaction ($F_{(6, 772)}$ = 2.296, p=0.033) in the P/C ratio, there were no significant differences between individual time points for any genotype when analysed with post-hoc Tukey tests, suggesting that in response to EGF stimulation, translocation occurs primarily between nuclear and perinuclear regions.
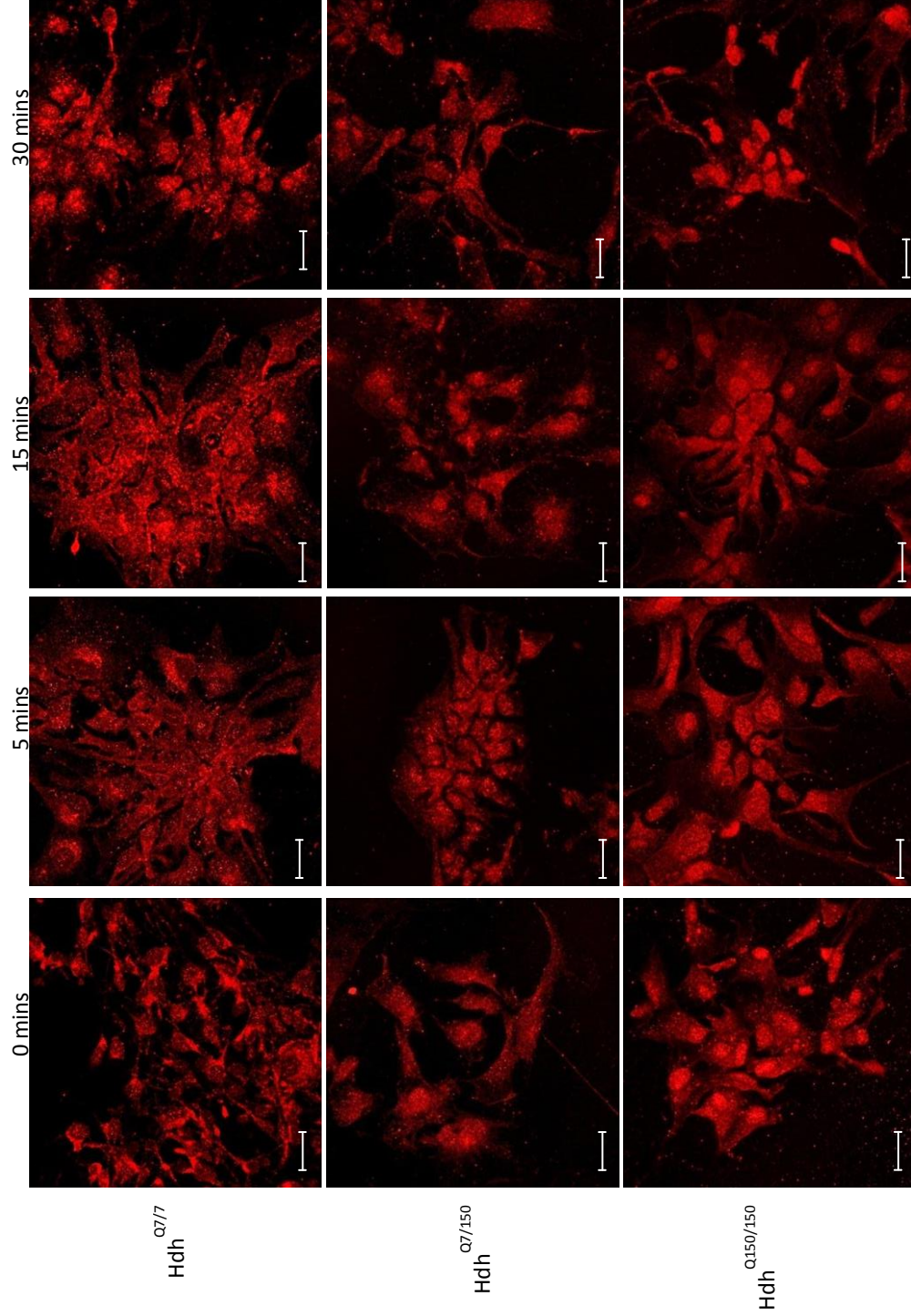
Figure 6.10 Subcellular localisation of an N-terminal epitope of HTT and mHTT in Hdh$^{Q7/7}$, Hdh$^{Q7/150}$ and Hdh$^{Q111/150}$ E14 primary striatal cell cultures. Cells were fixed following 0, 5, 15 and 30 minutes of stimulation with 100ng/ml EGF, labelled with Ab109115 against amino acids 1-30 of HTT, then analysed by confocal microscopy (see Sections 2.2.1.8 and 2.2.1.9 for further details). Scale bar = 20µm
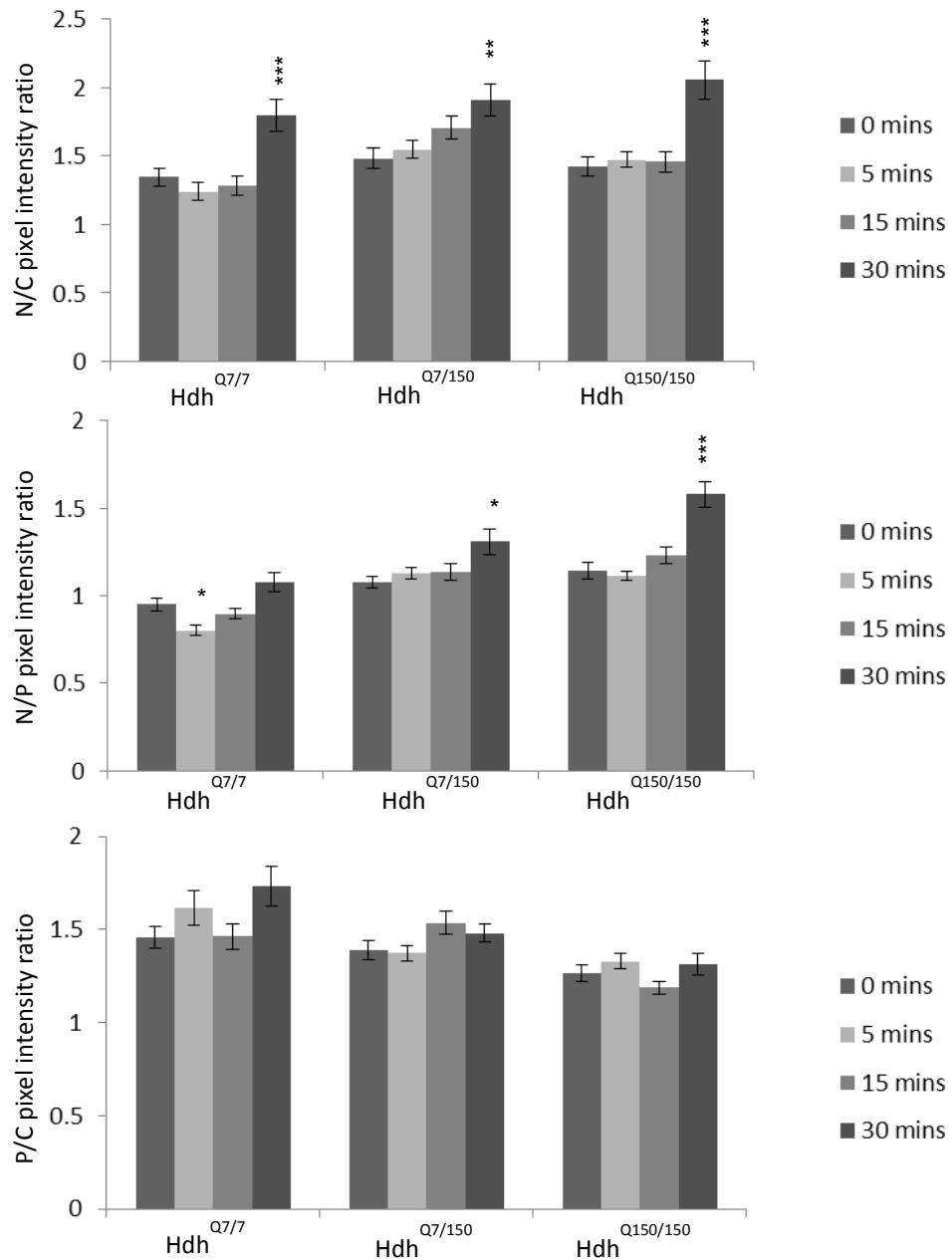
Figure 6.11 Quantitative analysis of immunofluorescence images in Figure 6.10. Nuclear/Cytoplasmic (N/C), Nuclear/Perinuclear (N/P) and Perinuclear/Cytoplasmic (P/C) mean pixel intensity ratios for Hdh$^{Q7/7}$, Hdh$^{Q7/150}$ and Hdh$^{Q111/150}$ primary embryonic striatal cells following 0, 5, 15 and 30 minutes of stimulation with 100ng/ml EGF. Mean pixel intensities were calculated from confocal microscopy images using GNU Image Manipulator (further details of the analysis can be found in Section 2.2.1.10). All images were randomised and analysed blind to genotype and length of time stimulated with EGF. Each condition consisted of 1 confocal microscopy image taken from 4-5 separate embryos of each genotype. A two-way ANOVA was carried out for main effects analysis, followed by planned one way ANOVAs and post-hoc Tukey tests. Error bars = SEM

* p<0.05   ** p<0.01   *** p<0.001

6.3.2.2 Mab2166

In accordance with previous observations (Sections 3.3.4.3 & 6.2.2.2), Mab2166 labels primarily a perinuclear epitope of HTT in Hdh^{Q150} primary cell lines, however in contrast to labelling with Ab109115 in Section 6.3.2.1, there was increased nuclear localisation of this HTT epitope in $Hdh^{Q150/150}$ cells only (Figures 6.12 & 6.13). Accordingly, there was a significant main effect of genotype in the N/C ratio (F (2, 699) = 14.106, p<0.001), and simple main effects suggest a trend towards differential HTT localisation between $Hdh^{Q7/7}$ and $Hdh^{Q7/150}$ cells (p=0.053), but both $Hdh^{Q7/7}$ and $Hdh^{Q7/150}$, and $Hdh^{Q7/150}$ and $Hdh^{Q150/150}$ cells were significantly different from each other (p=0.011 & p<0.001, respectively). However, although there was no main effect of EGF stimulation, there was a significant interaction with genotype (F (6, 699) = 3.565, p=0.002). Post-hoc Tukey tests indicate that this was due to a significant reduction in nuclear HTT in $Hdh^{Q7/7}$ cells at 15 minutes of EGF stimulation (p=0.013), but no effects in the other two genotypes, suggesting a suppressed response in these cells due to mHTT. An overlay of both Mab2166 and Ab109115 can be found in Figure 6.14, where the increased nuclear localisation of the N-terminal epitope detected by Ab109115 is particularly evident in comparison to the primarily perinuclear Mab2166.

There was a significant main effect of genotype (F (2, 699) = 50.882, p<0.001), EGF stimulation (F (3, 699) = 3.337, p=0.019), and a significant interaction between the two (F (6, 699) = 4.872, p<0.001) for the N/P ratio. Simple main effects analysis showed that all three genotypes were significantly different to each other (all p<0.04). There was a small reduction in the N/P ratio for $Hdh^{Q7/7}$ cells at 30 minutes from 5 minutes of EGF stimulation (p=0.025), but interestingly, the most significant effects were observed in $Hdh^{Q7/150}$ cells; there was a significant increase in the N/P ratio at 5 minutes (p=0.018) and again at 30 minutes (p=0.002), although this appeared to be due to a reduction in perinuclear intensity rather than an increase in nuclear HTT. Finally, there was a significant effect of genotype for the P/C ratio (F (2, 699) = 4.211, p=0.015), although there was only a significant difference between $Hdh^{Q7/7}$ and $Hdh^{Q150/150}$ cells when looking at simple main effects, suggesting a gene dosage effect. There was no significant effect of EGF stimulation, but there was a significant interaction with genotype (F (6, 669) = 2.266, p=0.036); however post-hoc analyses do

not identify any individual significant differences in the P/C over time in any of the three genotypes.

6.3.3 Supporting HTT localisation results using additional N-terminal antibodies, Ab675 and N17

A selection of Hdh^{Q150} primary cells were immunostained with two antibodies raised against amino acids 1-17 of HTT in order to compare the pattern of localisation in response to EGF stimulation with previous observations (Sections 3.3.3.3, 6.2.3 & Appendix II). Quantitative analysis could not be carried out for reasons described previously (Section 6.2.3).

The localisation of HTT epitopes detected by Ab675 can be found in Appendix VI. In comparison to previous observations when visualising HTT using the N17 antibody (Appendix II & 6.2.3), there is a slight reduction the nuclear epitope of HTT detected by N17 in both Hdh$^{Q7/150}$ and Hdh$^{Q150/150}$ cells at 30 minutes of stimulation (Figure 6.15). However, there is no apparent effect in Hdh$^{Q7/7}$ cells, which is a pattern that is more comparable to the previous data. In this case, detection by N17 presents with a spotted signal in these images, however as there is no consistent pattern of their localisation, and they are apparent in both the cell body and extracellular space, it is most likely that these are an artefact of non-specific antibody binding, possibly due to minor variations in cell fixation or due to re-use of the primary antibody over several samples.
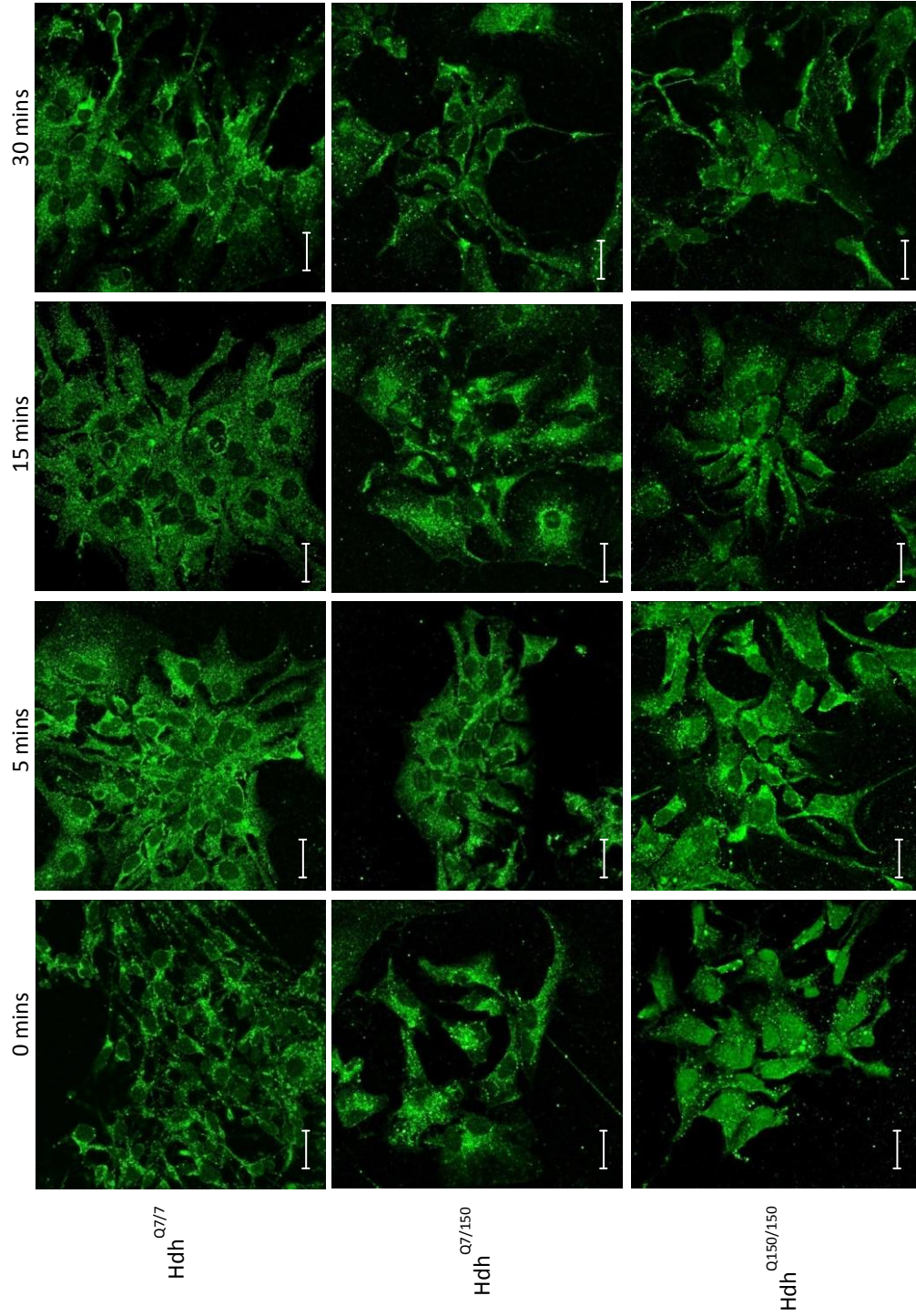
Figure 6.12 Subcellular localisation of an N-terminal epitope of HTT and mHTT in Hdh$^{Q7/7}$, Hdh$^{Q7/150}$ and Hdh$^{Q150/150}$ E14 primary striatal cell cultures. Cells were fixed following 0, 5, 15 and 30 minutes of stimulation with 100ng/ml EGF, labelled with Mab2166 against amino acids 181-810 of HTT, then analysed by confocal microscopy (see Sections 2.2.1.8 and 2.2.1.9 for further details). Scale bar = 20μm
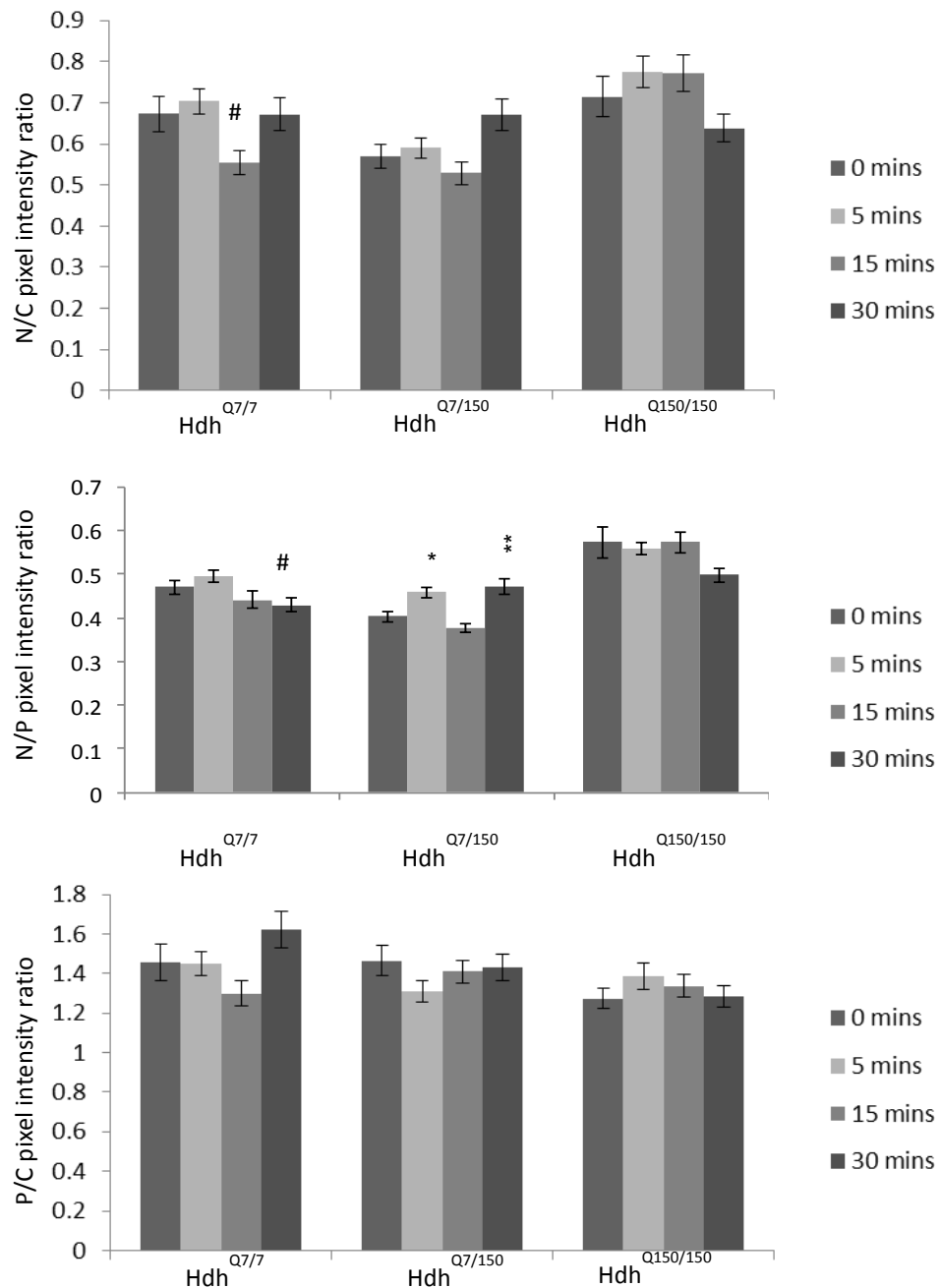
Figure 6.13 Quantitative analysis of immunofluorescence images in Figure 6.12. Nuclear/Cytoplasmic (N/C), Nuclear/Perinuclear (N/P) and Perinuclear/Cytoplasmic (P/C) mean pixel intensity ratios for $Hdh^{Q7/7}$, $Hdh^{Q7/150}$ and $Hdh^{Q150/150}$ primary embryonic striatal cells following 0, 5, 15 and 30 minutes of stimulation with 100ng/ml EGF. Mean pixel intensities were calculated from confocal microscopy images using GNU Image Manipulator (further details of the analysis can be found in Section 2.2.1.10). All images were randomised and analysed blind to genotype and length of time stimulated with EGF. Each condition consisted of 1 confocal microscopy images taken from 4-5 separate coverslips. A two-way ANOVA was carried out for main effects analysis, followed by planned one way ANOVAs and post-hoc Tukey tests. Error bars = SEM

* $p < 0.05$ ** $p < 0.01$ *** $p < 0.001$

Figure 6.14 Overlay of Ab109115 (Figure 6.10) and Mab2166 (Figure 6.12) in $Hdh^{Q7/7}$, $Hdh^{Q7/111}$ and $Hdh^{Q111/111}$ E14 primary striatal cell cultures following 0, 5, 15 and 30 minutes of stimulation with 100ng/ml EGF. Scale bar = 20μm
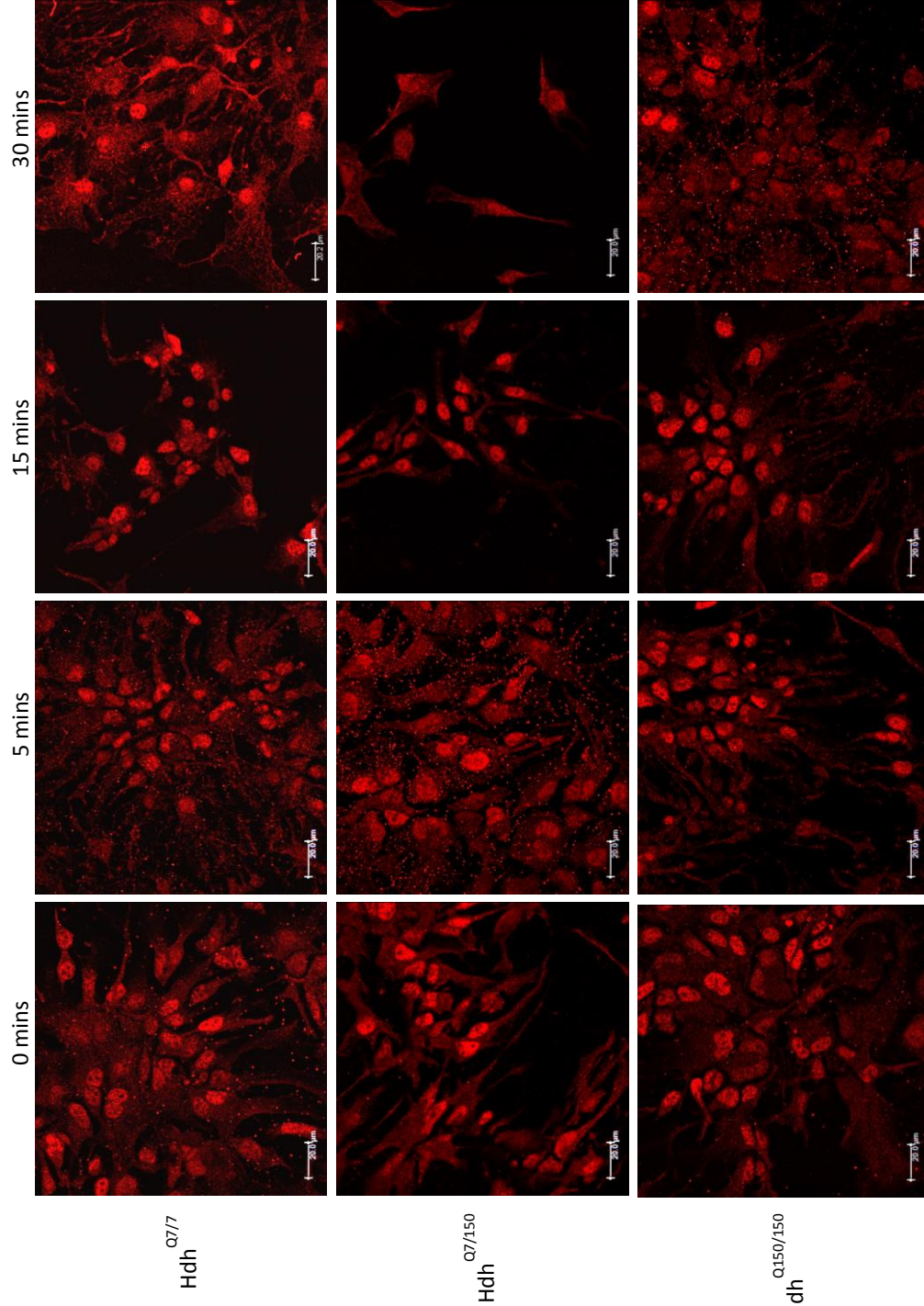
Figure 6.15 Subcellular localisation of an N-terminal epitope of HTT and mHTT in Hdh$^{Q7/7}$, Hdh$^{Q7/150}$ and Hdh$^{Q150/150}$ E14 primary striatal cell cultures. Cells were fixed following 0, 5, 15 and 30 minutes of stimulation with 100ng/ml EGF, labelled with N17 against amino acids 1-17 of HTT, then analysed by confocal microscopy (see Sections 2.2.1.8 and 2.2.1.9 for further details). Scale bar = 20μm

6.4 The localisation of a double phosphorylated epitope of HTT in response to EGF stimulation in Hdh^{Q111} and Hdh^{Q150} primary cells

In order to determine the effect of EGF stimulation on the localisation of phosphorylated HTT epitopes, primary E14 striatal cultures from Hdh^{Q111} and Hdh^{Q150} models were immunostained with the N17 s1316p antibody (see Table 2.1 and Section 3.4.3 for further details). The initial single anti-phosphorylated S13p and double anti-phosphorylated s1316p HTT antibodies were not available in order to try and replicate the findings from immortalised striatal cell cultures (Sections 3.4.1.3 &3.4.2.3).

> 6.4.1 The localisation of HTT phosphorylated on S13 and S16 in Hdh^{Q111} primary cell cultures.

In Hdh$^{Q7/7}$ cells, phosphorylated HTT is primarily cytoplasmic, whereas in Hdh$^{Q7/111}$ cells there is an increased intensity of nuclear staining, and Hdh$^{Q111/111}$ cells have a strong perinuclear signal (Figures 6.16 & 6.17), which is a similar pattern of localisation as seen in the immortalised striatal cell lines (Section 3.4.3). There is also a strong detection signal in the cell processes and at the plasma membrane; this also occurred in the *StHdh^{Q111}* cells when using the same antibody (Section 3.4.3), although it was not apparent to the same extent as in primary cell lines.

There was a significant main effect of genotype in the N/C (F (2, 415) = 11.794, p<0.001), N/P (F (2, 415) = 11.544, p<0.001,) and P/C ratios (F (2, 415) = 5.437, p=0.005). However, although there was a significant simple main effect between all three individual genotypes in the N/C ratio (all p<0.001), for the N/P and P/C ratios, the difference between Hdh$^{Q7/111}$ and Hdh$^{Q111/111}$ cells was not significant, suggesting a dominant mutant gene effect. There was a significant main effect of EGF stimulation on the N/C ratio (F (3, 415) = 10.795, p<0.001) and a significant interaction with genotype (F (6, 415) = 7.87, p<0.001), which was due to an increase in nuclear HTT phosphorylated on S13 and S16 in Hdh$^{Q7/7}$ cells at 5 minutes (p<0.001) and 15 minutes (p<0.001) of EGF stimulation; this increase in nuclear S1316p HTT was also observed in immortalised striatal *StHdh$^{Q7/7}$* cells (Section 3.4.3), although at a later time point. In contrast to the *StHdh^{Q111}* cell lines, there was no effect of EGF stimulation on the N/C ratio in Hdh$^{Q7/111}$ cells. However, there was a significant increase in nuclear

phosphorylated HTT in Hdh$^{Q111/111}$ cells from 5 minutes of EGF stimulation (p=0.005), which persisted for up to 30 minutes of EGF stimulation (p=0.002); this was not observed in immortalised cell lines.

The N/P ratio showed the same pattern of localisation as the N/C ratio; there was a significant main effect of EGF stimulation (F (3, 415) = 11.276, p<0.001) and a significant interaction with genotype (F (6, 415) = 9.452, p<0.001). This was due to the same increase in nuclear phosphorylated HTT in Hdh$^{Q7/7}$ cells detected in the N/C ratio at 5 (p=0.001) and 15 minutes (p<0.001). Again, there was no effect of EGF stimulation in Hdh$^{Q7/111}$ cells, but there was a significant increase in Hdh$^{Q111/111}$ cells at 5 (p=0.001), 15 (p<0.001) and 30 minutes (p=0.002) of EGF stimulation. Finally, there was no effect of EGF on the P/C ratio, or an interaction with genotypes, and there were no significant differences between each genotype at individual time points.
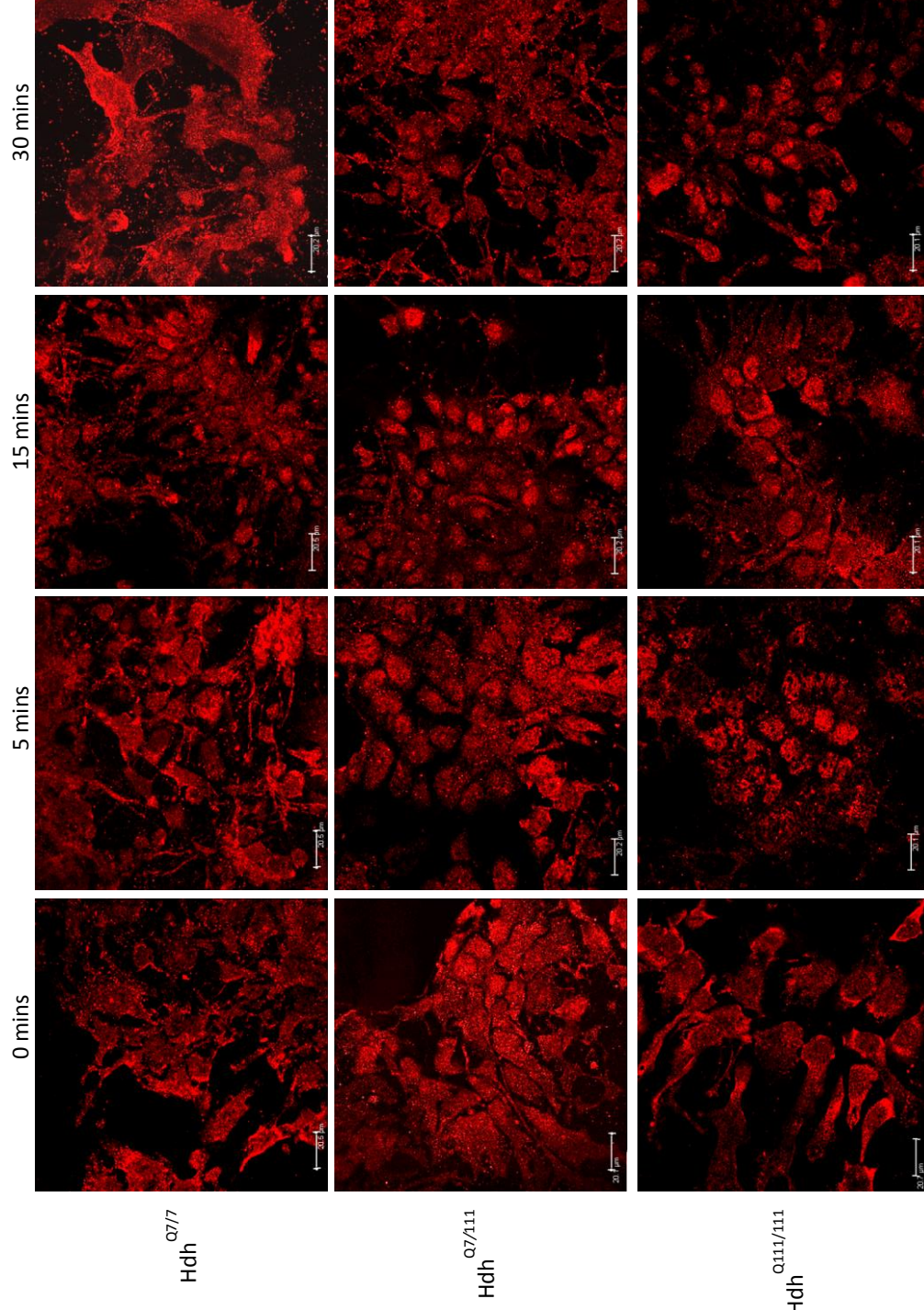
Figure 6.16 Subcellular localisation of an N-terminal epitope of HTT and mHTT phosphorylated on serines 13 and 16 in Hdh[Q7/7], Hdh[Q7/111] and Hdh[Q111/111] cell lines. Cells were fixed following 0, 5, 15 and 30 minutes of stimulation with 100ng/ml EGF, labelled with N17 s1316p against amino acids 1-17of HTT with phosphorylation on S13 and S16, then analysed by confocal microscopy (see Sections 2.2.1.8 and 2.2.1.9 for further details). Scale bar = 20µm
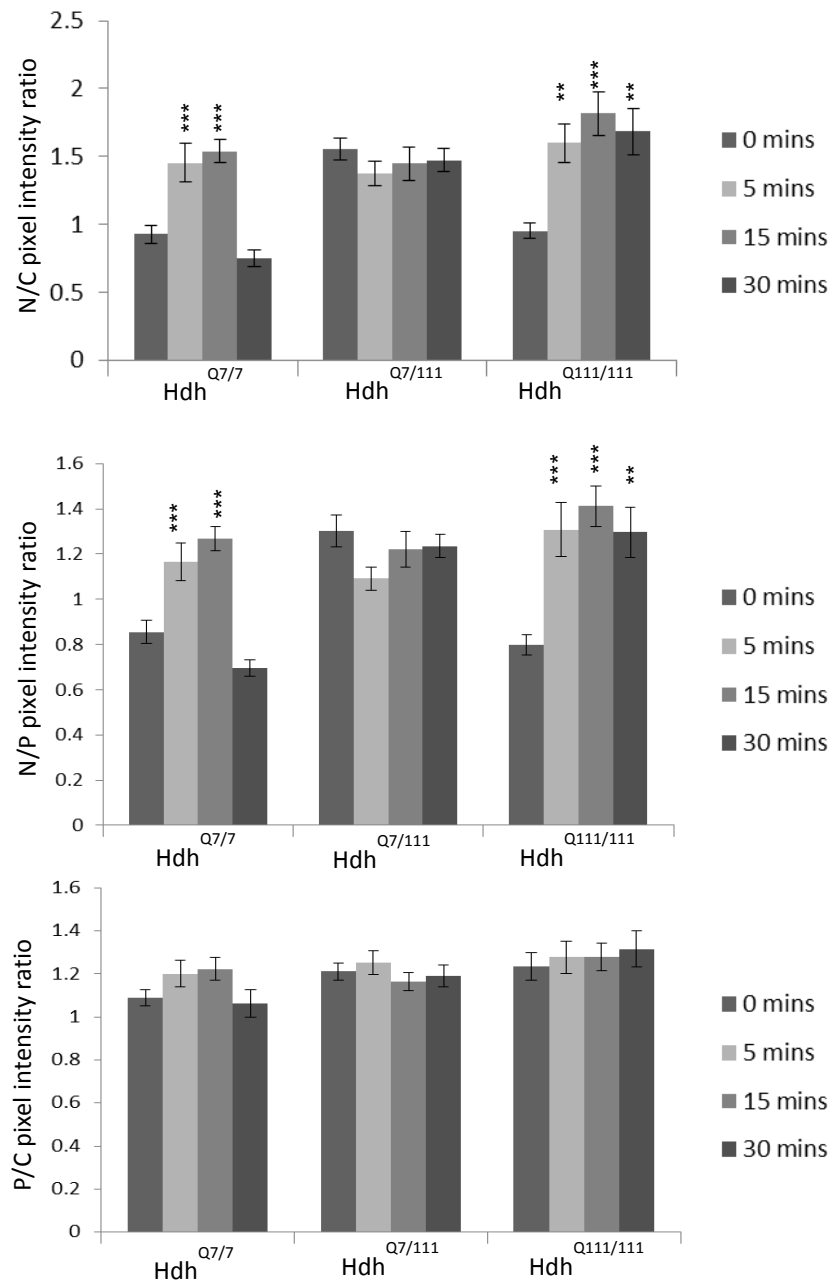
Figure 6.17 Quantitative analysis of immunofluorescence images in Figure 6.16. Nuclear/Cytoplasmic (N/C), Nuclear/Perinuclear (N/P) and Perinuclear/Cytoplasmic (P/C) mean pixel intensity ratios for $Hdh^{Q7/7}$, $Hdh^{Q7/111}$ and $Hdh^{Q111/111}$ primary embryonic striatal cells following 0, 5, 15 and 30 minutes of stimulation with 100ng/ml EGF. Mean pixel intensities were calculated from confocal microscopy images using GNU Image Manipulator (further details of the analysis can be found in Section 2.2.1.10). All images were randomised and analysed blind to genotype and length of time stimulated with EGF. Each condition consisted of 1 confocal microscopy images taken from 4-5 separate coverslips. A two-way ANOVA was carried out for main effects analysis, followed by planned one way ANOVAs and post-hoc Tukey tests. Error bars = SEM

* p<0.05   ** p<0.01   *** p<0.001

6.4.2 The localisation of HTT phosphorylated on S13 and S16 in Hdh^{Q150} primary cell cultures

The pattern of localisation of phosphorylated HTT epitopes in Hdh^{Q150} primary cultures differs substantially from Hdh^{Q111} cultures, and appeared to be considerably more variable (Figures 6.18 & 6.19). Initially, the localisation of phosphorylated HTT was more nuclear in Hdh$^{Q7/7}$ cells than it was previously in the Hdh^{Q111} model (Section 6.4.1). However, there is still increased detection of this epitope in the nucleus with mHTT load. In concordance with this, there was a significant effect of genotype in the N/C (F (2, 462) = 5.276, p=0.005), N/P (F (2, 462) = 2.987, p=0.05), and P/C ratios (F (2, 462) = 4.171, p=0.016). There was no effect of EGF in the N/C ratio, however there was a significant interaction with genotype (F (6, 462) = 2.952, p=0.008), which was a result of a significant reduction in the N/C ratio in Hdh$^{Q7/150}$ cells at 15 minutes of stimulation (p=0.045), compared with a large increase in the ratio in Hdh$^{Q150/Q150}$ at 30 minutes (p=0.006), and no effect in Hdh$^{Q7/7}$ cells.

In contrast, there was a significant main effect of EGF in the N/P ratio (F (3, 462) = 4.072, p=0.007), as well as a significant interaction with genotype (F (6, 462) = 3.113, p=0.005). There was a gradual increase in nuclear phosphorylated HTT in Hdh$^{Q7/7}$ cells over time, but this only reaches significance by 30 minutes of EGF stimulation (p=0.045), whereas there was no effect in Hdh$^{Q7/150}$ cells, and a significant increase in Hdh$^{Q150/150}$ cultures by only 5 minutes of EGF stimulation (p=0.013). This increase appears to be sustained for the full 30 minutes of stimulation, but does not maintain significance from baseline.

For the P/C ratio, there is a significant main effect of EGF stimulation (F (3, 462) = 2.864, p=0.036), but there is no significant interaction with genotype. Interestingly, there is again no significant effect in Hdh$^{Q7/7}$ cells, and there are opposing effects in Hdh$^{Q7/150}$ and Hdh$^{Q150/150}$ cells; there is a reduction in the P/C ratio in Hdh$^{Q7/150}$ cells at 15 minutes (p=0.036) and an increase in Hdh$^{Q150/150}$ cells at 30 minutes (p=0.018).
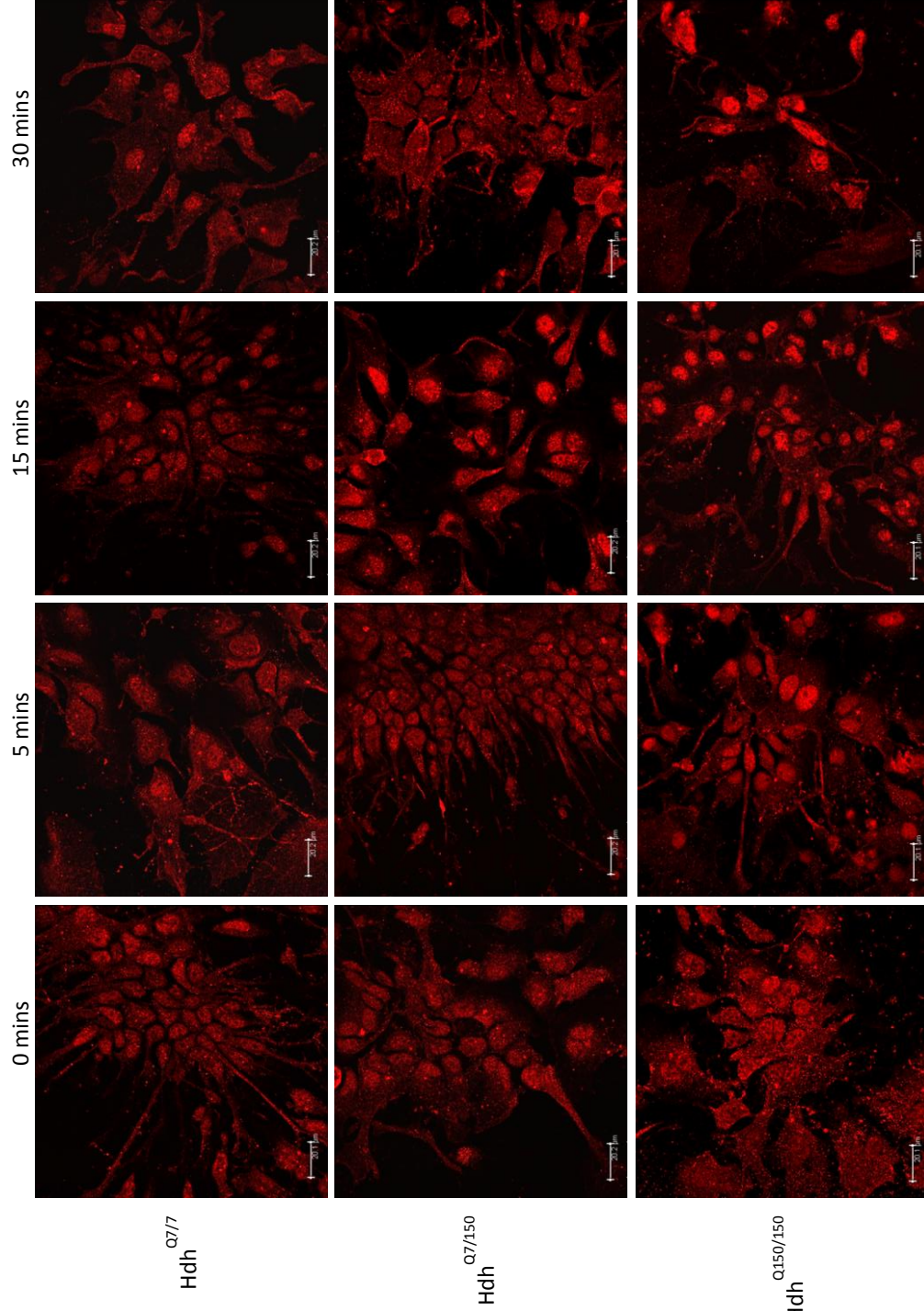
Figure 6.18 Subcellular localisation of an N-terminal epitope of HTT and mHTT phosphorylated on serines 13 and 16 in Hdh[Q7/7], Hdh[Q7/150] and Hdh[Q150/150] cell lines . Cells were fixed following 0, 5, 15 and 30 minutes of stimulation with 100ng/ml EGF, labelled with N17 s1316p against amino acids 1-17of HTT with phosphorylation on S13 and S16, then analysed by confocal microscopy (see Sections 2.2.1.8 and 2.2.1.9 for further details). Scale bar = 20µm
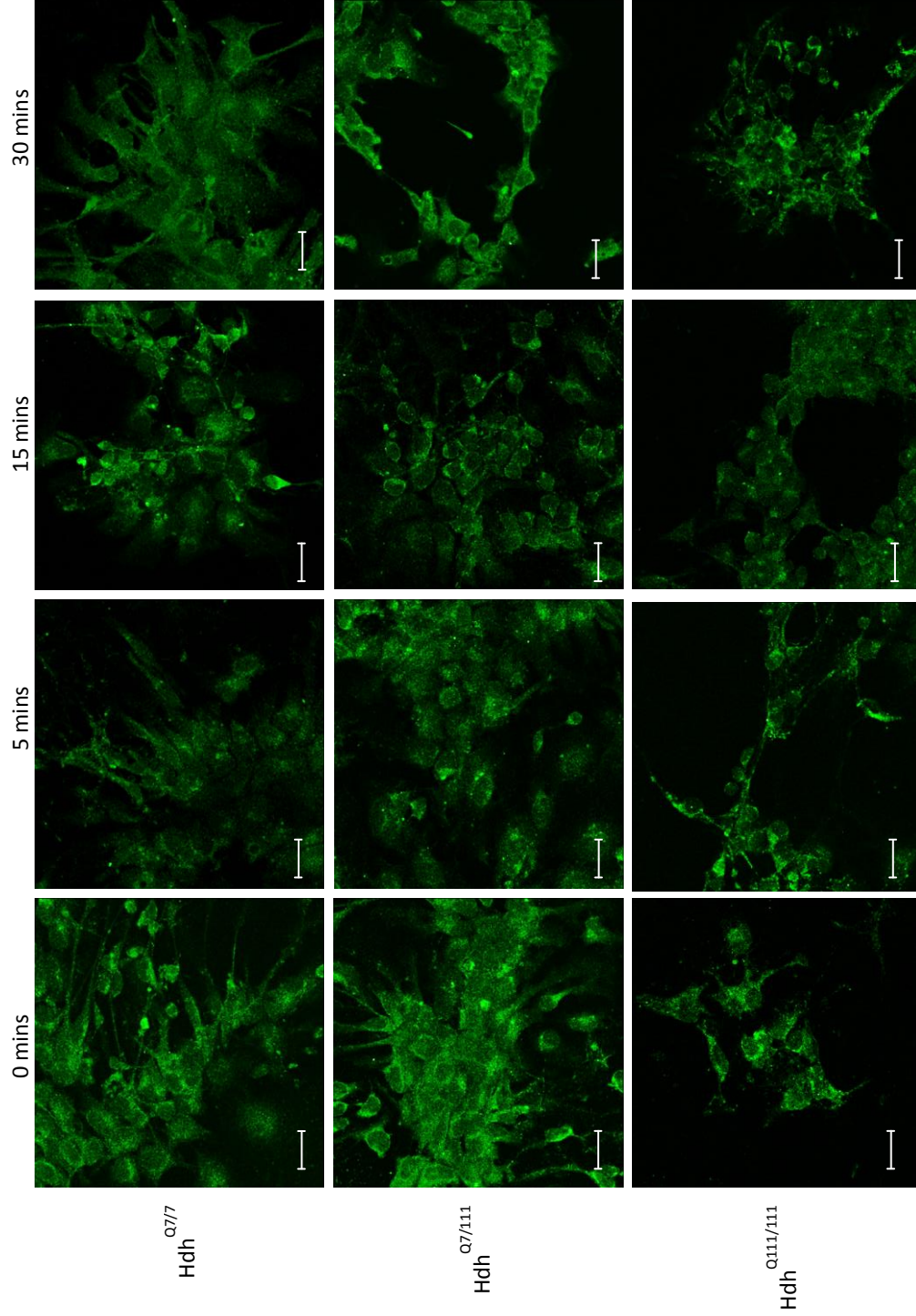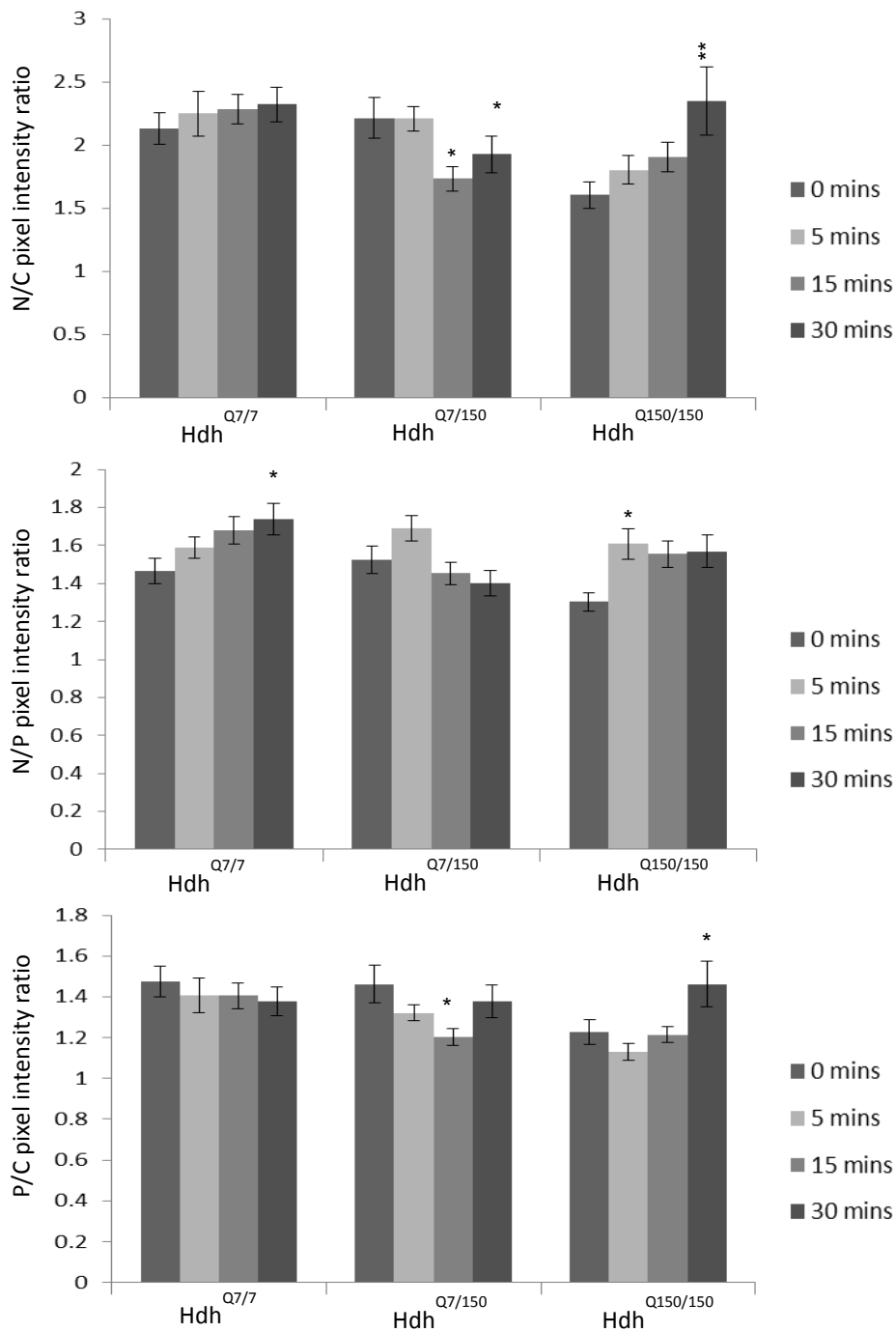
Figure 6.19 Quantitative analysis of immunofluorescence images in Figure 6.18. Nuclear/Cytoplasmic (N/C), Nuclear/Perinuclear (N/P) and Perinuclear/Cytoplasmic (P/C) mean pixel intensity ratios for Hdh$^{Q7/7}$, Hdh$^{Q7/150}$ and Hdh$^{Q150/150}$ primary embryonic striatal cells following 0, 5, 15 and 30 minutes of stimulation with 100ng/ml EGF. Mean pixel intensities were calculated from confocal microscopy images using GNU Image Manipulator (further details of the analysis can be found in Section 2.2.1.10). All images were randomised and analysed blind to genotype and length of time stimulated with EGF. Each condition consisted of 1 confocal microscopy images taken from 4-5 separate coverslips. A two-way ANOVA was carried out for main effects analysis, followed by planned one way ANOVAs and post-hoc Tukey tests. Error bars = SEM

* p<0.05   ** p<0.01   *** p<0.001

6.5 Transcriptional dysregulation in primary embryonic striatal cell cultures

In order to determine if the transcriptional profile of the *StHdh*^{Q111} cell model is comparable to primary cell models, the expression of a selection of differentially expressed genes that were identified in Chapter 5 were also investigated in primary E14 striatal cell cultures from Hdh^{Q111} and Hdh^{Q150} mouse models.

6.5.1 Transcriptional dysregulation in Hdh^{Q111} primary striatal cells

6.5.1.1 Genes with increased expression fold changes in *StHdh*$^{Q7/7}$ cells following EGF stimulation

Of the list of genes that had a larger transcriptional response following EGF stimulation in *StHdh*$^{Q7/7}$ cells, four were investigated in Hdh^{Q111} mouse model primary cells; a summary of the expression fold changes of these genes in response to EGF are presented in Table 6.2, and the full figures can be found in Appendix VII. In accordance with the effect seen in *StHdh*$^{Q7/7}$ cells (Section 5.2.3.2c)*,* there was a significant effect of EGF stimulation on *Fgf2* expression (F (1, 24) = 18.514, p<0.001), although this did not retain significance following post-hoc analysis .There was a trend towards an enhanced *Fgf2* expression response in Hdh$^{Q7/7}$ cells compared to both Hdh$^{Q7/111}$ and Hdh$^{Q111/111}$, as the increase in expression just failed to reach significance in Hdh$^{Q7/7}$ cells (p=0.061), but the magnitude of response was smaller in both Hdh$^{Q7/111}$ and Hdh$^{Q111/111}$ cells. In contrast to the immortalised cell model, where EGF stimulation elicited a significant response of *Myc* expression in *StHdh*$^{Q7/7}$ cells only, there was a significant effect of EGF stimulation on the expression of *Myc* in all three primary cell genotypes*;* Hdh$^{Q7/7}$ (p=0.003), Hdh$^{Q7/111}$ (p=0.009) and Hdh$^{Q111/111}$ cells (p=0.002). There was a significant main effect of genotype (F (2,24) = 3.561, p=0.044), suggesting that there was a trend towards an increased response in Hdh$^{Q7/111}$ and Hdh$^{Q111/111}$ cells, but this did not withstand post-hoc testing.

There was a significant effect of both genotype (F (2, 24) = 8.251, p=0.002) and EGF stimulation (F (1, 24) = 10.719, p=0.003) on the expression of *Smad7,* as well as a significant interaction between the two (F (2, 24) = 5.835, p=0.009). Although there was no increase in *Smad7* expression following EGF stimulation in Hdh$^{Q7/7}$ cells as there

was in *StHdh*^{Q7/7} cells (Section 5.2.3.2c), the expression of *Smad7* in Hdh^{Q111/111} cells was significantly lower than both Hdh^{Q7/7} (p<0.001) and Hdh^{Q7/111} cells (p=0.008) at baseline. However, unlike the pattern observed in *StHdh*^{Q111} cells, there was a significant increase in *Smad7* expression in Hdh^{Q111/111} cells following EGF stimulation (p=0.001), although this did not bring *Smad7* expression up to the same level as in Hdh^{Q7/7} and Hdh^{Q7/111} cells. Despite the lack of response to EGF stimulation, the suppressed expression of *Smad7* in the presence of mHTT in Hdh^{Q111/111} cells is consistent with reduced expression also observed in the *StHdh*^{Q111} cell model. There was no effect of either genotype or EGF stimulation on the expression of *Sox9*.

6.5.1.2 Genes with larger expression fold changes in *StHdh*^{Q111/111} cells following EGF stimulation

Four genes from the list with a larger expression change in *StHdh*^{Q111/111} cells following EGF stimulation (Section 5.2.3.2c) were investigated in primary cells from the Hdh^{Q111} mouse model; a summary of the expression fold changes of these genes in response to EGF are presented in Table 6.2, and the full figures can be found in Appendix VII. All three genotypes exhibited a significant increase in the expression of *Atf3* in response to EGF stimulation (all p<0.001), and there was a trend towards higher expression in both Hdh^{Q7/111} and Hdh^{Q111/111} cells compared to Hdh^{Q7/7} cells, although this did not reach significance. However, when calculating the fold change from each individual genotypic baseline, the expression fold change of *Atf3* in Hdh^{Q111/111} cells was twice as large as in Hdh^{Q7/7} cells following EGF stimulation, suggesting a trend towards a larger response in mutant cells.

Although there was no effect of EGF stimulation on Hdh^{Q111} cells, there was a significant effect of genotype ($F_{(2, 24)} = 5.021$, p=0.015) on *Id3* expression, and a significant interaction with EGF stimulation ($F_{(2, 24)} = 4.74$, p=0.018). The baseline level of *Id3* expression was significantly lower in Hdh^{Q111/111} cells compared to both Hdh^{Q7/7} (p=0.005) and Hdh^{Q7/111} cells (p=0.031). This is in contrast to the large reduction in *Id3* expression following EGF stimulation in *StHdh*^{Q111/111} cells (Section 5.2.3.2c), although is consistent with the phenotype of suppressed *Id3* expression in the presence of mHTT.

The expression of *Egr1* was significantly increased in all three genotypes following EGF stimulation (all p<0.001), which, similar to *Atf3*, resulted in a trend towards higher expression in Hdh$^{Q111/111}$ cells, although this did not reach significance. Similarly, EGF stimulation significantly increased *Fosl1* expression in all three genotypes (all p<0.001), but despite a trend towards a stronger transcriptional effect in both Hdh$^{Q7/111}$ and Hdh$^{Q111/111}$ cells, this was not significantly different to Hdh$^{Q7/7}$ *Fosl1* expression.

The expression of *Gadd45g*, *Cdc42ep3* and *Rasa1* were also examined in Hdh^{Q111} primary cells, as in the *StHdh^{Q111}* cell model these exhibited changes in expression following EGF stimulation in *StHdh$^{Q111/111}$* cells only (Section 5.2.3.2c). However, there was no significant effect of either genotype or EGF stimulation on the expression of any of these genes.

		Fold change following EGF stimulation		
		Hdh$^{Q7/7}$	Hdh$^{Q7/111}$	Hdh$^{Q111/111}$
A	*Fgf2*	2.17	1.56	1.18
	Myc	1.61 **	2.43 **	2 **
	Smad7	1.08	0.88	1.38 **
	Sox9	0.85	1.27	0.88
B	*Atf3*	14 ***	20 ***	30 ***
	Id3	0.31	0.48	1.47
	Fosl1	42.41 ***	61.64 ***	118.93 ***
	Egr1	18.08 ***	14.95 ***	27.4 ***
C	*Gadd45g*	1.01	0.93	1.91
	Cdc42ep3	0.93	1.2	1.32
	Rasa1	1.35	0.89	0.69

Table 6.2 A summary of the qRTPCR expression fold changes of a panel of genes in Hdh^{Q111} primary embryonic striatal cells following 2 hours stimulation with 100ng/ml EGF. The genes were previously identified in Chapter 5 as being either **A.** more highly expressed in *StHdh$^{Q7/7}$* cells, **B.** with a larger expression fold change in *StHdh$^{Q111/111}$* cells or **C.** having a change in expression in *StHdh$^{Q111/111}$* cells only, following EGF stimulation. Asterisks represent a significant change in expression from 0 mins EGF stimulation. Further details can be found in Appendix VII.
** p<0.01   *** p<0.001

6.5.2 Transcriptional dysregulation in Hdh^{Q150} primary striatal cells

6.5.1.1 Genes with larger expression fold changes in *StHdh$^{Q7/7}$* cells following EGF stimulation

A summary of the expression fold changes in response to EGF for these genes, and those in the following section are presented in Table 6.3, and the full figures can be found in Appendix VIII. Similar to both *StHdh^{Q111}* and Hdh^{Q111} models, there was a significant effect of EGF stimulation on the expression of *Fgf2* (F (1, 24) = 14.822, p=0.001) although this did not withstand post-hoc analysis; however there was a trend towards a larger increase in *Fgf2* expression in Hdh$^{Q150/150}$ cells (p=0.066), which is inconsistent with previous observations (Sections 5.2.3.2c & 6.5.1.1). There was also no effect of genotype, or an interaction with EGF stimulation. Post-hoc analyses also indicated that there were no significant differences in *Fgf2* expression between individual genotypes. Similarly, there was a significant effect of EGF stimulation on the expression of *Myc* (F (1, 24) = 8.641, p=0.007) that did not withstand post-hoc testing, and no effect of genotype or a significant interaction between genotype and EGF stimulation. However, similar to the pattern of expression of *Fgf2*, there is a trend towards a larger increase in *Myc* expression in Hdh$^{Q150/150}$ cells compared to Hdh$^{Q7/7}$ cells. In addition, there was no effect of either EGF or genotype on the expression of *Smad7* or *Sox9* in the Hdh^{Q150} model.

6.5.1.2 Genes with a larger expression fold change in *StHdh$^{Q111/111}$* cells following EGF stimulation

In contrast to previous findings on the expression of *Atf3* in the immortalised *StHdh^{Q111}* cell model (Section 5.2.3.2c), but in accordance with the expression pattern in Hdh^{Q111} primary cells (Section 6.5.1.2), there was a significant effect of EGF stimulation on the expression of *Atf3*, which was significant for each individual genotype (all p<0.001). However, there was no significant effect of genotype, but there was a trend towards a larger fold change in Hdh$^{Q150/150}$ cells following EGF stimulation than in Hdh$^{Q7/7}$ cells. In contrast to the lower expression of *Id3* observed in mHTT carrying cells in the *StHdh^{Q111}* and Hdh^{Q111} models, although the relative quantification of *Id3* expression

was twice as large in Hdh$^{Q7/7}$ cells compared to Hdh$^{Q150/150}$ cells, there was no significant effect of either EGF stimulation or genotype.

Similar to the expression of *Atf3* in the Hdh^{Q150} model, there was a significant effect of EGF stimulation on the expression of *Egr1* (F (1, 24) = 194.965, p<0.001), which remained significant following post-hoc analysis (all genotypes p<0.001). However, there was no effect of genotype, or a significant interaction between genotype and EGF stimulation. Nevertheless, there was still a trend towards an increased transcriptional response in Hdh$^{Q150/150}$ cells; the fold change from baseline in Hdh$^{Q7/7}$ cells was x26, whereas the fold change for Hdh$^{Q150/150}$ cells was x45. *Fosl1* expression was also significantly increased in all three genotypes following EGF stimulation (all p<0.001), but there was still no significant effect of genotype. In contrast to *Atf3* and *Egr1* expression, there was also no indication within the raw fold change data that there was a trend towards differential expression of *Fos1* due to genotype.

In accordance with the expression of *Gadd45g*, *Cdc42ep3* and *Rasa1* in Hdh^{Q111} cells (Section 6.5.1.2), there was no significant effect of either genotype or EGF stimulation, or a significant interaction between the two in Hdh^{Q150} cells.

		Fold change following EGF stimulation		
		Hdh$^{Q7/7}$	Hdh$^{Q7/150}$	Hdh$^{Q150/150}$
A	*Fgf2*	1.66	3.86	4.41
	Myc	1.47	2.11	3.08
	Smad7	1.32	1.52	0.96
	Sox9	0.95	1.48	1.51
B	*Atf3*	24.53 ***	22.7 ***	29 ***
	Id3	0.36	0.49	1.15
	Fosl1	44.1 ***	72.89 ***	44.35 ***
	Egr1	26.4 ***	34.34 ***	45.52 ***
C	*Gadd45g*	0.82	1.51	1.91
	Cdc42ep3	0.78	1.52	1.17
	Rasa1	1.29	1.4	1.17

Table 6.3 A summary of the qRTPCR expression fold changes of a panel of genes in Hdh^{Q150} primary embryonic striatal cells following 2 hours stimulation with 100ng/ml EGF. The genes were previously identified in Chapter 5 as being either **A.** more highly expressed in *StHdh*$^{Q7/7}$ cells, **B.** with a larger expression fold change in *StHdh*$^{Q111/111}$ cells or **C.** having a change in expression in *StHdh*$^{Q111/111}$ cells only, following EGF stimulation. Asterisks represent a significant change in expression from 0 mins EGF stimulation. Further details can be found in Appendix VII
** p<0.01   *** p<0.001

6.6 Investigating the activity of kinase signalling pathways previously found to be disrupted in *StHdh*$^{Q111/111}$ cells

The phosphorylation of AKT, MEK and P38 MAPK following 10 minutes of 100ng/ml EGF stimulation was assayed by ELISA in primary striatal cells from the Hdh^{Q111} mouse model of HD, as these pathways were found to be dysregulated in the immortalised *StHdh*^{Q111} cell model (Section 4.4.1).

EGF stimulation had a significant effect on AKT1 phosphorylation (F (1, 30) = 42.062, p<0.001), as it elicited a substantial increase in the phosphorylation of AKT1 in Hdh$^{Q7/7}$ (p=0.001) and Hdh$^{Q111/111}$ cells (p<0.001), although there was no significant effect in Hdh$^{Q7/111}$ cells (see Figure 6.20). In contrast to the findings in the immortalised cell lines, there was no significant difference in the level of AKT1 phosphorylation following

EGF stimulation between Hdh$^{Q7/7}$ and Hdh$^{Q111/111}$ cells. However, due to the lack of effect in Hdh$^{Q7/111}$ cells, the level of AKT1 phosphorylation in Hdh$^{Q7/7}$ and Hdh$^{Q111/111}$ cells following EGF stimulation was significantly higher than in Hdh$^{Q7/111}$ cells following EGF stimulation (p=0.003 and p=0.004, respectively). In accordance with this, when comparing the genotypic specific differences in phosphorylation by taking into account the baseline for each genotype, Hdh$^{Q7/111}$ cells had a significantly different phosphorylation change compared to both Hdh$^{Q7/7}$ (p=0.011) and Hdh$^{Q111/111}$ cells (p=0.016), whereas there was no significant difference in the phosphorylation change between Hdh$^{Q7/7}$ and Hdh$^{Q111/111}$ cells.

There was a significant increase in MEK1 phosphorylation following EGF stimulation in all three genotypes (all p<0.001), although there were no significant differences between genotypes at baseline. Despite suppressed MEK1 phosphorylation in Hdh$^{Q7/111}$ and Hdh$^{Q111/111}$ cells following EGF stimulation, only Hdh$^{Q7/111}$ cells were significantly lower than Hdh$^{Q7/7}$ following EGF stimulation (p=0.006), but were not significantly different to Hdh$^{Q111/111}$ cells. The same pattern of significance was found when analysing the extent of MEK1 phosphorylation when taking baseline phosphorylation into account.

There was no significant effect of EGF on the phosphorylation of P38 MAPK in Hdh$^{Q7/7}$ or Hdh$^{Q7/111}$ cells, but there was a significant increase in Hdh$^{Q111/111}$ cells (p=0.019), which is the same pattern observed in the immortalised cell model (Section 4.4.1). Although the resulting level of P38 MAPK was not significantly higher than the level of phosphorylated P38 MAPK in Hdh$^{Q7/7}$ or Hdh$^{Q111/111}$ cells following EGF stimulation, when taking the baseline levels of phosphorylation into account, the change in P38 MAPK phosphorylation following EGF stimulation was significantly different in Hdh$^{Q111/111}$ cells compared to both Hdh$^{Q7/7}$ (p=0.004) and Hdh$^{Q7/111}$ cells (p=0.021).
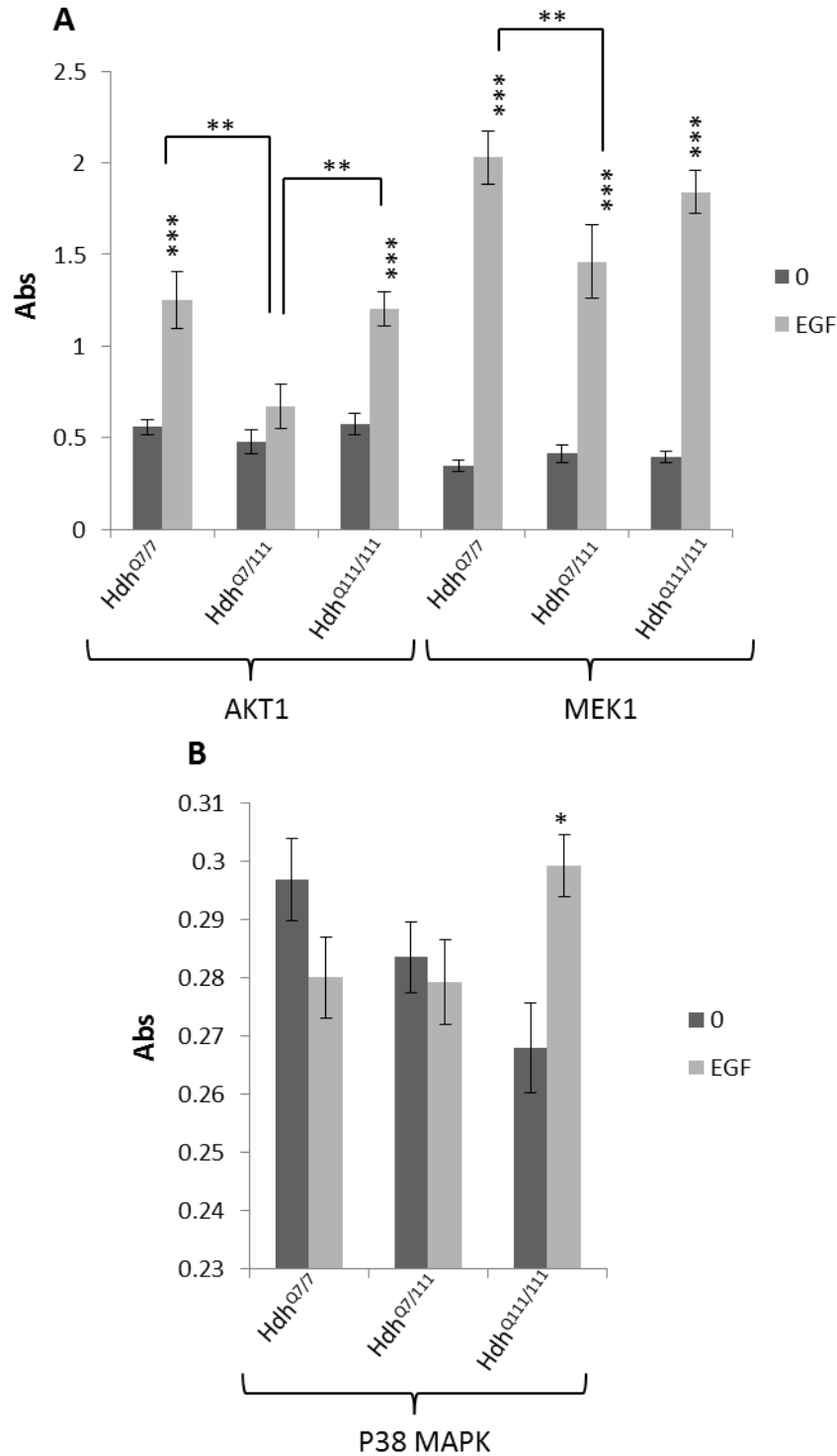
Figure 6.20 Mean absorbance (Abs) read at 450nm following a sandwich ELISA protocol in Hdh$^{Q7/7}$, Hdh$^{Q7/111}$ and Hdh$^{Q111/111}$ cells for detection of the phosphorylation of cell signalling markers **A.** AKT1 and MEK1, and **B.**P38 MAPK at 0 or 10 minutes stimulation with 100ng/ml EGF. Absorbance values were statistically analysed by two-way ANOVA for main effects, followed by a priori one-way ANOVAs to determine simple main effects, and post-hoc Tukey tests. (Error bars = SEM, Hdh$^{Q7/7}$ n = 5, Hdh$^{Q7/111}$ n = 6, Hdh$^{Q111/111}$ n = 7).

*p<0.05   **p<0.01   ***p<0.001

6.7 The expression of *Smad* genes and the phosphorylation of SMAD proteins in primary Hdh^{Q111} cells.

In order to determine if the dysregulation of the SMAD signalling pathway that was suggested to occur in the immortalised *StHdh*^{Q111} cell line (Section 5.3) was also present in primary cells from Hdh^{Q111} mice, the expression of *Smad* and *Smad*-related genes were analysed, and ELISA assays were performed in order to determine the levels of SMAD phosphorylation following TGFβ stimulation.

6.7.1 *Smad* gene expression

In contrast with the expression of *Smad* and *Smad*-related genes in *StHdh*^{Q111} cell lines, there were no significant differences in the expression of *Smad3, Smad6, Tgfβi* or *Tgfβr3* between any of the genotypes in Hdh^{Q111} primary striatal cells (Figure 6.21). There was a significant effect of EGF on the expression of *Smad6* ($F_{(1, 24)} = 18.036$, $p<0.001$) due to a reduction in *Smad6* expression following EGF stimulation. As *Smad6* is an inhibitory member of the *Smad* family, this is consistent with an increase in *Smad*-regulated activity; however, the reduction in *Smad6* expression did not withstand post-hoc testing.

Similarly, there was also a significant effect of EGF stimulation on *Tgfbi* expression ($F_{(1, 24)} = 10.389$, $p=0.004$) by eliciting an increase in expression in all three genotypes; despite this, there was no effect of EGF in *StHdh*^{Q111} cells on the expression of this gene (Section 5.3.1). However, the increase in *Tgfbi* expression did not remain significant during post-hoc testing. *Tgfbr3* expression showed a trend towards increased expression following EGF stimulation ($p=0.057$), but there were no significant differences in its expression between genotypes or following EGF stimulation.
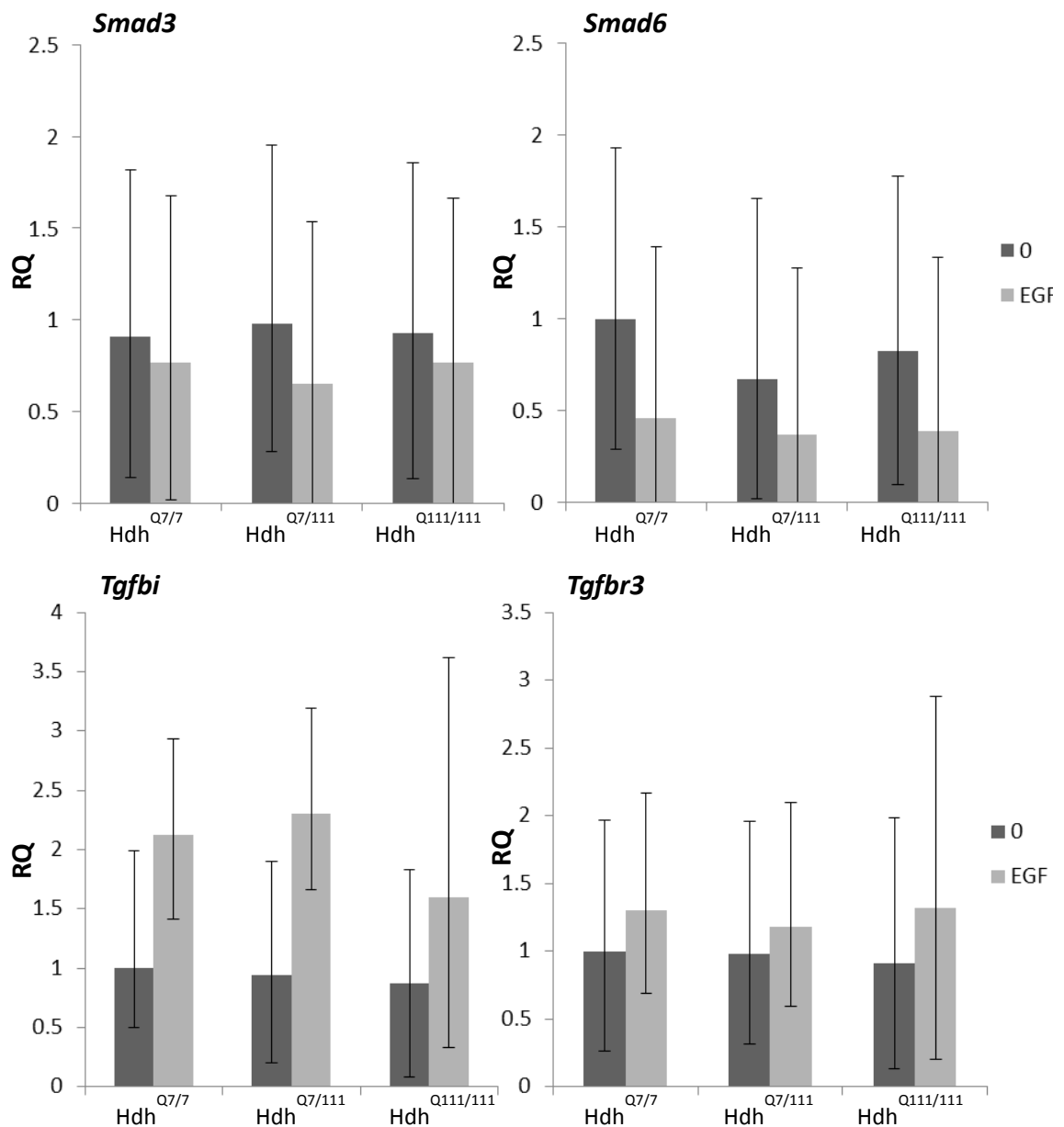
Figure 6.21 Relative Quantification (RQ) values representing the fold change in gene expression for Smad-related genes in Hdh[Q7/7], Hdh[Q7/111] and Hdh[Q111/111] primary embryonic striatal cells at 0 and 2 hours stimulation with 100ng/ml EGF. Delta cycle threshold (ΔC_t) values were analysed by two-way ANOVA and post-hoc Tukey tests. (Error bars = SEM, n=5)

6.7.2 SMAD2 activation

Due to very restricted numbers of Hdh^{Q111} mice that were available, there was not time within the duration of this project to collect substantial numbers of E14 striata for use in ELISA assays to accurately determine SMAD2 and SMAD3 phosphorylation following TGFβ stimulation in these cells. This restriction also prevented analysis of SMAD activation by western blot.

There was no significant difference in the level of total SMAD2 between genotypes, and there was no effect of EGF stimulation (Figure 6.22). However, there was a trend towards lower levels of total SMAD2 in Hdh$^{Q111/111}$ cells, but as the n was very low for both Hdh$^{Q7/7}$ and Hdh$^{Q111/111}$ cells, there would not have been enough power to detect a significant difference. There was a significant effect of TGFβ stimulation on SMAD2 phosphorylation (F $(1, 24)$ = 9.485, p=0.007), although in contrast to the immortalised *StHdh^{Q111}* cell line (Section 5.3.2.1), there was no difference in SMAD2 phosphorylation between genotypes. There was also no statistical difference in the extent of phosphorylation change following TGFβ stimulation when taking baseline phosphorylation levels into account, or in the ratio of phosphorylated SMAD2 to total SMAD2 between genotypes.
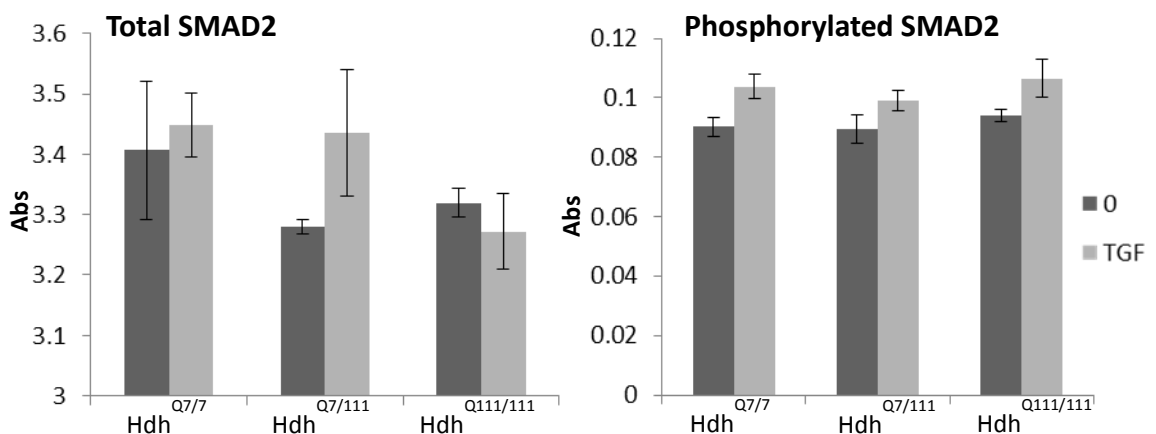
Figure 6.22 Mean absorbance (Abs) read at 450nm following a sandwich ELISA protocol in Hdh$^{Q7/7}$, Hdh$^{Q7/111}$ and Hdh$^{Q111/111}$ cells for the detection of total and phosphorylated SMAD2 following 0 and 30 minutes of 100ng/ml TGFβ stimulation. Absorbance values were statistically analysed by two-way ANOVA for main effects, followed by a priori one-way ANOVAs to determine simple main effects, and post-hoc Tukey tests. (Error bars = SEM, Hdh$^{Q7/7}$ n = 4, Hdh$^{Q7/111}$ n = 5, Hdh$^{Q111/111}$ n = 2).

6.7.3 SMAD3 activation

There was also no significant effect of either genotype or TGFβ stimulation between genotypes on the level of total SMAD3 (Figure 6.23). There was a significant effect of TGFβ stimulation on the phosphorylation of SMAD3 ($F (1, 24) = 5.196$, $p=0.037$), however this did not remain significant following post-hoc testing. There was no significant reduction in the phosphorylation of SMAD3 in Hdh$^{Q111/111}$ cells, as seen in StHdh$^{Q111/111}$ cells by ELISA assay (Section 5.3.2.2), although there was only an n=2 for Hdh$^{Q111/111}$ cells in this experiment; one sample exhibited a considerably higher phosphorylation response for SMAD3 following TGFβ, whereas the other was considerably lower, making any conclusions about SMAD3 phosphorylation in this model impossible to draw.

As expected due to the low n and non-significant results, there was also no difference in the ratio of phosphorylated to total SMAD3 between genotypes, and no difference in the extent of phosphorylation following TGFβ stimulation between genotypes.
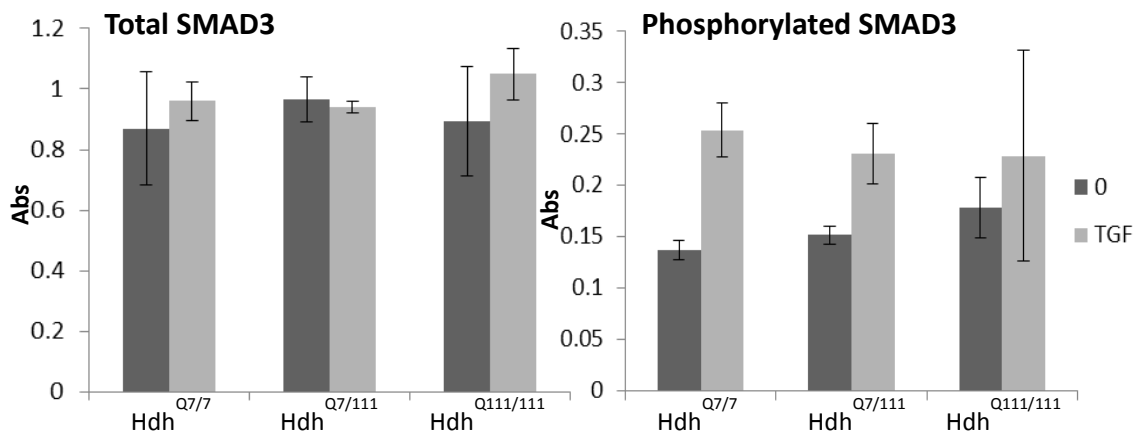
Figure 6.23 Mean absorbance (Abs) read at 450nm following a sandwich ELISA protocol in Hdh$^{Q7/7}$, Hdh$^{Q7/111}$ and Hdh$^{Q111/111}$ cells for the detection of total and phosphorylated SMAD3 following 0 and 30 minutes of 100ng/ml TGFβ stimulation. Absorbance values were statistically analysed by two-way ANOVA for main effects, followed by a priori one-way ANOVAs to determine simple main effects, and post-hoc Tukey tests. (Error bars = SEM, Hdh$^{Q7/7}$ n = 4, Hdh$^{Q7/111}$ n = 5, Hdh$^{Q111/111}$ n = 2).

6.8 Discussion

We have used primary embryonic E14 striatal cells from both the Hdh^{Q111} and Hdh^{Q150} mouse models of HD to repeat a panel of assays that were initially carried out in immortalised *StHdh*^{Q111} cell lines, in order to determine whether EGF stimulation would have a similar effect on gene expression and HTT localisation. We demonstrate that Hdh^{Q111} primary cells had a similar, but more subtle response to EGF stimulation compared to *StHdh*^{Q111} cells, but that the Hdh^{Q150} model exhibited some substantially different effects.

Similar to *StHdh*$^{Q7/7}$ cells, the localisation of the HTT epitope detected by Ab109115 was also primarily perinuclear in Hdh$^{Q7/7}$ cells, possibly reflecting the association of HTT with perinuclear organelles (Pal et al. 2006; del Toro et al. 2009; Hilditch-Maguire et al. 2000). There was also increased nuclear detection of this epitope with increased mHTT load in both cell lines, although in primary cells, this was harder to visualise due to smaller cell bodies and nuclei. However, EGF stimulation elicited a reduction of the nuclear epitope of HTT in Hdh$^{Q7/7}$ cells, an effect that also occurred in the immortalised line. In contrast with the immortalised line, there were no significant effects on either Hdh$^{Q7/111}$ or Hdh$^{Q111/111}$ cells following EGF stimulation; this suggests a dominant effect of mHTT on suppressing the response to EGF stimulation in these cells, whereas a gene dosage effect was apparent in *StHdh*^{Q111} lines. This may be due to the transformation that occurs in the process of immortalisation of cell lines, which may be altering the dominance of the *Htt* gene or has led to significant divergence between genotypes with increasing passage number. The possible mechanisms for the reduced response of HTT to EGF stimulation in the context of the expanded polyQ repeat have been discussed previously (Section 3.5).

In accordance with Ab109115, there was also a reduction of the epitope of HTT detected by Mab2166 in the nuclei of Hdh$^{Q7/7}$ cells following EGF stimulation, although this persisted for longer than the effect observed using Ab109115. This is likely to reflect the different epitopes of HTT that each antibody was raised against; Ab109115 was raised against amino acids 1-30, whereas the Mab2166 immunogen is further downstream of HTT between amino acids 118-181. Therefore Ab109115 may be more

able to detect shorter HTT N-terminal cleavage products that are enriched within cell nuclei (Hilditch-Maguire et al. 2000; Tao & Tartakoff 2001; Kegel et al. 2002), which Mab2166 cannot. In addition, the presence of further N-terminal HTT epitopes arising from aberrant splicing of exon 1 (Sathasivam et al. 2013) that would only be detectable by more N-terminal antibodies such as Ab109115, may also account for the differences in apparent HTT localisation detected by these two antibodies. Smaller fragments such as these can passively diffuse through the nuclear pore due to their small size (Hackam et al. 1998; Truant 2003; Terry et al. 2007; Bauer & Nukina 2009) and may be able to return to the nucleus more readily following EGF-stimulated translocation to the perinucleus and cytoplasm. Alternatively, the differences observed by each antibody may be due to alterations in the conformation of HTT, thus exposing alternate epitopes for antibody detection (Trettel et al. 2000; Wheeler 2000).

Also comparable to the $StHdh^{Q7/7}$ cells in Chapter 3, is the localisation of the epitope of HTT detected by the amino acid 1-17 antibodies N17 and Ab675; there is no effect of EGF stimulation on the localisation of the N17 signal, but there is a reduction in the nuclear detection of the epitope detected by Ab675 from 5 minutes of EGF stimulation in $Hdh^{Q7/7}$ cells. Interestingly, this also occurs in both $Hdh^{Q7/111}$ and $Hdh^{Q111/111}$ genotypes in the primary cell model, but not in mHTT carrying cells in the immortalised model. This could be an effect of the immortalisation process in $StHdh^{Q7/111}$ and $StHdh^{Q111/111}$ cells; as these lines are maintained in culture for prolonged periods of time, it may be expected that with increasing passage number there may also be karyotypic instability, as noted in other immortalised cell lines (Mi et al. 2005), which may in turn alter the cellular response to EGF stimulation and mHTT presence.

Hdh^{Q150} cells show a slightly different pattern of HTT localisation in response to EGF stimulation than both the immortalised and primary Hdh^{Q111} cells lines. There is a similar localisation of the HTT epitope detected by Ab109115 in $Hdh^{Q7/7}$ cells, and as has been noted in both $StHdh^{Q111}$ and Hdh^{Q111} lines, there is increasing nuclear localisation of this epitope with mHTT load. However, this is seen to a greater extent in Hdh^{Q150} cells than in the Hdh^{Q111} cells, and may reflect the more toxic effect and faster pathogenesis of the longer polyQ repeat that has been previously described (Lin 2001; Heng et al. 2007; Woodman et al. 2007; Weiss et al. 2008). There is also an evident

gene dosage effect, which has also been identified in adult Hdh^{Q150} mouse models (Heng et al. 2007). There is a small reduction in the nuclear localisation of Ab109115 following EGF stimulation in Hdh$^{Q7/7}$ cells only, concurrent with both Hdh^{Q111} and *StHdh*^{Q111} models. Conversely, all three genotypes exhibit a substantial increase in nuclear HTT at 30 minutes of EGF stimulation, which does not occur in the other two models; this is unlikely to be an effect of mHTT, as the nuclear filling also occurs in Hdh$^{Q7/7}$ cells within the Hdh^{Q150} model.

Despite the maintenance of both mouse lines in this project on a C57Bl/J6 background, the Hdh^{Q111} mouse line was constructed on a different strain background to the Hdh^{Q150} line (Wheeler 2000; Lin 2001; Woodman et al. 2007). Therefore there may be genetic differences in C57Bl/J6 stock contributing to each mouse line that may account for different effects observed in Hdh$^{Q7/7}$ cells from each strain, as substantial strain effects have been noted in HD mouse lines before (Lin 2001; Woodman et al. 2007). However, the effect of this is likely to be very small, and therefore this could also be a result of variation in microdissection and culture conditions. Ideally, this experiment would need to be replicated in a new cohort in order to determine if there is an effect of variability in strain background or experimental error. The increase in nuclear HTT at 30 minutes may reflect a stress response in these cells; in cultured HD patient lymphoblasts, HTT is released from perinuclear organelles and is translocated to cell nuclei in response to apoptotic stimulation (Sawa et al. 2005). A similar stress response may also be an effect of EGF stimulation at a concentration considerably higher than is found endogenously in these cells, thus eliciting HTT nuclear accumulation. This effect is also larger in Hdh$^{Q7/150}$ and Hdh$^{Q150/150}$ cells than in Hdh$^{Q7/7}$, which may be a result of an exaggerated stress response due to mHTT presence. In addition, there is a similar pattern of an increase of the nuclear epitope of HTT detected by Ab109115 in *StHdh*$^{Q111/111}$ cells at 30 minutes of EGF stimulation (Section 3.3.5), and an augmented stress response is a characteristic phenotype in this model (Trettel et al. 2000).

A nuclear increase in HTT is not apparent in Hdh$^{Q150/150}$ cells when detected by Mab2166, which is consistent with either the enrichment of shorter N-terminal fragments in cell nuclei (Hilditch-Maguire et al. 2000; Tao & Tartakoff 2001; Kegel et al. 2002), the presence of an aberrantly spliced exon 1 variant (Sathasivam et al. 2013) or

the altered conformation of HTT to a more amino-terminal accessible conformation, both of which Mab2166 may be less able to detect (Wheeler 2000; Thompson et al. 2009; Di Pardo et al. 2012). Comparable with both *StHdh*^{Q111} and Hdh^{Q111} cells, there is also a reduction in the nuclear epitope of HTT detected by Mab2166 in Hdh$^{Q7/7}$ cells only, although this effect is considerably less marked in the Hdh^{Q150} model. There is a slight reduction in nuclear HTT detected by Ab675 in Hdh$^{Q7/7}$ cells, but no effect in Hdh$^{Q7/150}$ or Hdh$^{Q150/150}$ lines, although there is also no nuclear filling at 30 minutes as was observed when using Ab109115. As these antibodies were previously found to exhibit similar patterns of localisation (Sections 3.3.3.3 & 3.3.4.3), the differences in an effect at 30 minutes may reflect variability between embryos and primary cell cultures. Similarly, N17 immunostaining exhibited a reduction in nuclear HTT in Hdh$^{Q150/150}$ cells at 30 minutes, which has not previously been noted. The sample size for the N17 and 675 experiments was very small, and therefore quantitative statistical analysis was not possible; therefore the inconsistency observed in HTT localisation in Hdh^{Q150} cells may not be accurately reflecting HTT localisation in response to EGF stimulation in these cells.

EGF stimulation elicits an increase in nuclear HTT phosphorylated on serines 13 and 16 in Hdh$^{Q7/7}$ cells from the Hdh^{Q111} model, although this occurs at an earlier time point than in the immortalised cell line. This also occurs in Hdh$^{Q111/111}$ cells, but interestingly not in the Hdh$^{Q7/111}$ cells; at baseline, there is already significantly more nuclear phosphorylated HTT in heterozygote cells, which may explain why a further nuclear increase of this epitope doesn't occur following EGF stimulation. This may be due to the transient nature of HTT phosphorylation or experimental error, although the same increase in nuclear location of this epitope in heterozygote cells was also observed in immortalised *StHdh*$^{Q7/111}$ cells. Therefore, differential localisation of phosphorylated epitopes could be an effect of mHTT presence; it has been found that mHTT is less efficiently phosphorylated on both serine 421 (Warby et al. 2009) and serines 13 and 16 (Thompson et al. 2009; Atwal et al. 2011). This phenotype may be penetrant in Hdh$^{Q111/111}$ cells only, thus appearing as though nuclear localisation of mHTT is reduced. In contrast, alternate conformations of mHTT may prevent the identification of phosphorylated epitopes in Hdh$^{Q111/111}$ cells until stimulation with EGF elicits a

response. In order to elucidate whether this was the case, it would have been useful to carry out subcellular fractionation and denaturing western blot analysis to determine whether the presence of HTT in each cellular compartment and the presence of any cleaved fragments may be contributing to the localisation phenotype. However, due to the poor sensitivity of the established fractionation protocol used previously (Section 3.3.6) and restricted availability of E14 striata, these experiments were not carried out. However, alterations in phosphorylated HTT localisation in response to EGF stimulation suggests that there is a response in Hdh^{Q111} primary cells that is similar to that seen in *StHdh^{Q111}* cells, and may be a mechanism by which gene expression and nuclear organisation are regulated (Holmberg et al. 2002; Ehrnhoefer et al. 2011).

EGF stimulation also elicited an increase in nuclear phosphorylated HTT over time in Hdh$^{Q7/7}$ cells from the Hdh^{Q150} model, but this did not occur until 30 minutes; this is likely to be result of variability in culture conditions or some variation in mouse background. Increased nuclear HTT in Hdh$^{Q7/150}$ compared to Hdh$^{Q150/150}$ cells was observed again, although to a lesser extent. There were also contrary effects of EGF stimulation on Hdh$^{Q7/150}$ and Hdh$^{Q150/150}$ cells as seen in the Hdh^{Q111} model; whether this is an effect of differing antibody binding efficiency, HTT conformation, or is a true representation of phosphorylated HTT localisation remains to be elucidated.

We have demonstrated that the localisation of HTT detected by N-terminal antibodies and anti-phosphorylated antibodies are similar in primary cell models as in the immortalised *StHdh^{Q111}* cell model, although the process of immortalisation appears to have transformed the immortalised cell line so that there is enhanced divergence between genotypes. However, there are still some alterations in response to EGF stimulation in primary cell lines carrying mHTT, suggesting a very early aberrant effect of the mutant protein in cellular signalling responses. There are some differences between Hdh^{Q111} and Hdh^{Q150} cells; however these appear to stem largely from baseline differences in all three genotypes rather than from a significant effect of a larger polyQ repeat. A more thorough discussion of the translocation kinetics and regulatory effects of HTT localisation can be found in Chapter 3.

As similarities with the immortalised cell line in terms of the localisation and phosphorylation of HTT could be identified in primary cells, the expression of several genes identified in Chapter 5 were also investigated in both Hdh^{Q111} and Hdh^{Q150} mouse model E14 striatal cells in order to determine if similar patterns of aberrant transcriptional control are present. Transcriptional dysregulation of SRY (sex determining region Y)-box 2 (*Sox2*) and signal transducer and activator of transcription 3 (*Stat3*) have been previously described in E13.5-15.5 $Hdh^{Q111/111}$ striatum, and are genes associated with embryonic brain maturation and development (Molero et al. 2009); this indicates that mHTT is initiating alterations in cell signalling from embryonic ages, consequently leading to adverse effects on brain development and function that may become associated with disease progression. We have also identified some evidence for transcriptional dysregulation in primary embryonic cells that may contribute to the development of later perturbations in HD mouse models. However, these experiments suffered from a low sample size, and consequently high variability, resulting in primarily the identification of trends rather than statistical significance.

Of the four genes that were tested that had a larger response to EGF stimulation in $StHdh^{Q7/7}$ cells in Chapter 5, two showed evidence of having a similar pattern of expression in Hdh^{Q111} cells; there was a trend towards increased sensitivity of the expression of *Fgf2* to EGF stimulation in $Hdh^{Q7/7}$ cells compared to both $Hdh^{Q7/111}$ and $Hdh^{Q111/111}$ cells, and there was also a pattern of expression that reflected a gene dosage effect. A summary of qRTPCR gene expression data for both primary cell lines compared to the original observations in $StHdh^{Q111}$ cells can be found in Table 6.4. *Fgf2* is an activator of MEK/ERK signalling and regulates neuronal proliferation and differentiation (Song & Ghosh 2004; Rudenko et al. 2010; Ishii et al. 2012; Li et al. 2012), as well as enhancing the differentiation and development of glia, potentially via MAPK signalling (Song & Ghosh 2004; Franzdottir et al. 2009; Li et al. 2012). FGF2 has been identified as a neuroprotective growth factor (Alzheimer & Werner 2002), and treatment of R6/2 mice with FGF2 or an FGF receptor agonist has been found to increase the number of proliferating cells in the subventricular zone, recruit new neurons to the striatum, reduce neuronal HTT aggregates and increase life span (Jin et al. 2005), in addition to alleviating anxiety and deficits in sociability in these mice

(Rudenko et al. 2010). Reduced expression of *Fgf2* may therefore be a mechanism by which embryonic brain development is impaired, and creates a predisposition to neurodegeneration by reducing the availability of neuroprotective factors.

	$StHdh^{Q111}$	Hdh^{Q111}	Hdh^{Q150}
Fgf2	↑$StHdh^{Q7/7}$	≈	χ
Myc	↑$StHdh^{Q7/7}$	χ	χ
Smad7	↑$StHdh^{Q7/7}$	✓	χ
Sox9	↑$StHdh^{Q7/7}$	χ	χ
Atf3	↑$StHdh^{Q111/111}$	✓	✓
Id3	↑$StHdh^{Q111/111}$	χ	≈
Fosl1	↑$StHdh^{Q111/111}$	✓	χ
Egr1	↑$StHdh^{Q111/111}$	✓	✓
Gadd45g	↑$StHdh^{Q111/111}$	χ	χ
Cdc42ep3	↑$StHdh^{Q111/111}$	χ	χ
Rasa1	↑$StHdh^{Q111/111}$	χ	χ

Table 6.4 A summary of the comparisons between both primary embryonic striatal cell lines, Hdh^{Q111} and $Hdh^{Q150,}$ against immortalised $StHdh^{Q111}$ cells for the pattern of qRTPCR gene expression data following 2 hours stimulation with 100ng/ml EGF. Column 2 indicates which genotype had a larger response in $StHdh^{Q111}$ cell lines. '✓' indicates concordance between primary and immortalised cell data, '≈' represents a trend in the same direction, and 'χ' indicates inconsistent findings.

Smad7 expression was also reduced in $Hdh^{Q111/111}$ embryonic striatal cells compared to both $Hdh^{Q7/7}$ and $Hdh^{Q7/111}$ cells; in immortalised cell lines, and there was also a reduction in *Smad7* expression in $StHdh^{Q111/111}$ cells, although this became evident

following EGF stimulation. In comparison, the reduction in *Smad7* expression in primary cell lines was apparent from baseline, and there was only an effect of EGF stimulation on *Smad7* expression Hdh[Q111/111] cells. *Smad7* is a competitive inhibitor of the TGFβ signalling pathway (Blanchette et al. 2001; Massague 2005; Kim et al. 2012); for example, its overexpression can prevent EGF-stimulated SMAD3 phosphorylation (Kim et al. 2012). In Chapter 5, we identified that there was reduced *Smad7* expression in *StHdh[Q111/111]* cells, in comparison with enhanced SMAD3 activation; therefore, alterations in *Smad7* regulation of the TGFβ pathway may be a mechanism for aberrant kinase signalling and transcriptional dysregulation in models of HD. There were no differences between genotypes for any of the four genes that were tested in the Hdh[Q150] line, despite a trend towards lower *Fgf2* expression at baseline, a suppressed response of *Smad7* expression to EGF stimulation and increased sensitivity of *Myc* expression following EGF stimulation in Hdh[Q150/150] cells. However, the high variability due to a low signal to noise ratio, and a consequent lack of statistical significance makes these results difficult to interpret.

Those genes with that were identified in Chapter 5 as having increased expression in *StHdh[Q111/111]* cells compared to *StHdh[Q7/7]* cells following EGF stimulation had promising results in the Hdh[Q111] primary cells. EGF stimulation elicited an increase in the expression of *Atf3*, *Egr1* and *Fosl1* in all three genotypes, and the magnitude of response compared to baseline expression was greater in Hdh[Q111/111] cells compared to wild type. These three genes are associated with transcription, and in particular *Atf3* and *Fosl1* form the AP1 complex that is involved in transcriptional regulation; the composition of which alters the control of gene expression by modifying DNA binding specificity (Shaulian & Karin 2002; Eferl & Wagner 2003). Early embryonic alterations in AP1 composition due to modifications of *Atf3* and *Fosl1* expression may therefore contribute to the transcriptional dysregulation observed in models of HD and human HD brain (Ross 2002; Zucker et al. 2005; Crocker et al. 2006; Crook & Housman 2011). *Egr1* expression was identified as being downstream of MEK signalling in the previous chapter, and it has also been associated with P38 MAPK activity (Kang et al. 2003; Lu et al. 2007). Therefore, its increased expression in Hdh[Q111/111] primary cells suggests that

there is potentially dysregulation of these kinase signalling pathways, which may be occurring as early as during embryonic brain development in HD.

A significant reduction of *Id3* expression following EGF stimulation in *StHdh^{Q111/111}* cells was seen in the previous chapter; however in the Hdh^{Q111} model, although there is significantly lower expression of *Id3* in Hdh^{Q111/111} cells compared to both Hdh^{Q7/7} and Hdh^{Q7/111} cells, there is no effect of EGF stimulation, whereas there is a trend towards a reduction in wild type and heterozygous lines. As *Id3* is a transcriptional repressor modulated by *Atf3*/*Smad* activity (Kang et al. 2003; Jin et al. 2011), it would have been expected that the enhanced *Atf3* activity in Hdh^{Q111/111} cells following EGF stimulation would elicit a consequent reduction in *Id3* expression. However, the lack of EGF effect in these cells suggests that there may be aberrant activity in other parts of the transcriptional machinery that is not maintaining a normal transcriptional equilibrium, the effects of which may accumulate over time.

The trend towards a more sensitive expression response to *Atf3* and *Egr1* to EGF stimulation was also maintained in Hdh^{Q150/150} cells, although there were high levels of variability. *Id3* expression also showed the same pattern as in the Hdh^{Q111} model; this suggests that the expression patterns of *Atf3*, *Egr1* and *Id3* may be an effect of the mHTT protein independent of polyQ length, and are not likely to be purely a result of immortalisation-induced transformation of cells. In contrast, *Fosl1* shows the opposite pattern of response; there is a gene dosage effect on the extent of *Fosl1* expression change following EGF stimulation, in which increased mHTT load reduces the response. Different polyQ lengths may therefore have differential effects on the expression of some genes, and may dictate the point at which cellular function switches from compensatory activity to pathogenic loss of function.

None of the effects observed in the immortalised striatal cell lines for genes that were identified as being altered in *StHdh^{Q111/111}* cells only following EGF stimulation (Chapter 5) could be replicated in either Hdh^{Q111} or Hdh^{Q150} primary cells, suggesting that these may be an effect of immortalisation; the immortalised cell line has previously been identified as having an increased sensitivity to metabolic stress (Ginés 2003), which may account for the larger expression effects in these cells. However, the tsA58 SV40

large T antigen that was used to immortalise Hdh^{Q111} cell lines has been found to have a limited transformation effect on striatal cells (Cattaneo & Conti 1998; Trettel et al. 2000), and there is a slight trend towards reduced *Cdc42ep3* and *Gadd45g* expression in both Hdh$^{Q111/111}$ and Hdh$^{Q150/150}$ cells, which suggests that with increased statistical power and reduced variability, an effect similar to that seen in immortalised cells may be identified. Unfortunately, the restricted availability of embryos prevented the use of a larger n or replication of gene expression experiments.

We also aimed to determine whether the same kinase signalling pathways that showed significant aberrant activity in *StHdh^{Q111}* cells were also disrupted in primary cells from the Hdh^{Q111} model; a summary of results can be seen in Table 6.5. Unfortunately, Hdh^{Q150} cell lines were no longer available for the remaining experiments. There was a significant effect of EGF stimulation on the phosphorylation of both AKT1 and MEK1 in Hdh$^{Q7/7}$ and Hdh$^{Q111/111}$ cells, although interestingly this was not significant in Hdh$^{Q7/111}$ cells. However, in contrast to the immortalised cell line, there was not a larger effect in Hdh$^{Q111/111}$ cells for the level of phosphorylated AKT1. Increased AKT activation has been identified previously in the Hdh^{Q111} mouse model, however these mice were 5-8 months old when this was determined (Ginés et al. 2003; Saavedra et al. 2010), which may suggest that this is a progressive phenotype that is not observable at embryonic stages; the increase in AKT phosphorylation in *StHdh^{Q111}* cells may be a result of their enhanced sensitivity to stressors (Ginés et al. 2003) that is exaggerating the phenotype. If the augmentation of AKT activation is more subtle in embryonic cells, then this may also be a mechanism by which some of the genes downstream of AKT signalling show less of a response in Hdh^{Q111} cells compared to the immortalised model. In addition, as AKT activity may regulate HTT phosphorylation on S13 and S16 (Thompson et al. 2009), the lack of a differential genotype effect in primary cells in response to EGF stimulation may account for differences in HTT phosphorylation and localisation between models.

	$StHdh^{Q111}$	Hdh^{Q111}
	Gene expression	
Smad3	$\uparrow StHdh^{Q111/111}$	χ
Smad6	$\uparrow StHdh^{Q111/111}$	χ
Tgfbr3	$\uparrow StHdh^{Q111/111}$	χ
Tgfbi	$\uparrow StHdh^{Q111/111}$	χ

	ELISA	
Phospho-AKT1	$\uparrow StHdh^{Q111/111}$	χ
Phospho-MEK1	$\uparrow StHdh^{Q7/7}$	≈
Phospho- P38 MAPK	$\uparrow StHdh^{Q111/111}$	✓

Total SMAD2	$\uparrow StHdh^{Q7/7}$	≈
Phospho-SMAD2	$\uparrow StHdh^{Q7/7}$	χ
Total SMAD3	$\uparrow StHdh^{Q7/7}$	χ
Phospho-SMAD3	$\uparrow StHdh^{Q7/7}$	χ

Table 6.5 A summary of the comparisons between Hdh^{Q111} primary embryonic striatal cells with immortalised *StHdh*^{Q111} cells for the expression of *Smad*-related genes, and for the activity of kinase signalling pathways as measured by ELISA assay. Column 2 indicates which genotype had a larger response in *StHdh*^{Q111} cell lines. '✓' indicates concordance between primary and immortalised cell data, '≈' represents a trend in the same direction, and 'χ' indicates inconsistent findings.

There was an equivalent level of MEK1 phosphorylation following EGF stimulation in Hdh$^{Q7/7}$ and Hdh$^{Q111/111}$ cells, although similar to the AKT1 assay, this effect was suppressed in Hdh$^{Q7/111}$ cells. To date, there is no literature regarding the activation of MEK1 in knock in mouse models of HD, however in the *StHdh*^{Q111} model, we found a suppression of MEK1 activation in response to EGF stimulation when mHTT was present. Treatment of a PC12 cell model of HD with a constituently active form of

MEK1 was found to be protective against cell death (Apostol et al. 2006), thus a reduction in MEK1 activation may be a mechanism for increased susceptibility to cell death in HD. In Hdh$^{Q111/111}$ cells, we see no reduction in MEK1 phosphorylation; however, disruption of this signalling pathway may follow a similar course as AKT phosphorylation, in that it is undetectable in embryonic cells, but may progressively worsen with disease development. It would have been useful to look at the levels of total AKT1 and MEK1 in order to calculate an active/total ratio, however, half of each embryonic striatum acted as its own baseline control while the other half was stimulated with EGF; therefore there was not enough extracted protein available to carry out additional ELISA assays with the same samples, and more Hdh^{Q111} embryos were not available to carry out these assays separately. Why there was a suppressed response in Hdh$^{Q7/111}$ cells would have been interesting to investigate further; a replication of this experiment would be required to determine if this was an effect of mHTT, or a spurious result due to experimental error.

The last kinase that was investigated in Hdh^{Q111} cells was P38 MAPK; in the *StHdh^{Q111}* model, we identified enhanced phosphorylation of P38 MAPK in *StHdh$^{Q111/111}$* cells. Similarly, there was an increased sensitivity to EGF stimulation in Hdh$^{Q111/111}$ primary cells on the phosphorylation of P38 MAPK. Activation of this kinase only occurred in the Hdh$^{Q111/111}$ cells, compared to no effect of EGF in either of the other two genotypes. Enhanced P38 MAPK signalling has been identified as an early phenotype in transgenic mouse models of HD (Gianfriddo et al. 2004; Saavedra et al. 2011; Fan et al. 2012), although this was noted from 1-3 months of age. Our results suggest that increased sensitivity within this pathway may be occurring prior to birth in mouse models of HD, but whether this may be a neuroprotective compensatory mechanism or not remains to be elucidated.

As several of the gene expression changes observed in the Hdh^{Q111} model resembled those seen in the *StHdh^{Q111}* model, we also investigated whether there were similar alterations in *Smad* gene expression and TGFβ-dependent phosphorylation (see Table 6.5 for a summary of the comparison of *Smad* expression and SMAD signalling data between Hdh^{Q111} and *StHdh$^{Q111/111}$* cell lines). Of the *Smad* genes that were tested, there were no significant differences in expression between genotypes, although EGF

stimulation did reduce *Smad6* expression and increase the expression of *Tgfbi.* As the TGFβ pathway plays a largely anti-proliferative role in cell regulation (Massague 2003; Massague 2005), it may be expected that expression of its associated genes would be low in embryonic stages of neuronal development; indeed, it has been found that suppression of SMAD2 and 3 signalling enhances conversion of human pluripotent stem cells to medium spiny neurons (Chambers et al. 2009; Carri et al. 2013). This may be reflected in the low expression values and high variability of *Smad*-associated genes in Hdh[Q111] cells. The immortalisation of the *StHdh[Q111]* cell line will have altered the developmental pathway of these cells, and consequently the expression of *Smad* and *Smad*-related genes. However, this does not rule out dysregulation of *Smad* expression at later developmental time points, which has not currently been investigated in mouse models of HD. It may have also been useful to assay a wider range of *Smad* genes in order to detect any dysregulation in the pathway as a whole, however time restrictions prevented this from being carried out, and so only those genes with the largest magnitude of effect in *StHdh[Q111]* cells from Chapter 5 were chosen to be followed up.

Finally, the phosphorylation of SMAD2 and SMAD3 were investigated in Hdh[Q111] cells following TGFβ stimulation; this was only able to be carried out by ELISA assay, as there was not enough available protein to perform additional western blot analyses. There were also very small sample sizes for each ELISA assay due to the limited availability of Hdh[Q111] mouse embryos and the concentration of protein that can be extracted per embryonic striata. There was a trend towards reduced total SMAD2 in Hdh[Q111/111] cells, similar to the effect seen in *StHdh[Q111/111]* cells; however due to low statistical power, this did not reach significance. There was an effect of TGFβ stimulation on the phosphorylation of SMAD2, but there was no evidence of a suppression of an effect in mHTT carrying cells as there was in the immortalised cell line. This may be due to the restricted role of SMAD2 in neuronal differentiation (Chambers et al. 2009; Carri et al. 2013), as the magnitude of response to stimulation was also considerably lower in primary cells than in the immortalised model. As the extent of the activation change was very small in this case, it would be difficult to identify an aberrant response in mutant cells.

Total SMAD3 and the phosphorylation of SMAD3 exhibited a similar pattern to SMAD2; unlike the immortalised cells, there was not a reduction in total SMAD3 in mHTT carrying cells in the Hdh^{Q111} model. Although there was an increase in the phosphorylation of SMAD3 following TGFβ stimulation, this did not differ between genotypes. However, there was a trend towards increased phosphorylated SMAD3 at baseline in $Hdh^{Q111/111}$ cells, but due to an n of only 2, it is not possible to draw any conclusions from these findings. The phosphorylated SMAD3 ELISA assay actually identified a suppressed phosphorylated SMAD3 response in $StHdh^{Q111/111}$ cells, whereas western blot analysis indicated hyperphosphorylation; therefore it would be of interest to investigate the expression and phosphorylation of SMAD proteins in primary embryonic striatal cells by alternative methods in order to more thoroughly characterise their activity. Nonetheless, these results may provide a starting point that suggests there may be a trend towards aberrant activity within the complex TGFβ signalling pathway in models of HD.

In conclusion, the characterisation of primary embryonic striatal cells from two knock-in mouse models of HD demonstrates some similarities in the localisation and phosphorylation of HTT epitopes with the immortalised $StHdh^{Q111}$ cell model. However, differences between wild-type cells from the Hdh^{Q111} and Hdh^{Q150} models make conclusions about the effect of polyQ length difficult to draw; replicating these experiments would be the best way to determine if these differences were due to minor variations within background mouse strains, or due to experimental error and technical variation. However, the characterisation of HTT localisation has indicated that there is mislocalisation of the mutant protein in both models from embryonic development, despite nuclear filling typically being described as a later phenotype (Wheeler 2000; Lin 2001; Fossale et al. 2002; Wheeler et al. 2002; Heng et al. 2007; Woodman et al. 2007; Menalled et al. 2009), suggesting that aberrant neurodevelopment may contribute to the later development of HD pathogenesis. In accordance with this, we have identified the transcriptional dysregulation of several genes in both mouse models of HD that are similar in their expression to the $StHdh^{Q111}$ cell lines. It has been postulated that transcriptional dysregulation may be the initiation point of the pathogenic cascade in HD (Hogel et al. 2012); this has been

demonstrated by the contribution of embryonic transcriptional dysregulation to altered striatal cell neurogenesis in Hdh^{Q111} mice (Molero et al. 2009), which is likely to lead to altered neuronal maturation and may therefore predispose affected cells to degeneration (Nguyen et al. 2013). We have identified additional genes that are differentially expressed in the presence of mHTT in response to growth factor signalling, which may have downstream effects on neuronal development and survival. Although we did not identify any differences in AKT1 or MEK1 phosphorylation in primary cells, this does not rule out a role for these pathways in disease progression. However, there is substantial hyperphosphorylation of P38 MAPK in Hdh$^{Q111/111}$ cells, which has been associated with the activity of other kinase signalling pathways, such as TGFβ (Massague 2003; Li et al. 2010), and the control of gene expression (Apostol et al. 2006; Yang et al. 2007; Martin et al. 2011). As such, aberrant activity in this pathway may influence the progression of HD phenotypes. We did not observe any apparent alterations in the expression of most *Smad* related genes, with the exception of *Smad7*. There were also no alterations in SMAD phosphorylation, although this may be due to the developmental stage of these cells, as well as this experiment having very low power, and therefore a reduced ability to find an effect. This is in addition to only being able to investigate a restricted panel of targets in comparison to *StHdh*^{Q111} cell lines.

Embryonic primary cells from mouse models of HD have been poorly characterised to date, however despite limitations in the availability of HD mouse model embryos, we have established that there are already perturbations in cell signalling, transcriptional control, and the regulation of HTT activity during the striatal development. This provides evidence for the importance of early neurodevelopment in the pathogenesis of HD, and may provide a basis for the vulnerability of striatal neurons to mHTT in later stages of the disease. However, although there are many similarities between primary cells and the immortalised cell line, there was also evidence that transformation of the immortalised cells may have made them more sensitive to growth factor stimulation, and alteration of their developmental pathways may have had an effect on transcriptional control. Therefore, although the *StHdh*$^{Q111/111}$ cells are a useful model,

characterisation of their phenotypes should be treated with caution when being applied to in vivo and primary models of HD, as well as the human disease.

Chapter 7: General discussion

7.1 Limitations of HTT localisation experiments

The determination of antibody specificity was the main limitation of these immunofluorescence experiments; we were unable to completely knock down the expression of HTT using siRNA transfection for the purposes of antibody validation. HTT is a long lived protein, and the half-life of wild type HTT is considerably longer than mHTT (J. Miller et al. 2010). It would therefore be difficult to increase the extent of siRNA transfection to the level of total HTT knock-down in this model without eliciting significant cellular toxicity due to the transfection reagent. Although there was a reduction in signal for the majority of antibodies that were tested following HTT knock-down, there was still substantial signal detection, particularly within the cytoplasm. We are therefore unable to state with any certainty that any of the antibodies that were utilised are specific to HTT. However, as there was a reduction in antibody detection following *Htt* siRNA transfection, a substantial proportion of their signal is still likely to be due to the detection of HTT. As the majority of the remaining signal following *Htt* siRNA transfection was cytoplasmic, this could be due to either enhanced non-specific binding of these antibodies within the cytoplasm, or may reflect the nuclear localisation of protein degradation systems (Thompson et al. 2009). Care should be taken when considering the pattern of cytoplasmic staining with these HTT antibodies, however as the majority of observable effects were between the nucleus and perinuclear area in these experiments, non-specific antibody detection within the cytoplasm is not likely to significantly contribute to these patterns. The DharmaFECT-only control immunofluorescence images differ slightly from the 0 minutes conditions in the growth factor experiments in terms of the nuclear staining intensity; this may be due to the interference of the transfection reagent within the cells, issues with non-specific binding, as well as inconsistencies between antibody batches and technical variation, as the siRNA experiments and growth factor experiments were conducted over a year apart. However, the pattern of increasing nuclear staining with mHTT load

was still present following treatment with DharmaFECT, suggesting that these controls are still likely to be representative of HTT localisation.

Despite using a panel of N-terminal HTT antibodies, this methodology is unable to determine whether the apparent changes in the subcellular localisation of HTT were due to dynamic shuttling of HTT between the nucleus and cytoplasm, or to changes in protein conformation and altered epitope availability. However, the differential localisation of phosphorylated HTT epitopes in comparison to non-phosphorylated epitopes suggests that alterations in apparent localisation may be due to conformational changes as a result of post-translational modifications. We only investigated phosphorylation of HTT at serines 13 and 16, however many other post-translational modifications of HTT have been identified that can alter its conformation and localisation (Steffan et al. 2004; Bauer & Nukina 2009; Warby et al. 2009), and therefore these cannot be ruled out as a mechanism of HTT regulation downstream of growth factor stimulation.

Additional investigation is required to determine whether the differences in antibody detection were due to conformation or localisation; the use of antibodies against C-terminal epitopes of HTT may provide additional information about whether conformational alterations are primarily restricted to N-terminal HTT, as the structure of this region is particularly flexible (Trettel et al. 2000; Wheeler 2000; Kim et al. 2009; Lotz et al. 2010; Seong et al. 2010; Zuccato et al. 2010; Długosz & Trylska 2011), or whether shuttling of HTT epitopes between cellular compartments encompasses the full length protein or occurs following proteolysis. Additionally, methods that can look directly at HTT conformation, such as time resolved fluorescence resonance energy transfer (TR-FRET), would be particularly useful to answer this question (Figure 7.1).

The subcellular fractionation experiments did not prove to be particularly informative; no alterations in full length HTT localisation were detectable by western blot, which may not be surprising as full length HTT is not able to traverse the nuclear pore in a manner as efficient as smaller N-terminal fragments (Hackam et al. 1998; Truant 2003; Terry et al. 2007; Bauer & Nukina 2009). Additionally, the majority of effects were identified between the perinuclear and nuclear regions; however the subcellular

fractionation protocol separated only nuclear and cytoplasmic fractions, therefore potentially obscuring these changes. Fractionation protocols that separate cellular regions more thoroughly may be a more desirable method of investigating HTT localisation by western blot. Conversely, the lack of change in HTT localisation by western blot may be reflective of alterations in HTT conformation in response to growth factor stimulation, rather than alterations in localisation.
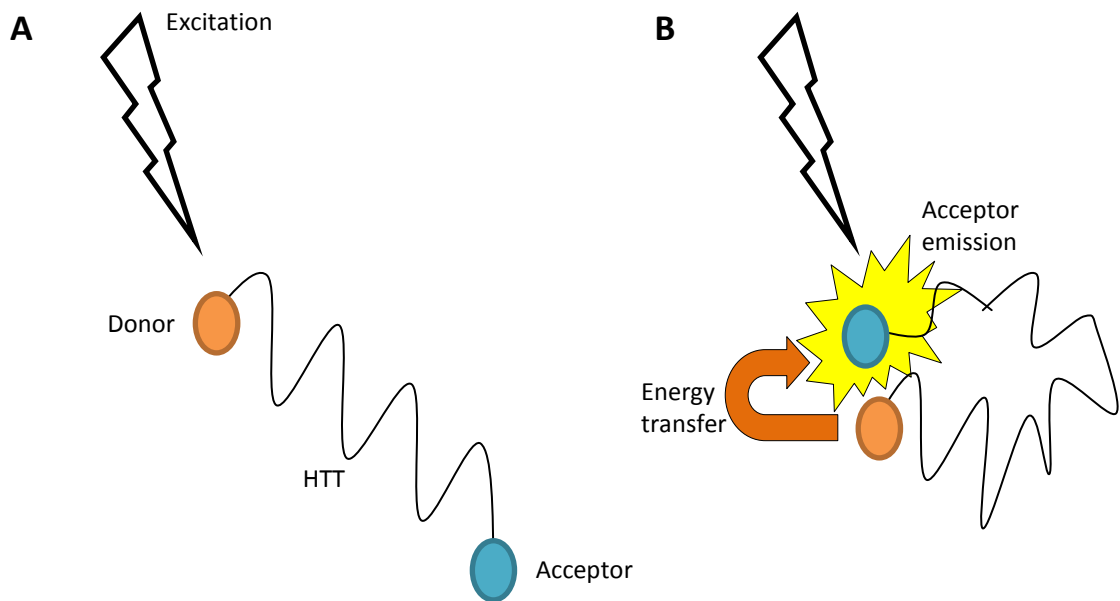
Figure 7.1 Cartoon depicting the principle behind TR-FRET in order to investigate changes in HTT conformation. **A.** A donor fluorophore is tagged to N-terminal HTT, and an acceptor is tagged to the C-terminal end. In an open conformation, following excitation from an external source, the two fluorophores are not in close enough proximity to each other in order for energy transfer to occur. **B**. Upon a conformation change, the proximity between donor and acceptor is reduced to between 1-10nm. Upon excitation of the donor, energy can be transferred to the acceptor molecule and a proximity-dependent fluorescent signal is emitted. TR-FRET involves the inclusion of a 50-150μs delay between excitation and emission measurement to allow for the degradation of short-lived background non-specific emissions. Live cell imaging following growth factor stimulation could therefore track potential alterations in HTT conformation over time.

No additional bands validated as HTT were detected by any of the antibodies that were tested by western blot, other than the full length epitope. Although HTT cleavage has been found to occur following DNA damage (Khoshnan et al. 2009), the presence of

HTT fragments in the *StHdh^{Q111}* model have not been characterised. It is therefore unclear whether our failure to detect additional forms of HTT is a result of minimal HTT cleavage and proteolysis in these cells, rapid degradation of cleaved products, or a methodological effect. As HTT is found to be cleaved as part of its normal function (Goldberg et al. 1996; Wellington et al. 1998; Kim et al. 2001; Gafni & Ellerby 2002; Graham, Deng, et al. 2006; Landles et al. 2010), it is likely that this may be a methodological effect; the protein gel was blotted for a long period of time in order to efficiently transfer the large, full length protein, but this process may have lost smaller fragments by diffusion through the membrane on to the chromatography paper. However, as this cell model does not exhibit mHTT toxicity, and cleavage products have not yet been characterised, mHTT cleavage and proteolysis may not be a central pathogenic mechanism in these cells, or may not occur at all.

7.2 Subcellular localisation of HTT and mHTT

The increased nuclear localisation of mHTT that we identify in these cells is consistent with other studies using this cell line (Trettel et al. 2000; Truant 2003; Atwal et al. 2007; Atwal et al. 2011), as well as with other models of HD (Hoogeveen et al. 1993; Dorsman et al. 1999; Hilditch-Maguire et al. 2000; Wheeler 2000; Kegel et al. 2002; Wheeler et al. 2002; Rockabrand et al. 2007; Seong et al. 2010). However, in mouse models of HD and in human HD caudate, HTT nuclear filling is described as a progressive phenotype that develops and worsens with disease progression (Gomez-Tortosa et al. 2001; Menalled et al. 2003; Woodman et al. 2007; Hickey et al. 2008; Heng et al. 2010; Bayram-Weston et al. 2012).We have demonstrated that the mislocalisation of mHTT is not only an age-associated phenotype, but is a pre-pathogenic phenotype present from embryonic stages of development. The increased nuclear localisation of HTT may affect transcriptional regulation (Zoghbi & Orr 2000; Bauer & Nukina 2009), nuclear organisation (Kegel et al. 2002; Sun et al. 2007), as well as loss-of-function effects within cytoplasmic-associated mechanisms (Zuccato et al. 2003; Zuccato et al. 2010). Therefore the mislocalisation of mHTT from embryogenesis may have implications for the understanding of HD developmental pathogenesis;

increased nuclear localisation of mHTT in striatal neurons may be initially tolerable, as its presence during brain development is likely to elicit compensatory mechanisms in order to maintain cell survival. The inability for these mechanisms to maintain survival-associated cell functions with cumulative mHTT insult may then lead to the observable pathogenic disease cascade. This underlying dysfunction may have implications for informing the development of subtle phenotypes that occur decades before the clinically defined age of onset.

In contrast to the localisation of HTT epitopes, we do not observe HTT hypophosphorylation in $StHdh^{Q7/111}$ and $StHdh^{Q111/111}$ cells, as has been described previously (Atwal et al. 2011). However, we also do not observe changes in the extent of phosphorylation following growth factor stimulation, despite previous work demonstrating that AKT activation may directly phosphorylate HTT (Thompson et al. 2009). Therefore, the detection of phosphorylated HTT in these experiments may reflect a saturation effect, thus any increase in HTT phosphorylation would not correlate with a concomitant increase in antibody detection. The discordance between these findings may be a result of high variability in $StHdh^{Q7/111}$ and $StHdh^{Q111/111}$ cells due to mHTT, the divergence of cell lines between different laboratories, or may be an effect of regulation by additional post-translational modifications. Despite the contrasting phosphorylated HTT evidence, aberrant phosphorylation has implications for the regulation of HTT localisation, cleavage and clearance, therefore contributing to cellular dysfunction that is present from embryonic development.

7.3 Effect of growth factor stimulation on HTT subcellular localisation

The regulation of HTT localisation and phosphorylation has been previously investigated following the activation or inhibition of downstream kinases, such as AKT and IKKβ (Thompson et al. 2009; Khoshnan et al. 2009; Atwal et al. 2011; Khoshnan & Patterson 2011), and the activity within signalling pathways has been investigated in the context of mHTT (Liu et al. 1997; Song et al. 2002; Ginés et al. 2003; Humbert 2003; Apostol et al. 2006; Kong et al. 2009; Liévens et al. 2008; Atwal et al. 2011). However, the effect of entire signalling transduction cascades, as elicited by growth

factor stimulation, on HTT localisation and phosphorylation has not been previously investigated. We demonstrate that stimulation with different growth factors leads to differential effects on the localisation of HTT. This suggests that HTT is a general downstream target of several kinase signalling pathways, which may regulate HTT localisation or conformation, and therefore its function. The differential effects of growth factor stimulation on the localisation of HTT may therefore implicate HTT as a regulatory mechanism by which cellular responses to diverse stimuli are modulated. Transcriptional regulation can be stimulated by growth factor activation of kinase signalling pathways (Lin et al. 2001; Apostol et al. 2006; Cabodi et al. 2009; Kong et al. 2009; Ro et al. 2010), and HTT localisation has been proposed to be a mechanism for transcriptional regulation (Zoghbi & Orr 2000; Bauer & Nukina 2009). Therefore, the ability for kinase signalling pathways to modulate HTT localisation may be a mechanism by which transcription is controlled. All three growth factors were less able to modify the apparent localisation of mHTT in $StHdh^{Q111/111}$ cells, suggesting that the expanded polyQ interferes with this process. However, the point in the pathway at which this may occur remains to be elucidated; the expanded polyQ may render mHTT less able to translocate or alter its conformation in response to kinase signalling, or mHTT may be aberrantly modulating signalling mechanisms upstream of transcriptional regulation. This may have implications for considering the mechanisms of mHTT mislocalisation; increased nuclear accumulation of mHTT is predominantly considered to be a result of increased cleavage and aberrant protein-protein associations (Bessert et al. 1995; Xia 2003; Truant et al. 2007; Desmond et al. 2013). However, if HTT is a regulatory target of signal transduction pathways, then mislocalisation of mHTT could also be a result of altered kinase signalling.

Differential cellular responses to growth factor stimulation in the context of mHTT also have implications for the consideration of therapeutic treatments. For example, BDNF replacement may have limited therapeutic benefit if cells are unable to appropriately respond to stimulation, and transcriptional dysregulation may persist due to continued mislocalisation of mHTT. Therefore, targets downstream of the growth factor receptor that directly modulate HTT localisation may be a more effective target, although these targets are yet to be identified.

7.4 Limitations of kinase signalling experiments

We observed dysregulation in several kinase signalling pathways in *StHdh*$^{Q111/111}$ cells, which is consistent with altered signalling modulating HTT localisation. However, the interpretation of some of the targets was limited by variability in their baseline activation. It was therefore difficult to determine the effect of mHTT on several kinases, and whether these differences were due to true variability of these pathways within this cell line, or were due to technical variation and error. This could be clarified by replicating these experiments and increasing statistical power. Non-specific binding of the antibodies utilised in the ELISA kits can also not be ruled out.

An additional limitation of the kinase signalling experiments was the use of only one method to assess kinase phosphorylation; ELISA assays are useful for the relative quantification of targets within cell populations, however the nature of the assay requires removal of the target away from the cellular context. Therefore investigation of the localisation of phosphorylated kinase targets would be of use to further characterise kinase signalling pathways that may be aberrantly controlled in mHTT carrying cells. Our experiment was also limited by only investigating a single time point of stimulation prior to collecting cell lysates. As discussed in Chapter 4, this may have influenced the observable alterations in kinase phosphorylation in response to each growth factor. Although these experiments have indicated which pathways may be altered in response to mHTT, they do not clarify how, or at which point in the pathway this disruption may occur. Manipulation of several points within a cascade would be required to elucidate where mHTT is exerting its effects.

7.5 Dysregulation of kinase signalling pathways

We demonstrate that in concordance with our HTT localisation data, there are several dysregulated kinase signalling pathways in *StHdh*$^{Q111/111}$ cells; the nature of which is consistent with previous characterisation studies of signalling pathways in HD models (Ginés et al. 2003; Kong et al. 2009; Molero et al. 2009; Ginés et al. 2010; Atwal et al. 2011; Saavedra et al. 2011; Ritch et al. 2012). EGF stimulation elicited the greatest

response in the investigated targets, however as the majority of these targets are shared between growth factor-induced pathways, the mechanism behind this is unclear. It may be a result of the single time point that was investigated; one mechanism for differentiating the effects of cellular inputs to similar pathways is by altering signalling kinetics (Ji et al. 2010), and therefore we may have looked at the time scale most appropriate for EGF signalling. Otherwise, NGF and BDNF stimulation may primarily act upon alternate signalling pathways in these cells that were not included in these experiments. As NGF and BDNF stimulation elicited a response in the apparent localisation of HTT, it is unlikely that the reduced effect observed in these signalling pathways is a result of suppressed receptor activation.

Although the nature of the interference caused by mHTT in these pathways cannot be elucidated from these findings, the alteration in both HTT localisation and the transcription of IE genes upon AKT1 and MEK1/2 inhibition supports our previous assertion that HTT localisation may be regulated by signal transduction pathways, and that this is turn may regulate transcription. The nature of this mechanism is likely to be complex; the inhibition of both AKT1 and MEK1/2 exerted similar effects on the localisation of HTT, suggesting that HTT may be a downstream component of several pathways, the synergism of which is required to regulate HTT function. Therefore an effective target for therapeutic intervention may be the restoration of the essential balance of pro- and anti-apoptotic mechanisms. For example, we identify enhanced AKT activation in $StHdh^{Q111/111}$ cells, which is concordant with the literature (Ginés et al. 2003; Kong et al. 2009; Atwal et al. 2011), and is considered to be a compensatory response and neuroprotective mechanism (Owada et al. 1997; Noshita et al. 2001; Chong et al. 2005). However, by inhibiting AKT1, the localisation of mHTT became less nuclear, and the overexpression of IE genes was suppressed. This suggests that despite being a neuroprotective anti-apoptotic pathway, the counter-intuitive inhibition of a hyper-activated AKT pathway may prove to be beneficial by restoring normal HTT localisation and IE gene expression by the re-balancing of pro- and anti-apoptotic pathways. As MEK inhibition elicited similar effects, and two pro-apoptotic pathways; P38 MAPK and STAT3, were also identified as being hyperphosphorylated in $StHdh^{Q111/111}$ cells, the use of a single kinase as a therapeutic target may prove to be

insufficient. Suppressing AKT alone may prove to have beneficial effects, however it may ultimately enhance mHTT toxicity by failing to counter pro-apoptotic mechanisms. Therefore, a multi-target approach to restore the balance of compensatory and synergistic signal transduction mechanisms may be an efficacious therapeutic approach.

Although AKT has been implicated in the phosphorylation of HTT on S13 and S16 (Thompson et al. 2009), we do not observe any loss of phosphorylation on these serines following AKT1 inhibition, and the nuclear localisation of these epitopes increased, which is consistent with enhanced phosphorylation. The same effect occurred following MEK1/2 inhibition, suggesting that similar to the regulation of HTT localisation, the regulation of HTT phosphorylation is likely to be downstream of multiple kinases. The phosphorylation of HTT on these serines and consequent nuclear translocation is considered to be neuroprotective by enhancing degradation and clearance (Thompson et al. 2009), which may be occurring following AKT and MEK inhibition. Interestingly, $StHdh^{Q7/7}$ and $StHdh^{Q111/111}$ cells exhibit differential responses to AKT1 and MEK1/2 inhibition; this may reflect an aberrant association between mechanisms regulating mHTT localisation with upstream kinase signalling pathways; however these mechanisms are yet to be determined.

7.6 Limitations of differential gene expression experiments

When considering the microarray data, the effect of NGF and EGF stimulation on gene expression was minimal in comparison to the genotype effect; the large genotype differences may have masked smaller, but potentially significant growth factor effects. In some cases, qRTPCR was not sensitive enough to validate the small expression changes of some genes following stimulation. As alterations in expression patterns for some genes could not be confirmed, the extent of the effect of growth factor stimulation could not be fully verified. Replication of these experiments with increased statistical power by increasing the n may allow for verification of small changes in expression by qRTPCR, or may definitively rule out the significance of genes that were detected by chance in the microarray. There were also extensive differences between

the baseline findings for the separate microarray experiments; this variation may have been a result of the large period of time between experiments, which may have resulted in batch effects, variation in RNA manipulations, or may be an effect of the different microarray chips that were used. It may have been advantageous to carry out these experiments in parallel to reduce extraneous variation, although this was not possible at the time. However, despite the variation, similar GO pathways were identified between experiments, indicating a degree of concordance for both NGF and EGF microarray experiments.

Despite potential alterations in SMAD proteins being identified from the EGF microarray experiment, the investigation of SMAD activity required stimulation with TGFβ to elicit phosphorylation. It could be expected that as potentially aberrant TGFβ pathway activity was highlighted following stimulation with EGF, then alterations in the downstream SMADs would also be identified following EGF stimulation, as these pathways can work synergistically (Jin et al. 2011; Kang et al. 2012). Baseline dysregulation of the TGFβ pathway in *StHdh*$^{Q111/111}$ cells may therefore have contributed to the alterations in gene expression observed following EGF stimulation; therefore EGF stimulation may be modulated by TGFβ activity, but did not activate the TGFβ pathway itself, and would therefore not enhance SMAD activity.

7.7 Differential gene expression

The differential effects of NGF and EGF stimulation on gene expression are consistent with the differential kinase signalling responses previously observed, and may reflect the diverse functions of these growth factors. Despite the dissimilar effects of NGF and EGF stimulation on gene expression in these cells, the transcriptional response was altered by mHTT for both growth factors. This suggests that mHTT interference is not specific to a particular pathway, but the nature of this interference remains unclear; however, influencing chromatin modification is the mechanism by which the broadest alterations to transcriptional regulation may occur. As HTT is a large and multifunctional protein, it is likely that several mechanisms contribute to transcriptional dysregulation following growth factor stimulation.

These findings have implications for the consideration of gene expression changes in models of HD; we demonstrate that by investigating the minority of upregulated genes, alternative, novel mechanisms for transcriptional dysregulation in HD may be identified, such as the TGFβ pathway and SMAD transcription factors. The genes that we identify as being differentially expressed in $StHdh^{Q111/111}$ cells have more putative TF binding sites in common than the genes identified in $StHdh^{Q7/7}$ cells; the increased responsiveness of these genes may therefore be due to compensatory responses. If the binding of some regulatory TFs is inhibited by mHTT, there is increased availability for binding by alternative TFs in the gene promoter region, which when not appropriately regulated, may lead to increased reactivity to transcriptional stimulation. As the genes associated with $StHdh^{Q7/7}$ cells had two TFs in common, *Egrf* and *Sp1*, which also had putative binding sites on the genes associated with $StHdh^{Q111/111}$ cells, these may be key TFs downstream of EGF signalling that had increased availability in $StHdh^{Q111/111}$ cells. Increased TF binding is inconsistent with the majority of the literature, where TFs are proposed to be sequestered by mHTT (Kazantsev et al. 1999; Steffan et al. 2000; Nucifora et al. 2001), or their binding is inhibited (Shimohata et al. 2000; Dunah et al. 2002; Li et al. 2002). However, our results suggest that altered transcriptional dysregulation in HD may not be as simple as a loss of TF function, but is more likely to be dysfunction of the regulatory mechanisms resulting from a combination of loss- and gain-of-function events. These events may be reflective of the loss of balance and coordination between signal transduction pathways.

There is currently limited and mixed evidence for the role of the TGFβ pathway in HD (Kandasamy et al. 2010; Battaglia et al. 2011; An et al. 2012), and to date there is no data regarding SMAD activity in the context of HD, or any potential associations with HTT. Therefore, our demonstration of SMAD expression and activation in this model implicates a novel pathway in the pathogenesis of HD. The TGFβ pathway is associated with immune reactivity and inflammation (Kandasamy et al. 2011), and these processes tend to be enhanced in mouse models and human HD (Dalrymple et al. 2007; Bjorkqvist et al. 2008; Hsiao et al. 2013), thus implicating a potential role for TGFβ in the development of HD phenotypes. TGFβ signalling plays a role within multiple cell types (Hata et al. 1998), and it would therefore be of interest to

investigate whether peripheral TGFβ and SMAD activation correlated with striatal dysfunction. If there was an association, these novel targets may be useful biomarkers for the development of HD pathology. In addition, the identification of additional pathways that may contribute to the HD phenotype also provides the potential for the development of new therapeutic targets.

7.8 Limitations of cell models

One of the main limitations of this project is the use of an immortalised cell model of HD to unearth potentially aberrant mechanisms that may play a role in the human disease. Although this model was derived from the knock-in Hdh^{Q111} mouse model, which is genetically similar to human HD, the immortalisation process elicits substantial modifications to these cells that may confer additional phenotypes to these cell lines that are not present in other models of HD. However, the *StHdh^{Q111}* cell line remains a useful and informative model, as previously its transcriptional profile has been found to be similar to that in mouse models and human HD caudate (Lee et al. 2007), and many of the signalling mechanisms identified in these cells have also been replicated in other models (Ginés et al. 2003; Kong et al. 2009; Molero et al. 2009; Ginés et al. 2010; Atwal et al. 2011; Saavedra et al. 2011; Ritch et al. 2012). This provides evidence that the transformation of these cells has not had a substantial effect so as to distance their molecular phenotype too far from mouse models and human HD. This cell line can also be grown at the non-permissive temperature of 39˚C, where the immortalising virus becomes inactive, and cell death can be assayed. However, this modification of the model was not appropriate for this project, as our focus was on the interference of mHTT within pre-pathogenic cellular processes rather than on modifications of its toxicity.

In order to determine whether the effects we observed in *StHdh^{Q111}* cells were a result of the immortalisation process, we aimed to replicate key experiments in primary embryonic striatal cells from both the Hdh^{Q111} and Hdh^{Q150} mouse models of HD. However, neither mouse model fully recapitulates the human disease, so any findings from primary cell cultures from these models will still require validation in human

derived cell lines, and potentially human post-mortem HD caudate. By using striatal dissections from embryonic mouse brain, the developing neurons are removed from their cellular context, which may potentially alter their signalling and transcriptional phenotypes. However, for the purposes of recapitulating aberrant signalling pathways and transcriptional mechanisms from immortalised striatal *StHdh*^{Q111} cells, the isolation of striatal neurons was not inappropriate. Cortical-striatal co-cultures may be of interest for future research, as connectivity between these two regions plays a large role in the functioning of the striatum and in HD pathogenesis.

One of the most restricting elements of the primary culture work was a lack of power; in order to gain sufficient numbers of each genotype for each experiment, a large cohort of mice was required. However, timed mating was restricted by factors such as colony size, and mating was not always successful. Therefore, many of the primary culture experiments carried out in this project were underpowered. It is therefore difficult to determine whether any differences that were observed between the mouse models and the immortalised cell model were due to model-specific effects (i.e. immortalisation or CAG repeat length), or were due to high variability in primary cells. The homozygous cells in the primary cultures tended to have less extreme phenotypes than *StHdh*$^{Q111/111}$ cells; this is likely due to the effect of divergence and transformation in the immortalised cells over many passages. It is therefore possible that the differences between wild type cells and homozygous cells in primary cultures may become more apparent with differentiation and age.

7.9 Replicating results in primary cell cultures

We demonstrate that some of the signalling and transcriptional effects observed in *StHdh*^{Q111} cell lines following growth factor stimulation can be replicated in Hdh^{Q111} primary cell cultures. Although we were unable to replicate several of the gene expression and kinase signalling events, the lack of power and high variability in the data means that these targets may not be immediately ruled out. Similarities between the models have been observed previously (Fossale et al. 2002; Ginés et al. 2003; Carnemolla et al. 2009; Sinha et al. 2010), and therefore support the use of

immortalised cell lines as a more accessible model for investigating molecular mechanisms of HD. However, we demonstrate that there are substantial differences between Hdh^{Q111} and Hdh^{Q150} primary cell lines in terms of HTT localisation; interestingly, these differences are also apparent in wild type cells from baseline, which suggests that some of the variation in HTT localisation may be due to either differences in mouse background strain, or to technical variation rather than CAG repeat length. The housing of mouse models changed during the course of the project due to infection; Hdh^{Q150} microdissections were carried out while mice were housed in the presence of the infection, and Hdh^{Q111} dissections were carried out later after colonies were transferred to a barrier unit. The infection may therefore have had implications for embryonic development or the establishment of dissections into culture. However, despite baseline differences, there is a differential effect of EGF stimulation between genotypes in both mouse models, suggesting that mHTT mislocalisation, and therefore dysregulation of HTT-associated functions, is a pre-pathogenic phenotype that is present from embryonic development. Nonetheless, this experiment will need to be replicated for both mouse models under similar conditions in order to determine the most likely source of variation between models.

When considering the gene expression data, Hdh^{Q150} cells exhibit a trend towards some similar transcriptional differences to the Hdh^{Q111} and *StHdh^{Q111}* models. However, there are also some variations in the pattern of gene expression changes following growth factor stimulation, such as for *Fosl1*. This may be an effect of the longer polyQ on the regulation of gene expression; different polyQ lengths may exert differential effects on the expression of some genes, and may therefore influence the point at which compensatory activity is overcome by pathogenic processes. The similarities that do exist between both models suggest that there is still a degree of reproducibility of the effect of mHTT during embryonic development, regardless of CAG repeat length.

Our findings have implications for the comparison of the developmental trajectories of mouse models of HD; knock-in models with longer CAG repeat lengths develop motor abnormalities and neuropathological features earlier than those with shorter repeat lengths (Heng et al. 2007; Woodman et al. 2007; Heng et al. 2010). These alterations in

pathogenic development may not be due exclusively to hastened and more severe pathology as a result of a longer polyQ, but may also be due to differential transcriptional events during embryogenesis and development that may alter the pathogenic trajectory. Mouse models of HD have similar transcriptional profiles by the late stages of disease development (Kuhn et al. 2007), which suggests that the endpoint of mHTT disruption is the same regardless of CAG length and genetic context. However, if the developmental pathogenesis differs with CAG length, this may have implications for early therapeutic interventions that target transcriptional dysregulation, as different targets may be more appropriate for different CAG repeat lengths.

7.10 Conclusion

We created a dynamic cell model in order to investigate the signalling and transcriptional changes that may be present in the immortalised striatal cell model of HD, but which may be too subtle to be identified in a static cell culture. The use of growth factor stimulation at levels much higher than would be found endogenously initiated a cellular response and exacerbated minor alterations between cell lines. These differences in responding may be not be apparent during disease development due to their subtlety, but may be part of a cumulative process of cellular dysfunction that ultimately contributes to disease progression. From this model, we have demonstrated that;

- Cellular dysfunction is not solely a degenerative process in models of HD, but is a pre-pathogenic mechanism that is present during embryogenesis and may play a role in aberrant development;
- This dysfunction includes mislocalisation of mHTT and phosphorylated mHTT, which may be a result of aberrant control of signal transduction pathways. In turn, the mislocalisation of mHTT epitopes may contribute to the transcriptional dysregulation observed in HD. Several pathogenic mechanisms are likely to contribute to these effects;

- The dysregulation of HTT localisation may be a result of aberrant kinase signalling pathways, which is a novel mechanism for transcriptional dysregulation in HD, and also implies that HTT could be a transcriptional regulator that is a downstream substrate of several major signalling pathways;

- By focusing on a subset of genes with a larger transcriptional response in *StHdh*$^{Q111/111}$ cells, we have implicated a novel pathway in the pathogenesis of HD; dysregulation of SMAD transcription factors may contribute to the transcriptional effects observed in HD, and involvement of this pathway may also account for some of the inflammatory and immune system HD phenotypes;

- Much of this evidence could be replicated in Hdh^{Q111} primary cell cultures, although a lack of power prevented clear conclusions from being drawn;

- Alterations in gene expression phenotypes suggest that polyQ length may lead to differential gene expression effects, which may contribute to the speed and nature of phenotypic development.

Although signalling pathways may therefore be efficient targets for therapeutic intervention, the nature of the complex network of pro- and anti-apoptotic pathways, including compensatory and pathogenic responses, means that the targeting of a single kinase may not be sufficient. The restoration of a balance between these pathways may be a more efficacious approach, and may involve counter-intuitive interventions, such the suppression of compensatory anti-apoptotic signalling pathways. However, the efficiency of these compensatory responses during development may be a mechanism that contributes to variability in the age of disease onset. TGFβ and the SMADs also have the potential to be new targets of interest, and may be useful therapeutic targets and possibly biomarkers. However, the nature of the association between HTT and this pathway has not yet been investigated.

In the future, it would be of interest to determine whether the apparent changes in HTT localisation were due to the dynamic shuttling of HTT, or to alterations in its conformation, as this could not be ascertained in this project. Alternative C-terminal antibodies may be of use, and TR-FRET may be particularly informative. In addition, assaying additional post-translational modifications of HTT in response to growth

factor stimulation, such as alternate phosphorylation sites, SUMOylation and ubiquitination, would further characterise this model.

The validation of these results in additional models would also be of interest; it is important to see if replication of these results occurs in human-derived cell lines, such as patient HD fibroblasts and iPSCs, as these more closely mimic the human disease. Studying these changes directly in animal models without exogenous stimulation may be limiting, as alterations in signalling pathways may be too small to detect in the early stages of development; however a longitudinal study to investigate their progression may be of use. In human patients, investigation would be limited to peripheral or post-mortem tissue. However, if any subtle changes in kinase activation can be detected peripherally, these may become useful biomarkers to track disease progression and therapeutic efficiency.

The involvement of the TGFβ pathway and SMAD TFs in HD requires characterisation, as little work has currently been done concerning their role in HD pathogenesis. As TFs, the SMADs may interact directly with HTT; an association that may be altered by the presence of an expanded polyQ in order to disrupt transcriptional regulation. Alternatively, TGFβ signalling may also alter the localisation of HTT in the same manner as EGF, NGF and BDNF signalling, and mislocalisation of mHTT may be responsible for the altered activity of SMAD TFs.

In conclusion;

- We have identified a potential mechanism for transcriptional dysregulation in models of HD that stems from aberrant cellular responses to stimulation, and we have implicated a novel signalling pathway in the pathogenesis of HD.
- Cellular dysfunction is present from embryogenesis, and therefore confers a developmental aspect in the consideration of HD progression, which may have implications for the development of therapeutic interventions and the development of biomarkers.
- Although the mechanisms behind these findings require further elucidation and validation in additional models of HD, they contribute to our understanding of

HD molecular pathogenesis, and provide a new perspective from which to consider mechanisms of transcriptional dysregulation in HD.

References

Abada, Y.K., Schreiber, R. & Ellenbroek, B., 2013. Motor, emotional and cognitive deficits in adult BACHD mice: a model for Huntington's disease. *Behavioural Brain Research*, 238, pp.243–51.

Aiken, C.T., Steffan, J.S. Guerrero, C.M., Khashwji, H., Lukacsovich, T., Simmons, D., Purcell, J.M., Menhaji, K., Zhu, Y-Z., Green, K., Laferla, F., Huang, L., Thompson, L.M. & Marsh, J.L., 2009. Phosphorylation of threonine 3: implications for Huntingtin aggregation and neurotoxicity. *The Journal of Biological Chemistry*, 284(43), pp.29427–36.

Alexandrow, M.G. & Moses, H.L., 1995. Transforming growth-factor-beta and cell-cycle regulation. *Cancer Research*, 55(7), pp.1452–1457.

Allen, S.J., Watson, J.J., Shoemark, D.K., Barua, N.U. & Patel, N.K., 2013. GDNF, NGF and BDNF as therapeutic options for neurodegeneration. *Pharmacology & Therapeutics*, 138(2), pp.155–75.

Almeida, S., Cunha-Oliveira, T., Laco, M., Oliveira, C.R. & Rego, A.C., 2010. Dysregulation of CREB Activation and Histone Acetylation in 3-Nitropropionic Acid-Treated Cortical Neurons: Prevention by BDNF and NGF. *Neurotoxicity Research*, 17(4), pp.399–405.

Altar, C.A., Laeng, P., Jurata, L.W., Brockman, J.A., Lemire, A., Bullard, J., Bukhman, Y.V., Young, T.A., Charles, V. & Pafreyman, M.G., 2004. Electroconvulsive seizures regulate gene expression of distinct neurotrophic signaling pathways. *The Journal of Neuroscience,* 24(11), pp.2667–77.

Alzheimer, C. & Werner, S., 2002. Fibroblast growth factors and neuroprotection. In *Molecular and Cellular Biology of Neuroprotection in the CNS*. 233 Spring ST, New York, NY 10013 USA: Kluwer Academic/Plenum Publ, pp. 335–351.

An, M.C., Zhang, N., Scott, G., Montoro, D., Wittkop, T., Mooney, S., Meloy, S. & Ellerby, L.M., 2012. Genetic Correction of Huntington's Disease Phenotypes in Induced Pluripotent Stem Cells. *Cell Stem Cell*, pp.253–263.

Andrade, M.A. & Bork, P., 1995. HEAT repeats in the Huntington's disease protein. *Nature Genetics*, 11(2), pp.116–116.

Andrew, S.E., Goldberg, Y.P., Kremer, B., Telenius, H., Theilmann, J., Adam, S., Starr, E., Squitieri, F., Lin, B., Kalchman, M.A., Graham, R.K. & Hayden, M.R., 1993. The relationship between trinucleotide (CAG) repeat length and clinical features of Huntington's disease. *Nature Genetics*, 4(4), pp.398–403.

Andrich, J., Arning, L., Wieczorek, S., Kraus, P.H., Gold, R. & Saft, C., 2008. Huntington's disease as caused by 34 CAG repeats. *Movement Disorders*, 23(6), pp.879–881.

Angelastro, J.M., Torocsik, B. & Greene, L.A., 2002. Nerve growth factor selectively regulates expression of transcripts encoding ribosomal proteins. *BMC Neuroscience*, 3.

Anglada-Huguet, M., Giralt, A., Perez-Navarro, E., Alberch, J. & Xifró, X., 2012. Activation of Elk-1 participates as a neuroprotective compensatory mechanism in models of Huntington's disease. *Journal of Neurochemistry*, 121(4), pp.639–48.

Apostol, B.L., Illes, K., Pallos, J., Bodai, L., Wu, J., Strand, A., Schweitzer, E.S., Olsen, J.M., Kazantsev, A., Marsh, J.L. & Thompson, L.M., 2006. Mutant huntingtin alters MAPK signaling pathways in PC12 and striatal cells: ERK1/2 protects against mutant huntingtin-associated toxicity. *Human Molecular Genetics*, 15(2), pp.273–85.

Aronin, N., Chase, K., Young, C., Sapp, E., Schwarz, C., Matta, N., Kornreich, R., Landwehrmeyer, B., Bird, E., Beal, M.F., Vonsattel, J.P., Smith, T., Carraway, R., Boyce, F.M., Young, A.B., Penney, J.B. & Difiglia, M., 1995. CAG expansion affects the expression of mutant huntingtin in the Huntingtons disease brain. *Neuron*, 15(5), pp.1193–1201.

Arrasate, M., Mitra, S., Schweitzer, E.S., Segal, M.R. & Finkbeiner, S., 2004. Inclusion body formation reduces levels of mutant huntingtin and the risk of neuronal death. *Nature*, 431(7010), pp.805–10.

Atwal, R.S., Xia, J., Pinchev, D., Taylor, J., Epand, R.M. & Truant, R., 2007. Huntingtin has a membrane association signal that can modulate huntingtin aggregation, nuclear entry and toxicity. *Human Molecular Genetics*, 16(21), pp.2600–15.

Atwal, R.S., Desmond, C.R., Caron, N., Maiuri, T., Xia, J., Sipione, S. & Truant, R., 2011. Kinase inhibitors modulate huntingtin cell localization and toxicity. *Nature Chemical Biology*, 7(7), pp.453–60.

Aylward, E.H., Li, Q., Stine, O.C., Ranen, N., Sherr, M., Barta, P.E., Bylsma, F.W., Pearlson, G.D. & Ross, C.A., 1997. Longitudinal change in basal ganglia volume in patients with Huntington's disease. *Neurology*, 48(2), pp.394–399.

Aylward, E.H., Sparks, B.F., Field, K.M., Yallapragada, V., Shpritz, B.D., Rosenblatt, A., Brandt, J., Gourley, L.M., Liang, K., Zhou, H., Margolis, R.L. & Ross, C.A., 2004. Onset and rate of striatal atrophy in preclinical Huntington disease. *Neurology*, 63(1), pp.66–72.

Aziz, N.A., van der Burg, J.M., Landwehrmeyer, G.B., Brundin, P., Stijnen, T. & Roos, R.A.C., 2008. Weight loss in Huntington disease increases with higher CAG repeat number. *Neurology*, 71(19), pp.1506–1513.

Bae, B.-I., Xu, H., Igarishi, S., Fujimuro, M., Agrawal, N., Taya, Y., Hayward, S.D., Moran, T.H., Montell, D., Ross, C.A., Snyder, S.H. & Sawa, A., 2005. p53 mediates cellular

dysfunction and behavioral abnormalities in Huntington's disease. *Neuron*, 47(1), pp.29–41.

Baliko, L., Csala, B. & Czopf, J., 2004. Suicide in Hungarian Huntington's disease patients. *Neuroepidemiology*, 23(5), pp.258–260.

Bangs, P., Burke, B., Powers, C., Craig, R., Purohit, A. & Doxsey, S., 1998. Functional analysis of Tpr: identification of nuclear pore complex association and nuclear localization domains and a role in mRNA export. *The Journal of Cell Biology*, 143(7), pp.1801–12..

Baquet, Z.C., Gorski, J.A. & Jones, K.R., 2004. Early striatal dendrite deficits followed by neuron loss with advanced age in the absence of anterograde cortical brain-derived neurotrophic factor. *Journal of Neuroscience*, 24(17), pp.4250–4258.

Bates, G. & Murphy, K.P., 2002. Mouse Models of Huntington's Disease. In G. P. Bates, P. Harper, & A. L. Jones, eds. *Huntington's Disease*. Oxford, UK: Oxford University Press, pp. 387–426.

Battaglia, G., Cannella, M., Riozzi, B., Orobello, S., Maat-Schieman, M.L., Aronica, E., Busceti, C.L., Ciarmiello, A., Alberti, S., Amico, E., Sassone, J., Sipione, S., Bruno, V., Frati, L., Nicoletti, F. & Squitieri, F., 2011. Early defect of transforming growth factor β1 formation in Huntington's disease. *Journal of Cellular and Molecular Medicine*, 15(3), pp.555–71.

Bauer, P.O. & Nukina, N., 2009. The pathogenic mechanisms of polyglutamine diseases and current therapeutic strategies. *Journal of Neurochemistry*, 110(6), pp.1737–65.

Bayliss, R., Littlewood, T., Strawn, L.A., Wente, S.R. & Stewart, M., 2002. GLFG and FxFG nucleoporins bind to overlapping sites on importin-beta. *Journal of Biological Chemistry*, 277(52), pp.50597–50606.

Bayram-Weston, Z., Torres, E.M., Jones, L., Dunnett, S.B. & Brooks, S.P., 2012. Light and electron microscopic characterization of the evolution of cellular pathology in the Hdh(CAG)150 Huntington's disease knock-in mouse. *Brain Research Bulletin*, 88(2-3), pp.189–98.

Becanovic, K., Pouladi, M.A., Lim, R., Kuhn, A., Pavlidis, P., Luthi-Carter, R., Hayden, M.R. & Leavitt, B.R., 2010. Transcriptional changes in Huntington disease identified using genome-wide expression profiling and cross-platform analysis. *Human Molecular Genetics*, 19(8), pp.1438–52.

Bechtel, N., Acharya, T., Sturrock, A., Jauffret, C., Say, M.J., Patel, A., Read, J.E., T'Hart, E., van den Bogaard, S.J.A., Duerr, A., Leavitt, B.R., Roos, R.A.C., Langbehn, D.R., Tabrizi, S.J., Reilmann, R., 2010. Speeded tapping assesses progression of Huntington's disease within one year - Results from the TRACK-HD study. *Journal of Neurology Neurosurgery and Psychiatry*, 81(1), p.A27.

Benjamini, Y. & Hochberg, Y., 1995. Controlling the false discovery rate - A practical and powerful approach to multiple testing. *Journal of the Royal Statistical Society Series B-Methodological*, 57(1), pp.289–300.

Benn, C.L., Sun, T., Sadri-Vakilim G., McFarland, K.N., DiRocco, D.P., Yohrling, G.J., Clark, T.W., Bouzou, B. & Cha, J-H. J., 2008. Huntingtin modulates transcription, occupies gene promoters in vivo, and binds directly to DNA in a polyglutamine-dependent manner. *The Journal of Neuroscience*, 28(42), pp.10720–33.

Berardelli, A., Noth, J., Thompson, P.D., Bollen, E.L.E.M., Curra, A., Deuschl, G., van Dijk, J.G., Topper, R., Schwarz, M. & Roos, R.A.S., 1999. Pathophysiology of chorea and bradykinesia in Huntington's disease. *Movement Disorders*, 14(3), pp.398–403.

Berrios, G.E., Wagle, A.C., Markova, I.S., Wagle, S.A., Rosser, A. & Hodges, J.R., 2002. Psychiatric symptoms in neurologically asymptomatic Huntington's disease gene carriers: a comparison with gene negative at risk subjects. *Acta Psychiatrica Scandinavica*, 105(3), pp.224–230.

Bessert, D. A., Gutridge, K.L, Dunbar, J.C. & Carlock, L.R., 1995. The identification of a functional nuclear localization signal in the Huntington disease protein. *Brain Research. Molecular Brain Research*, 33(1), pp.165–73.

Bjorkqvist, M., Wild, E.J., Thiele, J., Silvestroni, A., Andre, R., Lahiri, N., Raibon, E., Lee, R.V., Benn, C.L., Soulet, D., Magnusson, A., Woodman, B., Landles, C., Pouladi, M.A., Hayden, M.R., Khalili-Shirazi, A., Lowdell, M.W., Brundin, P., Bates, G.P., Leavitt, B.R., Moller, T. & Tabrizi, S.J., 2008. A novel pathogenic pathway of immune activation detectable before clinical onset in Huntington's disease. *Journal of Experimental Medicine*, 205(8), pp.1869–1877.

Blanchette, F., Rivard, N., Ruddm, P., Grondin, F., Attisano, L. & Dubois, C.M., 2001. Cross-talk between the p42/p44 MAP kinase and Smad pathways in transforming growth factor beta 1-induced furin gene transactivation. *The Journal of Biological Chemistry*, 276(36), pp.33986–94.

BlockGalarza, J., Chase, K.O., Sapp, E., Vaughn, K.T., Vallee, R.B., DiFigliam M. & Aronin, N., 1997. Fast transport and retrograde movement of huntingtin and HAP 1 in axons. *Neuroreport*, 8(9-10), pp.2247–2251.

Bonelli, R.M., Bonelli, C.M., Koeltringer, P.X. & Obermayer-Pietsch, B.X., 2002. Osteoporosis in Huntington's disease. *Neurology*, 58(7, 3), pp.A307–A308.

Borovecki, F., Lovrecic, L., Zhou, J., Jeong, H., Then, F., Rosas, H.D., Hersch, S.M., Hogarth, P., Bouzou, B., Jensen, R.V. & Krainc, D., 2005. Genome-wide expression profiling of human blood reveals biomarkers for Huntington's disease. *Proceedings of the National Academy of Sciences of the United States of America*, 102(31), pp.11023–11028.

Boudreau, R.L., McBride, J.L., Martins, I., Shen, S., Xing, Y., Carter, B.J. & Davidson, B.L., 2009. Nonallele-specific Silencing of Mutant and Wild-type Huntingtin Demonstrates Therapeutic Efficacy in Huntington's Disease Mice. *Molecular Therapy*, 17(6), pp.1053–1063.

Bourillot, P.-Y. & Savatier, P., 2010. Krüppel-like transcription factors and control of pluripotency. *BMC Biology*, 8, p.125.

Boutell, J.M., Thomas, P., Neal, J.W., Weston, V.J., Duce, J., Harper, P.S. & Jones, A.L., 1999. Aberrant interactions of transcriptional repressor proteins with the Huntington's disease gene product, huntingtin. *Human Molecular Genetics*, 8(9), pp.1647–1655.

Bowles, K.R., Brooks, S.P., Dunnett, S.B. & Jones, L., 2012. Gene expression and behaviour in mouse models of HD. *Brain Research Bulletin*, 88(2-3), pp.276–84.

Bradford, M., 1976. Rapid and sensitive method for quantitation of microgram quantities of protein utilizing principles of protein-dye binding. *Analytical Biochemistry*, 72(1-2), pp.248–254.

Brito, V., Puigdellivol, M., Giralt, A., del Toro, D, Alberch, J. & Ginés, S., 2013. Imbalance of p75 NTR/TrkB protein expression in Huntington's disease: implication for neuroprotective therapies. *Cell Death and Disease*, 4(e595), pp.1–15.

Brooks, S.P., Betteridgea, H., Trueman, R.C., Jones, L. & Dunnett, S.B., 2006. Selective extra-dimensional set shifting deficit in a knock-in mouse model of Huntington's disease. *Brain Research Bulletin*, 69(4), pp.452–457.Brooks, S., Higgs, G., et al., 2012. Longitudinal analysis of the behavioural phenotype in Hdh(CAG)150 Huntington's disease knock-in mice. *Brain Research Bulletin*, 88(2-3), pp.182–8..

Brooks, S.P., Janghra, N., Workman, V., Bayram-Weston, Z., Jones, L. & Dunnett, S.B., 2012. Longitudinal analysis of the behavioural phenotype in R6/1 (C57BL/6J) Huntington's disease transgenic mice. *Brain Research Bulletin*, 88(2-3), pp.94–103.

Brooks, S.P., Jones, L. & Dunnett, S.B., 2012. Comparative analysis of pathology and behavioural phenotypes in mouse models of Huntington's disease. *Brain Research Bulletin*, 88(2-3), pp.81–93.

Bruce, A.W., Donaldson, I.J., Wood, I.C., Yerbury, S.A., Sadowski, M.I., Chapman, M., Gottgens, B. & Buckley, N.J., 2004. Genome-wide analysis of repressor element 1 silencing transcription factor/neuron-restrictive silencing factor (REST/NRSF) target genes. *Proceedings of the National Academy of Sciences of the United States of America*, 101(28), pp.10458–10463.

Buckley, N.J., Johnson, R., Zuccato, C., Bithell, A. & Cattaneo, E., 2010. The role of REST in transcriptional and epigenetic dysregulation in Huntington's disease. *Neurobiology of Disease*, 39(1), pp.28–39.

van der Burg, J.M.M., Björkqvist, M. & Brundin, P., 2009. Beyond the brain: widespread pathology in Huntington's disease. *Lancet Neurology*, 8(8), pp.765–74.

Cabodi, S., Morello, V., Masi, A., Cicchi, R., Broggio, C., Distefano, P., Brunelli, E., Silengo, L., Pavone, F., Arcangeli, A., Turco, E., Tarone, G., Moro, L. & Defilippi, P., 2009. Convergence of integrins and EGF receptor signaling via PI3K/Akt/FoxO pathway in early gene Egr-1 expression. *Journal of Cellular Physiology*, 218(2), pp.294–303.

Caja, L., Sancho, P., Bertran, E. & Fabregat, I., 2011. Dissecting the effect of targeting the epidermal growth factor receptor on TGF-β-induced-apoptosis in human hepatocellular carcinoma cells. *Journal of Hepatology*, 55(2), pp.351–8.

Calonge, M.J. & Massagué, J., 1999. Smad4/DPC4 silencing and hyperactive Ras jointly disrupt transforming growth factor-beta antiproliferative responses in colon cancer cells. *The Journal of Biological Chemistry*, 274(47), pp.33637–43.

Campbell, M.C., Stout, J.C. & Finn, P.R., 2004. Reduced autonomic responsiveness to gambling task losses in Huntington's disease. *Journal of the International Neuropsychological Society*, 10(02), pp.239–245.

Canals, J.M., Checa, N., Marco, S., Akerud, P., Michels, A., Perez-Navarro, E., Tolosa, E., Arenas, E. & Alberch, J., 2001. Expression of brain-derived neurotrophic factor in cortical neurons is regulated by striatal target area. The *Journal of Neuroscience*, 21(1), pp.117–124.

Canals, J.M., Pineda, J.R., Torres-Peraza, J.F., Bosch, M., Martin-Ibanez, R., Munoz, M.T., Mengod, G., Ernfors, P. & Alberch, J., 2004. Brain-derived neurotrophic factor regulates the onset and severity of motor dysfunction associated with enkephalinergic neuronal degeneration in Huntington's disease. The *Journal of Neuroscience*, 24(35), pp.7727–7739.

Cannella, M., Gellera, C., Maglione, V., Giallonardo, P., Cislaghi, G., Muglia, M., Quattrone, A., Pierelli, F., Di Donato, S. & Squitieri, F., 2004. The gender effect in juvenile Huntington disease patients of Italian origin. *American Journal of Medical Genetics. Part B, Neuropsychiatric Genetics*, 125B(1), pp.92–8.

Cannella, M., Maglione, V., Martion, T., Ragona, G., Frati, L., Li, G-M. & Squitieri, F., 2009. DNA instability in replicating Huntington's disease lymphoblasts. *BMC Medical Genetics*, 10, p.11.

Carnemolla, A., Fossale, E., Agostoni, E., Michelazzi, S., Calligaris, R., De Maso, L., Del Sal, G., MacDonald, M.E. & Persichetti, F., 2009. Rrs1 is involved in endoplasmic reticulum stress response in Huntington disease. *The Journal of Biological Chemistry*, 284(27), pp.18167–73.

Carri, A.D., Onorati, M., Lelos, M.J., Castiglioni, V., Faedo, A., Menon, R., Camnasio, S., Vuono, R., Spaiardi, P., Talpo, F., Toselli, M., Martino, G., Barker, R.A., Dunnett,

S.B., Biella, G. & Cattaneo, E., 2013. Developmentally coordinated extrinsic signals drive human pluripotent stem cell differentiation toward authentic DARPP-32+ medium-sized spiny neurons. *Development*, 140(2), pp.301–12.

Carter, R.J., Lione, L.A., Humby, T., Mangiarini, L., Mahal, A., Bates, G.P., Dunnett, S.B. & Morton, A.J., 1999. Characterization of progressive motor deficits in mice transgenic for the human Huntington's disease mutation. *The Journal of Neuroscience*, 19(8), pp.3248–3257.

Cattaneo, E. & Conti, L., 1998. Generation and characterization of embryonic striatal conditionally immortalised ST14A cells. *Journal of Neuroscience Research*, 53(2), pp.223–234.

Cattaneo, E., Zuccato, C. & Tartari, M., 2005. Normal huntingtin function: an alternative approach to Huntington's disease. *Nature Reviews. Neuroscience*, 6(12), pp.919–30.

Cayzac, S., Delcasso, S., Paz, V., Jeantet, Y. & Cho, Y.H., 2011. Changes in striatal procedural memory coding correlate with learning deficits in a mouse model of Huntington disease. *Proceedings of the National Academy of Sciences of the United States of America*, 108(22), pp.9280–5.

Cha, J.-H.J., 2007. Transcriptional signatures in Huntington's disease. *Progress in Neurobiology*, 83(4), pp.228–48.

Chambers, S.M., Fasano, C.A., Papapetrou, E.P., Tomishima, M., Sadelain, M. & Studer, L., 2009. Highly efficient neural conversion of human ES and iPS cells by dual inhibition of SMAD signaling. *Nature Biotechnology*, 27(3), pp.275–280.

Chang, J.R., Ghafouri, M., Mukerjee, R., Bagashev, A., Chabrashvili, T. & Sawaya, B.E., 2012. Role of p53 in neurodegenerative diseases. *Neuro-degenerative Diseases*, 9(2), pp.68–80.

Chen, B.P.C., Liang, G.S., Whelan, J. & Hai, T.W., 1994. ATF3 and ATF3-delta-zip - Transcriptional repression versus activation by alternatively spliced isoforms. *Journal of Biological Chemistry*, 269(22), pp.15819–15826.

Chen, L.-W., Horng, L-Y., Wu, C-L., Sung, H-C. & Wi, R-T., 2012. Activating mitochondrial regulator PGC-1α expression by astrocytic NGF is a therapeutic strategy for Huntington's disease. *Neuropharmacology*, 63(4), pp.719–32.

Cheng, Y., Peng, Q., Hou, Z., Aggarwal, M., Zhang, J., Mori, S., Ross, C.A. & Duan, W., 2011. Structural MRI detects progressive regional brain atrophy and neuroprotective effects in N171-82Q Huntington's disease mouse model. *NeuroImage*, 56(3), pp.1027–34.

Chen-Plotkin, A.S., Sadri-Vakili, G., Yohrling, G.J., Bravernan, M.W., Berin, C.L., Glajch, K.E., DiRocco, D. P., Farrella, L.A., Krainc, D., Ginés, S., MacDonald, M.E. & Cha, J-

H. J., 2006. Decreased association of the transcription factor Sp1 with genes downregulated in Huntington's disease. *Neurobiology of Disease*, 22(2), pp.233–241.

Chisholm, L.Z., Flavin, K.T., Paulsen, J.S. & Ready, R., 2013. Psychological well-being in persons affected by Huntington's disease: a comparison of at-risk, prodromal, and symptomatic groups. *Journal of Health 1psychology*, 18(3), pp.408–18.

Chong, Z.Z., Li, F. & Maiese, K., 2005. Activating Akt and the brain's resources to drive cellular survival and prevent inflammatory injury. *Histology and Histopathology*, 20(1), pp.299–315.

Ciarmiello, A., Cannella, M., Lastoria, S, Simonelli, M., Frati, L., Rubinsztein, D.C. & Squitieri, F., 2006. Brain white-matter volume loss and glucose hypometabolism precede the clinical symptoms of Huntington's disease. *Journal of Nuclear Medicine*, 47(2), pp.215–222.

Conforti, P., Camnasio, S., Mutti, C., Valenza, M., Thompson, M., Fossale, E., Zeitlin, S., MacDonald, M.E., Zuccato, C. & Cattaneo, E., 2013. Lack of huntingtin promotes neural stem cells differentiation into glial cells while neurons expressing huntingtin with expanded polyglutamine tracts undergo cell death. *Neurobiology of Disease*, 50, pp.160–170.

Cong, S.Y., Pepers, B.A., Evert, B.O., Rubinsztein, D.C., Roos, R.A.C, van Ommen, G.J.B. & Dorsman, J.C., 2005. Mutant huntingtin represses CBP, but not p300, by binding and protein degradation. *Molecular and Cellular Neuroscience*, 30(4), pp.560–571.

Coré, N., Caubit, X., Metchat, A., Boned, A., Djabali, M. & Fasano, L., 2007. Tshz1 is required for axial skeleton, soft palate and middle ear development in mice. *Developmental Biology*, 308(2), pp.407–20.

Cornett, J., Cao, F., Wang, C-E., Ross, C.A., Bates, G.P., Li, S-H. & Li, X-J., 2005. Polyglutamine expansion of huntingtin impairs its nuclear export. *Nature Genetics*, 37(2), pp.198–204.

Cosgaya, J.M. & Aranda, A., 1999. The ras oncogene inhibits growth factor inducibility of early response genes, and promotes selectively expression of NGFI-A in a PC12 cell line. *FEBS Letters*, 445(2-3), pp.329–32.

Cowin, R.-M., Bui, N., Graham, D., Green, J.R., Grueninger, S., Yuya-Paylor, L.A., Syed, A.U., Weiss, A. & Paylor, R., 2011. Onset and progression of behavioral and molecular phenotypes in a novel congenic R6/2 line exhibiting intergenerational CAG repeat stability. *PloS One*, 6(12), p.e28409.

Crauford, D. & Snowden, J., 2002. Neuropsychological and neuropsychiatric aspects of Huntington's disease. In G. Bates, P. Harper, & L. Jones, eds. *Huntington's Disease*. Oxford, UK: Oxford University Press, pp. 62–94.

Crocker, S.F., Costain, W.J. & Robertson, H. a, 2006. DNA microarray analysis of striatal gene expression in symptomatic transgenic Huntington's mice (R6/2) reveals neuroinflammation and insulin associations. *Brain Research*, 1088(1), pp.176–86.

Crook, Z.R. & Housman, D., 2011. Huntington's Disease: Can Mice Lead the Way to Treatment? *Neuron*, 69(3), pp.423–435.

Cudkowicz, M. & Kowall, N.W., 1990. Degeneration of pyramidal projection neurons in Huntingtons-disease cortex. *Annals of Neurology*, 27(2), pp.200–204.

Dalrymple, A., Wild, E.J., Joubert, R., Sathasivam, K., Bjorkvist, M., Peterson, A., Jackson, G.S., Isaacs, J.D., Kristiansen, M., Bates, G.P., Leavitt, B.R., Keir, G., Ward, M. & Tabrizi, S., 2007. Proteomic profiling of plasma in Huntington's disease reveals neuroinflammatory activation and biomarker candidates. *Journal of Proteome Research*, 6(7), pp.2833–2840.

Datta, S.R., Dudek, H., Tao, X., Masters, S., Fu, H.A., Gotoh, Y. & Greenberg, M.E., 1997. Akt phosphorylation of BAD couples survival signals to the cell-intrinsic death machinery. *Cell*, 91(2), pp.231–241.

Davenport, C.B. & Muncey, E.B., 1916. Huntington's chorea in relation to heredity and eugenics. *American Journal of Insanity*, 73(2), pp.195–222.

Davies, S.W., Turmaine, M., Cozens, B.A., DiFiglia, M., Sharp, A.H., Ross, C.A., Scherzinger, E., Wanker, E.E., Mangiarini, L. & Bates, G.P., 1997. Formation of neuronal intranuclear inclusions underlies the neurological dysfunction in mice transgenic for the HD mutation. *Cell*, 90(3), pp.537–48.

Day, J.J. & Sweatt, J.D., 2010. DNA methylation and memory formation. *Nature Neuroscience*, 13(11), pp.1319–1323.

De Rooij, K.E., De Koning Gans, P.A.M., Skraastas, M.I., Belfroid, R.D., Vegter-Van Der Vlis, M., Roos, R.A., Bakker, E., van Ommen, G.J., Den Dunnen, J.T. & Losekoot, M., 1993. Dynamic mutation in Dutch Huntington's disease patients: increased paternal repeat instability extending to within the normal size range. *Journal of Medical Genetics*, 30(12), pp.996–1002.

De Rooij, K.E., De Koning Gans, P.A.M., Losekoot, M., Bakker, E., den Dunnen, J.T., Vegter-van der Vlis, M., Roos, R.A.C. & van Ommen, G.J.B., 1993. Borderline repeat expansion in Huntington's disease. *The Lancet*, 342(8885), pp.1491–1492.

De Rooij, K.E., Dorsman, J.C., Smoor, M.A., Den Dunnen, J.T. & van Ommen, G.J.B., 1996. Subcellular localization of the Huntington's disease gene product in cell lines by immunofluorescence and biochemical subcellular fractionation. *Human Molecular Genetics*, 5(8), pp.1093–1099.

Desmond, C.R., Atwal, R.S., Xia, J. & Truant, R., 2012. Identification of a karyopherin β1/β2 proline-tyrosine nuclear localization signal in huntingtin protein. *The Journal of Biological Chemistry*, 287(47), pp.39626–33.

Desmond, C.R., Maiuri, T. & Truant, R., 2013. A multifunctional, multi-pathway intracellular localization signal in Huntingtin. *Communicative & Integrative Biology*, 6(2), p.e23318.

Dey, N.D., Bombard, M.C., Roland, B. P., Davidson, S., Lu, M., Rossignol, J., Sandstrom, M.I., Skeel, R.L., Lescaudron, L. & Dunbar, G.L., 2010. Genetically engineered mesenchymal stem cells reduce behavioral deficits in the YAC 128 mouse model of Huntington's disease. *Behavioural Brain Research*, 214(2), pp.193–200.

Di Pardo, A., Maglione, V., Alpaugh, M., Horkey, M., Atwal, R.S., Sassone, J., Ciammola, A., Steffan, J.S., Fouad, K., Truant, R. & Sipione, S., 2012. Ganglioside GM1 induces phosphorylation of mutant huntingtin and restores normal motor behavior in Huntington disease mice. *Proceedings of the National Academy of Sciences of the United States of America*, 109(9), pp.3528–33.

DiFiglia, M., Sapp, E., Chase, K., Schwarz, C., Meloni, A., Young, C., Martin, E., Vonsattel, J.P., Carraway, R. & Reeves, S.A., 1995. Huntingtin is a cytoplasmic protein associated with vesicles in human and rat brain neurons. *Neuron*, 14(5), pp.1075–81.

DiFiglia, M., 1997. Aggregation of Huntingtin in Neuronal Intranuclear Inclusions and Dystrophic Neurites in Brain. *Science*, 277(5334), pp.1990–1993.

DiFiglia, M. & Lombroso, P.J., 2000. Genetics of Childhood Disorders: X. Huntington Disease. *Journal of the American Academy of Child & Adolescent Psychiatry*, 39(1), pp.120–122.

Dimaio, L., Squitieri, F., Napolitano, G., Campanella, G., Trofatter, J.A. & Conneally, P.M., 1993. Onset symptoms in 510 patients with Huntington's disease. *Journal of Medical Genetics*, 30(4), pp.289–292.

Ding, W.E.I., Shi, W.E. I., Belluschi, S., Groffen, J., Heisterkamp, N., Minoo, P. & Warburton, D., 2007. Sprouty2 downregulation plays a pivotal role in mediating crosstalk between TGF-B1 signaling and EGF as well as FGF receptor tyrosine kinase-ERK pathways in mesenchymal cells. *Journal of Cellular Physiology*, 212(3), pp.796–806.

Djoussé, L, Knowlton, B., Cupples, L.A., Marder, K., 2002. Weight loss in early stage of Huntington's disease. *Neurology*, 59(9), pp.1325–1330.

Djoussé, L., Knowlton, B., Hayden, M.R, Almqvist, E.W., Brinkman, R.R., Ross, C.A., Margolis, R.L., Rosenblatt, A., Durr, A., Dode, C., Morrison, P.J., Novelletto, A., Frontali, M., Trent, R.J.A., McCusker, E., Gomez-Tortosa, E., Cabrero, D.M., Jones, R., Zanko, A., Nance, M., Abramson, R.K., Suchowersky, O., Paulsen, J.S., Harrison,

M.B., Yang, Q., Cupples, L.A., Mysore, J., Gusella, J.F., MacDonald, M.E. & Myers, R.H., 2004. Evidence for a modifier of onset age in Huntington disease linked to the HD gene in 4p16. *Neurogenetics*, 5(2), pp.109–114.

Długosz, M. & Trylska, J., 2011. Secondary structures of native and pathogenic huntingtin N-terminal fragments. *The Journal of Physical Chemistry. B*, 115(40), pp.11597–608.

Dorsman, J.C., Smoor, M.A., Maat-Schieman, M.L., Bout, M., Siesling, S., van Duinen, S.G., Verschuuren, J.J., den Dunnen, J.T., Roos, R.A. & van Ommen, G.J., 1999. Analysis of the subcellular localization of huntingtin with a set of rabbit polyclonal antibodies in cultured mammalian cells of neuronal origin: comparison with the distribution of huntingtin in Huntington's disease autopsy brain. *Philosophical Transactions of the Royal Society of London. Series B, Biological Sciences*, 354(1386), pp.1061–7.

Dougherty, S.E., Reeves, J.L., Lesort, M., Detloff, P.J. & Cowell, R.M., 2013. Purkinje cell dysfunction and loss in a knock-in mouse model of Huntington disease. *Experimental Neurology*, 240, pp.96–102.

Douglas, I., Evans, S., Rawlins, M.D., Smeeth, L., Tabrizi, S. & Wexler, N.S., 2013. Juvenile Huntington's disease: a population-based study using the General Practice Research Database. *BMJ Open*, 3(4), pp.1–5.

Dragatsis, I., Levine, M.S. & Zeitlin, S., 2000. Inactivation of Hdh in the brain and testis results in progressive neurodegeneration and sterility in mice. *Nature Genetics*, 26(3), pp.300–306.

Duesterhus, P., Schimmelmann, B.G., Wittkugel, O. & Schulte-Markwort, M., 2004. Huntington disease: a case study of early onset presenting as depression. *Journal of the American Academy of Child and Adolescent Psychiatry*, 43(10), pp.1293–7.

Duff, K., Paulsen, J., Mills, J., Beglinger, L.J., Moder, D.J., Smith, M.M., Langbehn, D., Stout, J., Queller, S. & Harrington, D.L., 2010. Mild cognitive impairment in prediagnosed Huntington disease. *Neurology*, 75(6), pp.500–507.

Dumas, E.M., van den Bogaard, S.J.A., Ruber, M.E., Reilman, R.R., Stout, J.C., Craufurd, D., Hicks, S.L., Kennard, C., Tabrizi, S.J., van Buchem, M.A., van der Grond, J. & Roos, R.A.C., 2012. Early changes in white matter pathways of the sensorimotor cortex in premanifest Huntington's disease. *Human Brain Mapping*, 33(1), pp.203–212.

Dunah, A.W., Jeong, H., Griffin, A., Kim, Y-M., Standaert, D.G., Hersch, S.M., Mouradian, M.M., Young, A.B., Tanese, N. & Krainc, D., 2002. Sp1 and TAFII130 transcriptional activity disrupted in early Huntington's disease. *Science*, 296(5576), pp.2238–43.

Dunnett, S. & Bjorklund, A., 1999. Dissecting embryonic neural tissues for transplantation. In A. Boulton, G. Baker, & S. Dunnett, eds. *Neural Transplantation Methods*. Totowa, New Jersey, USA: Humana Press Inc, pp. 3–25.

Duyao, M.P., Ambrose, C.M., Myers, R.H., Novalletto, A., Persichetti, F., Frontali, M., Folstein, S., Ross, C., Franz, M., Abbott, M., Gray, J., Conneally, P., Young, A., Penney, J., Hollingsworth, Z., Shoulson, I., Lazzarini, A., Falek, A., Koroshetz, W., Sax, D., Bird, E., Vonsattel, J., Bonilla, E, Alvir, J., Bickham Conde, J., Cha, J-H., Dure, L., Gomez, F., Ramos, M., Sanchez-Ramos, J., Snodgrass, S., de Young, M., Wexler, N., Moscowitz, C., Penchaszadeh, G., Macfarlane, H., Anderson, M., Jenkins, B., Srinidhi, J., Barnes, G., Gusella, J. & MacDonald, M., 1993. Trinucleotide repeat length instability and age of onset in Huntington's disease. *Nature Genetics*, 4(4), pp.387–392.

Dyer, R.B. & McMurray, C.T., 2001. Mutant protein in Huntington disease is resistant to proteolysis in affected brain. *Nature Genetics*, 29(3), pp.270–278.

Eferl, R. & Wagner, E.F., 2003. AP-1: A double-edged sword in tumorigenesis. *Nature Reviews Cancer*, 3(11), pp.859–868.

Ehata, S., Hanyu, A., Hayashi, M., Aburatani, H., Kato, Y., Fujime, M., Saitoh, M., Miyazawa, K., Imamura, T. & Miyazono, K., 2007. Transforming growth factor-beta promotes survival of mammary carcinoma cells through induction of antiapoptotic transcription factor DEC1. *Cancer Research*, 67(20), pp.9694–703.

Ehrnhoefer, D.E., Sutton, L. & Hayden, M.R., 2011. Small changes, big impact: posttranslational modifications and function of huntingtin in Huntington disease. *The Neuroscientist*, 17(5), pp.475–92.

El Kochairi, I., Letovanec, I., Uffer, S., Munier, F.L., Chaubert, P. & Schorderet, D.F., 2006. Systemic investigation of keratoepithelin deposits in TGFBI/BIGH3-related corneal dystrophy. *Molecular Vision*, 12(April), pp.461–6.

Evans, S.J., Douglas, I., Rawlins, M.D., Wexler, N.S., Tabrizi, S.J. & Smeeth, L., 2013. Prevalence of adult Huntington's disease in the UK based on diagnoses recorded in general practice records. *Journal of Neurology, Neurosurgery, and Psychiatry*, pp.1–6.

Faber, P.W., Barnes, G.T., Srinidhi, J., Chen, J., Gusella, J.F. & MacDonald, M.E., 1998. Huntingtin interacts with a family of WW domain proteins. *Human Molecular Genetics*, 7(9), pp.1463–74.

Fan, F.Y., Jin, S.Q., Amundson, S.A., Tong, T., Fan, W.H., Zhao, H.C., Zhu, X.C., Mazzacurati, L., Li, X.X., Petrik, K.L., Fornace, A.J., Rajasekaran, B. & Zhan, Q.M., 2002. ATF3 induction following DNA damage is regulated by distinct signaling pathways and over-expression of ATF3 protein suppresses cells growth. *Oncogene*, 21(49), pp.7488–7496.

Fan, J., Gladding, C.M., Wang, L., Zhang, L.Y.J., Kaufman, A.M., Milnerwood, A.J. & Raymond, L.A., 2012. P38 MAPK is involved in enhanced NMDA receptor-dependent excitotoxicity in YAC transgenic mouse model of Huntington disease. *Neurobiology of Disease*, 45(3), pp.999–1009.

Farrer, L.A. & Meaney, F.J., 1985. An anthropometric assessment of Huntington's disease patients and families. *American Journal of Physical Anthropology*, 67(3), pp.185–194.

Farrer, L.A., Cupples, L.A., Kiely, D.K., Conneally, P.M. & Myers, R.H., 1992. Inverse relationship between age at onset of Huntington disease and paternal age suggests involvement of genetic imprinting. *American Journal of Human Genetics*, 50(3), pp.528–535.

Faught, E., Falgout, J.C. & Leli, D.A., 1983. Late-onset variant of Huntingtons-chorea. *Southern Medical Journal*, 76(10), pp.1266–1270.

Fedele, V., Roybon, L., Nordström, U., Li, J-Y. & Brundin, P., 2010. Neurogenesis in R6/2 mouse model of Huntington's disease is impaired at the level of NeuroD1. *Neuroscience*, 173, pp.76 – 81.

Ferrante, R.J., Kowall, N.W., Beal, M.F., Richardson, E.P., Bird, E.D. & Martin, J.B., 1985. Selective sparing of a class of striatal neurons in Huntingtons-disease. *Science*, 230(4725), pp.561–563.

Ferrante, R.J., Beal M.F., Kowall, N.W., Richardson, E.P. & Martin. J.B., 1987. Sparing of avetylcholinesterase-containing striatal neurons in Huntingtons-disease. *Brain Research*, 411(1), pp.162–166.

Ferrante, R.J., Kowall, N.W. & Richardson, E.P., 1991. Proliferative and degenerative changes in striatal spiny neurons in Huntington's disease : A combined study using the Section-Golgi method and calbindin D28k immunocytochemistry. *The Journal of Neuroscience*, 11(12), pp.3877–3887.

Ferrante, R.J., Gutekunst, C.A., Persichetti, F., McNeil, S.M., Kowall, N.W., Gusella, J.F., MacDonald, M.E., Beal, M.F. & Hersch, S.M., 1997. Heterogeneous topographic and cellular distribution of Huntington expression in the normal human neostriatum. *Journal of Neuroscience*, 17(9), pp.3052–3063.

Ferrante, R.J., Kubilus, J.K., Lee, J., Ryu, H., Beesen, A., Zucker, B., Smith, K., Kowall, N.W., Rata, R.R., Luthi-Carter, R. & Hersch, S.M., 2003. Histone deacetylase inhibition by sodium butyrate chemotherapy ameliorates the neurodegenerative phenotype in Huntington's disease mice. *The Journal of Neuroscience*, 23(28), pp.9418–9427.

Ferrante, R.J., 2009. Mouse models of Huntington's disease and methodological considerations for therapeutic trials. *Biochimica et Biophysica Acta*, 1792(6), pp.506–20.

Ferrer, I, Goutan, E., Marin, C., Rey, M.J. & Ribalta, T., 2000. Brain-derived neurotrophic factor in Huntington disease. *Brain Research*, 866(1-2), pp.257–261.

Ferrigno, P. & Silver, P. A., 2000. Polyglutamine expansions: proteolysis, chaperones, and the dangers of promiscuity. *Neuron*, 26(1), pp.9–12.

Feyeux, M., Bourgois-Rocha, F., Redfern, A., Giles, P., Lefort, N., Aubert, S., Bonnefond, C., Bugi, A., Ruiz, M., Deglon, N., Jones, L., Peschanski, M., Allen, N.D. & Perrier, A. L., 2012. Early transcriptional changes linked to naturally occurring Huntington's disease mutations in neural derivatives of human embryonic stem cells. *Human Molecular Genetics*, 21(17), pp.3883–3895.

Finch, J.S., Joseloff, E. & Bowden, G.T., 2002. JunB negatively regulates AP-1 activity and cell proliferation of malignant mouse keratinocytes. *Journal of Cancer Research and Clinical Oncology*, 128(1), pp.3–10.

Folstein, S.E., 1989. The psychopathology of Huntington's disease. *Journal of Nervous and Mental Disease*, 177(10), p.645.

Fortin, J. & Bernard, D.J., 2010. SMAD3 and EGR1 physically and functionally interact in promoter-specific fashion. *Cellular Signalling*, 22(6), pp.936–43.

Fossale, E., Wheeler, V.C., Vrbanac, V., Lebel, L-A., Teed, A., Mysore, J.S., Gusella, J.F., MacDonald, M.E. & Persichetti, F., 2002. Identification of a presymptomatic molecular phenotype in Hdh CAG knock-in mice. *Human Molecular Genetics*, 11(19), pp.2233–41

Fossale, E., Seong, I.S., Coser, K.R., Shioda, T., Kohane, I.S., Wheeler, V.C., Gusella, J.F., MacDonald, M.E. & Lee, J-M., 2011. Differential effects of the Huntington's disease CAG mutation in striatum and cerebellum are quantitative not qualitative. *Human Molecular Genetics*, 20(21), pp.4258–67..

Franzdottir, S.R., Engelen, D., Yuya-Aydemir, Y., Schmidt, I., Aho, A. & Klaembt, C., 2009. Switch in FGF signalling initiates glial differentiation in the Drosophila eye. *Nature*, 460(7256), pp.758–U106.

Fricker, M., Hollinshead, M., White, N. & Vaux, D., 1997. Interphase nuclei of many mammalian cell types contain deep, dynamic, tubular membrane-bound invaginations of the nuclear envelope. *Journal of Cell Biology*, 136(3), pp.531–544.

Frosst, P., Guan, T., Subauste, C., Hahn, K. & Gerace, L., 2002. Tpr is localized within the nuclear basket of the pore complex and has a role in nuclear protein export. *The Journal of Cell Biology*, 156(4), pp.617–30.

Fuentes, L.Q., Reyes, C.E., Sarmiento, J.M., Villanueva, C.I., Figueroa, C.D., Navarro, J. & González, C.B., 2008. Vasopressin up-regulates the expression of growth-related immediate-early genes via two distinct EGF receptor transactivation pathways. *Cellular Signalling*, 20(9), pp.1642–50.

Furtado, S., Suchowersky, O., Rewcasle, N.B., Graham, L., Klimek, M.L. & Garber, A., 1996. Relationship between trinucleotide repeats and neuropathological changes in Huntington's disease. *Annals of Neurology*, 39(1), pp.132–136.

Fusco, F.R., Chen, Q., Lamoreaux, W.J., Figueredo-Cardenas, G., Jiao, Y., Coffman, J.A., Surmeier, D.J., Honig, M.G., Carlock, L.R. & Reiner, A., 1999. Cellular localization of huntingtin in striatal and cortical neurons in rats: Lack of correlation with neuronal vulnerability in Huntington's disease. *Journal of Neuroscience*, 19(4), pp.1189–1202.

Gafni, J. & Ellerby, L.M., 2002. Calpain activation in Huntington's disease. *The Journal of Neuroscience*, 22(12), pp.4842–4849.

Gafni, J., Hermel, E., Young, J.E., Wellington, C.L., Hayden, M.R. & Ellerby, L.M., 2004. Inhibition of calpain cleavage of huntingtin reduces toxicity - Accumulation of calpain/caspase fragments in the nucleus. *Journal of Biological Chemistry*, 279(19), pp.20211–20220.

Gardian, G., Browne, S.E., Choi, D.K., Klivenyi, P, Gregorio, J., Kubilus, J.K., Ryu, H., Langley, B., Ratan, R.R., Ferrante, R.J. & Beal, M.F., 2005. Neuroprotective effects of phenylbutyrate in the N171-82Q transgenic mouse model of Huntington's disease. *The Journal of Biological Chemistry*, 280(1), pp.556–563.

Gauthier, L.R., Charrin, B.C., Borrell-Pages, M., Dompierrem J.P., Rangone, H., Cordelieres, F.P., De May, J., MacDonald, M.E., Lessmann, V., Humbert, S. & Saudou, F., 2004. Huntingtin controls neurotrophic support and survival of neurons by enhancing BDNF vesicular transport along microtubules. *Cell*, 118(1), pp.127–138.

Ghaleb, A.M., Nandan, M.O., Chanchevalap, S., Dalton, W.B., Hisamuddin, I.M. & Yang, V.W., 2005. Kruppel-like factors 4 and 5: the yin and yang regulators of cellular proliferation. *Cell Research*, 15(2), pp.92–96.

Gianfriddo, M., Melani, A., Turchi, D., Giovannini, M.G. & Pedata, F., 2004. Adenosine and glutamate extracellular concentrations and mitogen-activated protein kinases in the striatum of Huntington transgenic mice. Selective antagonism of adenosine A2A receptors reduces transmitter outflow. *Neurobiology of Disease*, 17(1), pp.77–88.

Ginés, S., Ivanova, E., Seong, I-S., Saura, C.A. & MacDonald, M.E., 2003. Enhanced Akt signaling is an early pro-survival response that reflects N-methyl-D-aspartate receptor activation in Huntington's disease knock-in striatal cells. *The Journal of Biological Chemistry*, 278(50), pp.50514–22.

Ginés, S., 2003. Specific progressive cAMP reduction implicates energy deficit in presymptomatic Huntington's disease knock-in mice. *Human Molecular Genetics*, 12(5), pp.497–508.

Ginés, S., Bosch, M., Marco, S., Gavaldà, N., Dìaz-Hernández, M., Lucas, J.J., Canals, J.M. & Alberch, J., 2006. Reduced expression of the TrkB receptor in Huntington's disease mouse models and in human brain. *The European Journal of Neuroscience*, 23(3), pp.649–58.

Ginés, S., Paoletti, P. & Alberch, J., 2010. Impaired TrkB-mediated ERK1/2 activation in huntington disease knock-in striatal cells involves reduced p52/p46 Shc expression. *The Journal of Biological Chemistry*, 285(28), pp.21537–48.

Giovannone, B., Sabbadini, G., DiMaio, L., Calabrese, O., Castaldo, I., Frontali, M., Novelletto, A. & Squitieri, F., 1997. Analysis of (CAG)n size heterogeneity in somatic and sperm cell DNA from intermediate and expanded Huntington disease gene carriers. *Human Mutation*, 10(6), pp.458–464.

Giralt, A., Puigdellivol, M., Carretón, O., Paoletti, P., Valero, J., Parra-Damas, A., Saura, C.A., Alberch, J. & Ginés, S., 2012. Long-term memory deficits in Huntington's disease are associated with reduced CBP histone acetylase activity. *Human Molecular Genetics*, 21(6), pp.1203–16.

Godin, J.D., Poizat, G., Hickey, M.A., Maschat, F. & Humbert, S., 2010. Mutant huntingtin-impaired degradation of beta-catenin causes neurotoxicity in Huntington's disease. *The EMBO Journal*, 29(14), pp.2433–45.

Gokce, O., Runne, H., Kuhn, A. & Luthi-Carter, R., 2009. Short-term striatal gene expression responses to brain-derived neurotrophic factor are dependent on MEK and ERK activation. *PloS One*, 4(4), p.e5292.

Goldberg, Y.P., Andrew, S.E., Theilmann, J., Kremer, B., Squitieri, F., Telenius, H., Brown, J. & Hayden, M.R., 1993. Familial predisposition to recurrent mutations causing Huntington's disease: genetic risk to sibs of sporadic cases. *Journal of Medical Genetics*, 30(12), pp.987–990.

Goldberg, Y.P., Ziesler, J., Almqvist, E., Sillence, D., Richards, F., Buchanan, J., Telenius, H. & Hayden, M.R., 1995. Increased instability of intermediate alleles in families with sporadic Huntingtons disease compared to intermediate alleles in the general-population - Implications for genetic-counseling. *American Journal of Human Genetics*, 57(4, S), p.136.

Goldberg, Y.P., Nicholson, D.W., Rasper, D.M., Kalchman, M.A., Koide, H.B., Graham, R.K., Bromm, M., KazemiEsfarjani, P., Thornberry, N.A., Vaillancourt, J.P. & Hayden M.R., 1996. Cleavage of huntingtin by apopain, a proapoptotic cysteine protease, is modulated by the polyglutamine tract. *Nature Genetics*, 13(4), pp.442–449.

Gomez-Tortosa, E., MacDonald, M.E., Friend, J.C., Taylor, S.A.M., Weiler, L.J., Cupples, L.A., Srinidhi, J., Gusellla, J.F., Bird, E.D., Vonsattel, J.P. & Myers, R.H., 2001. Quantitative neuropathological changes in presymptomatic Huntington's disease. *Annals of Neurology*, 49(1), pp.29–34.

Gomis, R.R., Alarcón, C., He, W., Wang, Q., Seoane, J., Lash, A. & Massagué, J., 2006. A FoxO-Smad synexpression group in human keratinocytes. *Proceedings of the National Academy of Sciences of the United States of America*, 103(34), pp.12747–52.

Gonitel, R., Moffitt, H., Sathasivam, K., Woodman, B., Detloff, P.J., Faull, R.L.M. & Bates, G.P., 2008. DNA instability in postmitotic neurons. *Proceedings of the National Academy of Sciences of the United States of America*, 105(9), pp.3467–3472.

Goodman, A.O.G., Murgatroydm P.R., Medina-Gomez, G., Wood, N.I., Finer, N., Vidal-Puig, A-J., Morton, A.J. & Barker, R.A., 2008. The metabolic profile of early Huntington's disease - a combined human and transgenic mouse study. *Experimental Neurology*, 210(2), pp.691–698.

Grafton, S.T., Mazziota, J.C., Pahl, J.J., St George Hyslop, P., Haines, J.L., Gusella, J., Hoffman, J.M., Baxter, L.R. & Phelps, M.E., 1992. Serial changes of cerebral glucose-metabolism and caudate size in persons at risk for Huntingtons-disease. *Archives of Neurology*, 49(11), pp.1161–1167.

Graham, R.K., Deng, Y., Slow, E.J., Haigh, B., Bissada, N., Lu, G., Pearson, J., Shehadeh, J., Bertram, L., Murphy, Z., Warby, S.C., Doty, C.N., Roy, S., Wellington, C.L., Leavitt, B.R., Raymond, L.A., Nicholson, D.W. & Hayden, M.R., 2006. Cleavage at the caspase-6 site is required for neuronal dysfunction and degeneration due to mutant huntingtin. *Cell*, 125(6), pp.1179–91

Graham, R.K., Slow, E.J., Deng, Y., Bissada, N., Lu, G., Pearson, J., Shehadeh, J., Leavitt, B.R., Raymond, L.A. & Hayden, M.R., 2006. Levels of mutant huntingtin influence the phenotypic severity of Huntington disease in YAC128 mouse models. *Neurobiology of Disease*, 21(2), pp.444–55.

Graham, R.K., Deng, Y., Carroll, J., Vaid, K., Cowan, C., Pouladi, M.A., Metzler, M., Bissada, N., Wang, L., Faull, R.L.M., Gray, M., Yang, X.W., Raymond, L.A. & Hayden, M.R ., 2010. Cleavage at the 586 Amino Acid Caspase-6 Site in Mutant huntingtin Influences Caspase-6 Activation In Vivo. *The Journal of Neuroscience*, 30(45), pp.15019–15029.

Gray, M., Shirasaki, D.I., Cepeda, C., Andre, V.M., Wilburn, B., Lu, X-H., Tao, J., Yamazaki, I., Li, S-H., Sun, Y.E., Li, X-J., Levine, M.S. & Yang, X.W., 2008. Full-Length Human Mutant Huntingtin with a Stable Polyglutamine Repeat Can Elicit Progressive and Selective Neuropathogenesis in BACHD Mice. *The Journal of Neuroscience*, 28(24), pp.6182–6195.

Greiner, E.R. & Yang, X.W., 2011. Huntington's disease: Flipping a switch on huntingtin. *Nature Chemical Biology*, 7(7), pp.412–4.

Groen, J.L., de Bie, R.M.A., Foncke, E.M.J., Roos, R.A.C., Leenders, K.L. & Tijssen, M.A.J., 2010. Late-onset Huntington disease with intermediate CAG repeats: true or false? *Journal of Neurology, Neurosurgery, and Psychiatry*, 81(2), pp.228–30.

Gu, X., Greiner, E.R., Mishra, R., Kodali, R., Osmand, A., Finkbeiner, S., Steffan, J.S., Thompson, L.M., Wetzel, R. & Yang, W.X., 2009. Serines 13 and 16 are critical determinants of full-length human mutant huntingtin induced disease pathogenesis in HD mice. *Neuron*, 64(6), pp.828–40.

Gunawardena, S., Her, L.S., Brusch, R.G., Laymon, R.A., Niesman, I.R., Gordesky-Gold, B., Sintasath, L., Bonini, N.M. & Goldstein, L.S.B., 2003. Disruption of axonal transport by loss of huntingtin or expression of pathogenic PolyQ proteins in Drosophila. *Neuron*, 40(1), pp.25–40.

Guo, P., Dong, X-Y., Zhao, K., Sun, X., Li, Q. & Dong, J-T., 2009. Opposing effects of KLF5 on the transcription of MYC in epithelial proliferation in the context of transforming growth factor beta. *The Journal of Biological Chemistry*, 284(41), pp.28243–52.

Gusella, J.F., Wexler, N.S., Conneally, P.M., Naylor, S.L., Anderson, M.A., Tanzi, R.E., Watkins, P.C., Ottina, K., Wallace, M.R., Sakaguchi, A.Y., Young, A.B., Shoulson, I., Bonilla, E. & Martin, J.B., 1983. A polymorphic DNA marker genetically linked to Huntington's disease. *Nature*, 306(5940), pp.234–238.

Gutekunst, C. A., Levey, A.I., Heilmann, C.J., Whaley, W.L., Yi, H., Nash, N.R., Rees, H.D., Madden, J.J. & Hersch, S.M., 1995. Identification and localization of huntingtin in brain and human lymphoblastoid cell lines with anti-fusion protein antibodies. *Proceedings of the National Academy of Sciences of the United States of America*, 92(19), pp.8710–4.

Gutekunst, C.A., Li, S.H., Yi, H., Mulroy, J.S., Kuemmerle, S., Jones, T., Rye, D., Ferrante, R.J., Hersch, S.M. & Li, X.J., 1999. Nuclear and neuropil aggregates in Huntington's disease: Relationship to neuropathology. *The Journal of Neuroscience*, 19(7), pp.2522–2534.

Hackam, A.S., Singaraja, R., Wellington, C.L., Metzler, M., McCutcheon, K., Zhang, T., Kalchmann, M. & Hayden, M.R. et al., 1998. The influence of huntingtin protein size on nuclear localization and cellular toxicity. *The Journal of cell Biology*, 141(5), pp.1097–105.

Hahn-Barma, V., Deweer, B., Durr, A., Dode, C., Feingold, J., Pillon, B., Agid, Y., Brice, A. & Dubois, B., et al., 1998. Are cognitive changes the first symptoms of Huntington's disease? A study of gene carriers. *Journal of Neurology Neurosurgery and Psychiatry*, 64(2), pp.172–177.

Hai, T., Wolford, C.C. & Chang, Y.-S., 2010. ATF3, a Hub of the Cellular Adaptive-Response Network, in the Pathogenesis of Diseases: Is Modulation of Inflammation a Unifying Component? *Gene Expression*, 15(1), pp.1–11.

Harper, P., 2002. Huntington's disease: a historical background. In G. Bates, P. Harper, & L. Jones, eds. *Huntington's Disease*. Oxford, UK: Oxford University Press, pp. 3–27.

Harris, G.J., Codori, A.M., Lewis, R.F., Schmidt, E., Bedi, A. & Brandt, J., 1999. Reduced basal ganglia blood flow and volume in pre-symptomatic, gene-tested persons at-risk for Huntington's disease. *Brain*, 122(9), pp.1667–1678.

Hata, a, Shi, Y. & Massagué, J., 1998. TGF-beta signaling and cancer: structural and functional consequences of mutations in Smads. *Molecular Medicine Today*, 4(6), pp.257–62.

Haugwitz, U., Bobkiewicz, W., Han, S-R., Beckmann, E., Veerachato, G., Shaid, S., Biehl, S., Dersch, K., Bhakdi, S. & Husmann, M., 2006. Pore-forming Staphylococcus aureus alpha-toxin triggers epidermal growth factor receptor-dependent proliferation. *Cellular Microbiology*, 8(10), pp.1591–600.

Havel, L.S., Wang, C-E., Wade, B., Huang, B, Li, S. & Li, X-J., 2011. Preferential accumulation of N-terminal mutant huntingtin in the nuclei of striatal neurons is regulated by phosphorylation. *Human Molecular Genetics*, 20(7), pp.1424–37.

Hayden, M.R., 1981. *Huntington's chorea*, New York, USA: Springer-Verlag.

Huntington's Disease Collaborative Research Group, 1993. A Novel Gene Containing a Trinucleotide That Is Expanded and Unstable on Huntington ' s Disease Chromosomes. *Cell*, 72, pp.971–983.

Hedreen, J.C., Peyser, C.E., Folstein, S.E. & Ross, C.A., 1991. Neuronal loss in layers-V and layers-VI of cerebral-cortex in Huntingtons-disease. *Neuroscience Letters*, 133(2), pp.257–261.

Heinsen, H., Rub, U., Bauer, M., Ulmar, G., Bethke, B., Schuler, M., Bocker, F., Eisenmenger, W., Gotz, M., Korr, H. & Schmitz, C., 1999. Nerve cell loss in the thalamic mediodorsal nucleus in Huntington's disease. *Acta Neuropathologica*, 97(6), pp.613–622.

Heng, M.Y., Tallaksen-Greene, S.J., Detloff, P.J. & Albin, R.L., 2007. Longitudinal evaluation of the Hdh(CAG)150 knock-in murine model of Huntington's disease. *The Journal of Neuroscience*, 27(34), pp.8989–98.

Heng, M.Y., Duong, D.K., Albin, R.L., Tallaksen-Greene, S.J., Hunter, J.M., Lesort, M.J., Osmand, A., Paulsen, H.L. & Detloff, P.J., 2010. Early autophagic response in a novel knock-in model of Huntington disease. *Human Molecular Genetics*, 19(19), pp.3702–20.

Henley, S.M.D., Wild, E.J, Hobbs, N.Z., Warren, J.D., Frost, C., Scahill, R.I., Ridgway, G.R., MacManus, D.G., Barker, R.A., Fox, N.C. & Tabrizi, S.J., 2008. Defective emotion

recognition in early HD is neuropsychologically and anatomically generic. *Neuropsychologia*, 46(8), pp.2152–2160.

Henley, S.M.D., Wild, E.J., Hobbs, N.J., Frost, C., MacManus, D.G., Barker, R.A., Fox, N.C. & Tabrizi, S.J., 2009. Whole-Brain Atrophy as a Measure of Progression in Premanifest and Early Huntington's Disease. *Movement Disorders*, 24(6), pp.932–936.

Hickey, M.A., Kosmalska, A., Enayati, J., Cohen, R., Zeitlin, S., Levine, M.S. & Chesselet, M-F., 2008. Extensive early motor and non-motor behavioral deficits are followed by striatal neuronal loss in knock-in Huntington's disease mice. *Neuroscience*, 157(1), pp.280–95.

Hilditch-Maguire, P., Trettel, F., Passani, L.A., Auerbach, A., Persichetti, F. & MacDonald, M.E., 2000. Huntingtin: an iron-regulated protein essential for normal nuclear and perinuclear organelles. *Human Molecular Genetics*, 9(19), pp.2789–97.

Ho, A.K., Sahakian, B.J., Brown, R.G., Barker, R.A., Hodges, J.R., Ane, M.N., Snowden, J., Thompson, J., Esmonde, T., Gentry, R., Moore, J.W. & Bodner, T., 2003. Profile of cognitive progression in early Huntington's disease. *Neurology*, 61(12), pp.1702–1706.

Hobbs, N.Z., Henley, S.M.D., Wild, E.J., Leung, K.K., Frost, C., Barker, R.A., Scahill, R.I., Barnes, J., Tabrizi, S.J. & Fox, N.C., 2009. Automated quantification of caudate atrophy by local registration of serial MRI: Evaluation and application in Huntington's disease. *Neuroimage*, 47(4), pp.1659–1665.

Hockly, E., Richon, V.M., Woodman, B., Smith, D.L., Zhou, X.B., Rosa, E., Sathasivam, K., Ghazi-Noori, S., Mahal, A., Lowden, P.A.S., Steffan, J.S., Marsh, J.L., Thompson, L.M., Lewis, C.M., Marks, P.A. & Bates, G.P., 2003. Suberoylanilide hydroxamic acid, a histone deacetylase inhibitor, ameliorates motor deficits in a mouse model of Huntington's disease. *Proceedings of the National Academy of Sciences of the United States of America*, 100(4), pp.2041–2046.

Hodges, A., Strand, A.D., Aragaki, A.K., Kuhn A., Sengstag, T., Hughes, G., Elliston, L.A., Hartog, C., Goldstein, D.R., Thu, D., Hollingsworth, Z.R., Collin, F., Synek, B., Holmans, P.A., Young, A.B., Wexler, N.S., Delorenzi, M., Kooperberg, C., Augood, S.J., Faull, R.L.M., Olsen, J.M., Jones, L. & Luthi-Carter, R., 2006. Regional and cellular gene expression changes in human Huntington's disease brain. *Human Molecular Genetics*, 15(6), pp.965–77.

Hodges, A., Hughes, G., Brooks, S., Elliston, L., Holmans, P., Dunnett, S.B. & Jones, L., 2008. Brain gene expression correlates with changes in behavior in the R6/1 mouse model of Huntington's disease. *Genes, Brain, and Behavior*, 7(3), pp.288–99.

Hodgson, J.G., Agopyan, N., Gutekunst, C-A., Leavitt, B.R., LePiane, F., Singaraja, R., Smith, D.J., Bissada, N., McCutcheon, K., Nasir, J., Jamot, L., Li, X-J., Stevens, M.E., Rosemond, E., Roder, J.C., Phillips, A.G., Rubin, E.M., Hersch, S.M. & Hayden, M.R., 1999. A YAC Mouse Model for Huntington's Disease with Full-Length Mutant Huntingtin, Cytoplasmic Toxicity, and Selective Striatal Neurodegeneration. *Neuron*, 23(1), pp.181–192.

Hogart, A., Lichtenberg, J., Ajay, S.S., Anderson, S., Margulies, E.H. & Bodine, D.M., 2012. Genome-wide DNA methylation profiles in hematopoietic stem and progenitor cells reveal overrepresentation of ETS transcription factor binding sites. *Genome Research*, 22(8), pp.1407–1418.

Hogel, M., Laprairie, R.B. & Denovan-Wright, E.M., 2012. Promoters are differentially sensitive to N-terminal mutant huntingtin-mediated transcriptional repression. *PloS One*, 7(7), p.e41152.

Holl, A.K., Wilkinson, L., Tabrizi, S.J., Painold, A. & Jahanshahi, M., 2013. Selective executive dysfunction but intact risky decision-making in early Huntington's disease. *Movement disorders*, 28(8), pp.1104–9.

Holmberg, C.I., Tran, S.E.F., Eriksson, J.E. & Sistonen, L., 2002. Multisite phosphorylation provides sophisticated regulation of transcription factors. *Trends in Biochemical Sciences*, 27(12), pp.619–27.

Hoogeveen, A.T., Willemsen, R., Meyer, N., De Rooij, K.E., Roos, R.A., van Ommen, G.J. & Galjaard, H., 1993. Characterization and localization of the Huntington disease gene product. *Human Molecular Genetics*, 2(12), pp.2069–73.

Hsiao, H.-Y., Chen, Y-C., Chen, H-M., Tu, P-H. & Chern, Y., 2013. A critical role of astrocyte-mediated nuclear factor-kappa B-dependent inflammation in Huntington's disease. *Human Molecular Genetics*, 22(9), pp.1826–1842.

Hsiao, S.P., Huang, K.M., Chang, H. Y. & Chen, S.L., 2009. P/CAF rescues the Bhlhe40-mediated repression of MyoD transactivation. *The Biochemical Journal*, 422(2), pp.343–52.

Hu, H., McCaw, E.A., Hebb, A.L.O., Gomez, G.T. & Denovan-Wright, E.M., 2004. Mutant huntingtin affects the rate of transcription of striatum-specific isoforms of phosphodiesterase 10A. *The European Journal of Neuroscience*, 20(12), pp.3351–63.

Humbert, S., 2003. Huntingtin phosphorylation and signaling pathways that regulate toxicity in Huntington's disease. *Clinical Neuroscience Research*, 3(3), pp.149–155.

Humbert, S., Bryson, E.A., Cordelie, F.P., Conners, N.C., Datta, S.R., Finkbeiner, S., Greenberg, M.E. & Saudou, F., 2002. The IGF-1 / Akt Pathway is neuroprotective in Huntington's disease and involves huntingtin phosphorylation by Akt. *Developmental Cell*, 2(6), pp.831–837.

Huntington Study Group, 1996. Unified Huntington's Disease Rating Scale: Reliability and consistency. *Movement Disorders*, 11(2), pp.136–142.

Iijima-ando, K., Wu, P., Drier, E.A., Iijima, K. & Yin, J.C.P., 2005. cAMP-response element-binding protein and heat-shock protein 70 additively suppress polyglutamine-mediated toxicity in Drosophila. *Proceedings of the National Academy of Sciences of the United States of America*, 102(29), pp.10261–10266.

Ishiguro, H., Yamada, K., Sawada, H., Nishii, K., Ichino, N., Sawada, M., Kurosawa, Y., Matsushita, N., Kobayashi, K., Goto, J., Hashida, H., Masuda, N., Kanazawa, I. & Nagatsu, T., 2001. Age-dependent and tissue-specific CAG repeat instability occurs in mouse knock-in for a mutant Huntington's Disease gene. *Journal of Neuroscience Research*, 65(4), pp.289 –297.

Ishii, K., Kanatsu-Shinohara, M., Toyokuni, S. & Shinohara, T., 2012. FGF2 mediates mouse spermatogonial stem cell self-renewal via upregulation of Etv5 and Bcl6b through MAP2K1 activation. *Development*, 139(10), pp.1734–43.

Jacobsen, J.C., Bawden, C.S, Rudiger, S.R., McLaughlan, C.J., Reid, S.J., Waldvogel, H.J., MacDonald, M.E., Gusella, J.F., Walker, S.K., Kelly, J.M., Webb, G.C., Faull, R.L.M., Rees, M.I. & Snell, R.G., 2010. An ovine transgenic Huntington's disease model. *Human Molecular Genetics*, 19(10), pp.1873–82.

Jana, N.R., Dikshit, P., Goswami, A., Kotliarova, S., Murata, S., Tanaka, K. & Nukina, N., 2005. Co-chaperone CHIP associates with expanded polyglutamine protein and promotes their degradation by proteasomes. *The Journal of Biological Chemistry*, 280(12), pp.11635–11640.

Jervis, G.A., 1963. Huntingtons chorea in childhood. *Archives of Neurology*, 9(3), p.244–257.

Ji, Y., Lu, Y., Yang, F., Shen, W., Tang, .T.T-T., Feng, L., Duan, S. & Lu, B., 2010. Acute and gradual increases in BDNF concentration elicit distinct signaling and functions in neurons. *Nature Neuroscience*, 13(3), pp.302–9.

Jin, K.L., LaFevre-Bernt, M., Sun, Y.J., Chen, S., Gafni, J., Crippen, D., Logvinova, A., Ross, C.A., Greenberg, D.A. & Ellerby, L.M., 2005. FGF-2 promotes neurogenesis and neuroprotection and prolongs survival in a transgenic mouse model of Huntington's disease. *Proceedings of the National Academy of Sciences of the United States of America*, 102(50), pp.18189–18194.

Jin, X., Yin, J., Kim, S-H., Sohn, Y-W., Beck, S., Lim, Y.C., Nam, D-H., Choi, Y-J. & Kim, H., 2011. EGFR-AKT-Smad signaling promotes formation of glioma stem-like cells and tumor angiogenesis by ID3-driven cytokine induction. *Cancer Research*, 71(22), pp.7125–34.

Johnen, H., González-Silva, L., Carramolino, L., Flores, J.M., Torres, M. & Salvador, J.M., 2013. Gadd45g is essential for primary sex determination, male fertility and testis development. *PloS One*, 8(3), p.e58751.

Johnson, R., Zuccato, C., Belyaev, N.D., Guest, D.J., Cattaneo, E. & Buckley, N.J., 2008. A microRNA-based gene dysregulation pathway in Huntington's disease. *Neurobiology of Disease*, 29(3), pp.438–45.

Kalchman, M.A., Graham, R.K., Xia, G., Koide, H.B., Hodgson, J.G., Graham, K.C., Goldberg, Y.P., Gietz, R.D., Pickart, C.M. & Hayden, M.R., 1996. Huntingtin is ubiquitinated and interacts with a specific ubiquitin-conjugating enzyme. *The Journal of Biological Chemistry*, 271(32), pp.19385–19394.

Kandasamy, M., Couillard-Despres, S., Raber, K.A., Stephan, M., Lehner, B., Winner, B., Kohl, Z., Rivera, F.J., Nguyen, H.P., Riess, O., Bogdahn, U., Winkler, J., von Hörsten, S. & Aigner, L., 2010. Stem cell quiescence in the hippocampal neurogenic niche is associated with elevated transforming growth factor-beta signaling in an animal model of Huntington disease. *Journal of Neuropathology and Experimental Neurology*, 69(7), pp.717–28.

Kandasamy, M., Reilmann, R., Winkler, J., Bogdahn, U. & Aigner, L., 2011. Transforming Growth Factor-Beta Signaling in the Neural Stem Cell Niche: A Therapeutic Target for Huntington's Disease. *Neurology Research International*, 2011, p.124256.

Kang, M., Choi, S., Jeong, S-J., Lee, S-A., Kwak, T.K., Kim, H., Jung, O., Lee, M-S., Ko, Y., Ryu, J., Choi, Y-J., Jeong, D., Lee, H.J., Ye, S-K., Kim, S-H. & Lee, J.W., 2012. Cross-talk between TGFβ1 and EGFR signalling pathways induces TM4SF5 expression and epithelial-mesenchymal transition. *The Biochemical Journal*, 443(3), pp.691–700.

Kang, Y., Chen, C.-R. & Massagué, J., 2003. A self-enabling TGFbeta response coupled to stress signaling: Smad engages stress response factor ATF3 for Id1 repression in epithelial cells. *Molecular Cell*, 11(4), pp.915–26.

Kaplan, D.R. & Miller, F.D., 2000. Neurotrophin signal transduction in the nervous system. *Current Opinion in Neurobiology*, 10(3), pp.381–391.

Kazantsev, A., Preisinger, E., Dranovsky, A., Goldgaber, D. & Housman, D., 1999. Insoluble detergent-resistant aggregates form between pathological and nonpathological lengths of polyglutamine in mammalian cells. *Proceedings of the National Academy of Sciences of the United States of America*, 96(20), pp.11404–11409.

Kegel, K.B., Meloni, A.R., Yi, Y., Kim, Y.J., Doyle, E., Cuiffo, B.G., Sapp, E., Wang, Y., Qin, Z-H., Chen, J.D., Nevins, J.R., Aronin, N. & DiFiglia, M., 2002. Huntingtin is present in the nucleus, interacts with the transcriptional corepressor C-terminal binding protein, and represses transcription. *The Journal of Biological Chemistry*, 277(9), pp.7466–76.

Kennedy, L., Evans, E., Chen, C-M., Cravenm L., Detloff, P.J., Ennis, M. & Shelbourne, P.F., 2003. Dramatic tissue-specific mutation length increases are an early molecular event in Huntington disease pathogenesis. *Human Molecular Genetics*, 12(24), pp.3359–67.

Khoshnan, A., Ko, J., Watkin, E.E., Paige, L.A., Reinhart, P.H. & Patterson, P.H., 2004. Activation of the IkB Kinase complex and nuclear Factor- kB contributes to mutant huntingtin neurotoxicity. *The Journal of Neuroscience*, 24(37), pp.7999–8008.

Khoshnan, A., Ko, J., Tescu, S., Brundin, P. & Patterson, P.H., 2009. IKKalpha and IKKbeta regulation of DNA damage-induced cleavage of huntingtin. *PloS One*, 4(6), p.e5768.

Khoshnan, A. & Patterson, P.H., 2011. The role of IκB kinase complex in the neurobiology of Huntington's disease. *Neurobiology of Disease*, 43(2), pp.305–11.

Kim, M., Roh, J-K., Yoon, B.W., Kang, L., Kim, Y.J., Aronin, N. & DiFiglia, M., 2003. Huntingtin is degraded to small fragments by calpain after ischemic injury. *Experimental Neurology*, 183(1), pp.109–115.

Kim, M.W., Chelliah, Y., Kim, S.W., Otwinowski, Z. & Bezprozvanny, I., 2009. Secondary Structure of Huntingtin Amino-Terminal Region. *Structure*, 17(9), pp.1205–1212.

Kim, S., Han, J., Lee, S.K., Koo, M., Cho, D.H., Bae, S.Y., Choi, M-Y., Kim, J.S., Kim, J-H., Choe, J-H., Yang, J-H., Nam, S.J. & Lee, J.E., 2012. Smad7 acts as a negative regulator of the epidermal growth factor (EGF) signaling pathway in breast cancer cells. *Cancer Letters*, 314(2), pp.147–54.

Kim, Y.J., Yi, Y., Sapp, E., Wang, Y.M., Cuiffo, B., Kegel, K.B., Qin, Z.H., Aronin, N. & DiFiglia, M., 2001. Caspase 3-cleaved N-terminal fragments of wild-type and mutant huntingtin are present in normal and Huntington's disease brains, associate with membranes, and undergo calpain-dependent proteolysis. *Proceedings of the National Academy of Sciences of the United States of America*, 98(22), pp.12784–12789.

Kim, Y.J., Sapp, E., Cuiffo, B.G., Sobin, L., Yoder, J., Kegel, K.B., Qin, Z.H., Detloff, P., Aronin, N., DiFiglia, M., 2006. Lysosomal proteases are involved in generation of N-terminal huntingtin fragments. *Neurobiology of Disease*, 22(2), pp.346–356.

Kipps, C.M., Duggins, A.J., Mahant, N., Gomes, L., Ashburner, J. & McCusker, E.A., 2005. Progression of structural neuropathology in preclinical Huntington's disease: a tensor based morphometry study. *Journal of Neurology Neurosurgery and Psychiatry*, 76(5), pp.650–655.

Kirkwood, S.C., Siemers, E., Hodes, M.E., Conneally, P.M., Christian, J.C. & Foroud, T., 2000. Subtle changes among presymptomatic carriers of the Huntington's disease gene. *Journal of Neurology Neurosurgery and Psychiatry*, 69(6), pp.773–779.

Klöppel, S., Stonnington, C.M., Petrovic, P., Mobbs, D., Tüscher, O., Craufurd, D., Tabrizi, S.J. & Frackowiak, R.S.J., 2010. Irritability in pre-clinical Huntington's disease. *Neuropsychologia*, 48(2), pp.549–57.

Ko, J., Ou, S. & Patterson, P.H., 2001. New anti-huntingtin monoclonal antibodies: implications for huntingtin conformation and its binding proteins. *Brain Research Bulletin*, 56(3-4), pp.319–29.

Koinuma, D., Tsutsumi, S., Kamimura, N., Imamura, T., Aburatani, H. & Miyazono, K., 2009. Promoter-wide analysis of Smad4 binding sites in human epithelial cells. *Cancer Science*, 100(11), pp.2133–42.

Kong, P.-J., Kil, M-O., Lee, H., Kim, S-S., Johnson, G.V.W. & Chun, W., 2009. Increased expression of Bim contributes to the potentiation of serum deprivation-induced apoptotic cell death in Huntington's disease knock-in striatal cell line. *Neurological Research*, 31(1), pp.77–83.

Kremer, B., Squitieri, F., Telenius, H., Andrew, S.E., Theilmann, J., Spence, N., Goldberg, Y.P. & Hayden, M.R., 1993. Molecular analysis of late onset Huntington's disease. *Journal of Medical Genetics*, 30(12), pp.991–995.

Kremer, B., Almqvist, E., Theilmann, J., Spence, N., Telenius, H., Goldberg, Y.P. & Hayden, M.R., 1995. Sex-dependent mechanisms for expansions and contractions of the CAG repeat on affected Huntington disease chromosomes. *American Journal of Human Genetics*, 57(2), pp.343–350.

Kremer, H.P.H., Roos, R.A.C., Dingjan, G.M., Bots, G.T.A.M., Bruyn, G.W. & Hofman, M.A, 1991. The hypothalamic lateral tuberal nucleus and the characteristics of neuronal loss in Huntingtons-disease. *Neuroscience Letters*, 132(1), pp.101–104.

Kretzschmar, M., Liu, F., Doody, J. & Massagué, J., 1997. The TGF-P family mediator Smad1 is phosphorylated directly and activated functionally by the BMP receptor kinase. *Genes and Development*, 11(8), pp.984–995.

Kuemmerle, S., Gutekunst, C.A., Klein, A.M., Li, X.J., Li, S.H., Beal, M.F., Hersch, S.M. & Ferrante, R.J., 1999. Huntington aggregates may not predict neuronal death in Huntington's disease. *Annals of Neurology*, 46(6), pp.842–9.

Kuhn, A., Goldstein, D.R., Hodges, A., Strand, A.D., Sengstag, T., Kooperberg, C., Becanovic, K., Pouladi, M.A., Sathasivam, K., Cha, J-H.J., Hannan, A.J., Hayden, M.R., Leavitt, B.R., Dunnett, S.B., Ferrante, R.J., Albin, R., Shelbourne, P., Delorenzi, M., Augood, S.J., Faull, R.L.M., Olsen, J.M., Gates, G.P., Jones, L. & Luthi-Carter, R., 2007. Mutant huntingtin's effects on striatal gene expression in mice recapitulate changes observed in human Huntington's disease brain and do not differ with mutant huntingtin length or wild-type huntingtin dosage. *Human Molecular Genetics*, 16(15), pp.1845–61.

Kuwert, T., Lange, H.W., Langen, K.J., Herzog, H., Aulich, A. & Feinendegen, L.E., 1990. Cortical and subcortical glucose consumption measured by PET in patients with Huntingtons-disease. *Brain*, 113, pp.1405–1423.

Kyriakis, J.M. & Avruch, J., 2001. Mammalian mitogen-activated protein kinase signal transduction pathways activated by stress and inflammation. *Physiological Reviews*, 81(2), pp.807–869.

Labuschagne, I., Jones, R., Callaghan, J., Whitehead, D., Duman, E.M., Say, M.J., Hart, E.P., Justo, D., Coleman, A., Dar Santos, R.C., Frost, C., Crauford, D., Tabrizi, S.J. & Stout, J.C., 2013. Emotional face recognition deficits and medication effects in pre-manifest through stage-II Huntington's disease. *Psychiatry Research*, 207(1-2), pp.118–26.

Landles, C., Sathasivam, K., Weiss, A., Woodman, B., Moffitt, H., Finkbeiner, S., Sun, B., Gafni, J., Ellerby, L.M., Trottier, Y., Richards, W.G., Osmand, A., Paganetti, P. & Bates, G.P., 2010. Proteolysis of mutant huntingtin produces an exon 1 fragment that accumulates as an aggregated protein in neuronal nuclei in Huntington disease. *The Journal of Biological Chemistry*, 285(12), pp.8808–23.

Landwehrmeyer, G.B., McNeil, S.M., Dure, L.S., Ge. P., Aizawa, H., Huang, Q., Ambrose, C.M., Duyao, M.P., Bird, E.D., Bonilla, E., Deyoung, M., Avilagonzales, A.J., Wexler, N.S., DiFiglia, M., Gusella, J.F., MacDonald, M.E., Penney, J.B., Young, A.B. & Vonsattel, J.P., 1995. Huntingtons-disease gene - Regional and cellular expression in brain of normal and affected individuals. *Annals of Neurology*, 37(2), pp.218–230.

Langbehn, D.R., Hayden, M.R. & Paulsen, J.S., 2010. CAG-repeat length and the age of onset in Huntington disease (HD): a review and validation study of statistical approaches. *American Journal of Medical Genetics. Part B, Neuropsychiatric Genetics*, 153B(2), pp.397–408.

Lange, H., Thorner, G., Hopf, A. & Schroder, K.F., 1976. Morphometric studies of neuropathological changes in choreatic diseases. *Journal of the Neurological Sciences*, 28(4), pp.401–425.

Lanska, D.J., Lanska, M.J., Lavine, L. & Schoenberg, B.S., 1988. Conditions associated with Huntingon's disease at death - A case-control study. *Archives of Neurology*, 45(8), pp.878–880.

Lawrence, A.D., Hodges, J.R., Rosser, A.E., Kershaw, A., Ffrench-Constant, C., Rubinsztein, D.C., Robbins, T.W. & Sahakian, B.J., 1998. Evidence for specific cognitive deficits in preclinical Huntington's disease. *Brain*, 121(7), pp.1329–1341.

Lee, J.-H., Lee, J-M., Ramos, E.M., Gillis, T., Mysore, J.S., Kishikawa, S., Hadzi, T., Hendricks, A.E., Hayden, M.R., Morrison, P.J., Nance, M., Ross, C.A., Margolis, R.L., Squitieri, F., Gellera, C., Gomez-Tortosa, E., Ayuso, C., Suchowersky, O., Trent, R.J.,McCusker, E., Novelletto, A., Frontali, M., Jones, R., Ashizawa, T., Frank, S.,

Saint-Hilaire, M-H., Hersch, S.M., Rosas, H.D., Lucente, D., Harrison, M.B., Zanko, A., Abramson, R.K., Marder, K., Sequeiros, J., Landwehrmeyer, G.B., Shoulson, I., Myers, R.H., MacDonald, M.E. & Gusella, J.F., 2012. TAA repeat variation in the GRIK2 gene does not influence age at onset in Huntington's disease. *Biochemical and Biophysical Research Communications*, 424(3), pp.404–8.

Lee, J.-M., Ivanova, E.V., Seong, I.S., Cashorali, T., Kohane, I., Gusella, J.F. & MacDonald, M.E., 2007. Unbiased gene expression analysis implicates the huntingtin polyglutamine tract in extra-mitochondrial energy metabolism. *PLoS Genetics*, 3(8), p.e135.

Lee, J.-M. Galkina, E.I., Levantovsky, R.M., Fossale, E., Anderson, M.A., Gillis, T., Mysore, J.S., Coser, K.R., Shioda, T., Zhang, B., Furia, M.D., Derry, J., Kohane, I.S., Seong, I.S., Wheeler, V.C., Gusella, J.F. & MacDonald, M.E., 2013. Dominant effects of the Huntingtons disease HTT CAG repeat length are captured in gene-expression data sets by a continuous analysis mathematical modeling strategy. *Human Molecular Genetics*, 22(16), pp.3227–3238.

Lee, S.-T., Chu, K., Im, W-S., Yoon, H-J., Im, J-Y., Park, J-E., Park, K-H., Jung, K-H., Lee, S.K., Kim, M. & Roh, J-K., 2011. Altered microRNA regulation in Huntington's disease models. *Experimental Neurology*, 227(1), pp.172–9.

Legleiter, J., Lotz, G.P., Miller, J., Ko, J., Ng, C., Williams, G.L., Finkbeiner, S., Patterson, P.H. & Muchowski, P.J., 2009. Monoclonal antibodies recognize distinct conformational epitopes formed by polyglutamine in a mutant huntingtin fragment. *The Journal of Biological Chemistry*, 284(32), pp.21647–58.

Levine, M.S., Cepeda, C., Hickey, M.A., Fleming, S.M. & Chesselet, M.F., 2004. Genetic mouse models of Huntington's and Parkinson's diseases: illuminating but imperfect. *Trends in Neurosciences*, 27(11), pp.691–697.

Levkovitz, Y. & Baraban, J.M., 2002. A dominant negative Egr inhibitor blocks nerve growth factor-induced neurite outgrowth by suppressing c-Jun activation: role of an Egr/c-Jun complex. *The Journal of Neuroscience*, 22(10), pp.3845–54.

Li, H-X., Han, M., Bernier, M., Zheng, B., Sun, S-G., Su, M., Zhang, R., Fu, J-R. & Wen, J-K., 2010. Krüppel-like factor 4 promotes differentiation by transforming growth factor-beta receptor-mediated Smad and p38 MAPK signaling in vascular smooth muscle cells. *The Journal of Biological Chemistry*, 285(23), pp.17846–56.

Li, S-H., Schilling, G., Young, W.S., Li, X-J., Margolis, R.L., Stine, O.C., Wagsterm M.V., Abbott, M.H., Franz, M.L., Ranen, N.G., Folstein, S.E., Hedreen, J.C. & Ross, C.A., 1993. Huntingtons-disease gene (IT-15) is widely expressed in human and rat tissues. *Neuron*, 11(5), pp.985–993.

Li, S-H., Cheng, A.L., Zhou, H., Lam, S., Rao, M., Li, H. & Li, X-J., 2002. Interaction of Huntington Disease Protein with Transcriptional Activator Sp1. *Molecular and Cellular Biology*, 22(5), pp.1277–1287.

Li, X., Newbern, J.M., Wu, Y., Morgan-Smith, M., Zhong, J., Charron, J. & Snider, W.D., 2012. MEK Is a Key Regulator of Gliogenesis in the Developing Brain. *Neuron*, 75(6), pp.1035–50.

Li, X.-J., Li, S-H., Sharp, A.H., Nucifora Jr, F.C., Schilling, G., Lanahan, A., Worley, P., Snyder, S.H. & Ross, C.A., 1995. A huntingtin-associated protein enriched in brain with implications for pathology. *Nature*, 378(6555), pp.398–402.

Li, X.-J., Friedman, M. & Li, S., 2007. Interacting proteins as genetic modifiers of Huntington disease. *Trends in Genetics*, 23(11), pp.531–533.

Li, X.-J. & Li, S., 2012. Influence of Species Differences on the Neuropathology of Transgenic Huntington's Disease Animal Models. *Journal of Genetics and Genomics*, 39(6), pp.239–245.

Liang, Y., Jiang, H., Ratovitski, T., Jie, C., Nakamur, M., Hirschhorn, R.R., Wang, X., Smith, W.W., Hai, T., Poirier, M.A. & Ross, C.A., 2009. ATF3 plays a protective role against toxicity by N-terminal fragment of mutant huntingtin in stable PC12 cell line. *Brain Research*, 1286, pp.221–9.

Liévens, J.-C., Iché, M., Laval, M., Faivre-Sarrailh, C. & Birman, S., 2008. AKT-sensitive or insensitive pathways of toxicity in glial cells and neurons in Drosophila models of Huntington's disease. *Human Molecular Genetics*, 17(6), pp.882–94.

Lim, M.J., Lin, T. & Jakowlew, S.B., 2005. Signaling mechanisms of transforming growth factor-β (TGF-β) in cancer : TGF-β induces apoptosis in lung cells by a Smad-dependent mechanism. In Y. Cheng, ed. *Tumor Suppressor Genes*. InTech, pp. 145–180.

Lin, B., Rommens, J.M., Graham, R.K., Kalchman, M., MacDonald, H., Nasir, J., Delaney, A., Godlberg, Y.P. & Hayden, M.R., 1993. Differential 3' polyadenylation of the Huntington disease gene results in two mRNA species with variable tissue expression. *Human Molecular Genetics*, 2(10), pp.1541–5.

Lin, C.-H., 2001. Neurological abnormalities in a knock-in mouse model of Huntington's disease. *Human Molecular Genetics*, 10(2), pp.137–144.

Lin, S.Y., Makino, K., Xia, W., Matin, A., Wen, Y., Kwong, K.Y., Bourguignon, L. & Hung, M.C., 2001. Nuclear localization of EGF receptor and its potential new role as a transcription factor. *Nature Cell Biology*, 3(9), pp.802–8.

Lione, L.A., Carter, R.J., Hunt, M.J., Bates, G.P., Morton, A.J. & Dunnett, S.B., 1999. Selective discrimination learning impairments in mice expressing the human Huntington's disease mutation. *The Journal of Neuroscience*, 19(23), pp.10428–10437.

Liot, G., Zala, D., Pla, P., Mottet, G., Piel, M. & Saudou, F., 2013. Mutant Huntingtin alters retrograde transport of TrkB receptors in striatal dendrites. *The Journal of Neuroscience*, 33(15), pp.6298–309.

Liu, L., van Groen, T., Kadish, I. & Tollefsbol, T.O., 2009. DNA methylation impacts on learning and memory in aging. *Neurobiology of Aging*, 30(4), pp.549–560.

Liu, Y., Mei, C., Sun, L., Li, X., Liu, M., Wang, L, Li, Z., Yin, P., Zhao, C., Shi, Y., Qiu, S., Fan, J. & Zha, X., 2011. The PI3K-Akt pathway regulates calpain 6 expression, proliferation, and apoptosis. *Cellular Signalling*, 23(5), pp.827–836.

Liu, Y.F., Deth, R.C. & Devys, D., 1997. SH3 Domain-dependent Association of Huntingtin with Epidermal Growth Factor Receptor Signaling Complexes. *The Journal of Biological Chemistry*, 272(13), pp.8121–8124.

Liu, Y.F., Dorow, D. & Marshall, J., 2000. Activation of MLK2-mediated signaling cascades by polyglutamine-expanded huntingtin. *The Journal of Biological Chemistry*, 275(25), pp.19035–19040.

Lotz, G.P., Legleiter, J., Aron, R., Mitchell, E.J., Huang, S-Y., Ng, C., Glabe, C., Thompson, L.M. & Muchowski, P.J., 2010. Hsp70 and Hsp40 functionally interact with soluble mutant huntingtin oligomers in a classic ATP-dependent reaction cycle. *The Journal of Biological Chemistry*, 285(49), pp.38183–93.

Lu, D., Chen, J. & Hai, T., 2007. The regulation of ATF3 gene expression by mitogen-activated protein kinases. *Biochemical Journal*, 401(2), pp.559–567.

Lunkes, A., Lindenberg, K.S., Ben-Haiem, L., Weber, C., Devys, D., Landwehrmeyer, G.B., Mandel, J.L. & Trottier, Y., 2002. Proteases acting on mutant Huntingtin generate cleaved products that differentially build up cytoplasmic and nuclear inclusions. *Molecular Cell*, 10(2), pp.259–269.

Luo, S.Q., Vacher, C., Davies, J.E & Rubinsztein, D.C., 2005. Cdk5 phosphorylation of huntingtin reduces its cleavage by caspases: implications for mutant huntingtin toxicity. *Journal of Cell Biology*, 169(4), pp.647–656.

Luthi-Carter, R., 2000. Decreased expression of striatal signaling genes in a mouse model of Huntington's disease. *Human Molecular Genetics*, 9(9), pp.1259–1271.

Luthi-Carter, R., Hanson, S.A., Strand, A.D., Bergstrom, D.A., Chun, W., Peters, N.L., Woods, A.M., Chan, E.Y., Kooperberg, C., Krainc, D., Young, A.B., Tapscott., S.J & Olsen, J.M., 2002. Dysregulation of gene expression in the R6/2 model of polyglutamine disease: parallel changes in muscle and brain. *Human Molecular Genetics*, 11(17), pp.1911–26.

Lutz, M., Krieglstein, K., Schmitt, S., Ten Dijke, P., Sebald, W., Wizenmann, A. & Knaus, P., 2004. Nerve growth factor mediates activation of the Smad pathway in PC12 cells. *European Journal of Biochemistry*, 271(5), pp.920–931.

MacDonald, M., Barnes, G., Srinidhi, J., Duyao, M.P., Ambrose, C.M., Myers, R.H., Conneally, P.M., Young, A., Koroshetz, W., Bird, E., Vonsattel, J.P., Bonilla, E., Moscowitz, C., Penchaszadeh, G., Brzustowicz, L., Alvir, J., Conde, J.B., Cha, J-H., Dure, L., Gomez, F., Snodgras, S.R., Young, M.D., Wexler, N.S., Macfarlane, H., Anderson, M.A., Jenkins, B. & Gusella, JF., 1993. Gametic but not somatic instability of CAG repeat length in Huntington ' s disease. *Journal of Medical Genetics*, 30(12), pp.982–986.

Macdonald, V., Halliday, G.M., Trent, R.J. & McCusker, E.A., 1997. Significant loss of pyramidal neurons in the angular gyrus of patients with Huntington's disease. *Neuropathology and Applied Neurobiology*, 23(6), pp.492–495.

MacDonald, V. & Halliday, G.M., 2002. Selective loss of pyramidal neurons in the pre-supplementary motor cortex in Parkinson's disease. *Movement Disorders*, 17(6), pp.1166–1173.

Macgibbon, G.A., Hamilton, L.C., Crocker, S.F., Costain, S.F., Murphy, K.M., Robertson, H.A. & Denovan-Wright, E.M., 2002. Immediate-Early gene response to Methamphetamine, Haloperidol, and Quinolinic Acid is not impaired in Huntington's disease transgenic mice. *Journal of Neuroscience Research*, 67(3), pp.372–378.

MacMillan, J.C., Snell, R.G., Tyler, A., Houlihan, G.D., Fenton, I., Cheadle, J.P., Lazarou, L.P., Shaw, D.J. & Harper, P.S., 1993. Molecular analysis and clinical correlations of the Huntington's disease mutation. *The Lancet*, 342(8877), pp.954–958.

Mahant, N., McCusker, E.A., Byth, K. & Graham, S., 2003. Huntington's disease - Clinical correlates of disability and progression. *Neurology*, 61(8), pp.1085–1092.

Maheshwari, M., Samanta, A., Godavarthi, S.K., Mukherjee, R. & Jana, N.R., 2012. Dysfunction of the Ubiquitin Ligase Ube3a May Be Associated with Synaptic Pathophysiology in a Mouse Model of Huntington Disease. *Journal of Biological Chemistry*, 287(35), pp.29949–29957.

Maiuri, T., Woloshansky, T., Xia, J. & Truant, R., 2013. The huntingtin N17 domain is a multifunctional CRM1 and Ran-dependent nuclear and cilial export signal. *Human Molecular Genetics*, 22(7), pp.1383–94.

Mangiarini, L., Sathasivam, K., Seller, M., Cozens, B., Harper, A., Hetherington, C., Lawton, M., Trottier, Y., Lehrach, H., Davies, S.W. & Bates, G.P., 1996. Exon 1 of the HD gene with an expanded CAG repeat is sufficient to cause a progressive neurological phenotype in transgenic mice. *Cell*, 87(3), pp.493–506.

Martin, E., Betuing, S., Pagès, C., Cambon, K., Auregan, G., Deglon, N., Roze, E. & Caboche, J., 2011. Mitogen- and stress-activated protein kinase 1-induced neuroprotection in Huntington's disease: role on chromatin remodeling at the PGC-1-alpha promoter. *Human Molecular Genetics*, 20(12), pp.2422–34.

Martin, J.B., Gusella, J.F., Ronthal, M., Herzog, A., Flier, J.S. & Amir, S., 1986. Huntington's Disease - Pathogenesis and management. *New England Journal of Medicine*, 315(20), pp.1267–1276.

Mashima, T., Udagawa, S. & Tsuruo, T., 2001. Involvement of transcriptional repressor ATF3 in acceleration of caspase protease activation during DNA damaging agent-induced apoptosis. *Journal of Cellular Physiology*, 188(3), pp.352–358.

Massague, J., 2003. Integration of Smad and MAPK pathways: a link and a linker revisited. *Genes and Development*, 17(24), pp.2993–2997.

Massague, J., 2005. Smad transcription factors. *Genes and Development*, 19(23), pp.2783–2810.

Massagué, J., 1998. TGF-beta signal transduction. *Annual Review of Biochemistry*, 67, pp.753–91.

Mattson, M.P., 2006. Neuronal life-and-death signaling, apoptosis, and neurodegenerative disorders. *Antioxidants and Redox Signaling*, 8(11-12), pp.1997–2006.

Mazarei, G., Neal, S.J., Becanovic, K., Luthi-Carter, R., Simpson, E.M. & Leavitt, B.R., 2010. Expression analysis of novel striatal-enriched genes in Huntington disease. *Human Molecular Genetics*, 19(4), pp.609–22.

McCampbell, A., Taylor, J.P., Taye, A.A., Robitschek, J., Li, M., Walcott, J., Merry, D., Chai, Y.H., Paulson, H., Sobue, G. & Fischbeck, K.H., 2000. CREB-binding protein sequestration by expanded polyglutamine. *Human Molecular Genetics*, 9(14), pp.2197–2202.

McFarland, K.N., Das, S., Sun, T.T., Leyfer, D., Xia, E., Sangrey, G.R., Kuhn, A., Luthi-Carter, R., Clark, T.W., Sadri-Vakili, G. & Cha, J-H.J., 2012. Genome-wide histone acetylation is altered in a transgenic mouse model of Huntington's disease. *PloS One*, 7(7), p.e41423.

Meade, C. A., Deng, Y-P., Fusco, F.R., Del Mar, N., Hersch, S., Goldowitz, D. & Reiner, A., 2002. Cellular localization and development of neuronal intranuclear inclusions in striatal and cortical neurons in R6/2 transgenic mice. *The Journal of Comparative Neurology*, 449(3), pp.241–69.

Melone, M.A.B., Calarco, A., Petillo, O., Margarucci, S., Colucci-D'Amato, L., Galderisi, G. & Peluso, G., 2013. Mutant huntingtin regulates EGF receptor fate in non-neuronal cells lacking wild-type protein. *Biochimica et Biophysica Acta*, 1832(1), pp.105–13.

Menalled, L.B., Sison, J.D., Wu, Y., Olivieri, M., Li, X-J., Li, H., Zeitlin, S. & Chesselet, M-F., 2002. Early motor dysfunction and striosomal distribution of huntingtin

microaggregates in Huntington's disease knock-in mice. *The Journal of Neuroscience*, 22(18), pp.8266–8276.

Menalled, L.B., Sison, J.D., Dragatsis, I., Zeitlin, S., Chesselet, M-F., 2003. Time course of early motor and neuropathological anomalies in a knock-in mouse model of Huntington's disease with 140 CAG repeats. *The Journal of Comparative Neurology*, 465(1), pp.11–26.

Menalled, L.B., El-Khodor, B.F., Patry, M., Suárez-Fariñas, M., Orenstein, S.J., Zahasky, B., Leahy, C., Wheeler, V., Yang, X.W., MacDonald, M., Morton, A.J., Bates, G., Leeds, J., Park, L., Howland, D., Signer, E., Tobin, A. & Brunner, D., 2009. Systematic behavioral evaluation of Huntington's disease transgenic and knock-in mouse models. *Neurobiology of Disease*, 35(3), pp.319–36.

Meng, F., Liu, L., Chin, P.C. & D'Mello, S.R., 2002. Akt is a downstream target of NF-kappa B. *The Journal of Biological Chemistry*, 277(33), pp.29674–80.

Mi, R., Luo, Y., Cai, J., Limke, T.L., Rao, M.S. & Höke, A., 2005. Immortalized neural stem cells differ from nonimmortalized cortical neurospheres and cerebellar granule cell progenitors. *Experimental Neurology*, 194(2), pp.301–19.

Miller, J., Arrasate, M., Shaby, B.A., Mitra, S., Masliah, E. & Finkbeiner, S., 2010. Quantitative relationships between huntingtin levels, polyglutamine length, inclusion body formation, and neuronal death provide novel insight into huntington's disease molecular pathogenesis. *The Journal of Neuroscience,* 30(31), pp.10541–50.

Miller, J.P., Holcomb, J., Al-Ramahi, I., de Haro, M., Gafni, J., Zhang, N., Kim, E., Sanhuezza, M., Torcassi, C., Kwak, S., Botas, J., Hughes, R.E. & Ellerby, L.M., 2010. Matrix Metalloproteinases Are Modifiers of Huntingtin Proteolysis and Toxicity in Huntington's Disease. *Neuron*, 67(2), pp.199–212.

Mishra, R., hoop, C.L., Kodali, R., Sahoo, B., van der Wel, P.C.A. & Wetzel, R., 2012. Serine phosphorylation suppresses huntingtin amyloid accumulation by altering protein aggregation properties. *Journal of Molecular Biology*, 424(1-2), pp.1–14.

Mochel, F., Charles, P., Seguin, F., Barritault, J., Coussieu, C., Perin, L., Le Bouc, Y., Gervais, C., Carcelain, G., Vassault, A., Feingold, J., Rabier, D. & Durr, A., 2007. Early Energy Deficit in Huntington Disease: Identification of a Plasma Biomarker Traceable during Disease Progression. *PLoS One*, 2(7).

Molero, A.E., Gokhan, S., Gonzalez, S., Feig, J.L., Alexandre, L.C. & Mehler, M.F., 2009. Impairment of developmental stem cell-mediated striatal neurogenesis and pluripotency genes in a knock-in model of Huntington's disease. *Proceedings of the National Academy of Sciences of the United States of America*, 106(51), pp.21900–5.

Morales, L.M., Estevez, J., Suarez, H., Villalobos, R., Debonilla, L.C. & Bonilla, E., 1989. Nutritional-evaluation of Huntington disease patients. *American Journal of Clinical Nutrition*, 50(1), pp.145–150.

Morton, A.J., Hunt, M.J., Hodges, A.K., Lewis, P.D., Redfern, A.J., Dunnett, S.B. & Jones, L., 2005. A combination drug therapy improves cognition and reverses gene expression changes in a mouse model of Huntington's disease. *The European Journal of Neuroscience*, 21(4), pp.855–70.

Morton, a J. & Avanzo, L., 2011. Executive decision-making in the domestic sheep. *PloS One*, 6(1), p.e15752.

Morton, a J., 2013. Circadian and sleep disorder in Huntington's disease. *Experimental Neurology*, 243, pp.34–44.

Myers, R.H., Sax, D.S., Schoenfeld, M., Bird, E.D., Wolf, P.A., Vonsattel, J.P., White, R.F. & Martin, J.B., 1985. Late onset of Huntington's disease. *Journal of Neurology, Neurosurgery & Psychiatry*, 48(6), pp.530–534.

Myers, R.H., Sax, D.S., Koroshetz, W.J., Mastromauro, C., Cupples, L.A., Kiely, D.K., Pettengill, F.K. & Bird, E.D., 1991. Factors associated with slow progression in Huntington's diseas. *Archives of Neurology*, 48(8), pp.800–804.

Myers, R.H., MacDonald, M.E., Koroshetz, W.J., Duyao, M.P., Ambrose, C.M., Taylor, S.A.M., Barnes, G., Srinidhi, J., Lin, C.S., Whaley, W.L., Lazzarini, A.M., Scwarz, M., Wolff, G., Bird, E.D., Vonsattel, J-P.G. & Gusella, J.F., 1993. De novo expansion of a (CAG)n repeat in sporadic Huntington's disease. *Nature Genetics*, 5(2), pp.168–173.

Nance, M.A., Mathias-Hagen, V., Breningstall, G., Wick, M.J. & McGlennen, R.C., 1999. Analysis of a very large trinucleotide repeat in a patient with juvenile Huntington's disease. *Neurology*, 52(2), pp.392–394.

Naver, B., Stub, C., Møller, M., Fenger, K., Hansen, A.K., Hasholt, L. & Sørensen, S.A., 2003. Molecular and behavioral analysis of the R6/1 Huntington's disease transgenic mouse. *Neuroscience*, 122(4), pp.1049–1057.

Ng, C.W., Yildirim, F., Yap, Y.S., Dalin, S., Matthews, B.J., Velez, P.J., Labadorf, A., Housman, D.E.. & Fraenkel, E., 2013. Extensive changes in DNA methylation are associated with expression of mutant huntingtin. *Proceedings of the National Academy of Sciences of the United States of America*, 110(6), pp.2354–9.

Nguyen, G.D., Gokhan, S., Molero, A.E. & Mehler, M.F., 2013. Selective Roles of Normal and Mutant Huntingtin in Neural Induction and Early Neurogenesis. *PloS One*, 8(5), p.e64368.

Nishitoh, H., Matsuzawa, A., Tobiume, K., Saegusa, K., Takeda, K., Inoue, K., Hori, S., Kakizuka, A. & Ichijo, H., 2002. ASK1 is essential for endoplasmic reticulum stress-

induced neuronal cell death triggered by expanded polyglutamine repeats. *Genes and Development*, 16(11), pp.1345–1355.

Nopoulos, P.C., Aylward, E.H., Ross, C.A., Johnson, H.J., Magnotta, V.A., Juhl, A.R., Pierson, R.K., Mills, J., Langbehn, D.R. & Paulsen, J.S., 2010. Cerebral cortex structure in prodromal Huntington disease. *Neurobiology of Disease*, 40(3), pp.544–554.

Nørremølle, A., Riess, O., Epplen, J.T., Fenger, K., Hasholt, L. & Sørensen, S.A., 1993. Trinucleotide repeat elongation in the Huntingtin gene in Huntington disease patients from 71 Danish families. *Human Molecular Genetics*, 2(9), pp.1475–1476.

Nørremølle, A., Hasholt, L., Peterson, C.B., Eiberg, H., Hasselbalch, S.G., Gideon, P., Nielsen, J.E., Sørensen, S.A., 2004. Mosaicism of the CAG repeat sequence in the Huntington disease gene in a pair of monozygotic twins. *American Journal of Medical Genetics. Part A*, 130A(2), pp.154–9.

Noshita, N., Lewen, A., Sugawara, T. & Chan, P.H., 2001. Evidence of phosphorylation of Akt and neuronal survival after transient focal cerebral ischemia in mice. *Journal of Cerebral Blood Flow and Metabolism*, 21(12), pp.1442–1450.

Novak, M.J.U. & Tabrizi, S.J., 2010. Huntington's disease. *BMJ*, 341(c3109), pp.34–40.

Nucifora, F.C., Sasaki, M., Peters, M.F., Huang, H., Cooper, J.K., Yamada, M., Takahashi, H., Tsuji, S., Troncoso, J., Dawson, V.L., Dawson, T.M. & Ross, C.A., 2001. Interference by Huntingtin and atrophin-1 with CBP-mediated transcription leading to cellular toxicity. *Science*, 291(5512), pp.2423–2428.

Okun, M.S. & Thommi, N., 2004. Americo Negrette (1924 to 2003): diagnosing Huntington disease in Venezuela. *Neurology*, 63(2), pp.340–3.

Olsen, J. V., Blagoev, B., Gnad, F., Macek, B., Kumar, C., Mortensen, P. & Mann, M., 2006. Global, in vivo, and site-specific phosphorylation dynamics in signaling networks. *Cell*, 127(3), pp.635–48.

Osborne, C.S., Chakalova, L., Brown, K.E., Carter, D., Horton, A., Debrand, E., Goyenechea, B., Mitchell, J.A., Lopes, S., Reik, W. & Fraser, P., 2004. Active genes dynamically colocalize to shared sites of ongoing transcription. *Nature Genetics*, 36(10), pp.1065–71.

Owada, Y, Utsunomiya, A., Yoshimoto, T. & Kondo, H., 1997. Expression of mRNA for Akt, serine-threonine protein kinase, in the brain during development and its transient enhancement following axotomy of hypoglossal nerve. *Journal of Molecular Neuroscience*, 9(1), pp.27–33.

Pal, A., Severin, F., Lommer, B., Shevchenko, A. & Zerial, M., 2006. Huntingtin-HAP40 complex is a novel Rab5 effector that regulates early endosome motility and is up-regulated in Huntington's disease. *Journal of Cell Biology*, 172(4), pp.605–618.

Pallier, P.N., Maywood, E.S., Zheng, Z., Chesham, J.E., Inyushkin, A.N., Dyball, R., Hastings, M.H. & Morton, A.J., 2007. Pharmacological imposition of sleep slows cognitive decline and reverses dysregulation of circadian gene expression in a transgenic mouse model of Huntington's disease. *The Journal of Neuroscience* , 27(29), pp.7869–78.

Pang, L., Zheng, C.F., Guan, K.L. & Slatiel, A.R., 1995. Nerve growth-factor stimulates a novel protein-kinase in PC-12 cells that phosphorylates and activates mitogen-activated protein-kinase kinase (MEK). *Biochemical Journal*, 307(2), pp.513–519.

Park, S.H., 2005. Fine tuning and cross-talking of TGF-beta signal by inhibitory Smads. *Journal of Biochemistry and Molecular Biology*, 38(1), pp.9–16.

Paulsen, J.S., Zimbelman, J.L., Hinton, S.C., Langbehn, D.R., Leveroni, C.L., Benjamin, M.L., Reynolds, N.C. & Rao, S.M., 2004. fMRI biomarker of early neuronal dysfunction in presymptomatic Huntington's disease. *American Journal of Neuroradiology*, 25(10), pp.1715–1721.

Paulsen, J.S., Hoth, K.F., Nehl, C. & Stierman, L., 2005. Critical periods of suicide risk in Huntington's disease. *American Journal of Psychiatry*, 162(4), pp.725–731.

Paulsen, J.S., Langbehn, D.R., Stout, J.C., Aylward, E., Ross, C.A., Nance, M., Guttman, M., Johnson, S., MacDonald, M., Beglinger, L.J., Duff, K., Kayson, E., Biglan, K., Shoulson, I., Oakes, D. & Hayden, M., 2008. Detection of Huntington's disease decades before diagnosis: the Predict-HD study. *Journal of Neurology, Neurosurgery & Psychiatry*, 79(8), pp.874–880.

Penney, J.B., Vonsattel, J.P., MacDonald, M.E., Gusella, J.F. & Myers, R.H., 1997. CAG repeat number governs the development rate of pathology in Huntington's disease. *Annals of Neurology*, 41(5), pp.689–692.

Pennuto, M., Palazzolo, I. & Poletti, A., 2009. Post-translational modifications of expanded polyglutamine proteins: impact on neurotoxicity. *Human Molecular Genetics*, 18(R1), pp.R40–7.

Perrin, V., Dufour, N., Raoul, C., Hassig, R., Brouillet, E., Aebischer, P., Luthi-Carter, R. & Déglon, N., 2009. Implication of the JNK pathway in a rat model of Huntington's disease. *Experimental Neurology*, 215(1), pp.191–200.

Persichetti, F., Carlee, L., Faber, P.W., McNeil, S.M., Ambrose, C.M., Srinidhi, J., Anderson, M., Barnes, G.T., Gusella, J.F. & MacDonald, M.E., 1996. Differential expression of normal and mutant Huntington's disease gene alleles. *Neurobiology of Disease*, 3(3), pp.183–190.

Perutz, M.F., Johnson, T., Suzuki, M. & Finch, J.T., 1994. Glutamine repeats as polar zippers - their possible role in inherited neurodegenerative disease. *Proceedings of the National Academy of Sciences of the United States of America*, 91(12), pp.5355–5358.

Peters-Libeu, C., Miller, J., Rutenber, E., Newhouse, Y., Krishman, P., Cheung, K., Hatters, D., Brooks, E., Widjaja, K., Tran, T., Mitra, S, Arrasate, M., Mosquera, L.A., Taylor, D., Weisgraber, K.H. & Finkbeiner, S., 2012. Disease-associated polyglutamine stretches in monomeric huntingtin adopt a compact structure. *Journal of Molecular Biology*, 421(4-5), pp.587–600.

Pineda, J.R., Pardo, R., Zala, D., Yu, H., Humbert, S. & Saudou, F., 2009. Genetic and pharmacological inhibition of calcineurin corrects the BDNF transport defect in Huntington's disease. *Molecular Brain*, 2(1), p.33.

Politis, M., Pavese, N., Tai, Y.F., Tabrizi, S.J., Barker, R.A. & Piccini, P., 2008. Hypothalamic involvement in Huntingtons disease: an in vivo PET study. *Brain*, 131(11), pp.2860–2869.

Pouladi, M.A., Xie, Y., Skitte, N.H., Ehrnhoefer, d.E., Graham, R.K., Kim, J.E., Bissada, N., Yang, W.W., Paganetti, P., Friedlander, R.M., Leavitt, B.R. & Hayden, M.R ., 2010. Full-length huntingtin levels modulate body weight by influencing insulin-like growth factor 1 expression. *Human Molecular Genetics*, 19(8), pp.1528–38.

Pratley, R.E., Salbe, A.D., Ravussin, E. & Caviness, J.N., 2000. Higher sedentary energy expenditure in patients with Huntington's disease. *Annals of Neurology*, 47(1), pp.64–70.

Qin, Z.H., Wang, Y.M., Sapp, E., Cuiffo, B., Wanker, E., Hayden, M.R., Kegel, K.B., Aronin, N. & DiFiglia, M., 2004. Huntingtin bodies sequester vesicle-associated proteins by a polyproline-dependent interaction. *The Journal of Neuroscience*, 24(1), pp.269–281.

Qiu, Z.H., Norfus, F., Singh, B., Swindell, M.K., Buzescu, R., Bejarano, M., Chopra, R., Zucker, B., Benn, C.L., DiRocco, D.P., Cha, J-H.J., Ferrante, R.J. & Hersch, S.M., 2006. Sp1 is up-regulated in cellular and transgenic models of Huntington disease, and its reduction is neuroprotective. *The Journal of Biological Chemistry*, 281(24), pp.16672–16680.

Ramadoss, S., Chen, X. & Wang, C.-Y., 2012. Histone demethylase KDM6B promotes epithelial-mesenchymal transition. *The Journal of Biological Chemistry*, 287(53), pp.44508–17.

Ramos, E.M., Latourelle, J.C., Lee, J-H., Gillis, T., Mysore, J.S., Squitieri, F., Di Pardo, A., Di Donato, S., Hayden, M.R., Morrison, P.J., Nance, M., Ross, C.A., Margolis, R.L., Gomez-Tortosa, E., Ayuso, C., Suchowersky, O., Trent, R.J., McCusker, E., Novelletto, A., Frontali, M., Jones, R., Ashizawa, T., Frank, S., Saint-Hilaire, M-H., Hersch, S.M., Rosas, H.D., Lucente, D., Harrison, M.B., Zanko, A., Marder, K., Gusella, J.F., Lee, J-M., Alonso, I., Sequeiros, J., Myers, R.H. & MacDonald, M.E., 2012. Population stratification may bias analysis of PGC-1α as a modifier of age at Huntington disease motor onset. *Human Genetics*, 131(12), pp.1833–40.

Ramos, E.M., Latourelle, J.C., Gillis, T., Mysore, J.S., Squitieri, F., Di Pardo, A., Si Donato, S., Gellera, C., Hayden, M.R., Morrison, P.J., Nance, M., Ross, C.A., Margolis, R.L., Gomez-Tortosa, E., Ayuso, C., Suchowersky, O., Trent, R.J., McCusker, E., Novelletto, A., Frontali, M., Jones, R., Ashizawa, T., Frank, S., Saint-Hilaire, M-H., Hersch, S.M., Rosas, H.D., Lucente, D., Harrison, M.B., Zanko, A., Abramson, R.K., Marder, K., Gusella, J.F., Lee, J-M., Alonso, I., Sequeiros, J., Myers, R.H. & MacDonald, M.E., 2013. Candidate glutamatergic and dopaminergic pathway gene variants do not influence Huntington's disease motor onset. *Neurogenetics*, [Online prior to publication]. Available at: http://www.ncbi.nlm.nih.gov/pubmed/23644918 [Accessed: 20th September 2013]

Ranen, N.G., Stine, O.C., Abbott, M.H., Sherr, M., Codori, A.M., Franz., M.L., Chao, N.I., Chung, A.S., Pleasant, N., Callahan, C., Kasch, L.M., Ghaffari, M., Chase, G.A., Kazazian, H.H., Brandt, J., Folstein, S.E. & Ross, C.A., 1995. Anticipation and instability of IT-15 (CAG)(n) repeats in parent-offspring pairs with Huntington disease. *American Journal of Human Genetics*, 57(3), pp.593–602.

Ransome, M.I. & Hannan, A.J., 2013. Impaired basal and running-induced hippocampal neurogenesis coincides with reduced Akt signaling in adult R6/1 HD mice. *Molecular and Cellular Neurosciences*, 54, pp.93–107.

Rasmussen, A., Macias, R., Yescas, P., Ochoa, A., Davila, G. & Alonso, E., 2000. Huntington disease in children: Genotype-phenotype correlation. *Neuropediatrics*, 31(4), pp.190–194.

Ratovitski, T., Gucek, M., Jiang, H., Chighladze, E., Waldron, E., D'Ambola, J., Hou, Z., Liang, Y., Poirierm M.A., Hirschhorn, R.R., Graham, R., Hayden, M.R., Cole, R.N. & Ross, C.A., 2009. Mutant Huntingtin N-terminal Fragments of Specific Size Mediate Aggregation and Toxicity in Neuronal Cells. *Journal of Biological Chemistry*, 284(16), pp.10855–10867.

Rattray, I., Smith, E., Gale, R., Matsumoto, K., Bates, G.P. & Modo, M., 2013. Correlations of behavioral deficits with brain pathology assessed through longitudinal MRI and histopathology in the R6/2 mouse model of HD. *PloS One*, 8(4), p.e60012.

Read, A.P., 1993. Huntington's disease, testing the test. *Nature Genetics*, 4(4), pp.329–330.

Reddy, P.H., Williams, M. & Tagle, D.A., 1999. Recent advances in understanding the pathogenesis of Huntington's disease. *Trends in Neurosciences*, 22(6), pp.248–255.

Reilly, C.E., 2001. Wild-type huntingtin up-regulates BDNF transcription in Huntington's disease. *Journal of Neurology*, 248(10), pp.920–922.

Reilmann, R., Kirsten, F., Quinn, L., Henningsen, H., Marder, K. & Gordon, A.M., 2001. Objective assessment of progression in Huntington's disease: A 3-year follow-up study. *Neurology*, 57(5), pp.920–924.

Reiner, A., Albin, R.L., Anderson, K.D., D'Amato, C.J., Penney, J.B. & Young, A.B., 1988. Differential loss of striatal projection neurons in Huntington disease. *Proceedings of the National Academy of Sciences of the United States of America*, 85(15), pp.5733–7.

Reppert, S.M. & Weaver, D.R., 2002. Coordination of circadian timing in mammals. *Nature*, 418(6901), pp.935–41.

Ribai, P., Nguyen, K., Hahn-Barma, V., Gourfinkel, I., Vidailhet, M., Legout, A., Dode, C., Brice, A. & Durr, A., 2007. Psychiatric and cognitive difficulties as indicators of juvenile Huntington disease onset in 29 patients. *Archives of Neurology*, 64(6), pp.813–819.

Ribchester, R.R., Thomson, D., Wood, N.I., Hinks, T., Gillingwater, T.H, Wishart, T.M., Court, F.A. & Morton, A.J., 2004. Progressive abnormalities in skeletal muscle and neuromuscular junctions of transgenic mice expressing the Huntington's disease mutation. *European Journal of Neuroscience*, 20(11), pp.3092–3114.

Ridley, R.M., Frith, C.D., Crow, T.J. & Conneally, P.M., 1988. Anticipation in Huntington's disease is inherited through the male line but may originate in the female. *Journal of Medical Genetics*, 25(9), pp.589–595.

Ritch, J.J., Valencia, A., Alexander, J., Sapp, E., Gatune, L., Sangrey, G.R., Sinha, S., Scherber, C.M., Zeitlin, S., Sadri-Vakili, G., Irimia, D., DiFiglia, M. & Kegel, K.B., 2012. Multiple phenotypes in Huntington disease mouse neural stem cells. *Molecular and Cellular Neuroscience*.

Ro, Y.-T., Jang, B-K., Shin, C.Y., Park, E.U., Kim, C.G. & Yang, S-I., 2010. Akt regulates the expression of MafK, synaptotagmin I, and syntenin-1, which play roles in neuronal function. *Journal of Biomedical Science*, 17, p.18.

Robbins, A.O., Ho, A.K. & Barker, R.A., 2006. Weight changes in Huntington's disease. *European Journal of Neurology*, 13(8), p.E7.

Robins Wahlin, T.-B., Backman, L., Lundin, A., Haegermark, A., Wonblad, B. & Anvret, M., 2000. High suicidal ideation in persons testing for Huntington's disease. *Acta Neurologica Scandinavica*, 102(3), pp.150–161.

Rockabrand, E., Slepko, N., Pantalone, A., Nukala, V.N., Kazantsev, A., Marsh, J.L., Sullivan, P.G., Steffan, J.S., Sensi, S.L. & Thompson, L.M., 2007. The first 17 amino acids of Huntingtin modulate its sub-cellular localization, aggregation and effects on calcium homeostasis. *Human Molecular Genetics*, 16(1), pp.61–77.

Rong, J., McGuire, J.R., Fang, Z-H., Sheng, G., Shim, J-Y., Li, S-H. & Li, X-J., 2006. Regulation of intracellular trafficking of huntingtin-associated protein-1 is critical for TrkA protein levels and neurite outgrowth. *The Journal of Neuroscience*, 26(22), pp.6019–30.

Rong, R., He, Q., Liu, Y., Sheikh, M.S. & Huang, Y., 2002. TC21 mediates transformation and cell survival via activation of phosphatidylinositol 3-kinase/Akt and NF-kappa B signaling pathway. *Oncogene*, 21(7), pp.1062–1070.

Roos, R.A.C., Bots, G. & Hermans, J., 1986. Quantitative-analysis of morphological features in Huntingtons-disease. *Acta Neurologica Scandinavica*, 73(2), pp.131–135.

Roos, R.A.C., Vegtervandervlis, M., Hermans, J., Elshove, H.M., Moll, A.C., Vandekamp, J.J.P. & Bruyn, G.W., 1991. Age at onset of Huntingtons-disease - effect of line of inheritance and patients sex. *Journal of Medical Genetics*, 28(8), pp.515–519.

Rosas, H.D., Liu, A.K., Hersch, S., Glessner, M., Ferrante, R.J., Salat, D.H., van der Kouwe, A., Jenkins, B.G., Dale, A.M. & Fischl, B., 2002. Regional and progressive thinning of the cortical ribbon in Huntington' s disease. *Neurology*, 58(5), pp.695–701.

Rosas, H.D., Koroshetz, W.J., Chen, Y.I., Skeuse, C., Vangel, M., Cudkowicz, M.E., Caplan, K., Marek, K., Seidman, L.J., Makris, N., Jenkins, B.G. & Goldstein, J.M., 2003. Evidence for more widespread cerebral pathology in early HD - An MRI-based morphometric analysis. *Neurology*, 60(10), pp.1615–1620.

Rosas, H.D., Hevelone, N.D., Zaleta, A.K., Greve, D.N., Salat, D.H. & Fischl. B., 2005. Regional cortical thinning in preclinical Huntington disease and its relationship to cognition. *Neurology*, 65(5), pp.745–747.

Rosas, H.D., Salat, D.H., Lee, S.Y., Zaleta, A.K., Pappu, V., Fischl, B., Greve, D., Hevelone, N. & Hersch, S.M., 2008. Cerebral cortex and the clinical expression of Huntington's disease: complexity and heterogeneity. *Brain*, 131(4), pp.1057–1068.

Rosini, P.. De Chiara, G., Bonini, P., Lucibello, M., Marcocci, M.E., Garaci. E., Cozzolino, F. & Torcia, M., 2004. Nerve growth factor-dependent survival of CESS B cell line is mediated by increased expression and decreased degradation of MAPK phosphatase 1. *The Journal of Biological Chemistry*, 279(14), pp.14016–14023.

Ross, C.A., 2002. Polyglutamine pathogenesis: Emergence of unifying mechanisms for Huntington's disease and related disorders. *Neuron*, 35(5), pp.819–822.

Ross, S., Tienhaara, A., Lee, M-S., Tsai, L-H. & Gill, G., 2002. GC box-binding transcription factors control the neuronal specific transcription of the cyclin-dependent kinase 5 regulator p35. *The Journal of Biological Chemistry*, 277(6), pp.4455–64.

Rothlind, J.C., Bylsma, F.W., Peyser. C., Folstein, S.E. & Brandt, J., 1993. Cognitive and motor correlates of everyday functioning in early Huntington's disease. *Journal of Nervous and Mental Disease*, 181(3), pp.194–199.

Roze, E., Betuing, S., Deyts, C., Marcon, E., Brami-Cherrier, K., Pagès, C., Humbert, S., Mérienne, K. & Caboche, J., 2008. Mitogen- and stress-activated protein kinase-1 deficiency is involved in expanded-huntingtin-induced transcriptional dysregulation and striatal death. *The FASEB Journal*, 22(4), pp.1083–93.

Rubinsztein, D.C., Leggo, J., Coles, R., Almqvist, E., Biancalana, V., Cassiman, J.J., Chotai, K., Connarty, M., Crauford, D., Curtis, A., Curtis, D., Davidson, M.J., Differ, A.M., Dode, C., Dodge, A., Frontali, M., Ranen, N.G., Stine, O.C., Sherr, M., Abbott, M.H., Franz, M.L., Graham, C.A., Harper, P.S., Hedreen, J.C. & Hayden, M.R., 1996. Phenotypic characterization of individuals with 30-40 CAG repeats in the Huntington disease (HD) gene reveals HD cases with 36 repeats and apparently normal elderly individuals with 36-39 repeats. *American Journal of Human Genetics*, 59(1), pp.16–22.

Rudenko, O., Tkach, V., Berezin, V. & Bock, E., 2010. Effects of FGF receptor peptide agonists on animal behavior under normal and pathological conditions. *Neuroscience Research*, 68(1), pp.35–43.

Ryu, H., Lee, J., Hagerty, S.W., Soh, B.Y., Mcalpin, S.E., Cormier, K.A., Smith, K.M. & Ferrante, R.J., 2006. ESET/SETDB1 gene expression and histone H3 (K9) trimethylation in Huntington's disease. *Gene*, 103(50), pp.19176–19181.

Saavedra, A., Garcia-Martinez, J.M., Xifró, X., Giralt, A., Torres-Peraza, J.F., Canals, J.M., Diaz-Hernández, M., Lucas, J.J., Alberch, J. & Pérez-Navarro, E., 2010. PH domain leucine-rich repeat protein phosphatase 1 contributes to maintain the activation of the PI3K/Akt pro-survival pathway in Huntington's disease striatum. *Cell Death and Differentiation*, 17(2), pp.324–35.

Saavedra, A., Giralt, A., Rué, L., Xifró, X., Xu, J., Ortega, Z., Lucas, J.J., Lombroso, P.J., Alberch, J. & Pérez-Navarro, E., 2011. Striatal-Enriched Protein Tyrosine Phosphatase Expression and Activity in Huntington's Disease: A STEP in the Resistance to Excitotoxicity. *The Journal of Neuroscience*, 31(22), pp.8150–8162.

Sackley, C., Hoppitt, T.J., Calvert, M., Gill, P., Eaton, B., Yao, G. & Pall, H., 2011. Huntington's Disease: Current Epidemiology and Pharmacological Management in UK Primary Care. *Neuroepidemiology*, 37(3-4), pp.216–221.

Sadri-Vakili, G., Menon, A.S., Farrel, L.A., Keller-McGandy, C.E., Cantuti-Castelvetri, I., Standaert, D.G., Augood, S.J., Yohrling, G.J. & Cha, J-H.J., 2006. Huntingtin inclusions do not down-regulate specific genes in the R6/2 Huntington's disease mouse. *The European Journal of Neuroscience*, 23(12), pp.3171–5.

Sadri-Vakili, G., Bouzou, B., Benn, C.L., Kim, M-O., Chawla, P., Overland, R.P., Glajch, K.E., Xia, E., Qiu, Z., Hersch, S.M., Clark, T.W., Yohrling, G.J. & Cha, J-H.J., 2007.

Histones associated with downregulated genes are hypo-acetylated in Huntington's disease models. *Human Molecular Genetics*, 16(11), pp.1293–1306.

Sapp, E., Penney, J., Young, A., Aronin, N., Vonsattel, J.P. & DiFiglia, M., 1999. Axonal transport of N-terminal huntingtin suggests early pathology of corticostriatal projections in Huntington disease. *Journal of Neuropathology and Experimental Neurology*, 58(2), pp.165–173.

Sapp, E., Valencia, A., Li, X., Aronin, N., Kegel, K.B., Vonsattel, J-P., Young, A.B., Wexler, N. & DiFiglia, M., 2012. Native mutant huntingtin in human brain: evidence for prevalence of full-length monomer. *The Journal of Biological Chemistry*, 287(16), pp.13487–99.

Sathasivam, K., Hobbs, C., Turmaine, M., Mangiarini, L., Mahal, A., Bertaux, F., Wanker, E.E., Doherty, P., Davies, S.W. & Bates, G.P., 1999. Formation of polyglutamine inclusions in non-CNS tissue. *Human Molecular Genetics*, 8(5), pp.813–22.

Sathasivam, K., Neueder, A., Gipson, T.A., Landles, C., Benjamin, A.C. Bondulich, M.K., Smith, D.L., Faull, R.L.M., Roos, R.A.C., Howland, D., Detloff, P.J., Housman, D.E. & Bates, G.P., 2013. Aberrant splicing of HTT generates the pathogenic exon 1 protein in Huntington disease. *Proceedings of the National Academy of Sciences of the United States of America*, 110(6), pp.2366–2370.

Saudou, F., Finkbeiner, S., Devys, D. & Greenberg, M.E., 1998. Huntingtin acts in the nucleus to induce apoptosis but death does not correlate with the formation of intranuclear inclusions. *Cell*, 95(1), pp.55–66.

Sawa, A., Nagata, E., Sutcliffe, S., Dulloor, P., Cascio, M.B., Ozeki, Y., Roy, S., Ross, C.A. & Snyder, S.H., 2005. Huntingtin is cleaved by caspases in the cytoplasm and translocated to the nucleus via perinuclear sites in Huntington's disease patient lymphoblasts. *Neurobiology of Disease*, 20(2), pp.267–74.

Scahill, R.I., Hobbs, N.Z., Say, M.J., Bechtel, N., Henley, S.M.D., Hyare, H., Langbehn, D.R., Jones, R., Leavitt, B.R., Roos, R.A.C., Durr, A., Johnson, H., Lehéricy, S., Crauford, D., Kennard, C., Hicks, S.L., Stout, J.C., Reilmann, R. & Tabrizi, S.J., 2013. Clinical impairment in premanifest and early Huntington's disease is associated with regionally specific atrophy. *Human Brain Mapping*, 34(3), pp.519–29.

Schilling, B., Gafni, J., Torcassi, C., Cong, X., Row, R.H., LaFevre-Bernt, M.A., Cusack, M.P., Ratovitski, T., Hirschhorn, R., Ross, C.A., Gibson, B.W. & Ellerby, L.M., 2006. Huntingtin phosphorylation sites mapped by mass spectrometry. Modulation of cleavage and toxicity. *The Journal of Biological Chemistry*, 281(33), pp.23686–97.

Schilling, G., Becher, M.W., Sharp, A.H., Jinnah, H.A., Duan, K., Kotzuk, J.A., Slunt, H.H., Ratovitski, T., Cooper, J.K., Jenkins, N.A., Copeland, N.G., Price, D.L., Ross, C.A. & Borchelt, D.R., 1999. Intranuclear inclusions and neuritic aggregates in transgenic mice expressing a mutant N-terminal fragment of huntingtin. *Human Molecular Genetics*, 8(3), pp.397–407.

Schilling, G., Savonenko, A.V., Coonfield, M.L., Morton, J.L., Vorovich, E., Gale, A., Neslon, C., Chan, N., Eaton, M., Fromholt, D., Ross, C.A. & Borchelt, D.R., 2004. Environmental, pharmacological, and genetic modulation of the HD phenotype in transgenic mice. *Experimental Neurology*, 187(1), pp.137–49.

Schoenfeld, M., Myers, R.H., Cupples, L.A., Berkman, B., Sax, D. S. & Clark, E., 1984. Increased rate of suicide among patients with Huntington's disease. *Journal of Neurology, Neurosurgery, and Psychiatry*, 47(12), pp.1283–1287.

Scotter, E.L., Goodfellow, C.E., Graham, E.S., Dragunow, M. & Glass, M., 2010. Neuroprotective potential of CB1 receptor agonists in an in vitro model of Huntington's disease. *British Journal of Pharmacology*, 160(3), pp.747–761.

Seong, I.S., Woda, J.M., Song, J-J., Lloret, A., Abeyrathne, P.D., Woo, C.J., Gregory, G., Lee, J-M., Wheeler, V.C., Walz, T., Kingston, R.E., Gusella, J.F., Conlon, R.A. & MacDonald, M.E., 2010. Huntingtin facilitates polycomb repressive complex 2. *Human Molecular Genetics*, 19(4), pp.573–83.

Seredenina, T. & Luthi-Carter, R., 2012. What have we learned from gene expression profiles in Huntington's disease? *Neurobiology of Disease*, 45(1), pp.83–98.

Sharp, A.H., Loev, S.J., Schilling, G., Li, S.H., Li, X.J., Bao, J., Wagster, M.V., Kotzuk, J.A., Steiner, J.P., Lo, A., Hedreen, J., Sisodia, S., Snyder, S.H., Dawson, T.M., Ryugo, D.K. & Ross, C.A., 1995. Widespread expression of Huntingtons-disease gene (IT15) protein product. *Neuron*, 14(5), pp.1065–1074.

Shaulian, E. & Karin, M., 2002. AP-1 as a regulator of cell life and death. *Nature Cell Biology*, 4(5), pp.E131–E136.

Shelbourne, P., 1999. A Huntington's disease CAG expansion at the murine Hdh locus is unstable and associated with behavioural abnormalities in mice. *Human Molecular Genetics*, 8(5), pp.763–774.

Shelbourne, P.F., Keller-McGandy, C., Bi, W.L., Yoon, S-R., Dubeau, L., Veitch, N.J., Vonsattel, J.P., Wexler, N.S., Arnheim, N. & Augood, S.J., 2007. Triplet repeat mutation length gains correlate with cell-type specific vulnerability in Huntington disease brain. *Human Molecular Genetics*, 16(10), pp.1133–42.

Shimohata, T., Nakajima, T., Yamada, M., Uchida, C., Onodera, O., Naruse, S., Kimura, T., Koide, R., Nozaki, K., Sano, Y., Ishiguro, H., Sakoe, K., Ooshima, T., Sato, A., Ikeuchi, T., Oyake, M., Sato, T., Aoyagi, Y., Hozumi, I., Nagatsu, T., Takiyama, Y., Nishizawa, M., Goto, J., Kanazawa, I., Davidson, I., Tanese, N., Takahashi, H. & Tsuji, S., 2000. Expanded polyglutamine stretches interact with TAFII130, interfering with CREB-dependent transcription. *Nature Genetics*, 26(1), pp.29–36.

Sinha, M., Ghose, J., Das, E. & Bhattarcharyya, N.P., 2010. Altered microRNAs in STHdh(Q111)/Hdh(Q111) cells: miR-146a targets TBP. *Biochemical and Biophysical Research Communications*, 396(3), pp.742–7.

Slow, E.J., 2003. Selective striatal neuronal loss in a YAC128 mouse model of Huntington disease. *Human Molecular Genetics*, 12(13), pp.1555–1567.

Slow, E.J., Graham, R.K., Osmand, A.P., Devon, R.S., Lu, G., Deng, Y., Pearson, J., Vaid, K., Bissada, N., Wetzel, R., Leavitt, B.R. & Hayden, M.R., 2005. Absence of behavioral abnormalities and neurodegeneration in vivo despite widespread neuronal huntingtin inclusions. *Proceedings of the National Academy of Sciences of the United States of America*, 102(32), pp.11402–7.

Snell, R.G., MacMillan, J.C., Cheadle, J.P., Fenton, I., Lazarou, L.P., Davies, P., MacDonald, M.E., Gusella, J.F., Harper, P.S. & Shaw, D.J., 1993. Relationship between trinucleotide repeat expansion and phenotypic variation in Huntington's disease. *Nature Genetics*, 4(4), pp.393–397.

Snowden, J.S., Craufurd, D., Thompson, J., & Neary, D., 2002. Psychomotor, executive, and memory function in preclinical Huntington's disease. *Journal of Clinical and Experimental Neuropsychology*, 24(2), pp.133–145.

Soldati, C., Bithell, A., Johnston, C., Wong, K-Y., Stanton, L.W. & Buckley, N.J., 2013. Dysregulation of REST-regulated coding and non-coding RNAs in a cellular model of Huntington's disease. *Journal of Neurochemistry*, 124(3), pp.418–30.

Song, C., Perides, G. & Liu, Y.F., 2002. Expression of full-length polyglutamine-expanded Huntingtin disrupts growth factor receptor signaling in rat pheochromocytoma (PC12) cells. *The Journal of Biological Chemistry*, 277(8), pp.6703–7.

Song, M.R. & Ghosh, A., 2004. FGF2-induced chromatin remodeling regulates CNTF-mediated gene expression and astrocyte differentiation. *Nature Neuroscience*, 7(3), pp.229–235.

Song, S., Maru, D.M., Ajani, J.A., Chan, C-H., Honjo, S., Lin, H-K., Correa, A., Hofstetter, W.L., Davila, M., Stroehlein, J. & Mishra, L., 2013. Loss of TGF-β Adaptor β2SP Activates Notch Signaling and SOX9 Expression in Esophageal Adenocarcinoma. *Cancer Research*, 73(7), pp.2159–69.

Song, X., Thalacker, F.W. & Nilsen-Hamilton, M., 2012. Synergistic and multidimensional regulation Of plasminogen activator inhibitor type 1 expression by transforming growth factor Type β and epidermal growth factor. *The Journal of Biological Chemistry*, 287(15), pp.12520–12528.

Soulé, J., Messaoudi, E. & Bramham, C.R., 2006. Brain-derived neurotrophic factor and control of synaptic consolidation in the adult brain. *Biochemical Society Transactions*, 34(Pt 4), pp.600–4.

Spargo, E., Everall, I.P. & Lantos, P.L., 1993. Neuronal loss in the Hippocampus in Huntingtons-disease - A comparison with HIV infection. *Journal of Neurology Neurosurgery and Psychiatry*, 56(5), pp.487–491.

Spektor, B., 2002. Differential D1 and D2 receptor-mediated effects on immediate early gene induction in a transgenic mouse model of Huntington's disease. *Molecular Brain Research*, 102(1-2), pp.118–128.

Squitieri, F., Berardelli, A., Nargi, E., Castellotti, B., Mariotti, C., Cannella, M., Lavitrano, M.L., de Grazia, U., Gellera, C. & Ruggieri, S., 2000. Atypical movement disorders in the early stages of Huntington's disease: clinical and genetic analysis. *Clinical Genetics*, 58(1), pp.50–56.

Squitieri, F., 2003. Homozygosity for CAG mutation in Huntington disease is associated with a more severe clinical course. *Brain*, 126(4), pp.946–955.

Squitieri, F., Cannella, M, Simonelli, M., Sassone, J., Martino, T., Venditti, E., Ciammola, A., Colonnese, C., Frati, L. & Ciarmiello, A., 2009. Distinct brain volume changes correlating with clinical stage, disease progression rate, mutation size, and age at onset prediction as early biomarkers of brain atrophy in Huntington's disease. *CNS Neuroscience and Therapeutics*, 15(1), pp.1–11.

Stack, E.C., Kubilus, J.K., Smith, K., Cormier, K., Del Signore, S.J., Guelin, E., Ryu, H., Hersch, S.M. & Ferrante, R.J., 2005. Chronology of behavioral symptoms and neuropathological sequela in R6/2 Huntington's disease transgenic mice. *Journal of Comparative Neurology*, 490(4), pp.354–370.

Stadler, S.C. & Allis, C.D., 2012. Linking epithelial-to-mesenchymal-transition and epigenetic modifications. *Seminars in Cancer Biology*, 22(5-6), pp.404–410.

Steffan, J.S., Kazantsev, A., Spasic-Boskovic, O., Greenwald, M., Zhu, Y.Z., Gohler, H., Wanker, E.E., Bates, G.P., Housman, D.E. & Thompson, L.M., 2000. The Huntington's disease protein interacts with p53 and CREB-binding protein and represses transcription. *Proceedings of the National Academy of Sciences of the United States of America*, 97(12), pp.6763–6768.

Steffan, J.S., Agrawal, N., Pallos, J., Rockabrand, E., Trotman, L.C., Slepko, N., Illes, K., Lukacsovich, T., Zhu, Y-Z., Cattaneo, E., Pandolfi, P.P., Thompson, L.M. & Marsh, J.L., 2004. SUMO modification of Huntingtin and Huntington's disease pathology. *Science,* 304(5667), pp.100–4.

Stout, J.C., Rodawalt, W.C. & Siemers, E.R., 2001. Risky decision making in Huntington's disease. *Journal of the International Neuropsychological Society*, 7(1), pp.92–101.

Stout, J.C., Paulsen, J.S., Queller, S., Solomon, A.C., Whitlock, K.B., Campbell, J.C., Carlozzi, N., Duff, K., Beglinger, L.J., Langbehn, D.R., Johnson, S.A., Biglan, K.M. & Aylward, E.H., 2011. Neurocognitive Signs in Prodromal Huntington Disease. *Neuropsychology*, 25(1), pp.1–14.

Strand, A.D., Baquet, Z.C., Aragaki, A.K., Holmans, P., Yang, L., Cleren, C., Beal, M.F., Jones, L., Kooperberg, C., Olsen, J.M. & Jones, K.R., 2007. Expression profiling of Huntington's disease models suggests that brain-derived neurotrophic factor

depletion plays a major role in striatal degeneration. *The Journal of Neuroscience*, 27(43), pp.11758–68.

Strong, T.V., Tagle, D.A., Valdes, J.M., Elmer, L.W., Boehm, K., Swaroop, M., Kaatz, K.W., Collins, F.S. & Albin, R.L., 1993. Widespread expression of the human and rat Huntington's disease gene in brain and nonneural tissues. *Nature Genetics*, 5(3), pp.259–265.

Suhr, S.T., Senut, M.C., Whitelegge, J.P., Faull, K.F., Cuizon, D.B. & Gage, F.H., 2001. Identities of sequestered proteins in aggregates from cells with induced polyglutamine expression. *The Journal of Cell Biology*, 153(2), pp.283–94.

Sun, J., Xu, H., Negi, S., Subramony, S.H. & Hebert, M.D., 2007. Differential effects of polyglutamine proteins on nuclear organization and artificial reporter splicing. *Journal of Neuroscience Research*, 85(11), pp.2306–2317.

Suopanki, J., Gotz, C., Lutsch, G., Schiller, J., Harjes, P., Herrmann, A. & Wanker, E.E., 2006. Interaction of huntingtin fragments with brain membranes - clues to early dysfunction in Huntington's disease. *Journal of Neurochemistry*, 96(3), pp.870–884.

Tabrizi, S.J., Langbehn, D.R., Leavitt, B.R., Roos, R.A.C., Durr, A., Crauford, D., Kennard, C., Hicks, S.L., Fox, N.C., Scahill, R.I., Borowsky, B., Tobin, A. J., Rosas, H.D., Johnson, H., Reilmann, R., Landwehrmeyer, B. & Stout, J.C., 2009. Biological and clinical manifestations of Huntington's disease in the longitudinal TRACK-HD study: cross-sectional analysis of baseline data. *Lancet Neurology*, 8(9), pp.791–801.

Tabrizi, S.J., Scahill, R.I., Durr, A., Roos, R.A.C., Leavitt, B.R., Jones, R., Landwehrmeyer, G.B., Fox, N.C., Johnson, H., Hicks, S.L., Kennard, C., Crauford, D., Frost, C., Langbehn, D.R., Reilmann, R. & Stout, J.C., 2011. Biological and clinical changes in premanifest and early stage Huntington's disease in the TRACK-HD study: the 12-month longitudinal analysis. *Lancet Neurology*, 10(1), pp.31–42.

Tabrizi, S.J., Reilmann, R., Roos, R.A.C., Durr, A., Leavitt, B., Owen, G., Jones, R., Johnson, H., Crauford, D., Hicks, S.L., Kennard, C., Landwehrmeyer, B., Stout, J.C., Borowsky, B., Scahill, R.I., Frost, C., Langbehn, D.R., 2012. Potential endpoints for clinical trials in premanifest and early Huntington's disease in the TRACK-HD study: analysis of 24 month observational data. *Lancet Neurology*, 11(1), pp.42–53.

Tabrizi, S.J., Scahill, R.I., Owen, G., Durr, A., Leavitt, B.R., Roos, R.A., Borowsky, B., Landwehrmeyer, B., Frost, C., Johnson, H., Craufurd, D., Reilmann, R., Stout, J.C. & Langbehn, D.R., 2013. Predictors of phenotypic progression and disease onset in premanifest and early-stage Huntington's disease in the TRACK-HD study: analysis of 36-month observational data. *The Lancet Neurology*, 12(7), pp.637–649.

Takano, H., Cancel, G., Ikeuchi, T., Lorenzetti, D., Mawad, R., Stevanin, G., Didierjean, O., Durr, A., Oyake, M., Shimohata, T., Sasaki, R., Koide, R., Igarashi, S., Hayashi, S., Takiyama, Y., Nishizawa, M., Tanaka, H., Zoghbi, H., Brice, A. & Tsuji, S., 1998. Close associations between prevalences of dominantly inherited spinocerebellar ataxias with CAG-repeat expansions and frequencies of large normal CAG alleles in Japanese and Caucasian populations. *American Journal of Human Genetics*, 63(4), pp.1060–1066.

Takano, H. & Gusella, J.F., 2002. The predominantly HEAT-like motif structure of huntingtin and its association and coincident nuclear entry with dorsal, an NF-kB/Rel/dorsal family transcription factor. *BMC Neuroscience*, 3(15).

Tallaksen-Greene, S.J., Crouse, A.B., Hunter, J.M., Detloff, P.J. & Albin, R.L., 2005. Neuronal intranuclear inclusions and neuropil aggregates in Hdh(CAG(150)) knockin mice. *Neuroscience*, 131(4), pp.843–852.

Tanaka, Y., Igarashi, S., Nakamura, M., Gafni, J., Torcassi, C., Schilling, G., Crippen, D., Wood, J.D., Sawa, A., Jenkins, N.A., Copeland, N.G., Borchelt, D.R., Ross, C.A. & Ellerby, L.M., 2006. Progressive phenotype and nuclear accumulation of an amino-terminal cleavage fragment in a transgenic mouse model with inducible expression of full-length mutant huntingtin. *Neurobiology of Disease*, 21(2), pp.381–91.

Tao, T. & Tartakoff, a M., 2001. Nuclear relocation of normal huntingtin. *Traffic*, 2(6), pp.385–94.

Tartari, M., Gissi, C., Lo Sardo, V., Zuccato, C., Picardi, E., Pesole, G. & Cattaneo, E., 2008. Phylogenetic comparison of huntingtin homologues reveals the appearance of a primitive polyQ in sea urchin. *Molecular Biology and Evolution*, 25(2), pp.330–338.

Tasset, I., Sánchez-López, F., Agüera, E., Fernández-Bolaños, R., Sánchez, F.M., Cruz-Guerrero, A., Gascón-Luna, F. & Túnez, I., 2012. NGF and nitrosative stress in patients with Huntington's disease. *Journal of the Neurological Sciences*, 315(1-2), pp.133–6.

Taylor, D.M., Moser, R., Régulier, E., Breuillaud, L., Dixon, M., Beeson, A.A., Elliston, L., Silva Santos, M.D-F., Kim, J., Jones, L., Goldstein, D.R., Ferrante, R.J. & Luthi-Carter, R., 2013. MAP kinase phosphatase 1 (MKP-1/DUSP1) is neuroprotective in Huntington's disease via additive effects of JNK and p38 inhibition. *The Journal of Neuroscience*, 33(6), pp.2313–25.

Tebbenkamp, A.T.N., Crosby, K.W., Siemienski, Z.B., Brown, H.H., Golde, T.E. & Borchelt, D.R., 2012. Analysis of proteolytic processes and enzymatic activities in the generation of huntingtin n-terminal fragments in an HEK293 cell model. *PloS One*, 7(12), p.e50750.

Telenius, H., Kremer, H.P., Theilmann, J., Andrew, S.E., Almqvist, E., Anvret, M., Greenberg, C., Greenberg, J., Lucotte, G. & Squitieri, F., 1993. Molecular analysis of juvenile Huntington disease: the major influence on (CAG)n repeat length is the sex of the affected parent. *Human Molecular Genetics*, 2(10), pp.1535–40.

Telenius, H., Kremer, B., Goldberg, Y.P., Theilmann, J., Andrew, S.E., Zeisler, T., Adam, S., Greenberg, C., Ives, E.J., Clarke, L.A. & Hayden, M.R., 1994. Somatic and gonadal mosaicism of the Huntington disease gene CAG repeat in brain and sperm. *Nature Genetics*, 6(4), pp.409–414.

Teng, A.C.T., Al-Montashiri, N.A.M., Cheng, B.L.M., Lou, P., Ozmizrak, P., Chen, H-H. & Stewart, A.F.R., 2011. Identification of a phosphorylation-dependent nuclear localization motif in interferon regulatory factor 2 binding protein 2. *PloS One*, 6(8), p.e24100.

Terry, L.J., Shows, E.B. & Wente, S.R., 2007. Crossing the nuclear envelope: Hierarchical regulation of nucleocytoplasmic transport. *Science*, 318(5855), pp.1412–1416.

Thieben, M.J., Duggins, A.J., Good, C.D., Gomes, L., Mahant, N., Richards, F., McCusker, E. & Frackowiak, R.S.J., 2002. The distribution of structural neuropathology in pre-clinical Huntington's disease. *Brain*, 125(8), pp.1815–1828.

Thomas, E., Coppola, G., Desplats, P.A., Tang, B., Soragni, E., Burnett, R., Gao, F., Fitzgerald, K.M., Borok, J.F., Herman, D., Geschwind, D.H. & Gottesfeld, J.M., 2008. The HDAC inhibitor 4b ameliorates the disease phenotype and transcriptional abnormalities in Huntington's disease transgenic mice. *Proceedings of the National Academy of Sciences of the United States of America*, 105(40), pp.15564–9.

Thompson, L.M., Aiken, C.T., Kaltenbach, L.S., Agrawal, N., Illes, K., Khoshnan, A., Martinez-Vincente, M., Arrasate, M., O'Rourke, J.G., Khashwji, H., Lukacsovich, T., Zhu, Y-Z., Lau, A.L., Massey, A., Hayden, M.R., Zeitlin, S.O., Finkbeiner, S., Green, K.N., LaFerla, F.M., Bates, G., Huang, L., Patterson, P.H., Lo, D.C., Cuervo, A.M., Marsh, J.L. & Steffan, J.S., 2009. IKK phosphorylates Huntingtin and targets it for degradation by the proteasome and lysosome. *The Journal of Cell Biology*, 187(7), pp.1083–99.

Thuault, S., Tam, E-J., Peinado, H., Cano, A., Heldin, C-H. & Moustakas, A., 2008. HMGA2 and Smads co-regulate SNAIL1 expression during induction of epithelial-to-mesenchymal transition. *The Journal of Biological Chemistry*, 283(48), pp.33437–46.

Toneff, T., Mende-Mueller, L., Wu, Y., Hwang, S-R., Bundey, R., Thompson, L.M., Chesselet, M-F. & Hook, V., 2002. Comparison of huntingtin proteolytic fragments in human lymphoblast cell lines and human brain. *Journal of Neurochemistry*, 82(1), pp.84–92.

Torcia, M., De Chiara, G., Nencioni, L., Ammendola, S., Labardi, D., Lucibello, M., Rosini, P., Marlier, L.N.J.L., Bonini, P., Dello Sbarba, P., Palamara, A.T., Zambrano, N., Russo, T., Garaci, E. & Cozzolino, F., 2001. Nerve growth factor inhibits apoptosis in memory B lymphocytes via inactivation of p38 MAPK, prevention of Bcl-2 phosphorylation, and cytochrome c release. *The Journal of Biological Chemistry*, 276(42), pp.39027–39036.

del Toro, D., Alberch, J., Lazaro-Dieguez, F., Martin-Ibanez, R., Xifro, X., Egea, G. & Canals, J.M., 2009. Mutant Huntingtin Impairs Post-Golgi Trafficking to Lysosomes by Delocalizing Optineurin/Rab8 Complex from the Golgi Apparatus. *Molecular Biology of the Cell*, 20(5), pp.1478–1492.

Traverse, S., Gomez, N., Paterson, H., Marshall. C. & Cohen, P., 1992. Sustained activation of the mitogen-activated protein (MAP) kinase cascade may be required for differentiation of PC12 cells - comparison of the effects of nerve growth-factor and epidermal growth-factor. *Biochemical Journal*, 288(2), pp.351–355.

Trettel, F., Rigamonti, D., Hilditch-Maguire, P., Wheeler, V.C., Sharp, A.H., Persichetti, F., Cattaneo, E. & MacDonald, M.E., 2000. Dominant phenotypes produced by the HD mutation in STHdh(Q111) striatal cells. *Human Molecular Genetics*, 9(19), pp.2799–809.

Truant, R., 2003. Nucleocytoplasmic transport of huntingtin and Huntington's disease. *Clinical Neuroscience Research*, 3(3), pp.157–164.

Truant, R., Atwal, R.S. & Burtnik, A., 2007. Nucleocytoplasmic trafficking and transcription effects of huntingtin in Huntington's disease. *Progress in Neurobiology*, 83(4), pp.211–27.

Trueman, R.C., Brooks, S.P., Jones, L. & Dunnett, S.B., 2007. The operant serial implicit learning task reveals early onset motor learning deficits in the Hdh(Q92) knock-in mouse model of Huntington's disease. *European Journal of Neuroscience*, 25(2), pp.551–558.

Trueman, R.C., Jones, L., Dunnett, S.B. & Brooks, S.P., 2012. Early onset deficits on the delayed alternation task in the Hdh(Q92) knock-in mouse model of Huntington's disease. *Brain Research Bulletin*, 88(2-3, SI), pp.156–162.

Trueman, R.C., Dunnett, S.B., Jones, L. & Brooks, S.P., 2012. Five choice serial reaction time performance in the Hdh(Q92) mouse model of Huntington's disease. *Brain Research Bulletin*, 88(2-3, SI), pp.163–170.

Tsai, J.C., Liu, L.X., Cooley, B.C., Dichiara, M.R., Topper, J.N. & Aird, W.C., 2000. The Egr-1 promoter contains information for constitutive and inducible expression in transgenic mice. *FASEB Journal*, 14(13), pp.1870–1872.

Tsvetkov, A.S., Arrasate, M., Barmada, S., Ando, D.M., Sharma, P., Shaby, B.A. & Finkbeiner, S., 2013. Proteostasis of polyglutamine varies among neurons and predicts neurodegeneration. *Nature Chemical Biology*, 9(9), pp.586–592.

Uchida, M., Shimatsu, Y., Onoe, K., Matsuyama, N., Niki, R., Ikeda, J.E. & Imai, H., 2001. Production of transgenic miniature pigs by pronuclear microinjection. *Transgenic Research*, 10(6), pp.577–582.

Vachharajani, S.N., Chaudhary, R.K., Prasad, S. & Roy, I., 2012. Length of polyglutamine tract affects secondary and tertiary structures of huntingtin protein. *International Journal of Biological Macromolecules*, 51(5), pp.920–5.

Valor, L.M., Guiretti, D., Lopez-Atalaya, J.P. & Barco, A., 2013. Genomic landscape of transcriptional and epigenetic dysregulation in early onset polyglutamine disease. *The Journal of Neuroscience*, 33(25), pp.10471–82.

Van Raamsdonk, J.M., Pearson, J., Slow, E.J., Hossain, S.M., Leavitt, B.R. & Hayden, M.R., 2005. Cognitive dysfunction precedes neuropathology and motor abnormalities in the YAC128 mouse model of Huntington's disease. *The Journal of Neuroscience*, 25(16), pp.4169–80.

Van Raamsdonk, J.M., Metzler, M., Slow, E., Pearson, J., Schwab, C., Carroll, J., Graha,. R.K., Leavitt, B.R. & Hayden, M.R., 2007. Phenotypic abnormalities in the YAC128 mouse model of Huntington disease are penetrant on multiple genetic backgrounds and modulated by strain. *Neurobiology of Disease*, 26(1), pp.189–200.

Vandjik, J.G., Vandervelde, E.A., Roos, R.A.C. & Bruyn, G.W., 1986. Juvenile Huntington disease. *Human Genetics*, 73(3), pp.235–239.

Varma, H., Cheng, R., Voisine, C., Hart, A.C. & Stockwell, B.R., 2007. Inhibitors of metabolism rescue cell death in Huntington's disease models. *Proceedings of the National Academy of Sciences of the United States of America*, 104(36), pp.14525–30.

Vonsattel, J.P., Myers, R.H., Stevens, T.J., Ferrante, R.J., Bird, E.D. & Richardson, E.P., 1985. Neuropathological classification of Huntingtons-disease. *Journal of Neuropathology and Experimental Neurology*, 44(6), pp.559–577.

Vonsattel, J.P.G. & DiFiglia, M., 1998. Huntington disease. *Journal of Neuropathology and Experimental Neurology*, 57(5), pp.369–384.

Vonsattel, J.P.G., Keller, C. & del Pilar Amaya, M., 2008. Neuropathology of Huntington's Disease. In C. Duyckaerts & I. Litvan, eds. *Dementias*. Elsevier, pp. 599–618.

Walker, F.O., 2007. Huntington's Disease. *Seminars in Neurology*, 27(2), pp.143–50.

Wang, J., Duncan, D., Shi, Z. & Zhang, B., 2013. WEB-based GEne SeT AnaLysis Toolkit (WebGestalt): update 2013. *Nucleic acids research*, 41(Web Server issue), pp.W77–83.

Wang, L., Ankati, H., Akubathini, S.K., Balderamos, M., Storey, C.A., Patel, A.V., Price, V., Kretzschmar, D., Bieh, E.R. & D'Mello, S.R., 2010. Identification of Novel 1,4-Benzoxazine Compounds That Are Protective in Tissue Culture and In Vivo Models of Neurodegeneration. *Journal of Neuroscience Research*, 88(9), pp.1970–1984.

Wang, R., Luo, Y., Ly, P.T.T., Cai, F., Zhou, W., Zou, H. & Song, W., 2012. Sp1 Regulates Human Huntingtin Gene Expression. *Journal of Molecular Neuroscience*, 47(2), pp.311–321.

Warby, S.C., Chan, E.Y., Metzler, M., Gan, L., Singaraja, R.R., Crocker, S.F., Robertson, H.A. & Hayden, M.R., 2005. Huntingtin phosphorylation on serine 421 is significantly reduced in the striatum and by polyglutamine expansion in vivo. *Human Molecular Genetics*, 14(11), pp.1569–77.

Warby, S.C., Doty, C.N., Graham, R.K., Shively, J., Singaraja, R.R. & Hayden, M.R., 2009. Phosphorylation of huntingtin reduces the accumulation of its nuclear fragments. *Molecular and Cellular Neurosciences*, 40(2), pp.121–7.

Warby, S.C., Visscher, H., Collins, J.A., Doty, C.N., Carter, C., Butland, S.L., Hayden, A.R., Kanazawa, I., Ross, C.J. & Hayden, M.R., 2011. HTT haplotypes contribute to differences in Huntington disease prevalence between Europe and East Asia. *European Journal of Human Genetics*, 19(5), pp.561–6.

Weiss, A., Klein, C., Woodman, B., Sathasivam, K., Bibel, M., Régulier, E., Bates, G.P. & Paganetti, P., 2008. Sensitive biochemical aggregate detection reveals aggregation onset before symptom development in cellular and murine models of Huntington's disease. *Journal of Neurochemistry*, 104(3), pp.846–58.

Wellington, C.L., Ellerby, L.M., Hackam, A.S., Margolis, R.L., Trifiro, M.A., Singaraja, R., McCutcheon, K., Salvesen, G.S., Propp, S.S., Bromm, M., Rowland, K.J., Zhang, T., Rasper, D., Roy, S., Thornberry, N., Pinsky, L., Kakizuka, A., Ross, C.A., Nicholson, D.W., Bredesen, D.E. & Hayden, M.R., 1998. Caspase cleavage of gene products associated with triplet expansion disorders generates truncated fragments containing the polyglutamine tract. *The Journal of Biological Chemistry*, 273(15), pp.9158–67.

Wellington, C.L., Singaraja, R. Ellerby, L., Savill, J., Roy, S., Leavitt, B., Cattaneo, E., Hackam, A., Sharp, A., Thornberry, N., Nicholson, D.W., Bredesen, D.E. & Hayden, M.R., 2000. Inhibiting caspase cleavage of huntingtin reduces toxicity and aggregate formation in neuronal and nonneuronal cells. *The Journal of Biological Chemistry*, 275(26), pp.19831–19838.

Weston, C.R. & Davis, R.J., 2002. The JNK signal transduction pathway. *Current Opinion in Genetics and Development*, 12(1), pp.14–21.

Wexler, A., 1995. *Mapping fate: a memoir of family, risk, and genetic research*, Berkeley and Los Angeles, USA; University of California Press.

Wexler, N.S., Young. A.B., Tanzi, R.E., Travers, H., Starostarubinstein, S., Penney, J.B., Snodgrass, S.R., Shoulson, I., Gomez, F., Arroyo, M.A.R., Penchaszadeh, G.K., Moreno, H., Gibbons, K., Faryniarz, A., Hobbs, W., Anderson, M.A., Bonilla, E., Conneally, P.M. & Gusella, J.F., 1987. Homozygotes for Huntingtons-disease. *Nature*, 326(6109), pp.194–197.

Wexler, N.S., 2012. Huntington's disease: advocacy driving science. *Annual Review of Medicine*, 63, pp.1–22.

Wheeler, V., 1999. Length-dependent gametic CAG repeat instability in the Huntington's disease knock-in mouse. *Human Molecular Genetics*, 8(1), pp.115–122.

Wheeler, V.C., 2000. Long glutamine tracts cause nuclear localization of a novel form of huntingtin in medium spiny striatal neurons in HdhQ92 and HdhQ111 knock-in mice. *Human Molecular Genetics*, 9(4), pp.503–513.

Wheeler, V.C., Gutekunst, C.A., Vrbanac, V., Lebel, L-A., Schilling, G., Hersch, S., Friedlander, R.M., Gusella, J.F., Vonsattel, J-P., Borchelt, D.R. & MacDonald, M.E., 2002. Early phenotypes that presage late-onset neurodegenerative disease allow testing of modifiers in Hdh CAG knock-in mice. *Human Molecular Genetics*, 11(6), pp.633–40.

Wheeler, V.C., Persichetti, F., McNeil, S.M., Mysore, J.S., Mysore, S.S., MacDonald, M.E., Myers, R.H., Gusella, J.F. & Wexler, N.S., 2007. Factors associated with HD CAG repeat instability in Huntington disease. *Journal of Medical Genetics*, 44(11), pp.695–701.

Woodman, B., Butler, R., Landles, C., Lupton, M.K., Tse, J., Hockly, E., Moffitt, H., Sathasivam, K. & Bates, G.P., 2007. The Hdh(Q150/Q150) knock-in mouse model of HD and the R6/2 exon 1 model develop comparable and widespread molecular phenotypes. *Brain Research Bulletin*, 72(2-3), pp.83–97.

Xia, J., 2003. Huntingtin contains a highly conserved nuclear export signal. *Human Molecular Genetics*, 12(>12), pp.1393–1403.

Xie, Y., Hayden, M.R. & Xu, B., 2010. BDNF overexpression in the forebrain rescues Huntington's disease phenotypes in YAC128 mice. *The Journal of Neuroscience*, 30(44), pp.14708–18.

Yamamoto, a, Lucas, J.J. & Hen, R., 2000. Reversal of neuropathology and motor dysfunction in a conditional model of Huntington's disease. *Cell*, 101(1), pp.57–66.

Yamanaka, T., Tosaki, A., Miyazaki, H., Kurosawa, M., Furukawa, Y., Yamada, M. & Nukina, N., 2010. Mutant huntingtin fragment selectively suppresses Brn-2 POU

domain transcription factor to mediate hypothalamic cell dysfunction. *Human Molecular Genetics*, 19(11), pp.2099–112.

Yang, D., Wang, C-E., Zhao, B., Li, W., Ouyang, Z., Liu, Z., Yang, H., Fan, P., O'Neill, A., Gu, W., Yi, H., Li, S., Lai, L. & Li, X-J., 2010. Expression of Huntington's disease protein results in apoptotic neurons in the brains of cloned transgenic pigs. *Human Molecular Genetics*, 19(20), pp.3983–94.

Yang, S.-H., Cheng, P-H., Banta, H., Piotrowska-Nitsche, K., Yang, J-J., Cheng, E.C.H., Snyder, B., Larkin, K., Liu, J., Orkin, J., Fang, Z-H., Smith, Y., Bachevalier, J., Zola, S.M., Li, S-H., Li, X-J. & Chan, A.W.S., 2008. Towards a transgenic model of Huntington's disease in a non-human primate. *Nature*, 453(7197), pp.921–4.

Yang, Y., Goldstein, B.G. Nakagawa, H. & Katz, J.P., 2007. Krüppel-like factor 5 activates MEK/ERK signaling via EGFR in primary squamous epithelial cells. *FASEB Journal*, 21(2), pp.543–50.

Yao, L.-C., Blitz, I.L., Peiffer, D.A., Phin, S., Wang, Y., Ogata, S., Cho, K.W.Y., Arora, K. & Warrior, R., 2006. Schnurri transcription factors from Drosophila and vertebrates can mediate Bmp signaling through a phylogenetically conserved mechanism. *Development,* 133(20), pp.4025–34.

Young, A.B., Shoulson, I., Penney, J.B., Starostarubinstein, S., Gomez., Travers, H., Ramossarroyo, M.A., Snodgrass, S.R., Bonilla, E., Moreno, H. & Wexler, N.S., 1986. Huntington's disease in Venezuela - neurologic features and functional decline. *Neurology*, 36(2), pp.244–249.

Yu, Z., Li, S-H, Evans, J., Pillarisetti, A., Li, H. & Li, X-J., 2003. Mutant Huntingtin causes context-dependent neurodegeneration in mice with Huntington's disease. *The Journal of Neuroscience*, 23(6), pp.2193–2202.

Zajac, M.S., Pang, T.Y.C., Wong, N., Weinrich, B., Leang, L.S.K., Craig, J.M., Saffery, R. & Hannan, A.J., 2010. Wheel running and environmental enrichment differentially modify exon-specific BDNF expression in the hippocampus of wild-type and pre-motor symptomatic male and female Huntington's disease mice. *Hippocampus*, 20(5), pp.621–36.

Zala, D., Colin, E., Rangone, H., Liot, G., Humbert, S. & Saudou, F., 2008. Phosphorylation of mutant huntingtin at S421 restores anterograde and retrograde transport in neurons. *Human Molecular Genetics*, 17(24), pp.3837–46.

Zawel, L., Yu, J., Torrance, C.J., Markowitz, S., Kinzler, K.W., Vogelstein, B. & Zhou, S., 2002. DEC1 is a downstream target of TGF-beta with sequence-specific transcriptional repressor activities. *Proceedings of the National Academy of Sciences of the United States of America*, 99(5), pp.2848–53.

Zhang, B., Kirov, S. & Snoddy, J., 2005. WebGestalt: an integrated system for exploring gene sets in various biological contexts. *Nucleic Acids Research*, 33(Web Server issue), pp.W741–8.

Zhang, H., Das, S., Li, Q-Z., Dragatsis, I., Repa, J., Zeitlin, S., Hajnoczky, G. & Bexprozvanny, I., 2008. Elucidating a normal function of huntingtin by functional and microarray analysis of huntingtin-null mouse embryonic fibroblasts. *BMC Neuroscience*, 9(38).

Zhang, J., Peng, Q, Li, Q, Jahanshad, N., Hou, Z., Jiang, M., Masuda, N., Langbehn, D.R., Miller, M.I., Mori, S., Ross, C.A. & Duan, W., 2010. Longitudinal characterization of brain atrophy of a Huntington's disease mouse model by automated morphological analyses of magnetic resonance images. *Neuroimage*, 49(3), pp.2340–2351.

Zhang, J.H., Zhang, D.S., McQuade, J.S., Behbehani, M., Tsien, J.Z. & Xu, M., 2002. c-fos regulates neuronal excitability and survival. *Nature Genetics*, 30(4), pp.416–420.

Zhang, Y., Leavitt, B.R., van Raamsdonk, J.M., Dragatsis, I., Goldowitz, D., MacDonald, M.E., Hayden, M.R. & Friedlander, R.M., 2006. Huntingtin inhibits caspase-3 activation. *EMBO Journal*, 25(24), pp.5896–5906.

Zheng, Z., Li, A., Holmes, B.N, Marasa, J.C. & Diamond, M.I., 2013. An N-terminal nuclear export signal regulates trafficking and aggregation of Huntingtin (Htt) protein exon 1. *The Journal of Biological Chemistry*, 288(9), pp.6063–71.

Zoghbi, H.Y. & Orr, H.T., 2000. Glutamine repeats and neurodegeneration. *Annual Review of Neuroscience*, 23, pp.217–247.

Zuccato, C., Ciammola, A., Rigamonti, D., Leavitt, B.R., Goffredo, D., Conti, L., MacDonald, M.E., Friedlander, R.M., Silani, V., Hayden, M.R., Timmusk, T., Sipione, S. & Cattaneo, E., 2001. Loss of huntingtin-mediated BDNF gene transcription in Huntington's disease. *Science*, 293(5529), pp.493–8.

Zuccato, C., Tartari, M., Crotti, A., Goffrefdo, D., Valenza, M., Conti, L., Cataudella, T., Leavitt, B.R., Hayden, M.R., Timmusk, T., Rigamonti, D. & Cattaneo, E., 2003. Huntingtin interacts with REST/NRSF to modulate the transcription of NRSE-controlled neuronal genes. *Nature Genetics*, 35(1), pp.76–83.

Zuccato, C. & Cattaneo, E., 2007. Role of brain-derived neurotrophic factor in Huntington's disease. *Progress in Neurobiology*, 81(5-6), pp.294–330.

Zuccato, C., Marullo, M., Conforti, P., MacDonald, M.E., Tartari, M. & Cattaneo, E., 2008. Systematic assessment of BDNF and its receptor levels in human cortices affected by Huntington's disease. *Brain Pathology*, 18(2), pp.225–238.

Zuccato, C., Valenza, M. & Cattaneo, E., 2010. Molecular mechanisms and potential therapeutical targets in Huntington's disease. *Physiological Reviews*, 90(3), pp.905–81.

Zucker, B., Luthi-Carter, R., Kama, J.A., Dunah, A.W., Stern, E.A., Fox, J.H., Standert, D.G., Young, A.B. & Augood, S.J., 2005. Transcriptional dysregulation in striatal projection- and interneurons in a mouse model of Huntington's disease: neuronal selectivity and potential neuroprotective role of HAP1. *Human Molecular Genetics*, 14(2), pp.179–89.

Appendices

Appendix I - *StHdh*^{Q111} cell lines immunostained with Ab109115 following EGF stimulation

Consistent with Ab675 (Section 3.3.3.3), there was a significant effect of both time (F (3,856) = 6.08, p<0.001) and cell type (F (2, 856) = 132.21, p<0.001) in the N/C ratio, as well as a significant interaction between the two (F (6, 856) = 3.81, p=0.001) when cells were stained with Ab109115 following EGF stimulation (Figures AI.1 & AI.2). This was also the case for both the N/P and P/C ratios (p<0.05 in all cases). Similar to the observations with Ab675 following EGF stimulation, there was also a reduction in nuclear HTT using this antibody in both *StHdh*$^{Q7/7}$ and *StHdh*$^{Q7/111}$ cells, although this was significant after 15 minutes of stimulation rather than 5, and was only apparent in the N/P ratio rather than the N/C ratio (*StHdh*$^{Q7/7}$ p=0.04, *StHdh*$^{Q7/111}$ p=0.018). This may be because this antibody detects an epitope of HTT that is more perinuclear than the epitope detected by Ab675. Although there is no significant reduction in nuclear mHTT in *StHdh*$^{Q111/111}$ cells, there is a trend towards it. However, the high variability suggests that the nuclear reduction of the N-terminal epitope of mHTT in response to growth factor stimulation is impaired due to the expanded polyQ. Although there was a significant effect of both cell type and time in the P/C ratio, further investigation revealed that there were no individual significant differences in any of the cell lines at any time point. Simple main effects analyses indicated that this difference is due to *StHdh*$^{Q111/111}$ cells having significantly higher P/C ratios than *StHdh*$^{Q7/7}$ cells (p=0.006), while the *StHdh*$^{Q7/111}$ cells lie between the two other genotypes, which is the same pattern of localisation seen with other N-terminal HTT antibodies.
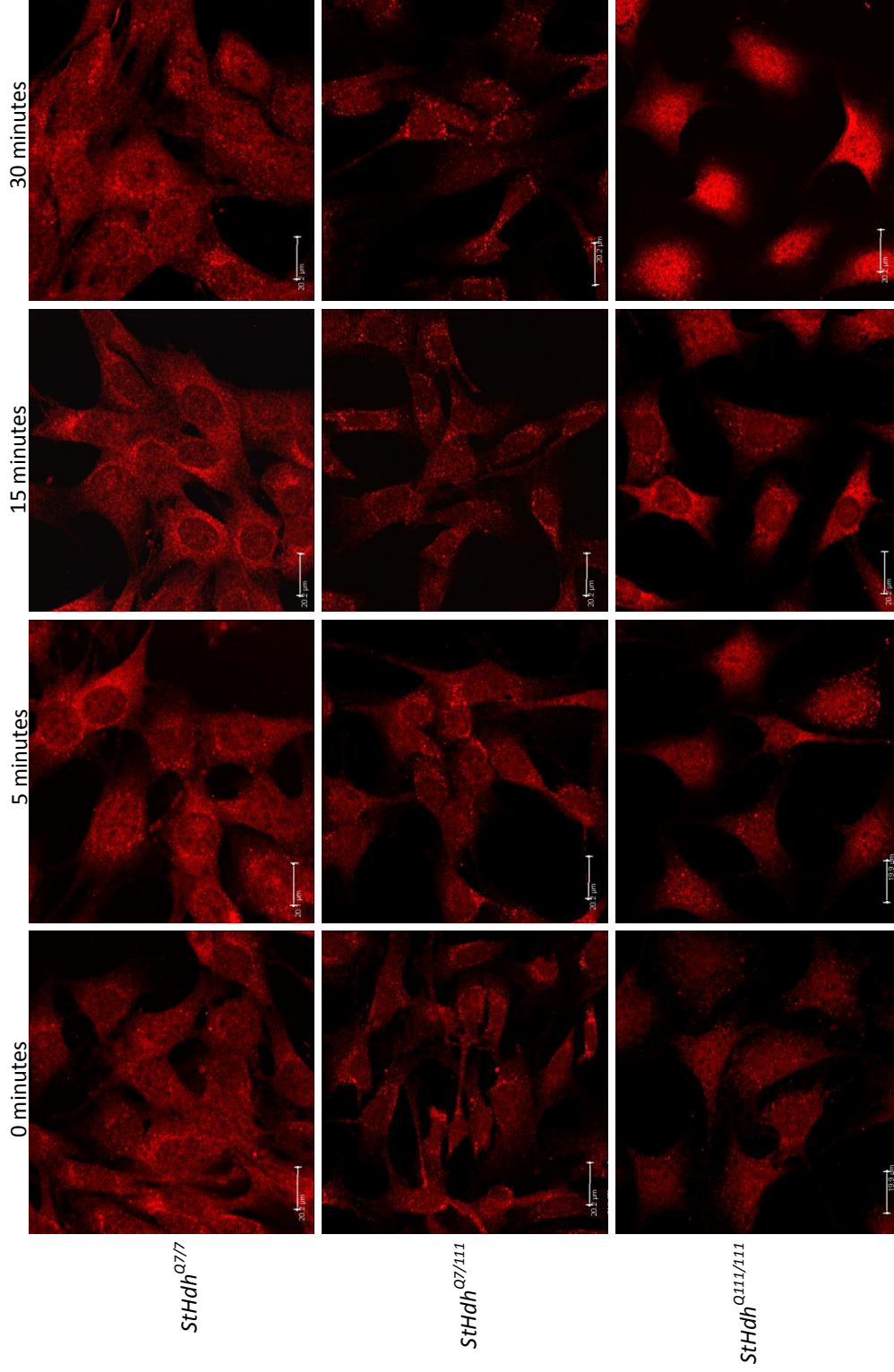
Figure AI.1 Subcellular localisation of an N-terminal epitope of HTT and mHTT in *StHdh*^{Q7/7}, *StHdh*^{Q7/111} and *StHdh*^{Q111/111} cell lines. Cells were fixed following 0, 5, 15 and 30 minutes of stimulation with 100ng/ml EGF, labelled with Ab109115 against amino acids 1-30 of HTT, then analysed by confocal microscopy (see Sections 2.2.1.8 and 2.2.1.9 for further details). Scale bar = 20μm

425
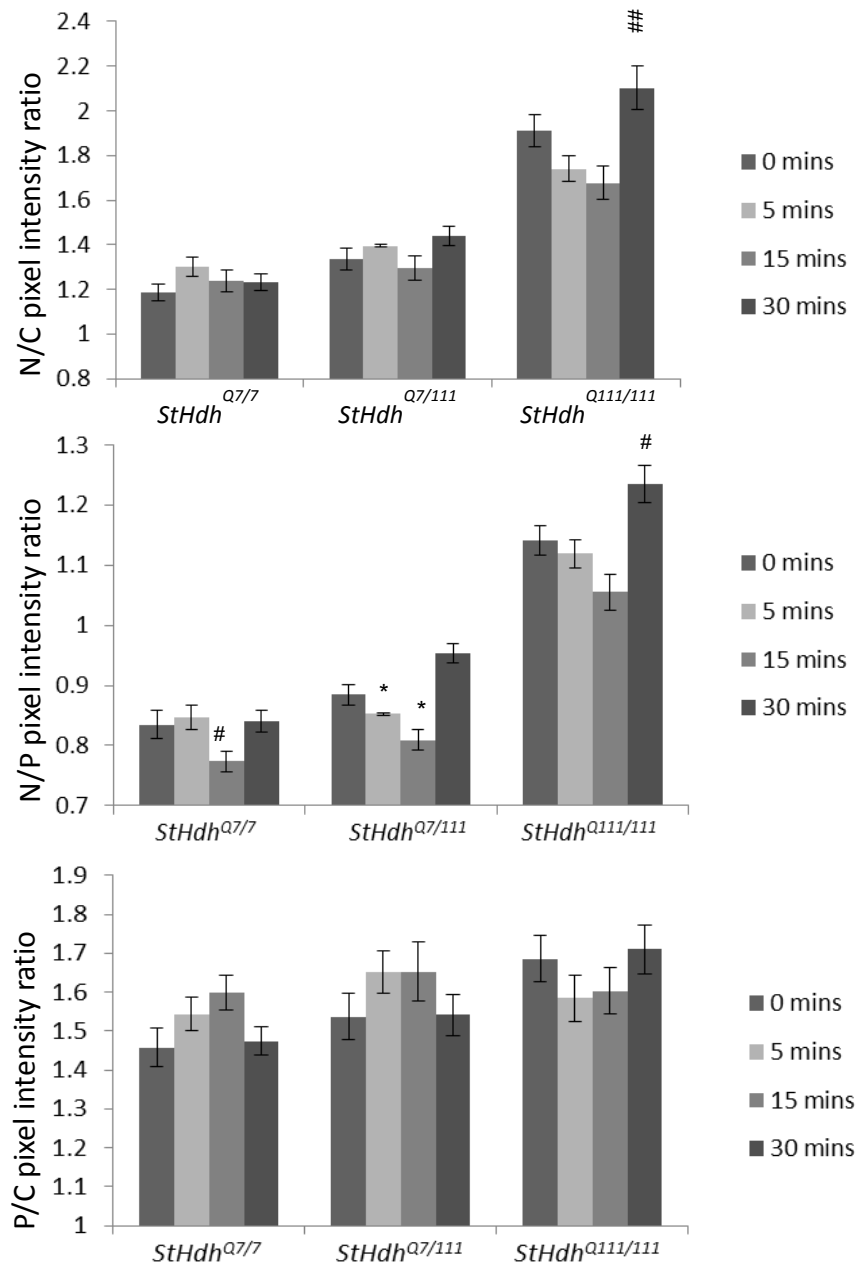
Figure AI.2 Quantitative analysis of immunofluorescence images in Figure AI.1. Nuclear/Cytoplasmic (N/C), Nuclear/Perinuclear (N/P) and Perinuclear/Cytoplasmic (P/C) mean pixel intensity ratios for $StHdh^{Q7/7}$, $StHdh^{Q7/111}$ and $StHdh^{Q111/111}$ cells following 0, 5, 15 and 30 minutes of stimulation with 100ng/ml EGF. Mean pixel intensities were calculated from confocal microscopy images using GNU Image Manipulator (further details of the analysis can be found in Section 2.2.1.10). All images were randomised and analysed blind to genotype and length of time stimulated with EGF. Each condition consisted of 9 confocal microscopy images taken from 3 separate coverslips. A 3x2 ANOVA was carried out for main effects analysis, followed by planned one way ANOVAs and post-hoc Tukey tests. Error bars = SEM.

* Denotes a significant difference from 0mins

\# Denotes a significant difference from 5mins

* p<0.05   ** p<0.01   *** p<0.001

Appendix II - *StHdh*^Q111^ **cell lines immunostained with N17 following EGF stimulation, and a replicate of Ab675 immunostaining carried out in parallel**

The N17 antibody was a kind gift from Ray Truant (McMaster University, Canada). It is a rabbit polyclonal antibody against the first 17 amino acids of the HTT protein, and would therefore be expected to yield similar results to Ab675 and Ab109115. Quantitative image analysis was not carried out with this antibody, as we did not have enough of it to carry out a sufficient number of replicates. However, it was still used to determine if it gave qualitatively comparable results. In comparison to the other N-terminal antibodies that were used here, N17 detects mostly nuclear HTT in all three genotypes (Figure AII.1). There is a slight increase in the amount of perinuclear HTT detected in *StHdh*^Q111/111^ cells as compared to *StHdh*^Q7/111^ and *StHdh*^Q7/7^ cells, but otherwise there is no qualitative difference. In addition, there is no observable effect of EGF stimulation for any of the genotypes. Additional coverslips from the same experiment were probed with Ab675 to determine if the effect of EGF was replicated, and there was reduced detection of this epitope of HTT in the nucleus by 15 minutes of stimulation in the StHdh^Q7/7^ cells, a small effect in the *StHdh*^Q7/111^ cells, and no observable difference in *StHdh*^Q111/111^ cells (Figure AII.2). This is similar to previous findings with the same antibody, Mab2166 and Ab109115 (Sections 3.3.3.3, 3.3.4.3 & 3.3.5). The lack of a visible effect when using N17 may therefore reflect the detection of a different epitope of HTT that either does not relocalise following EGF stimulation, or can be detected regardless of any changes in protein conformation. As the detection of this antibody was reduced in all three genotypes following *Htt* siRNA treatment (Section 3.3.2.3), the lack of response to EGF treatment is unlikely to be due to binding of N17 to non-specific targets.
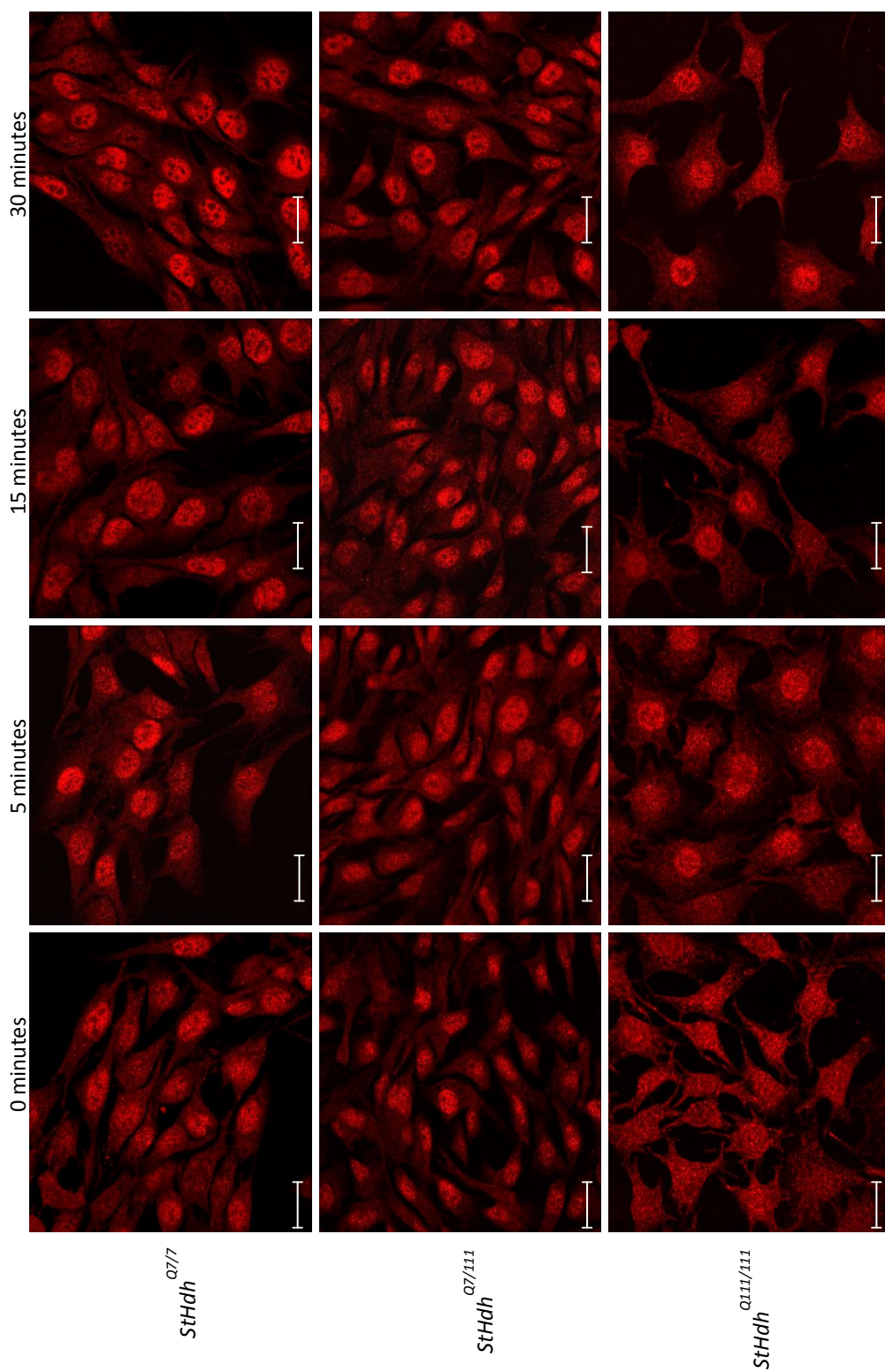
Figure AII.1 Subcellular localisation of an N-terminal epitope of HTT and mHTT in *StHdh*^Q7/7^, *StHdh*^Q7/111^ and *StHdh*^Q111/111^ cell lines. Cells were fixed following 0, 5, 15 and 30 minutes of stimulation with 100ng/ml EGF, labelled with N17 against amino acids 1-17 of HTT, then analysed by confocal microscopy (see Sections 2.2.1.8 and 2.2.1.9 for further details). Scale bar = 20μm
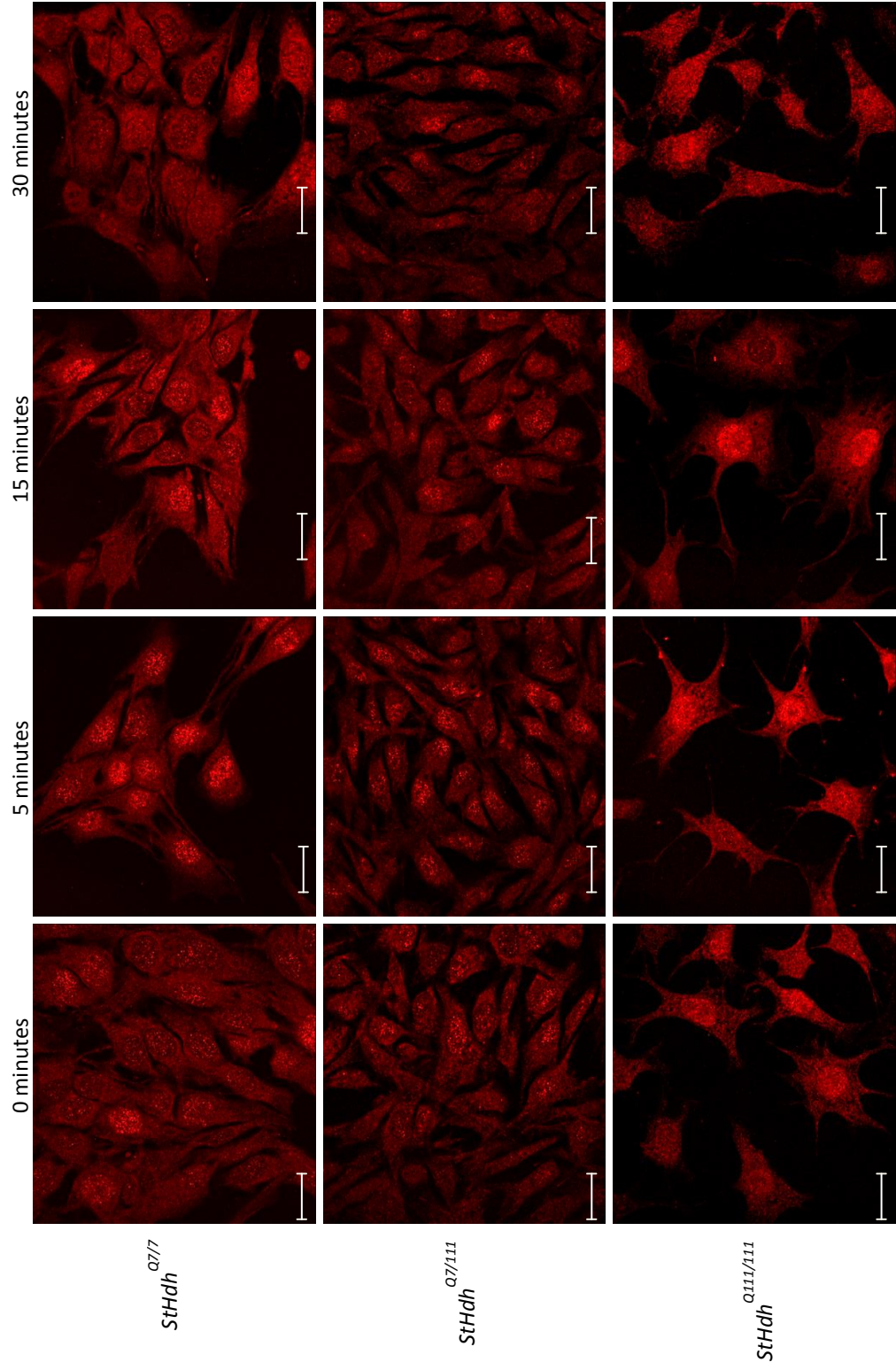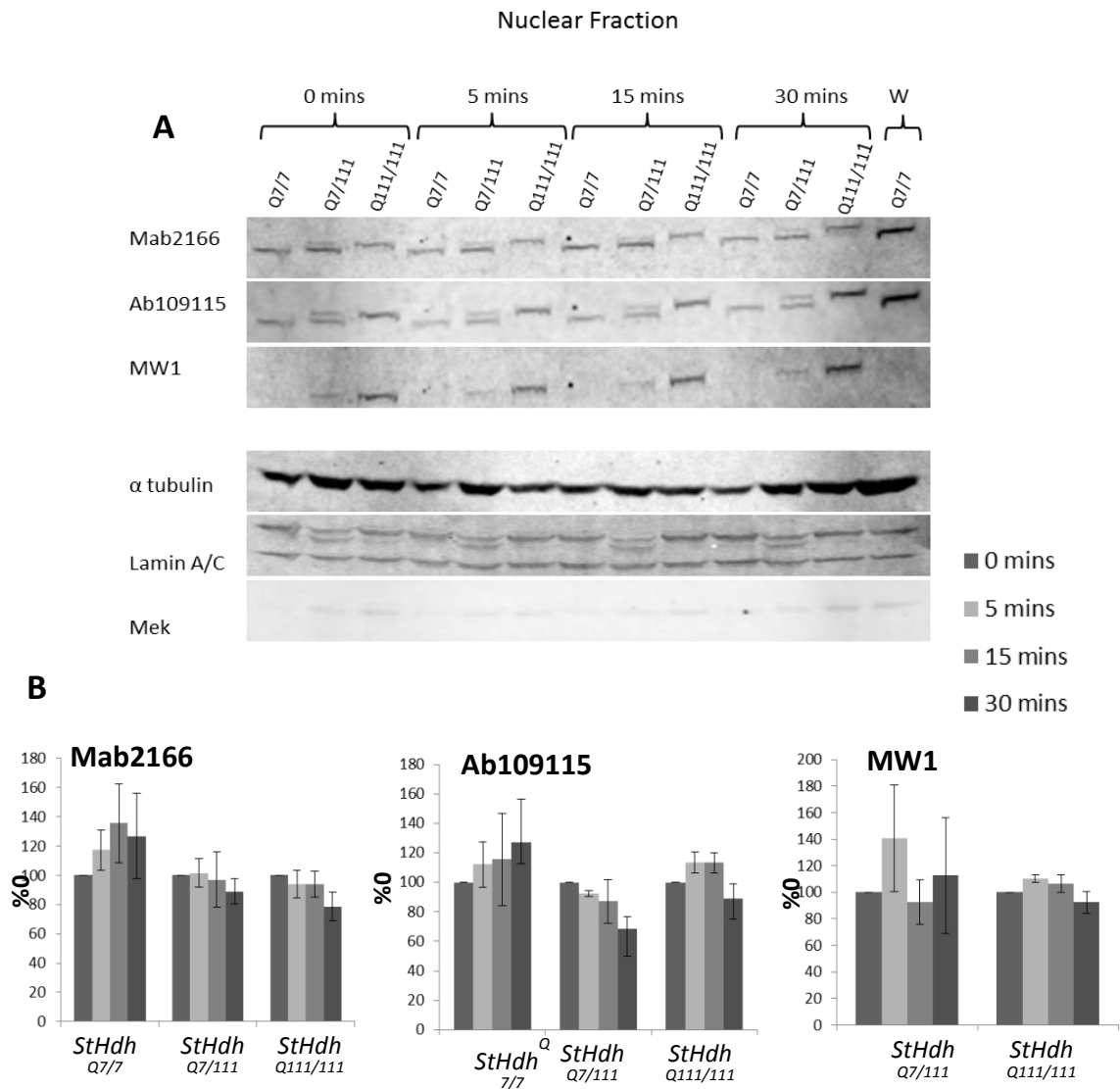
Figure AII.2 Replication of the subcellular localisation of an N-terminal epitope of HTT and mHTT in *StHdh*^{Q7/7}, *StHdh*^{Q7/111} and *StHdh*^{Q111/111} cell lines carried out in parallel with the experiment seen in Figure 3.21. Cells were fixed with Formalin following 0, 5, 15 and 30 minutes of stimulation with 100ng/ml EGF, then labelled with Ab675 against amino acids 1-17 of HTT, then analysed by confocal microscopy (see Sections 2.2.1.8 and 2.2.1.9 for further details). Scale bar = 20μm

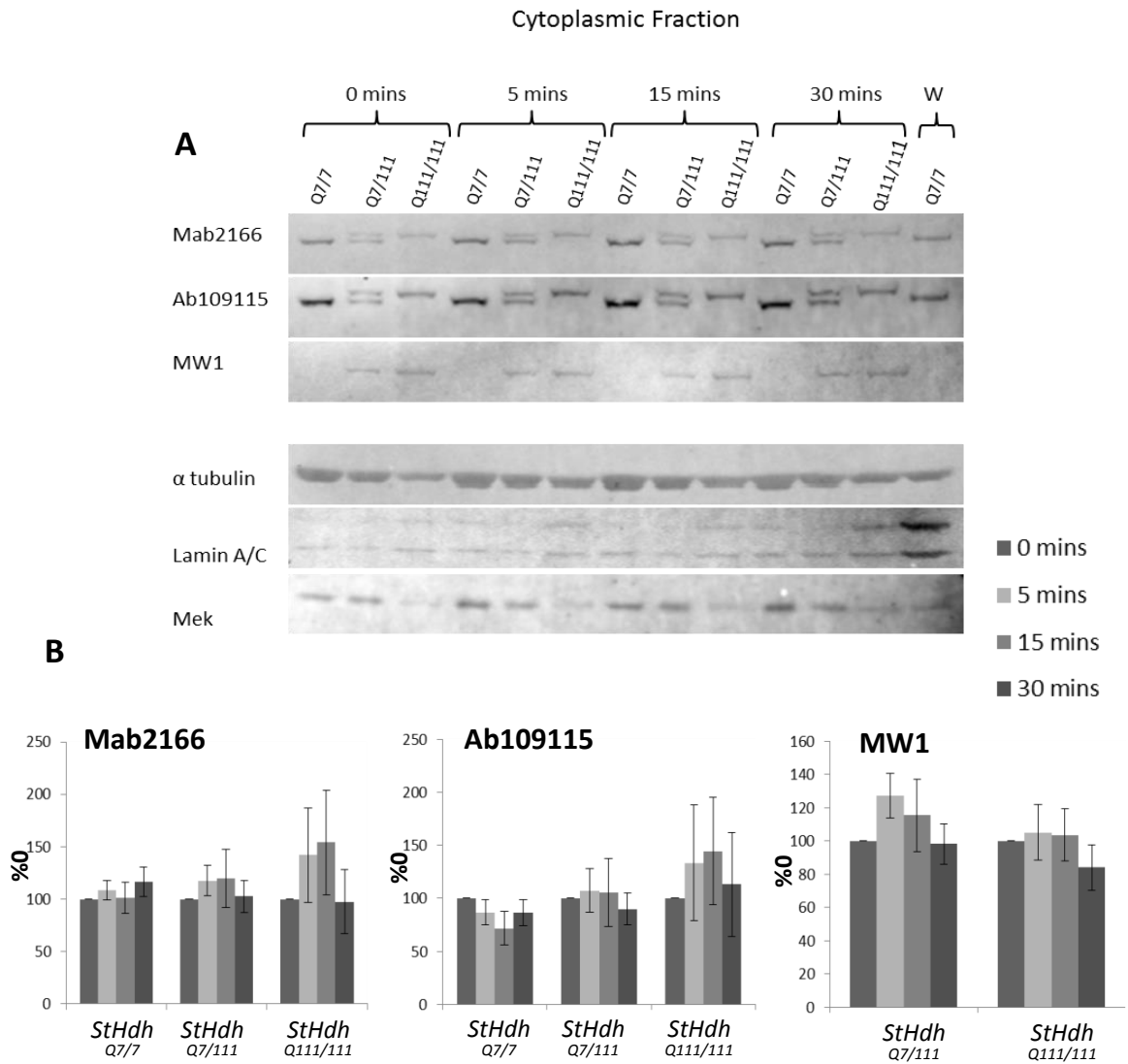## Appendix III - Subcellular fractionation following stimulation with NGF and EGF

Cytoplasmic Fraction
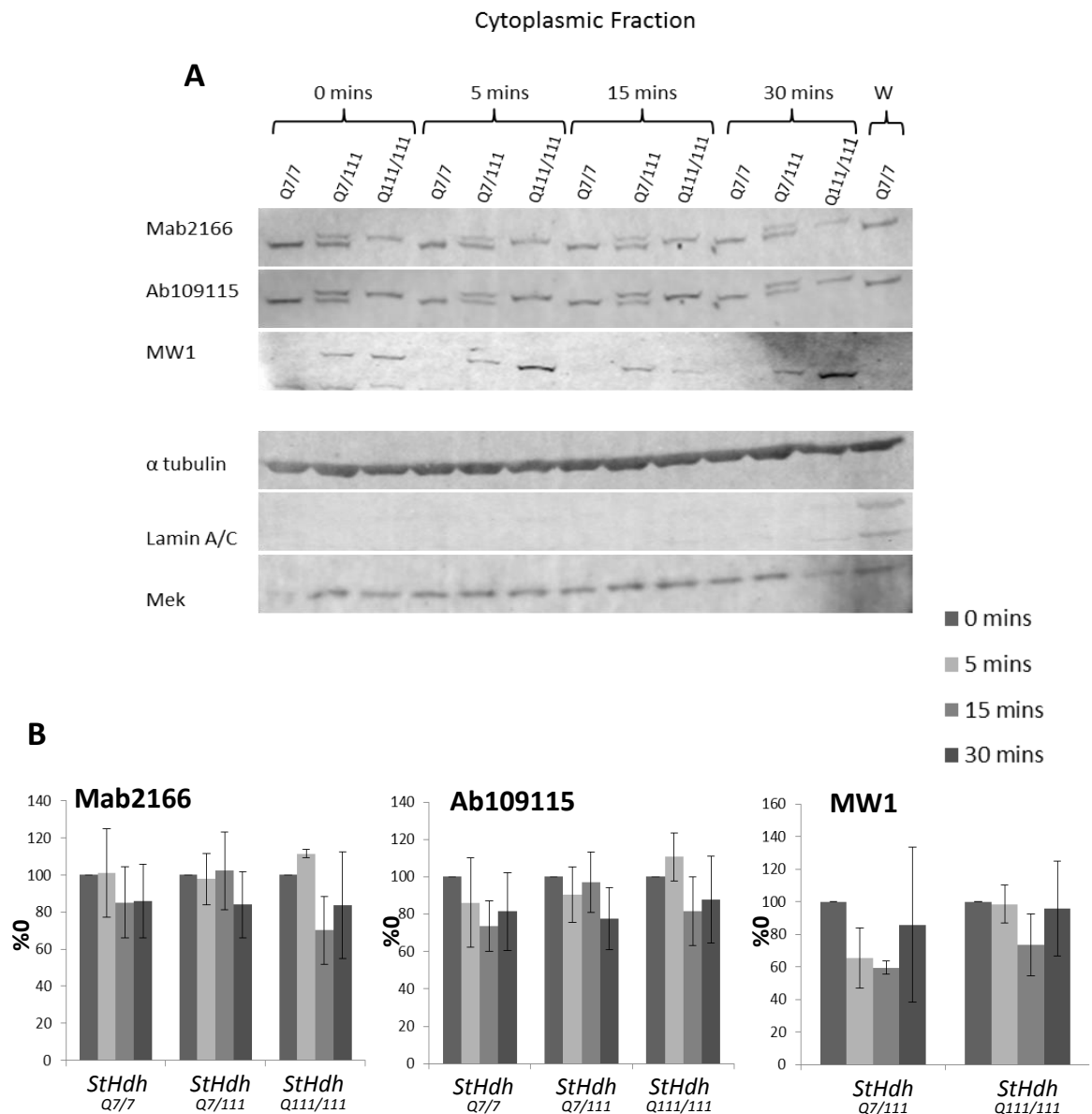
Figure AIII.1 A. Western blots of cytoplasmic fractions of *StHdh*$^{Q7/7}$, *StHdh*$^{Q7/111}$ and *StHdh*$^{Q111/111}$ cells stimulated with 100ng/ml NGF for 0, 5, 15 and 30 minutes before cell lysis and subcellular fractionation (see Section 2.2.2.3 for more details), and a whole cell lysate control (W). Blots were probed with Mab2166, stripped and re-probed with Ab109115, followed by MW1. Fractions were normalised to α-tubulin loading control, and purity of the fraction was assessed by the presence of cytoplasmic marker MEK and lack of the nuclear marker Lamin A/C. **B.** Licor Odyssey quantification of fluorescence intensities (FI) in *A* normalised to the loading control, and expressed as a percentage of 0 mins NGF stimulation (%0). Percentages were analysed by genotype individually by a one way ANOVA due to differences in band intensity between cell types, followed by post-hoc Tukey tests. (Error bars = SEM, n=3).
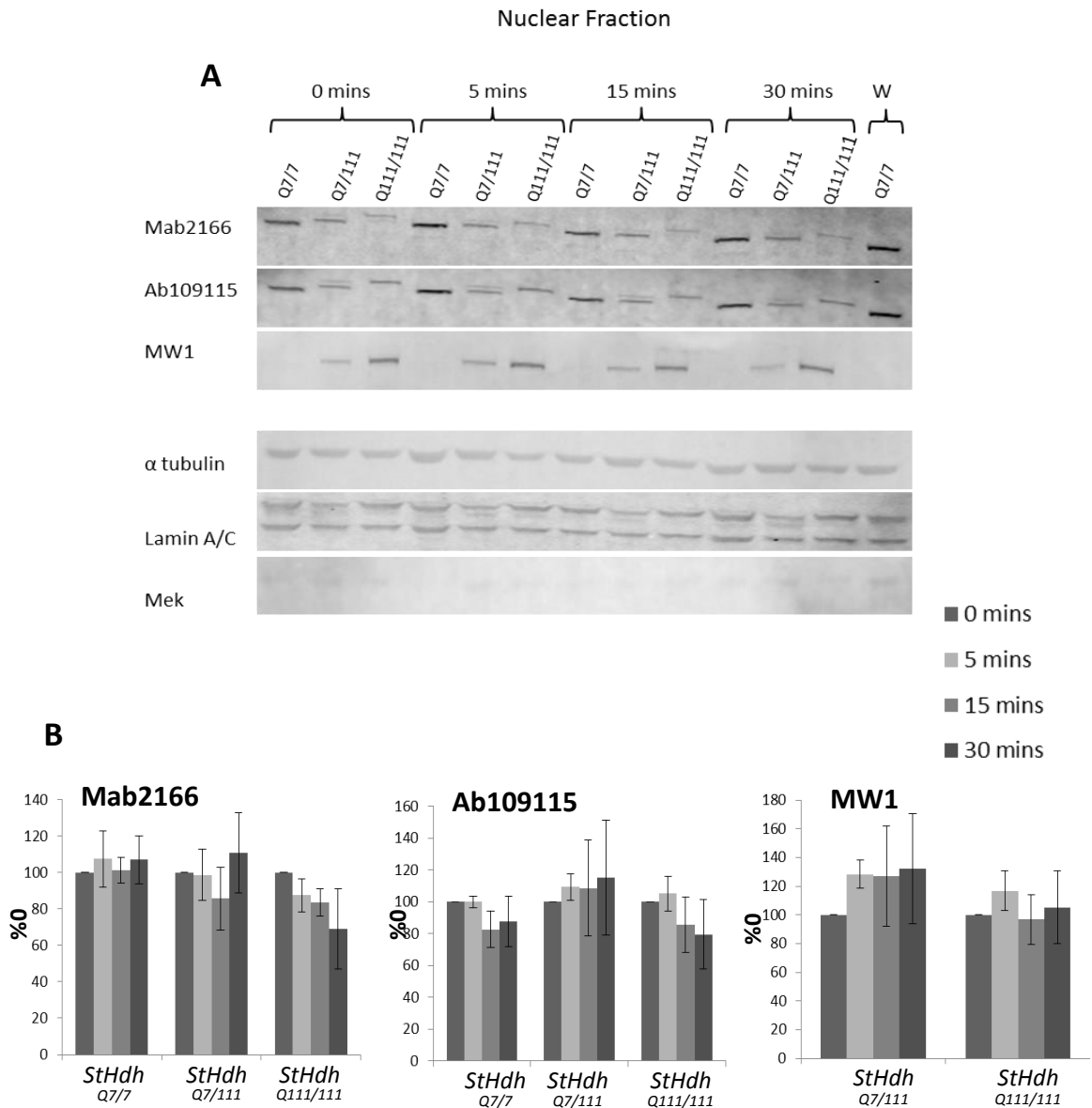
Figure AIII.2 **A**. Western blots of nuclear fractions of *StHdh*$^{Q7/7}$, *StHdh*$^{Q7/111}$ and *StHdh*$^{Q111/111}$ cells stimulated with 100ng/ml NGF for 0, 5, 15 and 30 minutes before cell lysis and subcellular fractionation (see Section 2.2.2.3 for more details), and a whole cell lysate control (W). Blots were probed with Mab2166, stripped and re-probed with Ab109115, followed by MW1. Fractions were normalised to α-tubulin loading control, and purity of the fraction was assessed by the presence of nuclear marker Lamin A/C and lack of the cytoplasmic marker MEK. **B.** Licor Odyssey quantification of fluorescence intensities (FI) in *A* normalised to the loading control, and expressed as a percentage of 0 mins NGF stimulation (%0). Percentages were analysed by genotype individually by a one way ANOVA due to differences in band intensity between cell types, followed by post-hoc Tukey tests (Error bars = SEM, n=3).

Figure AIII.3 A. Western blots of cytoplasmic fractions of $StHdh^{Q7/7}$, $StHdh^{Q7/111}$ and $StHdh^{Q111/111}$ cells stimulated with 100ng/ml EGF for 0, 5, 15 and 30 minutes before cell lysis and subcellular fractionation (see Section 2.2.2.3 for more details), and a whole cell lysate control (W). Blots were probed with Mab2166, stripped and re-probed with Ab109115, followed by MW1. Fractions were normalised to α-tubulin loading control, and purity of the fraction was assessed by the presence of cytoplasmic marker MEK and lack of the nuclear marker Lamin A/C. **B.** Licor Odyssey quantification of fluorescence intensities (FI) in *A* normalised to the loading control, and expressed as a percentage of 0 mins EGF stimulation (%0). Percentages were analysed by genotype individually by a one way ANOVA due to differences in band intensity between cell types, followed by post-hoc Tukey tests. (Error bars = SEM, n=3).

Figure AIII.4 **A**. Western blots of nuclear fractions of *StHdh*[Q7/7], *StHdh*[Q7/111] and *StHdh*[Q111/111] cells stimulated with 100ng/ml EGF for 0, 5, 15 and 30 minutes before cell lysis and subcellular fractionation (see Section 2.2.2.3 for more details), and a whole cell lysate control (W). Blots were probed with Mab2166, stripped and re-probed with Ab109115, followed by MW1. Fractions were normalised to α-tubulin loading control, and purity of the fraction was assessed by the presence of nuclear marker Lamin A/C and lack of the cytoplasmic marker MEK. **B**. Licor Odyssey quantification of fluorescence intensities (FI) in *A* normalised to the loading control, and expressed as a percentage of 0 mins EGF stimulation (%0). Percentages were analysed by genotype individually by a one way ANOVA due to differences in band intensity between cell types, followed by post-hoc Tukey tests (Error bars = SEM, n=3).

Appendix IV - Examples of full western blots from the *StHdh*^{Q111} cell line

Figure AIV.1 provides several examples of the full western blot membranes used in the *StHdh*^{Q111} cell line fractionation experiments (Chapter 3). The blots indicate that in these cells, only full length HTT was detected by both Ab109115 and Mab2166, thus making the presence of smaller N-terminal fragments in these cells difficult to ascertain.
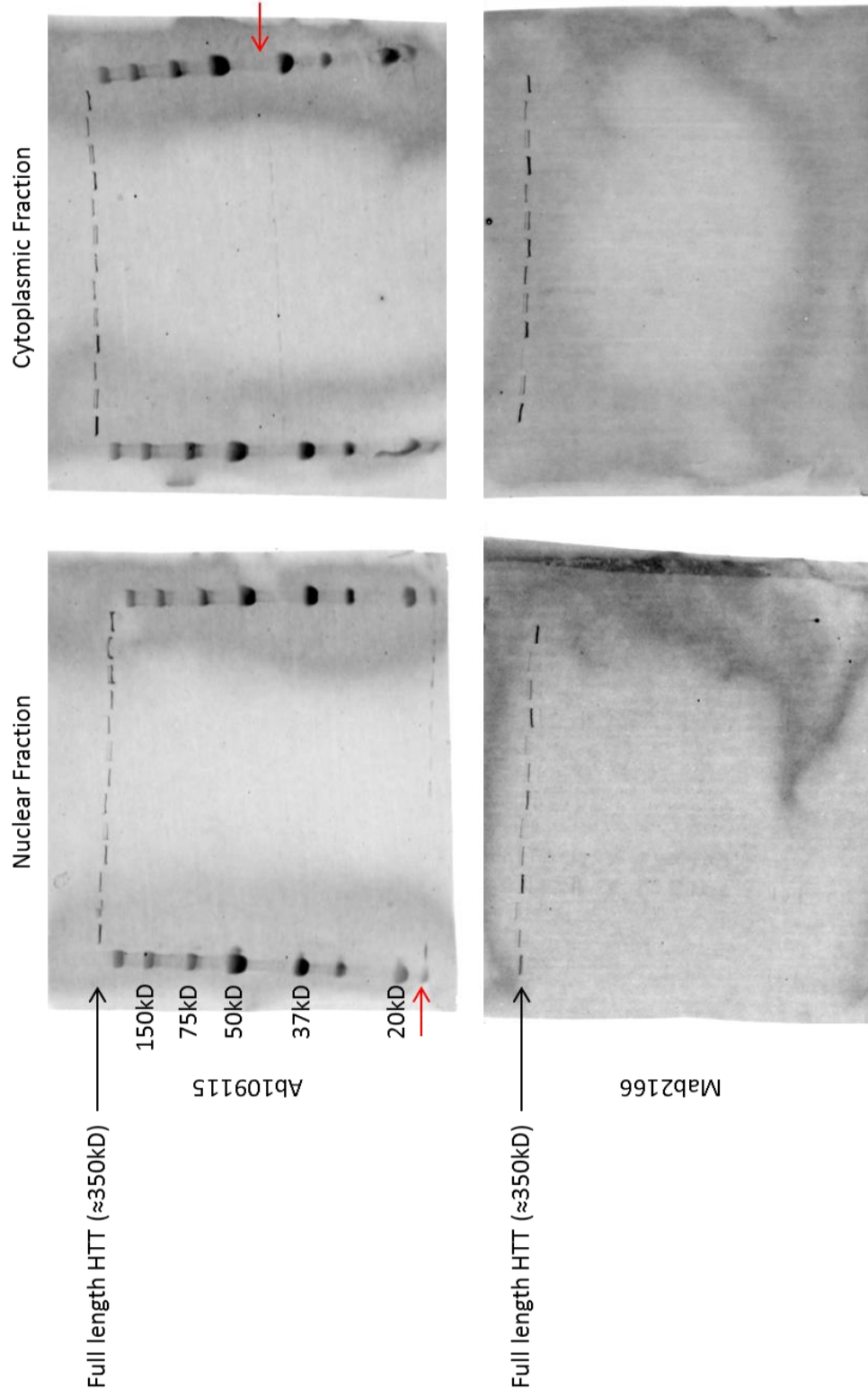
Figure AIV.1 Examples of fractionated *StHdh*^Q111 cell protein lysate western blot membranes probed with Ab109115 and Mab2166. A discernible band is only apparent for full length HTT at ≈350kD. For Ab109115, there is some faint detection of additional bands in both the nuclear and cytoplasmic fractions (indicated by red arrows), but these were not altered by *Htt* siRNA treatment and are variable between blots. Therefore they are likely to be due to non-specific binding.

435

Appendix V - Hdh^{Q111} primary embryonic striatal cell lines immunostained with Ab675 following EGF stimulation

Consistent with previous observations when using Ab675 (Sections 3.3.3.3 & 6.2.3), HTT localisation is more nuclear than when it is detected with either Ab109115 or Mab2166. When looking at Ab675, there is a reduction in nuclear HTT following 5 minutes of EGF stimulation in embryonic striatal cells from all three genotypes from the Hdh^{Q111} model, although this only persists to 15 minutes in Hdh^{Q7/7} cells (Figure AV.1). This is a similar pattern of response to EGF stimulation as was observed in *StHdh*^{Q111} cell lines (Section 3.3.3.3), and also suggests a reduced response to growth factor stimulation in mHTT cells. However, there are no apparent differences in the nuclear localisation of HTT at baseline.
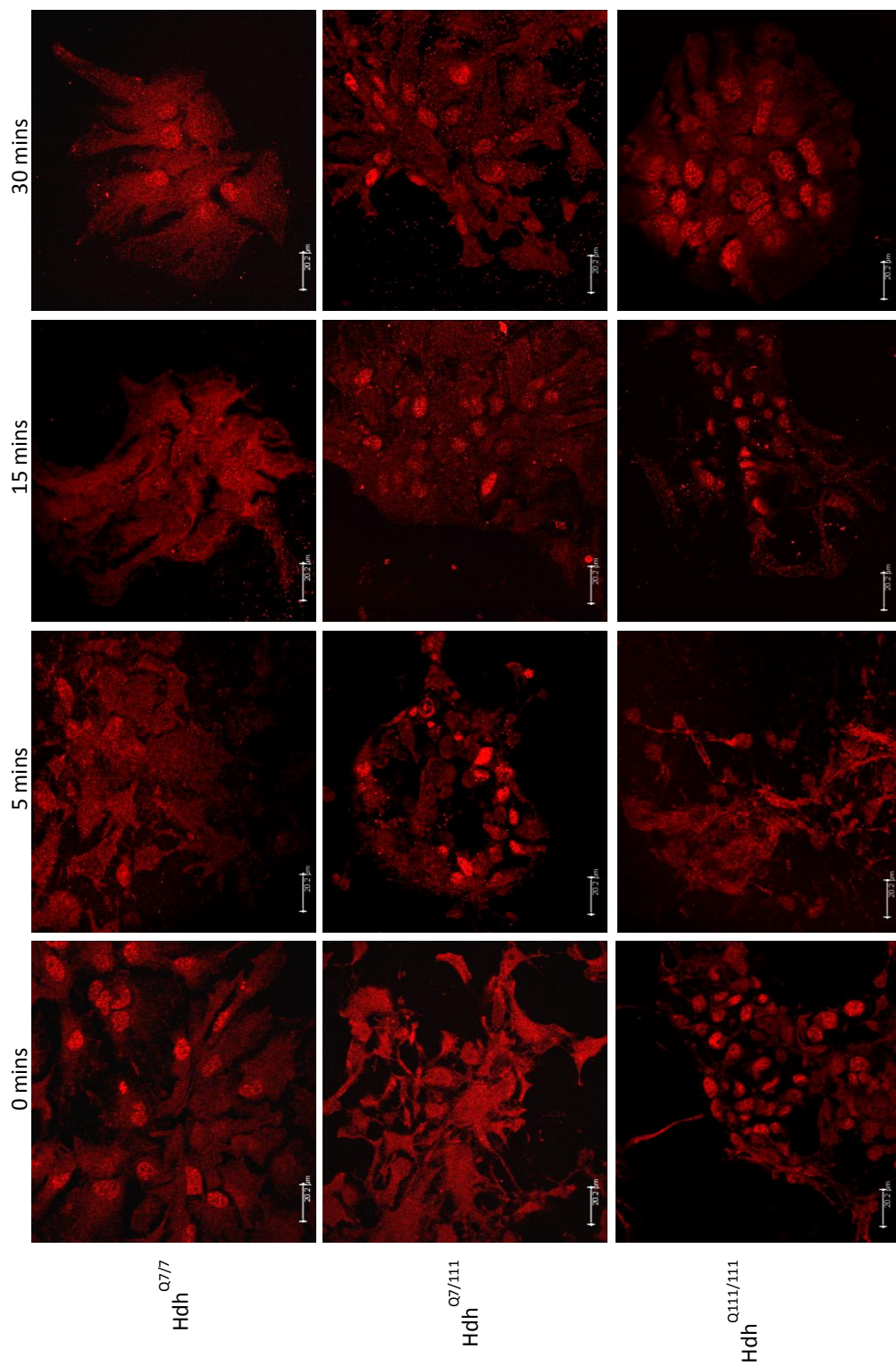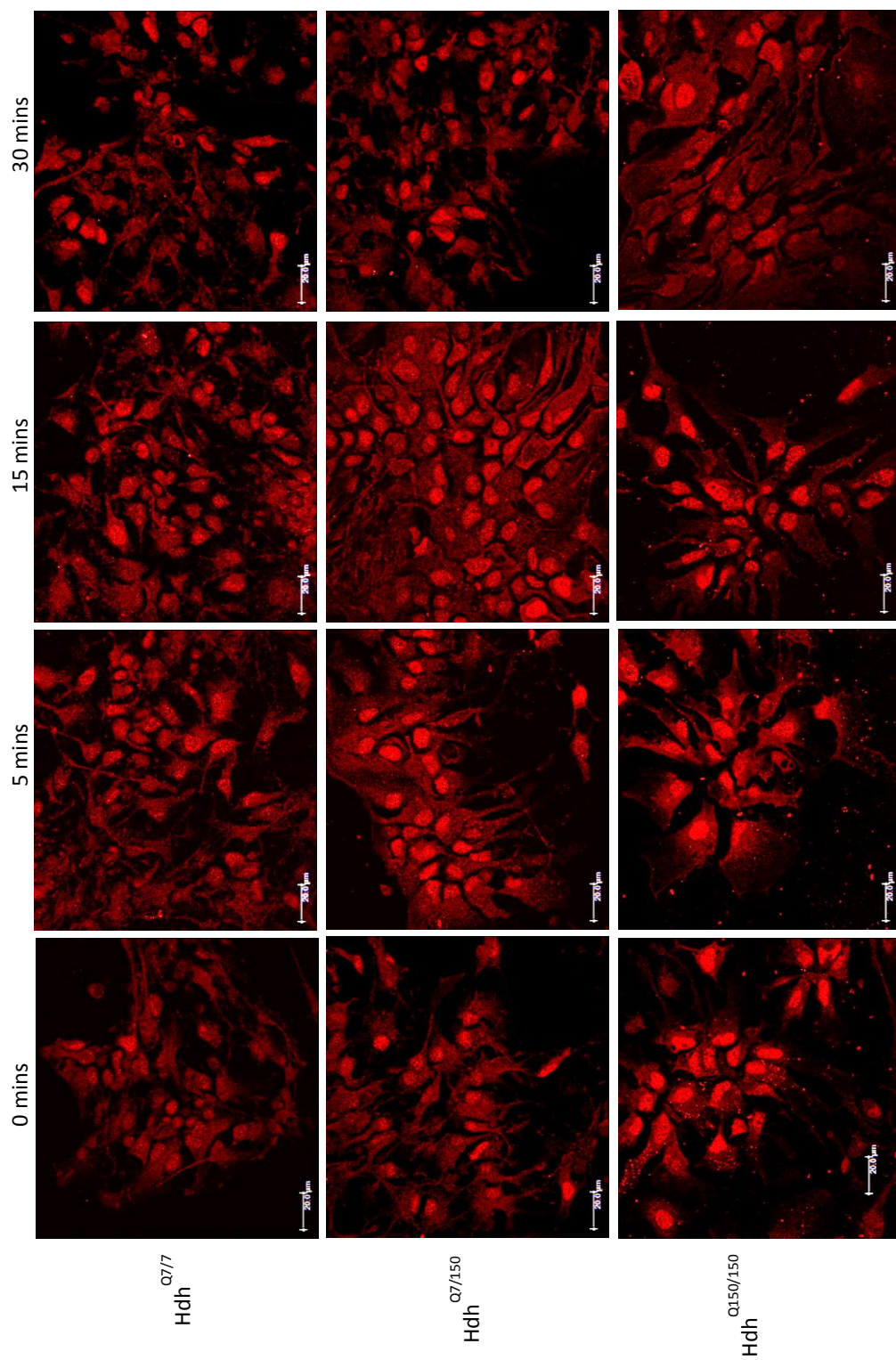
Figure AV.1 Subcellular localisation of an N-terminal epitope of HTT and mHTT in Hdh$^{Q7/7}$, Hdh$^{Q7/111}$ and Hdh$^{Q111/111}$ E14 primary striatal cell cultures. Cells were fixed following 0, 5, 15 and 30 minutes of stimulation with 100ng/ml EGF, labelled with Ab675 against amino acids 1-17 of HTT, then analysed by confocal microscopy (see Sections 2.2.1.8 and 2.2.1.9 for further details). Scale bar = 20μm

437

Appendix VI - Hdh^{Q150} primary embryonic striatal cell lines immunostained with Ab675 following EGF stimulation

Hdh^{Q150} primary cells exhibited an increased nuclear localisation of the HTT epitope detected by Ab675 with increasing mHTT gene dosage (Figure AVI.1). There was a slight reduction in nuclear HTT from 5 minutes following EGF stimulation in Hdh$^{Q7/7}$ cells, but there was no apparent effect in Hdh$^{Q7/150}$ or Hdh$^{Q150/150}$ cells until a slight reduction in nuclear localisation of this epitope at 30 minutes of EGF stimulation.

Figure AVI.1 Subcellular localisation of an N-terminal epitope of HTT and mHTT in Hdh$^{Q7/7}$, Hdh$^{Q7/150}$ and Hdh$^{Q150/150}$ E14 primary striatal cell cultures. Cells were fixed following 0, 5, 15 and 30 minutes of stimulation with 100ng/ml EGF, labelled with Ab675 against amino acids 1-17 of HTT, then analysed by confocal microscopy (see Sections 2.2.1.8 and 2.2.1.9 for further details). Scale bar = 20µm

Full expression data for a panel of genes in Hdh^{Q111} cells that were previously identified in *StHdh*^{Q111} cell lines (Chapter 5) as having either a larger fold change in *StHdh*$^{Q7/7}$ cells (Figure AVII.1), or a larger fold change in *StHdh*$^{Q111/111}$ cells (Figure AVII.2), as well as genes that showed a significant response in *StHdh*$^{Q111/111}$ cells only (Figure AVII.3) following 2 hours 100ng/ml EGF stimulation.
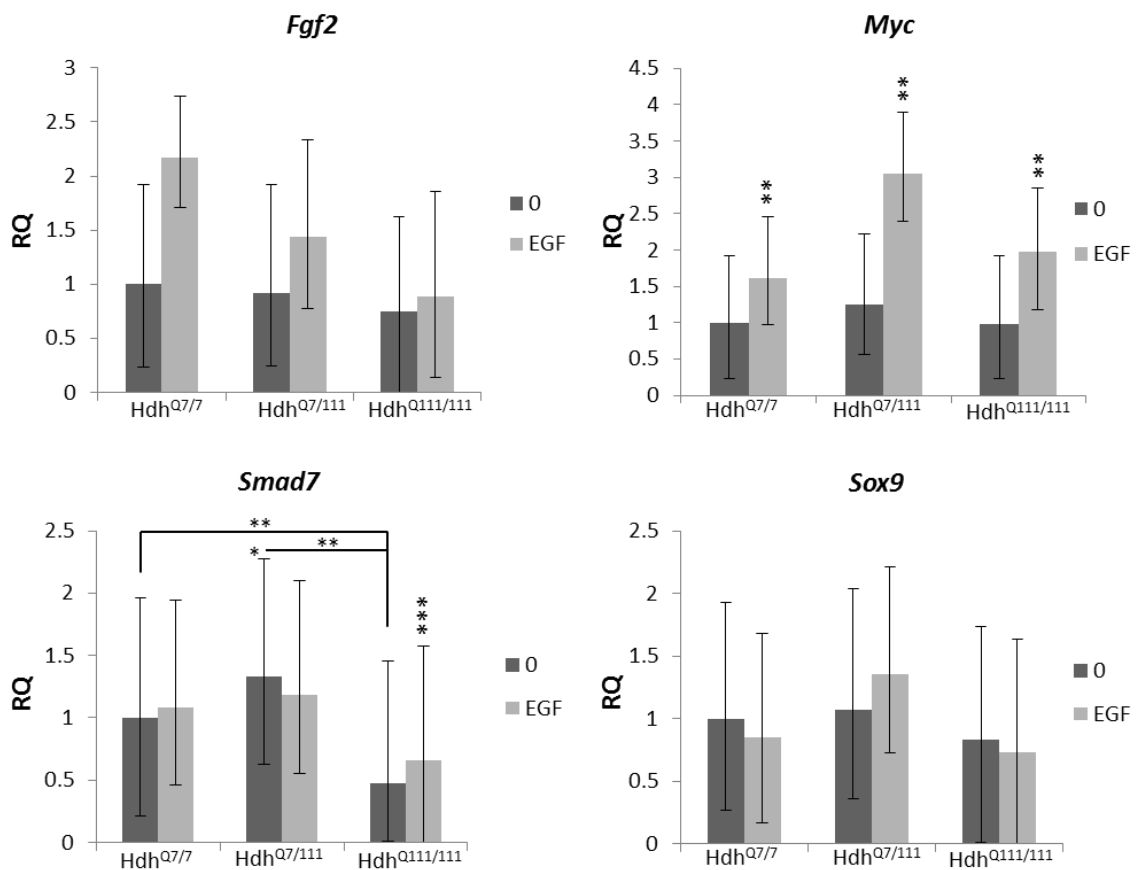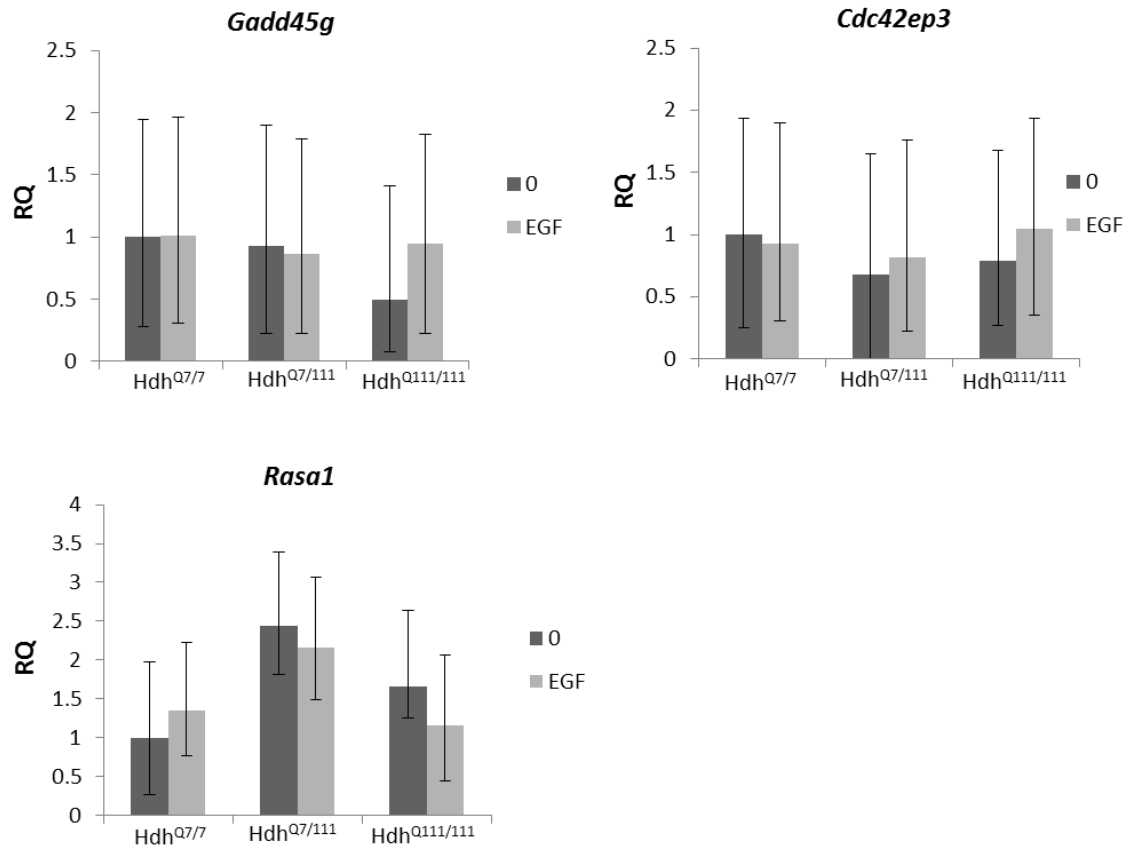

Figure AVII.1 Relative Quantification (RQ) values representing the fold change in gene expression for four genes in Hdh$^{Q7/7}$, Hdh$^{Q7/111}$ and Hdh$^{Q111/111}$ primary embryonic striatal cells at 0 and 2 hours stimulation with 100ng/ml EGF. The genes had been previously identified in Chapter 5 as having a larger change in expression following EGF stimulation in *StHdh*$^{Q7/7}$ cells than in *StHdh*$^{Q111/111}$ cells. Delta cycle threshold (ΔC_t) values were analysed by 3x2 ANOVA and post-hoc Tukey tests. (Error bars = SEM, n=5)

*p<0.05   **p<0.01   ***p<0.001
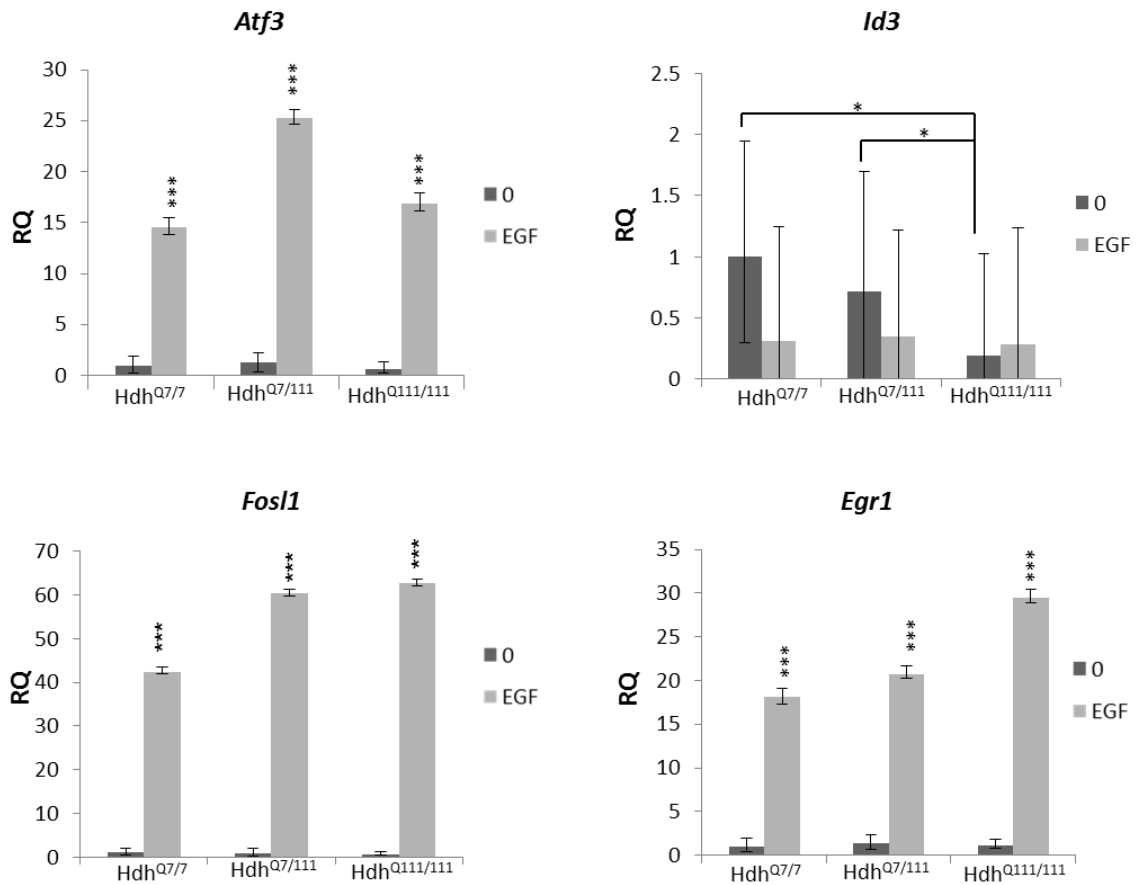
Figure AVII.2 Relative Quantification (RQ) values representing the fold change in gene expression for four genes in Hdh[Q7/7], Hdh[Q7/111] and Hdh[Q111/111] primary embryonic striatal cells at 0 and 2 hours stimulation with 100ng/ml EGF. The genes had been previously identified in Chapter 5 as having a larger change in expression following EGF stimulation in *StHdh*[Q111/111] cells than in *StHdh*[Q7/7] cells. Delta cycle threshold (ΔC_t) values were analysed by 3x2 ANOVA and post-hoc Tukey tests. (Error bars = SEM, n=5)
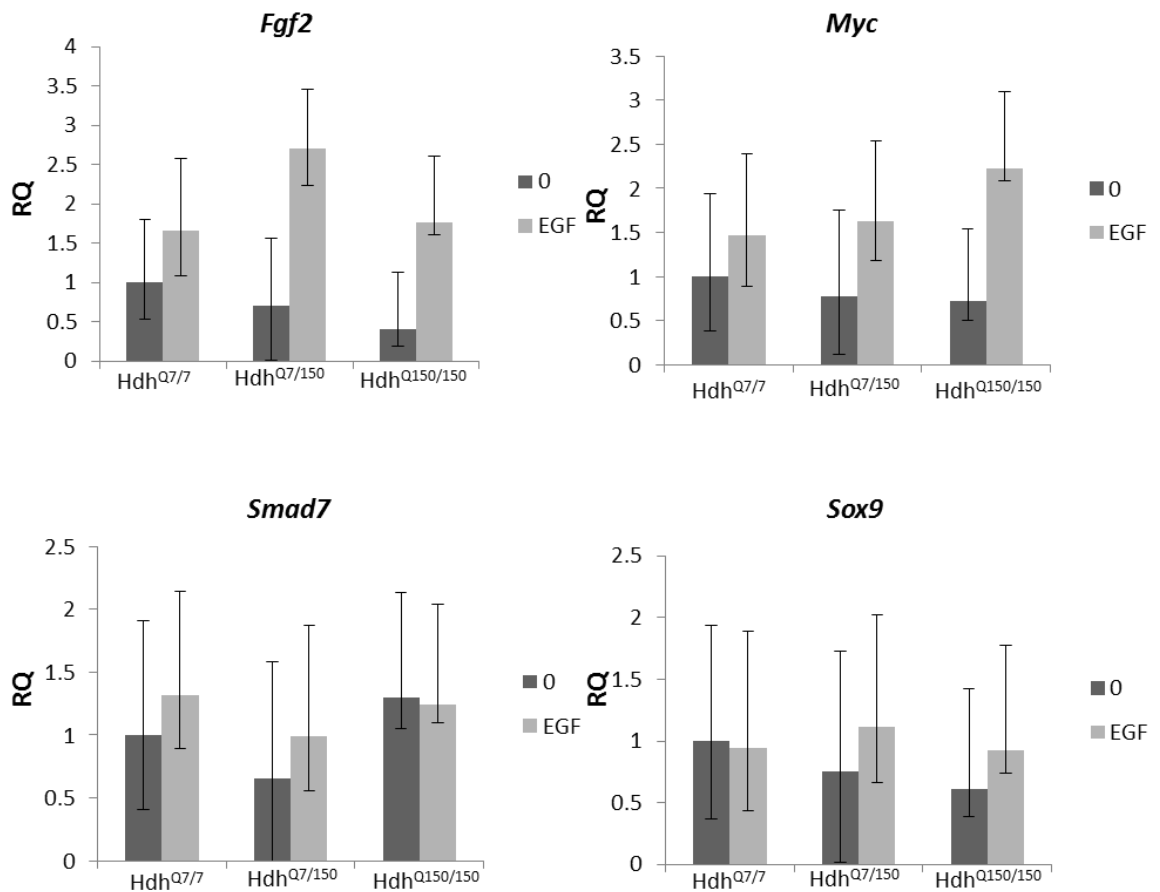
*p<0.05   **p<0.01   ***p<0.001

Figure AVII.3 Relative Quantification (RQ) values representing the fold change in gene expression for three genes in Hdh$^{Q7/7}$, Hdh$^{Q7/111}$ and Hdh$^{Q111/111}$ primary embryonic striatal cells at 0 and 2 hours stimulation with 100ng/ml EGF. The genes had been previously identified in Chapter 5 as having a change in expression following EGF stimulation in *StHdh*$^{Q111/111}$ cells only. Delta cycle threshold (ΔC_t) values were analysed by 3x2 ANOVA and post-hoc Tukey tests. (Error bars = SEM, n=5)

*p<0.05   **p<0.01   ***p<0.001

Full expression data for a panel of genes in Hdh^{Q150} cells that were previously identified in *StHdh*^{Q111} cell lines (Chapter 5) as having either a larger fold change in *StHdh*$^{Q7/7}$ cells (Figure AVIII.1), or a larger fold change in *StHdh*$^{Q111/111}$ cells (Figure AVIII.2), as well as genes that showed a significant response in *StHdh*$^{Q111/111}$ cells only (Figure AVIII.3) following 2 hours 100ng/ml EGF stimulation.
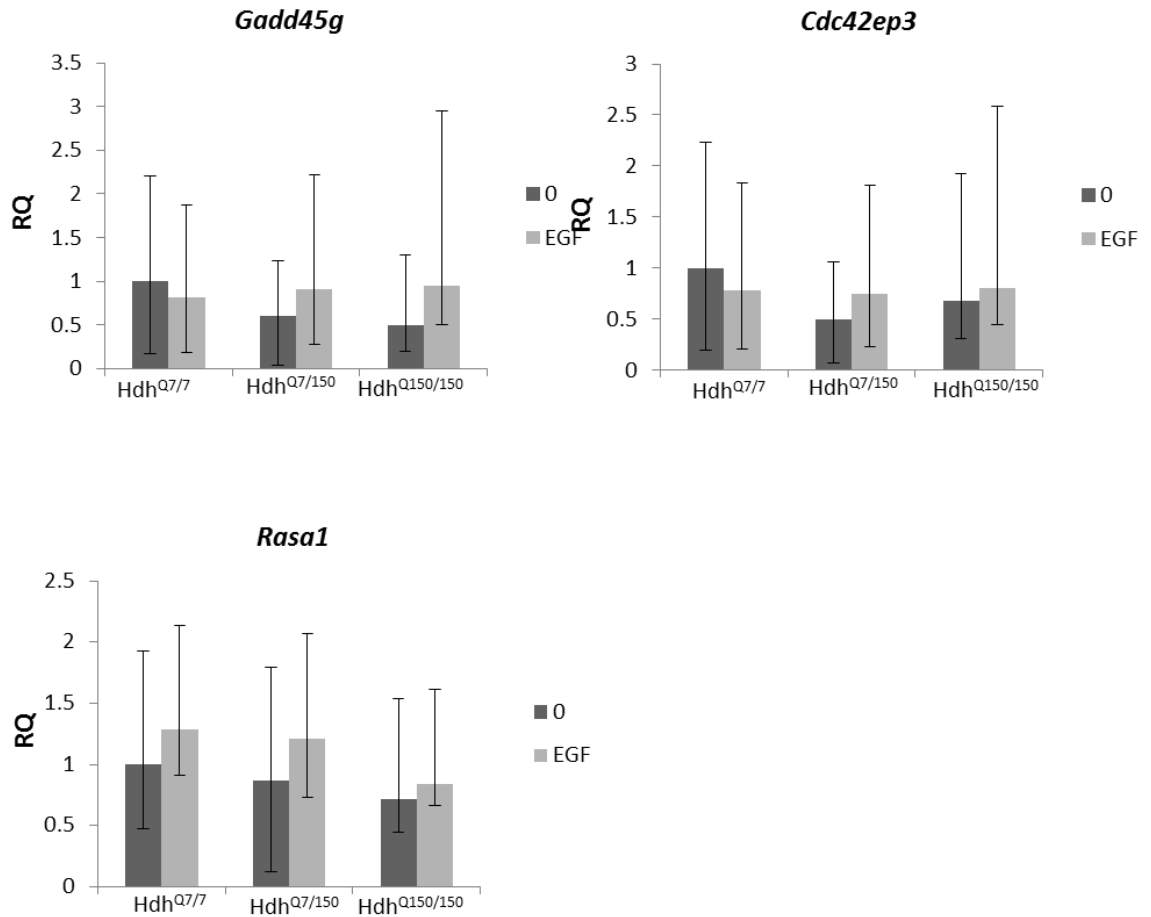

Figure AVIII.1 Relative Quantification (RQ) values representing the fold change in gene expression for four genes in Hdh$^{Q7/7}$, Hdh$^{Q7/150}$ and Hdh$^{Q150/150}$ primary embryonic striatal cells at 0 and 2 hours stimulation with 100ng/ml EGF. The genes had been previously identified in Chapter 5 as having a larger change in expression following EGF stimulation in *StHdh*$^{Q7/7}$ cells than in *StHdh*$^{Q111/111}$ cells. Delta cycle threshold (ΔC_t) values were analysed by 3x2 ANOVA and post-hoc Tukey tests. (Error bars = SEM, n=5)

*p<0.05   **p<0.01   ***p<0.001
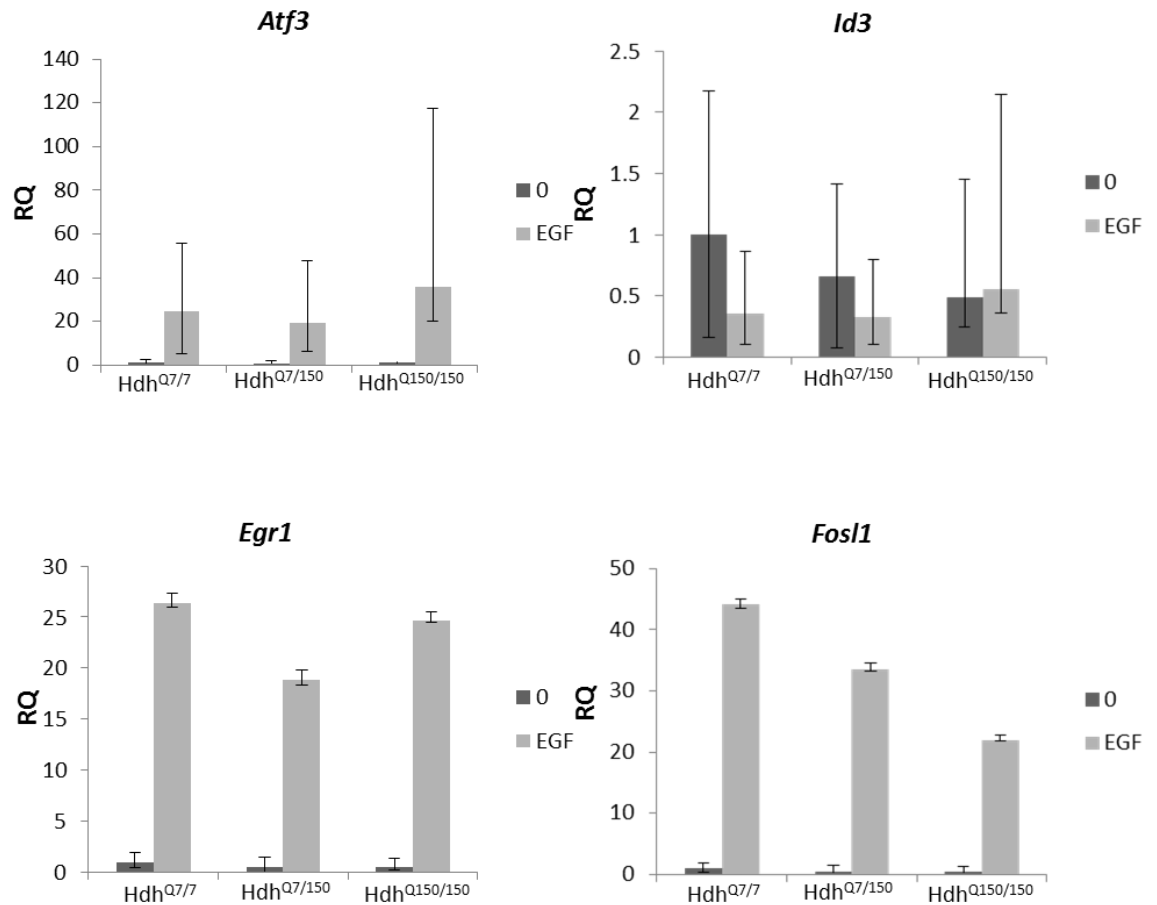
Figure AVIII.2 Relative Quantification (RQ) values representing the fold change in gene expression for four genes in Hdh[Q7/7], Hdh[Q7/150] and Hdh[Q150/150] primary embryonic striatal cells at 0 and 2 hours stimulation with 100ng/ml EGF. The genes had been previously identified in Chapter 5 as having a larger change in expression following EGF stimulation in *StHdh*[Q111/111] cells than in *StHdh*[Q7/7] cells. Delta cycle threshold (ΔC_t) values were analysed by 3x2 ANOVA and post-hoc Tukey tests. (Error bars = SEM, n=5)

*$p<0.05$ **$p<0.01$ ***$p<0.001$

Figure AVIII.3 Relative Quantification (RQ) values representing the fold change in gene expression for three genes in Hdh$^{Q7/7}$, Hdh$^{Q7/150}$ and Hdh$^{Q150/150}$ primary embryonic striatal cells at 0 and 2 hours stimulation with 100ng/ml EGF. The genes had been previously identified in Chapter 5 as having a change in expression following EGF stimulation in *StHdh*$^{Q111/111}$ cells only. Delta cycle threshold (ΔC_t) values were analysed by 3x2 ANOVA and post-hoc Tukey tests. (Error bars = SEM, n=5)

*p<0.05   **p<0.01   ***p<0.001